

**Developing new methods
for specific RNA modification**

Inaugural-Dissertation

zur Erlangung des Doktorgrades (Dr. rer. nat.)
der Mathematisch-Naturwissenschaftlichen Fakultät
der Universität zu Köln

vorgelegt von

Lisa Bornewasser

aus Bonn

Köln

2022

Berichtersteller:

Prof.'in Dr. Stephanie Kath-Schorr
Prof.'in Dr. Ines Neundorf

Tag der mündlichen Prüfung:

07.03.2023

Parts of this thesis have been published in the following journals:

Bornewasser, L.; Domnick, C.; Kath-Schorr, S., Stronger together for in-cell translation: natural and unnatural base modified mRNA, *Chem. Sci.* **2022**, *13*, 4753-4761 (doi: 10.1039/D2SC00670G).

Bornewasser, L.; Kath-Schorr, S., Preparation of Site-Specifically Spin-Labeled RNA by in Vitro Transcription Using an Expanded Genetic Alphabet, *Methods in Molecular Biology (Clifton, N.J.)* **2022**, *2439*, 223-240 (doi: 10.1007/978-1-0716-2047-2_15).

Domnick, C.; Eggert, F.; Wuebben, C.; Bornewasser, L.; Hagelueken, G.; Schiemann, O.; Kath-Schorr, S., EPR Distance Measurements on Long Non-coding RNAs Empowered by Genetic Alphabet Expansion Transcription, *Angew. Chem. Int. Ed.* **2020**, *59*, 7891-7896 (doi: 10.1002/anie.201916447).

„The question today is how one can convince
humanity to consent to their own survival.”

Marc-Uwe Kling, QualityLand

Abstract

Ribonucleic acids (RNAs), and messenger RNAs (mRNAs) in particular, have the potential to play a leading role in future therapeutic research. During the SARS-CoV-2 pandemic, mRNA vaccines have proven useful and highly effective. Therefore, it is of great interest to further investigate RNA and to broaden the current knowledge about RNA function, structure as well as modifications and their effects. Expansion of the genetic alphabet by use of unnatural bases (UB) can contribute to this, both by modifying RNA and extracting new information from the modified RNA.

In this thesis, unnatural base modifications were utilized for site-specific introduction of various functionalities into different RNA sequences. A valuable contribution was made towards structure elucidation of the non-coding and complex folded regulatory *Xist A-repeat region*. Here, incorporation of UB-attached nitroxide spin labels enabled inter-spin distance measurements and thus support for a previously proposed structure by targeting different labeling positions.

Multifaceted analysis of cellular applications was presented for protein-coding mRNA sequences carrying cyclopropene (CP)-functionalized UB modifications in their 3'-untranslated regions. Employing inverse electron demand Diels-Alder click chemistry, live-cell labeling of CP-modified mRNAs with tetrazine-conjugated fluorophores allowed excellent spatiotemporal mRNA visualization in cells. In addition, highly modified mRNA sequences with a combination of site-specific unnatural and random positioned natural base modifications were investigated regarding their influence on mRNA stability and functionality. A combined temporal quantification was performed for cellular mRNA levels and cellular expression of the mRNA-encoded reporter protein. The combination of unnatural and natural base modifications was shown to synergistically improve both mRNA stability in cells and cellular protein expression through outstanding mRNA translation efficiency.

Briefly, UB modifications proved advantageous for research on both coding and non-coding RNA. Moreover, site-specific UB modifications facilitated non-disruptive investigations on different parameters such as structure, function and visualization of RNA. The applications and methods developed in this thesis will support future RNA research and therapeutic development.

Zusammenfassung

Ribonukleinsäuren (RNAs), insbesondere Boten-RNAs (mRNAs), haben das Potenzial, in der künftigen therapeutischen Forschung eine führende Rolle zu spielen. Während der SARS-CoV-2 Pandemie haben sich mRNA-Impfstoffe als nützlich und hochwirksam erwiesen. Daher ist es von großem Interesse, RNA weiter zu erforschen und das derzeitige Wissen über Funktion, Struktur sowie Modifikationen an RNA und deren Auswirkungen auszubauen. Die Erweiterung des genetischen Alphabets durch die Verwendung unnatürlicher Basen (UB) kann dazu beitragen, sowohl durch die Modifizierung der RNA als auch durch die Gewinnung neuer Erkenntnisse aus der modifizierten RNA.

In dieser Arbeit wurden unnatürliche Basenmodifikationen für die ortsspezifische Einführung unterschiedlicher Funktionalitäten in verschiedene RNA-Sequenzen genutzt. Es wurde ein wertvoller Beitrag zur Strukturaufklärung der nicht kodierenden und komplex gefalteten regulatorischen *Xist A-Wiederholungsregion* geleistet. Hierbei ermöglichte der Einbau von UB-gebundenen Nitroxid-Spin-Sonden die Messung des Inter-Spin-Abstands. So wurde mithilfe von verschiedenen, gezielten Markierungspositionen eine zuvor vorgeschlagene Struktur bestärkt.

Für proteinkodierende mRNA-Sequenzen mit Cyclopropen (CP)-funktionalisierten UB-Modifikationen in ihren 3'-untranslatierten Regionen, wurden vielfältige Analysen zellulärer Anwendungen vorgestellt. Unter Verwendung der Klickchemie von Diels-Alder-Reaktionen mit inversem Elektronenbedarf ermöglichte die Markierung CP-modifizierter mRNAs mit Tetrazin-konjugierten Fluorophoren eine hervorragende räumlich-zeitliche Visualisierung der mRNA in Zellen. Darüber hinaus wurden hochgradig modifizierte mRNA-Sequenzen mit einer Kombination aus ortsspezifischen unnatürlichen und zufällig positionierten natürlichen Basenmodifikationen auf ihren Einfluss auf die mRNA-Stabilität und mRNA-Funktionalität hin untersucht. Es wurde eine kombinierte zeitliche Quantifizierung der zellulären mRNA-Spiegel und der zellulären Expression des mRNA-kodierten Reporterproteins durchgeführt. Es wurde gezeigt, dass die Kombination von unnatürlichen und natürlichen Basenmodifikationen sowohl die mRNA-Stabilität in den Zellen als auch die zelluläre Proteinexpression durch eine hervorragende mRNA-Translationseffizienz synergistisch verbessert.

UB-Modifikationen erwiesen sich als vorteilhaft für die Forschung sowohl an kodierender als auch an nicht-kodierender RNA. Darüber hinaus erleichterten ortsspezifische UB-Modifikationen nicht-disruptive Untersuchungen zu verschiedenen Parametern wie Struktur, Funktion und Visualisierung von RNA. Die in dieser Arbeit entwickelten Anwendungen und Methoden werden zu zukünftiger RNA-Forschung und therapeutischer Entwicklung unterstützend beitragen.

Vorwort

Die vorliegende Arbeit wurde im Zeitraum von September 2018 bis Dezember 2022 am Institut für Organische Chemie der Universität zu Köln, sowie zuvor am Institut für Life & Medical Sciences (LIMES) der Universität Bonn unter Anleitung von Frau Prof.'in Dr. Stephanie Kath-Schorr angefertigt.

Mein ausdrücklicher Dank gilt Prof.'in Dr. Stephanie Kath-Schorr, die mir die Arbeit an diesen spannenden Forschungsthemen ermöglicht hat. Ich bedanke mich für ihre fachliche sowie freundliche Unterstützung und engagierte Betreuung.

Frau Prof.'in Dr. Ines Neundorf danke ich herzlich für die Übernahme des Zweitgutachtens sowie für die Zweitbetreuung meiner Promotion an der Universität zu Köln.

Herrn Prof. Dr. Dr. (h.c.) Sanjay Mathur danke ich für die Übernahme des Prüfungsvorsitzes. Bei Herrn Dr. Jörg-Martin Neudörfl bedanke ich mich für die Schriftführung.

Bedanken möchte ich mich auch bei meinen Kolleg*innen und Freund*innen des Arbeitskreises Kath-Schorr. Ich danke euch für eure Unterstützung, die immer angenehme Arbeitsatmosphäre und schöne gemeinsame Zeiten. Besonders hervorheben möchte ich hierbei Dr. Frank Eggert, Dr. Christof Domnick, Hannah Depmeier und Eva Hoffmann.

Bei Dr. Frank Eggert und Dr. Christof Domnick möchte ich mich außerdem für ihre synthetischen Arbeiten bedanken, deren Produkte ich in meinen Arbeiten verwendet habe.

Zusätzlich möchte ich Dr. Christof Domnick für das Korrekturlesen dieser Arbeit danken.

Ebenfalls bedanke ich mich bei Prof. Dr. Günter Mayer und Prof. Dr. Michael Famulok am LIMES Institut der Universität Bonn. Ich bedanke mich für Ihre Großzügigkeit bei der Mitnutzung von Geräten und Laborplätzen. Auch möchte ich den Mitarbeitenden der Arbeitskreise Mayer und Famulok für eine angenehme Arbeitsatmosphäre und den wissenschaftlichen Austausch danken.

Ich danke allen Studierenden, die meine Arbeit im Rahmen von Praktika und Abschlussarbeiten begleitet haben.

Mein Dank gilt auch den Mitarbeitenden der zentralen Einrichtungen an der Universität zu Köln sowie der Universität Bonn.

Des Weiteren danke ich Kooperationspartner*innen für spannende Fragestellungen und den wissenschaftlichen Austausch.

Bedanken möchte ich mich bei meinen Freund*innen und meiner Familie. Ihr habt mich immer unterstützt und motiviert.

Mein Dank gilt meinen Eltern, Dr. Maria Luise und Norbert Konrad, meiner Schwester Nicole Konrad und meiner dazugewonnenen Familie auf der Seite meines Ehemannes, voran meinen Schwiegereltern Gisela und Berthold Bornewasser.

Mein besonderer Dank gilt meinem Ehemann Simon Bornewasser. Danke für deine ermutigende und liebevolle Unterstützung, deinen immerwährenden Rückhalt und dein unerschöpfliches Verständnis.

Contents

1 Theoretical Background.....	1
1.1 Coding and noncoding RNAs in light of the central dogma of molecular biology	1
1.2 Artificial nucleobases and natural occurring nucleobase modifications.....	3
1.2.1 Unnatural base pairs (UBPs): a brief history of the developments	4
1.2.2 Natural base modifications and structural features of mRNA	8
1.3 mRNA therapeutics and vaccines	16
1.4 RNA modifications for biochemical research	21
1.4.1 Labeling strategies for RNA.....	21
1.4.2 Bioorthogonal click-labeling applying inverse electron-demand Diels-Alder cycloadditions.....	22
1.4.3 Electron paramagnetic resonance (EPR) spectroscopy.....	24
2 Research Objectives	29
3 Results and Discussion	31
3.1 Cellular application analysis of site-specifically CP-modified mRNA.....	31
3.1.1 Preparation of site-specific UBP modified <i>mCh_DNA</i> and site-specific cyclopropene modified <i>mCh_mRNA</i> sequences in combination with natural base modifications	32
3.1.2 Cellular analysis of modified mRNAs	39
3.1.2.1 Live-cell iEDDA click labeling for fluorescence visualization of mCh_mRNA ..	39
3.1.2.2 Quantification of mRNA levels in cells by RT-qPCR and mCherry protein amounts from cellular expression	43
3.1.2.3 Cell viability analysis in the course of mRNA transfection and live-cell click reactions.....	56
3.2 <i>Xist</i> lncRNA <i>A-repeat region</i> for EPR structure elucidation employing site-specific RNA spin labeling.....	59
3.2.1 Preparation of site-specific UBP modified <i>Xist</i> DNA templates and nitroxide spin-labeled <i>Xist</i> RNA	61
3.2.2 cw-EPR and PELDOR distance measurements of the spin-labeled <i>Xist</i> lncRNA <i>A-repeat region</i>	66
4 Conclusion and Outlook	71
5 Material and Methods	75
5.1 Software and databases	75
5.2 Equipment.....	75
5.3 Consumables	77
5.4 Reagents and solutions.....	78
5.5 Buffers and media.....	79
5.6 Enzymes	80
5.7 Plasmids	81
5.8 Kits.....	81

5.9 Organisms	82
5.10 General biochemical methods.....	82
5.10.1 Agarose gel electrophoresis	82
5.10.2 Purification methods	83
5.10.3 Nucleic acid concentration determination	84
5.11 Bacterial culture	85
5.11.1 Transformation	85
5.11.2 Bacterial cultivation for plasmid preparation.....	85
5.11.3 Bacterial glycerol stock preparation	85
5.11.4 Plasmid preparation.....	85
5.11.5 Diagnostic restriction digest of plasmid DNA	86
5.12 Sequence design for DNA and RNA constructs	87
5.12.1 <i>mCh_mRNA</i> sequence design.....	87
5.12.2 RT-qPCR sequence design for <i>mCh_mRNA</i> analysis <i>in cellulo</i>	88
5.12.3 <i>Xist</i> lncRNA A repeat region sequence design	90
5.13 Preparation of DNA primers, oligonucleotides and hydrolysis probes.....	91
5.14 PCR for DNA template preparation	91
5.14.1 PCR for <i>mCherry</i> template DNA	91
5.14.2 PCR for <i>Xist</i> template DNA.....	94
5.15 <i>In vitro</i> transcription.....	95
5.15.1 <i>mCherry</i> RNA.....	95
5.15.2 <i>Xist</i> lncRNA	97
5.16 <i>In vitro</i> iEDDA click labeling on rTPT3 ^{CP} -modified <i>mCh_mRNA</i>	98
5.17 Cell culture maintenance.....	98
5.18 Cell transfection	99
5.19 Live-cell iEDDA click labeling on rTPT3 ^{CP} -modified <i>mCh_mRNA</i>	100
5.20 Cell fixation and counterstaining for microscopy.....	101
5.21 Confocal fluorescence microscopy.....	101
5.22 Quantification of cellular <i>mCherry</i> protein expression from <i>mCh_mRNA</i>	101
5.23 RT-qPCR of <i>mCh_mRNA</i> levels in cells.....	102
5.23.1 Cellular total RNA isolation from transfected cells.....	102
5.23.2 RT-qPCR analysis	103
5.23.3 Initial experiments for qPCR efficiencies.....	106
5.23.4 qPCR product extension for sequence validation.....	106
5.24 Sanger sequencing of UBP modified and unmodified DNA	110
5.25 Cell viability assay.....	111
5.26 EPR sample preparation	112
5.27 Data evaluation	112

5.27.1 Microscopy	112
5.27.2 Protein quantification	113
5.27.3 RT-qPCR.....	114
5.27.4 Cell viability assay	114
6 References.....	117
7 Appendix	145
7.1 Gel electrophoresis images.....	145
7.2 Sanger sequencing results.....	154
7.3 Microscopy images	159
7.4 <i>mCherry</i> protein quantification	163
7.4.1 <i>mCherry</i> protein quantification full data set figure	163
7.4.2 <i>mCherry</i> protein quantification data tables.....	163
7.5 RT-qPCR.....	188
7.5.1 RT-qPCR full data set figure.....	188
7.5.2 Initial experiments for qPCR efficiencies in singleplex vs. multiplex assays	189
7.5.3 RT-qPCR results for <i>mCh_mRNA</i> analysis.....	192
7.6 MT cell viability assay	228
7.6.1 MT cell viability assay data tables.....	228
7.6.2 MT cell viability assay linearity validation	229
7.7 cNLS mapper results for <i>mCherry</i> protein sequence.....	230
7.8 Sequences.....	231
7.8.1 Plasmid sequences	231
7.8.2 DNA Primers for PCR, qPCR and Sequencing	239
7.8.3 DNA Hydrolysis Probes for qPCR.....	241
7.8.4 Adapter and splint sequences for qPCR extension	242
7.8.5 DNA sequences	242
7.8.6 RNA sequences	246
7.9 List of abbreviations	250
7.10 List of tables.....	253
7.11 List of figures	261
8 Eidesstattliche Erklärung.....	265
9 Curriculum Vitae.....	267

1 Theoretical Background

1.1 Coding and noncoding RNAs in light of the central dogma of molecular biology

Formulated by Francis Crick in 1958, the central dogma of molecular biology states that genetic information flows in one direction, from DNA to RNA to protein (Figure 1).^[1] Described in a little more detail, the genetic information for the structure and organization of an organism is stored in DNA. From there it can be transcribed into transient copies of messenger RNA (mRNA), which are subsequently translated for the biosynthesis of protein. According to the nucleobase sequence in the mRNA, the genetic code is read by the ribosomes and in cooperation with transfer RNAs (tRNAs) converted into the amino acid sequence of the corresponding protein.

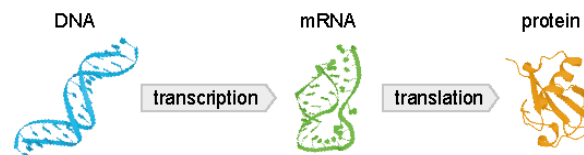


Figure 1. Genetic information flow according to the central dogma of molecular biology^[1].
PDB files: 1KBD, 1KAJ, 1NDD.

From today's point of view, the central dogma in its original formulation is no longer valid. Several additions and revisions have been made. For example, prion proteins have been shown to be able to self-replicate without DNA and RNA.^[2] Reverse transcription (RT) demonstrates that the flow of genetic information can also occur in reverse to the dogma, from RNA to DNA. Although RT was initially described as a retroviral capability, RT is now also known to occur in pro- and eukaryotes.^[3–7] Catalytically active RNA^[8,9] shows that, in addition to its ascribed role of coding, RNA can fulfill the additional role of catalysis. Furthermore, there are many different classes of non-coding RNAs (ncRNAs) that perform various tasks ranging from catalysis to signaling to regulation.^[9–11] To expand on the transcription and translation process described above (see Figure 2), tasks and involvement of ncRNAs can be added at various points and will be introduced shortly in the following.

Between transcription and translation, maturation of the primarily transcribed precursor-mRNA (pre-mRNA) takes place in eukaryotes. Besides protein-coding sections (exons), pre-mRNA also contains non-coding sequence sections (introns). During the splicing process, the introns are excised and the exons are reassembled, resulting in mature mRNA. The ribonucleoprotein (RNP) of the spliceosome forms at the intron-exon junctions of the pre-mRNA through the

binding of small nuclear RNAs (snRNA) and numerous protein factors.^[12] snRNAs within the spliceosome catalyze the transesterification reactions during splicing.^[12]

The ribosome, which is active during translation, is also an RNP in which ribosomal RNA (rRNA) catalyzes peptide-bond formation in an all-RNA active site of the ribosome.^[13,14] rRNA, as well as tRNAs, each undergo their own maturation processes involving other catalytically active or guiding RNAs^[15–18].

Post-transcriptional regulation of gene expression involves two short (20-24 nucleotides (nt)), non-coding types of RNA, microRNA (miRNAs) and small interfering RNA (siRNA). Both can act within the RNA-induced silencing complex (RISC), which is another RNP complex.^[19] Within RISC, miRNA and siRNA bind to mRNA sequences via partial base pairing and induce translational repression or cleavage and degradation of mRNA.^[19]

In conclusion, the purist progression diagram of the dogma can be extended to include the processes and actors mentioned above (Figure 2).

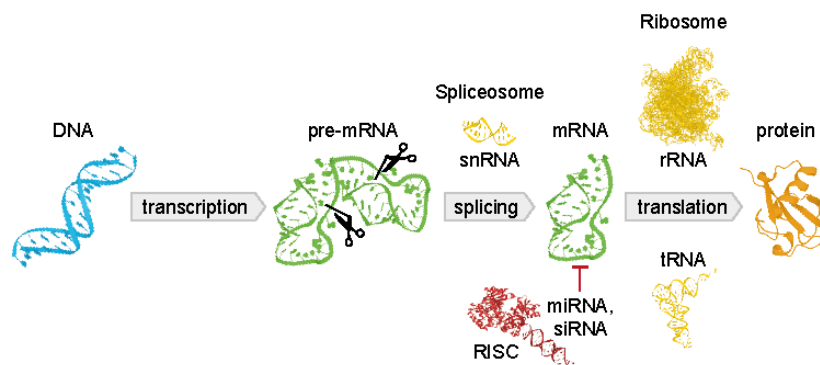


Figure 2. Extended view on the genetic information flow including catalytic and regulatory RNAs.
PDB files: 1KBD, 1KAJ, 1NDD, 2U2A, 2O44, 2F8S, 1EHZ.

Another class of ncRNAs are the long non-coding RNAs (lncRNAs), which differ from the previously mentioned ones, except for some rRNAs, due to their length of at least 200 nt up to 10 000 nt^[20]. lncRNAs are found in a variety of sequence contexts, both within or in close proximity to protein-coding sequences and far from the translational sequence.^[11,21–23] They are involved in transcription regulation, epigenetic modifications, protein or RNA stability, translation and signaling.^[21,24–27] However, to date, biological functions are only known for a small number of lncRNAs. Therefore, it is of great interest to further investigate the functions of lncRNAs. Structure elucidation and analysis of structure-function relationships are important factors in this regard.

Contrary to the central dogma formulated by Francis Crick, large parts of the RNA family play more complex and far more important roles than that of a mere intermediary. However, in its role as a messenger, mRNA is currently becoming increasingly important for therapeutic

research. Studies on therapeutically effective mRNA modifications and investigative tools to be combined with them are of great current interest.

1.2 Artificial nucleobases and natural occurring nucleobase modifications

Prior to the solution of the double helix structure of DNA by work of Rosalind Franklin, Maurice Wilkins, Francis Crick and James Watson in 1953^[28], a number of valuable discoveries were made through the research of other scientists. This includes the identification of the individual building blocks. Both DNA and RNA consist of four different nucleic bases, each bound to a sugar, the (deoxy-)ribose, and linked to each other via a phosphate backbone. Two single strands of DNA or RNA can form a double strand in which their opposing nucleobases pair via hydrogen bonds, known as Watson-Crick base pairing (see Figure 3).

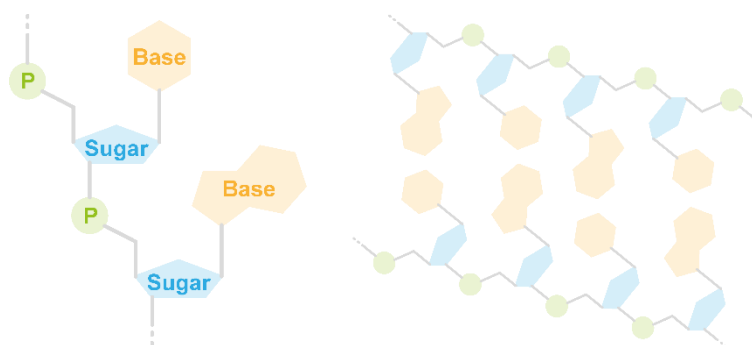


Figure 3. Schematic illustration of a DNA or RNA oligonucleotide strand (on the left) and the formation of a double strand via base pairing (on the right).

By changing and exchanging the building blocks, the chemical space of the nucleic acids is expanded. Altered structures and properties open up new possibilities for artificial nucleic acids and thus increase the toolbox for research and development in this field. Modifications can be introduced to the phosphate backbone, the base or sugar units of nucleic acids or even combinations thereof.

For the following sections, the exchange and modification of nucleobases will be considered, first introducing unnatural nucleobases and their historical development, followed by naturally occurring alterations to canonical nucleobases found in mRNAs.

1.2.1 Unnatural base pairs (UBPs): a brief history of the developments

The natural genetic code consists of a four-letter alphabet (adenine (**A**), thymine (**T**) or uracil (**U**), guanine (**G**) and cytosine (**C**)), in which two nucleobases each form a base pair (Figure 4, top). It can be augmented by adding an unnatural third base pair resulting in an expanded six-letter alphabet. Two distinct approaches for unnatural base pair (UBP) design and development have been demonstrated to date: mimicking naturally occurring bases with their purine and pyrimidine scaffolds as well as hydrogen bonds for Watson-Crick-like base pairing or creating a novel bio-orthogonal system that opposes existing natural schemes for structure and pairing. It all started when in 1962 Alexander Rich suggested a third base pair between **isoguanine** and **isocytosine** (**iso-G:iso-C**, Figure 4)^[29]. This isomeric UBP retaining canonical hydrogen bonds was thought to act orthogonally and only bond with each other but not the other four naturally occurring bases.^[29] Almost two decades later, **iso-G:iso-C** was synthesized and tested for enzymatic incorporation into DNA and RNA by Steven Benner and coworkers.^[30–32] Yet enzymatic misincorporation of **T/U** opposite **iso-C**, deamination of **iso-C** and ambivalent tautomeric forms of **iso-G** hampered enzymatic replication and transcription of **iso-G:iso-C** in the beginning.^[32]

By now, after years of continuous development, Benner and coworkers have established an artificially expanded genetic information system (AEGIS).^[33–36] Based on the idea that the positions of H-donors and H-acceptors on a nucleobase are interchangeable in their positions, Benner and coworkers have developed eight artificial bases, all of which bind in different donor-acceptor patterns via three hydrogen bonds per pair.^[34,37–39] These eight bases form the four UBPs **B:S**, **J:V**, **X:K**, and **P:Z** (Figure 4).^[34,37–39] Interestingly, **iso-G** is still part of this system but under a new name, namely **B**. Of these four UBPs, only **P:Z** has been used so far to produce six-letter AEGIS DNA containing the four natural letters **A,T,G,C** and additionally **P** and **Z**.^[40,41] In this context, the **P:Z** UBP has been applied in PCR amplifications, using **P**-modified primers in nested-PCRs or amplifying synthetic DNA strands with internal UB modifications of **P** and **Z**.^[40,41] Moreover, AEGIS laboratory *in vitro* evolution (AEGIS-LIVE) successfully enabled development of a **Z**- and **P**-modified DNA aptamer applying six-letter PCR amplification during cell-SELEX (Systematic Evolution of Ligands by Exponential Enrichment).^[42,43] In addition to replication, **P**- or **Z**-modified AEGIS DNA was also transcribed to RNA *in vitro*, and incorporation of r**Z** opposite d**P** and r**P** opposite d**Z** was demonstrated using T7 RNA polymerase.^[44] In 2019, Benner and coworkers reported “hachimoji” DNA and RNA which consists of eight (“hachi”) letters (“moji”) and includes the two UBPs **B:S** and **P:Z**.^[45] Enzymatic transcription of hachimoji template DNA using a mutated variant of T7 polymerase was presented for efficient preparation of the hachimoji version of the fluorescent spinach RNA aptamer.^[45] However, the hachimoji template DNA used was previously prepared by

solid-phase synthesis utilizing the corresponding UB phosphoramidites rather than enzymatically by eight-letter-PCR amplification.^[45]

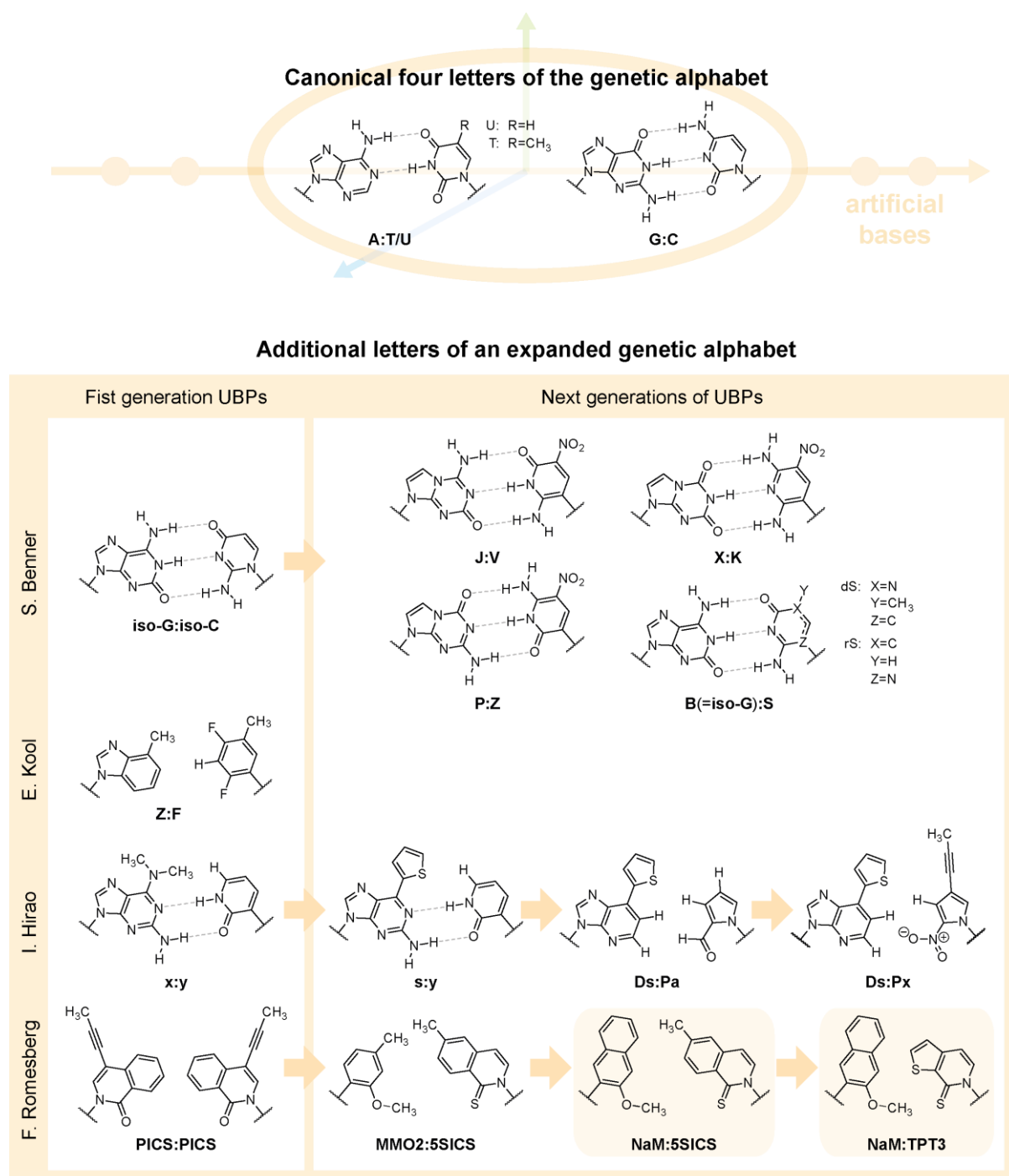


Figure 4. Artificial base pairs to expand the genetic alphabet. Top: The two natural base pairs **A:T/U** and **G:C** in the center of the coordinate system for nucleic acid building blocks. Bottom: Artificial base pairs that have been developed to expand the genetic alphabet. The two highlighted UBPs **NaM:5SICS**^[75] and **NaM:TPT3**^[80] have been used in this thesis.

As a note, the attachment of reporter groups to the AEGIS UBPs has not yet been reported. However, this may be reflected in the motivation for the research presented by the Benner

group, which was driven more by an interest in exploring the origins of life, the RNA-world model or more generally by a deeper insight into the evolutionary processes of nucleic acids,^[46-48] rather than in establishing research tools.

Due to their natural-like design and the resulting high similarity to the four canonical bases, hydrogen bonding artificial base pairs are often limited in their application. By maintaining hydrogen bonding patterns, mismatches with natural bases can occur more easily. Also, artificial base pairs based on hydrogen bonding can lack sufficiently strong discrimination compared to canonical bases when using natural enzymes for replication. Both will result in lower fidelity of enzymatic amplification, *i.e.*, retention of UBPs per DNA duplication, and thus rapid loss of base modification. However, reliable production and amplification of the modified template DNA is an important prerequisite for the application of UBs on DNA as well as RNA level. Alternative systems that can blend in with natural conditions, but also differ sufficiently from them, offer a promising alternative to hydrogen bond-based UBPs.

With the discovery by Eric Kool, a new aspect for UBP design and development came into play. In 1997, Kool and coworkers presented the isosteric unnatural base pair **Z:F** (Figure 4), in which **F** and **Z** mimicked the shape of the natural occurring pyrimidine and purine bases **T** and **A**, respectively, but did not allow hydrogen bonding.^[49] Thereby, they proved that nucleobase size and shape can be more important than hydrogen bonding and that template formation in DNA replication is not depended on hydrogen bonding.^[49]

Applying the different approaches for UBP design presented so far, in the year 2000 the group of Ichiro Hirao developed their first UBP **x:y** (Figure 4).^[50,51] The UBP design for **x:y** was also based on purine and pyridine scaffolds and combined hydrogen bonding with aspects of shape complementarity.^[50] In further development of the **x:y** UBP, a bulkier substituent was added to the purine scaffold to induce steric hindrance and thus avoid undesired mispairing with canonical bases.^[52] This led to the improved UBP **s:y**^[52] (Figure 4) which was successfully applied in a coupled *in vitro* transcription and cell-free translation system facilitating protein synthesis with a site-specific unnatural amino acid modification^[53]. Furthermore, site-specific RNA biotinylation and fluorescent labeling were achieved by T7 *in vitro* transcription utilizing the **s:y** UBP and functionalized **y** triphosphates (TP)s.^[54-56] However, due to mispairing problems of **y** with the canonical base **A**, replication of the **s:y** UBP was limited.^[52,57] For the development of new generations of UBPs, Hirao and coworkers then exchanged the pyridine base scaffold for the smaller pyrrole, and dispensed with hydrogen bonds for base pairing in favor of exclusive shape complementarity. In 2006, the **Pa:Ds** UBP (Figure 4) was shown to be the efficiently amplified and transcribed *in vitro* using Vent DNA and T7 RNA polymerase, respectively.^[58] In addition, it was applied for site-specific RNA biotinylation and fluorescent labeling of RNA and featured efficient incorporation rates ($\geq 90\%$) utilizing biotin- and

fluorescein-linked **Pa** TPs.^[58,59] Addressing limitations due to **Ds:Ds** self-pairing and **A:Pa** mispairing, additional modifications were made to substituents of the **Pa** base, resulting in the successor UBP **Px:Ds**^[60]. Current applications of the **Px:Ds** UBP (Figure 4) include qPCR^[61,62], high-affinity DNA aptamers^[63–65] and site-specific RNA click labeling^[66].

In contrast to Benner and Hirao, the group of Floyd Romesberg focused exclusively on hydrophobic interactions and shape complementarity in the development of their UBPs from the beginning and eschewed hydrogen bonding. In 1999, Romesberg and coworkers published the self-pairing orthogonal **PICS:PICS** UBP (Figure 4), which was characterized by a 20-fold increase in selectivity for **PICS:PICS** self-pairing compared to undesired mispairing between **PICS** and the four canonical bases.^[67] However, the used polymerase, the Klenow fragment of *E.coli* polymerase I, only insufficiently proceeded after **PICS** incorporation.^[67] In the time following, Romesberg and coworkers implemented large-scale screenings of 3600 candidates, testing for insertion, extension and amplification of hydrophobic UBP analogs.^[68–75] In addition, they performed structure-activity relationship (SAR) analysis using approaches from medicinal chemistry.^[76,77] In 2008, the UBP **5SICS:MMO2** (Figure 4) was published, resulting from further optimization of a precursor UBP identified during screening.^[74] Ongoing work to improve the replication efficiency of the **5SICS:MMO2** led to the **5SICS:NaM** UBP^[75] (Figure 4) which was characterized by its outstanding efficiency and fidelity in *Taq* PCR amplification and T7 *in vitro* transcription^[78,79]. Fidelity refers to the accuracy of replication of the template and includes UB retention per duplication, while efficiency means yield and describes how many times a template was duplicated.^[80] Further improvements were achieved by contraction of the distal ring of **5SICS**, resulting in the successor UBP **TPT3:NaM** (Figure 4), which allowed ‘natural-like’ PCR replication applying *OneTaq* DNA Polymerase (>99% retention, >99.98% fidelity).^[80] Romesberg’s efforts to engineer UBPs processed by native DNA and RNA polymerases focused in the creation of a semi-synthetic organism (SSO) using *E. coli* in 2014.^[81] The SSO aims to store and retrieve increased information which means that UBP modifications are not only retained in its DNA but also transcribed into the corresponding unnatural nucleotides in mRNA codons and tRNA anticodons and then translated to generate proteins with noncanonical amino acids (ncAA).^[82,83] In SSO optimizations to improve the replication efficiency and retention of the UBP in the DNA, as well as to increase the fidelity of the ncAA incorporation into proteins, several more UBP candidates have been identified to date and applied in combination with each other in the set-up of replication, transcription and translation.^[82,83]

With regard to nucleic acid labeling, Romesberg and coworkers reported efficient *in vitro* labeling of DNA using the **TPT3:NaM** UBP, specifically using d**TPT3**^{PA} TP (Figure 5, on the left) functionalized with a propargyl amine (PA) linker for subsequent NHS-chemistry modification.^[80]

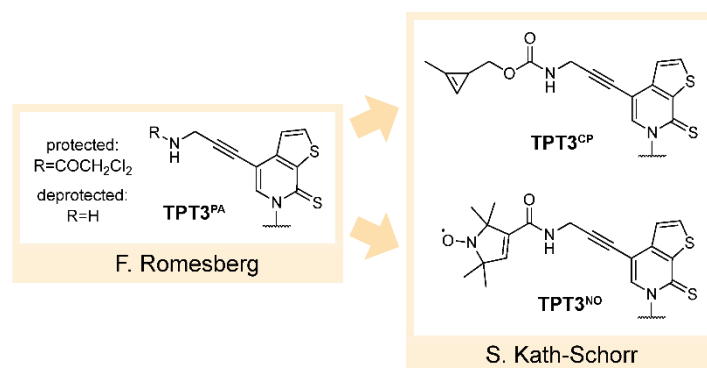


Figure 5. Functionalized unnatural bases for site-specific labeling.

Building on the earlier work of Romesberg and coworkers, the group of Stephanie Kath-Schorr has taken up the work on the **TPT3:NaM** UBP and further developed it for site-specific labeling of RNA *in vitro*. Various functionalized **rTPT3** building blocks and their incorporation into RNA via genetic alphabet expansion transcription^[76,78,79,84–87] (GENAEXT) enables a modular site-specific labeling system for RNA. During GENAEXT site-specific UB-modified RNA sequences are yielded by enzymatic *in vitro* transcription from UBP-modified template DNA applying a mixture of the canonical nucleoside triphosphates (NTPs) together with the UB TPs. These include the cyclopropene-modified **rTPT3^{CP}** and the nitroxide-modified **rTPT3^{NO}** published in 2016 and 2020, respectively (Figure 5, on the right).^[88,89] So far, **rTPT3^{CP}** TP has been applied for site-specific enzymatic RNA modification and was characterized by excellent efficiency and specificity.^[88,90] Post-transcriptional click labeling using inverse electron demand Diels-Alder cycloaddition (see chapter 1.4.2) facilitated effective *in vitro* visualization of RNA.^[88] Alternatively, the site-specific and direct incorporation of the nitroxide spin label-modified **rTPT3^{NO}** TP via GENAEXT enables structural studies of various RNAs by electron paramagnetic resonance (EPR) spectroscopy (see chapter 1.4.3 and for results in 3.2).^[89]

1.2.2 Natural base modifications and structural features of mRNA

In contrast to artificially modified or completely newly developed unnatural nucleobases that expand the genetic alphabet, there exist a whole range of natural occurring nucleobase modifications. Altered canonical nucleobases are found as natural RNA modifications in various types of RNA and throughout different species. The alterations occur through the introduction of modifications to the nucleobases and often include methylations or small functional groups, *e.g.*, hydroxyl groups. Most modifications have been found in tRNAs, with a total of 111 different modifications to nucleobases and the ribose sugar moiety, as well as combinations thereof.^[91–94] In mRNAs, on the other hand, twelve modifications (Figure 9) have been found so far, limited to the nucleobases.^[91,93,94] All twelve modifications found in natural

mRNA will be introduced individually in the second part of this chapter. Moreover, some of the modified nucleobases have been tested and used in synthetic RNA for therapeutic applications.^[95] The effects of the individual base modifications and their significance for synthetic mRNA applications will also be presented in the second section. First, however, the structural features of mRNA are reviewed, one of which already includes a natural base modification.

Structural features of mRNA in view of synthetic mRNA production

The general structure of eukaryotic mRNA consists of a central protein encoding sequence, plus framing, non-coding sequences, a 5'-cap, and a poly(A) tail at the 3'-end (see Figure 6). The protein-coding sequence begins with a base triplet that starts the translation process and ends with a base triplet that terminates the translation. Noncoding sequence segments, called untranslated regions (UTRs), line the coding mRNA sequence at both ends. The 5'-end of mRNAs is provided with a modified dinucleotide cap structure. A poly(A) tail, consisting of contiguous adenine nucleotides, is located at the 3'-end of mRNAs.

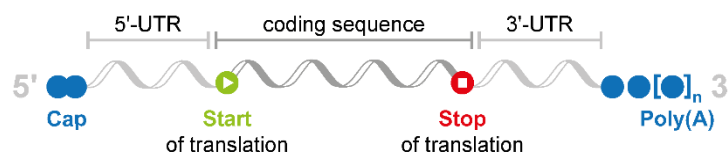


Figure 6. Structural features of mRNA. A central coding sequence is flanked on both sides by untranslated regions (UTRs). The mRNA comprises a 5'-terminal cap and a 3'-terminal poly(A) tail.

When preparing synthetic mRNAs for *in vivo* and *in cell* applications, the aforementioned structural features of mRNA need to be included. Enzymatic preparation of synthetic mRNAs is enabled by *in vitro* transcription (IVT). During IVT, the protein encoding sequence and the UTR sequences are transcribed from a DNA template in which these sequences are defined. Additionally, the structural features of cap and poly(A) tail can be included into the synthesized mRNA.

With an average length of 2.2 kb for mammalian mRNA,^[96] enzymatic production is the method of choice for long synthetic mRNA. By IVT, RNAs of basically any length can be prepared, whereas RNA obtained by solid phase synthesis is generally limited to a length of 120 nt (*biomers.net*, requested 08/2022).

In the following section, the previously named structural features of mRNA and its assembly are described in more detail. In addition, their significance for the function and mode of action of mRNA will be discussed.

To build up the 5'-terminal cap structure (Figure 7, on the left), the modified nucleotide **7-methyl-guanosine (7mG)** is co-transcriptionally attached to the first transcribed nucleotide of the nascent mRNA. Here, the linkage of 7mG occurs in an inverted 5'-5' triphosphate linkage.^[97,98] Subsequently, the first transcribed nucleotide is methylated the O2'-position of the respective ribose.^[97-101] Once installed, the **7mG-cap** mediates splicing, polyadenylation, and nuclear export, recruits translation factors, and initiates cap-dependent mRNA translation.^[97,98] In addition, the **7mG-cap** facilitates 5'-to-3' looping of mRNA during translation and protects the mRNA from 5'-to-3' degradation by exoribonucleases.^[102]

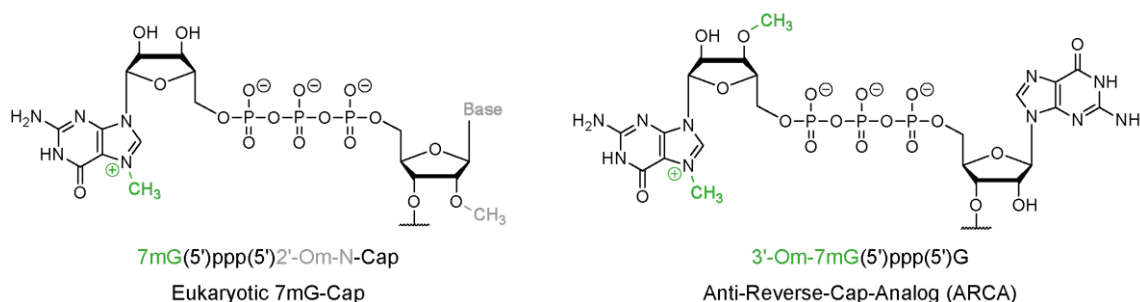


Figure 7. mRNA cap structures. Chemical structure of the eukaryotic **7mG-Cap** on the left. Chemical structure of the artificial Anti-Reverse Cap Analog (ARCA) on the right.

For capping of synthetic mRNAs, the anti-reverse cap analog (ARCA, Figure 7, on the right) is most commonly used.^[103-105] ARCA is a 5'-5' triphosphate-linked **7mG-G** dinucleotide with a **7mG**-modified terminal base that is additionally methylated at the O3'-position.^[105] In the preparation of synthetic RNA by IVT, the additional O3'-methylation ensures that ARCA can only be incorporated in the correct orientation at the 5'-end.^[105]

The structural element of the poly(A) tail at the 3'-end of eukaryotic mRNA was first described in 1970.^[106,107] The average length of poly(A) tails in eukaryotic mRNA amounts to ca. 200 nt.^[108] As of today, the poly(A) tail plays an important role in translation regulation and mRNA stability.^[109-112] The combination of the 5'-terminal **7mG-cap** and the poly(A) tail acts synergistically for translation stimulation.^[111] Increasing poly(A) tail length has been shown to reduce immunogenicity by shielding or decreasing **U** content in the sequence.^[113,114] In addition, higher protein expression was obtained from synthetic mRNA with longer poly(A) tails (64 vs. 120 nt poly(A) tail lengths).^[115] Moreover, the combination of ARCA and a 100 nt long poly(A) tail has been demonstrated to significantly improve protein translation in cell experiments.^[112] In the preparation of synthetic mRNAs, the use of commercially available

mRNA IVT kits allow both co-transcriptional capping and post-transcriptional poly(A) tailing using recombinant poly(A) polymerases. Alternatively, poly(A) tails can be co-transcribed during IVT using a DNA template encoding them.

In addition, the UTR sequences of an mRNA also influence its translation efficiency^[116,117] and stability^[117,118]. The way of UTR regulation is versatile. It can occur via UTR sequence motifs and their primary or secondary structure in interactions with specific binding proteins or via repeat elements within the UTRs and their binding interactions.^[117] Also binding of short complementary miRNAs and siRNAs to UTR sequence sections, especially located in 3'-UTRs, is known to trigger translation suppression and mRNA degradation.^[119] Due to its diversity, UTR regulation cannot be discussed in more detail here. However, two examples for regulatory sequence elements in UTRs will be given.

Eukaryotic 5'-UTR sequences comprise a consensus sequence flanking the start codon, known as Kozak sequence^[120–123]. It functions as a ribosomal binding site and regulates the efficiency of translation initiation.^[120–123] Changes within the Kozak sequence can lead to reduced translation efficiency.^[122]

In contrast, mRNAs with AU-rich elements in their 3'-UTR sequences have been shown to have a reduced half-life because the AU-rich sequences induce deadenylation and degradation of the mRNA.^[124,125] Additionally, AU-rich elements were found to be involved in miRNA binding and consequent mRNA instability.^[124,126]

For synthetic mRNAs, transfer and integration of UTR sequences from natural mRNAs known for high translation, such as human β -globin, was successfully applied.^[115,127]

Figure 8 provides an overview of the outlined structural mRNA features and sequence sections with regard to their effects on mRNA translation and stability.

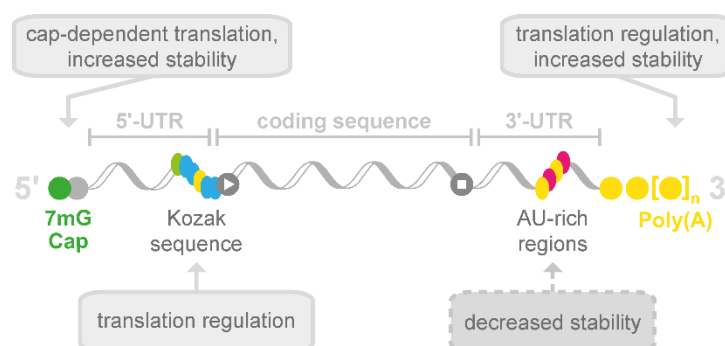


Figure 8. Structural mRNA features and their effects on mRNA translation and stability. Solid lines represent positive effects on translation and stability, dashed lines represent possible negative effects.

Natural base modifications and their effects on mRNA

In addition to the previously described structural features of mRNA, where a permanent base modification is included with the **7mG** cap, dynamic modifications occur within mRNA sequences. These modifications are added post-transcriptional to the nucleobases of the mRNA as well as possibly removed later, both within the coding sequence and in the UTRs. The added modifications may affect the structure and interactions of the mRNA as well as its translational efficiency and stability. With regard to synthetic mRNA, base modifications have also been deliberately used to achieve improved mRNA stability and translation efficiency. Another advantage of incorporating naturally occurring modified nucleobases in synthetic mRNA is their immune-cloaking effect, due to which undesirable immune responses to the exogenous mRNA are reduced. For instance, as little as 0.2-0.4% chemically modified bases, e.g. **5-methylcytidine (5mC)**, **pseudouridine (Ψ)**, or **N6-methyladenosine (6mA)**, were seen to reduce immunogenicity while increasing RNase cleavage resistance and thus stability of the modified mRNA.^[128,129] In addition, replacing unmodified canonical bases with modified bases, e.g., **C** and **U** with **5mC** and **Ψ** , has been shown to enhance the translation efficiency from the modified mRNAs.^[130–135]

In the following, each of the natural base modifications found in mRNA to date is briefly reviewed along with its significance as mRNA feature and for application in synthetic mRNA.

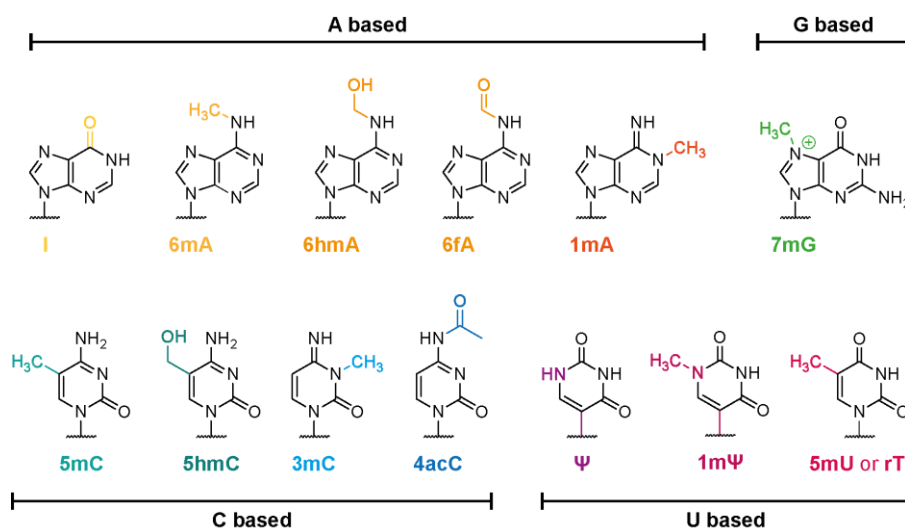


Figure 9. Modified natural nucleobases found in mRNA.

Inosine (I, Figure 9, top row), which was already discovered in 1957^[136], is found in both DNA and RNA and formed by hydrolytic deamination at the C6 position of **A**.^[137] I can form base pairs opposite **A**, **C** or **U** and function as a Wobble base.^[138] During the mRNA translation process, I is recognized as **G**.^[139–142] If the I-modification is located within the coding sequence,

the affected codons are altered, which in turn can cause a change in the translated protein sequence..^[139–142] However, most **I** modifications have been found to occur outside the coding sequence and predominantly in the UTRs of mRNA.^[139–142]

N6-methyladenosine (6mA), Figure 9, top row) represents the most common internal modification in mRNA^[143] and is a dynamic and reversible mark^[144]. Several enzymes have been identified that either synthesize **6mA** marks within a given consensus sequence (**6mA** writers)^[145–149], bind specifically to mRNA with the presence or absence of **6mA** marks (**6mA** readers)^[149–153] or remove marks by demethylation (**6mA** erasers)^[149,154–157]. In addition to direct demethylation, a human eraser enzyme has also been found to oxidize **6mA** marks to **N6-hydroxymethyladenosine (6hmA)**, Figure 9, top row) and **N6-formyl-adenosine (6fA)**, Figure 9, top row).^[158] However, the biological significance of **6hmA** and **6fA** is still unclear.^[91] **6hmA** and **6fA** both have relatively short half-lives (~3 h *in vitro*), before being non-enzymatically degraded to canonical **A**.^[158] Albeit for **6mA** marks, a number of different effects have been reported, and the mode of action of **6mA** depends on the modification site. **6mA** marks within the 5'-UTR allowed cap-independent mRNA translation^[159], whereas **6mA** marks within the coding sequence impeded mRNA translation^[160,161]. **6mA** within the coding sequence and 3'-UTR has been associated with mRNA destabilization and enhanced mRNA decay.^[160,162] In contrast, interactions with a certain reader protein have been shown to increase the stability and thus half-life of **6mA**-marked mRNAs.^[163] In synthetic mRNA, partial or full replacement of **A** with **6mA** successfully avoided undesired immunostimulation, but translation was not improved and even deteriorated.^[128–130,132,164–167]

Similar to **6mA**, **N1-methyladenosine (1mA)**, Figure 9, top row) modifications are also dynamic^[168–173] and are set or deleted as marks by writer or eraser proteins, respectively.^[157,172,174] Other than that, **1mA** modifications have been reported to affect **U-A** base pairing because the *N1*-methylation is positioned at the Watson-Crick interface.^[173,175–178] Furthermore, **1mA** marks putatively alter RNA structure by introducing a positive charge at physiological pH, which additionally enables charge-charge interactions.^[173,175–178] **1mA** modifications were found to be concentrated near the start codon of mRNAs, where they are included in highly structured regions.^[173] Modifications of **1mA** in synthetic mRNAs have been shown to increase translation initiation, improve early elongation, and enhance translation overall.^[173,177]

7-Methylguanosine (7mG), Figure 9, top row) is known to form the eukaryotic **7mG**-cap at the 5'-end of mRNAs^[97,98] and until recently **7mG** was thought to occur exclusively in the **7mG**-cap structure. However, in 2019, **7mG** modifications were detected within the coding sequence, 3'-UTR and rarely in the 5'-UTR of mRNAs.^[179] Associated experiments with depletion of the **7mG** writer showed decreased mRNA translation efficiency.^[179] Indirectly, this indicated that

7mG modifications in mRNAs could positively affect protein translation.^[179] Future work will help to clarify.

5-Methylcytidine (5mC), Figure 9, bottom row) modifications in mRNA are also dynamic and coordinated by the aforementioned three types of regulators of methylation: writers, readers and erasers.^[180,181] **5mC** marks were found to be enriched in 5'- and 3'-UTRs and peak near the start codon.^[182–184] The exact effect of **5mC** modifications on mRNA translation remains to be elucidated. On the one hand, it has been shown that increased **5mC** marks within the coding sequence lead to reduced translation whereas **5mC** marks concentrated in the 3'-UTR enhanced translation.^[185–188] On the other hand, it has also been reported that **5mC**-modified coding sequences do not negatively affect translation.^[189] In addition, replacement of **C** with **5mC** in combination with another modified base (**Ψ**, see below) resulted in greatly enhanced translation efficiency both *in vitro* and *in vivo*.^[130–135] Moreover, the interactions between **5mC**-reader proteins and modified mRNA influence nuclear export^[184] and mRNA stability in the cytoplasm^[190,191]. **5mC** further stabilizes synthetic mRNA and prevents degradation by avoiding immunostimulation.^[128,130,132,167,181] **5-Hydroxymethylcytidine (5hmC)**, Figure 9, bottom row) was discovered more recently and is generated by oxidation of **5mC**.^[192,193] *In vivo* experiments showed increased translation from **5hmC**-modified mRNAs.^[194] Experiments to exploit the positive effects on translation for synthetic **5hmC**-modified mRNA are pending.

3-Methylcytidine (3mC), Figure 9, bottom row) which was originally found in tRNA,^[195–197] was also found to be present as a modification in mRNA.^[198] Likewise, the methyltransferase associated with **3mC** marks in mRNA was identified in mammalian cell lines.^[198] It is discussed that **3mC** is involved in **C**-to-**U** editing in eukaryotes^[199], but this is not proven yet. The effect of **3mC** modifications in mRNA on structure and function are yet unknown.

N4-acetylcytidine (4acC), Figure 9, bottom row) was discovered to be present in mRNA in HeLa cells during a transcriptome-wide search in 2018.^[200] **4acC** was found within the coding sequence and was enriched first towards the 5'-end and second within wobble sites.^[200] The presence of **4acC** modifications increased mRNA stability and enhanced translation.^[200] In particular, **4acC** positioned in wobble sites improved translation efficiency.^[200] It remains to be seen whether **4acC** modifications will also be found in other eukaryotes and what application **4acC** will find in synthetic RNA.

Pseudouridine (Ψ), Figure 9, bottom row) was identified as early as 1951 and was the first post-translational RNA modification described.^[201] **Ψ** can be found in human and other mammalian mRNA, within coding sequences and the UTRs.^[202–204] **Ψ** is an isomer of **U** with an exchanged C-C glycosidic bond instead of the N-C bond in **U**. Because of its additional imine group, **Ψ** can form additional hydrogen bonds, enhance base-stacking, and thus stabilize RNA structures.^[205] **Ψ** is formed mainly by pseudouridine synthases catalyzing the isomerization

after the incorporation of **U** into RNA oligonucleotides.^[206,207] **Ψ** is found in the coding sequence and in both 3'- and 5'-UTRs of mRNAs.^[204] It has been shown that full replacement of **U** with **Ψ** in synthetic mRNA increased translation in mammalian cells.^[130] The combined replacement of **U** and **C** with **Ψ** and **5mC** enhanced translation most efficiently both *in vitro* and *in vivo*.^[130-135] Moreover, **Ψ** reduced immunostimulation in several signaling pathways.^[128,129,132,167]

N1-methylpseudouridine (1mΨ) (Figure 9, bottom row) is currently the most promising modification when it comes to synthetic mRNA for medical applications. **1mΨ** occurs naturally in eukaryotic 18S ribosomal RNA (rRNA) and archaeal tRNA,^[208-210] but has not been found in natural mRNA. However, it is included in this chapter because of its great current importance for use in mRNA vaccines. For mRNA vaccines against COVID-19, **U** was completely exchanged with **1mΨ** in the entire mRNA sequence.^[211,212] In addition, **1mΨ** has already been tested earlier in vaccines against Zika,^[213-215] HIV-1,^[215] influenza^[215] and Ebola^[216]. In a 2016 study, synthetic mRNAs modified with **1mΨ** were tested either alone or in combination with **5mC** in both mammalian cell lines and in mice.^[133] The combination of **1mΨ** and **5mC** extended the translational lifetimes of mRNAs, improved gene expression and cell viability, and also reduced cell cytotoxicity and cellular immunogenicity.^[133] Overall, **1mΨ/5mC** performed better than **Ψ/5mC**.^[133] **1mΨ** was also shown to alter translational dynamics by increasing ribosome pausing and density on modified mRNAs while circumventing immune-dependent translational inhibition.^[217]

5-methyluridine (5mU) (Figure 9, bottom row), also referred to as **ribothymidine (rT)**, was recently detected as an mRNA modification in human cells by high-throughput sequencing^[218,219]. Its potential application in synthetic RNAs has been explored previously, showing that **5mU** reduced immunogenicity but at the same time unimproved translation efficiency.^[130]

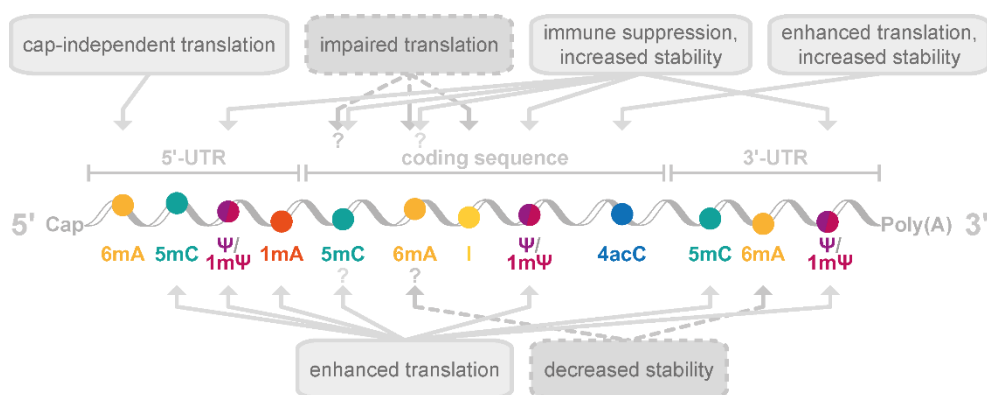


Figure 10. Nucleobase modifications and their effects on mRNA translation and stability. Solid lines represent positive effects on translation and stability, dashed lines represent negative effects. Question marks indicate contradictory effects that have been reported.

An overview of the structural features of mRNA and the different base modification in view of their respective effects when applied in synthetic or natural mRNAs is given in Figure 10.

With regard to mRNA as a therapeutic agent, natural base modifications represent a versatile tool that can be used to target mRNA properties such as stability and translation efficiency. Further research and insights into the use of natural base modifications in synthetic mRNA and their cellular application are therefore of great interest.

1.3 mRNA therapeutics and vaccines

mRNA therapeutics and, in particular, mRNA vaccines attract increasing interest in pharmaceutical development. As an alternative approach to DNA gene therapy and protein drugs, mRNA therapeutics offer several advantages. In the early 1970s, DNA was first tested as a nucleic acid therapeutic for the insertion of protein-coding genes via cell infection.^[220] However, the use of virus infection for DNA delivery into cells has been shown to carry the risk of genomic DNA damage and virus integration, possibly resulting in carcinogenesis.^[221] Even if virus-based DNA transfer is not used and alternative methods are employed, apart from integration of DNA at planned sites by homology-dependent processes, illegitimate DNA integration occurs at unpredictable sites, leading to genomic alterations and risks.^[222] As opposed to this, mRNA cannot be integrated into the genome and thus circumvents the risk of carcinogenesis^[223]. In addition, mRNA provides a dose-dependency that is more difficult to achieve with DNA gene therapy.^[224] In contrast to one-time DNA integration into the genome and subsequent cellular regulation of gene expression, the administration of mRNA therapeutics is repetitive and allows for variations in the amounts of mRNA administered and thus the amounts of protein translated from it. Furthermore, a natural degradation pathway ensures that mRNA therapeutics are only transiently active.^[225]

To enable protein expression from therapeutic mRNAs, the mRNA must first enter the cytosol of the target cell. Also, foreign mRNA outside the cell is most likely recognized by receptors of both immune and non-immune cells.^[226–230] Therefore, the mRNA needs to be packed up and has to cross the cell membrane, this often occurs via endocytosis^[231] (Figure 11). In addition to successful transport across the cell membrane, modified mRNA itself and mRNA packaging can further prevent naked exogenous mRNA from triggering innate immune responses that lead to inhibition of mRNA translation, mRNA degradation and inflammation.^[226–230]

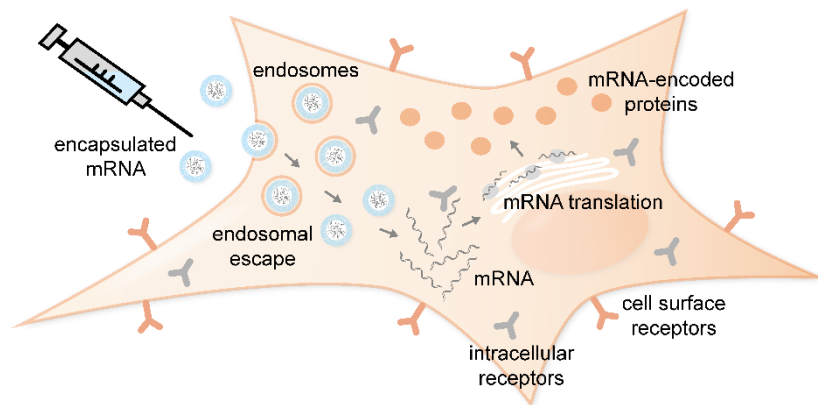


Figure 11. Endosomal take-up of encapsulated mRNA. After endosomal escape the mRNA is translated to produce the encoded protein. Cell surface and intracellular receptors can detect naked exogenous mRNA and trigger immune responses.

In the following section, the various therapeutic applications of mRNA are introduced first. In the subsequent section, the requirements and adaptations for mRNA as a therapeutic agent as well as their transport vehicles are described.

mRNA vaccines and therapeutics

Besides mRNA vaccines, a variety of mRNA therapeutics are in development. Yet it is only recently that mRNA vaccines attracted greater attention fighting the Covid-19 pandemic.^[232] However, for the various applications of mRNA therapeutics compared to mRNA vaccines, different effects are sought and different requirements must be met.

mRNA vaccines use antigen-encoding mRNAs to induce cellular and antibody-based immunity. Therefore, the mRNA vaccine is injected intradermally, intramuscularly or subcutaneously to transfect antigen-presenting cells such as dendritic cells (DCs) that populate skin tissue^[233] and skeletal muscle^[234]. Only a low level of expression of the encoded antigen is required for immunization as the immune system amplifies the antigenic signal via cell- and antibody-mediated immunity.^[224,235,236] Consequently, a low dose of mRNA is used in vaccines, which carries a lower risk of toxicity.^[224] In addition, tropism need not to be considered in the formulation of mRNA vaccines, and some degree of immunogenicity is desired.^[224]

The situation is different for mRNA therapeutics and will be outlined in the following. For both, mRNA cargo and its carriers a minimized immunogenicity is desirable.^[224] Due to a limited duration of action, a prolonged mRNA stability is preferable.^[224] To achieve high protein therapeutic thresholds, mRNA translation and expression of the encoded protein should be

maximized.^[224] Cell- or tissue-specific tropism as well as tissue bioavailability and circulatory half-life need to be considered.^[224] In the treatment of chronic diseases, the additional challenges of repeated dosing must be overcome. Protein replacement therapies are one such case and will be discussed lastly. Other therapies based on limited periods of mRNA delivery and protein expression, like mRNA vaccines, avoid the problems of chronic administration. These include cancer immunotherapy, gene editing and cellular reprogramming (Figure 12).

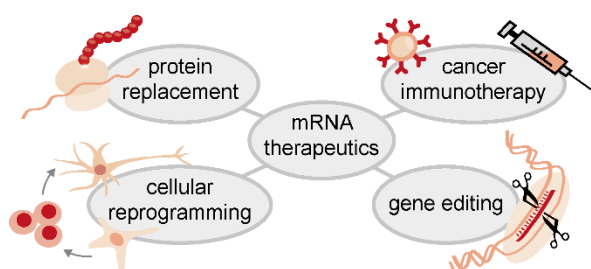


Figure 12. Overview of mRNA therapeutic strategies.

Two major types of mRNA cancer immunotherapy have been reported. The first one resembles mRNA vaccines, whereby antigen-presenting cells are transfected with mRNAs encoding tumor associated peptide antigens.^[237–240] The second type uses mRNAs to modify T cells with chimeric antigen receptors (CARs) and is therefore called CAR T cell therapy.^[241,242] CARs are protein fragments that are displayed on the surface of T cells and bind to specific tumor epitopes.^[243] CAR T cell therapy involves isolating of a patient's T cells, *ex vivo* transfection of the T cells with mRNAs encoding CARs, and re-introduction of the modified T cells into the patient to treat tumor cells.

Gene editing has been revolutionized by the discovery and application of CRISPR-Cas9 (clustered regularly interspaced short palindromic repeats; CRISPR associated protein 9).^[244,245] Precise DNA cutting requires two components, the nuclease Cas9 to cut DNA, and a short guide RNA (gRNA) that directs Cas9 to the desired cleavage site.^[244] In a combined approach, mRNA and CRISPR-Cas9 can be used for improved gene editing. To do this, the customized gRNA and the mRNA encoding Cas9 are co-delivered into cells. The major advantage of the combined approach with mRNA in contrast to DNA is the transient expression of Cas9, avoiding off-target cleavage found with prolonged expression of Cas9^[246]. Moreover, CRISPR-Cas9-mediated gene editing utilizing mRNA to encode Cas9 has also been applied to generate CAR T cells with improved properties for cancer immunotherapy.^[247–250]

Cellular reprogramming can be used to redirect cell fate and function. By introducing four transcription factors, known as the Yamanaka factors, human somatic cells could be reprogrammed into induced pluripotent stem cells.^[251] Instead of coding plasmids, a mixture of

mRNAs can be used to encode the Yamanaka factors.^[252,253] This mRNA approach has been shown to avoid gene integration that occurs with plasmid delivery^[252,253] and has been used to treat heart attacks^[254].

Among the other therapeutic strategies presented, protein replacement represents the most straightforward application of mRNA, namely the expression of a desired protein. Compared to the use of protein drugs, mRNA can increase molecular efficacy, because a single mRNA can be repeatedly translated into multiple copies of the same protein.^[255] However, maintaining a consistent amount of protein expressed from unchanged doses of mRNA becomes more difficult over the time course of therapy.^[224] Most chronic protein therapies report a drop in efficacy due to the rise of antibodies against the protein or delivery vehicle.^[224] Immune responses to lipid-encapsulated mRNAs proved problematic in early clinical trials.^[224] Likewise, it has been reported that parts of the lipid formulation for mRNA packing can cause inflammation^[256] and immunogenicity, resulting in accelerated blood clearance and pseudoallergies.^[257–260] In several preclinical studies for protein replacement therapies, chronic administration of lipid-encapsulated mRNA was found to be liver toxic.^[261–264] Therefore, chronic systemic administration of mRNA therapeutics, as for long-term protein replacement therapies, is not yet feasible and requires future research into improved delivery systems.

Requirements for therapeutic mRNA and its delivery vehicle

For therapeutically effective mRNA formulations, challenges and current limitations need to be addressed with regard to both the mRNA as cargo and its transport vehicle. As for the mRNA, its sequences can be adjusted accordingly. Incorporation of chemical base modifications have been shown to reduce these undesired immune reactions, increase mRNA stability and enhance translation (see chapter 1.2.2 for detailed descriptions). Alternatively, synthetic mRNAs without base modifications but with optimized sequences, obtained by **U**-depletion and codon replacement for **GC**-rich codons, were reported to yield enhanced translation and reduced immunogenicity *in vivo*.^[265,266] Moreover, self-amplifying mRNAs (saRNA)^[267–270] or circular mRNAs (circRNA)^[271–273] have been developed as alternative mRNA variants. saRNA encode not only their target protein, but also virus-derived replication enzymes that amplify the RNA after their own *in situ* translation. Thus, saRNAs increase the expression of their encoded proteins while decreasing the delivered amount of mRNA.^[268–270] circRNA have been shown to improve mRNA stability by protecting against exonucleases and to increase translation by extending mRNA longevity.^[271–273] In addition, after mRNA IVT preparation, high-performance liquid chromatography (HPLC) purification can be performed to remove side products such as double-stranded RNA (dsRNA), uncapped mRNA or mRNA fragments.^[274,275] Removal of these contaminations has also been shown to increase translation and prevent

inflammation.^[274,275] Just recently, engineering of a T7 RNA polymerase variant was reported which decreases immunostimulatory byproduct formation of dsRNA during IVT and thus may reduce the need for HPLC purification in the future.^[276]

Besides optimization of the mRNA, suitable packaging is required to improve the transport of the mRNA cargo into the cell because mRNA holds a negative charge that leads to electrostatic repulsion from the anionic cell membrane. The development of methods for systemic delivery that allow efficient cellular uptake and intracellular release while protecting mRNA during transport has long been investigated.

Liposomes represent a common transport vehicle for mRNA, and commercial products for lipofection allow easy and wide application. Liposomes are spherical vesicles of phospholipid bilayers formed by hydrophobic and hydrophilic interactions between the polar head group and the nonpolar tails of phospholipids (Figure 13, on the left).^[277] Cationic lipids enable loading of negatively charged mRNA molecules inside liposomes and offer good efficacies for *in vitro*^[135,278] and *in vivo*^[135,254,265,279] applications. However, toxic and immunogenic side effects have been reported causing inflammation^[280,281] and even liver damage following intravenous injections in mice^[282]. Instead of cationic lipids, ionizable lipids are used in newer compositions for liposomes. Ionizable lipids are positively charged at acidic pH for RNA loading and electrically neutral at physiological pH to reduce their toxicity.^[283] After cellular uptake, the ionizability also promotes endosomal escape and cargo release.^[283–286]

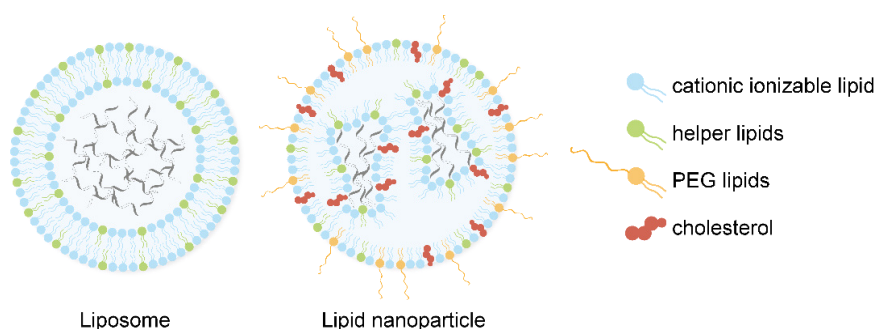


Figure 13. Composition and structure of lipid-based transport vehicles for mRNA.

State-of-the-art formulations for mRNA transport, advanced from pure liposomes to lipid nanoparticles (LNPs, see Figure 13, on the right) which comprise a mixture of ionizable lipids and a range of helper lipids, such as cholesterol, dioleoylphosphatidylethanolamine (DOPE), phosphatidylcholine (PC) and polyethylene glycol (PEG) lipids. Each of the aforementioned helper lipids contributes to the stability of LNPs and their delivery efficiency. Cholesterol increases vesicle stability *in vivo* and intracellular delivery by improving membrane-fluidity, elasticity and permeability.^[287–290] PC also contributes to an improved stability while DOPE

enhances endosomal release by membrane fusion and disruption.^[287,291] PEG lipids augment the LNPs colloidal stability in fluids improving not only the systemic delivery but also immunogenicity and *in vivo* retention of PEGylated LNPs.^[260,292–296] Furthermore, LNPs can be modified for tropism, either by modulating their polarity to target different organs depending on the charge of the LNPs^[297,298] or by incorporating antibodies on the LNP surface for specific targeting^[299].

As an alternative to LNPs, several other transport systems for mRNAs such as viral systems^[300,301], cationic polymers built of poly(L-lysine)^[302,303] or poly(ethyleneimine)^[304–306], cell systems^[307–311] and extracellular vesicles^[312–314] have been reported so far, but they have not yet been exploited for therapeutic applications. Some of them had certain drawbacks, such as undesirable immune responses in viral transport systems^[315] or increasing toxicity with increasing molecular weight of cationic polymers^[316]. Whereas natural vehicles such as cell systems and extracellular vesicles greatly benefit from biocompatibility and hypoimmunogenicity,^[307,308,314] but require quite elaborate manufacturing concepts.

So far, promising therapeutic approaches on the basis of mRNA have been developed. However, improvements are sought on both the mRNA as therapeutic agent and its delivery vehicle to improve and extend existing approaches. In achieving these goals, the given advantages of mRNA, its time-limited duration of action and efficiency, as well as avoidance of undesirable side effects and consequences by bypassing permanent modification of the genome, can be fully exploited. In the future, further properties such as translation efficiency and stability could be modulated and fine-tuned by cleverly chosen modifications of mRNA, e.g., modified nucleobases, to adapt mRNAs even more specifically to their application. Further research into mRNA modifications is needed for a better understanding of their effects and will contribute to the continued development and optimization of mRNA therapeutics.

1.4 RNA modifications for biochemical research

1.4.1 Labeling strategies for RNA

Specific investigations on biomolecules often require attachment of a selective modification or functionalization. Labeling and probing strategies enable a whole range of investigations from basic research to studies on biological processes and also biomedical applications. Examples include visualization, tracking and localization, quantification, isolation, or studies of structure and interactions. The choice of method depends on the system to be studied and the features to be investigated in it.

To minimize undesirable side effects on the system under study, a few site-specific modifications should be preferred over multiple random introductions of reporter groups. However, co-transcriptional and site-specific enzymatic introduction of functionalized nucleobases into long RNAs still remains a challenge.^[317]

1.4.2 Bioorthogonal click-labeling applying inverse electron-demand Diels-Alder cycloadditions

Bioorthogonal reactions allow selective labeling of biomolecules in their natural environment.^[318,319] Thereby, interfering side reactions with the biological environment are excluded. An aqueous environment, reducing conditions of cells or the presence of nucleophiles do not affect the reaction. In addition, bioorthogonal reactions meet the criteria of click chemistry, *i.e.*, they proceed rapidly, irreversibly, with high yields and high specificity, and generate minimal and inoffensive byproducts.^[320] Consequently, these reactions are suited to the covalent linkage of selected substrates and biomolecules, known as bioconjugation. Only recently, the Nobel Prize in Chemistry was awarded for the development of click chemistry and bioorthogonal chemistry, proving the actuality and importance of these methods.

Meeting the criteria above, the inverse electron-demand Diels-Alder cycloaddition (IEDDA, see Figure 14) represents a powerful tool for bioconjugation. In this reaction, strained alkenes react with 1,2,4,5-tetrazines in a Diels-Alder retro Diels-Alder cascade.^[321] From an initially formed bicyclic intermediate, the dihydropyridazine is obtained by elimination of nitrogen.^[321] Subsequently, isomerization by H-shift can take place.^[321] When asymmetric substrates are used, several stereoisomers can be formed. For simplification, the different isomers are not depicted here.

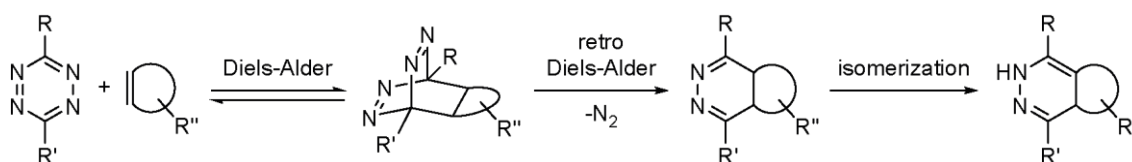


Figure 14. Reaction cascade for iEDDA click reactions between strained alkenes and 1,2,4,5-tetrazines.

One of the major advantages of bioconjugation using iEDDA click chemistry is that this reaction does not require the addition of a catalyst. In contrast, the commonly used Huisgen-like cycloaddition between alkynes and azides (CuAAC)^[322,323] uses copper(I) as a catalyst. However, since copper(I) has a toxic effect on cells^[319,321,324] and accelerates RNA degradation^[325], successful application of copper-catalyzed click chemistry is hindered *in vivo*.

Moreover, 1,2,4,5-tetrazines are particularly suitable for fluorescent labeling of biomolecules due to their quenching properties. With a characteristic absorption in the range of 500-525 nm,^[326] tetrazines suppress the fluorescence emission of conjugated fluorophores.^[327] This is ideal for green fluorescent dyes based on rhodamine or fluorescein, whose fluorescence emissions peak at 523 nm (Rhodamine Green) and 517 nm, respectively. As the tetrazine core is converted during the click reaction,^[321] a turn-on effect of fluorescence can be observed (Figure 15). Further advantages of this effect are a low background signal of the tetrazine-bound fluorophore before the reaction and an outstanding turn-on ratio after reaction completion.^[328–330] For cellular applications, no additional washing steps are required due to the excellent signal-to-noise ratio achieved by the turn-on effect.^[331] A variety of commercially available tetrazine-fluorophore conjugates and its widespread use highlight the importance of iEDDA for current research applications.

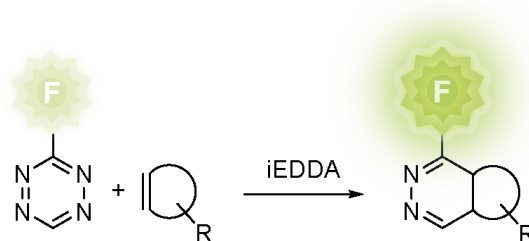


Figure 15. Turn-on effect of tetrazine-conjugated green fluorophores upon iEDDA reaction.

The most commonly used strained alkenes for iEDDA are cyclooctenes, norbornenes, and cyclopropenes. Among these, cyclopropene (CP) and norbornene modifications have both been employed by the Kath-Schorr group for effective RNA click labeling utilizing tetrazine-conjugated fluorophores *in vitro*.^[88,332,333] Two different applications have been shown for norbornene-moieties that were linked to both a natural and an unnatural nucleobase. By use of the norbornene-modified uridine cyanoethylphosphoramidite (CEP), called **Nor-U** (Figure 16, on the left), which was installed into a short siRNA prepared by solid-phase synthesis, first-time fluorescent iEDDA click labeling was demonstrated in live cells.^[334] In addition, by combining iEDDA click functionalization and unnatural bases, norbornene-modified nucleoside triphosphate of **TPT3**, called **Nor-UB** (Figure 16, on the right), was incorporated site-specifically into a short 30mer RNA oligonucleotide using enzymatic GENAEXT and reacted with tetrazine-conjugated fluorophores for *in vitro* visualization.^[332]

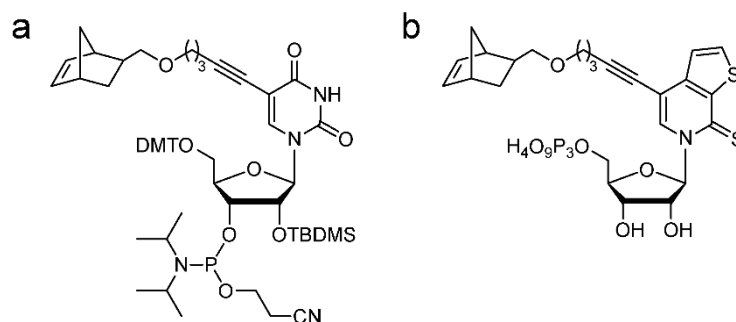


Figure 16. Chemical structures of norbornene-modified nucleobase building blocks. a) **Nor-U CEP**. b) **Nor-UB TP**.

The use of the more recently developed CP-modified unnatural base **rTPT3^{CP}**^[88] for site-specific labeling of functional mRNAs by GENAEXT (as presented in section 3.1) combines the previous projects in a logical continuation and allows both enzymatic preparation and iEDDA click visualization in live cells.

In addition to the advantages of iEDDA mentioned earlier, the method of enzymatic **rTPT3^{CP}** incorporation benefits from site specificity and the freely selectable modification site. Other published protocols for posttranscriptional fluorescent labeling of mRNA in cells^[335,336] either use CuAAC^[322,323] or strain-promoted azide-alkyne cycloadditions (SPAAC)^[337]. Besides the aforementioned drawbacks of CuAAC for applications on RNA and in cells, the methods presented using SPACC are limited in the positioning of the label, by either a single, terminal modification³⁰⁸ or randomized, multiple modifications throughout the poly(A) tail^[336]. Briefly, this is why a protocol is of great interest that allows for site-specific and enzymatic introduction of functionalized nucleotides into any RNA of interest, which can be complemented by subsequent attachment of reporter groups using biorthogonal click chemistry in live cells.

1.4.3 Electron paramagnetic resonance (EPR) spectroscopy

Electron paramagnetic resonance (EPR) spectroscopy can be used to study structural characteristics and dynamics of biomolecules under solution-state conditions. For this purpose, the biomolecules to be studied must be paramagnetic, *i.e.*, have unpaired electrons. EPR studies can be performed on biomolecules with intrinsic paramagnetic centers, such as manganese or iron metal ions bound in metal binding sites. If no such paramagnetic centers are present, they must be inserted artificially using spin labels. Trityl or nitroxide (NO) spin labels are often used for this purpose, the latter being more suitable for highly structured RNAs as they are less sterically demanding. NO labels are structurally derived from oxidized piperidine or pyrroline scaffolds (see Figure 17). An α -tetramethyl substitution provides improved stability of the radical by protecting against reduction in aqueous medium.

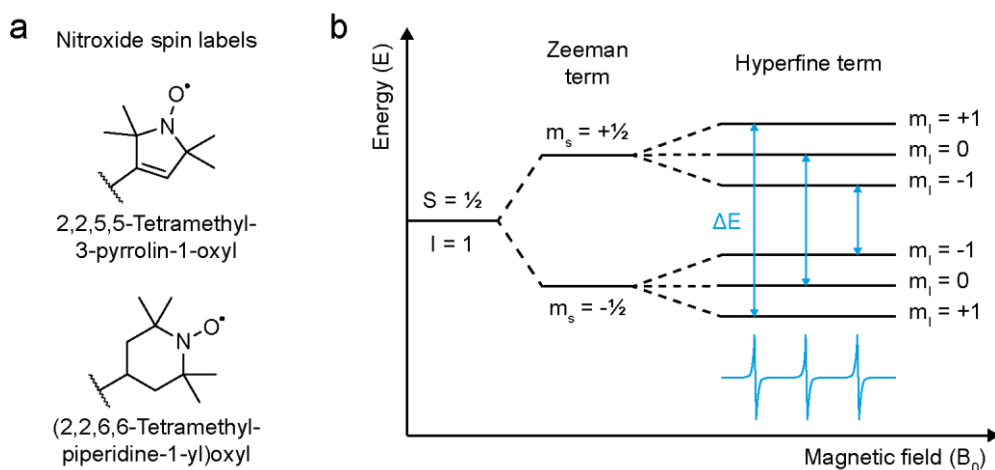


Figure 17. Nitroxide spin labels and energy diagram for nitroxides in an external magnetic field. a) Nitroxide spin labels based on pyrroline or piperidine scaffolds. b) Transition energies creating the nitroxide EPR spectrum after splitting of the energy levels of the electron spin moments.

In an externally applied magnetic field, the energy levels of the electron spin moments ($S = \frac{1}{2}$) split according to the Zeeman effect ($m_s = -\frac{1}{2}, +\frac{1}{2}$).^[338] Through the interaction with neighboring nuclear spins ($I = 1$ as in nitroxides), hyperfine coupling of the split energy levels is created, resulting in sub-states ($m_l = -1, 0, +1$) and distinct transition energies (ΔE) in between.^[338] By absorbing microwave radiation ($h\nu$), the unpaired electron can switch between the energy levels.^[338] This can be described in the equation $\Delta E = h\nu = g\beta_e B_0$ where h is Planck's constant, ν is the frequency, g is the electron's g -factor, β_e is the electron Bohr magneton and B_0 is the magnetic field. Consequently, either constant photon irradiation ($h\nu$) combined with a varying magnetic field (B_0) or, conversely, varying photon irradiation with a constant magnetic field can be used to record an EPR spectrum (see Figure 17).^[339]

To record continuous wave (cw) EPR spectra, a microwave field of constant frequency is applied and the external magnetic field is varied until the resonance condition is satisfied.^[338] Based on the multiplicity of the signals, the paramagnetic species present can be inferred from the spectrum obtained. For example, a NO cw-spectrum shows three peaks (see Figure 17). By integrating the signal peaks during the so-called spin counting, the amount of spin probes can be quantified. In addition, a qualitative estimation of the signal broadening and the changed relative intensities of the signal peaks can be made. The broader the signal becomes and the more the relative intensities change, the less dynamic is the measured spin label (Figure 18).^[339] This change in dynamics is observed when a spin label is immobilized due to its binding to a biomolecule.

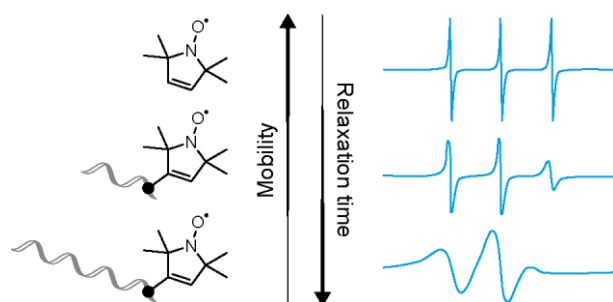


Figure 18. Relationship between relaxation times of differently mobile spin labels with exemplary corresponding cw-EPR spectra (adapted from NejatyJahromy *et al.*^[339]).

In the recording of pulsed EPR experiments, the magnetic field is kept constant and the spectrum is generated by simultaneously exciting a series of transition energies using a high-power microwave pulse of fixed frequency.^[338] One of the commonly used echo-detected field sweeps experiments in EPR is pulsed electron-electron double resonance (PELDOR). By the help of PELDOR experiments larger distance distributions between paramagnetic centers with distances down to 8 nm can be determined.^[340] Applying a special pulsed sequence to separate the dipole-dipole coupling from other contributions to the energy of the unpaired electrons,^[340] the PELDOR time trace of the echo intensity of the spins is recorded (Figure 19 b). For this purpose, sufficiently long relaxation times of the excited spins are required, which are achieved by cryogenic temperatures during the measurement.^[341] In the obtained PELDOR time trace, the modulation depth of the echo intensity gives information about the quantity of excited spins.^[340] Using the Fourier transform, a distance distribution can be determined from the PELDOR time trace (Figure 19 c).^[340] The obtained inter-spin distances give structural insight at the nanometer scale and can provide valuable information for the structural elucidation of biomolecules.

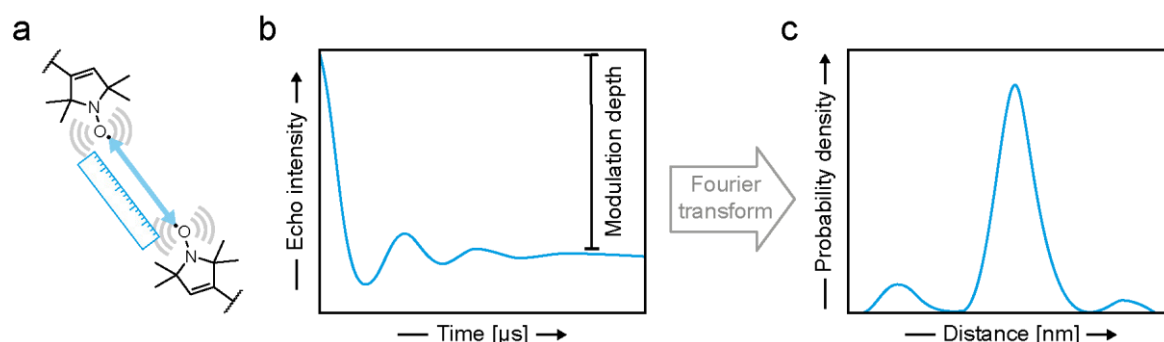


Figure 19. PELDOR experiments for inter-spin distance measurements (reproduced from Schiemann *et al.*^[344]). a) Schematic illustration of two nitroxide spin labels and their inter-spin distance. b) Exemplary PELDOR time trace of the echo intensity of the spins. c) Exemplary PELDOR-derived inter-spin distance distribution.

With regard to nucleic acids, a number of measurements on DNA and RNA duplexes, hairpin motifs and aptamer domains have been performed using PELDOR.^[342–349] In order to obtain relevant structural information by inter-spin distance measurements, spin labels must be introduced into the RNA in a site-specific manner. For this purpose, site-directed spin labeling (SDSL) strategies are applied. In the past, spin label-modified nucleobases were often introduced into sequences using solid-phase synthesis. This was done either by direct incorporation of a spin-label modified nucleobase or by post-synthetic attachment of a spin label to a previously introduced functionalized nucleobase.^[342,343,345,348,350,351] As an alternative to modified nucleobases, spin labels have also been introduced into nucleic acids site-specifically via the phosphate backbone or the sugar moiety.^[352–355]

By developing an enzymatic method for site-specific and direct spin labeling of RNA, limitations in the length of oligonucleotides produced by solid-phase synthesis and reduced efficiencies of post-synthetic ligation or coupling reactions can be addressed. The use of an extended genetic alphabet and the nitroxide modified UB **rTPT3^{NO}**, as presented in section 3.2, opens up unprecedented possibilities and enables EPR studies on previously inaccessible large and complex folded RNA.

2 Research Objectives

RNA, and mRNA especially, are noticeably coming to the fore of modern therapeutics. mRNA vaccines achieved great success fighting the global Covid-19 pandemic. Yet, there are many open starting points making it worthwhile and necessary to develop new visualization techniques and further investigate structure and function. Site-specific labeling approaches represent a powerful tool to study RNA both *in vitro* and in a cellular environment.

In this thesis, the versatile applications of an expanded genetic alphabet will be used to address visualization and detailed functional analysis of a protein-coding mRNA as well as structural studies of a regulatory lncRNA. For this purpose, modified unnatural base building blocks will be utilized which were derived from the unnatural base pair **TPT3:NaM** developed by the Romesberg group and advanced in the Kath-Schorr group.

First, mRNA visualization in cells as well as investigations into the influence of different modification patterns on mRNA stability and functionality were aimed. To this effect, site-specific cyclopropene labeling of a protein-coding mRNA sequence was aspired. Utilizing the earlier developed nucleoside triphosphate **rTPT3^{CP}** building block, mRNA sequences were prepared by genetic alphabet expansion transcription. In addition, a set of highly modified mRNA sequences carrying both natural and unnatural base modifications was intended. Therefore, further natural occurring base modifications of **pseudouridine** and **5-methylcytidine** were included in the mRNA. mRNA visualization by confocal fluorescence microscopy was enabled by live-cell iEDDA click labeling of cyclopropene-modified mRNA employing tetrazine-conjugated fluorophores. Moreover, a combined temporal analysis in cells was envisaged to assess mRNA functionality in terms of translation and protein expression together with transfection efficiency and mRNA stability. Additional cell health investigation was proposed to further evaluate this method's value with respect to potential *in vivo* applications in the future.

Furthermore, the structure of the complex folded *A-repeat region* from the long non-coding RNA *Xist* was investigated considering different structural proposals. To evaluate the proposals with regard to their accuracy, structural probing by pulsed EPR spectroscopy was intended. Using the nitroxide-modified unnatural base nucleoside triphosphate **rTPT3^{NO}**, enzymatic preparation and co-transcriptional site-directed spin labeling were aspired.

The aim of this study was to contribute to the structure elucidation of a regulatory active lncRNA and to diversify the toolbox for RNA visualization, complex analysis and fine-tuning of mRNA characteristics relating to mRNA therapeutics.

3 Results and Discussion

In the course of this study, unnatural nucleobases as part of an expanded genetic alphabet were applied in two different sequence contexts and for varying purposes. This is made possible by the use of a modular labeling system in which the same unnatural base is modified with different chemical functionalities. During *in vitro* preparation by GENAEXT, either a small chemical handle or a direct reporter group attached to the unnatural base was incorporated into different RNA sequences.

Section 3.1 describes the site-specific CP labeling of a series of mRNA sequences using the unnatural triphosphate rTPT3^{CP} for live-cell click labeling and mRNA visualization as well as the versatile cellular analysis of CP-modified mRNA in combination with natural base modifications Ψ and 5mC.

Section 3.2 presents the site-specific NO spin labeling of the *A repeat region* from the *Xist* lncRNA using the unnatural triphosphate rTPT3^{NO} with regard to structural considerations of the *Xist A-repeat region* applying PELDOR-derived intramolecular distance measurements.

The results of this study show that genetic alphabet expansion represents a powerful and versatile toolbox for multiple purposes and a variety of different RNA sequences, coding and non-coding. The methodological and experimental procedures presented will contribute to advance future research in the field of synthetic mRNA and structural research on lncRNA.

3.1 Cellular application analysis of site-specifically CP-modified mRNA

Artificial mRNAs have emerged as powerful and effective therapeutics.^[356] Further research is necessary to gain a deeper understanding of the role of artificial mRNAs in cellular processes. New methods that allow mRNA functionalization and their analysis in cells are therefore of great interest.

In the following, *in vitro* preparation (section 3.1.1) and cellular application (section 3.1.2) are presented for a range of artificial mRNAs. Using GENAEXT, the cyclopropene modified unnatural base rTPT3^{CP} [88] is incorporated site-specifically into the 3'-UTR of an mRNA as a small and reactive handle for click labeling. Optionally, natural base modifications of Ψ and 5mC were included in the mRNA and all mRNA sequences were comparatively tested for their cellular application.

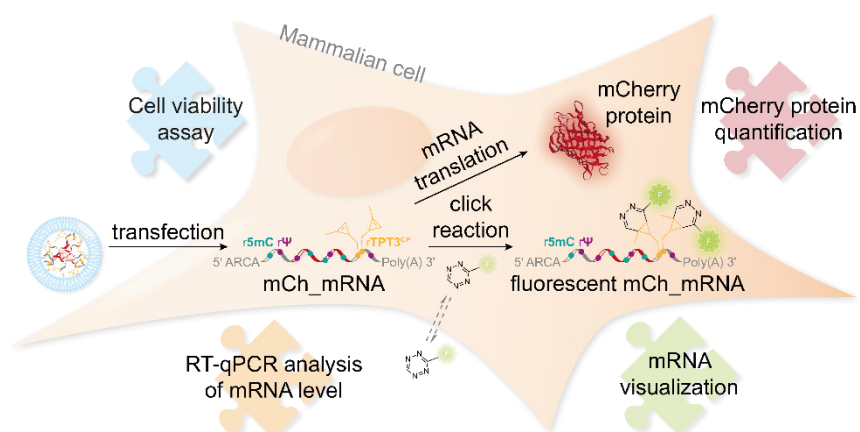


Figure 20. Schematic overview of the cellular application and analysis of CP-modified *mCh_mRNA*.

Figure 20 provides a conceptual overview of the multifaceted cellular function analysis and fluorescent visualization of *mCherry* encoding mRNA (*mCh_mRNA*). After preparation, *mCh_mRNA* is transfected into mammalian cells. Live-cell fluorescent click labeling of CP-modified *mCh_mRNA* enables visualization of mRNA by confocal fluorescence microscopy. Cellular mRNA levels are analyzed by RT-qPCR and mRNA stability is assessed over time. Quantification of the *mCherry* reporter protein expression is used to evaluate functionality of *mCh_mRNA* in terms of efficient mRNA translation and protein expression. In addition, the compatibility of the presented method for live-cell experiments was validated by measuring the cell viability in the experimental course of *mCh_mRNA* transfection and live-cell click labeling.

3.1.1 Preparation of site-specific UBP modified *mCh_DNA* and site-specific cyclopropene modified *mCh_mRNA* sequences in combination with natural base modifications

Sequence design of *mCh_mRNA*

In order to prepare site-specifically cyclopropene labeled RNA, the methyl-cyclopropene functionalized unnatural nucleoside triphosphate **rTPT3^{CP}** [88] (Figure 21) was used. **rTPT3^{CP}** TP was developed and synthesized by Dr. F. Eggert. [88] In previous work, **rTPT3^{CP}** TP has already been used for site-specific enzymatic introduction of CP-moieties into various RNA sequences of different lengths, for e.g. the *Xist* lncRNA *A-repeat region* or the catalytically active *glmS* ribozyme. [88,333] Applying iEDDA click reactions, these CP moieties were reacted *in vitro* with tetrazine-conjugated fluorophores, resulting in fluorescently labeled RNAs. [88,333]

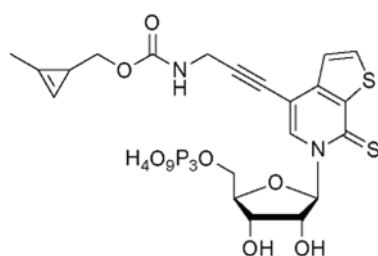


Figure 21. Chemical structure of the unnatural nucleoside triphosphate rTPT3^{CP} developed and synthesized by Dr. F. Eggert.^[68]

In the design and construction of the mRNA sequence, the red fluorescent *mCherry*^[357] protein was selected as the encoded reporter protein. The *mCherry* protein is a monomeric, rapidly maturing and highly photostable fluorescent protein derived from the *DsRed* protein from *Discosoma sp.*^[357] *mCherry* was chosen as a reporter protein for two reasons, first because of its strong red fluorescent signal, which contrasts with the green signal of click-labeled fluorescent mRNA, and second to allow fluorescence quantification of the *mCherry* protein to assess the functionality of the mRNA based on its cellular translation and protein expression (see section 3.1.2.2).

The sequence of the *mCh_mRNA* (see Figure 22) was designed to cover the *mCherry* protein coding sequence with additional flanking UTR sequences on the RNA's 3'- and 5'-end. The *mCherry* coding sequence and both UTR sequences were adapted from the *pmCherry-N1_AA-insert* plasmid without changes. UB modifications were placed outside the coding sequence towards the end of the 3'-UTR of the mRNA to not interfere with translation. In addition to site-specific UB modifications, mRNA sequences with natural base point mutations (PM) were prepared for comparison. Optionally for some mRNA sequences, natural base modifications of rΨ and r5mC were included as partial and random replacements of rU and rC within the complete mRNA, also including the protein coding sequence.

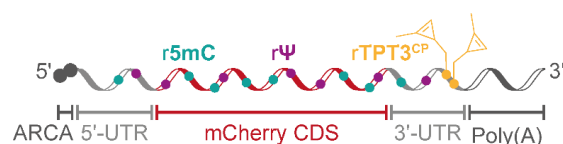


Figure 22. Schematic illustration for the sequence design of *mCh_mRNA*. A central *mCherry* protein coding sequence (CDS) is flanked on both sides by untranslated regions (UTRs). The mRNA contains an 5'-terminal Anti-Reverse Cap Analog (ARCA) and a 3'-terminal poly(A) tail.

Testing the influence of the position of the modification section within the mRNA's 3'-UTR sequence, another set of mRNA sequences (*mCh_mRNA_{UTR 2}*) was developed. Therefore, the UB modifications were positioned closer to the coding sequence and thus further away from the 3'-end. Additionally, the sequence following the modifications, which is the last 20 bases

of sequence of the 3'-terminal UTR, was exchanged. For the alternative sequence at the 3'-UTR end, a section was taken from the 3'-UTR sequence of the *pmCherry-C1* plasmid.

All different *mCh_mRNA* 3'-UTR sequences with site-specific UB modifications, canonical base point mutations, and optional natural base modifications generated in this study is listed in

Table 1.

Table 1. 3'-UTR sequences of different *mCh_mRNA* sequence constructs. **Y** stands for a rTPT3^{CP} point mutation, **G** stands for a rG point mutation. The underlined sequence shows the exchanged sequence part for *mCh_mRNA*_{UTR 2} variants. Purple and blue highlighted **U** and **G** represent partially replaced bases of rU by rΨ and rC by r5mC.

Sequence name	3'-UTR sequence
mCh_mRNA ^{WT}	AGCGGCCGCGACUCUAGAUCAUAAUCAGCCAUACCACAUUUGU
mCh_mRNA ^{WT, Ψ+5mC}	AG <u>C</u> GG <u>C</u> CG <u>C</u> G <u>C</u> GA <u>C</u> Ψ <u>C</u> ΨAG <u>A</u> Ψ <u>C</u> ΨAAΨ <u>C</u> AG <u>C</u> Ψ <u>A</u> Ψ <u>C</u> Ψ <u>C</u> Ψ <u>C</u> Ψ <u>C</u> Ψ
mCh_mRNA ^{1 CP}	AGCGGCCGCGACUCUAGAUCAUAAUCAGCC <u>Y</u> UACCACAUUUGU
mCh_mRNA ^{1 CP, Ψ+5mC}	AG <u>C</u> GG <u>C</u> CG <u>C</u> G <u>C</u> GA <u>C</u> Ψ <u>C</u> ΨAG <u>A</u> Ψ <u>C</u> ΨAAΨ <u>C</u> AG <u>C</u> Ψ <u>A</u> Ψ <u>C</u> Ψ <u>C</u> Ψ <u>C</u> Ψ <u>C</u> Ψ
mCh_mRNA ^{1 PM}	AGCGGCCGCGACUCUAGAUCAUAAUCAGCC <u>G</u> UACCACAUUUGU
mCh_mRNA ^{2 CP}	AGCGGCCGCGACUCUAGAUCAU <u>Y</u> UCAGCCAUACCAC <u>Y</u> UUUGU
mCh_mRNA ^{2 CP, Ψ+5mC}	AG <u>C</u> GG <u>C</u> CG <u>C</u> G <u>C</u> GA <u>C</u> Ψ <u>C</u> ΨAG <u>A</u> Ψ <u>C</u> ΨAAΨ <u>C</u> AG <u>C</u> Ψ <u>A</u> Ψ <u>C</u> Ψ <u>C</u> Ψ <u>C</u> Ψ <u>C</u> Ψ
mCh_mRNA ^{2 PM}	AGCGGCCGCGACUCUAGAUCAU <u>G</u> UCAGCCAUACCAC <u>G</u> JUUUGU
mCh_mRNA ^{WT} _{UTR 2}	AGCGGCCGCGACUCUAGAUCAU <u>GUUGUUGUUAACUUGUUU</u> AU
mCh_mRNA ^{1 CP} _{UTR 2}	AGCGGCCGCGACUCU <u>Y</u> GAUCAUAGUUGUUGUUAACUUGUUU <u>AU</u>
mCh_mRNA ^{1 PM} _{UTR 2}	AGCGGCCGCGACUCU <u>G</u> GAUCAUAGUUGUUGUUAACUUGUUU <u>AU</u>
mCh_mRNA ^{2 CP} _{UTR 2}	AGCGGCCGCG <u>Y</u> CUCUAGAUC <u>Y</u> UAGUUGUUGUUAACUUGUUU <u>AU</u>
mCh_mRNA ^{2 PM} _{UTR 2}	AGCGGCCGCG <u>G</u> CUCUAGAUC <u>G</u> UAGUUGUUGUUAACUUGUUU <u>AU</u>

Y = rTPT3^{CP}, **G** = rG, **ΨC** = rU/rC partially replaced by rΨ/r5mC

Preparation of mCh_DNA sequences

As shown in Figure 23, *mCh_DNA* acting as template for subsequent IVT was obtained by PCR amplification. For UB-modified *mCh_DNA* sequences, a six-letter PCR^[88,89,333] was performed. In a six-letter PCR, two unnatural nucleoside triphosphates are used in addition to the four canonical nucleoside triphosphates during amplification of the selected sequence. In combination with UB-modified template sequences or primers, their corresponding UB counterparts are incorporated opposite the UBs in the elongation phase of the PCR.

For the *mCh_DNA* sequence, site-specific UB-modifications were introduced into the amplicon applying a dNaM-modified reverse primer in the PCR reaction mix together with the UB nucleoside triphosphates, dTPT3 TP and dNaM TP. During PCR cycling, the reverse primer hybridizes to the plasmid and creates a dNaM:dA mismatch between primer and plasmid. After denaturing and elongation, the complementary DNA strand is filled up with the

dTPT3 UB counterpart, resulting in site-specifically dNaM:dTPT3 UBP-modified dsDNA. Utilizing a forward primer that is extended by the T7 promoter as an overhang sequence, the T7 promoter sequence, which is needed for subsequent IVT, is introduced on the other end of the dsDNA.

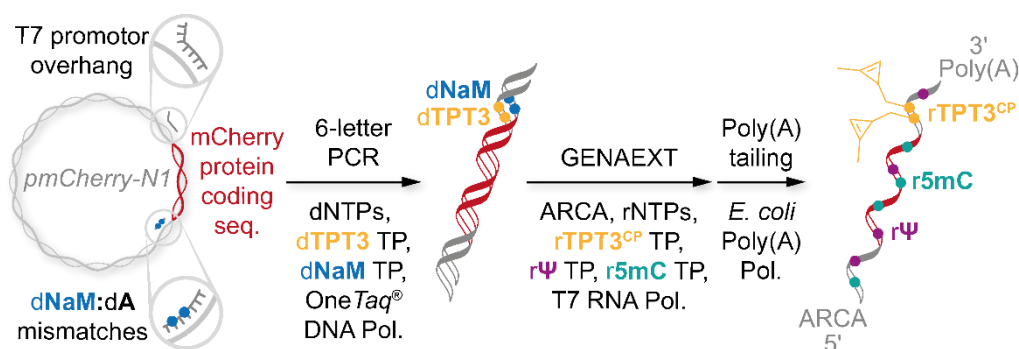


Figure 23. Schematic illustration for preparation of *mCh_DNA* by six-letter PCR, followed by GENAEXT for preparation of *mCh_mRNA*.

Six-letter PCR was performed for UBP-modified *mCh_DNA* and *mCh_DNA_{UTR2}*, whereas standard PCR reactions were performed for all non-UBP modified sequences including wild-type (WT) control sequences and canonical point mutations. PCR amplicons were obtained in good yields with high specificity for the expected sequence length as analyzed by agarose gel electrophoresis (see Figure 24 for *mCh_DNA*, and Figure 55 + Figure 56 in appendix for *mCh_DNA_{UTR2}*).

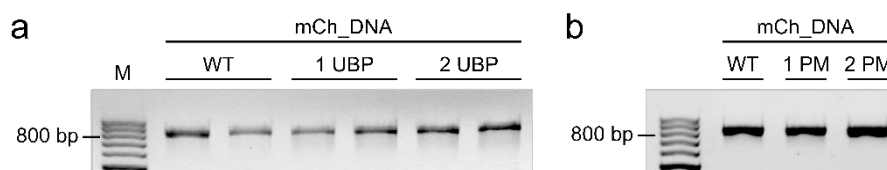


Figure 24. Agarose gel of different *mCh_DNA* sequences prepared by PCR. a) Unmodified and UB-modified *mCh_DNA*. b) Unmodified and natural base point-mutated *mCh_DNA*.

The sequence identity for each sequence was confirmed by Sanger sequencing for both, UBP-modified and unmodified *mCh_DNA* sequences (see section 7.2 for all sequencing results). For UBP-modified DNA sequences, site-specific termination of the sequencing reaction proved efficient UBP incorporation (Figure 25). In the case of double consecutive UBP modification in *mCh_DNA^{2UBP}*, the first of the two UBP modifications was indicated by termination of the sequencing reaction.

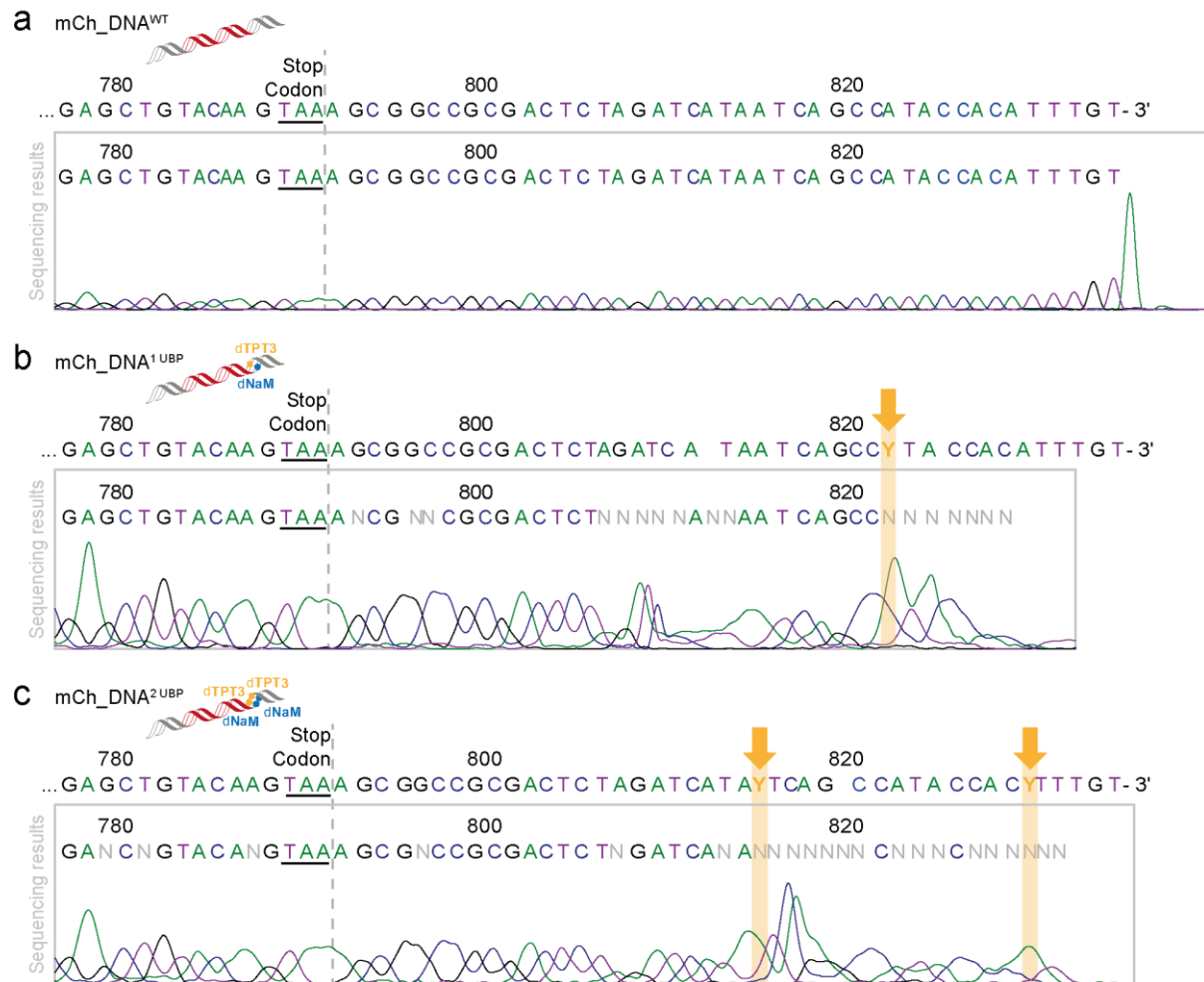


Figure 25. Sanger sequencing results of UBP-modified *mCh_DNA*. a) Sequencing results for unmodified *mCh_mRNA*^{WT}. b) Sequencing results for single UBP-modified *mCh_DNA*^{1UBP}. c) Sequencing results for double UBP-modified *mCh_DNA*^{2UBP}. Y marks the positions for a dTPT3 UB modification site.

Preparation of *mCh_mRNA* sequences

Site-specific CP-modified *mCh_mRNA* was prepared by co-transcriptional template directed incorporation of rTPT3^{CP} during GENAEXT at the opposite positions to the dNaM modifications in the DNA template. Analogously, WT control and canonical point mutated sequences were obtained under standard IVT reactions. For all *mCh_mRNA* sequences, the ARCA^[105,358,359] cap analog was introduced at the 5'-end co-transcriptionally. Likewise, all *mCh_mRNA* sequences were extended post-transcriptionally with a poly(A)-tail of approximately 150 nt length. In order to compare the influence of UB modifications with other stabilizing natural modifications, *mCh_mRNA* sequences were prepared including additional natural base modification (see Table 1). Therefore, rΨ and r5mC were co-transcriptionally installed at multiple random positions in the mRNA sequences replacing approximately 50% of the unmodified canonical nucleobases rU and rC.

mCh_mRNAs were obtained in good yields (up to 700 ng per 50 μ L IVT) with high specificity for the expected sequence lengths as analyzed by agarose gel electrophoresis (Figure 26 and for *mCh_mRNA*_{UTR2} Figure 59 in appendix). Moreover, the different mRNAs were prepared with consistent and mutually comparable lengths, fulfilling a necessary requirement for comparative cell application.

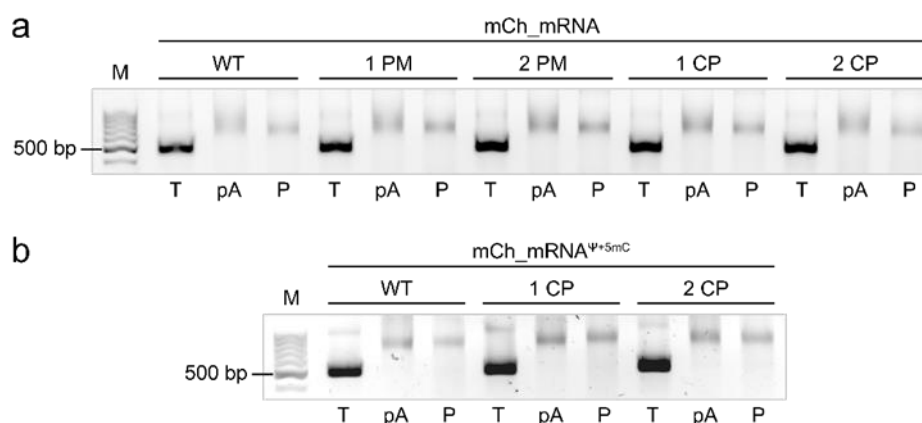


Figure 26. Agarose gels of *mCh_mRNA* transcripts without or with additional natural base modifications. a) Unmodified or UB-modified or natural base point-mutated *mCh_mRNA*. b) Unmodified or UB-modified *mCh_mRNA* with additional natural base modifications of r Ψ and r5mC.

Fluorescent labeling of CP-modified *mCh_mRNA* *in vitro*

Evaluating successful rTPT3^{CP} incorporation into transcribed mRNA sequences, fluorescent click labeling was performed for *in vitro* mRNA visualization (see Figure 27). All different *mCh_mRNA* sequences, either bearing the CP-modification or not, were incubated with a more than 60-fold molar excess of tetrazine-conjugated AF 488 fluorophores (TET-FL) and analyzed by preparative agarose gel electrophoresis and fluorescence scanning (Figure 28 and for *mCh_mRNA*_{UTR2} Figure 61 in appendix).

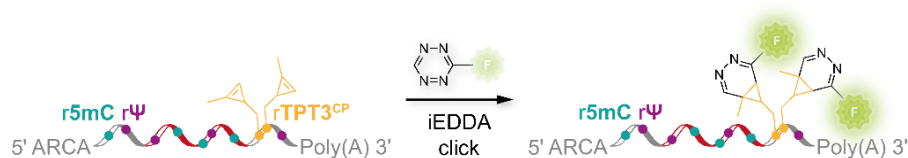


Figure 27. Schematic illustration of fluorescent iEDDA click labeling of CP-modified *mCh_mRNA*.

Only the *mCh_mRNA* sequences including rTPT3^{CP} modifications, showed a fluorescence signal. Single CP-modified and clicked *mCh_mRNA*^{1 CP} holds a strong fluorescence signal intensity, which is even exceeded by the double CP-modified and clicked *mCh_mRNA*^{2 CP}.

Whereas the unmodified control *mCh_mRNA*^{WT} does not show any fluorescence signal and is only visible after EtBr post-staining.

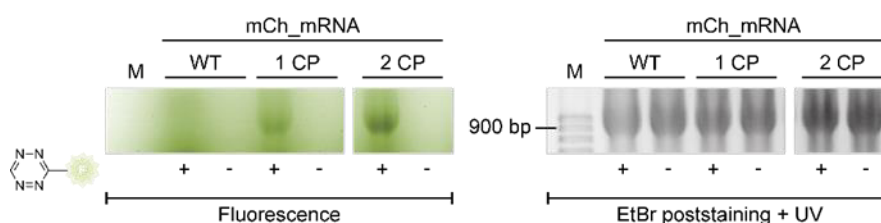


Figure 28. Agarose gel of *in vitro* click reaction of CP-modified *mCh_mRNA*. Fluorescence scan on the left. EtBr poststaining and UV visualization on the right.

Moreover, an additional experiment was performed in order to exclude unspecific rTPT3^{CP} TP incorporation^[90,333] during IVT mRNA preparation. Therefore, *mCh_mRNA*^{WT} was prepared by IVT from the unmodified *mCh_DNA*^{WT} template. Two identical samples were prepared, except that one IVT reaction included additional rTPT3^{CP} TP. The so transcribed *mCh_mRNAs* were then analogously incubated with TET-FL and analyzed by preparative agarose gel electrophoresis and fluorescence scanning (Figure 29). Neither *mCh_mRNA*^{WT} nor *mCh_mRNA*^{WT} transcribed in the presence of rTPT3^{CP} TP can be visualized in the fluorescence scan as compared to the strong fluorescent signal of click-labeled *mCh_mRNA*^{2 CP} that was included on the gel as fluorescent control.

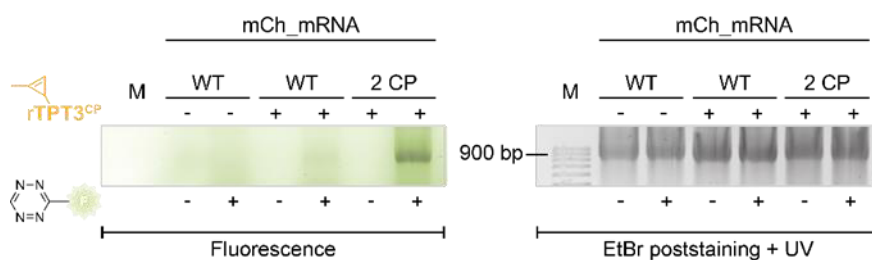


Figure 29. Agarose gel of *in vitro* click reaction checking for unspecific rTPT3^{CP} incorporation into unmodified *mCh_mRNA*^{WT}. Fluorescence scan on the left. EtBr poststaining and UV visualization on the right.

Briefly, correct and site-specific incorporation of rTPT3^{CP} TP into mRNAs transcribed from UBP-modified DNA templates was confirmed. CP-modified *mCh_mRNAs* held a strong fluorescent signal after iEDDA click labeling with TET-FL. Further, undesired untemplated incorporation of rTPT3^{CP} TP into mRNAs transcribed from unmodified DNA templates was successfully excluded.

3.1.2 Cellular analysis of modified mRNAs

Testing for cellular applications of *mCh_mRNA* transfected into mammalian cells, a multi-step analysis was devised and performed. CP-modified *mCh_mRNA* was fluorescently labeled in live cells utilizing iEDDA click reactions with tetrazine-conjugated fluorophores. Spatiotemporal fluorescence visualization of *mCh_mRNA* is presented in section 3.1.2.1.

Cellular *mCh_mRNA* levels after transfection were analyzed by RT-qPCR. In addition, a quantitative analysis of cellular mRNA translation and *mCherry* protein expression was accomplished. The combined results for quantification of relative *mCh_mRNA* levels as well as *mCherry* protein amounts expressed in transfected cells is shown in section 3.1.2.2.

For evaluation of cell health in the course of mRNA transfection and live-cell click labeling, a cell viability assay was carried out. Results of the cell viability assay are outlined in section 3.1.2.3.

3.1.2.1 Live-cell iEDDA click labeling for fluorescence visualization of *mCh_mRNA*

Following successful fluorescent labeling of CP-modified *mCh_mRNA in vitro* as previously described (see section 3.1.1), live-cell iEDDA click labeling was conducted in cells. Therefore, TET-FL was added to the cell medium of transfected HeLa cells at different time points after mRNA transfection initiating live-cell click labeling. Cell membrane permeable TET-FL^[334] reacts with the CP-moieties of UB-modified GENAEXT mRNAs resulting in green fluorescently labeled *mCh_mRNA*. Subsequently to live-cell click labeling and prior to confocal fluorescence microscopy, the cells were fixed by crosslinking with formaldehyde. The chosen time points for live-cell click labeling followed by fixation were 6, 24 and 48 h. Since the cell medium was changed 4 h after transfection according to the manufacturer's protocol for lipofection, the first time point for live-cell click labeling was set at 6 h after transfection. The two later time points were chosen at 24 and 48 h after transfection start in order to observe the time course of mRNA translation and mRNA distribution in cells. Cell fixation after live-cell click labeling allowed identical laser settings for all different samples at all different time points and hence a direct comparison of signal intensities between samples and time points. In addition, confocal fluorescence microscopy on fixed cells provided higher resolution and better light sensitivity as compared to live-cell microscopy.

For the *mCh_mRNA* sequence set (Figure 30 and Figures 74-76 in appendix), single CP-modifications in *mCh_mRNA*^{1 CP} were successfully demonstrated to be well suited for mRNA visualization holding bright green signals. Double CP-modified *mCh_mRNA*^{2 CP} even

exceeded these findings with increased signal intensities and improved signal-to-noise ratios facilitating excellent mRNA visualization.

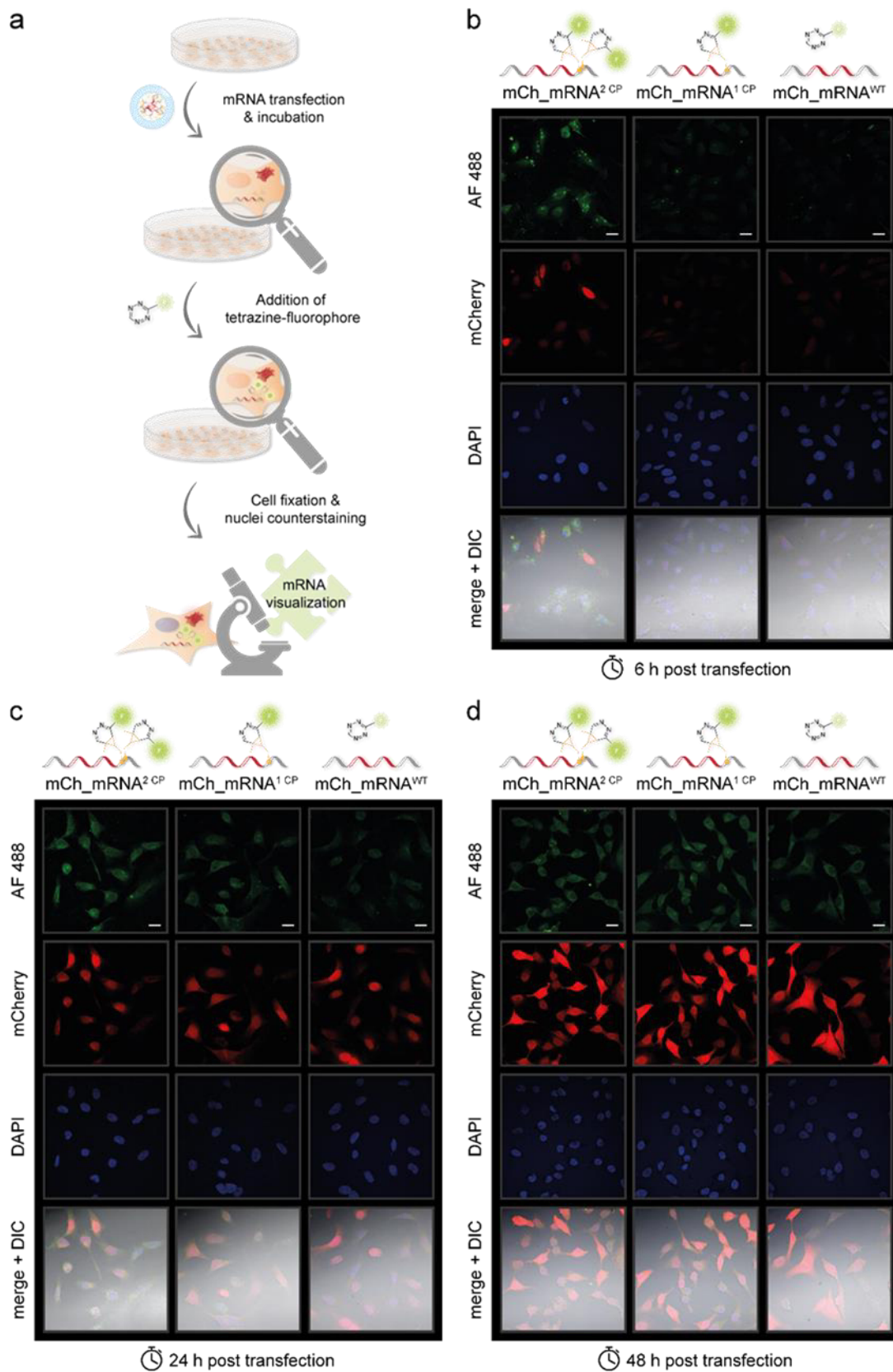


Figure 30. Confocal fluorescence microscopy images of cells transfected with CP-modified *mCh_mRNA* for live-cell click labeling and fluorescence mRNA visualization. Scale bars correspond to 20 μm .

The specificity of iEDDA linkage between TET-FL and the CP-moieties of *mCh_mRNA* was clearly demonstrated by the green signal seen in cells with CP-modified *mCh_mRNA* but not in control samples of unmodified *mCh_mRNA*^{WT}. Additional control samples such as the H₂O transfection control and untreated cells (Figure 80 in appendix) also do not show a green click-signal.

For clicked UB-modified *mCh_mRNA*, at the earliest time point, 6 h after the start of transfection (Figure 30 b), intense green signal spots can be seen. These most likely arise from concentrated mRNA still kept within the transfection vesicles. As previously reported^[334,360], lipid vesicles that have not completely resolved are present 6 h after cell transfection. Consequently, the mRNA accumulated within them explains local signal maxima. 24 h after the start of transfection (Figure 30 c), the mRNA was released from the lipid vesicles into the cell cytoplasm. This can be seen by a more evenly distributed green signal throughout the cytoplasm of the cells. At the latest time point chosen for mRNA visualization, 48 h after transfection start (Figure 30 d), a decreased signal-to-background ratio is observed. This is accompanied by a nonspecific increase in the green fluorescent signal, which can be detected in all samples, clicked CP-modified and unmodified *mCh_mRNA* sequence variants. The increasing nonspecific green signal seen 48 hours after transfection start can be explained by increased green autofluorescence of the cells. An increase in cellular stress levels^[361–365] due to swelling exogenous *mCherry* protein concentrations from prolonged incubation of the cells with *mCh_mRNA* may account for the enhanced cellular green autofluorescence.

Thus, the herein presented method provides a straightforward strategy for live-cell labeling and enables steady mRNA visualization featuring excellent signal intensities for at least 24 h after transfection start.

In addition to the images discussed, a z-stack series of click labeled *mCh_mRNA*^{2 CP} (Figure 31) was acquired. Therein, the green fluorescent mRNA can be evidently localized within the cell concomitant with the red fluorescent *mCherry* protein signal.

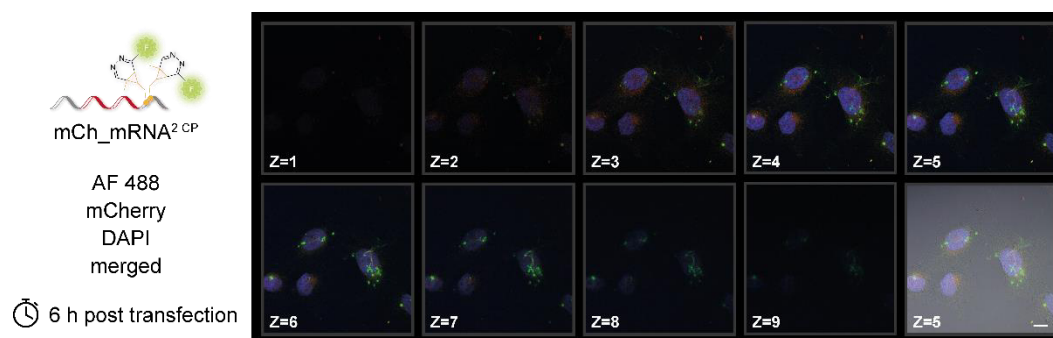


Figure 31. Z-stack series of *mCh_mRNA*^{2 CP} transfected cells at 6 h after transfection start. Scale bar in merged image of Z=5 (bottom right) corresponds to 20 μ m.

For both, *mCh_mRNA* and *mCherry* protein, strongest signal intensities are detected in mid-series images while the signals attenuate towards the cell periphery. Hereby, both the signal from the *mCherry* protein and the click-labeled *mCh_mRNA* can be localized within the imaged cells.

Moreover, close-up images of click labeled *mCh_mRNA*^{2CP} (Figure 32) were taken. Therein, one can nicely see how the presented approach of iEDDA click labeling enables even subcellular mRNA localization.

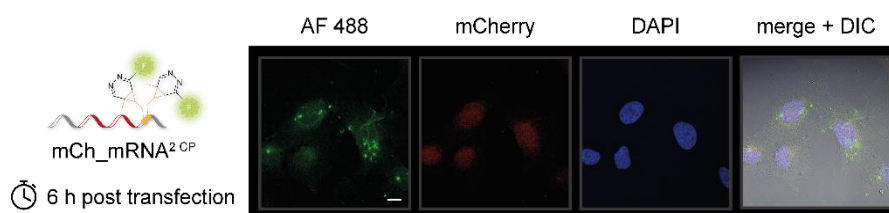


Figure 32. Close-up images of *mCh_mRNA*^{2CP} transfected cells at 6 h after transfection start. Scale bar corresponds to 20 μm .

Additionally, cell transfection and live-cell click labeling as well as microscopy analysis was performed in parallel for *mCh_mRNA*_{UTR 2} sequences and the previously reported results for *mCh_mRNA* were supported. For microscopy images of *mCh_mRNA*_{UTR 2} please see Figures 77-79 in appendix.

By confocal fluorescence microscopy analysis, not only CP-modified *mCh_mRNA* can be visualized in cells and used for mRNA localization. Red fluorescence of the mRNA encoded *mCherry* reporter protein allows qualitative evaluation of protein expression. This provides initial information about *mCh_mRNA* functionality by means of mRNA translation and protein expression in transfected cells, before *mCherry* protein quantification is discussed in section 3.1.2.2.

Red fluorescent signals were observed for all different *mCh_mRNA* sequence variants and increasing intensities thereof over progressing incubation time (Figure 30). Thus, efficient mRNA translation and protein expression *in cellulo* was demonstrated independent of *mCh_mRNA* sequence variants and modifications. Intensities of *mCherry* protein signals increased over time due to repeated mRNA translation and accumulation of expressed protein. Generally, for all different *mCh_mRNA* sequences, a more intense red fluorescent signal and hence higher concentration of *mCherry* protein was observed in the cell nuclei. Analysis of the *mCherry* protein amino acid sequence revealed a nuclear localization sequence (see section 7.7 in appendix) explaining this observation.

Taken together, fluorescent click labeling of CP-modified mRNA in live cells was successfully demonstrated. Even a single CP-modification was shown to enable mRNA visualization by fluorescence microscopy with good signal-to-noise ratios. Furthermore, double CP-modifications allowed exceptionally strong signal intensities. UB modifications within the 3'-UTR of *mCh_mRNA* sequences did not hinder expression of red fluorescent *mCherry* protein. iEDDA click labeling can be initiated at any time point by addition of TET-FL to the cell medium. In addition, no washing steps are needed prior to visualization or fixation. This makes it a straightforward procedure for spatiotemporal mRNA visualization in cells.

3.1.2.2 Quantification of mRNA levels in cells by RT-qPCR and *mCherry* protein amounts from cellular expression

Quantification of mRNA levels in cells by RT-qPCR

As qualitatively shown in microscopy, the CP-modified mRNA is functional, *i.e.*, it is translated in transfected cells and the mRNA encoded protein is expressed. Precisely for this purpose, in order not to affect the functionality of the *mCh_mRNA* with respect to protein translation, the UB modifications were solely placed in the 3'-UTR sequences and excluded from the reporter protein encoding sequence. Thereby, interference of the UB modifications with the cellular translation machinery and erroneous interactions such as mutating readthroughs, truncation or inhibition should be avoided. Optionally, additional natural base modifications of Ψ and **5mC** were installed throughout the entire *mCh_mRNA* sequences. These modified natural nucleobases were randomly incorporated into both flanking UTRs as well as into the coding sequence of the mRNA.

After mRNA and protein visualization by microscopy, in the following, cellular mRNA and protein levels are analyzed in detail. The effects of the various modifications and their combinations on the mRNA and protein level are investigated quantitatively.

In order to relatively quantify cellular levels of *mCh_mRNA*, reverse transcription coupled with quantitative PCR (RT-qPCR) was accomplished. For this purpose, two sets of qPCR primers and hydrolysis probes were designed. One set covered a sequence section at the 3'-end of the *mCh_mRNA* sequence, the other set targeted a sequence section at an mRNA internal position within the *mCherry* protein coding sequence (see Figure 33). For the 3'-end analysis, the sequence segment was placed outside the modification sites to exclude UB modifications for RT and thus avoid potential interference with efficient RT. By combining the *mCh_mRNA* quantification results from both sets, at the internal segment and at the 3'-end, information about mRNA stability and decay in cells can be obtained. The sample preparation procedure

was identical for all cells and independent of the fact that they were transfected with different *mCh_mRNA* sequences.



Figure 33. Schematic illustration for the two different sequence sections on *mCh_mRNA* chosen for RT-qPCR analysis.

After cell transfection and incubation, cells were lysed and the total cellular RNA was isolated. Subsequently, RT was performed applying a mixture of random primers and oligo(dT) primers. During RT, not only is *mCh_mRNA* reverse transcribed, but complementary DNA (cDNA) is generated for all (m)RNAs obtained by isolation of total cellular RNA. RT is initiated at sequence sites where either one of the random primers can hybridize to an mRNA sequence segment complementary to it or where the oligo(dT) primers hybridize to complementary sections within poly(A) tails. In subsequent qPCR, sections of selected target cDNA sequences are amplified. For this purpose, pairs of specific forward and reverse primers are used for each selected target cDNA sequence. Additionally, specific hydrolysis probes hybridize to complementary sequence segments included in the corresponding selected target cDNA sequences. During qPCR elongation cycles, the hydrolysis probes are degraded, producing a fluorescence signal corresponding to the amount of templating cDNA and thus the previous mRNA. By measuring the fluorescence signal intensities, the threshold cycle (C_t) is determined at which the amplification of the target sequence transitions to the exponential phase.

For this study, qPCR was accomplished in multiplex format, allowing simultaneous analysis of *mCh_mRNA* at its 3'-end and at the internal segment, both together with the mRNA of *glyceraldehyd-3-phosphat-dehydrogenase (GAPDH)* as the chosen reference gene. Data analysis uses the reference gene to normalize target mRNA levels to an endogenous mRNA that is stably expressed in all cells across transfection treatments. In this way, the ΔC_t values of all *mCh_mRNA* sequences are calculated. Then, the $\Delta\Delta C_t$ values are calculated by subtracting the ΔC_t value of the unmodified *mCh_mRNA*^{WT} at the 6 h analysis time point, in a sense as the control condition, from all other ΔC_t values of different *mCh_mRNA* sequences at different analysis time points. Fold changes in *mCherry* protein expression between cells transfected with different *mCh_mRNA* sequences were then given as $2^{-\Delta\Delta C_t}$ (Figure 34).

The lengths of qPCR amplicons were analyzed by agarose gel electrophoresis (see Figures 63-68 in appendix). Sequence identities of qPCR amplicons were additionally confirmed by Sanger sequencing (for sequencing results see section 7.2 in appendix). For this purpose, a sequence extension and amplification strategy was developed and carried out. All qPCR amplicons were extended by 130 nt applying a universal adapter oligonucleotide and

amplicon-specific splint oligonucleotides (for agarose gel analysis of the elongation process, please see Figures 69-71 in appendix). By appending the adapter sequence and applying a sequencing primer that hybridizes to the initial adapter sequence, the subsequent qPCR amplicon sequences were read starting with their first bases. This procedure enabled reliable sequencing results of the qPCR amplicon sequences using standard Sanger sequencing technology.

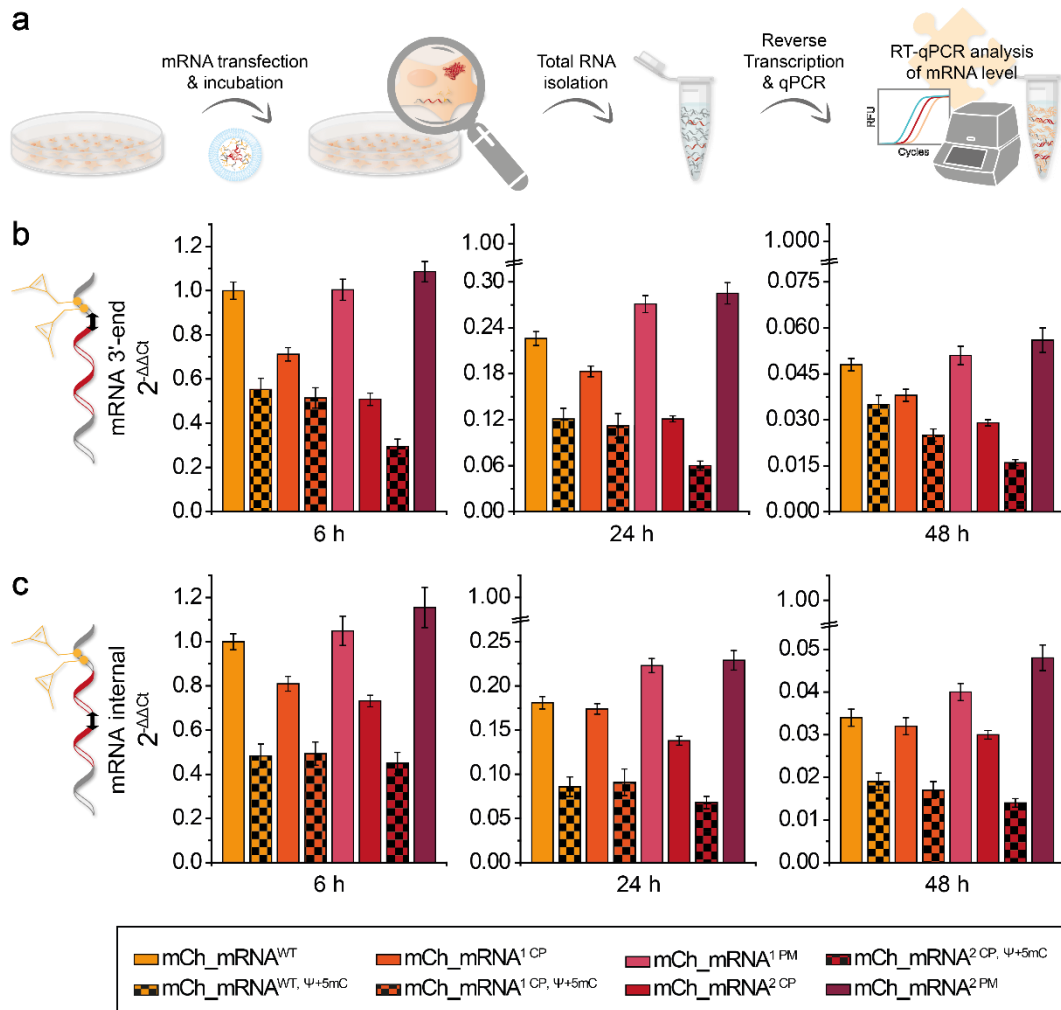


Figure 34. Results for RT-qPCR analysis of mCh_mRNA level in transfected cells at different time points. a) Schematic illustration of experimental workflow. b) Normalized mRNA fold change obtained by RT-qPCR analysis of mRNA levels using the 3'-end primer/probe set. c) Normalized mRNA fold change obtained for RT-qPCR analysis of mRNA levels using the internal primer/probe set.

For the evaluation of transfection efficiencies between different *mCh_mRNA* sequences, conclusions can be drawn from the earliest time point in analysis, 6 h post transfection start. At this time, most of the mRNA was still in the vesicles, as analyzed by fluorescence microscopy. Therefore, at the time point of 6 h after transfection, an assessment of the

transfected mRNA amounts is feasible without the possibility of parts of the mRNA being degraded and reduced by cellular influences by then.

As seen for both analysis sets, 3'-end and internal, reduced mRNA levels of 55% and less were found for mRNA sequences that contained the natural base modifications **rΨ** and **r5mC** (see bars with checkered pattern in Figure 34), compared with unmodified *mCh_mRNA*^{WT}. These findings are consistent with those published by Kauffman *et al.*, who also reported reduced levels for Ψ-modified mRNA^[366]. In addition, a lower amount at the earliest time point and thus a lower transfection rate was seen for CP-modified GENAEXT mRNAs. This effect was not as pronounced as that for natural base modifications; reduced levels of 81% and less were detected for CP-modified mRNA sequences. Whilst a gradation was observed in which the amounts of mRNA in cells decreased from *mCh_mRNA*^{WT} to *mCh_mRNA*^{1CP} and even further to *mCh_mRNA*^{2CP}, *i.e.*, with increasing number of CP-modifications (see Figure 35).

Similarly, results for 3'-end qPCR analysis of dual modified mRNA sequences with additional natural base modifications showed gradation from *mCh_mRNA*^{WT, Ψ+5mC} to *mCh_mRNA*^{1CP, Ψ+5mC} and even further to *mCh_mRNA*^{2CP, Ψ+5mC}, *i.e.*, again with increasing number of CP-modifications (see Figure 35). However, no reduction in cellular mRNA was detected with canonical base mutations of *mCh_mRNA*^{1PM} or *mCh_mRNA*^{2PM}. Consequently, as a first interim conclusion, the type of modification, the unnatural base **rTPT3**^{CP} or **rΨ**- and **r5mC**-modifications, seems to be crucial for this effect on reduced transfection efficiencies and not the position, because replacement of UB modifications with the canonical **rG** did not show the same effect and **rΨ**- and **r5mC**-modifications were randomly included in the whole mRNA sequence.

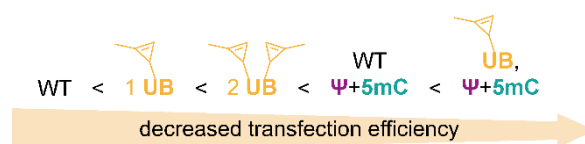


Figure 35. Decreased transfection efficiencies by different *mCh_mRNA* modification patterns.

In general, the cellular levels of all different *mCh_mRNAs* sequences progressively decreased over time due to proceeding mRNA degradation in the cells. At later time points, the previously discussed reduced mRNA levels for modified mRNA sequences, **rTPT3**^{CP} or **rΨ** and **r5mC**, are still present. However, a range of converging mRNA levels can be observed. As incubation time progressed after transfection initiation, a convergence of cellular mRNA levels was detected for both CP-modified sequences, *mCh_mRNA*^{1CP} and *mCh_mRNA*^{2CP}, in relation to unmodified *mCh_mRNA*^{WT}. As an exemplary calculation, mRNA levels of *mCh_mRNA*^{2CP} compared to *mCh_mRNA*^{WT} increased from 51% to 60% (3'-end analysis) and 73% to 88% (internal analysis) over time from 6 h to 48 h (see Figure 36). A possible explanation may be

the reduced degradation and hence increased cellular mRNA stability of CP-modified *mCh_mRNAs* in the transfected cells. The UB modification at the mRNA's 3'-end probably leads to a stalling event and thus terminate the exonucleolytic mRNA decay process in 3'→5' direction by the exosome^[367,368]. A similar convergency was found for natural base modified *mCh_mRNA*^{WT, Ψ +5mC} in comparison to unmodified *mCh_mRNA*^{WT} with increases of 55% to 73% (3'-end analysis) and 48% to 56% (internal analysis) (see Figure 36). Similar to the UB modifications, the natural base modifications likely reduce mRNA decay. In addition, r Ψ and r5mC can further increase mRNA stability and reduce mRNA degradation as they have been reported to confer resistance to RNase L cleavage and reduce stimulation of the cellular immune system.^[128,129,132,167,181]

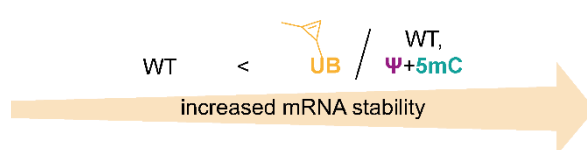


Figure 36. Increased mRNA stability by different *mCh_mRNA* modification patterns.

Since r Ψ and r5mC modifications were randomly incorporated into the coding sequence and UTRs of the mRNA sequence, impacts on reverse transcriptase activity by the modified natural bases can be excluded. Consequently, the observed effects are not a systematic error of the RT-qPCR assay and must originate from cell incubation. Taken together, differences in mRNA levels as well as converging levels of modified mRNA sequences are most likely reasoned by differences in lipofection and stalled mRNA degradation in cells, respectively, both caused by UB and natural base modifications.

Strikingly, the data did not show a convergence of mRNA levels between sequences with natural base modification and optionally additional UB modifications, e.g., *mCh_mRNA*^{2 CP, Ψ +5mC} and *mCh_mRNA*^{WT, Ψ +5mC}. Therefore, natural base modifications present in the entire mRNA sequence appeared to have a more dominant effect on slowing the mRNA decay as compared to only single or double UB modifications positioned at the 3'-end of the mRNA. Future studies on UB modifications and mRNA degradation could help to examine the strength of the influence by UB incorporation.

The ratios of mRNA levels of canonical base mutated sequences, *mCh_mRNA*^{1 PM} or *mCh_mRNA*^{2 PM}, to unmodified *mCh_mRNA*^{WT}, remained unchanged over progressing time. Thus, consistent with the conclusion previously drawn for transfection efficiencies, the type of modification, the unnatural base rTPT3^{CP}, is accountable for decreased mRNA decay and not the position. Since the rA↔rG exchange, in contrast to the rA↔rTPT3^{CP} mutation at the same position, has no discernible difference on the course of the mRNA level, it can be excluded

that the stabilizing effects of the UB modifications occurred only by random selection and mutation of a regulatory-active sequence site.

Consistent results were obtained for the second set of mRNA sequences with a partially replaced UTR sequence and the modification cassette shifted forward, *mCh_mRNA_{UTR 2}* (see Figures 82 and Figure 83 in appendix). Previously described findings on reduced transfection rates and increased mRNA stability for CP-modified mRNAs were confirmed. Similarly, the second set confirms the comparable transfection rates and unchanged mRNA levels over time for canonical base mutations in contrast to their corresponding site-specific rTPT3^{CP} modifications and their effect on increased mRNA stability.

Quantification of protein amounts in cells

In addition to cellular mRNA level analysis by RT-qPCR, concurrently the amounts of *mCherry* protein expressed *in cellulo* were measured. For this purpose, cells were transfected with *mCh_mRNAs* and incubated, after which the cells were lysed and the protein-containing lysate was isolated. The time points for cell lysis and protein isolation were set at 6, 24, and 48 h, analogous to the previous studies. The protein solutions obtained were analyzed by fluorescence measurements, and the amounts of *mCherry* protein present in the samples were calculated applying a standard *mCherry* dilution series added to each measurement. In order to obtain conclusive data on cellular protein expression, ten biologically independent experiments were performed in two sets each, testing UB- and natural base modifications (Figure 37) as well as the alternative 3'-UTR of *mCh_mRNA_{UTR 2}* (see Figure 81 in appendix). The *mCherry* protein levels from biologically independent experiments but transfections with identical *mCh_mRNA* sequences were averaged (n=20). All calculated *mCherry* protein amounts expressed from different *mCh_mRNA* sequence variants were normalized to the expression from unmodified *mCh_mRNA^{WT}* at 6 h after transfection start.

As it can be seen in Figure 37, in general, effective cellular translation and *mCherry* protein expression were demonstrated for all different *mCh_mRNA* sequence variants. All cell lysates from mRNA transfected cells display red fluorescent signals. Moreover, *mCherry* protein levels generally increased for all *mCh_mRNA* sequence variants in association with longer incubation times. This is due to repeated mRNA translation and accumulation of expressed *mCherry* protein in treated cells over time. However, when comparing the expression from different mRNA sequences and modification patterns, significant differences were ascertained. The discovered differences in protein expression from the different *mCh_mRNA* sequence variants will be discussed in the following section. To compare the expression levels of different mRNA sequences and modification patterns, the changes mentioned in the following section are

always referred to the unmodified *mCh_mRNA*^{WT} as standard. Overall, it was noticed that the general trends in differences in protein expression remain mainly unchanged over longer incubation times after cell transfection.

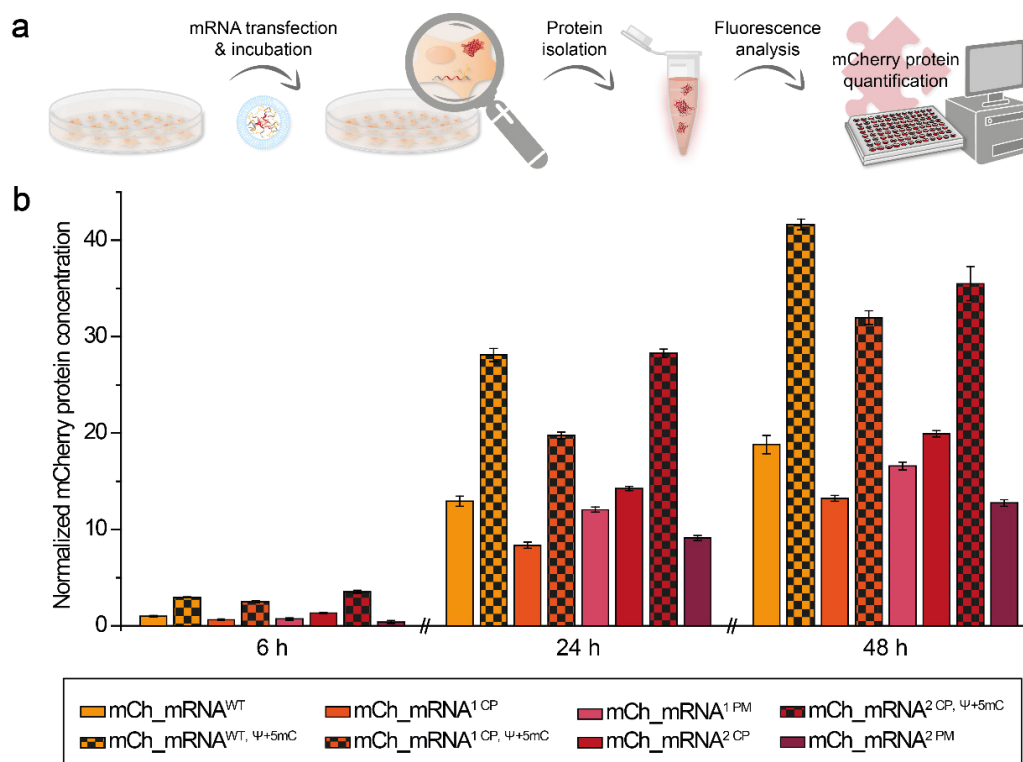


Figure 37. *mCherry* protein quantification analysis of cells transfected with different *mCh_mRNA* sequence variants at different time points. a) Schematic illustration of experimental workflow. b) Normalized *mCherry* protein concentrations obtained from different *mCh_mRNA* sequences modifications.

First of all, as shown before in confocal microscopy, CP-modified GENAEXT mRNAs, *mCh_mRNA*^{1CP} and *mCh_mRNA*^{2CP} did not affect the translational activity. No loss or impairment in mRNA function was detected for double CP-modified *mCh_mRNA*^{2CP} based on its cellular protein expression. On the contrary, a slightly improved expression was observed for *mCh_mRNA*^{2CP}. However, in contrast to *mCh_mRNA* level analysis by RT-qPCR, no gradation of protein expression from CP-modified mRNA was observed dependent on the number of CP modifications. While double CP-modified *mCh_mRNA*^{2CP} yielded slightly improved protein levels, the expression from single CP-modified *mCh_mRNA*^{1CP} was reduced to 69% or less.

Compared to the canonically modified sequences, *i.e.*, same modification site only **rA↔rG** exchanged instead of **rA↔rTPT3^{CP}**, it was the other way around. Slightly decreased expression levels were measured for *mCh_mRNA*^{1PM}, whereas more reduced protein levels were detected for double canonically mutated *mCh_mRNA*^{2PM}. Analogous to the interim conclusion for RT-qPCR, it is noted here that the change in protein level appears to be

dependent on the type of modification, introduction of the unnatural base, rather than the position of the modification.

A general increase in protein amounts was found for all cell samples transfected with natural base (r Ψ and r5mC) modified sequences. This emphasizes the impact of modified natural bases to create high translation efficiencies for the efficacy of therapeutic mRNA applications. Greatly improved expressions were noted for dual modified $mCh_mRNA^{1\text{CP}, \Psi+5mC}$ and $mCh_mRNA^{2\text{CP}, \Psi+5mC}$. However, the single CP-modified sequence variant of $mCh_mRNA^{1\text{CP}, \Psi+5mC}$ showed not quite as strong an improvement as the double CP-modified sequence variant of $mCh_mRNA^{2\text{CP}, \Psi+5mC}$. This is a comparable trend to the only CP-modified sequences. The sequence with double CP modification, with or without additional natural base modifications, features improved expression compared to the single CP modified sequence.

Altogether, highest multiplication of expressed *mCherry* protein levels was detected for dual modified $mCh_mRNA^{2\text{CP}, \Psi+5mC}$ and only natural base modified $mCh_mRNA^{WT, \Psi+5mC}$. At the earliest measured time point, 6 h after transfection start, $mCh_mRNA^{WT, \Psi+5mC}$ and $mCh_mRNA^{2\text{CP}, \Psi+5mC}$ showed a 3-fold and 3.5-fold increase, respectively. Over time, the multiplication decreased slightly, but the improved ratio remained as a trend. 48 h after transfection start, 2.2-fold and 1.9-fold amounts of *mCherry* protein were present for $mCh_mRNA^{WT, \Psi+5mC}$ and $mCh_mRNA^{2\text{CP}, \Psi+5mC}$, respectively.

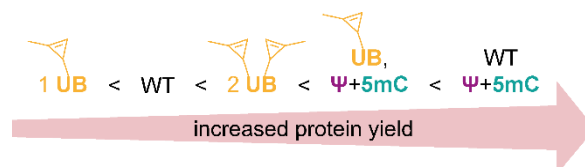


Figure 38. Increased protein yields expressed from *mCh_mRNA* with different modification patterns.

As an interim conclusion, double UB modification was found to increase protein yields, whereas single UB modification did not. The type of modification, *i.e.*, the UB rather than the position of the modification, was crucial to observe effects in protein expression, as verified by the PM mutation sequences. Natural base modifications generally increase protein yields. The combination of UB and natural base modification did not exceed the protein levels expressed from the sequence modified with natural bases only (see Figure 38).

For all different sequence variants of the mCh_mRNA_{UTR2} set, with partly exchanged 3'-UTR sequence and shifted modification sites, a general and strong reduction of expressed *mCherry* protein was observed (see Figure 81 in appendix). Overall, the determined values and ratios of the different modifications and sequences compared with the *mCh_mRNA* set differed significantly. Consequently, UTR sequence replacement and shifting the modification section

had a more drastic effect on protein expression levels than on mRNA transfection rates and mRNA stability in cells.

Because the cellular processes of mRNA translation and protein expression are complex and influenced by multiple factors, changes in protein levels due to the use of modified mRNA sequences cannot be easily attributed to single causes. Multi-causal changes in the interaction between the different mRNA variants and the cellular translational machinery are conceivable. These can be induced by the different types of modification, *i.e.*, UB or natural base modification, and their quantities, as well as their interplay, which may ultimately lead to altered mRNA folding and structural binding interactions with translation factors. Conclusive comparative considerations of the results from *mCh_mRNA* level analysis by RT-qPCR in connection with protein levels obtained by fluorescence quantification will be discussed in the following subsection.

Comparative considerations from *mCh_mRNA* level analysis by RT-qPCR in relation to *mCherry* protein quantification

In the following section, the previously discussed results of *mCh_mRNA* level and *mCherry* protein quantification will be considered together. A combined analysis is necessary because the amount of translated and expressed reporter protein is directly dependent on the amount of mRNA available in the cells. In order to assess the effects of different modifications in the *mCh_mRNA* sequences with regard to their translation efficiency conclusively and comprehensively, the protein amounts are to be brought into a relationship with the corresponding mRNA levels.

Therefore, *mCh_mRNA* and quantified *mCherry* protein amounts were normalized to the mRNA amount and expression level of unmodified *mCh_mRNA*^{WT}, which was set to 1 for both measures (Figure 39). This was done for the measured values at 48 h after transfection start. By then, the effects on cellular mRNA degradation and accumulated cellular mCherry protein expression are most apparent for comparison between the different *mCh_mRNA* sequences. In addition, only the data from the mCh_mRNA 3'-end qPCR set were used here for the mRNA level analysis because they more sensitively reflect 3'→5' mRNA degradation than the data of the mRNA internal qPCR set. For analysis of the correlation of cellular *mCh_mRNA* and *mCherry* protein amounts, protein/mRNA ratios were calculated from the normalized values.

In the following, selected data (see Figure 39 and Table 2) from the double CP-modified and unmodified sequences, with and without additional natural base modifications (*mCh_mRNA*^{2CP} and *mCh_mRNA*^{WT} vs. *mCh_mRNA*^{2CP, $\psi+5mC$} and *mCh_mRNA*^{WT, $\psi+5mC$}), will be discussed

further. These sequences were chosen because the overall highest protein levels were measured for them in combination with additional Ψ - and **5mC** modifications.

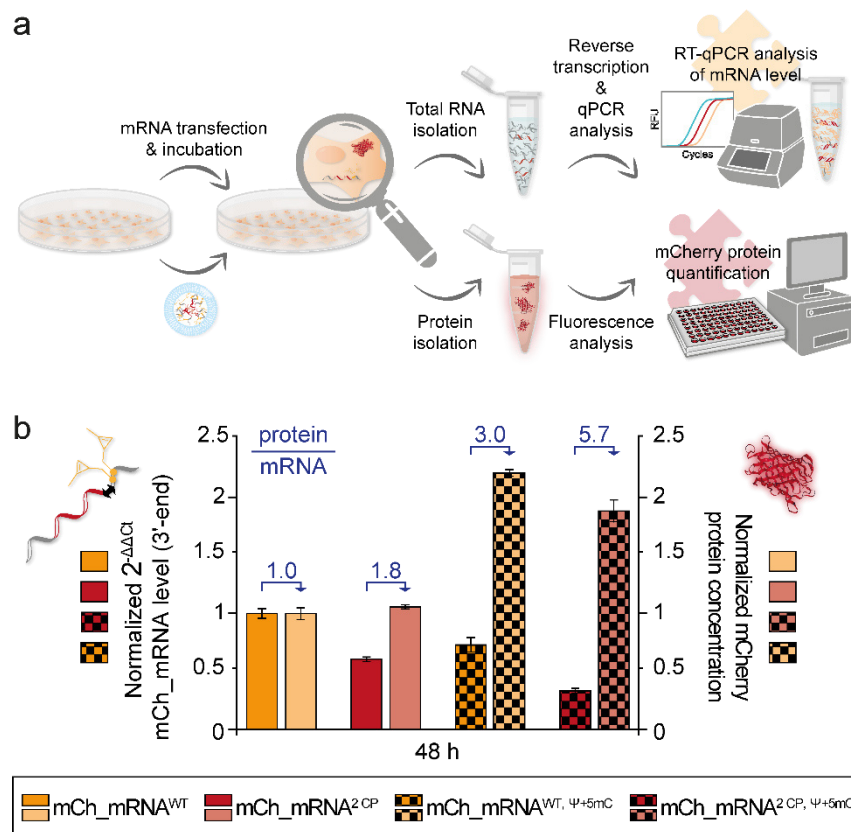


Figure 39. Comparison between cellular *mCh_mRNA* and *mCherry* protein levels for selected *mCh_mRNA* sequence variants. a) Schematic illustration of experimental workflow. b) Combined graph for normalized *mCh_mRNA* levels as analyzed by RT-qPCR using the 3'-end primer/probe set and normalized *mCherry* protein concentrations measured in transfected cells at 48 h after transfection start.

Table 2. Calculated protein/ mRNA ratios for selected *mCh_mRNA* sequence variants as analyzed by RT-qPCR using the 3'-end primer/probe set and *mCherry* protein fluorescence quantification at 48 h after transfection start.

Sequence name	Normalized mRNA level	Normalized protein level	Protein/mRNA ratio
mCh_mRNA ^{WT}	1	1	1
mCh_mRNA ^{2CP}	0.60	1.06	1.8
mCh_mRNA ^{WT, Ψ+5mC}	0.73	2.21	3.0
mCh_mRNA ^{2CP, Ψ+5mC}	0.33	1.89	5.7

For double CP-modified *mCh_mRNA*^{2CP} without additional natural base modifications, a reduction in the amount of cellular mRNA to 60% was observed. In contrast, an increase in protein expression was detected, which slightly exceeded the expression from the unmodified *mCh_mRNA*^{WT} control sequence. Thus, although comparatively less *mCh_mRNA*^{2CP} was

present in the transfected cells, improved protein translation and expression was found, resulting in a protein/mRNA ratio of 1.8.

In the presence of natural base modifications, a general decrease in cellular *mCh_mRNA* levels was detected by RT-qPCR. For *mCh_mRNA*^{WT, $\Psi+5mC$} , a decrease to 73% was observed, whereas for dual modified *mCh_mRNA*^{2 CP, $\Psi+5mC$} , the most drastic decrease to only 33% of cellular mRNA was found. However, protein quantification for *mCh_mRNA*^{WT, $\Psi+5mC$} and *mCh_mRNA*^{2 CP, $\Psi+5mC$} revealed 2.2-fold and 1.9-fold increased *mCherry* protein levels, respectively. All ratios mentioned referred to the unmodified *mCh_mRNA*^{WT} control sequence. This observation is made abundantly clear by calculated protein/mRNA ratios of 3.0 for *mCh_mRNA*^{WT, $\Psi+5mC$} and even 5.7 for *mCh_mRNA*^{2 CP, $\Psi+5mC$} .

Hereby, it has been conclusively shown that *mCh_mRNA* sequences carrying unnatural or natural base modifications significantly enhance cellular translation and expression of the encoded *mCherry* protein. The combination of both modifications in *mCh_mRNA*^{2 CP, $\Psi+5mC$} resulted in a synergistic effect and thus the strongest protein/mRNA ratio of 5.7 in comparison to all the different *mCh_mRNA* sequence variants investigated in this study. By comparing RT-qPCR and protein quantification results, it was demonstrated that the dual modified *mCh_mRNA*^{2 CP, $\Psi+5mC$} sequence was not only able to counterbalance the reduced mRNA levels, but even outperformed them with an exceedingly strong increase in protein expression. Hence, it was proven that the UB modifications can be incorporated into non-coding regions of mRNA sequences without negatively affecting the mRNA's biological function and translational activity. On the contrary, it was shown that the UB modifications positively influence cellular translation efficiency (see Figure 40).

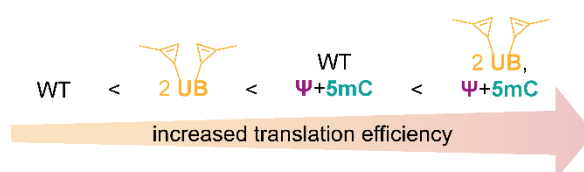


Figure 40. Increased translation efficiencies by different *mCh_mRNA* modification patterns.

It has been repeatedly shown that incorporation of natural base modifications into an mRNA sequence resulted in increased translation efficiency both *in vitro* and *in vivo*.^[132,135,369,370] So far, there is no definite explanation for this, but there are several explanatory approaches. One of them is an altered and enhanced interaction between modified mRNA and ribosomes during the translation process, leading to polysome formation, ribosome recycling or ribosome pausing.

Accompanied by increased protein expression from natural base modified mRNA, Sonenberg and coworkers found an increased formation of polysomes, which they explained by increased translation initiation and promoted ribosome recycling.^[217] In addition, polysome formation and growth were associated with decreased translation elongation rates and increased ribosome pausing.^[217] Ribosome pausing can have a substantial effect on the folding of nascent polypeptide chains,^[371] as intensified ribosome pausing enhances sequential folding of the growing peptide chain^[372] and thus the adoption of its correctly folded state. The modifications described in this study suggest an analogy. Modifications such as **rΨ** and **r5mC** incorporated into the mRNA likely increase protein expression through polysome formation and polysome growth, and the amount of correctly folded protein by ribosome pausing. Unnatural base modifications at the 3'-end of the mRNA may additionally contribute to this and explain the outstanding protein/mRNA ratio of twofold modified *mCh_mRNA*^{2 CP, Ψ+5mC}.

Furthermore, Romano and coworkers showed that efficient ribosome recycling induces optimal translation rates.^[373] According to the so-called 'closed-loop' model, interactions between the two ends of an mRNA strand can promote repeated translation of one and the same mRNA by repeatedly recycling terminating ribosomes back onto the same mRNA.^[373] An altered mRNA sequence and secondary structure induced by the incorporated natural and unnatural base modifications could enhance interactions with cellular recycling factors that stabilize the mRNA loop formation and thus promote multiple translation. This is further supported by the increased stability of **rΨ**-modified mRNA secondary structure due to enhanced H-bond formation^[374–376], which possibly results in altered dynamics of translating ribosomes.^[377,378] Moreover, UB modifications near the 3'-end of the mRNA can likely contribute to enhanced binding and loop formation because their different chemical structure allows for additional hydrophobic binding interactions specifically at the 3'-end of the mRNA strand. The strong increase in protein translation from dual modified *mCh_mRNA*^{2 CP, Ψ+5mC} (see Figure 39 and Table 2) can be explained hypothesizing that interactions of the UB modifications at the end of the 3'-UTR led to intensified loop formation, increased ribosome recycling and multiplied rounds of translation.

Besides altered mRNA-ribosome interactions, natural and unnatural base modifications may additionally affect translation regulation. This can occur either by increased translation activation or, conversely, by decreased translational repression. For formation of translationally active complexes as a part of gene expression, RNA-binding proteins (RBPs) represent connecting elements. RBPs bind to 3'-UTR *cis*-elements of the mRNA, in a sequence- and structure-dependent manner, to then mediate 3'-UTR function by recruiting effector proteins.^[379] Incorporation of natural and unnatural base modifications most likely results in altered mRNA and 3'-UTR structures^[181,374–376] that may increase the availability for RBP binding and thus translation activation. In addition, enhanced chemical diversity of incorporated

UB modifications located specifically in the 3'-UTR may allow for new binding interactions, hence promoting the formation of translationally active complexes.

While natural and unnatural base modifications included in the mRNA can enable the formation of new binding modes, they may in turn prevent others. In addition to previously described effects on ribosomal translation dynamics, natural base modifications were also shown to attenuate phosphorylation signals and reduce translational repression^[132,217]. During viral infection, RNA-dependent protein kinase (PKR) binds to exogenous RNA and then phosphorylates translation initiation factor 2, resulting in translational repression.^[380,381] However, reduced recognition and binding to PKR was observed for Ψ -modified mRNAs, which ultimately improved translation.^[132] This fits well with the observed increase in mRNA/protein ratios for natural base modified *mCh_mRNA* sequences, both with or without additional UB-modifications (see Figure 39 and Table 2). Besides PKR signaling, miRNAs represent another class of post-transcriptional regulators. Single-stranded miRNAs target the 3'-UTR and are a critical component of the effector ribonucleoprotein complexes RISC.^[19,382] RISC-mediated translational repression is guided by binding of the miRNA to complementary sequence sections in the 3'-UTR of mRNAs^[119,383] and can be divided into three steps: (i) site-specific cleavage, (ii) enhanced mRNA degradation and (iii) translation inhibition.^[383] The first step, also known as RNA interference (RNAi), requires a perfect or near-perfect match of miRNA and target sequence.^[383] Natural base modifications may prevent miRNA binding by altering the secondary structure of the modified mRNA due to enhanced thermodynamic stabilities^[376], resulting in inhibition of RNAi and translational repression. In particular, unnatural base modifications at the end of the 3'-UTR likely interfere with imperfect miRNA binding due to their hydrophobic character, which prevents incorrect base pairing with the canonical bases of miRNA and thus prevents RNAi and translation inhibition. Moreover, miRNA-binding sites located at the end of the 3'-UTR were reported to mediate a stronger repression compared to other sites.^[379,382] This could be a reason for the exceptionally high mRNA/protein ratio of dual modified *mCh_mRNA*^{2 CP, $\Psi+5mC$} , as the UB modifications at the end of the 3'-UTR can explain a significant reduction in potent miRNA-RISC-mediated translational repression. Over and above, since miRNA-mediated translational repression is a pre-requisite and directly linked to degradation of the target mRNA^[119,383], avoidance of miRNA translational repression also supports the increased stability of UB-modified *mCh_mRNA* sequences, as it was observed in the analysis of RT-qPCR data.

Future research will be required to conclusively answer the question of what specific mechanisms lead to both the increased mRNA stability in cells and the increased cellular mRNA translation and protein expression from the differently modified mRNA sequences.

3.1.2.3 Cell viability analysis in the course of mRNA transfection and live-cell click reactions

In order to assess cell health over time, after mRNA transfection and during live-cell click labeling, a non-lytic and bioluminescent cell viability assay was performed. In anticipation of future developments, such as *in vivo* applications, influences of the applied method on cell health should be obtained. The assay used is based on the reducing potential of viable cells. For this purpose, a substrate is supplied to the cells, the degradation of which in viable cells leads to the generation of a luminescence signal and enables constant measurements. The luminescence measured in the assay is not affected by the production of red or green fluorescence signals resulting from *mCherry* expression or click-labeled *mCh_mRNA*.

The measurement time of the assay started with the medium change, 6 h after cell transfection and was intended to cover the effects of cell transfection as well as the subsequent incubation period with opening of the vesicles and cellular mRNA translation. Also, the addition of TET-FL and the effect of live-cell click labeling of mRNA should be observed. Initial experiments were performed to measure the maximum time period in which the necessary linearity of the viability assay remained guaranteed (see section 7.6.2 in appendix). A period of approximately 30 h was determined. With reverence to the maximum assay measurement period, TET-FL was added to the cells 24 h after transfection start. As shown in the microscopy analysis, the lipid vesicles were open at this time and the mRNA was distributed in the cells, so that live-cell click labeling at 24 h post-transfection additionally allowed to evaluate the follow-up time.

The luminescence values measured over time of cells transfected with different *mCh_mRNA* sequences and control samples are presented in Figure 41. Since luminescence directly reflects the cellular reducing potential and thus viability, conclusion can be drawn from the measured luminescence values without conversions.

As previously reported, cell transfection by lipofection negatively affects cell viability because the commonly used cationic lipids can trigger pro-inflammatory immune responses and lead to systemic toxicities^[384,385]. Accordingly, slightly reduced luminescence signals were observed for all cells transfected with different *mCh_mRNA* sequence variants compared to the untreated cells control sample. As noted for the H₂O transfection control sample, cells treated with lipofection reagent but without mRNA encapsulated in it, also showed a reduction in measured cell viability, but to a lesser extent. Incorporation of natural base modifications into the mRNA sequences resulted in increased cell viability for cells transfected with these mRNA sequences.

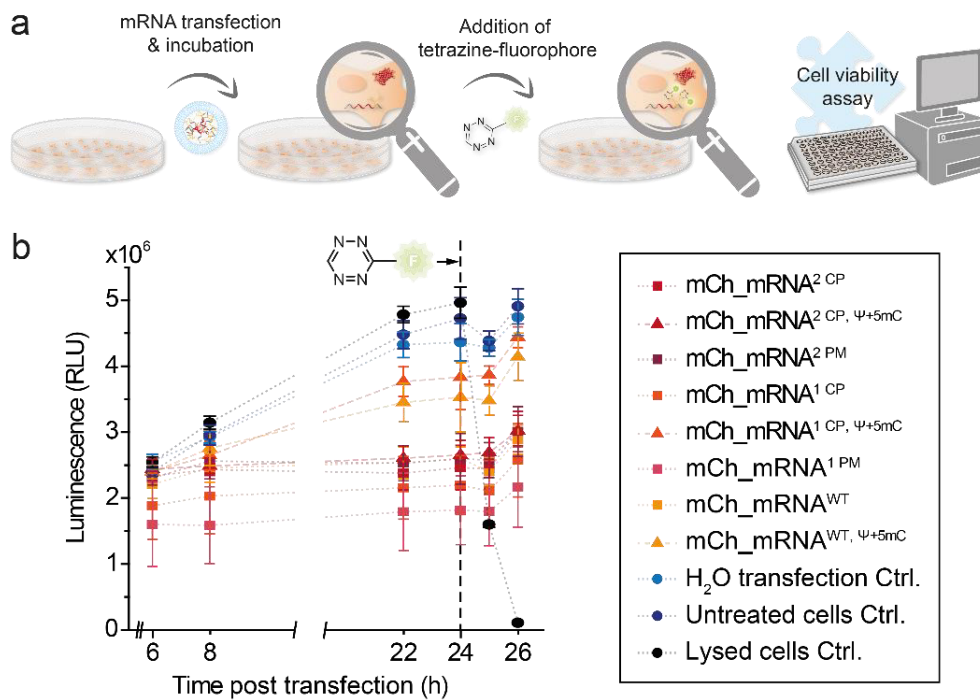


Figure 41. Cell viability evaluation of *mCh_mRNA* transfection and live-cell click labeling. a) Schematic illustration of experimental workflow. b) Measured luminescence over time reflecting the cell viability of cells transfected with *mCh_mRNA* sequence variants and control samples.

Incorporation of natural base modifications has repeatedly been shown to decrease the immunogenicity of synthetic RNAs^[128,130,131,134,167,369] and it was therefore anticipated that incorporation of **Ψ** and **5mC** into *mCh_mRNA* sequences result in a positive effect on cell health. In case of infectious diseases, the innate immune system can be activated by recognition of potentially pathogen-associated RNA.^[128] Immune responses leading to RNA degradation, but also cell inflammation and eventually apoptosis can arise. Cytosolic receptors such as retinoic acid inducible gene I (RIG-I) and membrane-bound pattern recognition receptors expressed on dendritic cells (DCs) and macrophages such as Toll-like receptors (TLRs) recognize and bind nucleic acids.^[128,167] Among these, TLR3, TLR7 and TLR8 were found to be stimulated by unmodified *in vitro* transcribed RNA, however RNAs including natural base modifications did not affect stimulation.^[131,134] Human DCs exposed to the same unmodified RNA secreted high levels of pro-inflammatory cytokines, whereas natural base modified sequences did not elicit cytokine secretion.^[131,134] Moreover, when testing various base modifications for suppression of RIG-I, it was suggested that, among other modified bases, **rΨ** and **r5mC** can individually suppress RIG-I.^[167] For **rΨ**-modified RNAs, it was also shown that RIG-I could bind to them but cannot induce conformational changes associated with RIG-I-activation.^[167] With respect to cell viability, complete substitution of **5mC** and **Ψ** for **C** and **U**, respectively, resulted in the most significant improvement, outperforming the effects of single substitutions of only one of the two modified natural bases.^[369]

Accordingly, higher luminescence signals were found for all *mCh_mRNA* sequence variants that contained **rΨ** and **r5mC** modifications. The highest values for transfected cells were seen for single CP-modified *mCh_mRNA*^{1 CP, Ψ+5mC} and unmodified *mCh_mRNA*^{WT, Ψ+5mC}, both with additional natural base modifications. These findings clearly demonstrate the positive impact of natural base modifications incorporated in the mRNA sequences on the transfected cells and emphasize the importance of natural base modifications for medical mRNA applications.

In addition, it was efficiently shown that UB modifications did not negatively affect cell viability, but could not additionally improve it. The viability values of cells transfected with UB-modified *mCh_mRNA* sequences are at least in the same range as those of unmodified *mCh_mRNA* sequence controls and canonical base mutated sequences. However, best results in terms of cell viability were observed for cells treated with UB-modified *mCh_mRNA* sequences that additionally included natural base modifications. Furthermore, it was found that addition of TET-FL did not impair cell viability either. At 1 h after addition of TET-FL to the cells, only a comparably small decrease in luminescence was detected for all samples. Subsequently, an increase in luminescence was observed for all samples. However, the lysed cell control, with alternative addition of Triton X-100 instead of TET-FL, displayed a remarkably strong decrease in measured luminescence and thus in cell viability 1 h after addition. In contrast to the transfected cell samples with addition of TET-FL, the luminescence of the lysed cell control continued to decrease sharply 2 h after addition.

In summary, the presented method for mRNA transfection of cells and subsequent live-cell click labeling by addition of TET-FL was shown to be well feasible in terms of cell viability. Transfected cells generally displayed reduced viability which is mostly assigned to lipofection and induced cellular stress responses thereof. In comparison of the mRNA cargo, UB modifications included in the mRNA did not affect cell viability. Incorporated natural base modifications of **Ψ** and **5mC** proved to be beneficial for cell health, as they generally increased the cell viability. mRNA sequences with combinations of natural and unnatural base modifications can be used as efficiently in the context of the conditions tested here, as they have a comparable small impact on cell viability as only natural base modified sequences.

3.2 *Xist* lncRNA A-repeat region for EPR structure elucidation employing site-specific RNA spin labeling

Studies on regulatory, ncRNAs with several hundred nucleotides in length, some of which may have additional complex foldings, have received increasing attention in recent years. Addressing this task, EPR spectroscopy allows for investigation on structural dynamics and folding of such RNAs.^[342,344,347,355,386–389] Using pulsed EPR techniques such as PELDOR^[390,391], intermolecular distances between two spin labels positioned in an RNA sequence of interest are measured^[343,345,346,391–403]. Therefore, specific spin label modifications must first be introduced into the RNA strand site-specifically. The use of functionalized UBs and GENAEXT for SDSL represents an alternative application of the previously introduced modular labeling system. With the help of an expanded genetic alphabet, information can be obtained not only for RNA visualization but also for structural investigation. In addition, the approach presented in the following demonstrates that this method of precise RNA modification can go hand in hand with computational studies, in this case for structure prediction.

Utilizing an expanded genetic alphabet for this purpose, common labeling limitations can be overcome and advantages of GENAEXT can be exploited. In the following, features of the GENAEXT approach using spin label modified unnatural nucleotides are comparatively highlighted. Co-transcriptional introduction of spin label modifications represents a fast and facile production of modified RNA. Direct incorporation of spin label modified unnatural nucleotides during *in vitro* transcription reduces preparation steps is preferred over solid phase RNA synthesis and additional post-transcriptional labeling reactions for the following reasons. For the RNA in general, limitations arise, first, due to the length constraints of solid phase synthesis^[403] and, second, due to the lower overall yield associated with an increasing number of preparation steps. With regard to the spin labels, both their integrity and quantity may be compromised, firstly due to the harsh reaction conditions during solid-phase synthesis leading to partial reduction of the nitroxides,^[404] and secondly due to less efficient post-transcriptional labeling caused by limited accessibility of modification sites in folded RNA^[405,406]. However, with enzymatic *in vitro* preparation, there are no length limitations and no subsequent steps are necessary due to direct incorporation. Co-transcriptional labeling proceeds under mild conditions and without being influenced by subsequent folding. Furthermore, as a key feature of GENAEXT, site-specificity enables a high accuracy for subsequent distance measurements, which is mandatory for the PELDOR experiment. Overall, the development of an *in vitro* protocol for direct and site-specific spin labeling of long and complexly folded RNA is of great benefit for EPR structure elucidation studies of additional RNA sequences.

For co-transcriptional and site-directed spin labeling applying the GENAEXT approach, the *A-repeat region* of the mouse *Xist* lncRNA was selected. Structural investigations on the *Xist A-repeat region* are highly desirable, as its structure has not been clearly elucidated to date.

The acronym *Xist* stands for X inactive specific transcript. *Xist* is accountable for X chromosome inactivation in female mammals and acts as a molecular scaffold for protein factor recruitment.^[407] Mouse *Xist* RNA consists of six conserved regions of tandem repeats, designated A through F.^[408,409] *Xist* repeat regions are conserved in mammalian vertebrates and thus also in humans.^[407] Corresponding to the repeat regions found in mouse *Xist* RNA, conserved equivalents are found in human *Xist* RNA, but they differ considerably in copy number of the repeats.^[407] However, the *Xist A-repeat region* represents an exception, as it is conserved from mouse to human, based on copy number and consensus sequence.^[407] In addition, the *Xist A-repeat region* is thought to be an important mediator of early gene silencing.^[409,410] It is further hypothesized that the structure of the repeats, rather than the sequence, is critical for silencing.^[409] For this reason, it is of great interest to further investigate the structure and folding of *Xist A-repeat region* RNA.

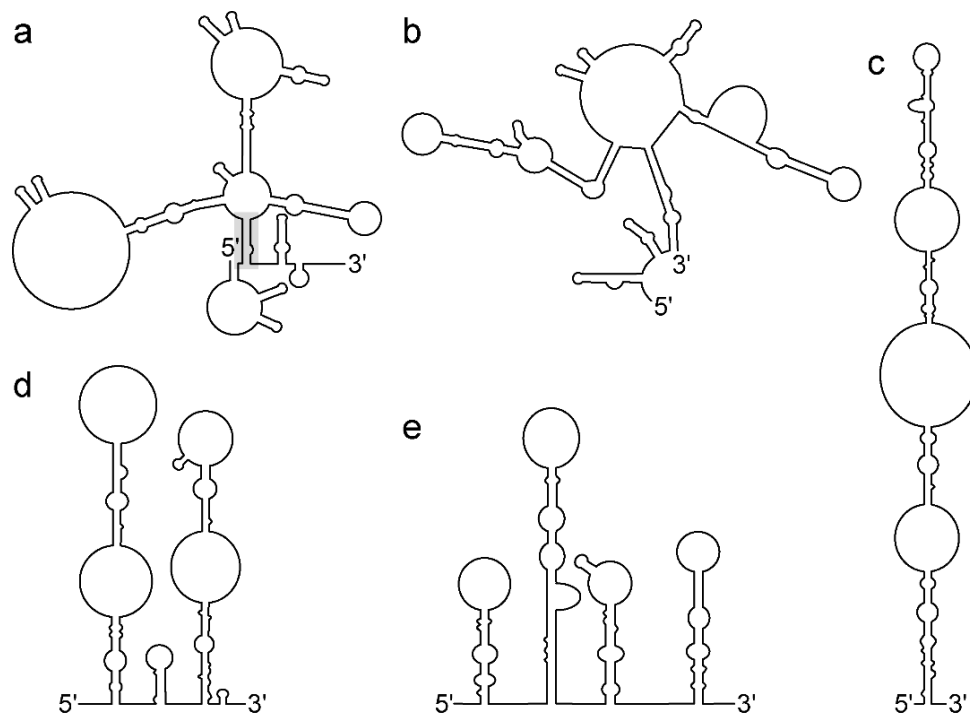


Figure 42. Different models for folding of the mouse *Xist* RNA *A-repeat region*. a) Structure model proposed by Fang *et al.*^[411] with highlighted duplex structure. b) Structure model proposed by Liu *et al.*^[413]. c-d) Structure models proposed by Maenner *et al.*^[412].

To date, different models have been proposed for the mouse *A-repeat* of *Xist* RNA (Figure 42)^[407,411–413]. Of these, the model by Fang *et al.*^[411] using Targeted Structure-Seq, a method combining *in vivo* DMS chemical probing with next-generation sequencing, assumes

a duplex formation between the 5'- and 3'-ends of the *Xist A-repeat region*^[411] which is investigated in the following (Figure 42 a, duplex structure is highlighted).

3.2.1 Preparation of site-specific UBP modified *Xist* DNA templates and nitroxide spin-labeled *Xist* RNA

In order to prepare site-specifically spin-labeled RNA, the pyrroline nitroxyl spin label functionalized unnatural nucleoside triphosphate **rTPT3^{NO}**^[414] (Figure 43) was used. **rTPT3^{NO}** TP was developed and synthesized by Dr. C. Domnick. In previous work, site-specific spin labeling using **rTPT3^{NO}** TP was performed on short self-complementary RNA duplexes and the self-cleaving *glmS* ribozyme.^[90,414,415]

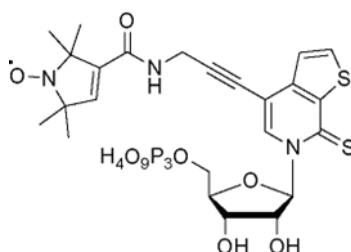


Figure 43. Chemical structure of the unnatural nucleoside triphosphate **rTPT3^{NO}** developed and synthesized by Dr. C. Domnick.^[414]

For EPR structure analysis of the *Xist A-repeat region*, a 377 nt long RNA sequence section was taken from the 426 nt long *Xist A-repeat region*. The selected sequence section from T366 to T740 of the *Xist* gene exon 1 was shortened compared to the full-length *A-repeat region* for two reasons. For the introduction of spin labels, the modifications sites had to be close to the 3'- and 5'-ends of the strand, because the templating modification sites in the precursor DNA were to be introduced via UB-modified PCR primers. Therefore, short 3'- and 5'-terminal sequence parts were truncated, which originally extended the proposed duplex structure by Fang *et al.* between the 5'- and 3'-ends beyond^[411]. For this purpose, two different truncation sites at the 3'-end were devised (see Figure 44, on the left, truncation sites are indicated). The first and longer sequence of 391 nt included an additional predicted hairpin structure at the 3'-end. In the second, slightly shorter sequence of 377 nt, this hairpin structure was also truncated. For the first and longer sequence, computational structure predictions performed with *mfold*^[416] revealed a more stable alternative folding in which the two ends of the sequence no longer formed a common duplex structure (Figure 44, on the right). For the second, shorter sequence, the *mfold* structure prediction showed much greater agreement with the structure proposed by Fang *et al.*^[411]. Moreover, the *mfold* structure calculation also indicated the

formation of the duplex postulated by Fang *et al.*^[411]. (Figure 44, center). Therefore, the shorter, 377 nt long sequence was chosen for this study.

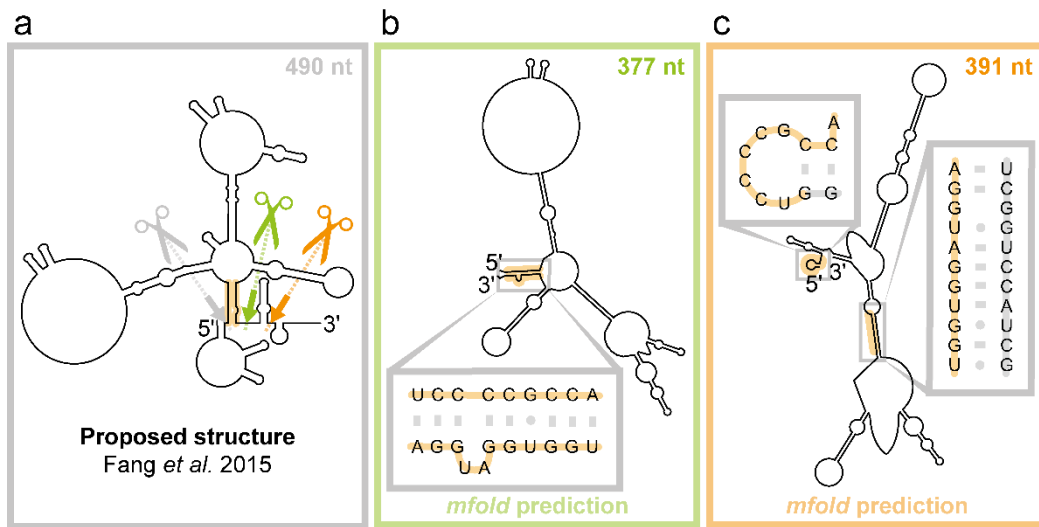


Figure 44. Structure predictions of truncated *Xist A-repeat region* RNA sequences. a) Structure of *Xist A-repeat* as proposed by Fang *et al.*^[411] with indicated truncation sites for different *Xist* sequence constructs. b) Structure prediction for shorter *Xist* sequence including the duplex structure proposed by Fang *et al.*^[411]. c) Structure prediction for longer *Xist* sequence showing an alternative folding and disruption of the duplex sequence sections.

Two different spin labeling constructs of the 377 nt long *Xist A-repeat region* RNA sequence section were designed to test the validity of the proposed folding by Fang *et al.*^[411]. Therefore, labeling positions were placed on both sides of the postulated duplex formed from the two sequence ends (see Figure 45). *Xist_RNA^{2NO}_5_3* includes one spin label at each of the 3'- and 5'-ends of the RNA sequence, giving the two labels a 363 nt distance from each other. Upon duplex formation, the two labeled ends of *Xist_RNA^{2NO}_5_3* come in close proximity and span the length of the duplex from both sides. In addition, *Xist_RNA^{2NO}_3_3* was prepared bearing two spin labels at the RNA's 3'-end, where the two labels are 11 nt apart. This covers the distance of the proposed duplex on one side from one end to the other.

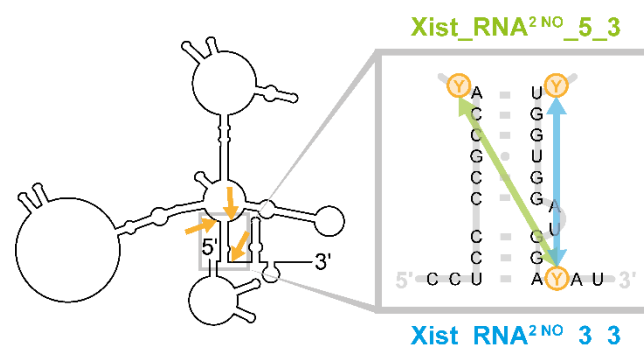


Figure 45. *Xist A-repeat region* folding as proposed by Fang *et al.*^[411] showing the selected spin labeling positions and the resulting inter-label distances of *Xist_RNA^{2NO}_3_3* or *Xist_RNA^{2NO}_5_3*.

In contrast, in almost all other structures of the *Xist* A-repeat region proposed by Maenner *et al.*^[412] or Liu *et al.*^[413], the two sequence ends and, accordingly, the two spin labels of *Xist*_RNA^{2NO}_5_3 are not in a short spatial proximity to each other (see Figure 46 a, b and d). A distinctly longer inter-label distance for the 3'- and 5'-label modifications may be stabilized by a hairpin-like structure in one of the proposed models by Maenner *et al.*^[412] (see Figure 46 c).

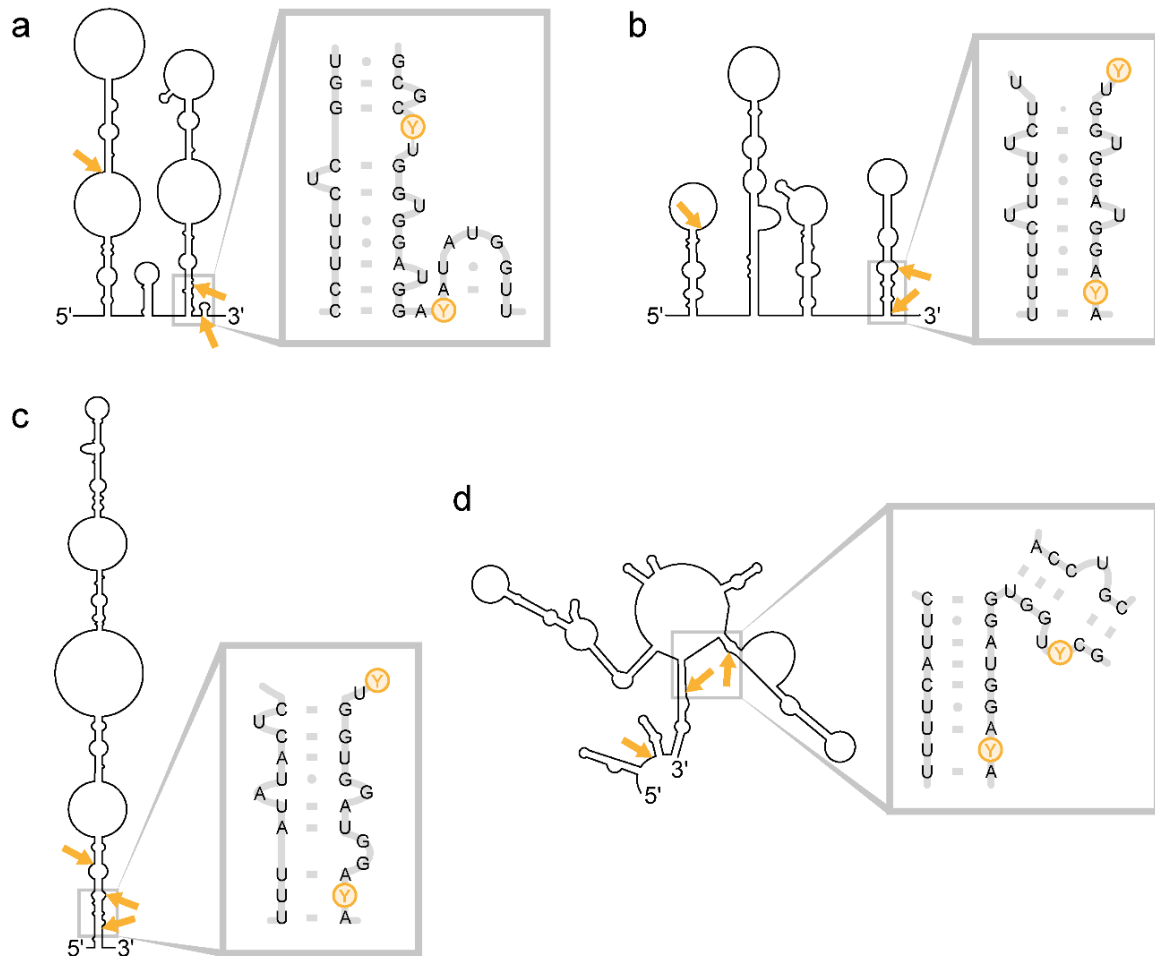


Figure 46. Alternative proposed structures of *Xist* A-repeat region with amplified substructures showing the spin label positions of *Xist*_RNA^{2NO}_3_3 or *Xist*_RNA^{2NO}_5_3. a)-c) Structures proposed by Maenner *et al.*^[412]. d) Structure proposed by Liu *et al.*^[413].

For the double spin label modifications at the 3'-end in *Xist*_RNA^{2NO}_3_3, there are several other proposed structures besides the assumed duplex structure by Fang *et al.*^[411], in which the 11 nt long 3'-3'-inter-label distance can be stabilized. All three different structure models proposed by Maenner *et al.*^[412] (Figure 46 a-c) hold possible stabilizations of the 3'-3'-inter-label distance by hairpin-like structures. Thus, measurable inter-label distances in a similar distance range compared to the duplex by Fang *et al.*^[411] are conceivable for these.

Only for the structure model proposed by Liu *et al.*^[413] comparable inter-label distances should not be measurable for both *Xist_RNA*^{2^{NO}_5_3} and *Xist_RNA*^{2^{NO}_3_3}, either due to too large distances or too much flexibility in spacing (see Figure 46 d).

In order to build up spin-labeled RNA sequences of the *Xist A-repeat region* for structural studies by PELDOR, UBP-modified *Xist_DNA* is first prepared, which is then used as a template for the preparation of *Xist_RNA* in subsequent *in vitro* transcription. An example illustration of the production of *Xist_DNA*^{2^{UBP}_5_3} and *Xist_RNA*^{2^{NO}_5_3} by six-letter PCR followed by GENAEXT is shown in Figure 47.

For preparation of templating DNA strands bearing site-specific UBP modifications, the mouse *Xist A-repeat region* sequence was amplified from the *pCMV-Xist-PA* plasmid in a six-letter PCR. UBP modifications were site-specifically introduced into the amplified DNA by use of UB-modified forward and reverse primers. Sites for UB point mutations primers were placed at **A:T** base pairing positions within the original sequence. The **A:T** base pairing positions, in contrast to G:C base pairing positions, were selected with the aim of exerting less influence on the secondary structure when a double rather than a triple base pair hydrogen bond is disrupted. For the preparation of *Xist_DNA*^{2^{UBP}_3_3}, a double d**NaM**-modified reverse primer was used in the PCR reaction mix together with d**TPT3** and d**NaM** TPs. For *Xist_DNA*^{2^{UBP}_5_3}, a single d**NaM**-modified reverse primer was used in the PCR reaction mix and combined with a single d**5SICS**-modified forward primer and the d**TPT3** and d**NaM** TPs.

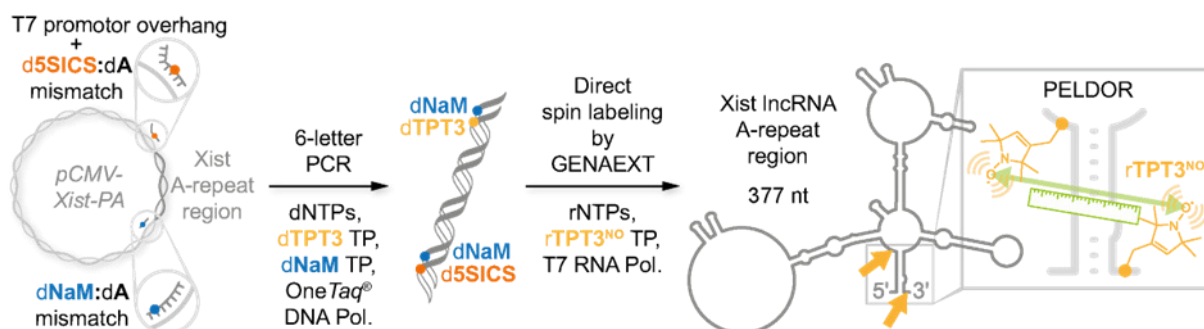


Figure 47. Preparation of UB-modified *Xist_DNA* by six-letter PCR amplification and subsequent preparation of spin label modified *Xist_RNA* by GENAEXT for inter-spin distance measurements by PELDOR.

A d**5SICS**-modified forward primer had to be used instead of a d**TPT3**-modified forward primer, since no d**TPT3** cyanoethyl phosphoramidite (CEP) was available for solid phase synthesis of d**TPT3**-modified DNA primers. Instead, the commercially available d**5SICS** CEP was purchased and given to the commercial manufacturer to be used in primer synthesis. As the d**5SICS** unnatural base also pairs with d**NaM**^[75] and represents the previously designed UBP

before this was optimized to the dTPT3:dNaM UBP, d5SICS-modified primers can be used together with dTPT3 TP and dNaM TP in a six-letter PCR reaction mix.

After PCR amplification, UBP-modified double stranded DNAs are obtained for both *Xist* sequences. *Xist_DNA^{2UBP}_5_3* includes two UBP modifications, one at its 3'-end and the other at its 5'-end. The templating strand of *Xist_DNA^{2UBP}_5_3* carries two dNaM UBs, whereas the counter strand comprises a mixture of d5SICS and dTPT3 (see Figure 47). During subsequent T7 IVT, only the templating dNaM-modified DNA strand is read, incorporating spin label modified rTPT3^{NO} TPs into the nascent RNA opposite dNaM. Therefore, the mixture of d5SICS and dTPT3 in *Xist_DNA^{2UBP}_5_3* does not affect the subsequent RNA preparation.

For *Xist_DNA^{2UBP}_3_3*, it is simpler. *Xist_DNA^{2UBP}_3_3* contains two dNaM:dTPT3 UBP modifications, both located at the same end of the DNA double strand.

In addition to the UBP modifications in the two *Xist* DNAs, 2'-O-methyl modifications were included for the last two nucleotides at the 5'-end of the templating DNA strand. This was done to prevent untemplated rTPT3^{NO} incorporation during subsequent IVT.^[90]

For both *Xist* sequences, *Xist_DNA^{2UBP}_5_3* and *Xist_DNA^{2UBP}_3_3*, PCR products were yielded with good yields and high specificity (see Figure 48).

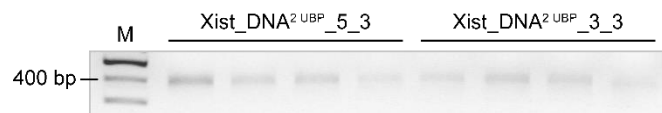


Figure 48. Agarose gel of PCR products of *Xist_DNA^{2UBP}_5_3* and *Xist_DNA^{2UBP}_3_3*.

Subsequent GENAEXT reactions utilizing rTPT3^{NO} TP and the previously prepared templating DNA sequences yielded the two different *Xist A-repeat region* RNA sequence constructs *Xist_RNA^{2NO}_3_3* and *Xist_RNA^{2NO}_5_3*. In order to obtain sufficient amounts of spin-labeled RNA, multiple IVT reactions had to be accomplished for each sequence construct. The transcribed RNA from multiple IVT reaction was combined and purified by preparative gel electrophoresis (see Figure 49).

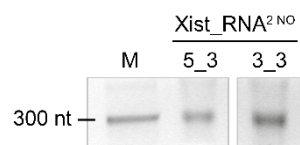


Figure 49. Agarose gel of *Xist_RNA^{2NO}_5_3* and *Xist_RNA^{2NO}_3_3* yielded by GENAEXT.

3.2.2 cw-EPR and PELDOR distance measurements of the spin-labeled *Xist* lncRNA A-repeat region

In the following section, EPR measurements of the two different *Xist* A-repeat region RNA sequence constructs *Xist_RNA*^{2NO}_{3_3} and *Xist_RNA*^{2NO}_{5_3} are presented and discussed. EPR experiments (cw-EPR, PELDOR) and data processing were performed by Dr. Christine Wuebben as part of a collaboration project with the research group of Prof. Dr. Olav Schiemann at the University of Bonn.

In addition, molecular dynamics (MD) simulations were performed and will be used to compare the distance information obtained with calculated structural information. MD simulations were performed by Prof. Dr. Stephanie Kath-Schorr. For this, a model duplex structure, which mimics the stem structure duplex formed by the 3'- and 5'-ends of the *Xist* A-repeat region as proposed by Fang *et al.*^[411], was constructed based on A-form RNA (for representative snapshots see Figure 50). All-atom MD simulations were accomplished in explicit solvent (TIP3P water model) using the GROMACS^[417–420] software package in combination with the CHARMM36^[421–423] force field. MD calculations were performed at 300 K with restraints on H-bonds or without restraints (except bond lengths). MD trajectories were calculated for *Xist_RNA*^{2NO}_{3_3} first with restraints on all base pairs for 50 ns, followed by 1 ms without restraints. For *Xist_RNA*^{2NO}_{5_3}, MD trajectories were calculated with restraints on all base pairs for 1 ms.

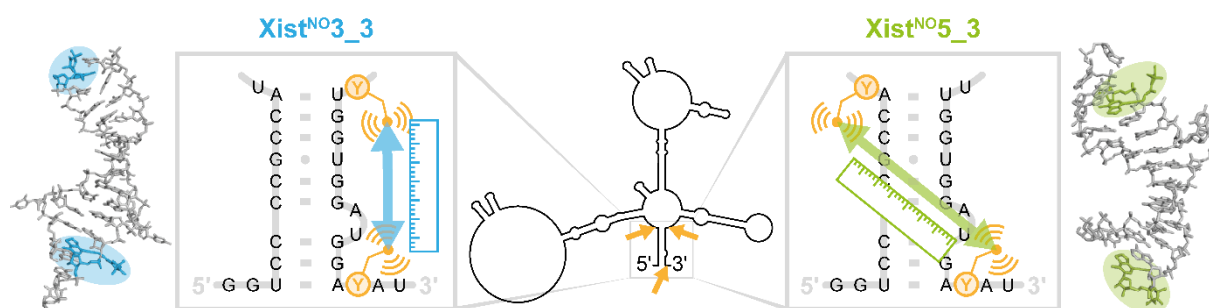


Figure 50. Representative snapshots (cluster analysis) of 1 ms MD simulation of the *Xist_RNA* duplex structures together with schematic illustrations for their label positions and inter-label distances.

cw-EPR measurements of the *Xist* lncRNA A-repeat region

Spin label mobility and spin labeling efficiency of the two different *Xist* A-repeat region RNA sequence constructs *Xist_RNA^{2NO}_3_3* and *Xist_RNA^{2NO}_5_3* were validated by cw-EPR spectroscopic analysis (Fig. 51). The obtained cw-EPR spectra showed an immobilized nitroxide signal, demonstrating the successful incorporation of spin labels into the RNA sequence constructs. Spin counting was performed by integration of the cw-EPR signal peaks. The comparison of the determined spin concentration and the concentration of *Xist_RNA* calculated from A_{260} absorbance, showed spin labeling efficiencies of 44% for *Xist_RNA^{2NO}_3_3* and 76% for *Xist_RNA^{2NO}_5_3*.

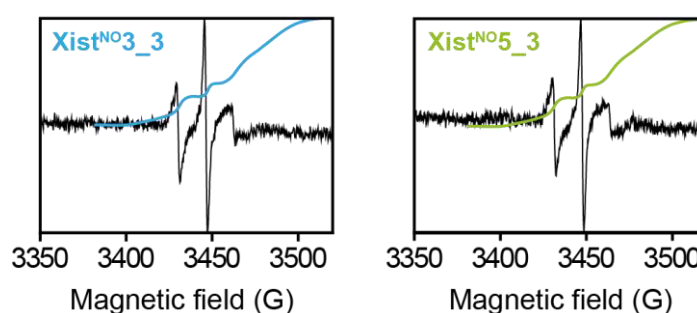


Figure 51. cw-EPR spectra for *Xist_RNA^{2NO}_3_3* and *Xist_RNA^{2NO}_5_3* with integrated signal peaks for spin counting.

PELDOR distance measurements of the *Xist* lncRNA A-repeat region

PELDOR experiments and data evaluations for both *Xist* A-repeat region RNA sequence constructs, *Xist_RNA^{2NO}_3_3* and *Xist_RNA^{2NO}_5_3*, yielded PELDOR time traces and inter-nitroxide (N-N) distance distributions (see Figure 52).

For the PELDOR time trace of *Xist_RNA^{2NO}_3_3* (Figure 52 a, top row), a modulation depth of 12% was attained which corresponds to the previously calculated labeling efficiency. The PELDOR-derived distance distribution peaks at 3.8 nm and overlaps exceedingly well with the peak of the 1 μ s MD simulation at 3.9 nm (Figure 52 b, top row). The well-overlapping distances from the PELDOR-derived distance distribution and the MD simulations support the duplex structure proposed by Fang *et al.*^[411]. However, because both spin markers are positioned at the 3'-end of the RNA sequence covering an intra-strand distance of 11 nt between them, the duplex structure proposed by Fang *et al.*^[411] is not the only structure for which strand-stabilizing folding would explain the resulting distance. Similar distances for the *Xist_RNA^{2NO}_3_3* spin labelled construct can be predicted for alternative stabilizing sequence folds by Maenner *et al.*^[412] (see above). Coexistence of different folds with similar intra-strand

N-N distances explain the increased width of the obtained PELDOR distance peak. Since the superposition of several similar distances would lead to a broadening of the peak, heterogeneous folding of the *Xist-A repeat region* RNA sequence can be inferred. In addition to the assumed duplex formation of Fang *et al.*^[411], the three structural models of Maenner *et al.*^[412] with similar 3'-3'-N-N distances (see Figure 46 a-c) are also conceivable.

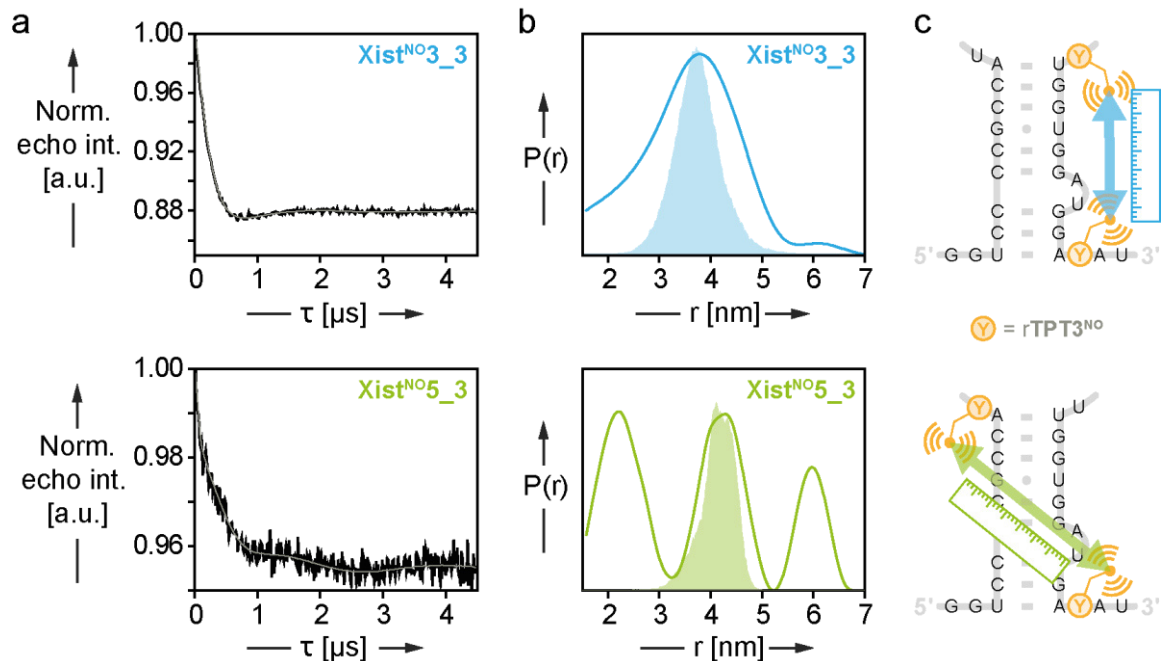


Figure 52. PELDOR derived distances for *Xist_RNA*^{2NO_3_3} and *Xist_RNA*^{2NO_5_3}. a) Background-corrected PELDOR time traces. b) Inter-label distance distributions (curves) overlaid with predicted N–N distance distributions (shadings) by MD simulations. c) Schematic illustrations of *Xist_RNA* duplex structures with label positions and inter-label distances.

The second *Xist_RNA*^{2NO_5_3} sequence construct was specifically designed to test the validity of the duplex structure proposed by Fang *et al.*^[411]. Only when the spin-labeled 3'- and 5'-ends of the RNA strand are in close proximity, a PELDOR-derived distance distribution should be obtained for the inter-strand 5'-3'-N-N distance. In almost all other proposed structures of the *Xist A-repeat region* sequence, the 3'- and 5'-ends of the RNA strand do not interact with each other, and the two spin labels would be positioned far apart (see above and see Figure 46 a, b and d). Only a distinctly longer inter-strand 5'-3'-N-N distance is founded by one of the three structure proposals by Maenner *et al.*^[413] (see above and see Figure 46 c). In addition, and in contrast to the previously described *Xist_RNA*^{2NO_3_3} sequence construct, the two spin labels are no longer positioned on the same site of the duplex with a short intra-strand distance. Instead, the spin-labeled 3'- and 5'-ends span the length of the proposed duplex from both sides. For this reason, no alternative stabilizing folding of only one of the two RNA strand ends should result in a stable and comparably short distance.

In the obtained PELDOR time trace for *Xist*_RNA^{2NO}_5_3, only a relatively low modulation depth of 4% is observed (see Figure 52 a, bottom row). The PELDOR-derived distance distribution for the *Xist*_RNA^{2NO}_5_3 indicates three different distances peaking at 2.2, 4.3 and 6.0 nm (see Figure 52 b, bottom row). The middle-distance peak at 4.3 nm perfectly overlaps with the MD calculated distance peak at 4.3 nm for the model duplex. Thus, duplex formation of the spin-labeled 3'- and 5'-ends of the RNA strand can be confirmed and the structure model by Fang *et al.*^[411] is the most valid one explaining the 4.3 nm distance.

In addition, the distance peak for 4.3 nm is much sharper and narrower compared to the broadened signal of the former discussed *Xist*_RNA^{2NO}_3_3. This suggests that the 4.3 nm distance of *Xist*_RNA^{2NO}_5_3 is formed by only one and not multiple similar structures. However, there are two other sharp signal peaks, for a shorter and a longer 3'-5'-N-N distance of 2.2 nm and 6.0 nm, respectively. Together with the 5'- and 3'-end inter-strand duplex postulated by Fang *et al.*^[411], there appear to be at least two, and probably more, structural folds forming a heterogeneous mixture. This is further supported by the low modulation depth of *Xist*_RNA^{2NO}_5_3, which contrasts with the previously mentioned good labeling efficiency (see above). In the presence of alternative folds, longer 3'-5'-N-N distances can arise, contributing to the intermolecular PELDOR background. These long distances are removed during data processing and thus reduce the signal modulation depth.

At this stage, the two additional distances at 2.2 and 6.0 nm cannot be conclusively clarified and assigned to structural proposals for the *Xist* A-repeat region. One of the previously discussed structural models proposed by Maenner *et al.*^[413] for the *Xist* A-repeat region (Figure 46 c) could explain both an alternative duplex formation of the 5'- and 3'-ends and the creation of a longer inter-spin distance. However, this structure and the resulting distance have not been calculated or verified with MD simulations. Consistent with the results for *Xist*_RNA^{2NO}_3_3, the measurement for *Xist*_RNA^{2NO}_5_3 also suggests heterogeneous folding of the *Xist* A repeat region.

With the obtained PELDOR-derived distance distributions for the two *Xist* A-repeat region RNA constructs, direct and site-specific spin labeling of a large RNA was successfully demonstrated. Furthermore, it was effectively shown that complex folded RNA structures such as the *Xist* A-repeat region can be addressed using this method and that nitroxide-modified rTPT3^{NO} can be used to introduce the spin labels site-specifically and with good yields. The presented approach of a nanometer-range ruler measuring distances in large and highly structured RNA represents a powerful instrument for the toolbox of structural RNA research. In the future, the presented approach can also be used to elucidate RNA structures that are difficult to access applying alternative methods such as crystallization.

Likewise, the applied method shows excellent agreement with structural MD-calculations and illustrates how well the combination of site-specific labeling via GENAEXT and *in silico* predictions can go hand in hand.

To date, this approach of site-directed spin labeling has been limited to structures under solution conditions. Since the nitroxide spin label linked to the UB is not stable in the cellular environment, alternative and more stable spin label conjugates need to be developed for in-cell applications. With the help of these, the promising tool of the nanometer-range ruler may find additional future application in the structural elucidation of complex RNAs in cells.

4 Conclusion and Outlook

Visualization and analysis of structure and function provide a deeper understanding of how RNA works. Since properties of functional biomolecules such as RNA are often influenced by multiple factors, it is important for an in-depth analysis to examine not only a single parameter but several parameters coherently and to consider their interplay. Adapted to these needs, the development of tools and methods for RNA visualization and investigations on structure and function will be of great interest for future research. In this regard, functionalized unnatural nucleotides as part of an expanded genetic alphabet enable new and promising possibilities for advanced RNA research and help to analyze multiple RNA characteristics simultaneously.

In this thesis, various unnatural base (UB)-modified RNA sequences were produced by genetic alphabet expansion transcription (GENAEXT) site-specifically installing functionalized UB nucleoside triphosphates. Efficient preparation and UB-incorporation were demonstrated, also several follow-up applications for UB-modified RNA sequences were presented. This was done for two different types of RNA, first for *mCherry* protein-coding mRNA (*mCh_mRNA*) sequences and second for the highly-structured *Xist* long non-coding (lnc)RNA *A-repeat* region.

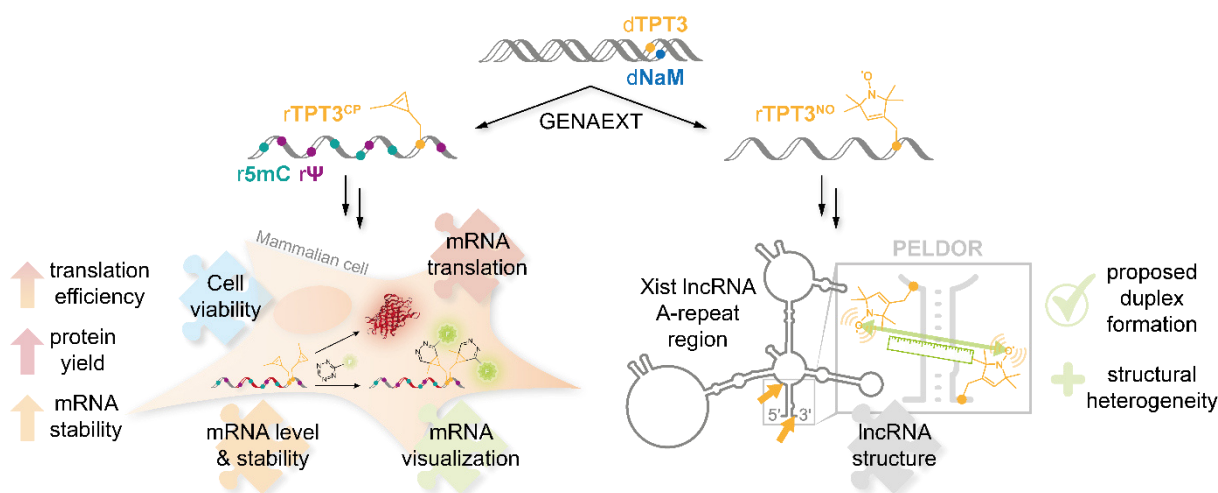


Figure 53. Applications of modified UBs and GENAEXT for site-specific RNA labeling. On the left: Combined labeling of a protein-coding mRNA using a CP-modified UB for fluorescent live-cell click labeling and modified natural bases for multifaceted cellular analysis. On the right: NO-labeling of a complex folded lncRNA sequence for structure investigations by EPR spectroscopy.

For a set of protein-coding *mCh_mRNA* sequences, site-specific cyclopropene (CP)-labeling was performed applying the CP-functionalized unnatural base nucleoside triphosphate **rTPT3^{CP}**. In order to preserve mRNA functionality in terms of unimpeded protein translation, CP-modifications were solely placed in the 3'-untranslated region (UTR). This represents an unprecedented strategy for site-specific 3'-UTR labeling of mRNAs. After mRNA lipofection in

mammalian cells, live-cell click labeling of CP-modified *mCh_mRNA* with tetrazine-conjugated fluorophores enabled mRNA visualization with excellent signal intensities. Moreover, CP-modifications were shown to not impede mRNA function with regard to cellular expression of the encoded reporter protein. For investigations of the influence of different modification patterns on mRNA stability and functionality, highly modified *mCh_mRNA* sequences were additionally prepared carrying the additional natural base modifications of **pseudouridine (Ψ)** and **5-methylcytidine (5mC)**. A multifaceted cellular analysis was performed testing the different *mCh_mRNA* sequence variants comparatively. Combined temporal quantification of cellular *mCh_mRNA* levels and the encoded *mCherry* reporter protein arising from cellular mRNA translation was implemented. RT-qPCR analysis revealed lower mRNA transfection rates but increased mRNA stability for modified sequences, both for natural and unnatural base modifications and a combination thereof. Furthermore, full functionality of all modified *mCh_mRNA* sequences was proven by quantification of the fluorescent *mCherry* protein. It was demonstrated that incorporation of natural base modifications strongly enhanced cellular protein expression. However, the most outstanding translation and expression efficiency was observed for dual modified *mCh_mRNA* with a double CP-modification and additional natural base modifications of Ψ and 5mC. In addition, natural base modifications proved beneficial for cell health with regard to increased cell viability and dual modified mRNA was found to be well suited for cellular applications. In summary, the combination of natural and unnatural base modifications for a highly modified mRNA resulted in a synergetic effect on increased mRNA stability, translation and expression efficiency as well as cell viability.

Future research on this topic will need to focus on elucidating the mechanisms that underly the increased mRNA stability and translation efficiency of modified sequences. On the one hand, the activity of ribosomes could be studied on the modified mRNA in cell-free translation systems. Thus, RNA-bound ribosomes can be quantified and provide an inference of polysome formation or kinetic studies can be performed to reveal ribosome pausing. On the other hand, the 3'-UTR sequence of *mCh_mRNA* could be selectively exchanged for a UTR sequence containing a known binding site for microRNA (miRNA) or RNA-binding proteins (RBPs). By selectively introducing the modifications in the miRNA or RBP binding sequence, the protein quantification shown in this work can be used to test whether altered translational regulation by RBPs or miRNAs due to modifications in their UTR binding sites alters protein levels. The RT-qPCR analysis shown here can be used to determine the mRNA level for the same mRNA sequences with miRNA- or RBP-binding sites in their UTRs and additionally clarify whether the 3'-UTR interactions are also related to the improved mRNA stability. Understanding the causes of increased translation efficiency and mRNA stability will be highly advantageous for potential applications to precisely fine-tune mRNA characteristics and further develop mRNA therapeutics.

Using the nitroxide (NO)-functionalized unnatural base nucleoside triphosphate **rTPT3^{NO}**, direct and site-specific spin labeling of the *Xist* lncRNA *A-repeat region* was performed. Different labeling positions were addressed aiming to probe different previously proposed structure models. Pulsed electron-electron double resonance (PELDOR) experiments yielded inter-spin distance distributions with high agreement to comparative molecular dynamics (MD) calculations. In addition, the PELDOR-derived distance distributions strongly supported one of the proposed structure models but also reflected a structural heterogeneity in solution. Hereby, a valuable contribution was made towards the structure elucidation of *Xist* lncRNA *A-repeat region*. Moreover, the method of direct and site-specific spin labeling utilizing functionalized UB building blocks was successfully transferred and extended to a long and complex folded RNA sequence for the first time. This project represents the foundation to overcome current limitations of solving structures only under solution conditions.

By further developing an UB-attached spin label that is stable under cellular conditions, site-specific spin labeling applying GENAEXT will extend the approach to highly interesting applications in cells. For this purpose, the trityl^[424] spin labels known from literature can be used. Due to its high reduction stability, this spin label is well suited for cellular applications and is already used for spin labeling of proteins and their EPR measurements in cells.^[425–431] However, due to its size, an unnatural base with attached trityl spin label is unlikely to be enzymatically incorporated. Therefore, an alternative approach for posttranscriptional RNA spin labeling has to be developed.

Various applications of site-specific UB-modified RNA sequences were presented. Worthwhile conclusions were drawn about structural folding of the regulatory important *Xist* lncRNA *A-repeat region* using UB-linked spin labels. Exceptionally high signal intensities for visualization of mRNA in cells was achieved utilizing CP-functionalized UBs for site-specific modification of long and functional mRNA sequences. On top of that, a remarkably improved mRNA function in the sense of translation efficiency was exposed for an mRNA sequence that carried a dual modification pattern of unnatural and natural base modifications. Thus, UB-modifications were shown to be perfectly suited to study multiple parameters of selected RNAs in cells while not limiting their function. Moreover, analysis of the interplay of different mRNA properties allowed to characterize the selected mRNA sequences more complexly. The applications and methods developed in this thesis will therefore support future RNA research and may contribute to the advancement of mRNA therapeutics.

5 Material and Methods

In the following section all materials and methods that have been applied in this study are listed and described.

5.1 Software and databases

The software applications and data bases that have been used for experimental designs, data evaluation, processing and depiction in this study are shown in Table 3 and Table 4.

Table 3. Software applications used in this study.

Software	Version	Source
CFX Maestro	4.1.2433.1219	<i>Bio-Rad</i>
ChemDraw	16.0.1.4	<i>PerkinElmer</i>
Creative Suite	3-5	<i>Adobe</i>
mfold	3.0	http://www.bioinfo.rpi.edu/applications/mfold
Office	2019	<i>Microsoft</i>
OligoCalc Oligo Properties Calculator	3.27	http://biotools.nubic.northwestern.edu/OligoCalc.html
OriginPro	8 SR1	<i>OriginLab Corporation</i>
Primer3	4.1.0	https://primer3.ut.ee/
Primer-BLAST		https://www.ncbi.nlm.nih.gov/tools/primer-blast/
PrimerQuest Tool		https://eu.idtna.com/Primerquest/Home/Index
Zen	3.3 blue edition	<i>Zeiss</i>

Table 4. Databases used in this study.

Database	Source
European Nucleotide Archive	https://www.ebi.ac.uk/ena/browser/search
GenBank	http://www.ncbi.nlm.nih.gov
UniProt	https://www.uniprot.org/
RTPrimerDB	http://www.rtpimerdb.org/index.php

5.2 Equipment

The equipment that has been used for experimental work in this study is shown in Table 5.

Table 5. Equipment used in this study.

Equipment	Model	Manufacturer
Agarose gel electrophoresis chamber	<i>Mini-Sub Cell GT</i>	<i>Bio-Rad</i>
	<i>EasyPhor Mini</i>	<i>Biozym</i>
Autoclave	n.a.	Custom-buit
	<i>D65</i>	<i>Systec</i>
Bacterial Culture Incubator	<i>BD 400</i>	<i>Binder</i>

Centrifuges	<i>Micro 2000</i> <i>5417 C</i> <i>5424 R</i> <i>5810 R</i> <i>Sorvall fresco</i>	<i>Hettich</i> <i>Eppendorf</i> <i>Eppendorf</i> <i>Eppendorf</i> <i>Thermo Fisher</i>
Block heater	<i>HBT-1-131</i> <i>isoBlock digital dry bath</i>	<i>HLC BioTech</i> <i>Benchmark</i>
Cell Culture Incubator	<i>Heracell 150</i>	<i>Heraeus</i>
Freeze-dryer	<i>Alpha 2-4 LD plus</i> <i>Alpha 1-2 LD plus</i>	<i>Martin Christ</i> <i>Martin Christ</i>
Freezers	<i>Premium NoFrost -20 °C</i> <i>-85°C Ultra Low Freezer</i> <i>C99085</i>	<i>Liebherr</i> <i>New Brunswick Scientific</i>
Gel documentation system	<i>Gel Doc 2000</i> <i>Genoplex</i> <i>BioDoc-It</i> <i>Chemostar Touch</i>	<i>Bio-Rad</i> <i>VWR</i> <i>UVP</i> <i>intas</i>
Incubator shaker	<i>Innova 4430</i>	<i>Thermo Fisher</i>
Laminar flow hood	<i>HeraSafe HS 18</i>	<i>Heraeus</i>
Micro scales	<i>AT261 Delta Range</i>	<i>Mettler Toledo</i>
Microscopes	<i>LSM 710</i> <i>Axiovert25</i>	<i>Carl Zeiss</i> <i>Carl Zeiss</i>
Microwave	<i>MW 7873</i>	<i>Severin</i>
Mini centrifuges	<i>SU1550</i> <i>MyFuge</i>	<i>Sunlab</i> <i>Benchmark</i>
PAGE chamber	<i>Mini Protean</i>	<i>Bio-Rad</i>
pH meter	<i>FiveEasy Plus</i>	<i>Mettler Toledo</i>
Phosphorimager	<i>FLA-3000</i>	<i>Fujifilm</i>
Pipettes	<i>2.5 µL, 10 µL, 20 µL, 100 µL, 200 µl, 1000 µL, Research Plus</i> <i>Acura manual 855</i> <i>8-channel pipette 20-200 µL</i>	<i>Eppendorf</i> <i>Socorex</i>
Plate reader	<i>EnSpire Multimode</i>	<i>Perkin Elmer</i>
Power Supply for gel electrophoresis	<i>P25</i> <i>E132</i> <i>PowerPac Basic</i>	<i>Biometra</i> <i>Consort</i> <i>Bio-Rad</i>
Spectrophotometer	<i>Nanodrop 2000c</i> <i>DS-11 FX</i>	<i>Thermo Fisher</i> <i>DeNovix</i>
Thermocycler	<i>LifeECO</i> <i>T3</i>	<i>Bioer</i> <i>Biometra</i>
Thermoshaker	<i>PocketBloc Thermomixer</i> <i>Thermomixer comfort</i>	<i>Bioer</i> <i>Eppendorf</i>
qPCR Thermal Cycler	<i>CFX96 Touch Real-Time PCR Detection System</i>	<i>Bio-Rad</i>
Vortex Mixer	<i>Vortex-Genie 2</i> <i>RS-VA 10</i>	<i>Scientific Industries</i> <i>Phoenix Instruments</i>
Water bath	<i>1004</i>	<i>GFL</i>

5.3 Consumables

Consumables that have been used for experimental work in this study are shown in Table 6.

Table 6. Consumables used in this study.

Consumable	Specification	Manufacturer
Adhesive foil for qPCR plate sealing	Microseal 'B' PCR Plate Sealing Film, adhesive, optical	<i>Bio-Rad</i>
Cell culture flask	T75, T25, PS, standard surface, sterile	<i>Sarstedt</i>
Centrifugal filters	<i>Amicon Ultra 3K</i>	<i>Merck</i>
Conical Tubes	15 mL, 50 mL, PP, DNA-free, DNase-free, RNase-free, sterile	<i>Sarstedt</i>
Cryotubes	2 mL, PP, round bottom, screw top, sterile	<i>Greiner Bio-One</i>
EPR tubes	3 mm quartz Q-band tubes	<i>SP Wilmad-Lab Glass</i>
Fluorescence assay plates	Black, low-binding, half area	<i>Corning</i>
Glass Pasteur pipettes	Soda lime glass, 225 mm	<i>Brand</i>
Microscope slides	Borosilicate glass, Ø 15 mm, thickness 1	<i>Marienfeld</i>
Microscope cover slips	Soda lime glass, corners grounded 90°, with frosted edge	<i>Carl Roth</i>
PCR reaction tubes	200 µL, transparent, PP, DNA-free, flat lid	<i>neoLab Migge</i>
Petri dishes	100x15 mm, PS, sterile	<i>Corning</i>
Pipette tips	10 µL, 200 µL, 1 mL, PP, non-sterile	<i>Carl Roth, Sarstedt</i>
Plastic syringe	10 mL, 50 mL, sterile	<i>Henke-Sass Wolf</i>
qPCR plates	96-well, hard-Shell, low profile, thin wall, skirted, white/white	<i>Bio-Rad</i>
Reaction tubes	1.5 mL and 2 mL, PP, transparent, SafeSeal cap, cap attached	<i>Sarstedt</i>
Serological pipettes	5 mL, 10 mL, 25 mL, 50 mL, PS, plugged, sterile, non-cytotoxic	<i>Sarstedt</i>
Spin columns	<i>G-25 Illustra MicroSpin</i>	<i>GE Healthcare, Cytiva</i>
Syringe filters	0.22 µm pore size, cellulose acetate filter, sterile	<i>Absolute Th. Geyer</i>
Tissue culture plates	24 well, PS, standard surface, sterile	<i>Sarstedt</i>
	96 well, PS, µClear bottom, chimney well	<i>Greiner Bio-One</i>

5.4 Reagents and solutions

Reagents and solutions that have been used for experimental work in this study are shown in Table 7 and Table 8.

Table 7. Reagents used in this study.

Reagent	Manufacturer
AF Dye 488 tetrazine	<i>Click Chemistry Tools</i>
Agar, bacteriology grade	<i>AppliChem</i>
Agarose LE	<i>Genaxxon</i>
Agarose High Resolution	<i>Sigma Aldrich</i>
Boric acid	<i>Alfa Aesar, Labochem International</i>
Bromophenol blue (BPB)	<i>Carl Roth</i>
4',6-Diamidino-2-phenylindole (DAPI)	<i>Merck</i>
Dimethylsulfoxide (DMSO)	<i>Sigma Aldrich</i>
Dithiothreitol (DTT)	<i>Sigma Aldrich</i>
D ₂ O (99.9%)	<i>Deutero</i>
Ethanol (EtOH) absolute	<i>VWR</i>
Ethidium bromide (EtBr)	<i>Carl Roth</i>
Ethylenediaminetetraacetic acid (EDTA)	<i>Carl Roth, Thermo Fisher, AppliChem</i>
Ethylene glycol-d ₆	<i>Sigma Aldrich</i>
Ficoll 400	<i>Sigma Aldrich</i>
Formamide (FA)	<i>Fluka</i>
<i>GeneRuler 100 bp</i> DNA Ladder	<i>Thermo Fisher</i>
<i>GeneRuler Ultra Low Range</i> DNA Ladder	<i>Thermo Fisher</i>
Glycerol	<i>Sigma Aldrich</i>
High resolution agarose	<i>Carl Roth</i>
Kanamycin sulfate	<i>Merck</i>
LB Broth (Lennox)	<i>Carl Roth</i>
MgCl ₂ x 6 H ₂ O	<i>Alfa Aesar</i>
Na ₂ HPO ₄	<i>Sigma Aldrich, Carl Roth</i>
NaCl	<i>Carl Roth</i>
NaH ₂ PO ₄	<i>Carl Roth</i>
d NaM CEP	<i>Berry & Associates Inc.</i>
d NaM TP	<i>MyChem LLC</i>
dNTPs	<i>Jena Bioscience</i>
rNTPs	<i>Jena Bioscience</i>
Phenylmethylsulfonyl fluoride (PMSF)	<i>Thermo Fisher Scientific</i>
<i>RNasin</i> or <i>RNasin plus</i>	<i>Promega, New England Biolabs</i>
<i>SYBR Safe</i> DNA stain	<i>Life Technologies</i>
d TPT3 TP	Synthesized and kindly provided by Dr. F. Eggert and Dr. C. Domnick
r TPT3 ^{CP} TP	Synthesized and kindly provided by Dr. F. Eggert and Dr. C. Domnick
Tris-(hydroxymethyl)-aminomethan (Tris)	<i>Carl Roth</i>
Triton X-100, 10% (w/v) aqueous solution	<i>Thermo Fisher Scientific</i>
Xylene cyanol (XC)	<i>Applichem</i>

Table 8. Solutions used in this study.

Solution	Manufacturer	Specification
0.05% Trypsin-EDTA (1x)	<i>Thermo Fisher Scientific</i>	
2x ARCA/NTP Mix (8 mM ARCA, 2 mM GTP, 2.5 mM UTP, 2.5 mM CTP, >2.5 mM ATP)	<i>New England Biolabs</i>	
2x <i>GoTaq® Probe qPCR Master Mix</i>	<i>Promega</i>	
r5mC TP (100 mM)	<i>Jena Bioscience</i>	
ATP (100 mM)	<i>Thermo Fisher Scientific</i>	
Foetal calf serum (FCS)	<i>Sigma-Aldrich</i>	Order No. F9665 (Charge: 054M3399)
Fluoro-Gel (with Tris buffer) mounting medium	<i>Electron Microscopy Sciences</i>	
Formaldehyde, 37 wt% solution in water, stabilized with 5-15 % methanol	<i>Acros Organics</i>	
MgCl ₂ (25 mM)	<i>Promega</i>	
LiCl (7.5 M) with EDTA (10 mM)	<i>New England Bioabs</i>	
Lipofectamine MessengerMAX	<i>Invitrogen</i>	
Minimum Essential Medium (MEM) non-essential amino acids (NEAA) (100x)	<i>Thermo Fisher Scientific</i>	
MT Cell Viability Substrate (1,000x)	<i>Promega</i>	
PCR Nucleotide Mix (10mM)	<i>Promega</i>	
Recombinant RNasin®	<i>Promega</i>	
Ribonuclease Inhibitor		
Sodium Pyruvate 100 mM (100x)	<i>Thermo Fisher Scientific</i>	
rΨ TP (100 mM)	<i>Jena Bioscience</i>	

5.5 Buffers and media

The buffers and media that have been used for experimental work in this study are shown in Table 9 and Table 10.

Table 9. Buffers used in this study.

Buffer	Composition	Manufacturer
10x CutSmart Buffer	500 mM KAc, 200 mM Tris-Ac, 100 mM MgAc ₂ , 100 µg/mL BSA, pH 7.9	<i>New England Biolabs</i>
10x DNase I Reaction Buffer	100 mM Tris, 25 mM MgCl ₂ , 5 mM CaCl ₂ , pH 7.6	<i>New England Biolabs</i>
10x <i>OneTaq</i> Standard Reaction Buffer	200 mM Tris-HCl, 220 mM NH ₄ Cl, 220 mM KCl, 18 mM MgCl ₂ , 0.6% IGEPAL CA-630, 0.5% Tween 20, pH 8.9	<i>New England Biolabs</i>

10x Phosphate buffer	1.45 M NaCl, 100 mM Na ₂ HPO ₄ , 100 mM NaH ₂ PO ₄ , pH 7.0	made in-house
10x Poly(A) Polymerase Reaction Buffer	unlisted concentrations of <i>HiScribe™ T7 ARCA mRNA Kit (with tailing)</i> component	New England Biolabs
10x T4 PNK Reaction Buffer	700 mM Tris-HCl, 100 mM MgCl ₂ , 50 mM DTT, pH 7.6	Thermo Fisher Scientific
10x T4 DNA Ligase Buffer	500 mM Tris-HCl, 100 mM MgCl ₂ , 10 mM ATP, 100 mM DTT, pH 7.5	Thermo Fisher Scientific
10x TBE	900 mM Tris, 900 mM boric acid, 20 mM EDTA, pH 8.0	made in-house
0.5x TBE	45 mM Tris, 45 mM boric acid, 1 mM EDTA, pH 8.0	made in-house
5x <i>GoScript™ Reaction Buffer</i>	unlisted concentrations of <i>GoTaq® Probe 2 step RT-qPCR System</i> component	<i>Promega</i>
5x Transcription buffer	200 mM Tris pH 7.9	made in-house
6x Agarose loading buffer	50 mM Tris, 15% (w/v) Ficoll 400, 6 mM EDTA, 0.25% (w/v) BPB, pH 8.3	made in-house
6x Agarose loading buffer, colourless	50 mM Tris, 15% (w/v) Ficoll 400, 6 mM EDTA	made in-house
6x TriTrack DNA Loading Dye	10 mM Tris-HCl, 0.03% BPB, 0.03% XC, 0.15% orange G, 60 % glycerol, 60 mM EDTA, pH 7.6	<i>Thermo Fisher Scientific</i>
PELDOR buffer	145 mM NaCl, 10 mM Na ₂ HPO ₄ , 10 mM NaH ₂ PO ₄ in D ₂ O	made in-house
RIPA Lysis and Extraction Buffer	1-3% Nonidet P-40 Substitute, 1-3% sodium 3- α ,12- α -dihydroxy-5- β -cholan-24-oate	<i>Thermo Fisher Scientific</i>

Table 10. Media used in this study.

Media	Manufacturer
Dulbecco's Modified Eagle Medium (DMEM) (1x) GlutaMAX	<i>Thermo Fisher Scientific</i>
Dulbecco's Phosphate Buffered Saline (DPBS) (1x)	<i>Thermo Fisher Scientific</i>
LB Medium (Lennox)	made in-house
Opti-MEM Reduced-Serum Medium (1x)	<i>Thermo Fisher Scientific</i>
SOC Medium	<i>Takara Bio</i>

5.6 Enzymes

The enzymes that have been used for experimental work in this study are shown in Table 11.

Table 11. Enzymes used in this study.

Enzyme	Manufacturer	Specification
DNase I (RNase-free, 2 U μ L ⁻¹)	<i>New England Biolabs</i>	
<i>E. coli</i> Poly(A) Polymerase (unlisted concentrations of <i>HiScribe™ T7 ARCA mRNA Kit (with tailing)</i> component)	<i>New England Biolabs</i>	

GoScript™ Reverse Transcriptase (unlisted concentrations of <i>GoTaq® Probe</i> <i>2 step RT-qPCR System</i> component)	<i>Promega</i>	
HpaI (5 U μL^{-1})	<i>New England Biolabs</i>	
Inorganic Pyrophosphatase (iPP)	<i>New England Biolabs</i>	
<i>OneTaq</i> DNA Polymerase	<i>New England Biolabs</i>	
<i>NanoLuc® Enzyme</i> (1,000x) (unlisted concentrations of <i>RealTime-Glo™</i> <i>MT Cell Viability Assay</i> component)	<i>Promega</i>	
T4 DNA Ligase	<i>Thermo Fisher Scientific</i>	
T4 Polynucleotide Kinase (PNK)	<i>Thermo Fisher Scientific</i>	
T7 RNA Polymerase	<i>made in-house</i>	AA sequence conforms with GenBank entry AY264774.1, “gene 1” and UniProt entry P00573
T7 RNA Polymerase Mix (unlisted concentrations of <i>HiScribe™ T7</i> <i>ARCA mRNA Kit (with tailing)</i> component)	<i>New England Biolabs</i>	

5.7 Plasmids

The plasmids that have been used for experimental work in this study are shown in Table 12.

Table 12. Plasmids used in this study.

Plasmids	Provided by	Publication DOI
<i>pCMV-Xist-PA</i>	Rudolf Jaenisch, Addgene ID # 26760	10.1016/s1097- 2765(00)80248-8
<i>pmCherry-C1</i>	Kath-Schorr lab	-
<i>pmCherry-N1_AA-insert</i>	Kath-Schorr lab	-

5.8 Kits

The kits that have been used for experimental work in this study are shown in Table 13.

Table 13. Kits used in this study.

Kits	Manufacturer
<i>BigDye™ Terminator v3.1 Cycle</i> <i>Sequencing Kit</i>	<i>Applied Biosystems</i>
<i>GoTaq® Probe 2 step RT-qPCR System</i>	<i>Promega</i>
<i>HiScribe™ T7 ARCA mRNA Kit (with tailing)</i>	<i>New England Biolabs</i>
<i>mCherry Quantification Kit</i>	<i>BioVision</i>
<i>NucleoSpin® Gel and PCR Clean-Up Kit</i>	<i>Macherey-Nagel</i>
<i>NucleoSpin® Plasmid Kit</i>	<i>Macherey-Nagel</i>
<i>NucleoSpin® RNA Kit</i>	<i>Macherey-Nagel</i>
<i>RealTime-Glo™ MT Cell Viability Assay</i>	<i>Promega</i>

5.9 Organisms

The organisms that have been used for experimental work in this study are shown in Table 14.

Table 14. Organism used in this study.

Organisms	Description	Manufacturer
HeLa	Human cervix adenocarcinoma cell line	CLS Cell Lines Services GmbH
Stellar competent cells	<i>E. coli</i> HST08 strain	Takara Bio

5.10 General biochemical methods

When working with ribonucleic acids care has to be taken to prevent degradation of the sample material caused by ribonucleases^[432]. Therefore, nitrile gloves had to be worn at all times and additionally be disinfected with 80% EtOH after donning. Further, disposable plastic ware was used. Reaction tubes (0.2 mL, 1.5 mL and 2 mL) and pipette tips (10 µL, 200 µL and 1 mL) were autoclaved and stored in sealed glasses and boxes. Conical tubes (15 mL and 50 mL) were purchased from the supplier classified as DNA-, DNase- and RNase-free and applied without additional treatment. Ultrapure water (referred to as ddH₂O) for direct use or employed in buffers was generated from deionized water and further treated in an ultrapure water system, *Barnstead MicroPure (Thermo Fisher Scientific)* and *Arium Mini (Sartorius)*, then autoclaved, sterile filtered and stored in aliquots at -20 °C.

5.10.1 Agarose gel electrophoresis

Analytical gel electrophoresis was performed with 1%, 2% or 4% (w/v) agarose gels. Therefore, a solution of 1 g, 2 g or 4 g, respectively, in 100 mL 0.5 x TBE buffer was prepared and microwaved (900 V, 2 min) until the agarose was fully dissolved. Agarose solutions were stored at 60 °C in a heating cabinet. Prior to casting, the agarose solutions were supplemented with either 1 mg mL⁻¹ EtBr or 1:50.000 (v/v) SYBR Safe stain. 25 mL of agarose solutions were used to cast a 16 or 20 pockets gel and the solution was allowed to solidify for 30 min at rt. Samples were prepared by mixing with an appropriate volume of concentrated loading buffer. 0.5 x TBE was used as running buffer. Gel electrophoresis was performed at 150 V const. for 20-30 min depending on the DNA or RNA sequence length. An appropriate DNA or RNA ladder

was included as a reference for analytical characterization. Agarose gels were visualized by UV illumination using a gel documentation system.

5.10.2 Purification methods

Preparative agarose gel electrophoresis

Agarose gels for preparative gel electrophoresis were prepared analogously to the previously described procedure for analytical gel electrophoresis, except that larger gel pockets were included for larger sample volumes. After gel electrophoresis, the samples were visualized by UV illumination on transilluminating sample table and selectively excised from the gel. Using the *Nucleo Spin Gel and PCR Clean-Up Kit*, gel pieces were mixed in loading buffer and heated to 50 °C until completely dissolved. The following work steps correspond to the protocol described below under silica-membrane spin columns.

Centrifugal filters

Amicon Ultra 3K centrifugal filter devices were used for concentration and buffer exchange of RNA samples. According to the manufacturer's protocol, RNA samples were added to the filter device and centrifuged for up to 30 min at 14000 x g for concentration. For buffer exchange, concentration steps were repeated several times in combination with reconstituting the concentrates in fresh buffer. After the last concentration step, the concentrate was recovered by an upside-down centrifugation step for 2 min at 1000 x g at the end.

G-25 gel filtration spin columns

G-25 Illustra MicroSpin gel filtration spin columns were used to clean-up and desalt DNA and RNA oligonucleotide samples after enzymatic reactions. According to the manufacturer's protocol the column was prepared in a first step by resuspending the Sephadex G-25 DNA grade F resin and removing excess storage buffer by centrifugation for 1 min at 735 x g. The sample (adjusted to 50 µL volume) was then added on top of the resin and a centrifugation step for 2 min at 735 x g was applied to elute the purified sample.

Silica-membrane spin columns

For purification of DNA and RNA oligonucleotide samples directly after enzymatic reactions or in combination with preparative gel electrophoresis, the *Nucleo Spin Gel and PCR Clean-Up Kit* was used. According to the manufacturer's protocol samples were mixed with loading buffer

and loaded onto silica-membrane spin columns by centrifugation for 30 s at 11000 x g. For larger sample volumes, columns were loaded up to three times. The flow-through after the first loading was loaded repeatedly. After repeated centrifugation-coupled washing steps with an EtOH-based washing buffer, each 30 s at 11000 x g, another centrifugation step for 1 min at 11000 x g was performed to dry the silica membrane. In addition, the spin columns were incubated for 5 min at 70 °C in a heating block evaporating residual EtOH. Clean samples were eluted in two steps, for which ddH₂O was added to the membrane, incubated for 1 min at rt or 5 min at 70 °C (for recovery of long DNA or RNA) and then centrifuged for 1 min at 11000 x g.

LiCl precipitation

LiCl precipitation was used to purify mRNA after enzymatic *in vitro* preparation. LiCl solution (7.5 mM LiCl, 10 mM EDTA) was added to the mRNA tailing mix at a ratio of 1:3. After incubation at -20 °C for 30 min or longer, the mRNA was pelleted by centrifugation at 4 °C for 15 min at top speed. The supernatant was removed, the pellet was rinsed with 500 µL of cold 70% EtOH, and another centrifugation step was performed at 4 °C for 10 min at top speed. Subsequently, the EtOH was removed and the mRNA pellet was incubated for 5 min at 70 °C in a heating block evaporating residual EtOH. The mRNA was then resuspended in 50 µL ddH₂O and incubated for 5-10 min at 65 °C in a heating block until completely dissolved.

5.10.3 Nucleic acid concentration determination

Nucleic acid concentrations were determined measuring the absorption at 260 nm (A_{260}) using a spectrophotometer and software-assisted calculation with OligoCalc^[433]. For UB-modified RNA or DNA oligonucleotides, their respective native sequences containing only canonical nucleobases were used. For calculations of mRNA sequences, an estimated number of 150 nucleotides A within the poly(A) tail was added to the defined sequences.

5.11 Bacterial culture

Bacterial culture was used to produce plasmid DNA for subsequent use as template DNA for PCR amplification. For this purpose, *E. coli* cells were transformed with *pmCherry-N1_AA-insert* and the amplified plasmid DNA was isolated from liquid bacterial cultures.

5.11.1 Transformation

For transformation of *E. coli* cells, a 50 μL aliquot of Stellar competent cells was thawed on ice, mixed with 5 ng *pmCherry-N1_AA-insert* plasmid DNA and incubated on ice for 30 min. A heat shock was performed for 45 s at 42 °C, followed by incubation of the cells on ice for 5 min. Then 950 μL SOC medium was added and the cells were incubated for 1 h at 37 °C and 800 rpm shaking. 100 μL of the cell suspension was spread on a pre-warmed agar plate supplemented with 50 $\mu\text{g mL}^{-1}$ Kanamycin. The agar plate with plated bacteria was then incubated overnight at 37 °C.

5.11.2 Bacterial cultivation for plasmid preparation

For bacterial cultivation, LB medium was inoculated with single clones picked from the agar plate. Therefor tubes with 4 mL LB medium supplemented with 50 $\mu\text{g mL}^{-1}$ Kanamycin were prepared, inoculated and subsequently incubated overnight at 37 °C and 180 rpm shaking.

5.11.3 Bacterial glycerol stock preparation

For bacterial glycerol stock preparation, 750 μL of overnight culture (described in X.2) was mixed with 750 μL of 50% glycerol in a screw top cryotube, that was pre-cooled to -20 °C. The bacterial glycerol stock was then frozen and kept at -80 °C.

5.11.4 Plasmid preparation

For plasmid preparation the *NucleoSpin Plasmid* Kit was used. First, bacterial cultures were transferred to 2 mL tubes and centrifuged for 30 s at 11000 x g to pellet the bacteria. All subsequent centrifugation steps were also performed at 11000 x g. For cell lysis, 250 μL Buffer A1 was added to the cell pellet and mixed to resuspend. Then, 250 μL SDS/alkaline lysis Buffer

A2 was added, mixed gently by inverting the tube and incubated at rt for 5 min. To neutralize the lysate, 300 μL *Buffer A3* was added and mixed. The resulting lysate was centrifuged for 10 min. The clear supernatant was carefully removed from the tube and loaded onto a *NucleoSpin plasmid column* by centrifugation for 1 min. Next, the silica membrane was washed in two steps. The first washing step was performed by adding 500 μL *Buffer AW*, pre-heated to 50 $^{\circ}\text{C}$, to the column and centrifugation for 1 min. For the second washing step, 600 μL of *Buffer A4* was added to the column and centrifuged for 1 min. After drying the silica membrane by centrifugation for 2 min, the plasmid DNA was eluted in two steps. For each step, 25 μL *Buffer AE*, pre-heated to 70 $^{\circ}\text{C}$, was added to the column, incubated at rt for 1 min and centrifuged for 1 min. Purified plasmid DNA was analyzed by a diagnostic restriction digest and Sanger sequencing.

5.11.5 Diagnostic restriction digest of plasmid DNA

In addition to Sanger sequencing, purified plasmid DNA was analyzed by a diagnostic restriction digest. For *pmCherry-N1_AA-insert* retransformation and plasmid preparation, linearization of the isolated plasmid DNA was accomplished followed by agarose gel electrophoresis analysis. The diagnostic restriction digest was performed in 10 μL scale using 5 μL isolated plasmid DNA and 1.25 U μL^{-1} *HpaI* restriction enzyme. A pipetting scheme for the restriction digest reaction mix is shown in Table 15.

Table 15. Pipetting scheme for diagnostic restriction digest.

Component	Stock concentration	Final concentration	V [μL]
Isolated <i>pmCherry-N1_AA-insert</i> plasmid DNA	varied	varied	5
<i>CutSmart Buffer</i>	10x	1x	1
<i>HpaI</i> restriction enzyme	5 U μL^{-1}	1.25 U μL^{-1}	0.25
ddH ₂ O	-	-	ad 10

The restriction digest reaction mix was incubated for 1 at 37 $^{\circ}\text{C}$, before crude reactions were analyzed on a 1% agarose gel.

5.12 Sequence design for DNA and RNA constructs

Target DNA and primer sequences were analyzed and designed using the A plasmid Editor (*ApE*) application^[434]. The gene sequence for *Xist* lncRNA was looked up in the GenBank^[435] sequence database. DNA sequences that were not copied from plasmid DNA, as for β -*Actin* and *GAPDH* qPCR analysis, were looked up in the European Nucleotide Archive (ENA) (β -*Actin*: X00351; *GAPDH*: X01677). For reconciliation with the coding DNA sequences, protein sequences of β -*Actin*, *GAPDH* and *mCherry* were taken from UniProt^[436] (β -*Actin*: P60709; *GAPDH*: P04406; *mCherry*: D1MPT3). Designed primers and qPCR hydrolysis probes were analyzed with regard to their specificity using the Primer3^[437–439] and Primer-BLAST^[440] online applications. The *mfold* web server^[416] was used for secondary structure and minimum free energy (ΔG) predictions of the designed DNA and resulting RNA sequences. By this, stable folding patterns that might prevent correct primer hybridization and denaturing during PCR cycling should be excluded.

5.12.1 *mCh_mRNA* sequence design

For studies on *mCh_mRNA* various DNA and RNA sequences were designed. All DNA sequences were planned for PCR amplification from the *pmCherry-N1_AA* insert plasmid. The two major sequences *mCh_DNA* and *mCh_DNA_{UTR 2}*, and their respective mRNA transcripts *mCh_mRNA* and *mCh_mRNA_{UTR 2}*, were built up with identical 5'-UTR and *mCherry* protein coding sequences but different 3'-UTR sequences. For *mCh_mRNA* the 3'-UTR was adopted without changes from the *pmCherry-N1_AA-insert* plasmid's UTR following the protein coding region. For *mCh_mRNA_{UTR 2}* this 3'-UTR was partly exchanged to a sequence adopted from the *pmCherry-C1* plasmid's 3'-UTR. Using the PrimerQuest Tool a PCR primer pair (*mCh_FW* and *mCh_RV*) was designed amplifying nucleotides 618 to 1432 from the *pmCherry-N1_AA-insert* plasmid for *mCh_DNA*. Additionally, the T7 promoter sequence and one additional **G** for an improved transcription start was added to the *mCh_FW* primer as a 5'-end overhang sequence. For preparation of *mCh_DNA_{UTR 2}* a different reverse primer (*mCh_RV_{UTR 2}*) was designed. Generating *mCh_DNA_{UTR 2}*, nucleotides 618 to 1412 are amplified from the *pmCherry-N1_AA-insert* plasmid. Additionally, the primer *mCh_RV_{UTR 2}* includes a 20 nt long 5'-overhang sequence adopted from the *pmCherry-C1* plasmid's 3'-UTR sequence (G1501 to T1520) which extends the resulting *mCh_DNA_{UTR 2}* PCR amplicon. Thus, two equally long DNA template and also mRNA transcript sequences can be prepared allowing for a comparison of different 3'-UTR sequences. Both templating *mCh_DNA* sequences were planned to consist of 834 bp and result in 817 nt long RNA transcripts. Within the 3'-UTRs of both sequences, *mCh_mRNA* and *mCh_mRNA_{UTR 2}*, UB-modifications and canonical base

point mutations were placed. Therefore, the two different reverse primers were also planned with one or two point mutations of either dT/dNaM ($mCh_RV^1^{dNaM}$, $mCh_RV^2^{dNaM}$, $mCh_RV^1_{UTR2}^{dNaM}$ or $mCh_RV^2_{UTR2}^{dNaM}$) or dT/dC ($mCh_RV^1^{PM}$, $mCh_RV^2^{PM}$, $mCh_RV^1_{UTR2}^{PM}$ or $mCh_RV^2_{UTR2}^{PM}$). Further, for mCh_mRNA sequences, a partial and randomized replacement of the canonical nucleobases **U** and **C** with modified natural bases **Ψ** and **5mC** throughout the complete mRNA sequence was conceived. This was planned to be implemented during *in vitro* transcription utilizing a rNTP mix supplemented with rΨ TP and r5mC TP.

5.12.2 RT-qPCR sequence design for *mCh_mRNA* analysis *in cellulo*

For RT-qPCR analysis of *mCh_mRNA* levels in transfected cells, two different sets of qPCR primers and hydrolysis probes were designed for *mCh_mRNA* analysis. One set was addressed to a section within the *mCherry* protein coding sequence ($mCh_qPCR^{internal}$), the other covered a sequence section closer to the 3'-end of the mRNA's sequence ($mCh_qPCR^{3'-end}$). The selected site for $mCh_qPCR^{3'-end}$ was placed close to the 3'-end of the RNA transcripts but prior to any modification sites. Thus, consistent conditions for reverse transcription were aimed avoiding defective reverse transcription of the UB modifications. Furthermore, a comparison of the RT-qPCR results for both sets, $mCh_qPCR^{internal}$ and $mCh_qPCR^{3'-end}$, was envisioned to assess evaluation of mRNA decay for the different *mCh_mRNA* sequence variants. *GAPDH* and *β-Actin* were chosen as reference genes for RT-qPCR data evaluation. Sequences for qPCR primers and hydrolysis probes for both reference genes were taken from published studies stored in the RTPriMerDB^[441–443] database (*β-Actin*: #2209; *GAPDH*: #2022). qPCR amplicon sizes and GC content for the two *mCh_qPCR* sequences were adjusted to those of the two reference genes and each other. *mCh_qPCR* primers and probes were initially designed using Primer 3^[437–439] and then manually modified to meet the following conditions. qPCR amplicon sizes were chosen between 111 to 130 bp. GC contents of the qPCR amplicons ranged between 52 to 62% (calculated with *ApE*^[434]). Primer and hydrolysis probe lengths and melting temperatures were adjusted in the same way. Primer lengths were set between 20 to 22 nt and primer melting temperatures was kept between 55 to 60 °C (calculated with *ApE*^[434]). Hydrolysis probe lengths were set between 23 to 29 nt and probe melting temperatures was kept between 65 to 66 °C (calculated with *ApE*^[434]). Hydrolysis probe melting temperatures were set 6 to 8 °C higher than those of the primers to ensure binding of the probes before the primers hybridize and PCR extension begins^[444]. In addition, a guanidine was excluded at the 5'-end of the hydrolysis probe adjacent to the fluorescent reporter in order to prevent quenching of the fluorophore^[444]. Further, no more Gs than Cs were included in the probe sequences according to the “Good practice guide for the application of quantitative PCR (qPCR)”^[444]. Ready-designed primer and

hydrolysis probe sequences were checked for their unique target gene specificity running a Primer-BLAST^[440] alignment. Amplicon sequence structures were predicted using *mfold*^[416] checking for secondary structure elements that might interfere with primer and probe binding. Enabling multiplex qPCR analysis, individual fluorescent dyes with separate excitation and emission wavelengths were chosen for each hydrolysis probe. HEX, FAM, Cy 3.5 and Cy 5 were used as 5'-end hydrolysis probe modifications for *mCh_qPCR^{internal}*, *mCh_qPCR^{3'-end}*, *β-Actin* and *GAPDH*, respectively.

For subsequent sequence verification by Sanger sequencing, a qPCR product extension strategy was planned as the original four qPCR amplicons were too short and efficient sequencing starting at their 5'-ends was intended. Therefore, phosphorylated original qPCR products should be ligated with sequence specific splint DNA oligonucleotides and a universal adapter DNA oligonucleotide to extend their 5'-ends. Therefore, an adapter sequence was taken partly from the CMV-promoter sequence from the *pmCherry-N1* plasmid. The complementary sequence of section C519 to A648 from *pmCherry-N1* was used to design a 130 nt long adapter DNA oligonucleotide. Its first 12 nt comprising sequence was copied as it stands for the ext-qPCR_FW amplification and sequencing primer. Melting temperature and GC content of this ext-qPCR_FW primer was 57 °C and 65%, respectively. The section of the last 14 nt from the adapter DNA oligonucleotide sequence was converted into its reverse complement and used as the 3'-end of all qPCR amplicon sequence specific splint DNA oligonucleotides. Its melting temperature was set to be 49 °C (calculated with *ApE*^[434]). The 5'-terminal sequences of the different qPCR amplicons were also converted into their reverse complements and used for the individual 5'-end sequence parts of the splint DNA oligonucleotides. Melting temperatures for these individual qPCR amplicon complementary sequences were kept between 49 to 50 °C (calculated with *ApE*^[434]) in accordance to the 3'-end sequence part of the splint DNA oligonucleotides. Complementary sequence lengths of the individual 5'-end parts ranged from 16 to 18 nt. Further, four different qPCR extension reverse primers (ext-qPCR_RV) had to be prepared for an additional PCR amplification step following splinted ligation. ext-qPCR_RV primers were designed converting the 3'-end terminal sequences of the corresponding original qPCR amplicons to their reverse complements. All four ext-qPCR_RV primers were chosen with a length between 21 to 23 nt, a melting temperature between 56 to 58 °C and a GC content ranging from 48 to 52% (calculated with *ApE*^[434]) in accordance to the universal ext-qPCR_FW primer. Extended qPCR products after splinted ligation and PCR amplification were scheduled to be 241 to 260 bp long.

5.12.3 *Xist* lncRNA A repeat region sequence design

For investigations on the A repeat region of *Xist* lncRNA, the sequence section of nucleotides 366 to 740 within exon 1 from the *M. musculus Xist* gene (GenBank NR_001463.3) were used. The *pCMV-Xist-PA* plasmid (Addgene #26760) was used for preparation of *Xist* A repeat region template DNA. DNA primers were designed covering the sequence of the *Xist* A repeat region from nucleotide 1058 to 1432 from the *pCMV-Xist-PA* plasmid. The templating *Xist_DNA* was planned to consist of 394 bp and result in a 377 nt long RNA transcript. For probing of the *Xist* lncRNA A region secondary structure, two different UBP-modified sequence constructs were planned. For *Xist_DNA*^{2UBP}_{5_3} one UBP-modification was placed at the 5'-end and a second UBP-modification was placed at the 3'-end of the oligonucleotide's coding strand. For *Xist_DNA*^{2UBP}_{3_3} two UBP-modification were positioned at the 3'-end of the oligonucleotide's coding strand stretching a distance of eleven nucleotides in between. For introduction of a UBP-modification at the 5'-end, a **d5SICS**-modification was set within the forward primer (*Xist_FW*^{d5SICS}). The **d5SICS** modification in the forward primer was chosen as an alternative to a **dTPT3** modification due to the fact that only **d5SICS** CEP but not **dTPT3** CEP was available for solid phase synthesis of the primers at that time. Additionally, the forward primer sequence for hybridization to the *pCMV-Xist-PA* plasmid was extended with the 18 nt long T7 promoter sequence as an overhang at its 5'-end. Improving the T7 transcription start, an extra nucleotide **G** was included after the promoter sequence and prior to the *Xist* sequence. For a single or double UBP-modification at the 3'-end, a single or double **dNaM**-modified reverse primer (*Xist_RV*^{dNaM} or *Xist_RV*^{2 dNaM}), were designed, respectively. UBP modifications within the primer sequences were chosen as **dA/dNaM** or **dT/d5SICS** point mutations of the corresponding unmodified primers. Thus, **dNaM:dT** (reverse primer:plasmid) or **d5SICS:dA** (forward primer:plasmid) mismatches will be induced during PCR amplification intending to disrupt an **A:T** base pairing position instead of a more stable G:C base pair. In addition, both reverse primers were ordered from *Ella Biotech* with 2'-O-methyl-modification for the last two nucleotides at the primer's 5'-end. This was planned to prevent untemplated incorporation of additional nucleotides after the 3'-end of the RNA transcript.

During sequence construct design, *mfold* secondary structure predictions were used choosing appropriate truncation sites. Cutting out a shorter sequence section from the *Xist* A region, the resulting RNA transcript was aimed to form a hairpin structure as proposed by Fang *et al.*^[411] consisting of the free 3'- and 5'-ends of the RNA strand.

5.13 Preparation of DNA primers, oligonucleotides and hydrolysis probes

Unmodified DNA primer, qPCR primer and hydrolysis probe oligonucleotides as well as DNA splint and adapter oligonucleotides were ordered and synthesized from *biomers.net* (Ulm, Germany). Unnatural nucleotide (d**5SICS**, d**NaM**) modified DNA primers were ordered and synthesized from by *Ella Biotech* (Martinsried, Germany). The required d**5SICS** and d**NaM** CEPs were purchased from *Berry & Associates Inc.* (Dexter, MI, USA) and provided for *Ella Biotech*. Synthetic DNA oligonucleotides from *biomers.net* or *Ella Biotech* were received as purified and freeze-dried compounds. After receipt, the DNA oligonucleotides were dissolved in ddH₂O to obtain 100 μ M stock solutions and stored at -20 °C.

5.14 PCR for DNA template preparation

For investigations on long RNA oligonucleotides, the RNA itself and its DNA template were prepared enzymatically. PCR approaches were used to generate dsDNA templates. Unmodified dsDNA templates were prepared under standard PCR conditions. For unnatural nucleotide modified dsDNA, an expanded six-letter PCR approach was performed. The required d**NaM** TP was purchased from *MyChem, LLC.* (San Diego, CA, USA). d**TPT3** TP was synthesized according to literature^[80] and kindly provided by Dr. F. Eggert and Dr. C. Domnick.

5.14.1 PCR for *mCherry* template DNA

PCR reactions generating *mCh_DNA* were performed in 100 μ L scales with final concentrations of 20 mM Tris-HCl pH 8.9, 22 mM NH₄Cl, 22 mM KCl, 1.8 mM MgCl₂, 0.06% IGEPAL CA-630, 0.05% Tween 20 (*OneTaq Standard Reaction Buffer*), 375 μ M each canonical dNTP, optionally 200 μ M d**NaM** TP and d**TPT3** TP, 1 μ M forward primer, 1 μ M reverse primer, 0.5 ng μ L⁻¹ *pmCherry-N1_AA-insert* as template and 0.025 U μ L⁻¹ *OneTaq* DNA Polymerase. Table 16 lists the different primer combinations that were used for different *mCh_DNA* sequences. A pipetting scheme for *mCh_DNA* PCR reaction mixes is shown in Table 17.

Table 16. Primer combinations for different *mCh_DNA* and *mCh_DNA_{UTR2}* sequences.

Sequences	Forward primer	Reverse primer
<i>mCh_DNA^{WT}</i>	<i>mCh_FW</i>	<i>mCh_RV</i>
<i>mCh_DNA^{1UBP}</i>		<i>mCh_RV^{1dNaM}</i>
<i>mCh_DNA^{1PM}</i>		<i>mCh_RV^{1PM}</i>
<i>mCh_DNA^{2UBP}</i>		<i>mCh_RV^{2dNaM}</i>
<i>mCh_DNA^{2PM}</i>		<i>mCh_RV^{2PM}</i>
<i>mCh_DNA^{WT}_{UTR2}</i>		<i>mCh_RV_{UTR2}</i>
<i>mCh_DNA^{1UBP}_{UTR2}</i>		<i>mCh_RV^{1dNaM}_{UTR2}</i>
<i>mCh_DNA^{1PM}_{UTR2}</i>		<i>mCh_RV^{1PM}_{UTR2}</i>
<i>mCh_DNA^{2UBP}_{UTR2}</i>		<i>mCh_RV^{2dNaM}_{UTR2}</i>
<i>mCh_DNA^{2PM}_{UTR2}</i>	<i>mCh_RV^{2PM}_{UTR2}</i>	

Table 17. Pipetting scheme for *mCh_DNA* PCR reaction mixes. **dNaM** TP and **dTPT3** TP were added to PCR reaction mixes for 6-letter PCR reactions only.

Component	Stock concentration	Final concentration	V [μ L]
<i>OneTaq Standard Reaction Buffer</i>	5x	1x	20
dNTP bundle	25 mM each	375 μ M each	1.5
dNaM TP	10 mM	0 or 200 μ M	0 or 2
dTPT3 TP	10 mM	0 or 200 μ M	0 or 2
<i>mCh_FW</i> forward primer	100 μ M	1 μ M	1
<i>mCh_RV</i> reverse primer	100 μ M	1 μ M	1
<i>pmCherry-N1_AA-insert</i>	50 ng μ L ⁻¹	0.5 ng μ L ⁻¹	1
<i>OneTaq</i> DNA polymerase	5 U μ L ⁻¹	0.025 U μ L ⁻¹	0.5
ddH ₂ O	-	-	ad 100

PCR cycling was performed with an initial denaturing step for 2 min at 94 °C, followed by 30 cycles of denaturing for 30 s at 94 °C, annealing at individual temperature for each sequence for 40 s and elongation for 1 min at 68 °C. A final elongation step was set for 3 min at 68 °C, before cooling to 4 °C at the end. Table 18 provides an overview of the general cycling conditions and the different annealing temperatures for the different *mCh_DNA* sequences.

Table 18. PCR cycling conditions for different *mCh_DNA* and *mCh_DNA_{UTR 2}* sequences.

Program segment	Sequences	T [°C]	t [s]	
Initial denaturation		94	120	
Denaturation		94	30	30 cycles
Annealing	<i>mCh_DNA^{WT}</i>	56	40	
	<i>mCh_DNA^{1 UB P}</i>	51		
	<i>mCh_DNA^{1 PM}</i>	55		
	<i>mCh_DNA^{2 UB P}</i>	46		
	<i>mCh_DNA^{2 PM}</i>	57		
	<i>mCh_DNA_{UTR 2}^{WT}</i>	61		
	<i>mCh_DNA_{UTR 2}^{1 PM}</i>	63		
<i>mCh_DNA_{UTR 2}^{2 PM}</i>	63			
Elongation		68	60	
Final elongation		68	180	
Hold		4	∞	

For *mCh_DNA_{UTR 2}^{1 UB P}* and *mCh_DNA_{UTR 2}^{2 UB P}*, the total number of 30 cycles was divided into five initial cycles with lower annealing temperatures followed by 25 cycles with increased annealing temperatures. Table 19 provides an overview of the cycling conditions for these two *mCh_DNA* sequences.

Table 19. PCR cycling conditions for *mCh_DNA_{UTR 2}^{UB P 1}* and *mCh_DNA_{UTR 2}^{UB P 2}*.

Program segment	Sequences	T [°C]	t [s]	
Initial denaturation		94	120	
Denaturation		94	30	5 cycles
Annealing	<i>mCh_DNA_{UTR 2}^{1 UB P}</i>	51	40	
	<i>mCh_DNA_{UTR 2}^{2 UB P}</i>	46		
Elongation		68	60	
Denaturation		94	30	
Annealing	<i>mCh_DNA_{UTR 2}^{1 UB P}</i>	55	40	
	<i>mCh_DNA_{UTR 2}^{2 UB P}</i>	51		
Elongation		68	60	
Final elongation		68	180	
Hold		4	∞	

mCh_DNA PCR products were analyzed by agarose gel electrophoresis and purified using the *NucleoSpin Gel and PCR Clean-Up Kit* according to the manufacturer's protocol.

5.14.2 PCR for *Xist* template DNA

PCR reactions generating *mCh_DNA* were performed in 100 μL scales with final concentrations of 20 mM Tris-HCl pH 8.9, 22 mM NH_4Cl , 22 mM KCl, 1.8 mM MgCl_2 , 0.06% IGEPAL CA-630, 0.05% Tween 20 (*OneTaq Standard Reaction Buffer*), 375 μM each canonical dNTP, optionally 200 μM dNaM TP and dTPT3 TP, 1 μM forward primer, 1 μM reverse primer, 0.5 $\text{ng } \mu\text{L}^{-1}$ *pCMV-Xist-PA* as template and 0.025 $\text{U } \mu\text{L}^{-1}$ *OneTaq* DNA Polymerase. Table 20 lists the different primer combinations that were used for different *mCh_DNA* sequences. A pipetting scheme for *mCh_DNA* PCR reaction mixes is shown in Table 21.

Table 20. Primer combinations for different *Xist_DNA* sequences.

Sequences	Forward primer	Reverse primer
<i>Xist_DNA</i> ^{2UBP} _{3_3}	<i>Xist_FW</i>	<i>Xist_RV</i> ^{2dNaM}
<i>Xist_DNA</i> ^{2UBP} _{5_3}	<i>Xist_FW</i> ^{1SSICS}	<i>Xist_RV</i> ^{1dNaM}

Table 21. Pipetting scheme for *Xist_DNA* PCR reaction mixes.

Component	Stock concentration	Final concentration	V [μL]
<i>OneTaq Standard Reaction Buffer</i>	5x	1x	20
dNTP bundle	25 mM each	375 μM each	1.5
dNaM TP	10 mM	0 or 200 μM	0 or 2
dTPT3 TP	10 mM	0 or 200 μM	0 or 2
<i>Xist_FW</i> forward primer	100 μM	1 μM	1
<i>Xist_RV</i> reverse primer	100 μM	1 μM	1
<i>pCMV-Xist-PA</i>	50 $\text{ng } \mu\text{L}^{-1}$	0.5 $\text{ng } \mu\text{L}^{-1}$	1
<i>OneTaq</i> DNA polymerase	5 $\text{U } \mu\text{L}^{-1}$	0.025 $\text{U } \mu\text{L}^{-1}$	0.5
ddH ₂ O	-	-	ad 100

PCR cycling was performed with an initial denaturing step for 2 min at 94 °C, followed by 30 cycles of denaturing for 30 s at 94 °C, annealing at individual temperature for the two different sequences for 40 s and elongation for 1 min at 68 °C. A final elongation step was set for 3 min

at 68 °C, before cooling to 4 °C at the end. Table 22 provides an overview of the general cycling conditions and the different annealing temperatures for the different *mCh_DNA* sequences.

Table 22. PCR cycling conditions for different *Xist_DNA* sequences.

Program segment	Sequences	T [°C]	t [s]	
Initial denaturation		94	120	
Denaturation		94	30	30 Cycles
	<i>Xist_DNA</i> ² _{UBP} _3_3	58	40	
	<i>Xist_DNA</i> ² _{UBP} _5_3	54	40	
Elongation		68	60	
Final elongation		68	180	
Hold		4	∞	

Xist_DNA PCR products were analyzed by agarose gel electrophoresis and purified using the *NucleoSpin Gel and PCR Clean-Up Kit* according to the manufacturer's protocol.

5.15 *In vitro* transcription

In order to prepare long RNA oligonucleotides, enzymatic *in vitro* transcription (IVT) methods were used. Unmodified ssRNA transcripts were prepared under standard IVT conditions. For unnatural nucleotide modified ssRNA, genetic alphabet expansion transcription (GENAEXT) was performed. The required rTPT3 TPs (rTPT3^{NO} TP, rTPT3^{CP} TP) were synthesized according to literature^[88,89] and kindly provided by Dr. C. Domnick and Dr. F. Eggert. For mRNA preparation, the IVT conditions were adapted and combined with co-transcriptional capping and post-transcriptional poly(A) tailing.

5.15.1 *mCherry* RNA

mCh_mRNA and *mCh_mRNA*_{UTR 2} *in vitro* transcriptions were performed using the *HiScribe T7 ARCA mRNA Kit (with tailing)* according to the manufacturer's protocol. During the IVT step, an ARCA-cap was incorporated at the RNA's 5'-end co-transcriptionally. IVT reactions generating *mCh_RNA* were performed in 20 µL scales with final concentrations of 4 mM ARCA, 1 mM GTP, 1.25 mM CTP, 1.25 mM UTP, >1.25 mM ATP and 50 ng µL⁻¹ template DNA. Buffer and enzyme specifications of the used *T7 RNA Polymerase Mix* were not given by the manufacturer and can therefore not be named here. A pipetting scheme for *mCh_RNA*

IVT reaction mixes is shown in Table 23. For preparation of CP-modified GENAEXT *mCh_mRNA*, rTPT3^{CP} TP was added to the IVT reaction mix at a concentration of 0.25 mM. Similarly, for optional natural base modifications, 1.25 mM rΨ TP and 1.25 mM r5mC TP were included in the IVT reaction mix. Except for unmodified *mCh_RNA*^{WT} and *mCh_RNA*^{WT}_{UTR 2'}, DTT and MgCl₂ were added to the IVT mix at concentrations of 5 mM and 2 mM, respectively, improving the yield for modified RNA sequences.

Table 23. Pipetting scheme for capped *mCh_RNA* IVT reaction mixes. rTPT3^{CP} TP was added to IVT reaction mixes for GENAEXT IVT reactions only. rΨ TP and r5mC TP were added if additional natural base modifications were required. DTT and MgCl₂ were included for IVT reaction preparing modified *mCh_RNA* sequences.

Component	Stock concentration	Final concentration	V [μL]
2x ARCA/NTP Mix	2x	1x	10
rTPT3 ^{CP} TP	10 mM	0 or 0.25 mM	0 or 0.5
rΨ TP	50 mM	0 or 1.25 mM	0 or 0.5
r5mC TP	50 mM	0 or 1.25 mM	0 or 0.5
DTT	100 mM	0 or 5 mM	0 or 1
MgCl ₂	50 mM	0 or 2 mM	0 or 0.8
<i>mCh_DNA</i> template	varied	50 ng μL ⁻¹	varied
T7 RNA Polymerase Mix	n.a.	n.a.	2
ddH ₂ O	-	-	ad 20

All IVT reactions were incubated for 30 min at 37 °C. Following, the template DNA was digested by adding 0.2 U μL⁻¹ DNase I to the IVT reaction mix and incubating for 15 min at 37 °C. Post-transcriptionally, the capped RNA was polyadenylated. Poly(A) tailing reactions were performed in 50 μL scales adding *Poly(A) Reaction Buffer* and *E. coli Poly(A) Polymerase* to the DNase-digested IVT mix. Buffer and enzyme specifications of the used *Poly(A) Reaction Buffer* and *E. coli Poly(A) Polymerase* were not given by the manufacturer and can therefore not be named here. A pipetting scheme for poly(A) tailing reactions is shown in Table 24.

Table 24. Pipetting scheme for poly(A) tailing reactions.

Component	Stock concentration	Final concentration	V [μL]
DNase-digested <i>mCh_RNA</i> IVT mix	-	-	20
ddH ₂ O	-	-	20
10x <i>Poly(A) Reaction Buffer</i>	10x	1x	5
<i>E. coli Poly(A) Polymerase</i>	n.a.	n.a.	5

Poly(A) tailing reactions were incubated for 30 min at 37 °C. Prepared *mCh_mRNA* samples were purified via LiCl precipitation according to the kit manufacturer's protocol.

5.15.2 *Xist* lncRNA

Xist_RNA in vitro transcriptions were performed in 100 μL scale with final concentrations of 40 mM Tris-HCl pH 7.9, 25 mM MgCl_2 , 5 mM DTT, 2.5 mM each canonical triphosphate, 0.8 mM rTPT3^{NO} TP, 0.5 U μL^{-1} RNasin, 3×10^{-4} U μL^{-1} iPP, 5 ng μL^{-1} *Xist_DNA* template and 5 U μL^{-1} T7 RNA polymerase. A pipetting scheme for *Xist_RNA* IVT reaction mixes is shown in Table 25.

Table 25. Pipetting scheme for *Xist_RNA* IVT reaction mixes.

Component	Stock concentration	Final concentration	V [μL]
<i>Tris-HCl</i> pH 7.9	200 mM	40 mM	20
MgCl_2	100 mM	25 mM	25
DTT	100 mM	5 mM	5
rNTP bundle	25 mM each	2.5 mM each	10
rTPT3 ^{NO} TP	10 mM	0.8 mM	8
<i>Xist_DNA</i> template	varied	5 ng μL^{-1}	varied
RNasin	40 U μL^{-1}	0.5 U μL^{-1}	1.2
iPP	0.1 U μL^{-1}	3×10^{-4} U μL^{-1}	0.3
<i>T7 RNA Polymerase</i>	50 U μL^{-1}	2.5 U μL^{-1}	5
ddH ₂ O	-	-	ad 100

IVT reactions were incubated for 4 h at 37 °C. Following, the template DNA was digested by adding *DNase I buffer* (final conc. of 10 mM Tris-HCl pH 7.6, 2.5 mM MgCl_2 , 0.5 mM CaCl_2) and 0.035 U μL^{-1} DNase I to the IVT reaction mix and incubating for 45 min at 37 °C. A pipetting scheme for DNase digestion reaction mixes is shown in Table 26.

Table 26. Pipetting scheme for DNase I digestion reaction mixes.

Component	Stock concentration	Final concentration	V [μL]
<i>Xist_RNA</i> IVT mix	n.a.	n.a.	100
<i>10x DNase I Reaction Buffer</i>	10x	1x	11
DNase I	2 U μL^{-1}	0.035 U μL^{-1}	2

DNase digested *Xist*_RNA samples were purified via preparative gel electrophoresis and recovered using the *NucleoSpin Gel and PCR Clean-Up Kit*.

5.16 *In vitro* iEDDA click labeling on rTPT3^{CP}-modified *mCh*_mRNA

For *in vitro* iEDDA click labeling of CP-modified mRNA, equimolar quantities of different *mCh*_mRNA sequence variants were incubated with a more than 60-fold molar excess of tetrazine-conjugated fluorophores. In total reaction volumes of 7 μ L, 8 pmol of each *mCh*_mRNA sequence variant was mixed with 500 pmol of AF Dye 488 tetrazine and incubated for 60 min at 25 °C in the dark. Control samples of *mCh*_mRNA sequence variants were treated equally with a compensatory volume of ddH₂O instead of AF Dye 488 tetrazine. An exemplary pipetting scheme for poly(A) tailing reactions is shown in Table 27.

Table 27. Exemplary pipetting scheme for *mCh*_mRNA *in vitro* click labeling.

Component	Stock concentration	Final concentration	V [μ L]
<i>mCh</i> _mRNA	varied	1.1 μ M	varied
AF Dye 488 tetrazine	500 μ M	0 or 71.4 μ M	0 or 1
ddH ₂ O	-	-	ad 7

After incubation, analytic gel electrophoresis was performed using a 2% agarose gel without EtBr supplement. The resulting mRNA bands were first analyzed by fluorescence scanning using the *Phosphorimager FLA-3000* ($\lambda_{\text{ex}} = 473$ nm $\lambda_{\text{em}} = 520$ nm), followed by EtBr post-staining and visualization using UV-illumination.

5.17 Cell culture maintenance

HeLa cells were cultured in *DMEM GlutaMAX* medium supplemented with 10% FCS, 1% MEM NEAA and 1% sodium pyruvate. Cells were kept in *T75* cell culture flasks at 37 °C and 5% CO₂. At regular intervals of two to three days, cells were split in ratios of 1:3 and 1:5 to maintain a cell confluence between 80-90%. For passage, cells were first washed with 8 mL PBS, then trypsinized with 2 mL Trypsin-EDTA and partly transferred into a new cell culture flask containing fresh medium.

5.18 Cell transfection

For *mCh_mRNA* cell transfections designated to fluorescence imaging, protein quantification or relative mRNA quantification analysis, HeLa cells were seeded the day before transfection in 24-well tissue culture plates at a density of 7×10^4 cells per well. For cells designated to fixed cell fluorescence imaging, additional glass coverslips were placed in each well before cell seeding. Transfections were performed in biological duplicates for each different *mCh_mRNA* sequence and control samples. Cells were transfected using *Lipofectamine MessengerMAX* according to the manufacturer's protocol. Therefore, for each well containing cells to be transfected, 1.5 μL *Lipofectamine MessengerMAX* was diluted in 23.5 μL *Opti-MEM Serum-Reduced Medium*. The diluted lipid mixture was vortexed thoroughly and incubated for 10 min at rt. In the same way, for each well containing cells to be transfected, 500 ng of *mCh_mRNA* was diluted in the appropriate amount of *Opti-MEM Serum-Reduced Medium* to obtain a total volume of 25 μL for each well. Depending on the total amount of wells containing cells to be transfected, the volumes for lipid dilution as well as mRNA dilution were scaled up proportionally and prepared as a whole at once. The diluted mRNA mixture was then added to the diluted lipid mixture in a 1:1 ratio, vortexed thoroughly and incubated for 5 min at rt. After incubation, the mRNA-lipid complex mixture was added dropwise to the surface of the cell medium of each well. Treated cells were incubated for 6, 24 or 48 h at 37 °C and 5% CO₂. At 4 h after transfection start, the cell medium was exchanged for fresh medium.

For *mCh_mRNA* transfections designated to cell viability analysis, HeLa cells were seeded the day before transfection in 96-well tissue culture plates with clear bottom at a density of 2.5×10^3 cells per well. Transfections were performed in biological triplicates for each different *mCh_mRNA* sequence and control samples. Cells were transfected in the same way as in 24-well plates using *Lipofectamine MessengerMAX*, only the amounts of *Lipofectamine MessengerMAX*, *mCh_mRNA* and *Opti-MEM Serum-Reduced Medium* were adjusted and reduced. For each well containing cells to be transfected, 0.3 μL *Lipofectamine MessengerMAX* was diluted in 4.7 μL *Opti-MEM Serum-Reduced Medium*. The diluted lipid mixture was vortexed thoroughly and incubated for 10 min at rt. In the same way, for each well containing cells to be transfected, 100 ng of *mCh_mRNA* was diluted in the appropriate amount of *Opti-MEM Serum-Reduced Medium* to obtain a total volume of 5 μL for each well. Depending on the total amount of wells containing cells to be transfected, the volumes for lipid dilution as well as mRNA dilution were scaled up proportionally and prepared as a whole at once. The diluted mRNA mixture was then added to the diluted lipid mixture in a 1:1 ratio, vortexed thoroughly and incubated for 5 min at rt. After incubation, the mRNA-lipid complex mixture was added dropwise to the surface of the cell medium of each well. Treated cells were incubated for 24 h at 37 °C and 5% CO₂. At 4 h after transfection start, the cell medium was

exchanged for fresh medium supplemented with *MT Cell Viability Substrate* and *NanoLuc Enzyme* from the *RealTime-Glo MT Cell Viability Assay Kit*.

Table 28 gives an overview of cell numbers for the different well plates and the corresponding amounts to prepare mRNA-lipid-complexes for cell transfection.

Table 28. Overview of cell numbers and corresponding amounts to prepare mRNA-lipid complexes for cell transfection.

Component		Single well in a 24-well plate	Single well in a 96-well plate
	Seeded cells	7×10^4 cells	2.5×10^3 cells
Lipid dilution	Lipofectamine	1.5 μ L	0.3 μ L
	Opti-MEM medium	ad 25 μ L	ad 5 μ L
mRNA dilution	<i>mCh_mRNA</i>	500 ng, varying V	100 ng, varying V
	Opti-MEM medium	ad 25 μ L	ad 5 μ L
mRNA-lipid complex	Lipid dilution	25 μ L	5 μ L
	mRNA dilution	25 μ L	5 μ L

5.19 Live-cell iEDDA click labeling on rTPT3^{CP}-modified *mCh_mRNA*

For live-cell iEDDA click labeling of CP-modified *mCh_mRNA* in transfected cells, cell membrane-permeable tetrazine-conjugated fluorophores were added to the transfected cells at 6, 24 or 48 h after transfection start. For cells designated to fixed cell fluorescence imaging, live-cell click labeling was performed in 24-well plates. 1 μ M AF Dye 488 tetrazine was added directly into the cell medium of each well and mixed with the medium by shaking the plate. Cells were incubated for 60 min at 37 °C and 5% CO₂ to allow the click reaction to proceed. Cells were then prepared for fluorescence imaging by washing, fixation and cell nuclei counterstaining.

For cells designated to cell viability analysis, live-cell click labeling was performed in 96-well plates. Cells were treated in the same way as in 24-well plates adding tetrazine-conjugated fluorophores to cells likewise, only the amount of AF Dye 488 tetrazine was adjusted and reduced. 1 μ M AF Dye 488 tetrazine was added directly into the cell medium of each well and mixed with the medium by shaking the plate. Cells were incubated for up to 2 h at 37 °C and 5% CO₂ to allow the click reaction to proceed and cell viability to be analyzed.

5.20 Cell fixation and counterstaining for microscopy

Following cell transfection and live-cell iEDDA click labeling, cells were washed, fixed and cell nuclei counterstained for fluorescence microscopy. First, cells were carefully washed once with 500 μL PBS buffer per well. For cell fixation, 500 μL of a 3.7% formaldehyde solution in PBS (1:10 dilution of 37% formaldehyde solution in PBS buffer) was added to each well and incubated for 10 min at rt. Cells were then washed trice with 500 μL PBS per well per washing step. Next, cell nuclei were counterstained by adding 1 mL of a 1 μg μL^{-1} aqueous DAPI solution per well and incubated for 2 min at rt. After that, cells were washed again trice with 500 μL PBS per well per washing step. The cover slips containing fixed cells were removed from the well-plate and mounted on microscope slides using Fluoro-Gel mounting medium. Mounted slides were allowed to dry overnight at rt in the dark and sealed with clear nail polish the next day.

5.21 Confocal fluorescence microscopy

Imaging of fixed cells after transfection with *mCh_mRNA* and live-cell iEDDA click labeling was performed on a *LSM 710* confocal laser scanning fluorescence microscope equipped with a 40x/1.4 DIC oil objective. Green fluorescence for AF 488 Dye labeled *mCh_mRNA* was recorded at $\lambda_{\text{ex}}/\lambda_{\text{em}} = 488 \text{ nm}/516 \text{ nm}$. Red fluorescence of translated and cellular expressed *mCherry* protein was recorded at $\lambda_{\text{ex}}/\lambda_{\text{em}} = 543 \text{ nm}/637 \text{ nm}$. Blue fluorescence of DAPI counterstained cell nuclei was recorded at $\lambda_{\text{ex}}/\lambda_{\text{em}} = 405 \text{ nm}/460 \text{ nm}$. Fluorescent channels were scanned consecutively to minimize crosstalk. For each channel and each image, a number of four scans were averaged to improve signal-to-noise ratios. In addition, z-stack images were taken with increments of 3.426 μm (corresponds to 1 AU).

5.22 Quantification of cellular *mCherry* protein expression from *mCh_mRNA*

For quantification of cellular *mCherry* protein expression, the *mCherry Quantification Kit* was used. Following *mCh_mRNA* cell transfection and incubation for translation and protein expression, the cell medium was removed from each well. For cell lysis, 130 μL *RIPA Lysis and Extraction Buffer* supplemented with 1 mM PMSF was added to each well and incubated on ice for 20 min. The resulting cell lysate buffer was then transferred from each well to individual 1.5 mL reaction tubes and centrifuged for 5 min at 10000 x g and 4 $^{\circ}\text{C}$. After

centrifugation, 100 μL of protein-containing supernatant was taken off from each tube and transferred either to fresh reaction tubes for intermediate storage at $-20\text{ }^{\circ}\text{C}$ or directly transferred to designated wells of a black 96-well plate. If samples were frozen, they needed to be thawed on ice gently before they were transferred to an assay plate. For each fluorescence measurement, a *mCherry* protein standard series was included in duplicate in the 96-well plate. For this purpose, a $10\text{ ng }\mu\text{L}^{-1}$ *mCherry* protein working solution was used to prepare a standard series of 0, 20, 40, 60, 80 and 100 ng *mCherry* protein per well. The volumes of each well for the standard series were adjusted to 100 μL volume with RIPA buffer. Fluorescence was measured at $\lambda_{\text{ex}}/\lambda_{\text{em}} = 587\text{ nm}/610\text{ nm}$ on the *EnSpire Multimode Plate Reader*, whose measurement chamber was pre-incubated to $25\text{ }^{\circ}\text{C}$.

5.23 RT-qPCR of *mCh_mRNA* levels in cells

In order to quantify *mCh_mRNA* amounts in transfected cells, total cellular RNA was isolated from lysed cells, then reverse transcribed and amplified in a quantitative real-time PCR. Cell lysis and total RNA isolation was performed using the *NucleoSpin RNA Kit* according to the manufacturer's protocol. Concentrations of isolated cellular total RNA were calculated from measured A_{260} absorptions. For reverse transcription and qPCR amplification the *GoTaq Probe 2-Step RT-qPCR System* was used. This allowed separate reaction steps, first reverse transcription and then qPCR analysis. Initial experiments were conducted to test cDNA dilution series in qPCR assays calculating qPCR efficiencies and comparing singleplex and multiplex assays. In addition, qPCR amplicon sequences were to be validated by Sanger sequencing. For that, an extension strategy was implemented.

5.23.1 Cellular total RNA isolation from transfected cells

For isolation of cellular total RNA from transfected cells, the *NucleoSpin RNA Kit* was used according to the manufacturer's protocol. After *mCh_mRNA* cell transfection and incubation, the cell medium was removed from each well. For cell lysis, 350 μL *RA1 Lysis Buffer* containing 10 mM DTT was added to each well and incubated for 1 h at $4\text{ }^{\circ}\text{C}$. The resulting cell lysate was then filtered through a *NucleoSpin Filter* by centrifugation for 1 min at 11000 x g to reduce viscosity and clear the lysate. The filtered lysate was mixed with 350 μL 70% EtOH before loading to a *NucleoSpin RNA Column* and centrifugation for 30 s at 11000 x g . After loading, the *NucleoSpin RNA Column's* silica membrane was desalted by adding 350 μL *Membrane Desalting Buffer* and centrifuging for 1 min at 11000 x g . To digest cellular DNA bound to the

silica membrane, a DNase digestion step was performed on the silica membrane. For that, rDNase was diluted in *rDNase Reaction Buffer*, applied directly onto the silica membrane and incubated at rt for 15 min. Subsequently the silica membrane was washed three times. For DNase inactivation and washing, 200 μL *Buffer RAW2* was first added to the column and centrifuged for 30 s at 11000 x g. Then, 600 μL (2nd wash) or 250 μL (3rd wash) of *Buffer RA3* was added to the column and centrifuged at 11000 x g for 30 s (2nd wash) or 2 min (3rd wash). Elution was performed in two steps; for each step, 30 μL ddH₂O was added to the column and centrifuged for 1 min at 11000 x g. Purified isolated cellular total RNA samples were intermediately stored at -20 °C.

5.23.2 RT-qPCR analysis

RT-qPCR analysis was performed in biological duplicates (n=2), starting from transfection to RNA isolation and reverse transcription. In addition, qPCR amplification was executed in technical triplicates. For each *mCh_mRNA* transfection condition and transfection control samples, RT reactions and respective No-Reverse-Transcriptase (NRT) controls were carried out separately. At first, RNA/primer mixes were prepared in total volumes of 7 μL on ice. 500 ng each of *Oligo(dT)₁₅ Primer* and *Random Primers* were added to 100 ng of isolated cellular total RNA from each transfection condition. The RNA/primer mixes were then incubated for 5 min at 70 °C and chilled for at least 5 min in an ice-water bath. In parallel, RT and NRT master mixes were prepared on ice. The NRT mix missed addition of reverse transcriptase, instead water was added in a compensatory amount. Depending on the number of RT or NRT samples, the respective master mix volumes of 13 μL per reaction or control sample were scaled up proportionally and prepared as a whole at once. RT reaction mixes and NRT control samples were obtained by mixing 7 μL RNA/primer mix with 13 μL RT or NRT master mix, respectively. 20 μL RT reaction samples included 5 ng μL^{-1} cellular total RNA, 25 ng μL^{-1} *Oligo(dT)₁₅ Primer*, 25 ng μL^{-1} *Random Primers*, 2 mM MgCl₂, 500 μM *PCR Nucleotide Mix*, 2.5 U μL^{-1} *Recombinant RNasin Ribonuclease Inhibitor*, *GoScript Reaction Buffer* and *GoScript Reverse Transcriptase* (unlisted concentrations for buffer and enzyme from the *GoTaq Probe 2-step RT-qPCR System* component). A pipetting scheme for RT reaction mixes or NRT controls is shown in Table 29. Table 30 provides an overview of the thermal program used for RT reactions. RT reaction and NRT control samples were incubated for 5 min at 25 °C hybridizing RNA and primers, following 45 min at 42 °C for reverse transcription, 15 min at 70 °C for enzyme inactivation and cooling to 4 °C at the end.

Table 29. Pipetting scheme for RT reaction mixes or NRT controls.

Component	Stock concentration	Final concentration	V [μL]
<i>Isolated cellular total RNA</i>	varied	5 ng μL^{-1}	varied
<i>Oligo(dT)₁₅ Primer</i>	0.5 $\mu\text{g } \mu\text{L}^{-1}$	25 ng μL^{-1}	1
<i>Random Primers</i>	0.5 $\mu\text{g } \mu\text{L}^{-1}$	25 ng μL^{-1}	1
<i>GoScript Reaction Buffer</i>	5x	1x	4
MgCl ₂	25 mM	2 mM	1.6
<i>PCR Nucleotide Mix</i>	10 mM	500 μM	1
<i>Recombinant RNasin</i>	100 U μL^{-1}	2.5 U μL^{-1}	0.5
<i>Ribonuclease Inhibitor</i>			
<i>GoScript Reverse Transcriptase</i>	20x	0 or 1x	0 or 1
ddH ₂ O	-	-	ad 20

Table 30. Thermal program for RT reactions.

Program segment	T [$^{\circ}\text{C}$]	t [min]
RNA/primer hybridization	25	5
Reverse transcription	42	45
Enzyme inactivation	70	15
Hold	4	∞

Obtained cDNA and NRT control samples were first diluted 1:2 by mixing 20 μL RT reaction mixes or NRT controls with 20 μL ddH₂O, respectively. 2.5 μL of diluted cDNA or NRT sample was further diluted in a ratio of 1:7 by addition of 17.5 μL ddH₂O. 5 μL of the second dilution was used for one qPCR reaction mix each. qPCR reactions mixes were pipetted in white 96-well PCR plates on ice. After addition of diluted cDNA or NRT samples, or 5 μL ddH₂O for NTC samples, 15 μL qPCR master mix was added to each well. The qPCR master mix therefor was prepared on ice by mixing *GoTaq Probe Master Mix* with the individual forward primers, reverse primers and probe oligonucleotides for each of the four target genes and sequences. Depending on the number of qPCR samples and controls, the qPCR master mix volume was scaled up proportionally and prepared as a whole at once. qPCR reactions were performed in multiplex assays and total volumes of 20 μL using 200 nM forward and reverse primers and 300 nM probe oligonucleotides. A pipetting scheme for RT reaction mixes or NRT controls is shown in Table 31.

Table 31. Pipetting scheme for qPCR reaction mixes.

Component	Stock concentration	Final concentration	V [μ L]
Diluted cDNA or NRT control	n.a.	n.a.	5
<i>GoTaq Probe Master Mix</i>	2x	1x	10
<i>mCh_qPCR^{internal}_FW primer</i>	12 μ M	200 nM	0.33
<i>mCh_qPCR^{3'-end}_FW primer</i>	12 μ M	200 nM	0.33
<i>GAPDH_qPCR_FW primer</i>	12 μ M	200 nM	0.33
<i>β-Actin_qPCR_FW primer</i>	12 μ M	200 nM	0.33
<i>mCh_qPCR^{internal}_RV primer</i>	12 μ M	200 nM	0.33
<i>mCh_qPCR^{3'-end}_RV primer</i>	12 μ M	200 nM	0.33
<i>GAPDH_qPCR_RV primer</i>	12 μ M	200 nM	0.33
<i>β-Actin_qPCR_RV primer</i>	12 μ M	200 nM	0.33
<i>mCh_qPCR^{internal}_probe</i>	18 μ M	300 nM	0.33
<i>mCh_qPCR^{3'-end}_probe</i>	18 μ M	300 nM	0.33
<i>GAPDH_qPCR_probe</i>	18 μ M	300 nM	0.33
<i>β-Actin_qPCR_probe</i>	18 μ M	300 nM	0.33
ddH ₂ O	-	-	ad 20

After pipetting, the qPCR plates were sealed with adhesive foil, briefly centrifuged and placed in the qPCR thermal cycler. PCR cycling was performed with an initial hot start and activation step for 2 min at 95 °C, followed by 40 cycles of denaturing for 15 s at 95 °C and combined annealing and elongation for 60 s at 60 °C, before cooling to 10 °C at the end. Table 32 provides an overview of the qPCR cycling conditions.

Table 32. PCR cycling conditions for qPCR analysis.

Program segment	T [°C]	t [s]	40 cycles
Hot Start / Activation	95	120	
Denaturation	95	15	
Annealing & Elongation	60	60	
Hold	10	∞	

After qPCR reaction completion, samples of qPCR amplicons were checked for lengths on analytic 4% agarose gels. In addition, qPCR amplicons were extended by splinted ligation. By this, subsequent Sanger sequencing enabled sequence validation of the intended qPCR target genes and sequences.

5.23.3 Initial experiments for qPCR efficiencies

Initial experiments applying the RT-qPCR protocol as described previously were performed in order to calculate qPCR efficiencies and compare them between singleplex and multiplex qPCR assays. In deviation from the previously described protocol, HeLa cells were transfected with unmodified *mCh_mRNA^{WT}* only, incubated for 24 h, then lysed and the total RNA was extracted as previously described. The obtained cDNA and NRT samples were first diluted 1:2 with ddH₂O. Five to six different volumes of subsequently prepared two-fold serial dilutions (0.156, 0.313, 0.625, 1.25, 2.5 and 5 μ L) were used in qPCR reactions. qPCR reaction mixes were pipetted and qPCR cycling was conducted as described previously. All initial qPCR reactions were performed in technical duplicates.

5.23.4 qPCR product extension for sequence validation

qPCR amplicons were to be extended in a splinted ligation approach to allow Sanger sequencing for qPCR product sequence validation. In a first step, samples of qPCR products were used as template DNA and amplified under standard PCR conditions. A separate PCR reaction was performed for amplification of each of the four target genes and sequences. 2 μ L of qPCR product mix were used in 100 μ L PCR reactions containing final concentrations of 20 mM Tris-HCl pH 8.9, 22 mM NH₄Cl, 22 mM KCl, 1.8 mM MgCl₂, 0.06% IGEPAL CA-630, 0.05% Tween 20 (*OneTaq Standard Reaction Buffer*), 375 μ M each canonical dNTP, 1 μ M forward primer, 1 μ M reverse primer and 0.025 U μ L⁻¹ *OneTaq* DNA Polymerase. For each of the four qPCR target genes and sequences their specific qPCR forward and reverse primers were used in the PCR reaction mix. A general pipetting scheme for PCR reaction mixes for qPCR product amplification is shown in Table 33.

Table 33. Pipetting scheme for PCR amplification of qPCR products.

Component	Stock concentration	Final concentration	V [μ L]
<i>OneTaq Standard Reaction Buffer</i>	5x	1x	20
dNTP bundle	25 mM each	375 μ M each	1.5
qPCR_FW forward primer	100 μ M	1 μ M	1
qPCR_RV reverse primer	100 μ M	1 μ M	1
qPCR product mix	n.a.	n.a.	2
<i>OneTaq DNA polymerase</i>	5 U μ L ⁻¹	0.025 U μ L ⁻¹	0.5
ddH ₂ O	-	-	ad 100

PCR cycling was performed with an initial denaturing step for 2 min at 94 °C, followed by 30 cycles of denaturing for 30 s at 94 °C, annealing for 40 s at 60 °C and elongation for 30 s at 68 °C. A final elongation step was set for 5 min at 68 °C, before cooling to 4 °C at the end. Table 34 provides an overview of the general cycling conditions.

Table 34. PCR cycling conditions for PCR amplification of qPCR products.

Program segment	T [°C]	t [s]	
Initial denaturation	94	120	
Denaturation	94	30	30 cycles
Annealing	60	40	
Elongation	68	30	
Final elongation	68	300	
Hold	4	∞	

PCR products were checked for lengths by analytic 4% agarose gel electrophoresis and purified using the *NucleoSpin Gel and PCR Clean-Up Kit* according to the manufacturer's protocol. Purified PCR products were then phosphorylated in 50 µL scale containing final concentrations of 2 µM clean PCR product, 70 mM Tris-HCl pH 7.6, 10 mM MgCl₂, 5 mM DTT (*T4 PNK Reaction Buffer*), 1 mM ATP and 0.2 U µL⁻¹ *T4 Polynucleotide Kinase*. Separate phosphorylation reactions were performed for each of the four different sequences. A general pipetting scheme for PCR reaction mixes for qPCR product amplification is shown in Table 35.

Table 35. General pipetting scheme for *T4 PNK* phosphorylation reactions.

Component	Stock concentration	Final concentration	V [µL]
<i>T4 PNK Reaction Buffer</i>	10x	1x	5
ATP	10 mM	1 mM	5
clean PCR product	varied	2 µM	varied
<i>T4 Polynucleotide Kinase</i>	10 U µL ⁻¹	0.2 U µL ⁻¹	1
ddH ₂ O	-	-	ad 50

Phosphorylation reactions were incubated at 37 °C for 30 min and then heated to 65 °C for 20 min for enzyme inactivation. Table 36 gives an overview of the incubation steps for *T4 PNK* phosphorylation.

Table 36. Incubation steps for *T4 PNK* phosphorylation reactions.

Incubation Step	T [°C]	t [min]
Phosphorylation	37	30
Enzyme inactivation	65	20

Phosphorylated PCR products were purified using *G-25 Illustra MicroSpin* gel filtration columns according to the manufacturer's protocol, lyophilized and resuspended in 10 μL ddH₂O. Splinted ligations were performed using a universal adapter and a sequence specific splint DNA oligonucleotide for each qPCR amplicon. Separate ligation reactions were performed for each of the four different sequences. Ligation reactions were performed in 20 μL scale containing 50 mM Tris-HCl pH 7.5, 10 mM MgCl₂, 1 mM ATP, 10 mM DTT (*T4 DNA Ligase Buffer*), 2.5 μM qPCR_adapter DNA oligonucleotide, 2.5 μM splint DNA oligonucleotide, 2.5 μM phosphorylated and purified qPCR product and 40 U μL^{-1} T4 DNA Ligase. A general pipetting scheme for splinted ligation reactions is shown in Table 37.

Table 37. General pipetting scheme for splinted ligation reactions.

Component	Stock concentration	Final concentration	V [μL]
<i>T4 DNA Ligase Buffer</i>	10x	1x	2
qPCR_adapter	100 μM	2.5 μM	0.5
qPCR_splint	100 μM	2.5 μM	0.5
phosphorylated PCR product	10 μM	2.5 μM	5
<i>T4 DNA Ligase</i>	400 U μL^{-1}	40 U μL^{-1}	2
ddH ₂ O	-	-	ad 20

Ligation reaction mixes were first prepared without adding of the enzyme, heated to 95 °C for 2 min, then incubated at 50 °C for 5 min, before slowly cooling to 16 °C at a cooling rate of 1 °C min⁻¹. T4 DNA ligase was then added, the reaction mix was incubated overnight at 16 °C, and heated to 95 °C for 2 min at the end for enzyme inactivation. Table 38 provides an overview of the incubation steps for T4 DNA ligation.

Table 38. Incubation steps for *T4 DNA ligase* splinted ligation reaction.

Incubation Step	T [°C]	t [min]	Cooling rate
Denaturing	95	2	
Annealing	50	5	
Slow cooling	50 → 16	34	1 °C min ⁻¹
Ligation	16	o/n	
Enzyme inactivation	95	2	

Ligation products were purified via preparative agarose gel electrophoresis. Subsequently, the ligation products were amplified by PCR. For each of the four sequences, separate PCR reactions were accomplished using sequence-specific reverse primer in combination with a universal forward primer. PCR reactions were performed in 100 µL scale containing final concentration of 20 mM Tris-HCl pH 8.9, 22 mM NH₄Cl, 22 mM KCl, 1.8 mM MgCl₂, 0.06 % IGEPAL CA-630, 0.05% Tween 20 (*OneTaq*® Standard Reaction Buffer), 375 µM each canonical dNTP, 1 µM ext-qPCR_FW forward primer, 1 µM reverse primer and 0.025 U µL⁻¹ *OneTaq* DNA Polymerase. A general pipetting scheme for PCR reaction mixes for extended qPCR product amplification is shown in Table 39.

Table 39. General pipetting scheme for PCR amplification of extended qPCR products.

Component	Stock concentration	Final concentration	V [µL]
<i>OneTaq Standard Reaction Buffer</i>	5x	1x	20
dNTP bundle	25 mM each	375 µM each	1.5
ext-qPCR_FW forward primer	100 µM	1 µM	1
ext-qPCR_RV reverse primer	100 µM	1 µM	1
ligated qPCR product	varied	0.7 ng µL ⁻¹	varied
<i>OneTaq</i> DNA polymerase	5 U µL ⁻¹	0.025 U µL ⁻¹	0.5
ddH ₂ O	-	-	ad 100

PCR cycling was performed with an initial denaturing step for 2 min at 94 °C, followed by 30 cycles of denaturing for 30 s at 94 °C, annealing for 40 s at 57 °C and elongation for 30 s at 68 °C. A final elongation step was set for 5 min at 68 °C, before cooling to 4 °C at the end. Table 40 provides an overview of the general cycling conditions.

Table 40. PCR cycling conditions for PCR amplification of extended qPCR products.

Program segment	T [°C]	t [s]	
Initial denaturation	94	120	
Denaturation	94	30	30 cycles
Annealing	57	40	
Elongation	68	30	
Final elongation	68	300	
Hold	4	∞	

PCR products were checked for length by analytic 4% agarose gel electrophoresis and purified using the *NucleoSpin Gel and PCR Clean-Up Kit* according to the manufacturer's protocol. Purified PCR products were then used for Sanger sequencing.

5.24 Sanger sequencing of UBP modified and unmodified DNA

For sequence validation of PCR and qPCR products, purified amplicons were analyzed by Sanger sequencing. All PCR and qPCR amplicons were previously purified using the *NucleoSpin Gel and PCR Clean-Up Kit*. Sequencing of unmodified DNA was entirely performed at *GATC Services (Eurofins Genomics, Germany)* using the self-designed *mCh_Seq* sequencing primer and the *T7_Seq* sequencing primer provided by the company. For sequencing of UBP-modified DNA, the *BigDye Terminator v3.1 Cycle Sequencing Kit* was used to perform cycle sequencing according to the *Cologne Center for Genomics's* protocol. Sequencing reactions were performed in 10 μL scale containing 4 $\text{ng } \mu\text{L}^{-1}$ *mCh_DNA* template and 0.25 μM *mCh_FW* primer in 1:40 diluted *BigDye Terminator 3.1 Ready Reaction Mix* and 1:4.4 diluted *BigDye Terminator 3.1. 5x Sequencing Buffer*. A pipetting scheme for *BigDye Terminator v3.1 Cycle Sequencing* reaction mixes is shown in Table 41.

Table 41. Pipetting scheme for *BigDye Terminator v3.1 Cycle Sequencing* reaction mixes.

Component	Stock concentration	Final concentration	V [μL]
<i>BigDye Terminator 3.1 Ready Reaction Mix</i>	n.a.	n.a.	0.25
<i>BigDye Terminator 3.1. 5x Sequencing Buffer</i>	5x	1.125x	2.25
<i>mCh_FW</i> primer	10 μM	0.25 μM	0.25
<i>mCh_DNA</i> template	varied	4 $\text{ng } \mu\text{L}^{-1}$	varied
ddH ₂ O	-	-	ad 10

Cycling was performed with 32 cycles of denaturing for 10 s at 96 °C, annealing for 5 s at 66 °C and extension for 4 min at 60 °C, before cooling to 4 °C at the end. Table 42 provides an overview of the cycling conditions.

Table 42. Cycling conditions for *BigDye Terminator v3.1* Cycle Sequencing reaction mixes.

Program segment	T [°C]	t [s]	32 cycles
Denaturation	96	10	
Annealing	66	5	
Extension	60	240	
Hold	4	∞	

After that, samples were submitted to the *Cologne Center for Genomics* (University of Cologne, Germany) for purification and capillary electrophoresis.

5.25 Cell viability assay

To evaluate cell viability associated with *mCh_mRNA* transfection and live-cell click labeling in HeLa cells, the non-lytic and bioluminescent *RealTime-Glo™ MT Cell Viability Assay* was used. This assay allows measurement of the cell's reducing potential and thus metabolism (MT) by coupling it to the generation of luminescent signals. Viable cells can reduce and convert an added pro-substrate into a substrate used by likewise added luciferase to generate a luminescent signal. The *RealTime-Glo™ MT Cell Viability Assay* was performed in a single cell experiment (n=1) with triplicate samples for the different transfection and treatment conditions.

As previously described, cells were seeded in 96-well tissue culture plates with clear bottom, transfected with *mCh_mRNA* and incubated at 37 °C and 5% CO₂. At 4 h after transfection start, the cell medium was exchanged. For that, 4 mL of fresh cell medium were mixed with 4 µL each of the *MT Cell Viability Substrate* (1000x stock conc.) and *NanoLuc Enzyme* (1000x stock conc.). 100 µL of fresh medium supplemented with *MT Cell Viability Substrate* and *NanoLuc Enzyme* was added to each well allowing for the continuous-read format of the assay. The cells were then incubated at 37 °C and 5% CO₂ again. At 6, 8, 22 and 24 h after transfection start, the cell plate was temporarily removed from the incubator and luminescence was measured with an integration time of 0.1 s on the *EnSpire Multimode Plate Reader*, whose measurement chamber preheated to 37 °C. After the last measurement at 24 h post transfection start, 1 µM AF Dye 488 tetrazine was added to the cell medium. As a control for

the maximum loss of luminescence signal due to cell lysis, 2 μL of Triton X-100 (10% solution in ddH₂O) was added simultaneously to formally untreated cells. Subsequently, the cells were incubated again at 37 °C and 5% CO₂ for 2 h. At 1 and 2 h after AF Dye 488 tetrazine addition, *i.e.* 25 and 26 h after transfection start, the cell plate was again temporarily removed from the incubator and luminescence was measured as previously described.

Initial experiments were performed to measure assay linearity over time. For this purpose, cell seeding, transfection and addition of *MT Cell Viability Substrate* and *NanoLuc Enzyme* was performed as previously described. Measured luminescence values for control samples with untreated cells and H₂O transfection were used to evaluate maximum assay incubation times.

5.26 EPR sample preparation

After purification by preparative agarose gel electrophoresis and *Xist_RNA* recovery using silica-spin columns, eluates from multiple columns were combined and centrifuged at 18620 x g for 10 min to pellet silica carry-over. Larger *Xist_RNA* sample volumes were concentrated using *Amicon Ultra 3K centrifugal filter devices* according to the manufacturers' protocol. Concentrated *Xist_RNA* was reconstituted in 450 μL PELDOR buffer and concentrated again for buffer exchange. This step was repeated. *Xist_RNA* was then recovered by an upside-down centrifugation step and the obtained sample was brought to 50 μL volume by addition of PELDOR buffer. For *Xist_RNA*^{2^{NO}}_3_3 MgCl₂ was also added to a final concentration of 1 mM. For hybridization, *Xist_RNA* was then heated to 70 °C for 5 min and subsequently chilled to 18 °C at a cooling rate of 2 °C min⁻¹. Finally, 12.5 μL of ethylene glycol-d₆ was added and the *Xist_RNA* samples were transferred into 3 mm quartz Q-band EPR tubes and flash-cooled in liquid nitrogen until PELDOR measurements were performed.

5.27 Data evaluation

5.27.1 Microscopy

For image editing, raw microscopy images were first exported to tagged image file format (TIF) using *Zen 3.3 (blue edition)* software and then processed using *Photoshop CS5*. Signals from different channels for fluorescence and transmitted light were separated into individual image layers. Tonal correction was applied to each layer. The tonal correction for red (cellular

mCherry protein expression) and green (labeled *mCh_mRNA*) image layers was performed using uniform parameters for all different biological samples, treatment controls and different time points. Similarly, brightness adjustments for red and green image layers were performed using uniform parameters for all different biological samples, treatment controls and different time points. The layers for blue (counterstained cell nuclei) and transmitted light signals were processed individually for each image during tonal correction and brightness adjustments. To enhance the visibility of blue signals, the blue signal layers was copied, converted to a greyscale image and additionally placed behind the blue signal layer. Opacity of the blue greyscale layer were reduced to 10% and the blend mode of the blue greyscale layer was changed to “luminosity”. For the transmitted light signals, tonal correction, brightness and contrast adjustments were performed for each image individually. In order to create merged images, the blend modes of all fluorescent signal layers were changed to “screen”. Scale bar graphics were inserted as fixed size boxes in new image layers of the processed images. For this purpose, scale bars were first calculated for the corresponding raw microscopy images using the *Zen 3.3 (blue edition)*, then their pixel size was measured to create the fixed size boxes.

5.27.2 Protein quantification

Data evaluation for *mCherry* protein quantifications was performed using *Excel*. For each plate and its individual *mCherry* protein standard series, calculations for the standard series were performed initially. First, mean fluorescence values for each concentration of the *mCherry* protein standard series duplicates were calculated. Next, the *mCherry* standard series was plotted using the calculated mean values and a line of best fit was applied to it. The quality of the line of best fit was characterized by the coefficient of determination R^2 . Measured fluorescence values from samples within the same plate, were background subtracted. For this, the mean value of the 0 ng *mCherry* fluorescence readings of the plate’s standard series was subtracted from all readings. After that, each background corrected fluorescence value was divided by the slope of the line of best fit. By this, amounts of *mCherry* protein in ng per well were obtained. For biological duplicates, a mean value of the amount of *mCherry* protein was calculated. Subsequently, mean values of *mCherry* protein amounts from biologically independent experiments but transfections using identical *mCh_mRNA* sequences were averaged (n=20 for *mCh_mRNA*^{WT}, *mCh_mRNA*^{1CP} and *mCh_mRNA*^{2CP}; n=10 for *mCh_mRNA*^{1PM}, *mCh_mRNA*^{2PM}, *mCh_mRNA*^{WT, $\psi+5mC$} , *mCh_mRNA*^{1CP, $\psi+5mC$} , *mCh_mRNA*^{2CP, $\psi+5mC$} , *mCh_mRNA*^{WT_{UTR 2}}, *mCh_mRNA*^{1CP_{UTR 2}}, *mCh_mRNA*^{2CP_{UTR 2}}, *mCh_mRNA*^{1PM_{UTR 2}}, *mCh_mRNA*^{2PM_{UTR 2}}). Their error values were calculated using Gaussian error propagation. Lastly, all *mCherry* protein amounts expressed from various *mCh_mRNA*

sequences were normalized to the expression from mCh_mRNA^{WT} and for that divided by the mCherry protein amount of mCh_mRNA^{WT} . Using *Origin*, normalized mCherry protein amounts and their corresponding error values were plotted as bar graphs comparing different mCh_mRNA sequences at different time points.

5.27.3 RT-qPCR

C_t values for each target gene and sequence were determined by the *CFX Maestro* software supplied with the qPCR thermal cycler. Further evaluation steps were performed using *Excel*. First, mean C_t values of the two biological duplicates and their technical triplicates along with their standard deviation (s.d.) were calculated for each of the four target genes and sequences, separately for each mCh_mRNA sequence transfection condition and each qPCR assay plate. Due to unstable results for β -Actin C_t values throughout the acquired qPCR data set, further calculations were performed with *GAPDH* as the only reference gene. ΔC_t values for each mCh_mRNA sequence were obtained by subtracting the C_t mean values of *GAPDH_qPCR* from C_t mean values of $mCh_qPCR^{internal}$ or $mCh_qPCR^{3'-end}$, respectively. Following, ΔC_t values of the different mCh_mRNA sequences from two biologically independent transfection experiments were averaged ($n=2$), separately for analysis using either the $mCh_qPCR^{internal}$ or $mCh_qPCR^{3'-end}$ primer/probe set. $\Delta\Delta C_t$ values of the different mCh_mRNA sequences were then calculated subtracting the averaged ΔC_t value of unmodified mCh_mRNA^{WT} at 6 h post transfection from all other averaged ΔC_t values of varying modified mCh_mRNA sequences at varying time points post transfection. Finally, fold changes in mCh_mRNA amounts between the different mCh_mRNA sequences were given as $2^{-\Delta\Delta C_t}$ values. Gaussian error propagation was applied to calculate all corresponding error values starting with the ΔC_t calculations. Using *Origin*, $2^{-\Delta\Delta C_t}$ values and their corresponding error values were plotted as bar graphs comparing different mCh_mRNA sequences at different time points.

For initial qPCR experiments, mean C_t values and their s.d. were calculated from the obtained C_t values of duplicate samples. Mean C_t values were plotted against the logarithm of volumes of the cDNA dilution series. Lines of best fit were computed and qPCR efficiencies were calculated as $(10^{-\frac{1}{\text{slope}} - 1}) \times 100$.

5.27.4 Cell viability assay

The *MT Cell Viability Assay* was performed in a single cell experiment ($n=1$) with triplicate samples for each transfection and treatment condition. All calculations were performed using *Excel*. A background mean value was calculated for each time point from the luminescent

signals measured in five wells containing only medium and no cells. All other luminescence signals measured for different transfection and treatment condition and at different time points were background corrected by subtracting the background mean value of the corresponding time point. Subsequently, mean values and their s.d. were calculated for triplicate samples. Using *Origin*, the background corrected, mean luminescence values and their s.d. were plotted against time.

In order to evaluate maximum assay incubation times and assay linearity over time, measured luminescence values for control samples with untreated cells and H₂O transfection from initial experiments were used. Using *Excel*, mean values and their s.d. were first calculated for triplicate samples. Luminescence mean values were plotted against time and then the corresponding lines of best fit were calculated. The quality of the lines of best fit was characterized by the coefficient of determination R².

6 References

- [1] F. H. C. Crick. The biological replication of macromolecules. *Symp. Soc. Exp. Biol.* **1958**, 138.
- [2] Tuite, M. F.; Serio, T. R. The prion hypothesis: from biological anomaly to basic regulatory mechanism. *Nat Rev Mol Cell Biol* **2010**, *11*, 823–833. DOI: 10.1038/nrm3007.
- [3] Finnegan, D. J. Eukaryotic transposable elements and genome evolution. *Trends in Genetics* **1989**, *5*, 103–107. DOI: 10.1016/0168-9525(89)90039-5.
- [4] Inouye, S.; Inouye, M. Structure, function, and evolution of bacterial reverse transcriptase. *Virus Genes* **1995**, *11*, 81–94. DOI: 10.1007/BF01728650.
- [5] Inouye, S.; Hsu, M.-Y.; Eagle, S.; Inouye, M. Reverse transcriptase associated with the biosynthesis of the branched RNA-linked msDNA in *Myxococcus xanthus*. *Cell* **1989**, *56*, 709–717. DOI: 10.1016/0092-8674(89)90593-X.
- [6] Nakamura, T. M.; Morin, G. B.; Chapman, K. B.; Weinrich, S. L.; Andrews, W. H.; Lingner, J.; Harley, C. B.; Cech, T. R. Telomerase catalytic subunit homologs from fission yeast and human. *Science (New York, N.Y.)* **1997**, *277*, 955–959. DOI: 10.1126/science.277.5328.955.
- [7] Teng, S. C.; Kim, B.; Gabriel, A. Retrotransposon reverse-transcriptase-mediated repair of chromosomal breaks. *Nature* **1996**, *383*, 641–644. DOI: 10.1038/383641a0.
- [8] Alonso, D.; Mondragón, A. Mechanisms of catalytic RNA molecules. *Biochem Soc Trans* **2021**, *49*, 1529–1535. DOI: 10.1042/BST20200465.
- [9] Scott, W. G. Ribozymes. *Current Opinion in Structural Biology* **2007**, *17*, 280–286. DOI: 10.1016/j.sbi.2007.05.003.
- [10] Fu, X.-D. Non-coding RNA: a new frontier in regulatory biology. *Natl Sci Rev* **2014**, *1*, 190–204. DOI: 10.1093/nsr/nwu008.
- [11] Mattick, J. S.; Makunin, I. V. Non-coding RNA. *Hum Mol Genet* **2006**, *15 Spec No 1*, R17-29. DOI: 10.1093/hmg/ddl046.
- [12] Krämer, A. The structure and function of proteins involved in mammalian pre-mRNA splicing. *Annual review of biochemistry* **1996**, *65*, 367–409. DOI: 10.1146/annurev.bi.65.070196.002055.
- [13] Muth, G. W.; Ortoleva-Donnelly, L.; Strobel, S. A. A single adenosine with a neutral pKa in the ribosomal peptidyl transferase center. *Science (New York, N.Y.)* **2000**, *289*, 947-950. DOI: 10.1126/science.289.5481.947.
- [14] Nissen, P.; Hansen, J.; Ban, N.; Moore, P. B.; Steitz, T. A. The structural basis of ribosome activity in peptide bond synthesis. *Science (New York, N.Y.)* **2000**, *289*, 920-930. DOI: 10.1126/science.289.5481.920.
- [15] Esakova, O.; Krasilnikov, A. S. Of proteins and RNA: the RNase P/MRP family. *RNA* **2010**, *16*, 1725–1747. DOI: 10.1261/rna.2214510.
- [16] Tollervey, D.; Kiss, T. Function and synthesis of small nucleolar RNAs. *Current Opinion in Cell Biology* **1997**, *9*, 337–342. DOI: 10.1016/S0955-0674(97)80005-1.
- [17] Morrissey, J. Birth of the snoRNPs: the evolution of RNase MRP and the eukaryotic pre-rRNA-processing system. *Trends in Biochemical Sciences* **1995**, *20*, 78–82. DOI: 10.1016/S0968-0004(00)88962-8.
- [18] Lafontaine, D. L.J.; Tollervey, D. Birth of the snoRNPs: the evolution of the modification-guide snoRNAs. *Trends in Biochemical Sciences* **1998**, *23*, 383–388. DOI: 10.1016/S0968-0004(98)01260-2.
- [19] Kawamata, T.; Tomari, Y. Making RISC. *Trends in Biochemical Sciences* **2010**, *35*, 368-376. DOI: 10.1016/j.tibs.2010.03.009.
- [20] Gibb, E. A.; Brown, C. J.; Lam, W. L. The functional role of long non-coding RNA in human carcinomas. *Mol Cancer* **2011**, *10*, 38. DOI: 10.1186/1476-4598-10-38.

- [21] Geisler, S.; Collier, J. RNA in unexpected places: long non-coding RNA functions in diverse cellular contexts. *Nat Rev Mol Cell Biol* **2013**, *14*, 699–712. DOI: 10.1038/nrm3679.
- [22] Ponjavic, J.; Oliver, P. L.; Lunter, G.; Ponting, C. P. Genomic and transcriptional co-localization of protein-coding and long non-coding RNA pairs in the developing brain. *PLoS Genetics* **2009**, *5*, e1000617. DOI: 10.1371/journal.pgen.1000617.
- [23] Ransohoff, J. D.; Wei, Y.; Khavari, P. A. The functions and unique features of long intergenic non-coding RNA. *Nat Rev Mol Cell Biol* **2018**, *19*, 143–157. DOI: 10.1038/nrm.2017.104.
- [24] Long, Y.; Wang, X.; Youmans, D. T.; Cech, T. R. How do lncRNAs regulate transcription? *Science advances* **2017**, *3*, eaao2110. DOI: 10.1126/sciadv.aao2110.
- [25] Lee, J. T. Epigenetic regulation by long noncoding RNAs. *Science* **2012**, *338*, 1435–1439. DOI: 10.1126/science.1231776.
- [26] Peng, W.-X.; Koirala, P.; Mo, Y.-Y. LncRNA-mediated regulation of cell signaling in cancer. *Oncogene* **2017**, *36*, 5661–5667. DOI: 10.1038/onc.2017.184.
- [27] Karakas, D.; Ozpolat, B. The Role of LncRNAs in Translation. *Non-Coding RNA* **2021**, *7*, 16. DOI: 10.3390/ncrna7010016.
- [28] WATSON, J. D.; CRICK, F. H. Molecular structure of nucleic acids; a structure for deoxyribose nucleic acid. *Nature* **1953**, *171*, 737–738. DOI: 10.1038/171737a0.
- [29] Alexander Rich. On the Problems of Evolution and Biochemical Information Transfer. In *Horizons in Biochemistry*; Michael Kasha, B. P., Ed.; Academic Press, 1962; pp 103-126.
- [30] Switzer, C.; Moroney, S. E.; Benner, S. A. Enzymatic incorporation of a new base pair into DNA and RNA. *J. Am. Chem. Soc.* **1989**, *111*, 8322–8323. DOI: 10.1021/ja00203a067.
- [31] Piccirilli, J. A.; Krauch, T.; Moroney, S. E.; Benner, S. A. Enzymatic incorporation of a new base pair into DNA and RNA extends the genetic alphabet. *Nature* **1990**, *343*, 33-37. DOI: 10.1038/343033a0.
- [32] Switzer, C. Y.; Moroney, S. E.; Benner, S. A. Enzymatic recognition of the base pair between isocytidine and isoguanosine. *Biochemistry* **1993**, *32*, 10489–10496. DOI: 10.1021/bi00090a027.
- [33] Benner, S. A.; Karalkar, N. B.; Hoshika, S.; Laos, R.; Shaw, R. W.; Matsuura, M.; Fajardo, D.; Moussatche, P. Alternative Watson-Crick Synthetic Genetic Systems. *Cold Spring Harb Perspect Biol* **2016**, *8*, a023770. DOI: 10.1101/cshperspect.a023770.
- [34] Benner, S. A. Understanding nucleic acids using synthetic chemistry. *Accounts of Chemical Research* **2004**, *37*, 784–797. DOI: 10.1021/ar040004z.
- [35] Kim, H.-J.; Leal, N. A.; Hoshika, S.; Benner, S. A. Ribonucleosides for an artificially expanded genetic information system. *The Journal of organic chemistry* **2014**, *79*, 3194-3199. DOI: 10.1021/jo402665d.
- [36] Biondi, E.; Benner, S. A. Artificially Expanded Genetic Information Systems for New Aptamer Technologies. *Biomedicines* **2018**, *6*, 53. DOI: 10.3390/biomedicines6020053.
- [37] Benner, S. A.; Yang, Z.; Chen, F. Synthetic Biology, Tinkering Biology, and Artificial Biology. What are We Learning? *Comptes Rendus Chimie* **2011**, *14*, 372–387. DOI: 10.1016/j.crci.2010.06.013.
- [38] Karalkar, N. B.; Benner, S. A. The challenge of synthetic biology. Synthetic Darwinism and the aperiodic crystal structure. *Current Opinion in Chemical Biology* **2018**, *46*, 188-195. DOI: 10.1016/j.cbpa.2018.07.008.
- [39] Lutz, M. J.; Held, H. A.; Hottiger, M.; Hübscher, U.; Benner, S. A. Differential discrimination of DNA polymerase for variants of the non-standard nucleobase pair between xanthosine and 2,4-diaminopyrimidine, two components of an expanded genetic alphabet. *Nucl Acids Res* **1996**, *24*, 1308–1313. DOI: 10.1093/nar/24.7.1308.

- [40] Yang, Z.; Chen, F.; Chamberlin, S. G.; Benner, S. A. Expanded genetic alphabets in the polymerase chain reaction. *Angew. Chem. Int. Ed. Engl.* **2010**, *49*, 177–180. DOI: 10.1002/anie.200905173.
- [41] Yang, Z.; Chen, F.; Alvarado, J. B.; Benner, S. A. Amplification, mutation, and sequencing of a six-letter synthetic genetic system. *J. Am. Chem. Soc.* **2011**, *133*, 15105–15112. DOI: 10.1021/ja204910n.
- [42] Sefah, K.; Yang, Z.; Bradley, K. M.; Hoshika, S.; Jiménez, E.; Zhang, L.; Zhu, G.; Shanker, S.; Yu, F.; Turek, D.; *et al.* In vitro selection with artificial expanded genetic information systems. *PNAS* **2014**, *111*, 1449–1454. DOI: 10.1073/pnas.1311778111.
- [43] Zhang, L.; Yang, Z.; Sefah, K.; Bradley, K. M.; Hoshika, S.; Kim, M.-J.; Kim, H.-J.; Zhu, G.; Jiménez, E.; Cansiz, S.; *et al.* Evolution of functional six-nucleotide DNA. *J. Am. Chem. Soc.* **2015**, *137*, 6734–6737. DOI: 10.1021/jacs.5b02251.
- [44] Leal, N. A.; Kim, H.-J.; Hoshika, S.; Kim, M.-J.; Carrigan, M. A.; Benner, S. A. Transcription, reverse transcription, and analysis of RNA containing artificial genetic components. *ACS Synthetic Biology* **2015**, *4*, 407–413. DOI: 10.1021/sb500268n.
- [45] Hoshika, S.; Leal, N. A.; Kim, M.-J.; Kim, M.-S.; Karalkar, N. B.; Kim, H.-J.; Bates, A. M.; Watkins, N. E.; SantaLucia, H. A.; Meyer, A. J.; *et al.* Hachimoji DNA and RNA: A genetic system with eight building blocks. *Science* **2019**, *363*, 884–887. DOI: 10.1126/science.aat0971.
- [46] Benner, S. Uniting Natural History with the Molecular Sciences. The Ultimate Multidisciplinarity. *Accounts of Chemical Research* **2017**, *50*, 498–502. DOI: 10.1021/acs.accounts.6b00496.
- [47] Benner, S. A.; Bell, E. A.; Biondi, E.; Brasser, R.; Carell, T.; Kim, H.-J.; Mojzsis, S. J.; Omran, A.; Pasek, M. A.; Trail, D. When Did Life Likely Emerge on Earth in an RNA-First Process? *ChemSystemsChem* **2020**, *2*, e1900035. DOI: 10.1002/syst.201900035.
- [48] Benner, S. A.; Kim, H.-J.; Yang, Z. Setting the stage: the history, chemistry, and geobiology behind RNA. *Cold Spring Harb Perspect Biol* **2012**, *4*, a003541. DOI: 10.1101/cshperspect.a003541.
- [49] Guckian, K. M.; Kool, E. T. Highly Precise Shape Mimicry by a Difluorotoluene Deoxynucleoside, a Replication-Competent Substitute for Thymidine. *Angew. Chem. Int. Ed. Engl.* **1997**, *36*, 2825–2828. DOI: 10.1002/anie.199728251.
- [50] Ishikawa, M.; Hirao, I.; Yokoyama, S. Synthesis of 3-(2-deoxy- β -d-ribofuranosyl)pyridin-2-one and 2-amino-6-(N,N-dimethylamino)-9-(2-deoxy- β -d-ribofuranosyl)purine derivatives for an unnatural base pair. *Tetrahedron Letters* **2000**, *41*, 3931–3934. DOI: 10.1016/S0040-4039(00)00520-7.
- [51] Ohtsuki, T.; Kimoto, M.; Ishikawa, M.; Mitsui, T.; Hirao, I.; Yokoyama, S. Unnatural base pairs for specific transcription. *Proceedings of the National Academy of Sciences of the United States of America* **2001**, *98*, 4922–4925. DOI: 10.1073/pnas.091532698.
- [52] Fujiwara, T.; Kimoto, M.; Sugiyama, H.; Hirao, I.; Yokoyama, S. Synthesis of 6-(2-thienyl)purine nucleoside derivatives that form unnatural base pairs with pyridin-2-one nucleosides. *Bioorganic & Medicinal Chemistry Letters* **2001**, *11*, 2221–2223. DOI: 10.1016/S0960-894X(01)00415-2.
- [53] Hirao, I.; Ohtsuki, T.; Fujiwara, T.; Mitsui, T.; Yokogawa, T.; Okuni, T.; Nakayama, H.; Takio, K.; Yabuki, T.; Kigawa, T.; *et al.* An unnatural base pair for incorporating amino acid analogs into proteins. *Nat Biotechnol* **2002**, *20*, 177–182. DOI: 10.1038/nbt0202-177.
- [54] Moriyama, K.; Kimoto, M.; Mitsui, T.; Yokoyama, S.; Hirao, I. Site-specific biotinylation of RNA molecules by transcription using unnatural base pairs. *Nucleic Acids Research* **2005**, *33*, e129. DOI: 10.1093/nar/gni128.
- [55] Kawai, R.; Kimoto, M.; Ikeda, S.; Mitsui, T.; Endo, M.; Yokoyama, S.; Hirao, I. Site-specific fluorescent labeling of RNA molecules by specific transcription using unnatural base pairs. *J. Am. Chem. Soc.* **2005**, *127*, 17286–17295. DOI: 10.1021/ja0542946.

- [56] Hirao, I. Placing extra components into RNA by specific transcription using unnatural base pair systems. *BioTechniques* **2006**, *40*, 711, 713, 715 passim. DOI: 10.2144/000112187.
- [57] Kimoto, M.; Hirao, I. Genetic alphabet expansion technology by creating unnatural base pairs. *Chem. Soc. Rev.* **2020**, *49*, 7602–7626. DOI: 10.1039/D0CS00457J.
- [58] Hirao, I.; Kimoto, M.; Mitsui, T.; Fujiwara, T.; Kawai, R.; Sato, A.; Harada, Y.; Yokoyama, S. An unnatural hydrophobic base pair system: site-specific incorporation of nucleotide analogs into DNA and RNA. *Nat Methods* **2006**, *3*, 729–735. DOI: 10.1038/nmeth915.
- [59] Kimoto, M.; Sato, A.; Kawai, R.; Yokoyama, S.; Hirao, I. Site-specific incorporation of functional components into RNA by transcription using unnatural base pair systems. *Nucleic acids symposium series (2004)* **2009**, 73–74. DOI: 10.1093/nass/nrp037.
- [60] Kimoto, M.; Kawai, R.; Mitsui, T.; Yokoyama, S.; Hirao, I. An unnatural base pair system for efficient PCR amplification and functionalization of DNA molecules. *Nucleic Acids Research* **2009**, *37*, e14. DOI: 10.1093/nar/gkn956.
- [61] Yamashige, R.; Kimoto, M.; Mitsui, T.; Yokoyama, S.; Hirao, I. Monitoring the site-specific incorporation of dual fluorophore-quencher base analogues for target DNA detection by an unnatural base pair system. *Org. Biomol. Chem.* **2011**, *9*, 7504–7509. DOI: 10.1039/C1OB06118F.
- [62] Yamashige, R.; Kimoto, M.; Okumura, R.; Hirao, I. Visual Detection of Amplified DNA by Polymerase Chain Reaction Using a Genetic Alphabet Expansion System. *J. Am. Chem. Soc.* **2018**, *140*, 14038–14041. DOI: 10.1021/jacs.8b08121.
- [63] Kimoto, M.; Yamashige, R.; Matsunaga, K.-i.; Yokoyama, S.; Hirao, I. Generation of high-affinity DNA aptamers using an expanded genetic alphabet. *Nat Biotechnol* **2013**, *31*, 453–457. DOI: 10.1038/nbt.2556.
- [64] Matsunaga, K.-i.; Kimoto, M.; Hirao, I. High-Affinity DNA Aptamer Generation Targeting von Willebrand Factor A1-Domain by Genetic Alphabet Expansion for Systematic Evolution of Ligands by Exponential Enrichment Using Two Types of Libraries Composed of Five Different Bases. *J. Am. Chem. Soc.* **2017**, *139*, 324–334. DOI: 10.1021/jacs.6b10767.
- [65] Hirao, I.; Kimoto, M.; Lee, K. H. DNA aptamer generation by ExSELEX using genetic alphabet expansion with a mini-hairpin DNA stabilization method. *Biochimie* **2018**, *145*, 15–21. DOI: 10.1016/j.biochi.2017.09.007.
- [66] Someya, T.; Ando, A.; Kimoto, M.; Hirao, I. Site-specific labeling of RNA by combining genetic alphabet expansion transcription and copper-free click chemistry. *Nucleic Acids Research* **2015**, *43*, 6665–6676. DOI: 10.1093/nar/gkv638.
- [67] McMinn, D. L.; Ogawa, A. K.; Wu, Y.; Liu, J.; Schultz, P. G.; Romesberg, F. E. Efforts toward Expansion of the Genetic Alphabet: DNA Polymerase Recognition of a Highly Stable, Self-Pairing Hydrophobic Base. *J. Am. Chem. Soc.* **1999**, *121*, 11585–11586. DOI: 10.1021/ja9925150.
- [68] Wu, Y.; Ogawa, A. K.; Berger, M.; McMinn, D. L.; Schultz, P. G.; Romesberg, F. E. Efforts toward Expansion of the Genetic Alphabet: Optimization of Interbase Hydrophobic Interactions. *J. Am. Chem. Soc.* **2000**, *122*, 7621–7632. DOI: 10.1021/ja0009931.
- [69] Tae, E. L.; Wu, Y.; Xia, G.; Schultz, P. G.; Romesberg, F. E. Efforts toward expansion of the genetic alphabet: replication of DNA with three base pairs. *J. Am. Chem. Soc.* **2001**, *123*, 7439–7440. DOI: 10.1021/ja010731e.
- [70] Berger, M.; Luzzi, S. D.; Henry, A. A.; Romesberg, F. E. Stability and selectivity of unnatural DNA with five-membered-ring nucleobase analogues. *J. Am. Chem. Soc.* **2002**, *124*, 1222–1226. DOI: 10.1021/ja012090t.
- [71] Matsuda, S.; Romesberg, F. E. Optimization of interstrand hydrophobic packing interactions within unnatural DNA base pairs. *J. Am. Chem. Soc.* **2004**, *126*, 14419–14427. DOI: 10.1021/ja047291m.

- [72] Leconte, A. M.; Matsuda, S.; Hwang, G. T.; Romesberg, F. E. Efforts towards expansion of the genetic alphabet: pyridone and methyl pyridone nucleobases. *Angewandte Chemie (International ed. in English)* **2006**, *45*, 4326–4329. DOI: 10.1002/anie.200601272.
- [73] Matsuda, S.; Fillo, J. D.; Henry, A. A.; Rai, P.; Wilkens, S. J.; Dwyer, T. J.; Geierstanger, B. H.; Wemmer, D. E.; Schultz, P. G.; Spraggon, G.; *et al.* Efforts toward expansion of the genetic alphabet: structure and replication of unnatural base pairs. *J. Am. Chem. Soc.* **2007**, *129*, 10466–10473. DOI: 10.1021/ja072276d.
- [74] Leconte, A. M.; Hwang, G. T.; Matsuda, S.; Capek, P.; Hari, Y.; Romesberg, F. E. Discovery, characterization, and optimization of an unnatural base pair for expansion of the genetic alphabet. *Journal of the American Chemical Society* **2008**, *130*, 2336–2343. DOI: 10.1021/ja078223d.
- [75] Seo, Y. J.; Hwang, G. T.; Ordoukhanian, P.; Romesberg, F. E. Optimization of an unnatural base pair toward natural-like replication. *Journal of the American Chemical Society* **2009**, *131*, 3246–3252. DOI: 10.1021/ja807853m.
- [76] Malyshev, D. A.; Romesberg, F. E. The expanded genetic alphabet. *Angewandte Chemie International Edition* **2015**, *54*, 11930–11944. DOI: 10.1002/anie.201502890.
- [77] Feldman, A. W.; Romesberg, F. E. Expansion of the Genetic Alphabet: A Chemist's Approach to Synthetic Biology. *Accounts of Chemical Research* **2018**, *51*, 394–403. DOI: 10.1021/acs.accounts.7b00403.
- [78] Malyshev, D. A.; Seo, Y. J.; Ordoukhanian, P.; Romesberg, F. E. PCR with an expanded genetic alphabet. *Journal of the American Chemical Society* **2009**, *131*, 14620–14621. DOI: 10.1021/ja906186f.
- [79] Seo, Y. J.; Matsuda, S.; Romesberg, F. E. Transcription of an expanded genetic alphabet. *Journal of the American Chemical Society* **2009**, *131*, 5046–5047. DOI: 10.1021/ja9006996.
- [80] Li, L.; Degardin, M.; Lavergne, T.; Malyshev, D. A.; Dhimi, K.; Ordoukhanian, P.; Romesberg, F. E. Natural-like replication of an unnatural base pair for the expansion of the genetic alphabet and biotechnology applications. *Journal of the American Chemical Society* **2014**, *136*, 826–829. DOI: 10.1021/ja408814g.
- [81] Malyshev, D. A.; Dhimi, K.; Lavergne, T.; Chen, T.; Dai, N.; Foster, J. M.; Corrêa, I. R.; Romesberg, F. E. A semi-synthetic organism with an expanded genetic alphabet. *Nature* **2014**, *509*, 385–388. DOI: 10.1038/nature13314.
- [82] Feldman, A. W.; Dien, V. T.; Karadeema, R. J.; Fischer, E. C.; You, Y.; Anderson, B. A.; Krishnamurthy, R.; Chen, J. S.; Li, L.; Romesberg, F. E. Optimization of Replication, Transcription, and Translation in a Semi-Synthetic Organism. *J. Am. Chem. Soc.* **2019**, *141*, 10644–10653. DOI: 10.1021/jacs.9b02075.
- [83] Feldman, A. W.; Romesberg, F. E. In Vivo Structure-Activity Relationships and Optimization of an Unnatural Base Pair for Replication in a Semi-Synthetic Organism. *J. Am. Chem. Soc.* **2017**, *139*, 11427–11433. DOI: 10.1021/jacs.7b03540.
- [84] Leconte, A. M.; Romesberg, F. E. Amplify this! DNA and RNA get a third base pair. *Nat Methods* **2006**, *3*, 667–668. DOI: 10.1038/nmeth0906-667.
- [85] Hirao, I.; Mitsui, T.; Kimoto, M.; Yokoyama, S. An efficient unnatural base pair for PCR amplification. *Journal of the American Chemical Society* **2007**, *129*, 15549–15555. DOI: 10.1021/ja073830m.
- [86] Mitsui, T.; Kimoto, M.; Harada, Y.; Yokoyama, S.; Hirao, I. An efficient unnatural base pair for a base-pair-expanded transcription system. *Journal of the American Chemical Society* **2005**, *127*, 8652–8658. DOI: 10.1021/ja0425280.
- [87] Hirao, I.; Harada, Y.; Kimoto, M.; Mitsui, T.; Fujiwara, T.; Yokoyama, S. A two-unnatural-base-pair system toward the expansion of the genetic code. *Journal of the American Chemical Society* **2004**, *126*, 13298–13305. DOI: 10.1021/ja047201d.

- [88] Eggert, F.; Kath-Schorr, S. A cyclopropene-modified nucleotide for site-specific RNA labeling using genetic alphabet expansion transcription. *Chem. Commun.* **2016**, *52*, 7284–7287. DOI: 10.1039/C6CC02321E.
- [89] Domnick, C.; Eggert, F.; Wuebben, C.; Bornewasser, L.; Hagelueken, G.; Schiemann, O.; Kath-Schorr, S. EPR Distance Measurements on Long Non-coding RNAs Empowered by Genetic Alphabet Expansion Transcription. *Angew. Chem. Int. Ed. Engl.* **2020**, *59*, 7891–7896. DOI: 10.1002/anie.201916447.
- [90] Eggert, F. Functionalization of nucleic acids using an expanded genetic alphabet, Universitäts- und Landesbibliothek Bonn, 2020.
- [91] McCown, P. J.; Ruszkowska, A.; Kunkler, C. N.; Breger, K.; Hulewicz, J. P.; Wang, M. C.; Springer, N. A.; Brown, J. A. Naturally occurring modified ribonucleosides. *Wiley Interdisciplinary Reviews: RNA* **2020**, *11*, e1595. DOI: 10.1002/wrna.1595.
- [92] Lorenz, C.; Lünse, C. E.; Mörl, M. tRNA Modifications: Impact on Structure and Thermal Adaptation. *Biomolecules* **2017**, *7*. DOI: 10.3390/biom7020035.
- [93] Boccaletto, P.; Machnicka, M. A.; Purta, E.; Piatkowski, P.; Baginski, B.; Wirecki, T. K.; Crécy-Lagard, V. de; Ross, R.; Limbach, P. A.; Kotter, A.; *et al.* MODOMICS: a database of RNA modification pathways. 2017 update. *Nucleic Acids Research* **2018**, *46*, D303–D307. DOI: 10.1093/nar/gkx1030.
- [94] Cantara, W. A.; Crain, P. F.; Rozenski, J.; McCloskey, J. A.; Harris, K. A.; Zhang, X.; Vendeix, F. A. P.; Fabris, D.; Agris, P. F. The RNA Modification Database, RNAMDB: 2011 update. *Nucleic Acids Research* **2011**, *39*, D195–201. DOI: 10.1093/nar/gkq1028.
- [95] Gao, M.; Zhang, Q.; Feng, X.-H.; Liu, J. Synthetic modified messenger RNA for therapeutic applications. *Acta Biomaterialia* **2021**, *131*, 1–15. DOI: 10.1016/j.actbio.2021.06.020.
- [96] Verma, R. S. *Genes V.* By Benjamin Lewin Oxford University Press, Oxford and New York, 1994, 1,272 pp. *Am. J. Med. Genet.* **1995**, *57*, 121. DOI: 10.1002/ajmg.1320570125.
- [97] Galloway, A.; Cowling, V. H. mRNA cap regulation in mammalian cell function and fate. *Biochimica et biophysica acta. Gene regulatory mechanisms* **2019**, *1862*, 270–279. DOI: 10.1016/j.bbagr.2018.09.011.
- [98] Topisirovic, I.; Svitkin, Y. V.; Sonenberg, N.; Shatkin, A. J. Cap and cap-binding proteins in the control of gene expression. *Wiley Interdisciplinary Reviews: RNA* **2011**, *2*, 277–298. DOI: 10.1002/wrna.52.
- [99] Akichika, S.; Hirano, S.; Shichino, Y.; Suzuki, T.; Nishimasu, H.; Ishitani, R.; Sugita, A.; Hirose, Y.; Iwasaki, S.; Nureki, O.; *et al.* Cap-specific terminal N6-methylation of RNA by an RNA polymerase II-associated methyltransferase. *Science* **2019**, *363*. DOI: 10.1126/science.aav0080.
- [100] Boulias, K.; Toczyłowska-Socha, D.; Hawley, B. R.; Liberman, N.; Takashima, K.; Zaccara, S.; Guez, T.; Vasseur, J.-J.; Debart, F.; Aravind, L.; *et al.* Identification of the m6Am Methyltransferase PCIF1 Reveals the Location and Functions of m6Am in the Transcriptome. *Molecular cell* **2019**, *75*, 631–643.e8. DOI: 10.1016/j.molcel.2019.06.006.
- [101] Sendinc, E.; Valle-Garcia, D.; Dhall, A.; Chen, H.; Henriques, T.; Navarrete-Perea, J.; Sheng, W.; Gygi, S. P.; Adelman, K.; Shi, Y. PCIF1 Catalyzes m6Am mRNA Methylation to Regulate Gene Expression. *Molecular cell* **2019**, *75*, 620–630.e9. DOI: 10.1016/j.molcel.2019.05.030.
- [102] Ramanathan, A.; Robb, G. B.; Chan, S.-H. mRNA capping: biological functions and applications. *Nucleic Acids Research* **2016**, *44*, 7511–7526. DOI: 10.1093/nar/gkw551.
- [103] Ziemniak, M.; Strenkowska, M.; Kowalska, J.; Jemielity, J. Potential therapeutic applications of RNA cap analogs. *Future medicinal chemistry* **2013**, *5*, 1141–1172. DOI: 10.4155/fmc.13.96.
- [104] Jemielity, J.; FOWLER, T.; Zuberek, J.; STEPINSKI, J.; LEWDOROWICZ, M.; NIEDZWIECKA, A.; STOLARSKI, R.; Darzynkiewicz, E.; RHOADS, R. E. Novel

- "anti-reverse" cap analogs with superior translational properties. *RNA* **2003**, *9*, 1108–1122. DOI: 10.1261/rna.5430403.
- [105] JANUSZ STEPINSKI; CLINT WADDELL; RYSZARD STOLARSKI; EDWARD DARZYNKIEWICZ; ROBERT E. RHOADS. Synthesis and properties of mRNAs containing the novel "anti-reverse" cap analogs 7-methyl(3'-O-methyl)GpppG and 7-methyl(3'-deoxy)GpppG. *RNA* **2001**, *7*, 1486–1495.
- [106] Kates, J. Transcription of the Vaccinia Virus Genome and the Occurrence of Polyriboadenylic Acid Sequences in Messenger RNA. *Cold Spring Harbor Symposia on Quantitative Biology* **1970**, *35*, 743–752. DOI: 10.1101/SQB.1970.035.01.090.
- [107] LIM, L.; CANELLAKIS, E. S. Adenine-rich polymer associated with rabbit reticulocyte messenger RNA. *Nature* **1970**, *227*, 710–712. DOI: 10.1038/227710a0.
- [108] Passmore, L. A.; Collier, J. Roles of mRNA poly(A) tails in regulation of eukaryotic gene expression. *Nat Rev Mol Cell Biol* **2022**, *23*, 93–106. DOI: 10.1038/s41580-021-00417-y.
- [109] Chang, H.; Lim, J.; Ha, M.; Kim, V. N. TAIL-seq: genome-wide determination of poly(A) tail length and 3' end modifications. *Molecular cell* **2014**, *53*, 1044–1052. DOI: 10.1016/j.molcel.2014.02.007.
- [110] Eckmann, C. R.; Rammelt, C.; Wahle, E. Control of poly(A) tail length. *Wiley Interdisciplinary Reviews: RNA* **2011**, *2*, 348–361. DOI: 10.1002/wrna.56.
- [111] Gallie, D. R. The cap and poly(A) tail function synergistically to regulate mRNA translational efficiency. *Genes Dev.* **1991**, *5*, 2108–2116. DOI: 10.1101/gad.5.11.2108.
- [112] Mockey, M.; Gonçalves, C.; Dupuy, F. P.; Lemoine, F. M.; Pichon, C.; Midoux, P. mRNA transfection of dendritic cells: synergistic effect of ARCA mRNA capping with Poly(A) chains in cis and in trans for a high protein expression level. *Biochemical and Biophysical Research Communications* **2006**, *340*, 1062–1068. DOI: 10.1016/j.bbrc.2005.12.105.
- [113] Koski, G. K.; Karikó, K.; Xu, S.; Weissman, D.; Cohen, P. A.; Czerniecki, B. J. Cutting edge: innate immune system discriminates between RNA containing bacterial versus eukaryotic structural features that prime for high-level IL-12 secretion by dendritic cells. *Journal of immunology (Baltimore, Md. : 1950)* **2004**, *172*, 3989–3993. DOI: 10.4049/jimmunol.172.7.3989.
- [114] Weissman, D.; Karikó, K. mRNA: Fulfilling the Promise of Gene Therapy. *Molecular therapy : the journal of the American Society of Gene Therapy* **2015**, *23*, 1416–1417. DOI: 10.1038/mt.2015.138.
- [115] Holtkamp, S.; Kreiter, S.; Selmi, A.; Simon, P.; Koslowski, M.; Huber, C.; Türeci, O.; Sahin, U. Modification of antigen-encoding RNA increases stability, translational efficacy, and T-cell stimulatory capacity of dendritic cells. *Blood* **2006**, *108*, 4009–4017. DOI: 10.1182/blood-2006-04-015024.
- [116] van der Velden, A. W.; Thomas, A. A. The role of the 5' untranslated region of an mRNA in translation regulation during development. *The International Journal of Biochemistry & Cell Biology* **1999**, *31*, 87–106. DOI: 10.1016/S1357-2725(98)00134-4.
- [117] Mignone, F.; Gissi, C.; Liuni, S.; Pesole, G. Untranslated regions of mRNAs. *Genome Biol* **2002**, *3*, REVIEWS0004. DOI: 10.1186/gb-2002-3-3-reviews0004.
- [118] Bashirullah, A.; Cooperstock, R. L.; Lipshitz, H. D. Spatial and temporal control of RNA stability. *Proceedings of the National Academy of Sciences of the United States of America* **2001**, *98*, 7025–7028. DOI: 10.1073/pnas.111145698.
- [119] Wilczynska, A.; Bushell, M. The complexity of miRNA-mediated repression. *Cell Death Differ* **2015**, *22*, 22–33. DOI: 10.1038/cdd.2014.112.
- [120] Kozak, M. Possible role of flanking nucleotides in recognition of the AUG initiator codon by eukaryotic ribosomes. *Nucl Acids Res* **1981**, *9*, 5233–5252. DOI: 10.1093/nar/9.20.5233.

- [121] Kozak, M. Compilation and analysis of sequences upstream from the translational start site in eukaryotic mRNAs. *Nucl Acids Res* **1984**, *12*, 857–872. DOI: 10.1093/nar/12.2.857.
- [122] Kozak, M. Point mutations define a sequence flanking the AUG initiator codon that modulates translation by eukaryotic ribosomes. *Cell* **1986**, *44*, 283–292. DOI: 10.1016/0092-8674(86)90762-2.
- [123] Kozak, M. Recognition of AUG and alternative initiator codons is augmented by G in position +4 but is not generally affected by the nucleotides in positions +5 and +6. *The EMBO Journal* **1997**, *16*, 2482–2492. DOI: 10.1093/emboj/16.9.2482.
- [124] Chen, C.-Y. A.; Shyu, A.-B. AU-rich elements: characterization and importance in mRNA degradation. *Trends in Biochemical Sciences* **1995**, *20*, 465–470. DOI: 10.1016/s0968-0004(00)89102-1.
- [125] Wilson, G. M.; Brewer, G. The Search for Trans-Acting Factors Controlling Messenger RNA Decay. In *Progress in Nucleic Acid Research and Molecular Biology*; Moldave, K., Ed.; Academic Press, 1998; pp 257–291.
- [126] Jing, Q.; Huang, S.; Guth, S.; Zarubin, T.; Motoyama, A.; Chen, J.; Di Padova, F.; Lin, S.-C.; Gram, H.; Han, J. Involvement of microRNA in AU-rich element-mediated mRNA instability. *Cell* **2005**, *120*, 623–634. DOI: 10.1016/j.cell.2004.12.038.
- [127] Karikó, K.; Kuo, A.; Barnathan, E. Overexpression of urokinase receptor in mammalian cells following administration of the in vitro transcribed encoding mRNA. *Gene Ther* **1999**, *6*, 1092–1100. DOI: 10.1038/sj.gt.3300930.
- [128] Freund, I.; Eigenbrod, T.; Helm, M.; Dalpke, A. H. RNA Modifications Modulate Activation of Innate Toll-Like Receptors. *Genes* **2019**, *10*, 92. DOI: 10.3390/genes10020092.
- [129] Anderson, B. R.; Muramatsu, H.; Jha, B. K.; Silverman, R. H.; Weissman, D.; Karikó, K. Nucleoside modifications in RNA limit activation of 2'-5'-oligoadenylate synthetase and increase resistance to cleavage by RNase L. *Nucleic Acids Research* **2011**, *39*, 9329–9338. DOI: 10.1093/nar/gkr586.
- [130] Karikó, K.; Muramatsu, H.; Welsh, F. A.; Ludwig, J.; Kato, H.; Akira, S.; Weissman, D. Incorporation of pseudouridine into mRNA yields superior nonimmunogenic vector with increased translational capacity and biological stability. *Molecular therapy : the journal of the American Society of Gene Therapy* **2008**, *16*, 1833–1840. DOI: 10.1038/mt.2008.200.
- [131] Karikó, K.; Buckstein, M.; Ni, H.; Weissman, D. Suppression of RNA recognition by Toll-like receptors: the impact of nucleoside modification and the evolutionary origin of RNA. *Immunity* **2005**, *23*, 165–175. DOI: 10.1016/j.immuni.2005.06.008.
- [132] Anderson, B. R.; Muramatsu, H.; Nallagatla, S. R.; Bevilacqua, P. C.; Sansing, L. H.; Weissman, D.; Karikó, K. Incorporation of pseudouridine into mRNA enhances translation by diminishing PKR activation. *Nucleic Acids Research* **2010**, *38*, 5884–5892. DOI: 10.1093/nar/gkq347.
- [133] Andries, O.; Mc Cafferty, S.; Smedt, S. C. de; Weiss, R.; Sanders, N. N.; Kitada, T. N(1)-methylpseudouridine-incorporated mRNA outperforms pseudouridine-incorporated mRNA by providing enhanced protein expression and reduced immunogenicity in mammalian cell lines and mice. *Journal of controlled release : official journal of the Controlled Release Society* **2015**, *217*, 337–344. DOI: 10.1016/j.jconrel.2015.08.051.
- [134] Karikó, K.; Weissman, D. Naturally occurring nucleoside modifications suppress the immunostimulatory activity of RNA: implication for therapeutic RNA development. *Current Opinion in Drug Discovery & Development* **2007**, *10*, 523–532.
- [135] Kormann, M. S. D.; Hasenpusch, G.; Aneja, M. K.; Nica, G.; Flemmer, A. W.; Herber-Jonat, S.; Huppmann, M.; Mays, L. E.; Illenyi, M.; Schams, A.; *et al.* Expression of therapeutic proteins after delivery of chemically modified mRNA in mice. *Nat Biotechnol* **2011**, *29*, 154–157. DOI: 10.1038/nbt.1733.

- [136]WARREN, L.; FLAKS, J. G.; BUCHANAN, J. M. Biosynthesis of the purines. XX. Integration of enzymatic transformylation reactions. *Journal of Biological Chemistry* **1957**, *229*, 627–640.
- [137]Alseth, I.; Dalhus, B.; Bjørås, M. Inosine in DNA and RNA. *Current opinion in genetics & development* **2014**, *26*, 116–123. DOI: 10.1016/j.gde.2014.07.008.
- [138]Wright, D. J.; Force, C. R.; Znosko, B. M. Stability of RNA duplexes containing inosine-cytosine pairs. *Nucleic Acids Research* **2018**, *46*, 12099–12108. DOI: 10.1093/nar/gky907.
- [139]Athanasias, A.; Rich, A.; Maas, S. Widespread A-to-I RNA editing of Alu-containing mRNAs in the human transcriptome. *PLOS Biology* **2004**, *2*, e391. DOI: 10.1371/journal.pbio.0020391.
- [140]Kim, D. D. Y.; Kim, T. T. Y.; Walsh, T.; Kobayashi, Y.; Matisse, T. C.; Buyske, S.; Gabriel, A. Widespread RNA editing of embedded alu elements in the human transcriptome. *Genome research* **2004**, *14*, 1719–1725. DOI: 10.1101/gr.2855504.
- [141]Levanon, E. Y.; Hallegger, M.; Kinar, Y.; Shemesh, R.; Djinovic-Carugo, K.; Rechavi, G.; Jantsch, M. F.; Eisenberg, E. Evolutionarily conserved human targets of adenosine to inosine RNA editing. *Nucleic Acids Research* **2005**, *33*, 1162–1168. DOI: 10.1093/nar/gki239.
- [142]Licht, K.; Hartl, M.; Amman, F.; Anrather, D.; Janisiw, M. P.; Jantsch, M. F. Inosine induces context-dependent recoding and translational stalling. *Nucleic Acids Research* **2019**, *47*, 3–14. DOI: 10.1093/nar/gky1163.
- [143]Rottman, F.; Shatkin, A. J.; Perry, R. P. Sequences containing methylated nucleotides at the 5' termini of messenger RNAs: Possible implications for processing. *Cell* **1974**, *3*, 197–199. DOI: 10.1016/0092-8674(74)90131-7.
- [144]Iyer, L. M.; Zhang, D.; Aravind, L. Adenine methylation in eukaryotes: Apprehending the complex evolutionary history and functional potential of an epigenetic modification. *BioEssays : news and reviews in molecular, cellular and developmental biology* **2016**, *38*, 27–40. DOI: 10.1002/bies.201500104.
- [145]Bokar, J. A.; Shambaugh, M. E.; Polayes, D.; Matera, A. G.; Rottman, F. M. Purification and cDNA cloning of the AdoMet-binding subunit of the human mRNA (N6-adenosine)-methyltransferase. *RNA* **1997**, *3*, 1233–1247.
- [146]Ping, X.-L.; Sun, B.-F.; Wang, L.; Xiao, W.; Yang, X.; Wang, W.-J.; Adhikari, S.; Shi, Y.; Lv, Y.; Chen, Y.-S.; *et al.* Mammalian WTAP is a regulatory subunit of the RNA N6-methyladenosine methyltransferase. *Cell Res* **2014**, *24*, 177–189. DOI: 10.1038/cr.2014.3.
- [147]Dominissini, D.; Moshitch-Moshkovitz, S.; Schwartz, S.; Salmon-Divon, M.; Ungar, L.; Osenberg, S.; Cesarkas, K.; Jacob-Hirsch, J.; Amariglio, N.; Kupiec, M.; *et al.* Topology of the human and mouse m6A RNA methylomes revealed by m6A-seq. *Nature* **2012**, *485*, 201–206. DOI: 10.1038/nature11112.
- [148]Meyer, K. D.; Saletore, Y.; Zumbo, P.; Elemento, O.; Mason, C. E.; Jaffrey, S. R. Comprehensive analysis of mRNA methylation reveals enrichment in 3' UTRs and near stop codons. *Cell* **2012**, *149*, 1635–1646. DOI: 10.1016/j.cell.2012.05.003.
- [149]Shi, H.; Wei, J.; He, C. Where, When, and How: Context-Dependent Functions of RNA Methylation Writers, Readers, and Erasers. *Molecular cell* **2019**, *74*, 640–650. DOI: 10.1016/j.molcel.2019.04.025.
- [150]Wu, B.; Su, S.; Patil, D. P.; Liu, H.; Gan, J.; Jaffrey, S. R.; Ma, J. Molecular basis for the specific and multivalent recognitions of RNA substrates by human hnRNP A2/B1. *Nat Commun* **2018**, *9*, 420. DOI: 10.1038/s41467-017-02770-z.
- [151]Liu, N.; Zhou, K. I.; Parisien, M.; Dai, Q.; Diatchenko, L.; Pan, T. N6-methyladenosine alters RNA structure to regulate binding of a low-complexity protein. *Nucleic Acids Research* **2017**, *45*, 6051–6063. DOI: 10.1093/nar/gkx141.

- [152] Liu, N.; Dai, Q.; Zheng, G.; He, C.; Parisien, M.; Pan, T. N(6)-methyladenosine-dependent RNA structural switches regulate RNA-protein interactions. *Nature* **2015**, *518*, 560–564. DOI: 10.1038/nature14234.
- [153] Alarcón, C. R.; Goodarzi, H.; Lee, H.; Liu, X.; Tavazoie, S.; Tavazoie, S. F. HNRNPA2B1 Is a Mediator of m(6)A-Dependent Nuclear RNA Processing Events. *Cell* **2015**, *162*, 1299–1308. DOI: 10.1016/j.cell.2015.08.011.
- [154] Fedeles, B. I.; Singh, V.; Delaney, J. C.; Li, D.; Essigmann, J. M. The AlkB Family of Fe(II)/ α -Ketoglutarate-dependent Dioxygenases: Repairing Nucleic Acid Alkylation Damage and Beyond. *J. Biol. Chem.* **2015**, *290*, 20734–20742. DOI: 10.1074/jbc.R115.656462.
- [155] Zheng, G.; Dahl, J. A.; Niu, Y.; Fedorcsak, P.; Huang, C.-M.; Li, C. J.; Vågbø, C. B.; Shi, Y.; Wang, W.-L.; Song, S.-H.; *et al.* ALKBH5 is a mammalian RNA demethylase that impacts RNA metabolism and mouse fertility. *Molecular cell* **2013**, *49*, 18–29. DOI: 10.1016/j.molcel.2012.10.015.
- [156] Zhang, X.; Wei, L.-H.; Wang, Y.; Xiao, Y.; Liu, J.; Zhang, W.; Yan, N.; Amu, G.; Tang, X.; Zhang, L.; *et al.* Structural insights into FTO's catalytic mechanism for the demethylation of multiple RNA substrates. *PNAS* **2019**, *116*, 2919–2924. DOI: 10.1073/pnas.1820574116.
- [157] Wei, J.; Liu, F.; Lu, Z.; Fei, Q.; Ai, Y.; He, P. C.; Shi, H.; Cui, X.; Su, R.; Klungland, A.; *et al.* Differential m6A, m6Am, and m1A Demethylation Mediated by FTO in the Cell Nucleus and Cytoplasm. *Molecular cell* **2018**, *71*, 973–985.e5. DOI: 10.1016/j.molcel.2018.08.011.
- [158] Fu, Y.; Jia, G.; Pang, X.; Wang, R. N.; Wang, X.; Li, C. J.; Smemo, S.; Dai, Q.; Bailey, K. A.; Nobrega, M. A.; *et al.* FTO-mediated formation of N6-hydroxymethyladenosine and N6-formyladenosine in mammalian RNA. *Nat Commun* **2013**, *4*, 1798. DOI: 10.1038/ncomms2822.
- [159] Meyer, K. D.; Patil, D. P.; Zhou, J.; Zinoviev, A.; Skabkin, M. A.; Elemento, O.; Pestova, T. V.; Qian, S.-B.; Jaffrey, S. R. 5' UTR m(6)A Promotes Cap-Independent Translation. *Cell* **2015**, *163*, 999–1010. DOI: 10.1016/j.cell.2015.10.012.
- [160] Patil, D. P.; Pickering, B. F.; Jaffrey, S. R. Reading m6A in the Transcriptome: m6A-Binding Proteins. *Trends in Cell Biology* **2018**, *28*, 113–127. DOI: 10.1016/j.tcb.2017.10.001.
- [161] Choi, J.; Jeong, K.-W.; Demirci, H.; Chen, J.; Petrov, A.; Prabhakar, A.; O'Leary, S. E.; Dominissini, D.; Rechavi, G.; Soltis, S. M.; *et al.* N(6)-methyladenosine in mRNA disrupts tRNA selection and translation-elongation dynamics. *Nat Struct Mol Biol* **2016**, *23*, 110–115. DOI: 10.1038/nsmb.3148.
- [162] Berlivet, S.; Scutenaire, J.; Deragon, J.-M.; Bousquet-Antonelli, C. Readers of the m6A epitranscriptomic code. *Biochimica et biophysica acta. Gene regulatory mechanisms* **2019**, *1862*, 329–342. DOI: 10.1016/j.bbagr.2018.12.008.
- [163] Huang, H.; Weng, H.; Sun, W.; Qin, X.; Shi, H.; Wu, H.; Zhao, B. S.; Mesquita, A.; Liu, C.; Yuan, C. L.; *et al.* Recognition of RNA N6-methyladenosine by IGF2BP proteins enhances mRNA stability and translation. *Nat Cell Biol* **2018**, *20*, 285–295. DOI: 10.1038/s41556-018-0045-z.
- [164] Chen, Y. G.; Chen, R.; Ahmad, S.; Verma, R.; Kasturi, S. P.; Amaya, L.; Broughton, J. P.; Kim, J.; Cadena, C.; Pulendran, B.; *et al.* N6-Methyladenosine Modification Controls Circular RNA Immunity. *Molecular cell* **2019**, *76*, 96–109.e9. DOI: 10.1016/j.molcel.2019.07.016.
- [165] Lu, M.; Zhang, Z.; Xue, M.; Zhao, B. S.; Harder, O.; Li, A.; Liang, X.; Gao, T. Z.; Xu, Y.; Zhou, J.; *et al.* N6-methyladenosine modification enables viral RNA to escape recognition by RNA sensor RIG-I. *Nat Microbiol* **2020**, *5*, 584–598. DOI: 10.1038/s41564-019-0653-9.

- [166] Qiu, W.; Zhang, Q.; Zhang, R.; Lu, Y.; Wang, X.; Tian, H.; Yang, Y.; Gu, Z.; Gao, Y.; Yang, X.; *et al.* N6-methyladenosine RNA modification suppresses antiviral innate sensing pathways via reshaping double-stranded RNA. *Nat Commun* **2021**, *12*, 1582. DOI: 10.1038/s41467-021-21904-y.
- [167] Durbin, A. F.; Wang, C.; Marcotrigiano, J.; Gehrke, L. RNAs Containing Modified Nucleotides Fail To Trigger RIG-I Conformational Changes for Innate Immune Signaling. *mBio* **2016**, *7*. DOI: 10.1128/mBio.00833-16.
- [168] Khoddami, V.; Yerra, A.; Mosbrugger, T. L.; Fleming, A. M.; Burrows, C. J.; Cairns, B. R. Transcriptome-wide profiling of multiple RNA modifications simultaneously at single-base resolution. *PNAS* **2019**, *116*, 6784–6789. DOI: 10.1073/pnas.1817334116.
- [169] Li, X.; Xiong, X.; Wang, K.; Wang, L.; Shu, X.; Ma, S.; Yi, C. Transcriptome-wide mapping reveals reversible and dynamic N(1)-methyladenosine methylome. *Nat Chem Biol* **2016**, *12*, 311–316. DOI: 10.1038/nchembio.2040.
- [170] McCown, P. J.; Wang, M. C.; Jaeger, L.; Brown, J. A. Secondary Structural Model of Human MALAT1 Reveals Multiple Structure-Function Relationships. *International Journal of Molecular Sciences* **2019**, *20*, 5610. DOI: 10.3390/ijms20225610.
- [171] Safra, M.; Sas-Chen, A.; Nir, R.; Winkler, R.; Nachshon, A.; Bar-Yaacov, D.; Erlacher, M.; Rossmannith, W.; Stern-Ginossar, N.; Schwartz, S. The m1A landscape on cytosolic and mitochondrial mRNA at single-base resolution. *Nature* **2017**, *551*, 251–255. DOI: 10.1038/nature24456.
- [172] Schwartz, S. m1A within cytoplasmic mRNAs at single nucleotide resolution: a reconciled transcriptome-wide map. *RNA* **2018**, *24*, 1427–1436. DOI: 10.1261/rna.067348.118.
- [173] Dominissini, D.; Nachtergaele, S.; Moshitch-Moshkovitz, S.; Peer, E.; Kol, N.; Ben-Haim, M. S.; Dai, Q.; Di Segni, A.; Salmon-Divon, M.; Clark, W. C.; *et al.* The dynamic N(1)-methyladenosine methylome in eukaryotic messenger RNA. *Nature* **2016**, *530*, 441–446. DOI: 10.1038/nature16998.
- [174] Woo, H.-H.; Chambers, S. K. Human ALKBH3-induced m1A demethylation increases the CSF-1 mRNA stability in breast and ovarian cancer cells. *Biochimica et biophysica acta. Gene regulatory mechanisms* **2019**, *1862*, 35–46. DOI: 10.1016/j.bbagr.2018.10.008.
- [175] Lu, L.; Yi, C.; Jian, X.; Zheng, G.; He, C. Structure determination of DNA methylation lesions N1-meA and N3-meC in duplex DNA using a cross-linked protein-DNA system. *Nucleic Acids Research* **2010**, *38*, 4415–4425. DOI: 10.1093/nar/gkq129.
- [176] Parsyan, A.; Svitkin, Y.; Shahbazian, D.; Gkogkas, C.; Lasko, P.; Merrick, W. C.; Sonenberg, N. mRNA helicases: the tacticians of translational control. *Nat Rev Mol Cell Biol* **2011**, *12*, 235–245. DOI: 10.1038/nrm3083.
- [177] Roundtree, I. A.; Evans, M. E.; Pan, T.; He, C. Dynamic RNA Modifications in Gene Expression Regulation. *Cell* **2017**, *169*, 1187–1200. DOI: 10.1016/j.cell.2017.05.045.
- [178] Zur, H.; Tuller, T. New universal rules of eukaryotic translation initiation fidelity. *PLoS computational biology* **2013**, *9*, e1003136. DOI: 10.1371/journal.pcbi.1003136.
- [179] Zhang, L.-S.; Liu, C.; Ma, H.; Dai, Q.; Sun, H.-L.; Luo, G.; Zhang, Z.; Zhang, L.; Hu, L.; Dong, X.; *et al.* Transcriptome-wide Mapping of Internal N7-Methylguanosine Methylome in Mammalian mRNA. *Molecular cell* **2019**, *74*, 1304-1316.e8. DOI: 10.1016/j.molcel.2019.03.036.
- [180] Chen, Y.-S.; Yang, W.-L.; Zhao, Y.-L.; Yang, Y.-G. Dynamic transcriptomic m5 C and its regulatory role in RNA processing. *Wiley Interdisciplinary Reviews: RNA* **2021**, *12*, e1639. DOI: 10.1002/wrna.1639.
- [181] Xue, C.; Zhao, Y.; Li, L. Advances in RNA cytosine-5 methylation: detection, regulatory mechanisms, biological functions and links to cancer. *Biomark Res* **2020**, *8*, 43. DOI: 10.1186/s40364-020-00225-0.
- [182] Amort, T.; Rieder, D.; Wille, A.; Khokhlova-Cubberley, D.; Riml, C.; Trixl, L.; Jia, X.-Y.; Micura, R.; Lusser, A. Distinct 5-methylcytosine profiles in poly(A) RNA from mouse

- embryonic stem cells and brain. *Genome Biol* **2017**, *18*, 1. DOI: 10.1186/s13059-016-1139-1.
- [183] Squires, J. E.; Patel, H. R.; Nousch, M.; Sibbritt, T.; Humphreys, D. T.; Parker, B. J.; Suter, C. M.; Preiss, T. Widespread occurrence of 5-methylcytosine in human coding and non-coding RNA. *Nucleic Acids Research* **2012**, *40*, 5023–5033. DOI: 10.1093/nar/gks144.
- [184] Yang, X.; Yang, Y.; Sun, B.-F.; Chen, Y.-S.; Xu, J.-W.; Lai, W.-Y.; Li, A.; Wang, X.; Bhattarai, D. P.; Xiao, W.; *et al.* 5-methylcytosine promotes mRNA export - NSUN2 as the methyltransferase and ALYREF as an m5C reader. *Cell Res* **2017**, *27*, 606–625. DOI: 10.1038/cr.2017.55.
- [185] Hoernes, T. P.; Clementi, N.; Faserl, K.; Glasner, H.; Breuker, K.; Lindner, H.; Hüttenhofer, A.; Erlacher, M. D. Nucleotide modifications within bacterial messenger RNAs regulate their translation and are able to rewire the genetic code. *Nucleic Acids Research* **2016**, *44*, 852–862. DOI: 10.1093/nar/gkv1182.
- [186] Schumann, U.; Zhang, H.-N.; Sibbritt, T.; Pan, A.; Horvath, A.; Gross, S.; Clark, S. J.; Yang, L.; Preiss, T. Multiple links between 5-methylcytosine content of mRNA and translation. *BMC Biol* **2020**, *18*, 40. DOI: 10.1186/s12915-020-00769-5.
- [187] Cui, X.; Liang, Z.; Shen, L.; Zhang, Q.; Bao, S.; Geng, Y.; Zhang, B.; Leo, V.; Vardy, L. A.; Lu, T.; *et al.* 5-Methylcytosine RNA Methylation in Arabidopsis Thaliana. *Molecular Plant* **2017**, *10*, 1387–1399. DOI: 10.1016/j.molp.2017.09.013.
- [188] Huang, T.; Chen, W.; Liu, J.; Gu, N.; Zhang, R. Genome-wide identification of mRNA 5-methylcytosine in mammals. *Nat Struct Mol Biol* **2019**, *26*, 380–388. DOI: 10.1038/s41594-019-0218-x.
- [189] Hoernes, T. P.; Heimdörfer, D.; Köstner, D.; Faserl, K.; Nußbaumer, F.; Plangger, R.; Kreutz, C.; Lindner, H.; Erlacher, M. D. Eukaryotic Translation Elongation is Modulated by Single Natural Nucleotide Derivatives in the Coding Sequences of mRNAs. *Genes* **2019**, *10*, 84. DOI: 10.3390/genes10020084.
- [190] Chen, X.; Li, A.; Sun, B.-F.; Yang, Y.; Han, Y.-N.; Yuan, X.; Chen, R.-X.; Wei, W.-S.; Liu, Y.; Gao, C.-C.; *et al.* 5-methylcytosine promotes pathogenesis of bladder cancer through stabilizing mRNAs. *Nat Cell Biol* **2019**, *21*, 978–990. DOI: 10.1038/s41556-019-0361-y.
- [191] Yang, Y.; Wang, L.; Han, X.; Yang, W.-L.; Zhang, M.; Ma, H.-L.; Sun, B.-F.; Li, A.; Xia, J.; Chen, J.; *et al.* RNA 5-Methylcytosine Facilitates the Maternal-to-Zygotic Transition by Preventing Maternal mRNA Decay. *Molecular cell* **2019**, *75*, 1188-1202.e11. DOI: 10.1016/j.molcel.2019.06.033.
- [192] van Haute, L.; Powell, C. A.; Minczuk, M. Dealing with an Unconventional Genetic Code in Mitochondria: The Biogenesis and Pathogenic Defects of the 5-Formylcytosine Modification in Mitochondrial tRNAMet. *Biomolecules* **2017**, *7*, 24. DOI: 10.3390/biom7010024.
- [193] Wang, R.; Luo, Z.; He, K.; Delaney, M. O.; Chen, D.; Sheng, J. Base pairing and structural insights into the 5-formylcytosine in RNA duplex. *Nucleic Acids Research* **2016**, *44*, 4968–4977. DOI: 10.1093/nar/gkw235.
- [194] Delatte, B.; Wang, F.; Ngoc, L. V.; Collignon, E.; Bonvin, E.; Deplus, R.; Calonne, E.; Hassabi, B.; Putmans, P.; Awe, S.; *et al.* RNA biochemistry. Transcriptome-wide distribution and function of RNA hydroxymethylcytosine. *Science* **2016**, *351*, 282–285. DOI: 10.1126/science.aac5253.
- [195] Hall, R. H. Isolation of 3-methyluridine and 3-methylcytidine from soluble ribonucleic acid. *Biochemical and Biophysical Research Communications* **1963**, *12*, 361–364. DOI: 10.1016/0006-291X(63)90105-0.
- [196] Iwanami, Y.; Brown, G. M. Methylated bases of ribosomal ribonucleic acid from HeLa cells. *Archives of Biochemistry and Biophysics* **1968**, *126*, 8–15. DOI: 10.1016/0003-9861(68)90553-5.

- [197] Maden, B.E.H.; Salim, M. The methylated nucleotide sequences in HeLa cell ribosomal RNA and its precursors. *Journal of Molecular Biology* **1974**, *88*, 133–152. DOI: 10.1016/0022-2836(74)90299-X.
- [198] Xu, L.; Liu, X.; Sheng, N.; Oo, K. S.; Liang, J.; Chionh, Y. H.; Xu, J.; Ye, F.; Gao, Y.-G.; Dedon, P. C.; *et al.* Three distinct 3-methylcytidine (m³C) methyltransferases modify tRNA and mRNA in mice and humans. *J. Biol. Chem.* **2017**, *292*, 14695–14703. DOI: 10.1074/jbc.M117.798298.
- [199] Rubio, M. A. T.; Gaston, K. W.; McKenney, K. M.; Fleming, I. M. C.; Paris, Z.; Limbach, P. A.; Alfonzo, J. D. Editing and methylation at a single site by functionally interdependent activities. *Nature* **2017**, *542*, 494–497. DOI: 10.1038/nature21396.
- [200] Arango, D.; Sturgill, D.; Alhusaini, N.; Dillman, A. A.; Sweet, T. J.; Hanson, G.; Hosogane, M.; Sinclair, W. R.; Nanan, K. K.; Mandler, M. D.; *et al.* Acetylation of Cytidine in mRNA Promotes Translation Efficiency. *Cell* **2018**, *175*, 1872–1886.e24. DOI: 10.1016/j.cell.2018.10.030.
- [201] COHN, W. E.; VOLKIN, E. Nucleoside-5'-Phosphates from Ribonucleic Acid. *Nature* **1951**, *167*, 483–484. DOI: 10.1038/167483a0.
- [202] Schwartz, S.; Bernstein, D. A.; Mumbach, M. R.; Jovanovic, M.; Herbst, R. H.; León-Ricardo, B. X.; Engreitz, J. M.; Guttman, M.; Satija, R.; Lander, E. S.; *et al.* Transcriptome-wide mapping reveals widespread dynamic-regulated pseudouridylation of ncRNA and mRNA. *Cell* **2014**, *159*, 148–162. DOI: 10.1016/j.cell.2014.08.028.
- [203] Li, X.; Zhu, P.; Ma, S.; Song, J.; Bai, J.; Sun, F.; Yi, C. Chemical pulldown reveals dynamic pseudouridylation of the mammalian transcriptome. *Nat Chem Biol* **2015**, *11*, 592–597. DOI: 10.1038/nchembio.1836.
- [204] Carlile, T. M.; Rojas-Duran, M. F.; Zinshteyn, B.; Shin, H.; Bartoli, K. M.; Gilbert, W. V. Pseudouridine profiling reveals regulated mRNA pseudouridylation in yeast and human cells. *Nature* **2014**, *515*, 143–146. DOI: 10.1038/nature13802.
- [205] Davis, D. R. Stabilization of RNA stacking by pseudouridine. *Nucleic Acids Res* **1995**, *23*, 5020–5026. DOI: 10.1093/nar/23.24.5020.
- [206] Borchardt, E. K.; Martinez, N. M.; Gilbert, W. V. Regulation and Function of RNA Pseudouridylation in Human Cells. *Annual review of genetics* **2020**, *54*, 309–336. DOI: 10.1146/annurev-genet-112618-043830.
- [207] Johnson, L.; Söll, D. In vitro biosynthesis of pseudouridine at the polynucleotide level by an enzyme extract from Escherichia coli. *Proceedings of the National Academy of Sciences of the United States of America* **1970**, *67*, 943–950. DOI: 10.1073/pnas.67.2.943.
- [208] Brand, R. C.; Klootwijk, J.; Planta, R. J.; Maden, B. E. Biosynthesis of a hypermodified nucleotide in *Saccharomyces carlsbergensis* 17S and HeLa-cell 18S ribosomal ribonucleic acid. *Biochem J* **1978**, *169*, 71–77. DOI: 10.1042/bj1690071.
- [209] Gupta, R. Halobacterium volcanii tRNAs. Identification of 41 tRNAs covering all amino acids, and the sequences of 33 class I tRNAs. *Journal of Biological Chemistry* **1984**, *259*, 9461–9471.
- [210] Pang, H.; Ihara, M.; Kuchino, Y.; Nishimura, S.; Gupta, R.; Woese, C. R.; McCloskey, J. A. Structure of a modified nucleoside in archaeobacterial tRNA which replaces ribosylthymine. 1-Methylpseudouridine. *Journal of Biological Chemistry* **1982**, *257*, 3589–3592.
- [211] Morais, P.; Adachi, H.; Yu, Y.-T. The Critical Contribution of Pseudouridine to mRNA COVID-19 Vaccines. *Frontiers in Cell and Developmental Biology* **2021**, *9*, 789427. DOI: 10.3389/fcell.2021.789427.
- [212] Nance, K. D.; Meier, J. L. Modifications in an Emergency: The Role of N1-Methylpseudouridine in COVID-19 Vaccines. *ACS central science* **2021**, *7*, 748–756. DOI: 10.1021/acscentsci.1c00197.

- [213] Pardi, N.; Hogan, M. J.; Pelc, R. S.; Muramatsu, H.; Andersen, H.; DeMaso, C. R.; Dowd, K. A.; Sutherland, L. L.; Scearce, R. M.; Parks, R.; *et al.* Zika virus protection by a single low-dose nucleoside-modified mRNA vaccination. *Nature* **2017**, *543*, 248–251. DOI: 10.1038/nature21428.
- [214] Richner, J. M.; Himansu, S.; Dowd, K. A.; Butler, S. L.; Salazar, V.; Fox, J. M.; Julander, J. G.; Tang, W. W.; Shrestha, S.; Pierson, T. C.; *et al.* Modified mRNA Vaccines Protect against Zika Virus Infection. *Cell* **2017**, *168*, 1114–1125.e10. DOI: 10.1016/j.cell.2017.02.017.
- [215] Pardi, N.; Hogan, M. J.; Naradikian, M. S.; Parkhouse, K.; Cain, D. W.; Jones, L.; Moody, M. A.; Verkerke, H. P.; Myles, A.; Willis, E.; *et al.* Nucleoside-modified mRNA vaccines induce potent T follicular helper and germinal center B cell responses. *The Journal of Experimental Medicine* **2018**, *215*, 1571–1588. DOI: 10.1084/jem.20171450.
- [216] Meyer, M.; Huang, E.; Yuzhakov, O.; Ramanathan, P.; Ciaramella, G.; Bukreyev, A. Modified mRNA-Based Vaccines Elicit Robust Immune Responses and Protect Guinea Pigs From Ebola Virus Disease. *The Journal of Infectious Diseases* **2018**, *217*, 451–455. DOI: 10.1093/infdis/jix592.
- [217] Svitkin, Y. V.; Cheng, Y. M.; Chakraborty, T.; Presnyak, V.; John, M.; Sonenberg, N. N1-methyl-pseudouridine in mRNA enhances translation through eIF2 α -dependent and independent mechanisms by increasing ribosome density. *Nucleic Acids Research* **2017**, *45*, 6023–6036. DOI: 10.1093/nar/gkx135.
- [218] Carter, J.-M.; Emmett, W.; Mozos, I. R.; Kotter, A.; Helm, M.; Ule, J.; Hussain, S. FICC-Seq: a method for enzyme-specified profiling of methyl-5-uridine in cellular RNA. *Nucleic Acids Research* **2019**, *47*, e113. DOI: 10.1093/nar/gkz658.
- [219] Cheng, Q.-Y.; Xiong, J.; Ma, C.-J.; Dai, Y.; Ding, J.-H.; Liu, F.-L.; Yuan, B.-F.; Feng, Y.-Q. Chemical tagging for sensitive determination of uridine modifications in RNA. *Chemical science* **2020**, *11*, 1878–1891. DOI: 10.1039/c9sc05094a.
- [220] Friedmann, T.; Roblin, R. Gene therapy for human genetic disease? *Science (New York, N.Y.)* **1972**, *175*, 949–955. DOI: 10.1126/science.175.4025.949.
- [221] Chen, Y.; Williams, V.; Filippova, M.; Filippov, V.; Duerksen-Hughes, P. Viral carcinogenesis: factors inducing DNA damage and virus integration. *Cancers* **2014**, *6*, 2155–2186. DOI: 10.3390/cancers6042155.
- [222] Würtele, H.; Little, K. C. E.; Chartrand, P. Illegitimate DNA integration in mammalian cells. *Gene Ther* **2003**, *10*, 1791–1799. DOI: 10.1038/sj.gt.3302074.
- [223] Cavazzana, M.; Six, E.; Lagresle-Peyrou, C.; André-Schmutz, I.; Hacein-Bey-Abina, S. Gene Therapy for X-Linked Severe Combined Immunodeficiency: Where Do We Stand? *Human gene therapy* **2016**, *27*, 108–116. DOI: 10.1089/hum.2015.137.
- [224] Rohner, E.; Yang, R.; Foo, K. S.; Goedel, A.; Chien, K. R. Unlocking the promise of mRNA therapeutics. *Nat Biotechnol* **2022**, *40*, 1586–1600. DOI: 10.1038/s41587-022-01491-z.
- [225] Hajj, K. A.; Whitehead, K. A. Tools for translation: non-viral materials for therapeutic mRNA delivery. *Nat Rev Mater* **2017**, *2*, 1–17. DOI: 10.1038/natrevmats.2017.56.
- [226] Hornung, V.; Ellegast, J.; Kim, S.; Brzózka, K.; Jung, A.; Kato, H.; Poeck, H.; Akira, S.; Conzelmann, K.-K.; Schlee, M.; *et al.* 5'-Triphosphate RNA is the ligand for RIG-I. *Science* **2006**, *314*, 994–997. DOI: 10.1126/science.1132505.
- [227] Loo, Y.-M.; Gale, M. Immune signaling by RIG-I-like receptors. *Immunity* **2011**, *34*, 680–692. DOI: 10.1016/j.immuni.2011.05.003.
- [228] Diebold, S. S.; Kaisho, T.; Hemmi, H.; Akira, S.; Reis e Sousa, C. Innate antiviral responses by means of TLR7-mediated recognition of single-stranded RNA. *Science* **2004**, *303*, 1529–1531. DOI: 10.1126/science.1093616.
- [229] Heil, F.; Hemmi, H.; Hochrein, H.; Ampenberger, F.; Kirschning, C.; Akira, S.; Lipford, G.; Wagner, H.; Bauer, S. Species-specific recognition of single-stranded RNA via toll-like receptor 7 and 8. *Science* **2004**, *303*, 1526–1529. DOI: 10.1126/science.1093620.

- [230] Lee, B. L.; Barton, G. M. Trafficking of endosomal Toll-like receptors. *Trends in Cell Biology* **2014**, *24*, 360–369. DOI: 10.1016/j.tcb.2013.12.002.
- [231] Lorenz, C.; Fotin-Mleczek, M.; Roth, G.; Becker, C.; Dam, T. C.; Verdurmen, W. P. R.; Brock, R.; Probst, J.; Schlake, T. Protein expression from exogenous mRNA: uptake by receptor-mediated endocytosis and trafficking via the lysosomal pathway. *RNA biology* **2011**, *8*, 627–636. DOI: 10.4161/rna.8.4.15394.
- [232] Vitiello, A.; Ferrara, F. Brief review of the mRNA vaccines COVID-19. *Inflammopharmacol* **2021**, *29*, 645–649. DOI: 10.1007/s10787-021-00811-0.
- [233] Malissen, B.; Tamoutounour, S.; Henri, S. The origins and functions of dendritic cells and macrophages in the skin. *Nat Rev Immunol* **2014**, *14*, 417–428. DOI: 10.1038/nri3683.
- [234] Langlet, C.; Tamoutounour, S.; Henri, S.; Luche, H.; Ardouin, L.; Grégoire, C.; Malissen, B.; Williams, M. CD64 expression distinguishes monocyte-derived and conventional dendritic cells and reveals their distinct role during intramuscular immunization. *Journal of immunology (Baltimore, Md. : 1950)* **2012**, *188*, 1751–1760. DOI: 10.4049/jimmunol.1102744.
- [235] Midoux, P.; Pichon, C. Lipid-based mRNA vaccine delivery systems. *Expert Review of Vaccines* **2015**, *14*, 221–234. DOI: 10.1586/14760584.2015.986104.
- [236] Deering, R. P.; Kommareddy, S.; Ulmer, J. B.; Brito, L. A.; Geall, A. J. Nucleic acid vaccines: prospects for non-viral delivery of mRNA vaccines. *Expert Opinion on Drug Delivery* **2014**, *11*, 885–899. DOI: 10.1517/17425247.2014.901308.
- [237] Oberli, M. A.; Reichmuth, A. M.; Dorkin, J. R.; Mitchell, M. J.; Fenton, O. S.; Jaklenec, A.; Anderson, D. G.; Langer, R.; Blankschtein, D. Lipid Nanoparticle Assisted mRNA Delivery for Potent Cancer Immunotherapy. *Nano Letters* **2017**, *17*, 1326–1335. DOI: 10.1021/acs.nanolett.6b03329.
- [238] Broos, K.; van der Jeught, K.; Puttemans, J.; Goyvaerts, C.; Heirman, C.; Dewitte, H.; Verbeke, R.; Lentacker, I.; Thielemans, K.; Breckpot, K. Particle-mediated Intravenous Delivery of Antigen mRNA Results in Strong Antigen-specific T-cell Responses Despite the Induction of Type I Interferon. *Molecular Therapy - Nucleic Acids* **2016**, *5*, e326. DOI: 10.1038/mtna.2016.38.
- [239] Nair, S. K.; Heiser, A.; Boczkowski, D.; Majumdar, A.; Naoe, M.; Lebkowski, J. S.; Vieweg, J.; Gilboa, E. Induction of cytotoxic T cell responses and tumor immunity against unrelated tumors using telomerase reverse transcriptase RNA transfected dendritic cells. *Nat Med* **2000**, *6*, 1011–1017. DOI: 10.1038/79519.
- [240] Perche, F.; Benvegna, T.; Berchel, M.; Lebegue, L.; Pichon, C.; Jaffrès, P.-A.; Midoux, P. Enhancement of dendritic cells transfection in vivo and of vaccination against B16F10 melanoma with mannosylated histidylated lipopolyplexes loaded with tumor antigen messenger RNA. *Nanomedicine : nanotechnology, biology, and medicine* **2011**, *7*, 445–453. DOI: 10.1016/j.nano.2010.12.010.
- [241] Eshhar, Z.; Waks, T.; Bendavid, A.; Schindler, D. G. Functional expression of chimeric receptor genes in human T cells. *Journal of Immunological Methods* **2001**, *248*, 67–76. DOI: 10.1016/S0022-1759(00)00343-4.
- [242] Kalos, M.; June, C. H. Adoptive T cell transfer for cancer immunotherapy in the era of synthetic biology. *Immunity* **2013**, *39*, 49–60. DOI: 10.1016/j.immuni.2013.07.002.
- [243] Hegde, M.; Corder, A.; Chow, K. K. H.; Mukherjee, M.; Ashoori, A.; Kew, Y.; Zhang, Y. J.; Baskin, D. S.; Merchant, F. A.; Brawley, V. S.; *et al.* Combinational targeting offsets antigen escape and enhances effector functions of adoptively transferred T cells in glioblastoma. *Molecular therapy : the journal of the American Society of Gene Therapy* **2013**, *21*, 2087–2101. DOI: 10.1038/mt.2013.185.
- [244] Doudna, J. A.; Charpentier, E. Genome editing. The new frontier of genome engineering with CRISPR-Cas9. *Science* **2014**, *346*, 1258096. DOI: 10.1126/science.1258096.
- [245] Wiedenheft, B.; Sternberg, S. H.; Doudna, J. A. RNA-guided genetic silencing systems in bacteria and archaea. *Nature* **2012**, *482*, 331–338. DOI: 10.1038/nature10886.

- [246] Tsai, S. Q.; Zheng, Z.; Nguyen, N. T.; Liebers, M.; Topkar, V. V.; Thapar, V.; Wyvekens, N.; Khayter, C.; Iafrate, A. J.; Le, L. P.; *et al.* GUIDE-seq enables genome-wide profiling of off-target cleavage by CRISPR-Cas nucleases. *Nat Biotechnol* **2015**, *33*, 187–197. DOI: 10.1038/nbt.3117.
- [247] Liu, X.; Zhang, Y.; Cheng, C.; Cheng, A. W.; Zhang, X.; Li, N.; Xia, C.; Wei, X.; Liu, X.; Wang, H. CRISPR-Cas9-mediated multiplex gene editing in CAR-T cells. *Cell Res* **2017**, *27*, 154–157. DOI: 10.1038/cr.2016.142.
- [248] Ren, J.; Liu, X.; Fang, C.; Jiang, S.; June, C. H.; Zhao, Y. Multiplex Genome Editing to Generate Universal CAR T Cells Resistant to PD1 Inhibition. *Clin Cancer Res* **2017**, *23*, 2255–2266. DOI: 10.1158/1078-0432.CCR-16-1300.
- [249] Rupp, L. J.; Schumann, K.; Roybal, K. T.; Gate, R. E.; Ye, C. J.; Lim, W. A.; Marson, A. CRISPR/Cas9-mediated PD-1 disruption enhances anti-tumor efficacy of human chimeric antigen receptor T cells. *Sci Rep* **2017**, *7*, 737. DOI: 10.1038/s41598-017-00462-8.
- [250] Eyquem, J.; Mansilla-Soto, J.; Giavridis, T.; van der Stegen, S. J. C.; Hamieh, M.; Cunanan, K. M.; Odak, A.; Gönen, M.; Sadelain, M. Targeting a CAR to the TRAC locus with CRISPR/Cas9 enhances tumour rejection. *Nature* **2017**, *543*, 113–117. DOI: 10.1038/nature21405.
- [251] Takahashi, K.; Yamanaka, S. Induction of pluripotent stem cells from mouse embryonic and adult fibroblast cultures by defined factors. *Cell* **2006**, *126*, 663–676. DOI: 10.1016/j.cell.2006.07.024.
- [252] Mandal, P. K.; Rossi, D. J. Reprogramming human fibroblasts to pluripotency using modified mRNA. *Nat Protoc* **2013**, *8*, 568–582. DOI: 10.1038/nprot.2013.019.
- [253] Warren, L.; Manos, P. D.; Ahfeldt, T.; Loh, Y.-H.; Li, H.; Lau, F.; Ebina, W.; Mandal, P. K.; Smith, Z. D.; Meissner, A.; *et al.* Highly efficient reprogramming to pluripotency and directed differentiation of human cells with synthetic modified mRNA. *Cell Stem Cell* **2010**, *7*, 618–630. DOI: 10.1016/j.stem.2010.08.012.
- [254] Zangi, L.; Lui, K. O.; Gise, A. von; Ma, Q.; Ebina, W.; Ptaszek, L. M.; Später, D.; Xu, H.; Tabebordbar, M.; Gorbатов, R.; *et al.* Modified mRNA directs the fate of heart progenitor cells and induces vascular regeneration after myocardial infarction. *Nat Biotechnol* **2013**, *31*, 898–907. DOI: 10.1038/nbt.2682.
- [255] WARNER, J. R.; KNOPF, P. M.; RICH, A. A multiple ribosomal structure in protein synthesis. *Proceedings of the National Academy of Sciences of the United States of America* **1963**, *49*, 122–129. DOI: 10.1073/pnas.49.1.122.
- [256] Ndeupen, S.; Qin, Z.; Jacobsen, S.; Bouteau, A.; Estanbouli, H.; Igyártó, B. Z. The mRNA-LNP platform's lipid nanoparticle component used in preclinical vaccine studies is highly inflammatory. *iScience* **2021**, *24*, 103479. DOI: 10.1016/j.isci.2021.103479.
- [257] Vlatkovic, I. Non-Immunotherapy Application of LNP-mRNA: Maximizing Efficacy and Safety. *Biomedicines* **2021**, *9*, 530. DOI: 10.3390/biomedicines9050530.
- [258] Shi, D.; Beasock, D.; Fessler, A.; Szebeni, J.; Ljubimova, J. Y.; Afonin, K. A.; Dobrovolskaia, M. A. To PEGylate or not to PEGylate: Immunological properties of nanomedicine's most popular component, polyethylene glycol and its alternatives. *Advanced Drug Delivery Reviews* **2022**, *180*, 114079. DOI: 10.1016/j.addr.2021.114079.
- [259] Besin, G.; Milton, J.; Sabnis, S.; Howell, R.; Mihai, C.; Burke, K.; Benenato, K. E.; Stanton, M.; Smith, P.; Senn, J.; *et al.* Accelerated Blood Clearance of Lipid Nanoparticles Entails a Biphasic Humoral Response of B-1 Followed by B-2 Lymphocytes to Distinct Antigenic Moieties. *Immunohorizons* **2019**, *3*, 282–293. DOI: 10.4049/immunohorizons.1900029.
- [260] Bigini, P.; Gobbi, M.; Bonati, M.; Clavenna, A.; Zucchetti, M.; Garattini, S.; Pasut, G. The role and impact of polyethylene glycol on anaphylactic reactions to COVID-19 nano-vaccines. *Nat. Nanotechnol.* **2021**, *16*, 1169–1171. DOI: 10.1038/s41565-021-01001-3.

- [261] Ramaswamy, S.; Tonnu, N.; Tachikawa, K.; Limphong, P.; Vega, J. B.; Karmali, P. P.; Chivukula, P.; Verma, I. M. Systemic delivery of factor IX messenger RNA for protein replacement therapy. *PNAS* **2017**, *114*, E1941–E1950. DOI: 10.1073/pnas.1619653114.
- [262] An, D.; Frassetto, A.; Jacquinet, E.; Eybye, M.; Milano, J.; DeAntonis, C.; Nguyen, V.; Laureano, R.; Milton, J.; Sabnis, S.; *et al.* Long-term efficacy and safety of mRNA therapy in two murine models of methylmalonic acidemia. *EBioMedicine* **2019**, *45*, 519–528. DOI: 10.1016/j.ebiom.2019.07.003.
- [263] Karadagi, A.; Cavedon, A. G.; Zemack, H.; Nowak, G.; Eybye, M. E.; Zhu, X.; Guadagnin, E.; White, R. A.; Rice, L. M.; Frassetto, A. L.; *et al.* Systemic modified messenger RNA for replacement therapy in alpha 1-antitrypsin deficiency. *Sci Rep* **2020**, *10*, 7052. DOI: 10.1038/s41598-020-64017-0.
- [264] Prieve, M. G.; Harvie, P.; Monahan, S. D.; Roy, D.; Li, A. G.; Blevins, T. L.; Paschal, A. E.; Waldheim, M.; Bell, E. C.; Galperin, A.; *et al.* Targeted mRNA Therapy for Ornithine Transcarbamylase Deficiency. *Molecular therapy : the journal of the American Society of Gene Therapy* **2018**, *26*, 801–813. DOI: 10.1016/j.ymthe.2017.12.024.
- [265] Thess, A.; Grund, S.; Mui, B. L.; Hope, M. J.; Baumhof, P.; Fotin-Mleczek, M.; Schlake, T. Sequence-engineered mRNA Without Chemical Nucleoside Modifications Enables an Effective Protein Therapy in Large Animals. *Molecular therapy : the journal of the American Society of Gene Therapy* **2015**, *23*, 1456–1464. DOI: 10.1038/mt.2015.103.
- [266] Vaidyanathan, S.; Azizian, K. T.; Haque, A. K. M. A.; Henderson, J. M.; Hendel, A.; Shore, S.; Antony, J. S.; Hogrefe, R. I.; Kormann, M. S. D.; Porteus, M. H.; *et al.* Uridine Depletion and Chemical Modification Increase Cas9 mRNA Activity and Reduce Immunogenicity without HPLC Purification. *Molecular therapy. Nucleic acids* **2018**, *12*, 530–542. DOI: 10.1016/j.omtn.2018.06.010.
- [267] Kim, D. Y.; Atasheva, S.; McAuley, A. J.; Plante, J. A.; Frolova, E. I.; Beasley, D. W. C.; Frolov, I. Enhancement of protein expression by alphavirus replicons by designing self-replicating subgenomic RNAs. *PNAS* **2014**, *111*, 10708–10713. DOI: 10.1073/pnas.1408677111.
- [268] Huysmans, H.; Zhong, Z.; Temmerman, J. de; Mui, B. L.; Tam, Y. K.; Mc Cafferty, S.; Gitsels, A.; Vanrompay, D.; Sanders, N. N. Expression Kinetics and Innate Immune Response after Electroporation and LNP-Mediated Delivery of a Self-Amplifying mRNA in the Skin. *Molecular Therapy - Nucleic Acids* **2019**, *17*, 867–878. DOI: 10.1016/j.omtn.2019.08.001.
- [269] Fuller, D. H.; Berglund, P. Amplifying RNA Vaccine Development. *The New England journal of medicine* **2020**, *382*, 2469–2471. DOI: 10.1056/NEJMcibr2009737.
- [270] McKay, P. F.; Hu, K.; Blakney, A. K.; Samnuan, K.; Brown, J. C.; Penn, R.; Zhou, J.; Bouton, C. R.; Rogers, P.; Polra, K.; *et al.* Self-amplifying RNA SARS-CoV-2 lipid nanoparticle vaccine candidate induces high neutralizing antibody titers in mice. *Nat Commun* **2020**, *11*, 3523. DOI: 10.1038/s41467-020-17409-9.
- [271] Santer, L.; Bär, C.; Thum, T. Circular RNAs: A Novel Class of Functional RNA Molecules with a Therapeutic Perspective. *Molecular therapy : the journal of the American Society of Gene Therapy* **2019**, *27*, 1350–1363. DOI: 10.1016/j.ymthe.2019.07.001.
- [272] Wesselhoef, R. A.; Kowalski, P. S.; Anderson, D. G. Engineering circular RNA for potent and stable translation in eukaryotic cells. *Nat Commun* **2018**, *9*, 2629. DOI: 10.1038/s41467-018-05096-6.
- [273] Wesselhoef, R. A.; Kowalski, P. S.; Parker-Hale, F. C.; Huang, Y.; Bisaria, N.; Anderson, D. G. RNA Circularization Diminishes Immunogenicity and Can Extend Translation Duration In Vivo. *Molecular cell* **2019**, *74*, 508–520.e4. DOI: 10.1016/j.molcel.2019.02.015.
- [274] Karikó, K.; Muramatsu, H.; Ludwig, J.; Weissman, D. Generating the optimal mRNA for therapy: HPLC purification eliminates immune activation and improves translation of

- nucleoside-modified, protein-encoding mRNA. *Nucleic Acids Research* **2011**, *39*, e142. DOI: 10.1093/nar/gkr695.
- [275] Nelson, J.; Sorensen, E. W.; Mintri, S.; Rabideau, A. E.; Zheng, W.; Besin, G.; Khatwani, N.; Su, S. V.; Miracco, E. J.; Issa, W. J.; *et al.* Impact of mRNA chemistry and manufacturing process on innate immune activation. *Science advances* **2020**, *6*, eaaz6893. DOI: 10.1126/sciadv.aaz6893.
- [276] Dousis, A.; Ravichandran, K.; Hobert, E. M.; Moore, M. J.; Rabideau, A. E. An engineered T7 RNA polymerase that produces mRNA free of immunostimulatory byproducts. *Nat Biotechnol* **2022**, 1–9. DOI: 10.1038/s41587-022-01525-6.
- [277] Torchilin, V. P. Recent advances with liposomes as pharmaceutical carriers. *Nature reviews. Drug discovery* **2005**, *4*, 145–160. DOI: 10.1038/nrd1632.
- [278] Rejman, J.; Tavernier, G.; Bavarsad, N.; Demeester, J.; Smedt, S. C. de. mRNA transfection of cervical carcinoma and mesenchymal stem cells mediated by cationic carriers. *Journal of controlled release : official journal of the Controlled Release Society* **2010**, *147*, 385–391. DOI: 10.1016/j.jconrel.2010.07.124.
- [279] Karikó, K.; Muramatsu, H.; Keller, J. M.; Weissman, D. Increased erythropoiesis in mice injected with submicrogram quantities of pseudouridine-containing mRNA encoding erythropoietin. *Molecular therapy : the journal of the American Society of Gene Therapy* **2012**, *20*, 948–953. DOI: 10.1038/mt.2012.7.
- [280] Ma, Z.; Li, J.; He, F.; Wilson, A.; Pitt, B.; Li, S. Cationic lipids enhance siRNA-mediated interferon response in mice. *Biochemical and Biophysical Research Communications* **2005**, *330*, 755–759. DOI: 10.1016/j.bbrc.2005.03.041.
- [281] Plataniias, L. C. Mechanisms of type-I- and type-II-interferon-mediated signalling. *Nat Rev Immunol* **2005**, *5*, 375–386. DOI: 10.1038/nri1604.
- [282] Landesman-Milo, D.; Peer, D. Toxicity profiling of several common RNAi-based nanomedicines: a comparative study. *Drug Deliv. and Transl. Res.* **2014**, *4*, 96–103. DOI: 10.1007/s13346-013-0158-7.
- [283] Han, X.; Zhang, H.; Butowska, K.; Swingle, K. L.; Alameh, M.-G.; Weissman, D.; Mitchell, M. J. An ionizable lipid toolbox for RNA delivery. *Nat Commun* **2021**, *12*, 7233. DOI: 10.1038/s41467-021-27493-0.
- [284] Semple, S. C.; Akinc, A.; Chen, J.; Sandhu, A. P.; Mui, B. L.; Cho, C. K.; Sah, D. W. Y.; Stebbing, D.; Crosley, E. J.; Yaworski, E.; *et al.* Rational design of cationic lipids for siRNA delivery. *Nat Biotechnol* **2010**, *28*, 172–176. DOI: 10.1038/nbt.1602.
- [285] Cullis, P. R.; Hope, M. J. Lipid Nanoparticle Systems for Enabling Gene Therapies. *Molecular therapy : the journal of the American Society of Gene Therapy* **2017**, *25*, 1467-1475. DOI: 10.1016/j.ymthe.2017.03.013.
- [286] Semple, S. C.; Klimuk, S. K.; Harasym, T. O.; Dos Santos, N.; Ansell, S. M.; Wong, K. F.; Maurer, N.; Stark, H.; Cullis, P. R.; Hope, M. J.; *et al.* Efficient encapsulation of antisense oligonucleotides in lipid vesicles using ionizable aminolipids: formation of novel small multilamellar vesicle structures. *Biochimica et Biophysica Acta (BBA) - Biomembranes* **2001**, *1510*, 152–166. DOI: 10.1016/s0005-2736(00)00343-6.
- [287] Cheng, X.; Lee, R. J. The role of helper lipids in lipid nanoparticles (LNPs) designed for oligonucleotide delivery. *Advanced Drug Delivery Reviews* **2016**, *99*, 129–137. DOI: 10.1016/j.addr.2016.01.022.
- [288] Briuglia, M.-L.; Rotella, C.; McFarlane, A.; Lamprou, D. A. Influence of cholesterol on liposome stability and on in vitro drug release. *Drug Deliv. and Transl. Res.* **2015**, *5*, 231-242. DOI: 10.1007/s13346-015-0220-8.
- [289] Gregoriadis, G.; Davis, C. Stability of liposomes in vivo and in vitro is promoted by their cholesterol content and the presence of blood cells. *Biochemical and Biophysical Research Communications* **1979**, *89*, 1287–1293. DOI: 10.1016/0006-291X(79)92148-X.

- [290] Kirby, C.; Clarke, J.; Gregoriadis, G. Effect of the cholesterol content of small unilamellar liposomes on their stability in vivo and in vitro. *Biochem J* **1980**, *186*, 591–598. DOI: 10.1042/bj1860591.
- [291] Li, W.; Szoka, F. C. Lipid-based nanoparticles for nucleic acid delivery. *Pharm Res* **2007**, *24*, 438–449. DOI: 10.1007/s11095-006-9180-5.
- [292] Pasut, G.; Zalipsky, S. *Polymer-Protein Conjugates: From Pegylation and Beyond*; Elsevier: Amsterdam, 2020.
- [293] Klibanov, A. L.; Maruyama, K.; Torchilin, V. P.; Huang, L. Amphipathic polyethyleneglycols effectively prolong the circulation time of liposomes. *FEBS letters* **1990**, *268*, 235–237. DOI: 10.1016/0014-5793(90)81016-H.
- [294] Gref, R.; Minamitake, Y.; Peracchia, M. T.; Trubetsky, V.; Torchilin, V.; Langer, R. Biodegradable long-circulating polymeric nanospheres. *Science (New York, N.Y.)* **1994**, *263*, 1600–1603. DOI: 10.1126/science.8128245.
- [295] Yang, Q.; Lai, S. K. Anti-PEG immunity: emergence, characteristics, and unaddressed questions. *Wiley Interdisciplinary Reviews: Nanomedicine and Nanobiotechnology* **2015**, *7*, 655–677. DOI: 10.1002/wnan.1339.
- [296] Zhang, P.; Sun, F.; Liu, S.; Jiang, S. Anti-PEG antibodies in the clinic: Current issues and beyond PEGylation. *Journal of controlled release : official journal of the Controlled Release Society* **2016**, *244*, 184–193. DOI: 10.1016/j.jconrel.2016.06.040.
- [297] Cheng, Q.; Wei, T.; Farbiak, L.; Johnson, L. T.; Dilliard, S. A.; Siegwart, D. J. Selective organ targeting (SORT) nanoparticles for tissue-specific mRNA delivery and CRISPR-Cas gene editing. *Nat. Nanotechnol.* **2020**, *15*, 313–320. DOI: 10.1038/s41565-020-0669-6.
- [298] Dilliard, S. A.; Cheng, Q.; Siegwart, D. J. On the mechanism of tissue-specific mRNA delivery by selective organ targeting nanoparticles. *PNAS* **2021**, *118*, e2109256118. DOI: 10.1073/pnas.2109256118.
- [299] Veiga, N.; Goldsmith, M.; Granot, Y.; Rosenblum, D.; Dammes, N.; Kedmi, R.; Ramishetti, S.; Peer, D. Cell specific delivery of modified mRNA expressing therapeutic proteins to leukocytes. *Nat Commun* **2018**, *9*, 4493. DOI: 10.1038/s41467-018-06936-1.
- [300] Giacca, M.; Zacchigna, S. Virus-mediated gene delivery for human gene therapy. *Journal of controlled release : official journal of the Controlled Release Society* **2012**, *161*, 377–388. DOI: 10.1016/j.jconrel.2012.04.008.
- [301] Ramani, K.; Hassan, Q.; Venkaiah, B.; Hasnain, S. E.; Sarkar, D. P. Site-specific gene delivery in vivo through engineered Sendai viral envelopes. *Proceedings of the National Academy of Sciences of the United States of America* **1998**, *95*, 11886–11890. DOI: 10.1073/pnas.95.20.11886.
- [302] Wu, G. Y.; Wu, C. H. Receptor-mediated in vitro gene transformation by a soluble DNA carrier system. *Journal of Biological Chemistry* **1987**, *262*, 4429–4432. DOI: 10.1016/S0021-9258(18)61209-8.
- [303] Chen, S.; Huang, S.; Li, Y.; Zhou, C. Recent Advances in Epsilon-Poly-L-Lysine and L-Lysine-Based Dendrimer Synthesis, Modification, and Biomedical Applications. *Front. Chem.* **2021**, *9*, 659304. DOI: 10.3389/fchem.2021.659304.
- [304] Akinc, A.; Thomas, M.; Klibanov, A. M.; Langer, R. Exploring polyethylenimine-mediated DNA transfection and the proton sponge hypothesis. *The Journal of Gene Medicine* **2005**, *7*, 657–663. DOI: 10.1002/jgm.696.
- [305] Boussif, O.; Lezoualc'h, F.; Zanta, M. A.; Mergny, M. D.; Scherman, D.; Demeneix, B.; Behr, J. P. A versatile vector for gene and oligonucleotide transfer into cells in culture and in vivo: polyethylenimine. *Proceedings of the National Academy of Sciences of the United States of America* **1995**, *92*, 7297–7301. DOI: 10.1073/pnas.92.16.7297.
- [306] Lungwitz, U.; Breunig, M.; Blunk, T.; Göpferich, A. Polyethylenimine-based non-viral gene delivery systems. *European Journal of Pharmaceutics and Biopharmaceutics* **2005**, *60*, 247–266. DOI: 10.1016/j.ejpb.2004.11.011.

- [307] Wang, H.; Alarcón, C. N.; Liu, B.; Watson, F.; Searles, S.; Lee, C. K.; Keys, J.; Pi, W.; Allen, D.; Lammerding, J.; *et al.* Genetically engineered and enucleated human mesenchymal stromal cells for the targeted delivery of therapeutics to diseased tissue. *Nat. Biomed. Eng* **2022**, *6*, 882–897. DOI: 10.1038/s41551-021-00815-9.
- [308] Ye, B.; Zhao, B.; Wang, K.; Guo, Y.; Lu, Q.; Zheng, L.; Li, A.; Qiao, J. Neutrophils mediated multistage nanoparticle delivery for prompting tumor photothermal therapy. *J Nanobiotechnol* **2020**, *18*, 138. DOI: 10.1186/s12951-020-00682-7.
- [309] Glassman, P. M.; Hood, E. D.; Ferguson, L. T.; Zhao, Z.; Siegel, D. L.; Mitragotri, S.; Brenner, J. S.; Muzykantov, V. R. Red blood cells: The metamorphosis of a neglected carrier into the natural mothership for artificial nanocarriers. *Advanced Drug Delivery Reviews* **2021**, *178*, 113992. DOI: 10.1016/j.addr.2021.113992.
- [310] Geng, Y.; Duan, H.; Xu, L.; Witman, N.; Yan, B.; Yu, Z.; Wang, H.; Tan, Y.; Lin, L.; Li, D.; *et al.* BMP-2 and VEGF-A modRNAs in collagen scaffold synergistically drive bone repair through osteogenic and angiogenic pathways. *Commun Biol* **2021**, *4*, 82. DOI: 10.1038/s42003-020-01606-9.
- [311] Levy, O.; Zhao, W.; Mortensen, L. J.; LeBlanc, S.; Tsang, K.; Fu, M.; Phillips, J. A.; Sagar, V.; Anandakumaran, P.; Ngai, J.; *et al.* mRNA-engineered mesenchymal stem cells for targeted delivery of interleukin-10 to sites of inflammation. *Blood* **2013**, *122*, e23-32. DOI: 10.1182/blood-2013-04-495119.
- [312] Sahoo, S.; Adamiak, M.; Mathiyalagan, P.; Kenneweg, F.; Kafert-Kasting, S.; Thum, T. Therapeutic and Diagnostic Translation of Extracellular Vesicles in Cardiovascular Diseases: Roadmap to the Clinic. *Circulation* **2021**, *143*, 1426–1449. DOI: 10.1161/CIRCULATIONAHA.120.049254.
- [313] O'Brien, K.; Breyne, K.; Ughetto, S.; Laurent, L. C.; Breakefield, X. O. RNA delivery by extracellular vesicles in mammalian cells and its applications. *Nat Rev Mol Cell Biol* **2020**, *21*, 585–606. DOI: 10.1038/s41580-020-0251-y.
- [314] Kalluri, R.; LeBleu, V. S. The biology, function, and biomedical applications of exosomes. *Science* **2020**, *367*. DOI: 10.1126/science.aau6977.
- [315] Nayak, S.; Herzog, R. W. Progress and prospects: immune responses to viral vectors. *Gene Ther* **2010**, *17*, 295–304. DOI: 10.1038/gt.2009.148.
- [316] Lv, H.; Zhang, S.; Wang, B.; Cui, S.; Yan, J. Toxicity of cationic lipids and cationic polymers in gene delivery. *Journal of Controlled Release* **2006**, *114*, 100–109. DOI: 10.1016/j.jconrel.2006.04.014.
- [317] Depmeier, H.; Hoffmann, E.; Bornewasser, L.; Kath-Schorr, S. Strategies for Covalent Labeling of Long RNAs. *ChemBioChem* **2021**, *22*, 2826–2847. DOI: 10.1002/cbic.202100161.
- [318] Scinto, S. L.; Bilodeau, D. A.; Hincapie, R.; Lee, W.; Nguyen, S. S.; Xu, M.; Ende, C. W. am; Finn, M. G.; Lang, K.; Lin, Q.; *et al.* Bioorthogonal chemistry. *Nat Rev Methods Primers* **2021**, *1*, 1–23. DOI: 10.1038/s43586-021-00028-z.
- [319] Sletten, E. M.; Bertozzi, C. R. From mechanism to mouse: a tale of two bioorthogonal reactions. *Accounts of Chemical Research* **2011**, *44*, 666–676. DOI: 10.1021/ar200148z.
- [320] Kolb, H. C.; Finn, M. G.; Sharpless, K. B. Click Chemistry: Diverse Chemical Function from a Few Good Reactions. *Angew. Chem. Int. Ed. Engl.* **2001**, *40*, 2004–2021. DOI: 10.1002/1521-3773(20010601)40:11<2004:AID-ANIE2004>3.0.CO;2-5.
- [321] Knall, A.-C.; Slugovc, C. Inverse electron demand Diels-Alder (IEDDA)-initiated conjugation: a (high) potential click chemistry scheme. *Chem. Soc. Rev.* **2013**, *42*, 5131-5142. DOI: 10.1039/C3CS60049A.
- [322] Tornøe, C. W.; Christensen, C.; Meldal, M. Peptidotriazoles on solid phase: 1,2,3-triazoles by regioselective copper(i)-catalyzed 1,3-dipolar cycloadditions of terminal alkynes to azides. *The Journal of organic chemistry* **2002**, *67*, 3057–3064. DOI: 10.1021/jo011148j.

- [323] Rostovtsev, V. V.; Green, L. G.; Fokin, V. V.; Sharpless, K. B. A Stepwise Huisgen Cycloaddition Process: Copper(I)-Catalyzed Regioselective “Ligation” of Azides and Terminal Alkynes. *Angew. Chem.* **2002**, *114*, 2708–2711. DOI: 10.1002/1521-3757(20020715)114:14<2708:AID-ANGE2708>3.0.CO;2-0.
- [324] Jewett, J. C.; Bertozzi, C. R. Cu-free click cycloaddition reactions in chemical biology. *Chem. Soc. Rev.* **2010**, *39*, 1272–1279. DOI: 10.1039/B901970G.
- [325] Bashkin, J. K.; Jenkins, L. A. The Role of Metals in the Hydrolytic Cleavage of DNA and RNA. *Comments on Inorganic Chemistry* **1994**, *16*, 77–93. DOI: 10.1080/02603599408035852.
- [326] Yang, J.; Liang, Y.; Šečkutė, J.; Houk, K. N.; Devaraj, N. K. Synthesis and reactivity comparisons of 1-methyl-3-substituted cyclopropene mini-tags for tetrazine bioorthogonal reactions. *Chemistry – A European Journal* **2014**, *20*, 3365–3375. DOI: 10.1002/chem.201304225.
- [327] Devaraj, N. Advancing Tetrazine Bioorthogonal Reactions through the Development of New Synthetic Tools. *Synlett* **2012**, *23*, 2147–2152. DOI: 10.1055/s-0032-1317043.
- [328] Wiczorek, A.; Buckup, T.; Wombacher, R. Rigid tetrazine fluorophore conjugates with fluorogenic properties in the inverse electron demand Diels-Alder reaction. *Org. Biomol. Chem.* **2014**, *12*, 4177–4185. DOI: 10.1039/C4OB00245H.
- [329] Devaraj, N. K.; Hilderbrand, S.; Upadhyay, R.; Mazitschek, R.; Weissleder, R. Bioorthogonal Turn-On Probes for Imaging Small Molecules inside Living Cells. *Angew. Chem.* **2010**, *122*, 2931–2934. DOI: 10.1002/ange.200906120.
- [330] Siegl, S. J.; Galeta, J.; Dzijak, R.; Vázquez, A.; Del Río-Villanueva, M.; Dračinský, M.; Vrabel, M. An Extended Approach for the Development of Fluorogenic trans-Cyclooctene-Tetrazine Cycloadditions. *ChemBioChem* **2019**, *20*, 886–890. DOI: 10.1002/cbic.201800711.
- [331] Wiczorek, A.; Werther, P.; Euchner, J.; Wombacher, R. Green- to far-red-emitting fluorogenic tetrazine probes - synthetic access and no-wash protein imaging inside living cells. *Chemical science* **2017**, *8*, 1506–1510. DOI: 10.1039/C6SC03879D.
- [332] Domnick, C.; Eggert, F.; Kath-Schorr, S. Site-specific enzymatic introduction of a norbornene modified unnatural base into RNA and application in post-transcriptional labeling. *Chem. Commun.* **2015**, *51*, 8253–8256. DOI: 10.1039/C5CC01765C.
- [333] Eggert, F.; Kulikov, K.; Domnick, C.; Leifels, P.; Kath-Schorr, S. Illuminated by foreign letters - Strategies for site-specific cyclopropene modification of large functional RNAs via in vitro transcription. *Methods* **2017**, *120*, 17–27. DOI: 10.1016/j.ymeth.2017.04.021.
- [334] Pyka, A. M.; Domnick, C.; Braun, F.; Kath-Schorr, S. Diels-Alder cycloadditions on synthetic RNA in mammalian cells. *Bioconjugate Chemistry* **2014**, *25*, 1438–1443. DOI: 10.1021/bc500302y.
- [335] Croce, S.; Serdjukow, S.; Carell, T.; Frischmuth, T. Chemoenzymatic Preparation of Functional Click-Labeled Messenger RNA. *ChemBioChem* **2020**, *21*, 1641–1646. DOI: 10.1002/cbic.201900718.
- [336] Anhäuser, L.; Hüwel, S.; Zobel, T.; Rentmeister, A. Multiple covalent fluorescence labeling of eukaryotic mRNA at the poly(A) tail enhances translation and can be performed in living cells. *Nucleic Acids Res* **2019**, *47*, e42. DOI: 10.1093/nar/gkz084.
- [337] Agard, N. J.; Prescher, J. A.; Bertozzi, C. R. A strain-promoted 3 + 2 azide-alkyne cycloaddition for covalent modification of biomolecules in living systems. *Journal of the American Chemical Society* **2004**, *126*, 15046–15047. DOI: 10.1021/ja044996f.
- [338] Sahu, I. D.; Lorigan, G. A. Electron Paramagnetic Resonance as a Tool for Studying Membrane Proteins. *Biomolecules* **2020**, *10*, 763. DOI: 10.3390/biom10050763.
- [339] NejatyJahromy, Y.; Schubert, E. *Demystifying EPR: A Rookie Guide to the Application of Electron Paramagnetic Resonance Spectroscopy on Biomolecules*; PROGRESS IN BIOLOGICAL SCIENCES, 2014.

- [340] Jeschke, G. Distance Measurements in the Nanometer Range by Pulse EPR. *ChemPhysChem* **2002**, *3*, 927–932. DOI: 10.1002/1439-7641(20021115)3:11<927:AID-CPHC927>3.0.CO;2-Q.
- [341] Torricella, F.; Pierro, A.; Mileo, E.; Belle, V.; Bonucci, A. Nitroxide spin labels and EPR spectroscopy: A powerful association for protein dynamics studies. *Biochimica et biophysica acta. Proteins and proteomics* **2021**, *1869*, 140653. DOI: 10.1016/j.bbapap.2021.140653.
- [342] Piton, N.; Mu, Y.; Stock, G.; Prisner, T. F.; Schiemann, O.; Engels, J. W. Base-specific spin-labeling of RNA for structure determination. *Nucleic Acids Research* **2007**, *35*, 3128–3143. DOI: 10.1093/nar/gkm169.
- [343] Kerzhner, M.; Abdullin, D.; Więcek, J.; Matsuoka, H.; Hagelueken, G.; Schiemann, O.; Famulok, M. Post-synthetic Spin-Labeling of RNA through Click Chemistry for PELDOR Measurements. *Chemistry – A European Journal* **2016**, *22*, 12113–12121. DOI: 10.1002/chem.201601897.
- [344] Schiemann, O.; Piton, N.; Plackmeyer, J.; Bode, B. E.; Prisner, T. F.; Engels, J. W. Spin labeling of oligonucleotides with the nitroxide TPA and use of PELDOR, a pulse EPR method, to measure intramolecular distances. *Nat Protoc* **2007**, *2*, 904–923. DOI: 10.1038/nprot.2007.97.
- [345] Gophane, D. B.; Endeward, B.; Prisner, T. F.; Sigurdsson, S. T. A semi-rigid isoindoline-derived nitroxide spin label for RNA. *Org. Biomol. Chem.* **2018**, *16*, 816–824. DOI: 10.1039/c7ob02870a.
- [346] Halbmaier, K.; Seikowski, J.; Tkach, I.; Höbartner, C.; Sezer, D.; Bennati, M. High-resolution measurement of long-range distances in RNA: pulse EPR spectroscopy with TEMPO-labeled nucleotides. *Chemical science* **2016**, *7*, 3172–3180. DOI: 10.1039/C5SC04631A.
- [347] Krstić, I.; Hänsel, R.; Romainczyk, O.; Engels, J. W.; Dötsch, V.; Prisner, T. F. Long-range distance measurements on nucleic acids in cells by pulsed EPR spectroscopy. *Angew. Chem. Int. Ed. Engl.* **2011**, *50*, 5070–5074. DOI: 10.1002/anie.201100886.
- [348] Kerzhner, M.; Matsuoka, H.; Wuebben, C.; Famulok, M.; Schiemann, O. High-Yield Spin Labeling of Long RNAs for Electron Paramagnetic Resonance Spectroscopy. *Biochemistry* **2018**, *57*, 2923–2931. DOI: 10.1021/acs.biochem.8b00040.
- [349] Grytz, C. M.; Marko, A.; Cekan, P.; Sigurdsson, S. T.; Prisner, T. F. Flexibility and conformation of the cocaine aptamer studied by PELDOR. *Physical chemistry chemical physics : PCCP* **2016**, *18*, 2993–3002. DOI: 10.1039/C5CP06158J.
- [350] Büttner, L.; Seikowski, J.; Wawrzyniak, K.; Ochmann, A.; Höbartner, C. Synthesis of spin-labeled riboswitch RNAs using convertible nucleosides and DNA-catalyzed RNA ligation. *Bioorganic & medicinal chemistry* **2013**, *21*, 6171–6180. DOI: 10.1016/j.bmc.2013.04.007.
- [351] Höbartner, C.; Sicoli, G.; Wachowius, F.; Gophane, D. B.; Sigurdsson, S. T. Synthesis and characterization of RNA containing a rigid and nonperturbing cytidine-derived spin label. *The Journal of organic chemistry* **2012**, *77*, 7749–7754. DOI: 10.1021/jo301227w.
- [352] Saha, S.; Jagtap, A. P.; Sigurdsson, S. T. Site-directed spin labeling of 2'-amino groups in RNA with isoindoline nitroxides that are resistant to reduction. *Chem. Commun.* **2015**, *51*, 13142–13145. DOI: 10.1039/c5cc05014f.
- [353] Kaminker, I.; Bye, M.; Mendelman, N.; Gislason, K.; Sigurdsson, S. T.; Goldfarb, D. Distance measurements between manganese(II) and nitroxide spin-labels by DEER determine a binding site of Mn(2+) in the HP92 loop of ribosomal RNA. *Physical chemistry chemical physics : PCCP* **2015**, *17*, 15098–15102. DOI: 10.1039/C5CP01624J.
- [354] Qin, P. Z.; Butcher, S. E.; Feigon, J.; Hubbell, W. L. Quantitative analysis of the isolated GAAA tetraloop/receptor interaction in solution: a site-directed spin labeling study. *Biochemistry* **2001**, *40*, 6929–6936. DOI: 10.1021/bi010294g.

- [355] Schiemann, O.; Weber, A.; Edwards, T. E.; Prisner, T. F.; Sigurdsson, S. T. Nanometer distance measurements on RNA using PELDOR. *Journal of the American Chemical Society* **2003**, *125*, 3434–3435. DOI: 10.1021/ja0274610.
- [356] Weng, Y.; Li, C.; Yang, T.; Hu, B.; Zhang, M.; Guo, S.; Xiao, H.; Liang, X.-J.; Huang, Y. The challenge and prospect of mRNA therapeutics landscape. *Biotechnology Advances* **2020**, *40*, 107534. DOI: 10.1016/j.biotechadv.2020.107534.
- [357] Shaner, N. C.; Campbell, R. E.; Steinbach, P. A.; Giepmans, B. N. G.; Palmer, A. E.; Tsien, R. Y. Improved monomeric red, orange and yellow fluorescent proteins derived from *Discosoma* sp. red fluorescent protein. *Nat Biotechnol* **2004**, *22*, 1567–1572. DOI: 10.1038/nbt1037.
- [358] Peng, Z.-H.; Sharma, V.; Singleton, S. F.; Gershon, P. D. Synthesis and application of a chain-terminating dinucleotide mRNA cap analog. *Organic Letters* **2002**, *4*, 161–164. DOI: 10.1021/ol0167715.
- [359] Jemielity, J.; FOWLER, T.; Zuberek, J.; STEPINSKI, J.; LEWDOROWICZ, M.; NIEDZWIECKA, A.; STOLARSKI, R.; Darzynkiewicz, E.; RHOADS, R. E. Novel "anti-reverse" cap analogs with superior translational properties. *RNA* **2003**, *9*, 1108–1122. DOI: 10.1261/rna.5430403.
- [360] Kirschman, J. L.; Bhosle, S.; Vanover, D.; Blanchard, E. L.; Loomis, K. H.; Zurla, C.; Murray, K.; Lam, B. C.; Santangelo, P. J. Characterizing exogenous mRNA delivery, trafficking, cytoplasmic release and RNA-protein correlations at the level of single cells. *Nucleic Acids Res* **2017**, *45*, e113. DOI: 10.1093/nar/gkx290.
- [361] Surre, J.; Saint-Ruf, C.; Collin, V.; Oregna, S.; Ramjeet, M.; Matic, I. Strong increase in the autofluorescence of cells signals struggle for survival. *Sci Rep* **2018**, *8*, 12088. DOI: 10.1038/s41598-018-30623-2.
- [362] Kolenc, O. I.; Quinn, K. P. Evaluating Cell Metabolism Through Autofluorescence Imaging of NAD(P)H and FAD. *Antioxidants & redox signaling* **2019**, *30*, 875–889. DOI: 10.1089/ars.2017.7451.
- [363] Heikal, A. A. Intracellular coenzymes as natural biomarkers for metabolic activities and mitochondrial anomalies. *Biomarkers in medicine* **2010**, *4*, 241–263. DOI: 10.2217/bmm.10.1.
- [364] Bartolomé, F.; Abramov, A. Y. Measurement of Mitochondrial NADH and FAD Autofluorescence in Live Cells. In *Probing mitochondrial function*; Weissig, V., Edeas, M., Eds.; Humana Pr: New York, NY, 2015; pp 263–270.
- [365] Fiszer-Kierzkowska, A.; Vydra, N.; Wysocka-Wycisk, A.; Kronekova, Z.; Jarzab, M.; Lisowska, K. M.; Krawczyk, Z. Liposome-based DNA carriers may induce cellular stress response and change gene expression pattern in transfected cells. *BMC molecular biology* **2011**, *12*, 27. DOI: 10.1186/1471-2199-12-27.
- [366] Kauffman, K. J.; Mir, F. F.; Jhunjunwala, S.; Kaczmarek, J. C.; Hurtado, J. E.; Yang, J. H.; Webber, M. J.; Kowalski, P. S.; Heartlein, M. W.; DeRosa, F.; *et al.* Efficacy and immunogenicity of unmodified and pseudouridine-modified mRNA delivered systemically with lipid nanoparticles in vivo. *Biomaterials* **2016**, *109*, 78–87. DOI: 10.1016/j.biomaterials.2016.09.006.
- [367] Chlebowski, A.; Lubas, M.; Jensen, T. H.; Dziembowski, A. RNA decay machines: the exosome. *Biochimica et biophysica acta* **2013**, *1829*, 552–560. DOI: 10.1016/j.bbagr.2013.01.006.
- [368] Zinder, J. C.; Lima, C. D. Targeting RNA for processing or destruction by the eukaryotic RNA exosome and its cofactors. *Genes Dev.* **2017**, *31*, 88–100. DOI: 10.1101/gad.294769.116.
- [369] Warren, L.; Manos, P. D.; Ahfeldt, T.; Loh, Y.-H.; Li, H.; Lau, F.; Ebina, W.; Mandal, P. K.; Smith, Z. D.; Meissner, A.; *et al.* Highly efficient reprogramming to pluripotency and directed differentiation of human cells with synthetic modified mRNA. *Cell Stem Cell* **2010**, *7*, 618–630. DOI: 10.1016/j.stem.2010.08.012.

- [370] Parr, C. J. C.; Wada, S.; Kotake, K.; Kameda, S.; Matsuura, S.; Sakashita, S.; Park, S.; Sugiyama, H.; Kuang, Y.; Saito, H. N 1-Methylpseudouridine substitution enhances the performance of synthetic mRNA switches in cells. *Nucleic Acids Research* **2020**, *48*, e35. DOI: 10.1093/nar/gkaa070.
- [371] Collart, M. A.; Weiss, B. Ribosome pausing, a dangerous necessity for co-translational events. *Nucleic Acids Research* **2020**, *48*, 1043–1055. DOI: 10.1093/nar/gkz763.
- [372] Komar, A. A. A pause for thought along the co-translational folding pathway. *Trends in Biochemical Sciences* **2009**, *34*, 16–24. DOI: 10.1016/j.tibs.2008.10.002.
- [373] Marshall, E.; Stansfield, I.; Romano, M. C. Ribosome recycling induces optimal translation rate at low ribosomal availability. *J. R. Soc. Interface.* **2014**, *11*, 20140589. DOI: 10.1098/rsif.2014.0589.
- [374] Decatur, W. A.; Fournier, M. J. rRNA modifications and ribosome function. *Trends in Biochemical Sciences* **2002**, *27*, 344–351. DOI: 10.1016/S0968-0004(02)02109-6.
- [375] Ofengand, J. Ribosomal RNA pseudouridines and pseudouridine synthases. *FEBS letters* **2002**, *514*, 17–25. DOI: 10.1016/S0014-5793(02)02305-0.
- [376] Kierzek, E.; Malgowska, M.; Lisowiec, J.; Turner, D. H.; Gdaniec, Z.; Kierzek, R. The contribution of pseudouridine to stabilities and structure of RNAs. *Nucleic Acids Research* **2014**, *42*, 3492–3501. DOI: 10.1093/nar/gkt1330.
- [377] Mauger, D. M.; Cabral, B. J.; Presnyak, V.; Su, S. V.; Reid, D. W.; Goodman, B.; Link, K.; Khatwani, N.; Reynders, J.; Moore, M. J.; *et al.* mRNA structure regulates protein expression through changes in functional half-life. *PNAS* **2019**, *116*, 24075–24083. DOI: 10.1073/pnas.1908052116.
- [378] Li, X.; Ma, S.; Yi, C. Pseudouridine: the fifth RNA nucleotide with renewed interests. *Current Opinion in Chemical Biology* **2016**, *33*, 108–116. DOI: 10.1016/j.cbpa.2016.06.014.
- [379] Mayr, C. Regulation by 3'-Untranslated Regions. *Annual review of genetics* **2017**, *51*, 171–194. DOI: 10.1146/annurev-genet-120116-024704.
- [380] Ehrenfeld, E.; Hunt, T. Double-stranded poliovirus RNA inhibits initiation of protein synthesis by reticulocyte lysates. *Proceedings of the National Academy of Sciences of the United States of America* **1971**, *68*, 1075–1078. DOI: 10.1073/pnas.68.5.1075.
- [381] Hunt, T.; Ehrenfeld, E. Cytoplasm from poliovirus-infected HeLa cells inhibits cell-free haemoglobin synthesis. *Nature: New biology* **1971**, *230*, 91–94. DOI: 10.1038/newbio230091a0.
- [382] Grimson, A.; Farh, K. K.-H.; Johnston, W. K.; Garrett-Engele, P.; Lim, L. P.; Bartel, D. P. MicroRNA targeting specificity in mammals: determinants beyond seed pairing. *Molecular cell* **2007**, *27*, 91–105. DOI: 10.1016/j.molcel.2007.06.017.
- [383] Gu, S.; Kay, M. A. How do miRNAs mediate translational repression? *Silence* **2010**, *1*, 11. DOI: 10.1186/1758-907X-1-11.
- [384] Granot, Y.; Peer, D. Delivering the right message: Challenges and opportunities in lipid nanoparticles-mediated modified mRNA therapeutics-An innate immune system standpoint. *Seminars in Immunology* **2017**, *34*, 68–77. DOI: 10.1016/j.smim.2017.08.015.
- [385] Wadhwa, A.; Aljabbari, A.; Lokras, A.; Foged, C.; Thakur, A. Opportunities and Challenges in the Delivery of mRNA-based Vaccines. *Pharmaceutics* **2020**, *12*. DOI: 10.3390/pharmaceutics12020102.
- [386] Endeward, B.; Marko, A.; Denysenkov, V. P.; Sigurdsson, S.T.; Prisner, T. F. Chapter Fourteen - Advanced EPR Methods for Studying Conformational Dynamics of Nucleic Acids. In *Methods in Enzymology : Structures of Large RNA Molecules and Their Complexes*; Woodson, S. A., Allain, F. H.T., Eds.; Academic Press, 2015; pp 403–425.
- [387] Schiemann, O.; Cekan, P.; Margraf, D.; Prisner, T. F.; Sigurdsson, S. T. Relative Orientation of Rigid Nitroxides by PELDOR: Beyond Distance Measurements in Nucleic Acids. *Angew. Chem.* **2009**, *121*, 3342–3345. DOI: 10.1002/ange.200805152.

- [388] Kamble, N. R.; Gränz, M.; Prisner, T. F.; Sigurdsson, S. T. Noncovalent and site-directed spin labeling of duplex RNA. *Chem. Commun.* **2016**, *52*, 14442–14445. DOI: 10.1039/c6cc08387k.
- [389] Piton, N.; Schiemann, O.; Mu, Y.; Stock, G.; Prisner, T.; Engels, J. W. Synthesis of spin-labeled RNAs for long range distance measurements by peldor. *Nucleosides, nucleotides & nucleic acids* **2005**, *24*, 771–775. DOI: 10.1081/NCN-200060139.
- [390] Milov, A.; Salikhov, K.; Shirov, M. Application of ELDOR in electron-spin echo for paramagnetic center space distribution in solids. *Fiz. Tverd. Tela* **1981**, 975–982.
- [391] Martin, R. E.; Pannier, M.; Diederich, F.; Gramlich, V.; Hubrich, M.; Spiess, H. W. Determination of End-to-End Distances in a Series of TEMPO Diradicals of up to 2.8 nm Length with a New Four-Pulse Double Electron Electron Resonance Experiment. *Angew. Chem. Int. Ed. Engl.* **1998**, *37*, 2833–2837. DOI: 10.1002/(SICI)1521-3773(19981102)37:20<2833:AID-ANIE2833>3.0.CO;2-7.
- [392] Sicoli, G.; Wachowius, F.; Bennati, M.; Höbartner, C. Probing secondary structures of spin-labeled RNA by pulsed EPR spectroscopy. *Angew. Chem. Int. Ed. Engl.* **2010**, *49*, 6443–6447. DOI: 10.1002/anie.201000713.
- [393] Babaylova, E. S.; Ivanov, A. V.; Malygin, A. A.; Vorobjeva, M. A.; Venyaminova, A. G.; Polienko, Y. F.; Kirilyuk, I. A.; Krumkacheva, O. A.; Fedin, M. V.; Karpova, G. G.; *et al.* A versatile approach for site-directed spin labeling and structural EPR studies of RNAs. *Org. Biomol. Chem.* **2014**, *12*, 3129–3136. DOI: 10.1039/c3ob42154f.
- [394] Weinrich, T.; Jaumann, E. A.; Scheffer, U.; Prisner, T. F.; Göbel, M. W. A Cytidine Phosphoramidite with Protected Nitroxide Spin Label: Synthesis of a Full-Length TAR RNA and Investigation by In-Line Probing and EPR Spectroscopy. *Chemistry – A European Journal* **2018**, *24*, 6202–6207. DOI: 10.1002/chem.201800167.
- [395] Shelke, S. A.; Sigurdsson, S. T. Site-Directed Spin Labelling of Nucleic Acids. *Eur. J. Org. Chem.* **2012**, *2012*, 2291–2301. DOI: 10.1002/ejoc.201101434.
- [396] Esquiaqui, J. M.; Sherman, E. M.; Ye, J.-D.; Fanucci, G. E. Chapter Thirteen - Site-Directed Spin-Labeling Strategies and Electron Paramagnetic Resonance Spectroscopy for Large Riboswitches. In *Methods in Enzymology : Structures of Large RNA Molecules and Their Complexes*; Woodson, S. A., Allain, F. H.T., Eds.; Academic Press, 2015; pp 287–311.
- [397] Esquiaqui, J. M.; Sherman, E. M.; Ye, J.-D.; Fanucci, G. E. Conformational Flexibility and Dynamics of the Internal Loop and Helical Regions of the Kink-Turn Motif in the Glycine Riboswitch by Site-Directed Spin-Labeling. *Biochemistry* **2016**, *55*, 4295–4305. DOI: 10.1021/acs.biochem.6b00287.
- [398] Duss, O.; Yulikov, M.; Jeschke, G.; Allain, F. H.-T. EPR-aided approach for solution structure determination of large RNAs or protein-RNA complexes. *Nat Commun* **2014**, *5*, 3669. DOI: 10.1038/ncomms4669.
- [399] Babaylova, E. S.; Malygin, A. A.; Lomzov, A. A.; Pyshnyi, D. V.; Yulikov, M.; Jeschke, G.; Krumkacheva, O. A.; Fedin, M. V.; Karpova, G. G.; Bagryanskaya, E. G. Complementary-addressed site-directed spin labeling of long natural RNAs. *Nucleic Acids Research* **2016**, *44*, 7935–7943. DOI: 10.1093/nar/gkw516.
- [400] Wuebben, C.; Vicino, M. F.; Mueller, M.; Schiemann, O. Do the P1 and P2 hairpins of the Guanidine-II riboswitch interact? *Nucleic Acids Research* **2020**, *48*, 10518–10526. DOI: 10.1093/nar/gkaa703.
- [401] Endeward, B.; Hu, Y.; Bai, G.; Liu, G.; Prisner, T. F.; Fang, X. Long-range distance determination in fully deuterated RNA with pulsed EPR spectroscopy. *Biophysical journal* **2022**, *121*, 37–43. DOI: 10.1016/j.bpj.2021.12.007.
- [402] Heinz, M.; Erlenbach, N.; Stelzl, L. S.; Thierolf, G.; Kamble, N. R.; Sigurdsson, S. T.; Prisner, T. F.; Hummer, G. High-resolution EPR distance measurements on RNA and DNA with the non-covalent G spin label. *Nucleic Acids Research* **2020**, *48*, 924–933. DOI: 10.1093/nar/gkz1096.

- [403] Wachowius, F.; Höbartner, C. Chemical RNA modifications for studies of RNA structure and dynamics. *ChemBioChem* **2010**, *11*, 469–480. DOI: 10.1002/cbic.200900697.
- [404] Shelke, S. A.; Sigurdsson, S. T. Site-Directed Spin Labelling of Nucleic Acids. *Eur. J. Org. Chem.* **2012**, *2012*, 2291–2301. DOI: 10.1002/ejoc.201101434.
- [405] Lebars, I.; Vileno, B.; Bourbigot, S.; Turek, P.; Wolff, P.; Kieffer, B. A fully enzymatic method for site-directed spin labeling of long RNA. *Nucleic Acids Research* **2014**, *42*, e117. DOI: 10.1093/nar/gku553.
- [406] Wawrzyniak-Turek, K.; Höbartner, C. Deoxyribozyme-Mediated Ligation for Incorporating EPR Spin Labels and Reporter Groups into RNA. In *Methods in Enzymology: Structures of Large RNA Molecules and Their Complexes*; Woodson, S. A., Allain, F. H.T., Eds.; Academic Press, 2015; pp 85–104.
- [407] Pintacuda, G.; Young, A. N.; Cerase, A. Function by Structure: Spotlights on Xist Long Non-coding RNA. *Front. Mol. Biosci.* **2017**, *4*, 90. DOI: 10.3389/fmolb.2017.00090.
- [408] Brockdorff, N. X-chromosome inactivation: closing in on proteins that bind Xist RNA. *Trends in Genetics* **2002**, *18*, 352–358. DOI: 10.1016/S0168-9525(02)02717-8.
- [409] Wutz, A.; Rasmussen, T. P.; Jaenisch, R. Chromosomal silencing and localization are mediated by different domains of Xist RNA. *Nat Genet* **2002**, *30*, 167–174. DOI: 10.1038/ng820.
- [410] Patil, D. P.; Chen, C.-K.; Pickering, B. F.; Chow, A.; Jackson, C.; Guttman, M.; Jaffrey, S. R. m(6)A RNA methylation promotes XIST-mediated transcriptional repression. *Nature* **2016**, *537*, 369–373. DOI: 10.1038/nature19342.
- [411] Fang, R.; Moss, W. N.; Rutenberg-Schoenberg, M.; Simon, M. D. Probing Xist RNA Structure in Cells Using Targeted Structure-Seq. *PLoS Genetics* **2015**, *11*, e1005668. DOI: 10.1371/journal.pgen.1005668.
- [412] Maenner, S.; Blaud, M.; Fouillen, L.; Savoye, A.; Marchand, V.; Dubois, A.; Sanglier-Cianfèrani, S.; van Dorsselaer, A.; Clerc, P.; Avner, P.; et al. 2-D structure of the A region of Xist RNA and its implication for PRC2 association. *PLOS Biology* **2010**, *8*, e1000276. DOI: 10.1371/journal.pbio.1000276.
- [413] Liu, F.; Somarowthu, S.; Pyle, A. M. Visualizing the secondary and tertiary architectural domains of lncRNA RepA. *Nat Chem Biol* **2017**, *13*, 282–289. DOI: 10.1038/nchembio.2272.
- [414] Domnick, C. Expanding the toolbox of modified nucleobases and click chemistry for investigations on non-coding RNA, Universitäts- und Landesbibliothek Bonn, 2019.
- [415] Domnick, C.; Eggert, F.; Wuebben, C.; Bornewasser, L.; Hagelueken, G.; Schiemann, O.; Kath-Schorr, S. EPR Distance Measurements on Long Non-coding RNAs Empowered by Genetic Alphabet Expansion Transcription. *Angew. Chem. Int. Ed. Engl.* **2020**, *59*, 7891–7896. DOI: 10.1002/anie.201916447.
- [416] Zuker, M. Mfold web server for nucleic acid folding and hybridization prediction. *Nucleic Acids Research* **2003**, *31*, 3406–3415. DOI: 10.1093/nar/gkg595.
- [417] Berendsen, H.J.C.; van der Spoel, D.; van Drunen, R. GROMACS: A message-passing parallel molecular dynamics implementation. *Computer Physics Communications* **1995**, *91*, 43–56. DOI: 10.1016/0010-4655(95)00042-E.
- [418] van der Spoel, D.; Lindahl, E.; Hess, B.; Groenhof, G.; Mark, A. E.; Berendsen, H. J. C. GROMACS: fast, flexible, and free. *Journal of computational chemistry* **2005**, *26*, 1701-1718. DOI: 10.1002/jcc.20291.
- [419] Pronk, S.; Páll, S.; Schulz, R.; Larsson, P.; Bjelkmar, P.; Apostolov, R.; Shirts, M. R.; Smith, J. C.; Kasson, P. M.; van der Spoel, D.; et al. GROMACS 4.5: a high-throughput and highly parallel open source molecular simulation toolkit. *Bioinformatics* **2013**, *29*, 845–854. DOI: 10.1093/bioinformatics/btt055.
- [420] Abraham, M. J.; Murtola, T.; Schulz, R.; Páll, S.; Smith, J. C.; Hess, B.; Lindahl, E. GROMACS: High performance molecular simulations through multi-level parallelism from

- laptops to supercomputers. *SoftwareX* **2015**, 1-2, 19–25. DOI: 10.1016/j.softx.2015.06.001.
- [421] Best, R. B.; Zhu, X.; Shim, J.; Lopes, P. E. M.; Mittal, J.; Feig, M.; Mackerell, A. D. Optimization of the additive CHARMM all-atom protein force field targeting improved sampling of the backbone ϕ , ψ and side-chain $\chi(1)$ and $\chi(2)$ dihedral angles. *Journal of Chemical Theory and Computation* **2012**, 8, 3257–3273. DOI: 10.1021/ct300400x.
- [422] Denning, E. J.; Priyakumar, U. D.; Nilsson, L.; Mackerell, A. D. Impact of 2'-hydroxyl sampling on the conformational properties of RNA: update of the CHARMM all-atom additive force field for RNA. *Journal of computational chemistry* **2011**, 32, 1929–1943. DOI: 10.1002/jcc.21777.
- [423] Raman, E. P.; Lemkul, J. A.; Best, R. B.; MacKerell, A. D., JR. http://mackerell.umaryland.edu/charmm_ff.shtml.
- [424] Reginsson, G. W.; Kunjir, N. C.; Sigurdsson, S. T.; Schiemann, O. Trityl radicals: spin labels for nanometer-distance measurements. *Chemistry – A European Journal* **2012**, 18, 13580–13584. DOI: 10.1002/chem.201203014.
- [425] Jassoy, J. J.; Berndhäuser, A.; Duthie, F.; Kühn, S. P.; Hagelueken, G.; Schiemann, O. Versatile Trityl Spin Labels for Nanometer Distance Measurements on Biomolecules In Vitro and within Cells. *Angew. Chem. Int. Ed. Engl.* **2017**, 56, 177–181. DOI: 10.1002/anie.201609085.
- [426] Fleck, N.; Heubach, C. A.; Hett, T.; Haege, F. R.; Bawol, P. P.; Baltruschat, H.; Schiemann, O. SLIM: A Short-Linked, Highly Redox-Stable Trityl Label for High-Sensitivity In-Cell EPR Distance Measurements. *Angew. Chem. Int. Ed. Engl.* **2020**, 59, 9767–9772. DOI: 10.1002/anie.202004452.
- [427] Bonucci, A.; Ouari, O.; Guigliarelli, B.; Belle, V.; Mileo, E. In-Cell EPR: Progress towards Structural Studies Inside Cells. *ChemBioChem* **2020**, 21, 451–460. DOI: 10.1002/cbic.201900291.
- [428] Yang, Y.; Pan, B.-B.; Tan, X.; Yang, F.; Liu, Y.; Su, X.-C.; Goldfarb, D. In-Cell Trityl-Trityl Distance Measurements on Proteins. *The journal of physical chemistry letters* **2020**, 11, 1141–1147. DOI: 10.1021/acs.jpcllett.9b03208.
- [429] Fleck, N.; Heubach, C.; Hett, T.; Spicher, S.; Grimme, S.; Schiemann, O. Ox-SLIM: Synthesis of and Site-Specific Labelling with a Highly Hydrophilic Trityl Spin Label. *Chemistry – A European Journal* **2021**, 27, 5292–5297. DOI: 10.1002/chem.202100013.
- [430] Ketter, S.; Gopinath, A.; Rogozhnikova, O.; Trukhin, D.; Tormyshev, V. M.; Bagryanskaya, E. G.; Joseph, B. In Situ Labeling and Distance Measurements of Membrane Proteins in *E. coli* Using Finland and OX063 Trityl Labels. *Chemistry – A European Journal* **2021**, 27, 2299–2304. DOI: 10.1002/chem.202004606.
- [431] Hasanbasri, Z.; Singewald, K.; Gluth, T. D.; Driesschaert, B.; Saxena, S. Cleavage-Resistant Protein Labeling With Hydrophilic Trityl Enables Distance Measurements In-Cell. *The journal of physical chemistry. B* **2021**, 125, 5265–5274. DOI: 10.1021/acs.jpcc.1c02371.
- [432] Nielsen, H. Working with RNA. *RNA*; Humana Press, 2011; pp 15–28.
- [433] Kibbe, W. A. OligoCalc: an online oligonucleotide properties calculator. *Nucleic Acids Research* **2007**, 35, W43-6. DOI: 10.1093/nar/gkm234.
- [434] Davis, M. W.; Jorgensen, E. M. ApE, A Plasmid Editor: A Freely Available DNA Manipulation and Visualization Program. *Front. Bioinform.* **2022**, 2. DOI: 10.3389/fbinf.2022.818619.
- [435] Benson, D. A.; Cavanaugh, M.; Clark, K.; Karsch-Mizrachi, I.; Lipman, D. J.; Ostell, J.; Sayers, E. W. GenBank. *Nucleic Acids Research* **2013**, 41, D36-42. DOI: 10.1093/nar/gks1195.
- [436] The UniProt Consortium; Bateman, A.; Martin, M.-J.; Orchard, S.; Magrane, M.; Agivetova, R.; Ahmad, S.; Alpi, E.; Bowler-Barnett, E. H.; Britto, R.; *et al.* UniProt: the

- universal protein knowledgebase in 2021. *Nucleic Acids Research* **2021**, *49*, D480-D489. DOI: 10.1093/nar/gkaa1100.
- [437] Untergasser, A.; Cutcutache, I.; Koressaar, T.; Ye, J.; Faircloth, B. C.; Remm, M.; Rozen, S. G. Primer3--new capabilities and interfaces. *Nucleic Acids Research* **2012**, *40*, e115. DOI: 10.1093/nar/gks596.
- [438] Koressaar, T.; Remm, M. Enhancements and modifications of primer design program Primer3. *Bioinformatics* **2007**, *23*, 1289–1291. DOI: 10.1093/bioinformatics/btm091.
- [439] Kõressaar, T.; Lepamets, M.; Kaplinski, L.; Raime, K.; Andreson, R.; Remm, M. Primer3_masker: integrating masking of template sequence with primer design software. *Bioinformatics* **2018**, *34*, 1937–1938. DOI: 10.1093/bioinformatics/bty036.
- [440] Ye, J.; Coulouris, G.; Zaretskaya, I.; Cutcutache, I.; Rozen, S.; Madden, T. L. Primer-BLAST: a tool to design target-specific primers for polymerase chain reaction. *BMC Bioinformatics* **2012**, *13*, 134. DOI: 10.1186/1471-2105-13-134.
- [441] Pattyn, F.; Speleman, F.; Paepe, A. de; Vandesompele, J. RTPrimerDB: the real-time PCR primer and probe database. *Nucleic Acids Research* **2003**, *31*, 122–123. DOI: 10.1093/nar/gkg011.
- [442] Pattyn, F.; Robbrecht, P.; Paepe, A. de; Speleman, F.; Vandesompele, J. RTPrimerDB: the real-time PCR primer and probe database, major update 2006. *Nucleic Acids Research* **2006**, *34*, D684-8. DOI: 10.1093/nar/gkj155.
- [443] Lefever, S.; Vandesompele, J.; Speleman, F.; Pattyn, F. RTPrimerDB: the portal for real-time PCR primers and probes. *Nucleic Acids Research* **2009**, *37*, D942-5. DOI: 10.1093/nar/gkn777.
- [444] Tania Nolan; Jim Huggett; Elena Sanchez; Rebecca Sanders; Nicholas Redshaw; Tim Wilkes. *Good practice guide for the application of quantitative PCR (qPCR)*, 2013.
- [445] Kosugi, S.; Hasebe, M.; Tomita, M.; Yanagawa, H. Systematic identification of cell cycle-dependent yeast nucleocytoplasmic shuttling proteins by prediction of composite motifs. *PNAS* **2009**, *106*, 10171–10176. DOI: 10.1073/pnas.0900604106.
- [446] Brockdorff, N.; Ashworth, A.; Kay, G. F.; McCabe, V. M.; Norris, D. P.; Cooper, P. J.; Swift, S.; Rastan, S. The product of the mouse Xist gene is a 15 kb inactive X-specific transcript containing no conserved ORF and located in the nucleus. *Cell* **1992**, *71*, 515-526. DOI: 10.1016/0092-8674(92)90519-I.

7 Appendix

7.1 Gel electrophoresis images

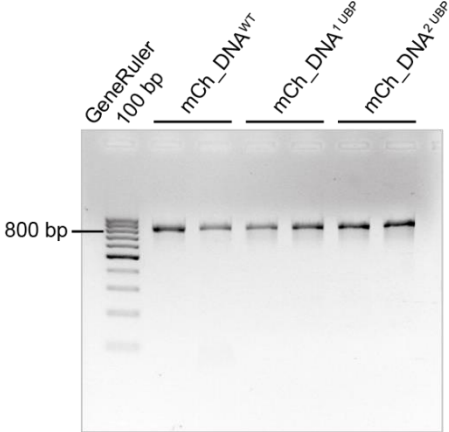


Figure 54. Agarose gel of unmodified and UB-modified *mCh_DNA* PCR products.

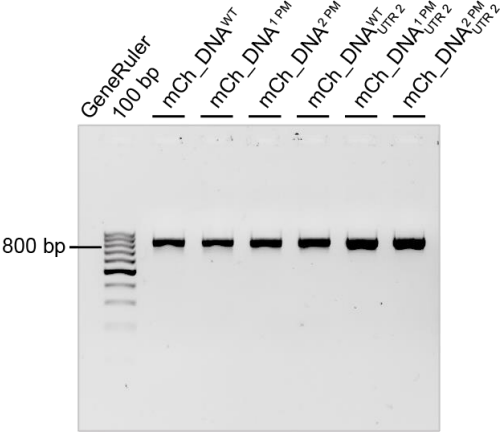


Figure 55. Agarose gel of unmodified and point mutated *mCh_DNA* and *mCh_DNA_{UTR 2}* PCR products.

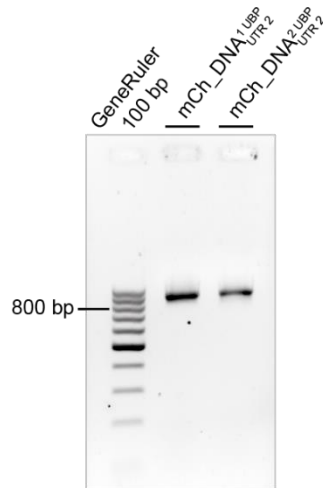


Figure 56. Agarose gel of UB-modified *mCh_DNA_{UTR 2}* PCR products.

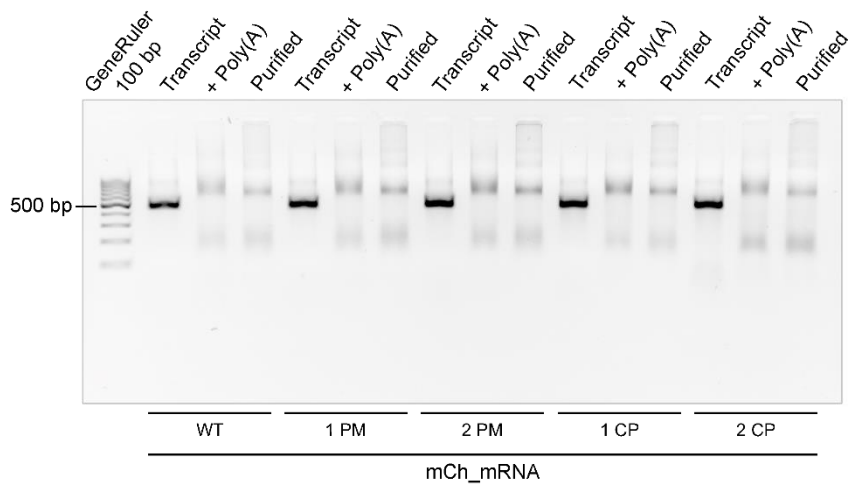


Figure 57. Agarose gel of unmodified, UB-modified and point mutated *mCh_mRNA*. Samples for gel analysis were taken after DNase digestion after IVT (Transcript), after Poly(A) tailing (Poly(A)) and after LiCl precipitation for mRNA purification (Purified).

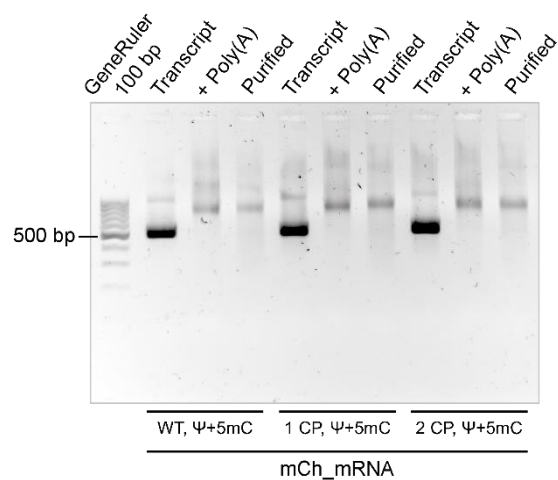


Figure 58. Agarose gel of *mCh_mRNA* with natural base modifications and UB modifications. Samples for gel analysis were taken after DNase digestion after IVT (Transcript), after Poly(A) tailing (Poly(A)) and after LiCl precipitation for mRNA purification (Purified).

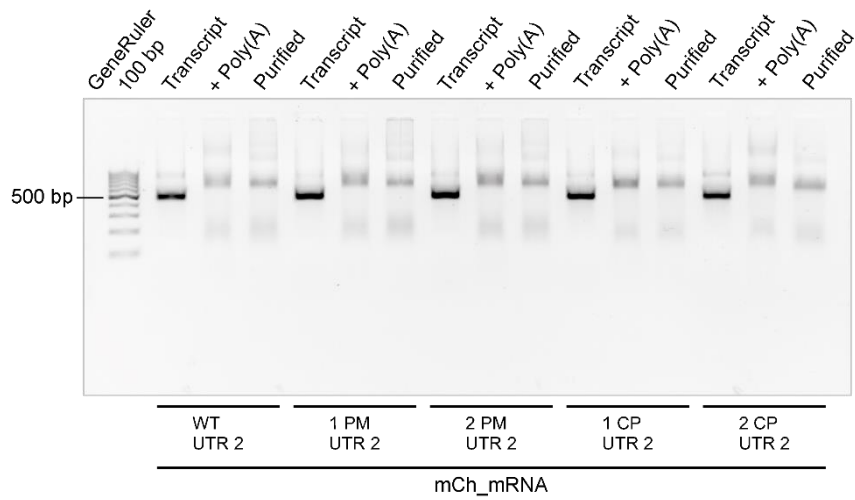


Figure 59. Agarose gel of unmodified, UB-modified and point mutated *mCh_mRNA*_{UTR 2}. Samples for gel analysis were taken after DNase digestion after IVT (Transcript), after Poly(A) tailing (Poly(A)) and after LiCl precipitation for mRNA purification (Purified).

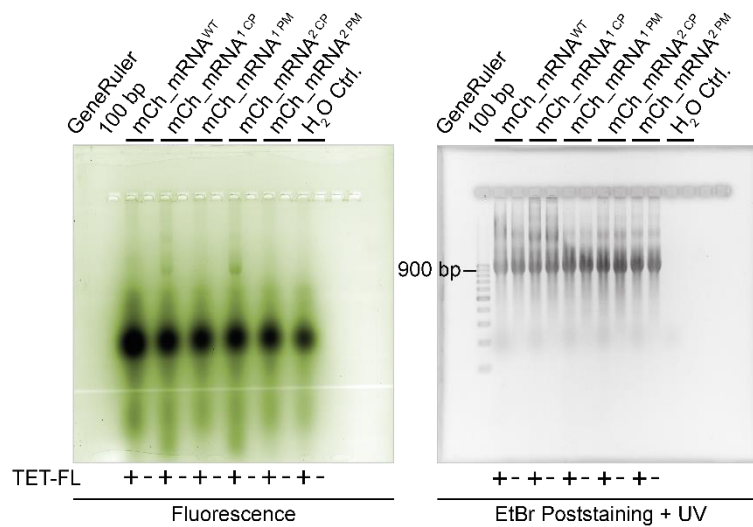


Figure 60. Agarose gel for *in vitro* fluorescent click labeling of *mCh_mRNA* with CP-modifications and point mutations. Fluorescence scan on the left, EtBr poststained gel and UV visualization on the right.

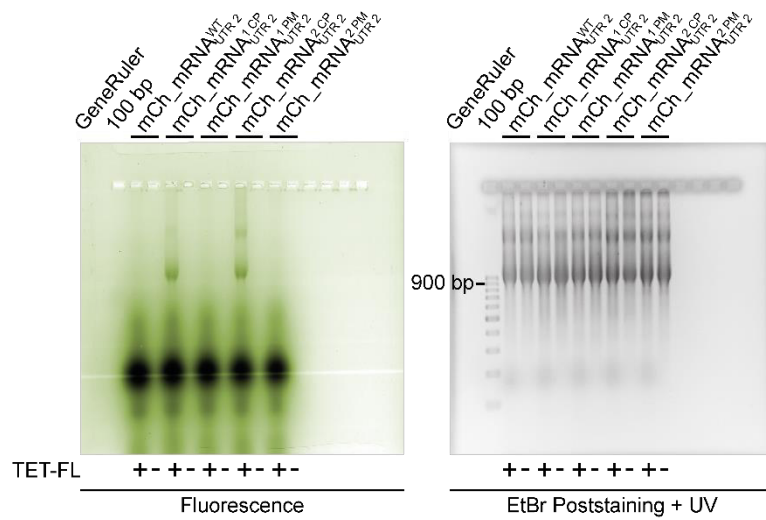


Figure 61. Agarose gel for *in vitro* fluorescent click labeling of *mCh_mRNA_{UTR2}* with CP-modifications and point mutations. Fluorescence scan on the left, EtBr poststained gel and UV visualization on the right.

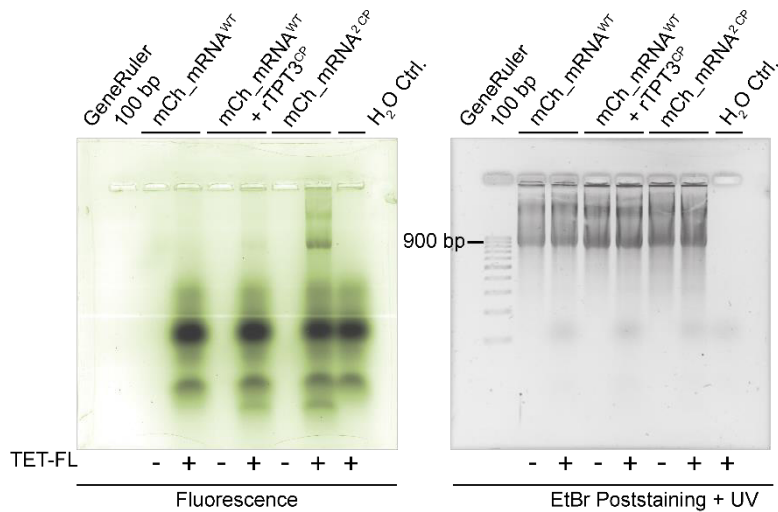


Figure 62. Agarose gel for analysis of specific rTPT3^{CP} incorporation and *in vitro* fluorescent click labeling of *mCh_mRNA*. Fluorescence scan on the left, EtBr poststained gel and UV visualization on the right.

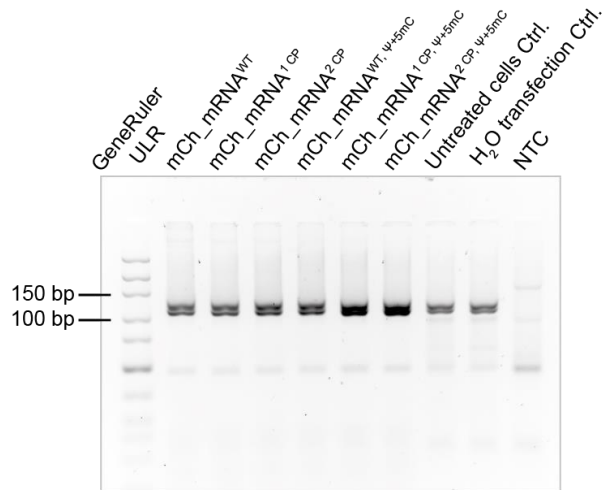


Figure 63. Agarose gel of RT-qPCR products for 6 h analysis of cells transfected with *mCh_mRNA* sequence variants.

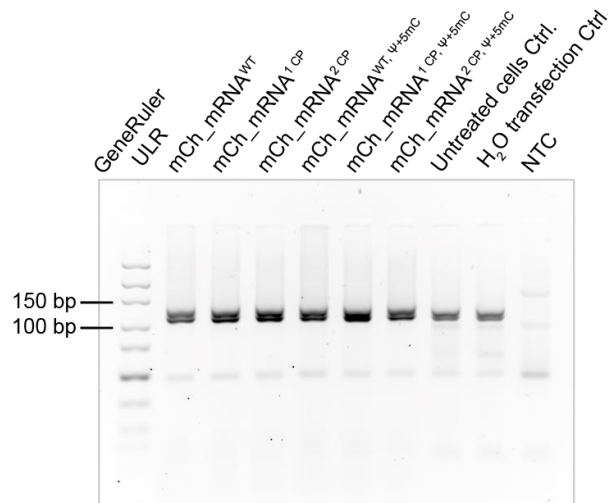


Figure 64. Agarose gel of RT-qPCR products for 24 h analysis of cells transfected with *mCh_mRNA* sequence variants.

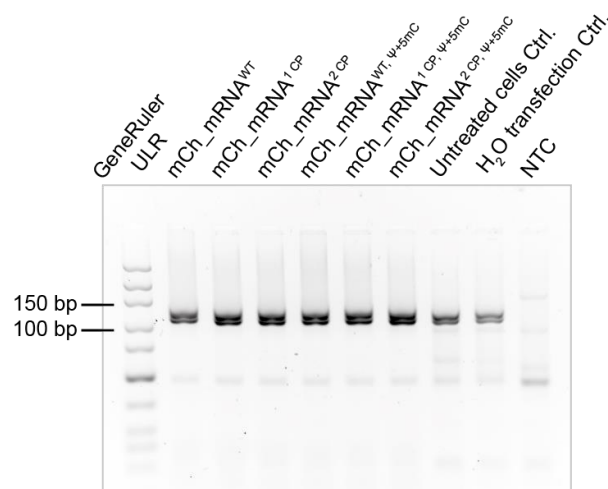


Figure 65. Agarose gel of RT-qPCR products for 48 h analysis of cells transfected with *mCh_mRNA* sequence variants.

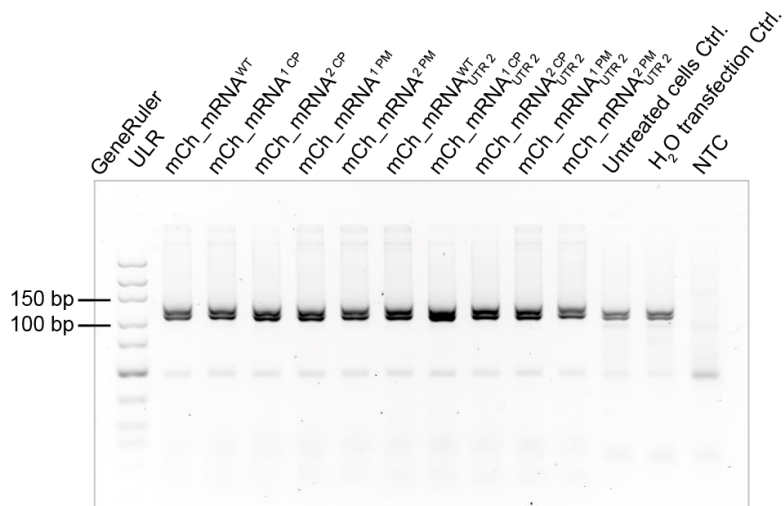


Figure 66. Agarose gel of RT-qPCR products for 6 h analysis of cells transfected with *mCh_mRNA* and *mCh_mRNA_{UTR2}* sequence variants.

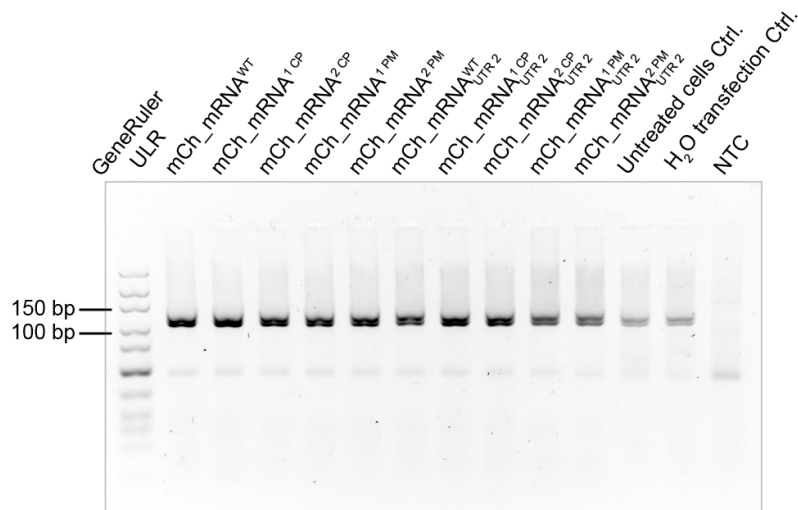


Figure 67. Agarose gel of RT-qPCR products for 24 h analysis of cells transfected with *mCh_mRNA* and *mCh_mRNA_{UTR2}* sequence variants.

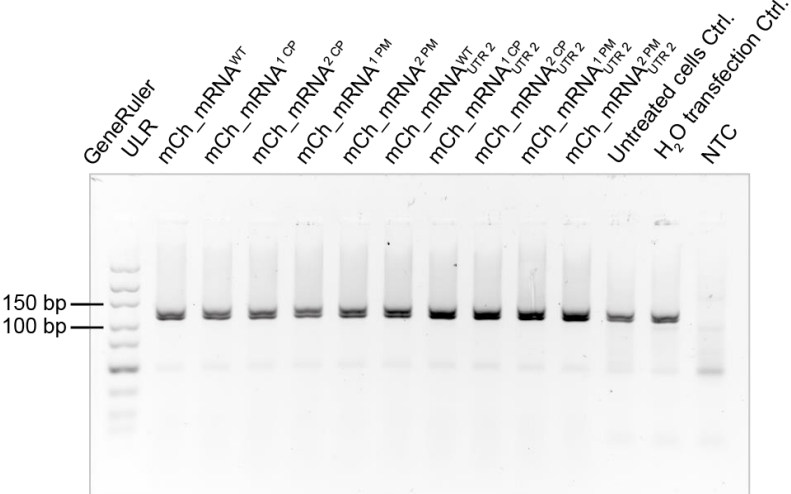


Figure 68. Agarose gel of RT-qPCR products for 48 h analysis of cells transfected with *mCh_mRNA* and *mCh_mRNA_{UTR 2}* sequence variants.

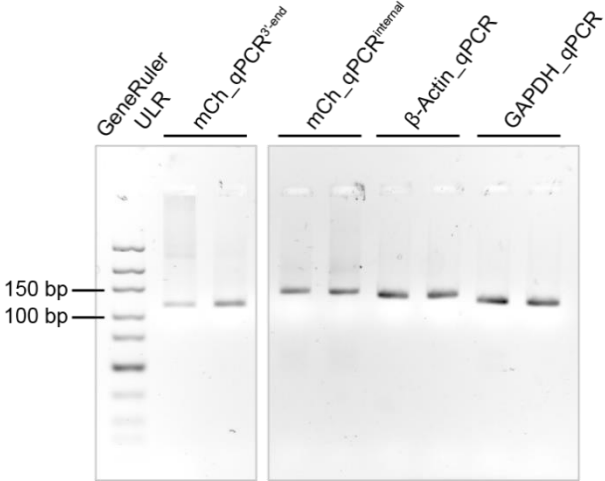


Figure 69. Agarose gel of PCR amplified RT-qPCR products for sequence elongation.

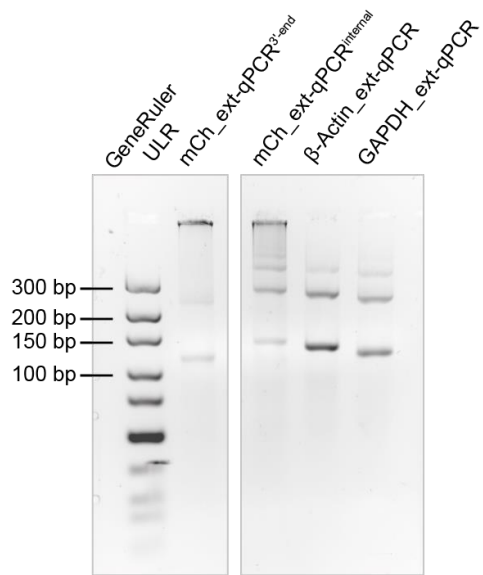


Figure 70. Agarose gel of extended RT-qPCR products after ligation with adapter sequences.

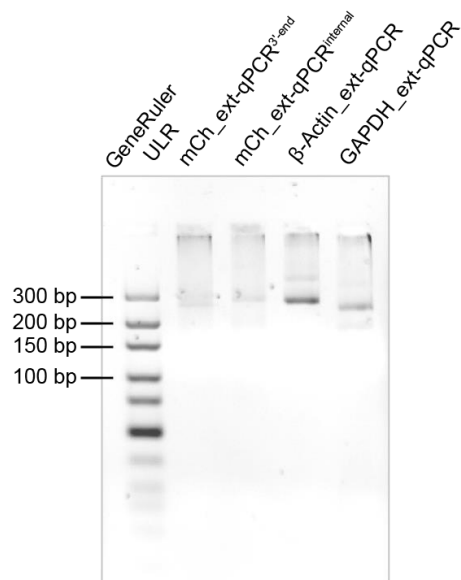


Figure 71. Agarose gel of PCR amplified extended RT-qPCR products.

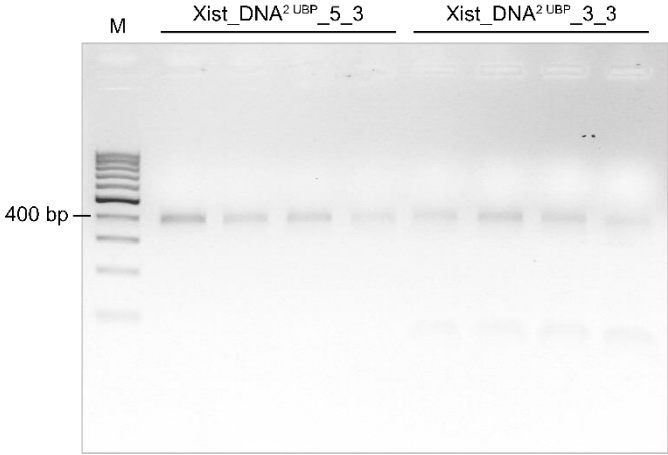


Figure 72. Agarose gel of UB-modified *Xist_DNA* PCR products.

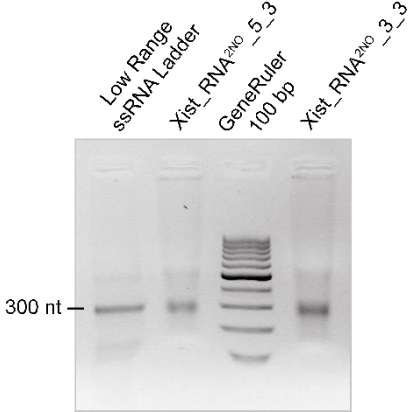


Figure 73. Agarose gel of NO-modified *Xist_RNA*.

7.2 Sanger sequencing results

pmCherry-N1_AA-insert

(AA-insertion highlighted; mutated stop codon underlined; mCherry protein coding region underlined)

5'-aGCaGaGCTGGTTtaGTGAaCCGTCAGATCCGCTAGCGCTACCGGaCTCAGATCTCGA
 GCTCAAGCTTTCGAATTCTGCAGTCGACGGTACCGCGGGCCCGGGATCCACCGGTTCGC
 CACCATGGTGAGCAAGGGGCGAGGAGGATAACATGGCCATCATCAAGGAGTTCATGCGC
 TTCAAGGTGCACATGGAGGGCTCCGTGAACGGCCACGAGTTCGAGATCGAGGGCGAG
 GGCGAGGGCCGCCCTACGAGGGCACCCAGACCGCCAAGCTGAAGGTGACCAAGGGT
 GGCCCCCTGCCCTTCGCCTGGGACATCCTGTCCCCTCAGTTCATGTACGGCTCCAAGG
 CCTACGTGAAGCACCCCGCCGACATCCCCGACTACTTGAAGCTGTCCTTCCCCGAGGG
 CTTCAAGTGGGAGCGCGTGATGAACTTCGAGGACGGCGGCGTGGTGACCGTGACCCA
 GGACTCCTCCCTGCAGGACGGCGAGTTCATCTACAAGGTGAAGCTGCGCGGCACCAAC
 TTCCCCTCCGACGGCCCCGTAATGCAGAAGAAGACCATGGGCTGGGAGGCCTCCTCCG
 AGCGGATGTACCCCGAGGACGGCGCCCTGAAGGGCGAGATCAAGCAGAGGCTGAAGC
 TGAAGGACGGCGGCCACTACGACGCTGAGGTCAAGACCACCTACAAGGCCAAGAAGC
 CCGTGCAGCTGCCCGGCGCCTACAACGTCAACATCAAGTTGGACATCACCTCCCACAA
 CGAGGACTACACCATCGTGGAACAGTACGAACGCGCCGAGGGCCGCGCCACTCCACCGG
 CGGCATGGACGAGCTGTACAAGTAAAGCGGCCGCGACTCTAGATCATAATCAGCCATA
 CCACATTTGTAGAGTTTTACTTGCTTTAAAAAaCCTCCACACCTCCCCTGAACCTGA
 AACATAAAATGAATGCAATTGTTGTTGTTAACTTGTTTATTGCAGCTTATAATGGTTACAA
 ATAAAGCAATAGCATCACAAATTTACAAATAAAGCATTTTTTTCaCTGCATTCTAGTTgtG
 gTTtGTCCAAaCTCATCAATGTATCTTAAGGCGTAAaTTGTAAGCGTTAAaTTTTtGTTAAa
 TTcnnGTTAAaTTTTTggtAAaTCAGcTcATTTTTtAaCCAanaGgCCGAAaTCGGcAAanTCCcT
 TanAAatCAAa-3'

mCh_DNA^{WT}

(stop codon underlined; mCherry protein coding region underlined)

T7_seq primer results:

5'-antctgCagTCGAACGGTACCGCGGggCCCggGATCCACCGGTGCGCCACCATGGTGAGC
 AAGGGCGAGGAGGATAACATGGCCATCATCAAGGAGTTCATGCGCTTCAAGGTGCACA
 TGGAGGGCTCCGTGAACGGCCACGAGTTCGAGATCGAGGGCGAGGGCGAGGGCCGC
 CCCTACGAGGGCACCCAGACCGCCAAGCTGAAGGTGACCAAGGGTGGCCCCCTGCC
 TTCGCCTGGGACATCCTGTCCCCTCAGTTCATGTACGGCTCCAAGGCCTACGTGAAGCA
 CCCC GCCGACATCCCCGACTACTTGAAGCTGTCCTTCCCCGAGGGCTTCAAGTGGGAG
 CGCGTGATGAACTTCGAGGACGGCGGCGTGGTGACCGTGACCCAGGACTCCTCCCTG
 CAGGACGGCGAGTTCATCTACAAGGTGAAGCTGCGCGGCACCAACTTCCCCTCCGACG
 GCCCGTAATGCAGAAGAAGACCATGGGCTGGGAGGCCTCCTCCGAGCGGATGTACC
 CCGAGGACGGCGCCCTGAAGGGCGAGATCAAGCAGAGGCTGAAGCTGAAGGACGGCG
 GCCACTACGACGCTGAGGTCAAGACCACCTACAAGGCCAAGAAGCCCGTGCAGCTGCC
 CGGCGCCTACAACGTCAACATCAAGTTGGACATCACCTCCCACAACGAGGACTACACCA
 TCGTGGAACAGTACGAACGCGCCGAGGGCCGCGCCACTCCACCGGCGGCATGGACGAGC
 TGTAACAAGTAAAGCGGCCGCGACTCTAGATCATAATCAGCCAtaCCc-3'

mCh_seq primer results:

5'-atGgnnGAgCTGTACaAGTAAAGCGGCCGCGACTCTAGATCATAATCAGCCATAACCACA
 TTT-3'

mCh_DNA¹ PM

(stop codon underlined; mCherry protein coding region underlined, mutated base highlighted)

T7_seq primer results:

GngTCGaangGtcCGCGGGGCCCGGGATcACCGGTCGCCACCATGGTGAGCAAGGGCGA
 GGAGGATAACATGGCCATCATCAAGGAGTTCATGCGCTTCAAGGTGCACATGGAGGGC
 TCCGTGAACGGCCACGAGTTCGAGATCGAGGGCGAGGGCGAGGGCCGCCCTACGAG
 GGCACCCAGACCGCCAAGCTGAAGGTGACCAAGGGTGGCCCCCTGCCCTTCGCCTGG
 GACATCCTGTCCCCTCAGTTCATGTACGGCTCCAAGGCCTACGTGAAGCACCCCGCCG
 ACATCCCCGACTACTTGAAGCTGTCCTTCCCCGAGGGCTTCAAGTGGGAGCGCGTGAT
 GAACTTCGAGGACGGCGGCGTGGTGACCGTGACCCAGGACTCCTCCCTGCAGGACGG
 CGAGTTCATCTACAAGGTGAAGCTGCGCGGCACCAACTTCCCCTCCGACGGCCCCGTA
 ATGCAGAAGAAGACCATGGGCTGGGAGGCCTCCTCCGAGCGGATGTACCCCGAGGAC
 GGCGCCCTGAAGGGCGAGATCAAGCAGAGGCTGAAGCTGAAGGACGGCGGCCACTAC
 GACGCTGAGGTCAAGACCACCTACAAGGCCAAGAAGCCCGTGCAGCTGCCCGGCGCC
 TACAACGTCAACATCAAGTTGGACATCACCTCCCACAACGAGGACTACACCATCGTGGA
 ACAGTACGAACGCGCCGAGGGCCGCACTCCACCGGCGGCATGGACGAGCTGTACAA
 GTAAAGCGGCCGCGACTCTAGATCATAATCAGc

mCh_seq primer results:

cgaagctgtacaagtaaagcggccgactctagatcataatcagccgtaccacatt

mCh_DNA² PM

(stop codon underlined; mCherry protein coding region underlined, mutated bases highlighted)

T7_seq primer results:

gTcgaacGGtnnCGCGGGgCCCGGGancCACCGGtncGCCACCATGGTGAGCAAGGGCGAG
 GAGGATAACATGGCCATCATCAAGGAGTTCATGCGCTTCAAGGTGCACATGGAGGGCT
 CCGTGAACGGCCACGAGTTCGAGATCGAGGGCGAGGGCGAGGGCCGCCCTACGAG
 GGCACCCAGACCGCCAAGCTGAAGGTGACCAAGGGTGGCCCCCTGCCCTTCGCCTGG
 GACATCCTGTCCCCTCAGTTCATGTACGGCTCCAAGGCCTACGTGAAGCACCCCGCCG
 ACATCCCCGACTACTTGAAGCTGTCCTTCCCCGAGGGCTTCAAGTGGGAGCGCGTGAT
 GAACTTCGAGGACGGCGGCGTGGTGACCGTGACCCAGGACTCCTCCCTGCAGGACGG
 CGAGTTCATCTACAAGGTGAAGCTGCGCGGCACCAACTTCCCCTCCGACGGCCCCGTA
 ATGCAGAAGAAGACCATGGGCTGGGAGGCCTCCTCCGAGCGGATGTACCCCGAGGAC
 GGCGCCCTGAAGGGCGAGATCAAGCAGAGGCTGAAGCTGAAGGACGGCGGCCACTAC
 GACGCTGAGGTCAAGACCACCTACAAGGCCAAGAAGCCCGTGCAGCTGCCCGGCGCC
 TACAACGTCAACATCAAGTTGGACATCACCTCCCACAACGAGGACTACACCATCGTGGA
 ACAGTACGAACGCGCCGAGGGCCGCACTCCACCGGCGGCATGGACGAGCTGTACAA
 GTAAAGCGGCCGCGACTCTAGATCATAGTCAGct

mCh_seq primer results:

acgagctgtacaagtaaagcggccgactctagatcatagtcagccataccacgtttgt

mCh_DNA^{WT}_{UTR 2}

(stop codon underlined; mCherry protein coding region underlined)

T7_seq primer results:

gTCGaangGtaCnGCGGGGCCCGggnatCCACCGGTCGCCACCATGGTGAGCAAGGGCGA
 GGAGGATAACATGGCCATCATCAAGGAGTTCATGCGCTTCAAGGTGCACATGGAGGGC
 TCCGTGAACGGCCACGAGTTCGAGATCGAGGGCGAGGGCGAGGGCCGCCCTACGAG
 GGCACCCAGACCGCCAAGCTGAAGGTGACCAAGGGTGGCCCCCTGCCCTTCGCCTGG
 GACATCCTGTCCCCTCAGTTCATGTACGGCTCCAAGGCCTACGTGAAGCACCCCGCCG
 ACATCCCCGACTACTTGAAGCTGTCCTTCCCCGAGGGCTTCAAGTGGGAGCGCGTGAT
 GAACTTCGAGGACGGCGGCGTGGTGACCGTGACCCAGGACTCCTCCCTGCAGGACGG
 CGAGTTCATCTACAAGGTGAAGCTGCGCGGCACCAACTTCCCCTCCGACGGCCCCGTA
 ATGCAGAAGAAGACCATGGGCTGGGAGGCCTCCTCCGAGCGGATGTACCCCGAGGAC
 GGCGCCCTGAAGGGCGAGATCAAGCAGAGGCTGAAGCTGAAGGACGGCGGCCACTAC
 GACGCTGAGGTCAAGACCACCTACAAGGCCAAGAAGCCCGTGCAGCTGCCCGGCGCC
 TACAACGTCAACATCAAGTTGGACATCACCTCCCACAACGAGGACTACACCATCGTGGA
 ACAGTACGAACGCGCCGAGGGCCGCCACTCCACCGGCGGCATGGACGAGCTGTACAA
 GTAAAGCGGCCGCGACTCTAGATCATAGTTGTTGTAcctTtnnttt

mCh_seq primer results:

tGgnnGAgCTGTaCaAGTAAAGCGGCCGCGACTCTAGATCATAGTTGTTGTTAACTTGT

mCh_DNA^{1 PM}_{UTR 2}

(stop codon underlined; mCherry protein coding region underlined, mutated base highlighted)

T7_seq primer results:

GcAgTCGaacGgGtaccGCGGGGCCCGgGgatCCACCGGTCGCCACCATGGTGAGCAAGGG
 CGAGGAGGATAACATGGCCATCATCAAGGAGTTCATGCGCTTCAAGGTGCACATGGAG
 GGCTCCGTGAACGGCCACGAGTTCGAGATCGAGGGCGAGGGCGAGGGCCGCCCTAC
 GAGGGCACCCAGACCGCCAAGCTGAAGGTGACCAAGGGTGGCCCCCTGCCCTTCGCC
 TGGGACATCCTGTCCCCTCAGTTCATGTACGGCTCCAAGGCCTACGTGAAGCACCCCG
 CCGACATCCCCGACTACTTGAAGCTGTCCTTCCCCGAGGGCTTCAAGTGGGAGCGCGT
 GATGAACTTCGAGGACGGCGGCGTGGTGACCGTGACCCAGGACTCCTCCCTGCAGGA
 CGGCGAGTTCATCTACAAGGTGAAGCTGCGCGGCACCAACTTCCCCTCCGACGGCCCC
 GTAATGCAGAAGAAGACCATGGGCTGGGAGGCCTCCTCCGAGCGGATGTACCCCGAG
 GACGGCGCCCTGAAGGGCGAGATCAAGCAGAGGCTGAAGCTGAAGGACGGCGGCCAC
 TACGACGCTGAGGTCAAGACCACCTACAAGGCCAAGAAGCCCGTGCAGCTGCCCGGC
 GCCTACAACGTCAACATCAAGTTGGACATCACCTCCCACAACGAGGACTACACCATCGT
 GGAACAGTACGAACGCGCCGAGGGCCGCCACTCCACCGGCGGCATGGACGAGCTGTA
 CAAGTAAAGCGGCCGCGACTCTGGATCATAGTTGTTGTA

mCh_seq primer results:

gcatggacgagctgtacaagttaaagcggccgcgactctggatcatagttgttgaactgtttat

mCh_DNA²PM_{UTR 2}

(stop codon underlined; mCherry protein coding region underlined, **mutated bases** highlighted)

T7_seq primer results:

gngTcgaacgGtnCGCGGGCCCGGGATcCaCCGgnccGCCACCATGGTGAGCAAGGGCGAG
 GAGGATAACATGGCCATCATCAAGGAGTTCATGCGCTTCAAGGTGCACATGGAGGGCT
 CCGTGAACGGCCACGAGTTCGAGATCGAGGGCGAGGGCGAGGGCCGCCCTACGAG
 GGCACCCAGACCGCCAAGCTGAAGGTGACCAAGGGTGGCCCCCTGCCCTTCGCCTGG
 GACATCCTGTCCCCTCAGTTCATGTACGGCTCCAAGGCCTACGTGAAGCACCCCGCCG
 ACATCCCCGACTACTTGAAGCTGTCCTTCCCCGAGGGCTTCAAGTGGGAGCGCGTGAT
 GAACTTCGAGGACGGCGGCGTGGTGACCGTGACCCAGGACTCCTCCCTGCAGGACGG
 CGAGTTCATCTACAAGGTGAAGCTGCGCGGCACCAACTTCCCCTCCGACGGCCCCGTA
 ATGCAGAAGAAGACCATGGGCTGGGAGGCCTCCTCCGAGCGGATGTACCCCGAGGAC
 GGCGCCCTGAAGGGCGAGATCAAGCAGAGGCTGAAGCTGAAGGACGGCGGCCACTAC
 GACGCTGAGGTCAAGACCACCTACAAGGCCAAGAAGCCCGTGCAGCTGCCCGGCGCC
 TACAACGTCAACATCAAGTTGGACATCACCTCCCACAACGAGGACTACACCATCGTGGA
 ACAGTACGAACGCGCCGAGGGCCGCCACTCCACCGCGGCATGGACGAGCTGTACAA
 GTAAAGCGGCCGCGGCTCTAGATCGTAGTTGTGAAnnTttttT

mCh_seq primer results:

acgaagctgtacaagtaaagcgccgctctagatcgtagtgtgttaactgttta

mCh_DNA¹UBP

(stop codon underlined; mCherry protein coding region underlined, **UB position** highlighted)

nnnnnnnnCGCGGnnnnGGnnCnnCCGGTCGCCACCATGGTGAGCAAGGGCGAGGAGGA
 TAAnnTGGCCATCATCAAGGAGTTCATGCGCTTCAAGGTGCACATGGAGGGCTCCGTGA
 ACGGCCACGAGTTCGAGATCGAGGGCGAGGGCGAGGGCCGCCCTACGAGGGCACC
 CAGACCGCCAAGCTGAAGGTGACCAAGGGTGGCCCCCTGCCCTTCGCCTGGGACATC
 CTGTCCCCTCAGTTCATGTACGGCTCCAAGGCCTACGTGAAGCACCCCGCCGACATCC
 CCGACTACTTGAAGCTGTCCTTCCCCGAGGGCTTCAAGTGGGAGCGCGTGATGAACTT
 CGAGGACGGCGGCGTGGTGACCGTGACCCAGGACTCCTCCCTGCAGGACGGCGAGTT
 CATCTACAAGGTGAAGCTGCGCGGCACCAACTTCCCCTCCGACGGCCCCGTAATGCAG
 AAGAAGACCATGGGCTGGGAGGCCTCCTCCGAGCGGATGTACCCCGAGGACGGCGCC
 CTGAAGGGCGAGATCAAGCAGAGGCTGAAGCTGAAGGACGGCGGCCACTACGACGCT
 GAnGTCAAGACCACCTACAAGGCCAAGAAGCCCGTGCAGCTGCCCGGCGCCTACAACG
 TCAACATCAAGTTGGACATCACCTCCCACAACGAGGACTACACCATCGTGnAACAGTAC
 GAACGCGCCGAGGGCCGCCACTCCACCGCGGCATGGACGAGCTGTACAAGTAAAnC
 GnnCGCGACTCTnnnnnnnnAATCAGCCnnnnnn

mCh_DNA²UBP

(stop codon underlined; mCherry protein coding region underlined, **UB position** highlighted)

nnnnnnnnnnnnGnnCCnCCGGTCGCCnCCATGGTGAGCAAGGGCGAGGAGGATAACATG
 GCCATCATCAAGGAGTTCATGCGCTTCAAGGTGCACATGGAGGGCTCCGTGAACGGCC
 ACGAGTTCGAGATCGAGGGCGAGGGCGAGGGCCGCCCTACGAGGGCACCCAGACC
 GCCAAGCTGAAGGTGACCAAGGGTGGCCCCCTGCCCTTCGCCTGGGACATCCTGTCCC
 CTCAGTTCATGTACGGCTCCAAGGCCTACGTGAAGCACCCCGCCGACATCCCCGACTA
 CTTGAAGCTGTCCTTCCCCGAGGGCTTCAAGTGGGAGCGCGTGATGAACTTCGAGGAC

GGCGGCGTGGTGACCGTGACCCAGGACTCCTCCCTGCAGGACGGCGAGTTCATCTAC
 AAGGTGAAGCTGCGCGGCACCAACTTCCCCTCCGACGGCCCCGTAATGCAGAAGAAGA
 CCATGGGCTGGGAGGCCTCCTCCGAGCGGATGTACCCCGAGGACGGCGCCCTGAAGG
 GCGAGATCAAGCAGAnGCTGAAGCTGAAGGACGGCGGCCACTACGACGCTGAnGTCAA
 GACCACCTACAAGGCCAAGAAGCCCGTGCAGCTGCCCGGCGCCTACAACGTCAACATC
 AAGTTGGACATCACCTCCCACnACGAGGACTACACCATCGTGGAACAGTACGAACGCG
 CCGAGGGCCGCACTCCACCGGCGGCATGGACGAnCnGTACAnGTAAAGCGnCCGCGA
 CTCTnGATCAnAnnnnnnnCnnnCnnnnnn

mCh_ext-qPCR^{internal}

5'-tTGgcagTCtAGGCGAtCGCgATGGCCTGAGTCTAGAGCTCGAgTTcnaAgCTtAagACGTC
 aGCTGCCATCCCgACTACTTGAAnCTGtCCTTCCCcgAgGgCTtcaagTGGgAaCgCGTGATGA
 ACTTCgAGGACGGCGGCgTGgTGACCGTGACCCAGGACTCctCCCTGCAGGACGGCaAg
 TTCATCTACaAGGTGA-3'

mCh_ext-qPCR^{3'-end}

5'-aGGCGAtcGcGATGGCCTGAGTCTAgAGCTCGAGTTCGAAgCTtAagACGTCngCTGCCA
 TATCAGtTTGGACaTcCaCTCCcAcAacGAGGACTACaCCaTcgtGgAacAGTACgAAcGCgC
 CgAGGGCCgCCacTCCaCCGGcGGcatGgacaAgCTGTACAAGTAAagcG-3'

GAPDH_ext-qPCR

5'-tTGgCAGTCTAGGCGATCGcgATGGCCTGAGTCTAGAGCTCgAgTTCgAagCTtAAGACG
 TCagCTGCcaTAgCCtCAagATCATCAgCaaTGCctCctGcaCCaCCAactGcTTAACaCCCctgAn
 nnAGGTCATCCaTGACaaCTTTGgTATCgtGgAAGGACTCatGAccaCagtcca-3'

β -Actin_ext-qPCR

5'-tcaCTTGGCAGTCTAGGCGATCGCGATGGCCTGAGTCTAGAGCTCGAGTTCGAAGCTT
 AAgACgTCAgCTGCcatGGTCATCACCATTGgcAATGAgCGGTTCCgctGCCcgGaGGCACTC
 TTCCagCCTTCTTCCgGGGcATGGAaTcCtGtGgCATCcacnaaACTaCcTTCAacTCcnTCatga
 agTGtga -3'

7.3 Microscopy images

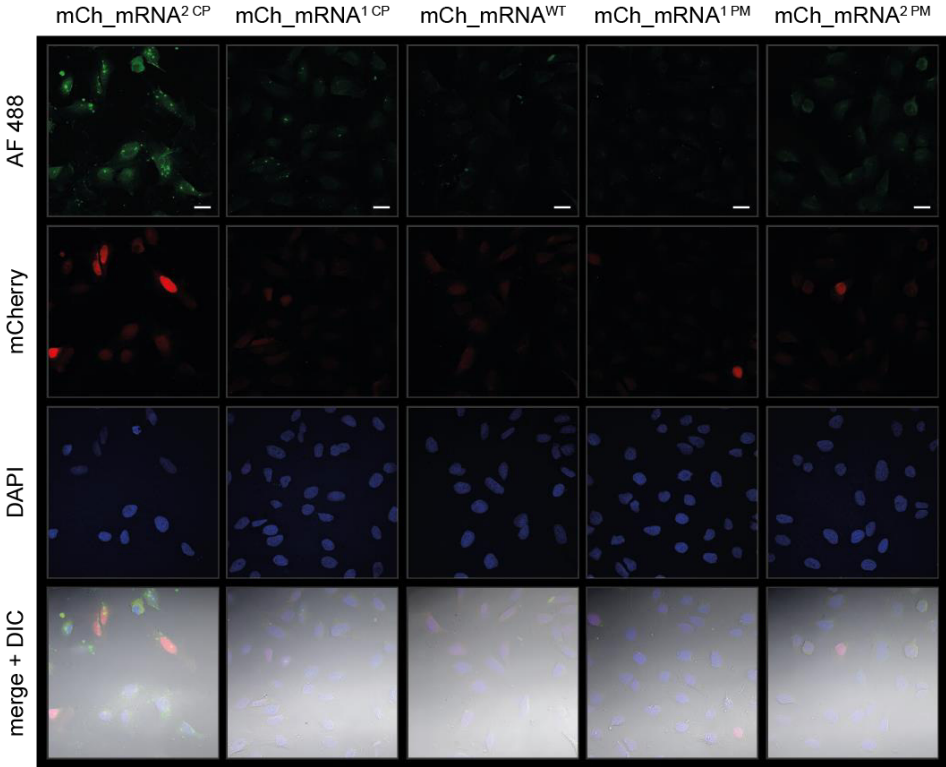


Figure 74. Confocal fluorescence microscopy images of cells transfected with *mCh_mRNA* variants at 6 h after transfection start. Scale bars correspond to 20 μ m.

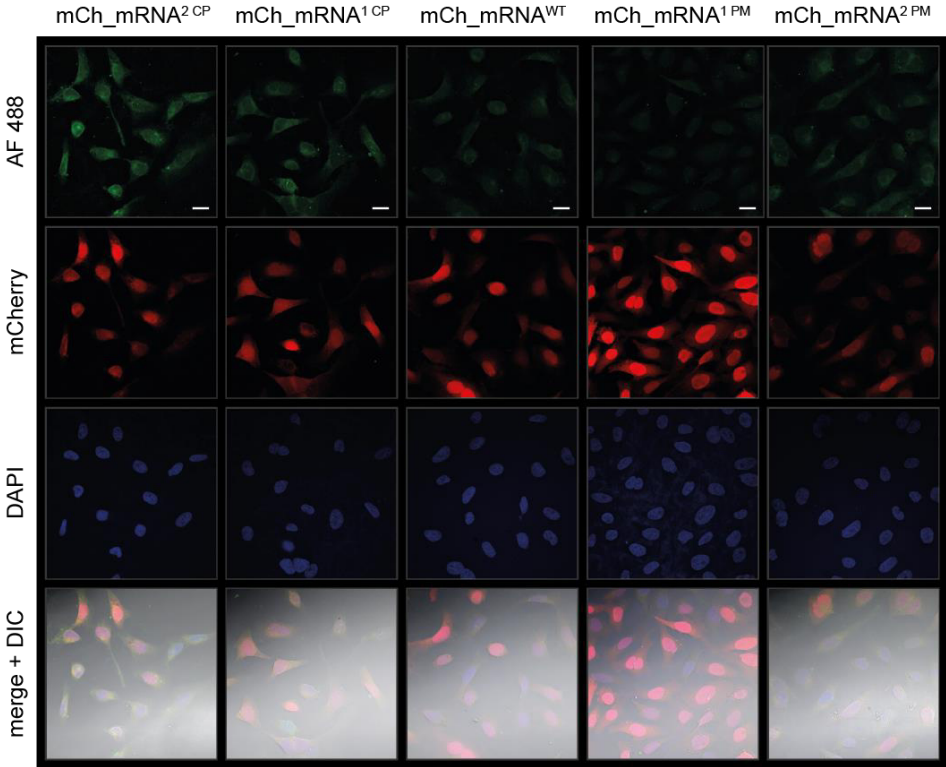


Figure 75. Confocal fluorescence microscopy images of cells transfected with *mCh_mRNA* variants at 24 h after transfection start. Scale bars correspond to 20 μ m.

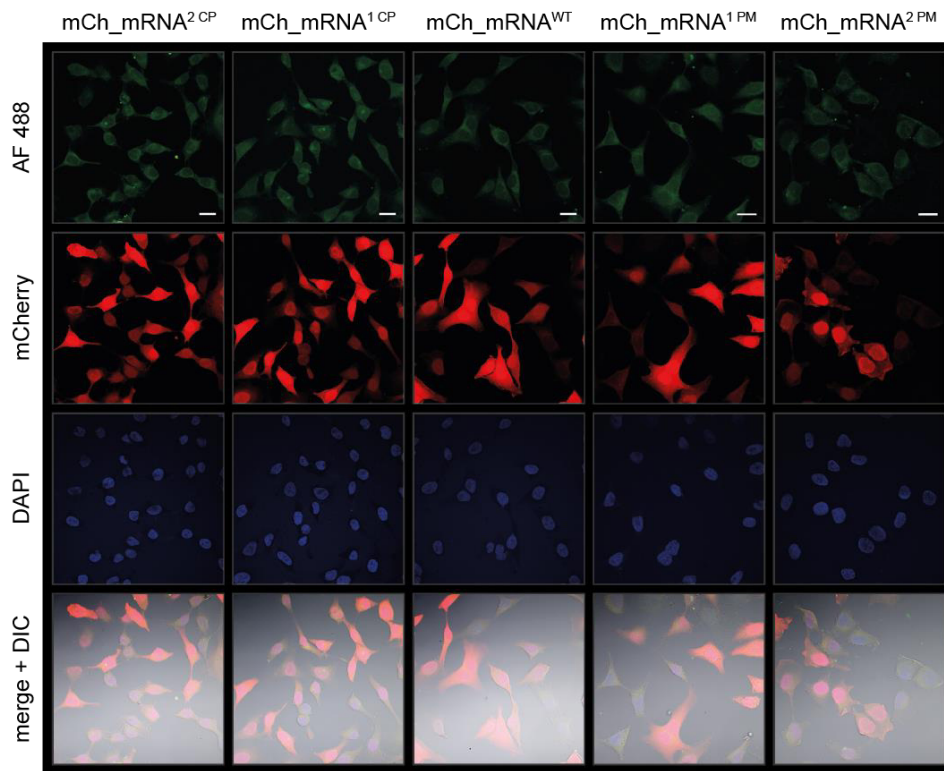


Figure 76. Confocal fluorescence microscopy images of cells transfected with *mCh_mRNA* variants at 48 h after transfection start. Scale bars correspond to 20 μm .

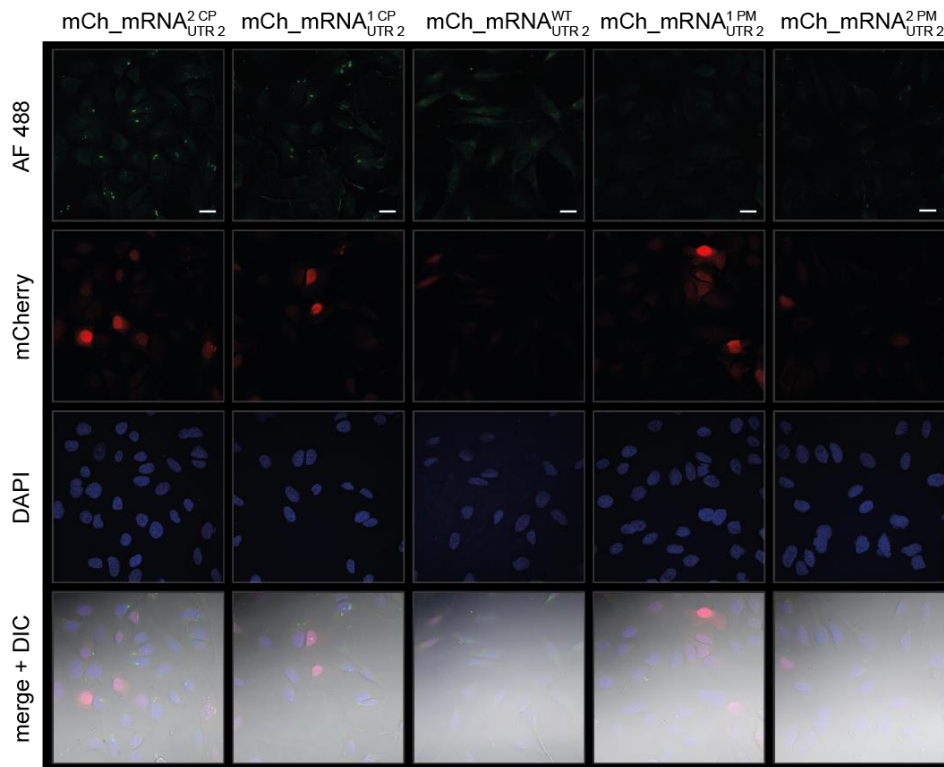


Figure 77. Confocal fluorescence microscopy images of cells transfected with *mCh_mRNA*_{UTR2} variants at 6 h after transfection start. Scale bars correspond to 20 μm .

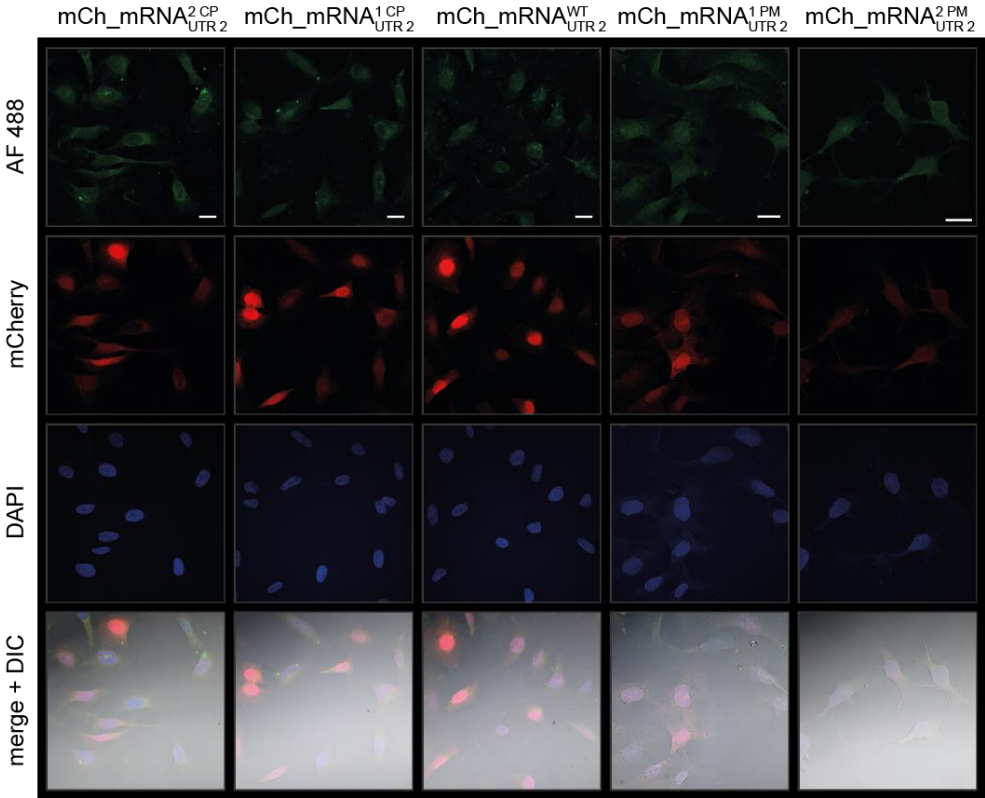


Figure 78. Confocal fluorescence microscopy images of cells transfected with *mCh_mRNA_{UTR 2}* variants at 24 h after transfection start. Scale bars correspond to 20 μ m.

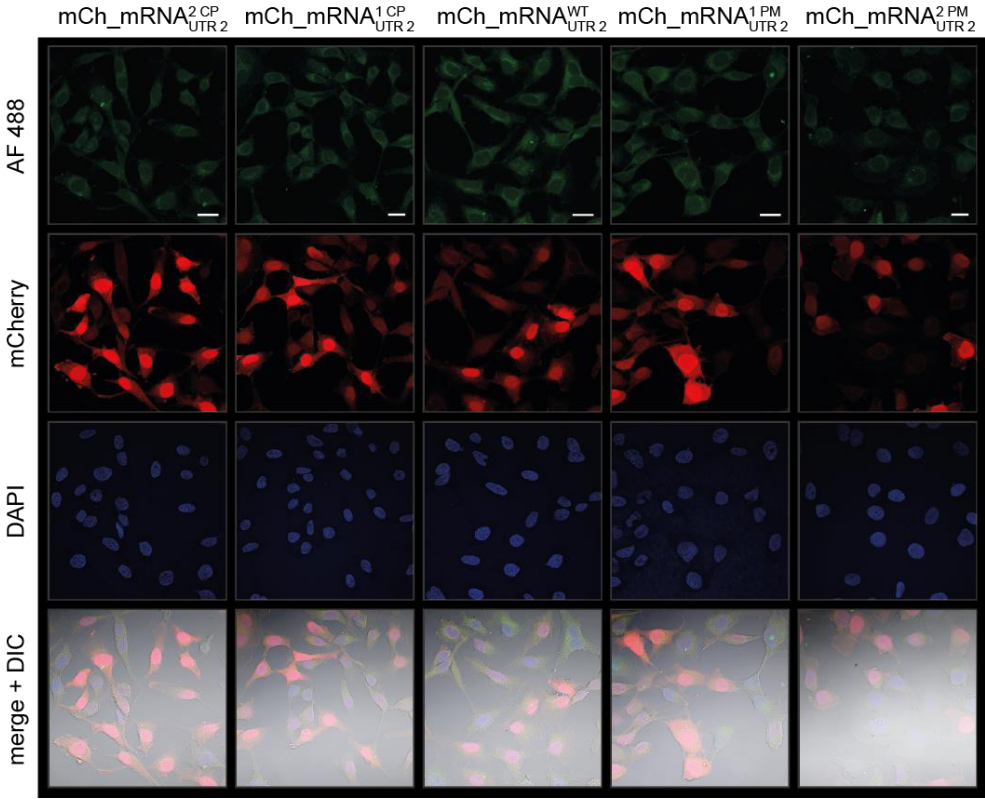


Figure 79. Confocal fluorescence microscopy images of cells transfected with *mCh_mRNA_{UTR 2}* variants at 48 h after transfection start. Scale bars correspond to 20 μ m.

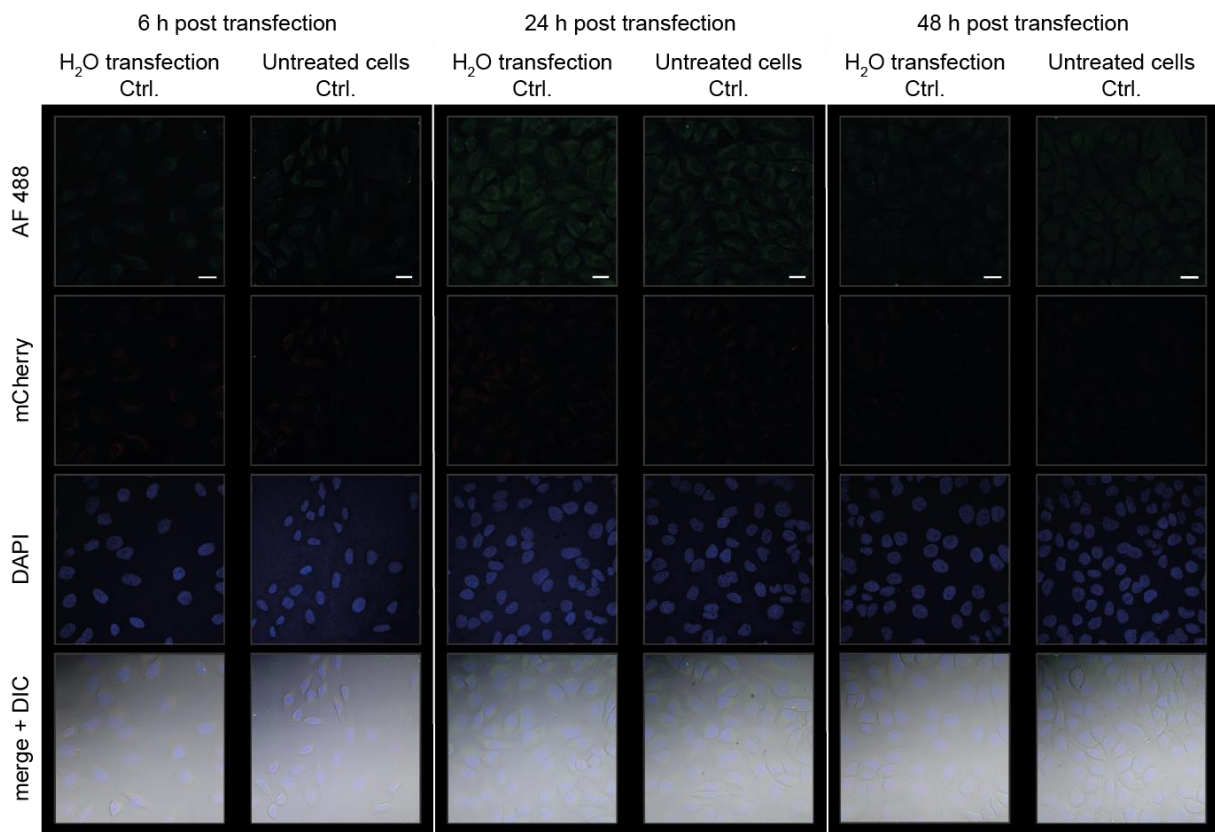


Figure 80. Confocal fluorescence microscopy images of transfection controls and untreated cell controls at 6, 24 and 48 h after transfection start. Scale bars correspond to 20 μ m.

7.4 *mCherry* protein quantification

7.4.1 *mCherry* protein quantification full data set figure

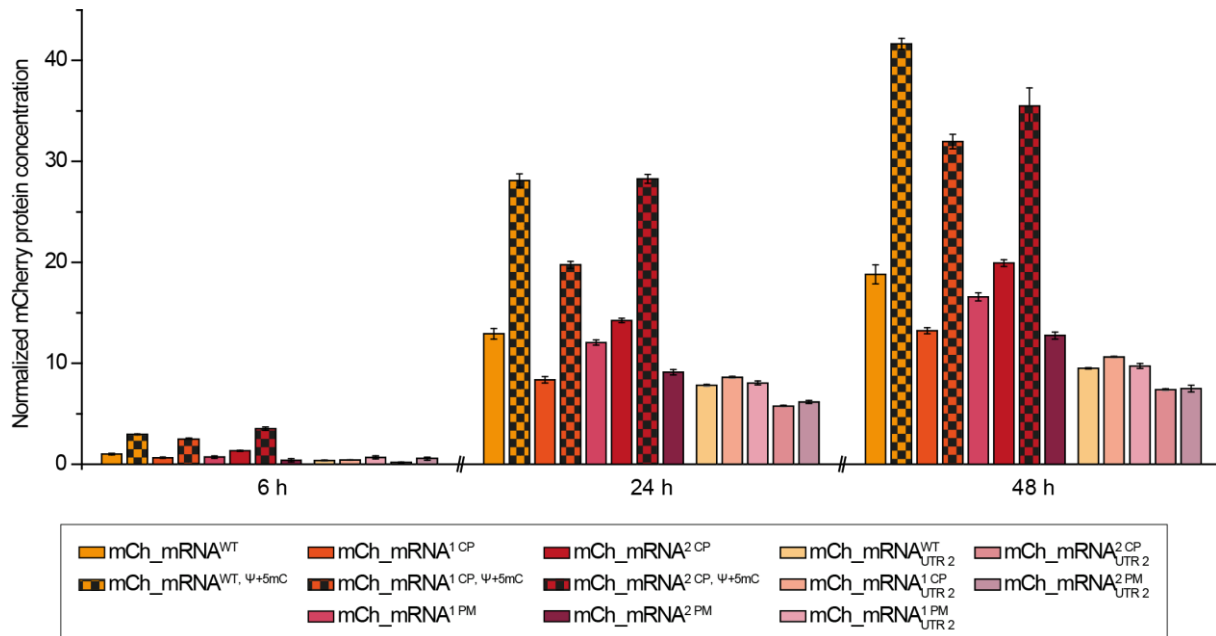


Figure 81. *mCherry* protein quantification of cells transfected with *mCh_mRNA* and *mCh_mRNA_{UTR2}* sequences analyzed at 6, 24 and 48 h after transfection start.

7.4.2 *mCherry* protein quantification data tables

	WT #1	WT #2	1 CP #1	1 CP #2	2 CP #1	2 CP #2	1 PM #1	1 PM #2	2 PM #1	2 PM #2
6 h <i>mCh_mRNA</i>	72	57	0	120	96	90	95	0	82	2
6 h <i>mCh_mRNA_{UTR2}</i>	80	94	74	74	77	0	74	135	47	74
24 h <i>mCh_mRNA</i>	416	365	227	364	391	501	426	460	397	351
24 h <i>mCh_mRNA_{UTR2}</i>	351	211	319	376	250	270	372	314	321	245
48 h <i>mCh_mRNA</i>	561	608	196	509	576	645	583	564	402	553
48 h <i>mCh_mRNA_{UTR2}</i>	355	331	444	511	464	378	443	467	427	347

	H ₂ O Transf. Ctrl. #1	H ₂ O Transf. Ctrl. #2	Untr. Cells Ctrl. #1	Untr. Cells Ctrl. #2
6 h H ₂ O Transf. Ctrl.	41	78		
6 h Untr. Cells Ctrl.			16	66
24 h H ₂ O Transf. Ctrl.	51	0		
24 h Untr. Cells Ctrl.			2	43
48 h H ₂ O Transf. Ctrl.	83	25		
48 h Untr. Cells Ctrl.			55	29

Table 43. Raw fluorescence values measured from cells transfected with *mCh_mRNA* or *mCh_mRNA_{UTR2}* variants and control values from exp. #1.

mCherry protein standard [ng/well]	0	20	40	60	80	100
Standard curve #1	60	119	208	396	587	620
Standard curve #2	80	82	331	148	499	544

Background (mean value for 0 ng/well)	70
Slope line of best fit	6.52
Coefficient of determination R ²	0.988

Table 44. *mCherry* protein standard curve values and calculated parameters from *mCh_mRNA* or *mCh_mRNA_{UTR2}* exp. #1.

	WT #1	WT #2	1 CP #1	1 CP #2	2 CP #1	2 CP #2	1 PM #1	1 PM #2	2 PM #1	2 PM #2
6 h <i>mCh_mRNA</i>	5	25	0	0	5	0	0	30	35	0
6 h <i>mCh_mRNA_{UTR2}</i>	46	0	32	16	0	0	15	76	42	41
24 h <i>mCh_mRNA</i>	300	398	137	260	336	349	336	313	251	246
24 h <i>mCh_mRNA_{UTR2}</i>	270	187	276	259	171	192	195	256	204	258
48 h <i>mCh_mRNA</i>	516	470	285	292	506	529	310	511	350	394
48 h <i>mCh_mRNA_{UTR2}</i>	347	343	381	398	200	250	384	361	348	145

	H ₂ O Transf. Ctrl. #1	H ₂ O Transf. Ctrl. #2	Untr. Cells Ctrl. #1
6 h H ₂ O Transf. Ctrl.	0	0	
6 h Untr. Cells Ctrl.			0
24 h H ₂ O Transf. Ctrl.	0	0	
24 h Untr. Cells Ctrl.			0
48 h H ₂ O Transf. Ctrl.	5	0	
48 h Untr. Cells Ctrl.			26

Table 45. Raw fluorescence values measured from cells transfected with *mCh_mRNA* or *mCh_mRNA_{UTR2}* variants and control values from exp. #2.

mCherry protein standard [ng/well]	0	20	40	60	80	100
Standard curve #1	0	118	94	214	306	317
Standard curve #2	0	33	145	198	318	429

Background (mean value for 0 ng/well)	0
Slope line of best fit	3.68
Coefficient of determination R ²	0.996

Table 46. *mCherry* protein standard curve values and calculated parameters from *mCh_mRNA* or *mCh_mRNA_{UTR2}* exp. #2.

	WT #1	WT #2	1 CP #1	1 CP #2	2 CP #1	2 CP #2	1 PM #1	1 PM #2	2 PM #1	2 PM #2
6 h <i>mCh_mRNA</i>	132	115	63	1	124	147	137	71	23	52
6 h <i>mCh_mRNA_{UTR2}</i>	77	88	12	38	51	55	40	91	47	36
24 h <i>mCh_mRNA</i>	872	830	236	374	543	577	635	741	505	605
24 h <i>mCh_mRNA_{UTR2}</i>	439	326	304	462	221	296	377	466	330	336
48 h <i>mCh_mRNA</i>	1050	1193	331	512	608	787	957	1141	698	827
48 h <i>mCh_mRNA_{UTR2}</i>	493	490	447	472	379	485	437	528	473	411

	H ₂ O Transf. Ctrl. #1	H ₂ O Transf. Ctrl. #2	Untr. Cells Ctrl. #1	Untr. Cells Ctrl. #2
6 h H ₂ O Transf. Ctrl.	73	28		
6 h Untr. Cells Ctrl.			2	69
24 h H ₂ O Transf. Ctrl.	4	15		
24 h Untr. Cells Ctrl.			45	39
48 h H ₂ O Transf. Ctrl.	27	32		
48 h Untr. Cells Ctrl.			1	54

Table 47. Raw fluorescence values measured from cells transfected with *mCh_mRNA* or *mCh_mRNA_{UTR 2}* variants and control values from exp. #3.

mCherry protein standard [ng/well]	0	20	40	60	80	100
Standard curve #1	38	136	170	256	424	432
Standard curve #2	43	95	192	336	346	430
Background (mean value for 0 ng/well)		40.5				
Slope line of best fit		4.60				
Coefficient of determination R ²		0.992				

Table 48. *mCherry* protein standard curve values and calculated parameters from *mCh_mRNA* or *mCh_mRNA_{UTR 2}* exp. #3.

	WT #1	WT #2	1 CP #1	1 CP #2	2 CP #1	2 CP #2	1 PM #1	1 PM #2	2 PM #1	2 PM #2
6 h mCh_mRNA	89	65	0	69	104	157	93	82	26	60
6 h mCh_mRNA _{UTR2}	31	75	52	59	17	56	101	78	53	90
24 h mCh_mRNA	985	1075	323	509	761	869	967	996	656	718
24 h mCh_mRNA _{UTR2}	607	537	438	543	363	436	515	560	406	486
48 h mCh_mRNA	1561	1424	492	592	1204	1259	1335	1480	1047	1170
48 h mCh_mRNA _{UTR2}	851	776	600	671	599	547	817	700	563	613

	H ₂ O Transf. Ctrl. #1	H ₂ O Transf. Ctrl. #2	Untr. Cells Ctrl. #1	Untr. Cells Ctrl. #2
6 h H ₂ O Transf. Ctrl.	60	9		
6 h Untr. Cells Ctrl.			0	44
24 h H ₂ O Transf. Ctrl.	59	8		
24 h Untr. Cells Ctrl.			34	39
48 h H ₂ O Transf. Ctrl.	43	17		
48 h Untr. Cells Ctrl.			76	10

Table 49. Raw fluorescence values measured from cells transfected with *mCh_mRNA* or *mCh_mRNA_{UTR 2}* variants and control values from exp. #4.

mCherry protein standard [ng/well]	0	20	40	60	80	100
Standard curve #1	49	122	266	282	289	548
Standard curve #2	50	102	301	304	393	413
Background (mean value for 0 ng/well)		49.5				
Slope line of best fit		4.84				
Coefficient of determination R ²		0.976				

Table 50. *mCherry* protein standard curve values and calculated parameters from *mCh_mRNA* or *mCh_mRNA_{UTR 2}* exp. #4.

	WT #1	WT #2	1 CP #1	1 CP #2	2 CP #1	2 CP #2	1 PM #1	1 PM #2	2 PM #1	2 PM #2
6 h mCh_mRNA	42	125	19	13	92	103	8	36	94	98
6 h mCh_mRNA _{UTR2}	13	0	21	41	0	0	26	89	43	42
24 h mCh_mRNA	694	670	117	390	833	683	659	782	582	574
24 h mCh_mRNA _{UTR2}	487	407	396	332	173	316	381	471	329	332
48 h mCh_mRNA	1194	1031	373	606	1219	1024	1234	1205	806	991
48 h mCh_mRNA _{UTR2}	610	566	597	570	390	321	635	653	526	480

	H ₂ O Transf. Ctrl. #1	H ₂ O Transf. Ctrl. #2	Untr. Cells Ctrl. #1	Untr. Cells Ctrl. #2
6 h H ₂ O Transf. Ctrl.	0	0		
6 h Untr. Cells Ctrl.			0	0
24 h H ₂ O Transf. Ctrl.	1	0		
24 h Untr. Cells Ctrl.			0	0
48 h H ₂ O Transf. Ctrl.	15	0		
48 h Untr. Cells Ctrl.			0	7

Table 51. Raw fluorescence values measured from cells transfected with *mCh_mRNA* or *mCh_mRNA_{UTR 2}* variants and control values from exp. #5.

mCherry protein standard [ng/well]	0	20	40	60	80	100	
Standard curve #1		10	104	263	367	523	616
Standard curve #2		13	135	241	389	480	653
Background (mean value for 0 ng/well)		11.5					
Slope line of best fit		6.31					
Coefficient of determination R ²		1					

Table 52. *mCherry* protein standard curve values and calculated parameters from *mCh_mRNA* or *mCh_mRNA_{UTR 2}* exp. #5.

	WT #1	WT #2	1 CP #1	1 CP #2	2 CP #1	2 CP #2	1 PM #1	1 PM #2	2 PM #1	2 PM #2
6 h mCh_mRNA	91	106	55	22	180	155	116	92	102	1
6 h mCh_mRNA _{UTR2}	52	46	49	67	57	31	52	38	54	34
24 h mCh_mRNA	717	647	226	371	750	975	696	742	463	614
24 h mCh_mRNA _{UTR2}	409	383	424	388	256	322	457	462	331	299
48 h mCh_mRNA	1072	833	279	520	1138	1243	1162	1196	799	866
48 h mCh_mRNA _{UTR2}	610	543	555	551	369	318	543	615	484	502

	H ₂ O Transf. Ctrl. #1	H ₂ O Transf. Ctrl. #2	Untr. Cells Ctrl. #1	Untr. Cells Ctrl. #2
6 h H ₂ O Transf. Ctrl.	63	0		
6 h Untr. Cells Ctrl.			37	0
24 h H ₂ O Transf. Ctrl.	43	0		
24 h Untr. Cells Ctrl.			45	9
48 h H ₂ O Transf. Ctrl.	62	4		
48 h Untr. Cells Ctrl.			37	13

Table 53. Raw fluorescence values measured from cells transfected with *mCh_mRNA* or *mCh_mRNA_{UTR 2}* variants and control values from exp. #6.

mCherry protein standard [ng/well]	0	20	40	60	80	100
Standard curve #1	4	106	202	304	435	507
Standard curve #2	0	154	222	387	394	564
Background (mean value for 0 ng/well)	2					
Slope line of best fit	5.18					
Coefficient of determination R ²	0.999					

Table 54. *mCherry* protein standard curve values and calculated parameters from *mCh_mRNA* or *mCh_mRNA_{UTR2}* exp. #6.

	WT #1	WT #2	1 CP #1	1 CP #2	2 CP #1	2 CP #2	1 PM #1	1 PM #2	2 PM #1	2 PM #2
6 h <i>mCh_mRNA</i>	72	124	51	56	90	67	140	96	107	79
6 h <i>mCh_mRNA_{UTR2}</i>	77	47	101	95	87	46	68	89	95	75
24 h <i>mCh_mRNA</i>	589	517	244	421	372	216	534	548	449	414
24 h <i>mCh_mRNA_{UTR2}</i>	514	492	604	625	365	423	463	433	343	381
48 h <i>mCh_mRNA</i>	692	691	301	443	320	333	668	726	513	603
48 h <i>mCh_mRNA_{UTR2}</i>	511	516	635	720	399	377	515	530	356	396

	H ₂ O Transf. Ctrl. #1	H ₂ O Transf. Ctrl. #2	Untr. Cells Ctrl. #1	Untr. Cells Ctrl. #2
6 h H ₂ O Transf. Ctrl.	20	1		
6 h Untr. Cells Ctrl.			33	61
24 h H ₂ O Transf. Ctrl.	15	33		
24 h Untr. Cells Ctrl.			88	120
48 h H ₂ O Transf. Ctrl.	38	8		
48 h Untr. Cells Ctrl.			76	45

Table 55. Raw fluorescence values measured from cells transfected with *mCh_mRNA* or *mCh_mRNA_{UTR2}* variants and control values from exp. #7.

mCherry protein standard [ng/well]	0	20	40	60	80	100
Standard curve #1	17	251	281	415	564	669
Standard curve #2	53	170	361	438	632	706
Background (mean value for 0 ng/well)	35					
Slope line of best fit	7.24					
Coefficient of determination R ²	0.993					

Table 56. *mCherry* protein standard curve values and calculated parameters from *mCh_mRNA* or *mCh_mRNA_{UTR2}* exp. #7.

	WT #1	WT #2	1 CP #1	1 CP #2	2 CP #1	2 CP #2	1 PM #1	1 PM #2	2 PM #1	2 PM #2
6 h <i>mCh_mRNA</i>	91	103	0	51	22	6	45	39	30	8
6 h <i>mCh_mRNA_{UTR2}</i>	42	23	96	85	13	23	81	55	73	80
24 h <i>mCh_mRNA</i>	587	616	231	378	260	389	536	538	395	480
24 h <i>mCh_mRNA_{UTR2}</i>	443	447	545	620	372	304	421	395	309	303
48 h <i>mCh_mRNA</i>	632	700	366	516	306	334	723	692	580	628
48 h <i>mCh_mRNA_{UTR2}</i>	549	446	714	682	474	409	474	515	401	374

	H ₂ O Transf. Ctrl. #1	H ₂ O Transf. Ctrl. #2	Untr. Cells Ctrl. #1	Untr. Cells Ctrl. #2
6 h H ₂ O Transf. Ctrl.	34	41		
6 h Untr. Cells Ctrl.			20	45
24 h H ₂ O Transf. Ctrl.	65	0		
24 h Untr. Cells Ctrl.			35	0
48 h H ₂ O Transf. Ctrl.	8	0		
48 h Untr. Cells Ctrl.			37	0

Table 57. Raw fluorescence values measured from cells transfected with *mCh_mRNA* or *mCh_mRNA_{UTR 2}* variants and control values from exp. #8.

mCherry protein standard [ng/well]	0	20	40	60	80	100
Standard curve #1	39	207	264	361	507	654
Standard curve #2	31	119	341	440	467	734
Background (mean value for 0 ng/well)		35				
Slope line of best fit		6.72				
Coefficient of determination R ²		0.994				

Table 58. *mCherry* protein standard curve values and calculated parameters from *mCh_mRNA* or *mCh_mRNA_{UTR 2}* exp. #8.

	WT #1	WT #2	1 CP #1	1 CP #2	2 CP #1	2 CP #2	1 PM #1	1 PM #2	2 PM #1	2 PM #2
6 h <i>mCh_mRNA</i>	0	2	0	59	4	0	32	39	0	41
6 h <i>mCh_mRNA_{UTR2}</i>	0	8	0	9	14	55	0	18	57	14
24 h <i>mCh_mRNA</i>	589	528	161	411	276	256	384	555	378	366
24 h <i>mCh_mRNA_{UTR2}</i>	437	326	526	583	275	359	430	441	285	285
48 h <i>mCh_mRNA</i>	545	566	205	389	246	298	546	571	358	492
48 h <i>mCh_mRNA_{UTR2}</i>	355	299	511	548	326	319	399	264	256	228

	H ₂ O Transf. Ctrl. #1	H ₂ O Transf. Ctrl. #2	Untr. Cells Ctrl. #1	Untr. Cells Ctrl. #2
6 h H ₂ O Transf. Ctrl.	0	0		
6 h Untr. Cells Ctrl.			0	0
24 h H ₂ O Transf. Ctrl.	0	0		
24 h Untr. Cells Ctrl.			0	0
48 h H ₂ O Transf. Ctrl.	0	0		
48 h Untr. Cells Ctrl.			0	0

Table 59. Raw fluorescence values measured from cells transfected with *mCh_mRNA* or *mCh_mRNA_{UTR 2}* variants and control values from exp. #9.

mCherry protein standard [ng/well]	0	20	40	60	80	100
Standard curve #1	0	67	202	307	456	511
Standard curve #2	0	102	197	273	369	557
Background (mean value for 0 ng/well)		0				
Slope line of best fit		5.16				
Coefficient of determination R ²		0.998				

Table 60. *mCherry* protein standard curve values and calculated parameters from *mCh_mRNA* or *mCh_mRNA_{UTR 2}* exp. #9.

	WT #1	WT #2	1 CP #1	1 CP #2	2 CP #1	2 CP #2	1 PM #1	1 PM #2	2 PM #1	2 PM #2
6 h mCh_mRNA	1	18	0	25	6	0	19	0	0	51
6 h mCh_mRNA _{UTR2}	0	21	31	22	54	0	0	21	54	0
24 h mCh_mRNA	655	510	228	371	299	435	623	712	409	523
24 h mCh_mRNA _{UTR2}	519	391	585	529	402	383	436	506	359	318
48 h mCh_mRNA	506	572	283	389	298	330	554	526	458	397
48 h mCh_mRNA _{UTR2}	390	363	615	585	312	414	337	396	254	256

	H ₂ O Transf. Ctrl. #1	H ₂ O Transf. Ctrl. #2	Untr. Cells Ctrl. #1	Untr. Cells Ctrl. #2
6 h H ₂ O Transf. Ctrl.	0	0		
6 h Untr. Cells Ctrl.			0	0
24 h H ₂ O Transf. Ctrl.	0	0		
24 h Untr. Cells Ctrl.			0	0
48 h H ₂ O Transf. Ctrl.	0	0		
48 h Untr. Cells Ctrl.			0	0

Table 61. Raw fluorescence values measured from cells transfected with *mCh_mRNA* or *mCh_mRNA_{UTR 2}* variants and control values from exp. #10.

mCherry protein standard [ng/well]	0	20	40	60	80	100
Standard curve #1	0	15	122	312	436	506
Standard curve #2	0	69	245	236	282	502

Background (mean value for 0 ng/well)	0
Slope line of best fit	4.72
Coefficient of determination R ²	0.991

Table 62. *mCherry* protein standard curve values and calculated parameters from exp. *mCh_mRNA* or *mCh_mRNA_{UTR 2}* Exp. #10.

	WT #1	WT #2	1 CP #1	1 CP #2	2 CP #1	2 CP #2
6 h mCh_mRNA	130	116	109	83	131	148
24 h mCh_mRNA	869	1083	572	549	846	767
48 h mCh_mRNA	1317	1468	775	834	1203	1204

	WT Ψ +5mC #1	WT Ψ +5mC #2	1 CP Ψ +5mC #1	1 CP Ψ +5mC #2	2 CP Ψ +5mC #1	2 CP Ψ +5mC #2
6 h mCh_mRNA	190	222	130	126	128	144
24 h mCh_mRNA	1850	1980	637	611	929	890
48 h mCh_mRNA	2540	2509	901	921	1154	1141

	H ₂ O Transf. Ctrl. #1	H ₂ O Transf. Ctrl. #2	Untr. Cells Ctrl. #1	Untr. Cells Ctrl. #2
6 h H ₂ O Transf. Ctrl.	13	71		
6 h Untr. Cells Ctrl.			44	67
24 h H ₂ O Transf. Ctrl.	26	2		
24 h Untr. Cells Ctrl.			61	64
48 h H ₂ O Transf. Ctrl.	35	48		
48 h Untr. Cells Ctrl.			37	47

Table 63. Raw fluorescence values measured from cells transfected with *mCh_mRNA* variants with or without natural base modifications and control values from exp. #1.

mCherry protein standard [ng/well]	0	20	40	60	80	100
Standard curve #1	6	127	262	347	354	450
Standard curve #2	86	138	238	307	386	383
Background (mean value for 0 ng/well)	46					
Slope line of best fit	4.68					
Coefficient of determination R ²	0.978					

Table 64. *mCherry* protein standard curve values and calculated parameters from exp. *mCh_mRNA* variants with or without natural base modifications exp. #1.

	WT #1	WT #2	1 CP #1	1 CP #2	2 CP #1	2 CP #2
6 h mCh_mRNA	121	98	96	92	189	161
24 h mCh_mRNA	1236	1447	667	746	1405	1343
48 h mCh_mRNA	1936	2360	1201	1219	1880	2339
	WT Ψ +5mC #1	WT Ψ +5mC #2	1 CP Ψ +5mC #1	1 CP Ψ +5mC #2	2 CP Ψ +5mC #1	2 CP Ψ +5mC #2
6 h mCh_mRNA	231	249	138	106	217	346
24 h mCh_mRNA	1681	1845	1216	1234	1869	1793
48 h mCh_mRNA	2716	2921	2364	1868	2777	2471

	H ₂ O Transf. Ctrl. #1	H ₂ O Transf. Ctrl. #2	Untr. Cells Ctrl. #1	Untr. Cells Ctrl. #2
6 h H ₂ O Transf. Ctrl.	18	0		
6 h Untr. Cells Ctrl.			2	40
24 h H ₂ O Transf. Ctrl.	6	27		
24 h Untr. Cells Ctrl.			36	3
48 h H ₂ O Transf. Ctrl.	19	25		
48 h Untr. Cells Ctrl.			13	21

Table 65. Raw fluorescence values measured from cells transfected with *mCh_mRNA* variants with or without natural base modifications and control values from exp. #2.

mCherry protein standard [ng/well]	0	20	40	60	80	100
Standard curve #1	0	143	215	304	466	595
Standard curve #2	0	150	256	385	365	514
Background (mean value for 0 ng/well)		0				
Slope line of best fit		5.53				
Coefficient of determination R ²		0.997				

Table 66. mCherry protein standard curve values and calculated parameters from exp. *mCh_mRNA* variants with or without natural base modifications exp. #2.

	WT #1	WT #2	1 CP #1	1 CP #2	2 CP #1	2 CP #2
6 h mCh_mRNA	0	92	0	27	76	37
24 h mCh_mRNA	404	1017	432	545	1159	1141
48 h mCh_mRNA	594	1465	812	794	1477	1405
	WT Ψ +5mC #1	WT Ψ +5mC #2	1 CP Ψ +5mC #1	1 CP Ψ +5mC #2	2 CP Ψ +5mC #1	2 CP Ψ +5mC #2
6 h mCh_mRNA	91	65	75	64	147	178
24 h mCh_mRNA	1704	1275	1080	1078	1685	1643
48 h mCh_mRNA	1687	1832	1541	1504	330	1835

	H ₂ O Transf. Ctrl. #1	H ₂ O Transf. Ctrl. #2	Untr. Cells Ctrl. #1	Untr. Cells Ctrl. #2
6 h H ₂ O Transf. Ctrl.	0	0		
6 h Untr. Cells Ctrl.			0	0
24 h H ₂ O Transf. Ctrl.	0	0		
24 h Untr. Cells Ctrl.			0	0
48 h H ₂ O Transf. Ctrl.	0	0		
48 h Untr. Cells Ctrl.			0	0

Table 67. Raw fluorescence values measured from cells transfected with *mCh_mRNA* variants with or without natural base modifications and control values from exp. #3.

mCherry protein standard [ng/well]	0	20	40	60	80	100
Standard curve #1	0	55	187	271	411	472
Standard curve #2	0	72	199	215	402	481
Background (mean value for 0 ng/well)		0				
Slope line of best fit		4.77				
Coefficient of determination R ²		0.995				

Table 68. mCherry protein standard curve values and calculated parameters from exp. *mCh_mRNA* variants with or without natural base modifications exp. #3.

	WT #1	WT #2	1 CP #1	1 CP #2	2 CP #1	2 CP #2
6 h mCh_mRNA	38	22	21	76	83	112
24 h mCh_mRNA	313	761	439	521	1036	999
48 h mCh_mRNA	504	1389	897	950	1584	1198

	WT Ψ +5mC #1	WT Ψ +5mC #2	1 CP Ψ +5mC #1	1 CP Ψ +5mC #2	2 CP Ψ +5mC #1	2 CP Ψ +5mC #2
6 h mCh_mRNA	177	131	111	78	167	246
24 h mCh_mRNA	1082	1087	1042	909	1667	1352
48 h mCh_mRNA	1446	1788	1442	1492	2055	1862

	H ₂ O Transf. Ctrl. #1	H ₂ O Transf. Ctrl. #2	Untr. Cells Ctrl. #1	Untr. Cells Ctrl. #2
6 h H ₂ O Transf. Ctrl.	0	0		
6 h Untr. Cells Ctrl.			0	52
24 h H ₂ O Transf. Ctrl.	5	0		
24 h Untr. Cells Ctrl.			0	15
48 h H ₂ O Transf. Ctrl.	0	55		
48 h Untr. Cells Ctrl.			0	0

Table 69. Raw fluorescence values measured from cells transfected with *mCh_mRNA* variants with or without natural base modifications and control values from exp. #4.

mCherry protein standard [ng/well]	0	20	40	60	80	100
Standard curve #1	0	139	282	418	480	605
Standard curve #2	0	121	283	286	475	648

Background (mean value for 0 ng/well)	0
Slope line of best fit	6.18
Coefficient of determination R ²	0.998

Table 70. *mCherry* protein standard curve values and calculated parameters from exp. *mCh_mRNA* variants with or without natural base modifications exp. #4.

	WT #1	WT #2	1 CP #1	1 CP #2	2 CP #1	2 CP #2
6 h mCh_mRNA	101	68	43	62	104	106
24 h mCh_mRNA	503	673	216	291	950	992
48 h mCh_mRNA	287	1092	548	616	1460	1400

	WT Ψ +5mC #1	WT Ψ +5mC #2	1 CP Ψ +5mC #1	1 CP Ψ +5mC #2	2 CP Ψ +5mC #1	2 CP Ψ +5mC #2
6 h mCh_mRNA	110	85	140	79	171	126
24 h mCh_mRNA	915	1114	643	667	1024	951
48 h mCh_mRNA	1520	1689	975	959	1538	1449

	H ₂ O Transf. Ctrl. #1	H ₂ O Transf. Ctrl. #2	Untr. Cells Ctrl. #1	Untr. Cells Ctrl. #2
6 h H ₂ O Transf. Ctrl.	0	0		
6 h Untr. Cells Ctrl.			0	0
24 h H ₂ O Transf. Ctrl.	20	0		
24 h Untr. Cells Ctrl.			0	0
48 h H ₂ O Transf. Ctrl.	0	0		
48 h Untr. Cells Ctrl.			0	0

Table 71. Raw fluorescence values measured from cells transfected with *mCh_mRNA* variants with or without natural base modifications and control values from exp. #5.

mCherry protein standard [ng/well]	0	20	40	60	80	100
Standard curve #1	0	101	159	315	389	535
Standard curve #2	0	103	219	324	434	523
<hr/>						
Background (mean value for 0 ng/well)	0					
Slope line of best fit	5.33					
Coefficient of determination R ²	1					

Table 72. *mCherry* protein standard curve values and calculated parameters from exp. *mCh_mRNA* variants with or without natural base modifications exp. #5.

	WT #1	WT #2	1 CP #1	1 CP #2	2 CP #1	2 CP #2
6 h mCh_mRNA	89	90	46	34	118	65
24 h mCh_mRNA	524	647	327	367	1142	1073
48 h mCh_mRNA	1110	1468	742	789	1751	1608
<hr/>						
	WT Ψ +5mC #1	WT Ψ +5mC #2	1 CP Ψ +5mC #1	1 CP Ψ +5mC #2	2 CP Ψ +5mC #1	2 CP Ψ +5mC #2
6 h mCh_mRNA	65	107	50	73	84	127
24 h mCh_mRNA	1071	1145	687	713	1152	1242
48 h mCh_mRNA	1710	1992	1175	1167	1584	1451

	H ₂ O Transf. Ctrl. #1	H ₂ O Transf. Ctrl. #2	Untr. Cells Ctrl. #1	Untr. Cells Ctrl. #2
6 h H ₂ O Transf. Ctrl.	0	0		
6 h Untr. Cells Ctrl.			0	0
24 h H ₂ O Transf. Ctrl.	0	0		
24 h Untr. Cells Ctrl.			0	2
48 h H ₂ O Transf. Ctrl.	0	0		
48 h Untr. Cells Ctrl.			0	0

Table 73. Raw fluorescence values measured from cells transfected with *mCh_mRNA* variants with or without natural base modifications and control values from exp. #6.

mCherry protein standard [ng/well]	0	20	40	60	80	100
Standard curve #1	0	96	260	314	449	505
Standard curve #2	6	117	203	344	484	465
<hr/>						
Background (mean value for 0 ng/well)	3					
Slope line of best fit	5.34					
Coefficient of determination R ²	0.994					

Table 74. *mCherry* protein standard curve values and calculated parameters from exp. *mCh_mRNA* variants with or without natural base modifications exp. #6.

	WT #1	WT #2	1 CP #1	1 CP #2	2 CP #1	2 CP #2
6 h mCh_mRNA	94	177	169	186	144	148
24 h mCh_mRNA	683	857	875	872	1009	900
48 h mCh_mRNA	1019	1347	1523	1476	1488	1454

	WT Ψ +5mC #1	WT Ψ +5mC #2	1 CP Ψ +5mC #1	1 CP Ψ +5mC #2	2 CP Ψ +5mC #1	2 CP Ψ +5mC #2
6 h mCh_mRNA	441	443	359	362	373	321
24 h mCh_mRNA	2732	3041	1951	2176	2071	1891
48 h mCh_mRNA	4304	4424	2931	2923	3027	2894

	H ₂ O Transf. Ctrl. #1	H ₂ O Transf. Ctrl. #2	Untr. Cells Ctrl. #1	Untr. Cells Ctrl. #2
6 h H ₂ O Transf. Ctrl.	65	37		
6 h Untr. Cells Ctrl.			101	92
24 h H ₂ O Transf. Ctrl.	71	101		
24 h Untr. Cells Ctrl.			93	87
48 h H ₂ O Transf. Ctrl.	119	96		
48 h Untr. Cells Ctrl.			83	81

Table 75. Raw fluorescence values measured from cells transfected with *mCh_mRNA* variants with or without natural base modifications and control values from exp. #7.

mCherry protein standard [ng/well]	0	20	40	60	80	100	
Standard curve #1		87	226	298	488	633	787
Standard curve #2		112	243	413	514	575	739

Background (mean value for 0 ng/well)	99.5
Slope line of best fit	7.96
Coefficient of determination R ²	0.991

Table 76. *mCherry* protein standard curve values and calculated parameters from exp. *mCh_mRNA* variants with or without natural base modifications exp. #7.

	WT #1	WT #2	1 CP #1	1 CP #2	2 CP #1	2 CP #2
6 h mCh_mRNA	45	67	104	58	35	87
24 h mCh_mRNA	592	728	734	796	794	771
48 h mCh_mRNA	970	1270	1288	1390	1323	1321

	WT Ψ +5mC #1	WT Ψ +5mC #2	1 CP Ψ +5mC #1	1 CP Ψ +5mC #2	2 CP Ψ +5mC #1	2 CP Ψ +5mC #2
6 h mCh_mRNA	298	290	229	233	259	266
24 h mCh_mRNA	2512	2818	1696	1880	1961	1759
48 h mCh_mRNA	4006	4200	2715	2682	2752	2671

	H ₂ O Transf. Ctrl. #1	H ₂ O Transf. Ctrl. #2	Untr. Cells Ctrl. #1	Untr. Cells Ctrl. #2
6 h H ₂ O Transf. Ctrl.	2	0		
6 h Untr. Cells Ctrl.			0	0
24 h H ₂ O Transf. Ctrl.	0	15		
24 h Untr. Cells Ctrl.			2	9
48 h H ₂ O Transf. Ctrl.	13	0		
48 h Untr. Cells Ctrl.			0	29

Table 77. Raw fluorescence values measured from cells transfected with *mCh_mRNA* variants with or without natural base modifications and control values from exp. #8.

mCherry protein standard [ng/well]	0	20	40	60	80	100
Standard curve #1	0	120	250	345	492	627
Standard curve #2	5	138	226	356	526	596
Background (mean value for 0 ng/well)		2.5				
Slope line of best fit		6.14				
Coefficient of determination R ²		0.999				

Table 78. *mCherry* protein standard curve values and calculated parameters from exp. *mCh_mRNA* variants with or without natural base modifications exp. #8.

	WT #1	WT #2	1 CP #1	1 CP #2	2 CP #1	2 CP #2
6 h mCh_mRNA	59	37	99	132	81	88
24 h mCh_mRNA	284	683	884	827	1057	889
48 h mCh_mRNA	369	1137	1274	1273	1208	1091
	WT Ψ +5mC #1	WT Ψ +5mC #2	1 CP Ψ +5mC #1	1 CP Ψ +5mC #2	2 CP Ψ +5mC #1	2 CP Ψ +5mC #2
6 h mCh_mRNA	117	110	247	176	246	242
24 h mCh_mRNA	709	727	928	1154	2096	1883
48 h mCh_mRNA	1075	1142	2000	2521	2477	2139

	H ₂ O Transf. Ctrl. #1	H ₂ O Transf. Ctrl. #2	Untr. Cells Ctrl. #1	Untr. Cells Ctrl. #2
6 h H ₂ O Transf. Ctrl.	32	76		
6 h Untr. Cells Ctrl.			0	0
24 h H ₂ O Transf. Ctrl.	18	0		
24 h Untr. Cells Ctrl.			0	0
48 h H ₂ O Transf. Ctrl.	18	71		
48 h Untr. Cells Ctrl.			0	0

Table 79. Raw fluorescence values measured from cells transfected with *mCh_mRNA* variants with or without natural base modifications and control values from exp. #9.

mCherry protein standard [ng/well]	0	20	40	60	80	100
Standard curve #1	32	131	206	383	545	634
Standard curve #2	0	161	284	369	576	774
Background (mean value for 0 ng/well)		16				
Slope line of best fit		6.84				
Coefficient of determination R ²		0.997				

Table 80. *mCherry* protein standard curve values and calculated parameters from exp. *mCh_mRNA* variants with or without natural base modifications exp. #9.

	WT #1	WT #2	1 CP #1	1 CP #2	2 CP #1	2 CP #2
6 h mCh_mRNA	91	150	176	143	133	191
24 h mCh_mRNA	355	813	898	848	1063	869
48 h mCh_mRNA	469	1186	1307	1314	1164	1175
	WT Ψ +5mC #1	WT Ψ +5mC #2	1 CP Ψ +5mC #1	1 CP Ψ +5mC #2	2 CP Ψ +5mC #1	2 CP Ψ +5mC #2
6 h mCh_mRNA	196	152	291	281	321	316

24 h mCh_mRNA	761	719	1040	1216	1984	1847
48 h mCh_mRNA	1137	1115	1977	2409	2341	2299

	H ₂ O Transf. Ctrl. #1	H ₂ O Transf. Ctrl. #2	Untr. Cells Ctrl. #1	Untr. Cells Ctrl. #2
6 h H ₂ O Transf. Ctrl.	66	153		
6 h Untr. Cells Ctrl.			95	48
24 h H ₂ O Transf. Ctrl.	93	50		
24 h Untr. Cells Ctrl.			88	85
48 h H ₂ O Transf. Ctrl.	77	52		
48 h Untr. Cells Ctrl.			107	18

Table 81. Raw fluorescence values measured from cells transfected with *mCh_mRNA* variants with or without natural base modifications and control values from exp. #10.

mCherry protein standard [ng/well]	0	20	40	60	80	100
Standard curve #1	70	204	290	372	654	635
Standard curve #2	86	283	298	425	549	807

Background (mean value for 0 ng/well)	78
Slope line of best fit	7.31
Coefficient of determination R ²	0.985

Table 82. *mCherry* protein standard curve values and calculated parameters from exp. *mCh_mRNA* variants with or without natural base modifications exp. #10.

	WT	error	1 CP	error	2 CP	error	1 PM	error	2 PM	error
6 h mCh_mRNA	-0.84	1.15	-1.53	9.20	3.53	0.46	-3.45	7.29	-4.30	6.14
6 h mCh_mRNA _{UTR2}	2.61	1.07	0.61	0.00	-4.83	5.91	5.29	4.68	-1.46	2.07
24 h mCh_mRNA	49.16	3.91	34.59	10.51	57.68	8.44	57.22	2.61	46.63	3.53
24 h mCh_mRNA _{UTR2}	32.37	10.74	42.57	4.37	29.15	1.53	41.88	4.45	32.67	5.83
48 h mCh_mRNA	78.92	3.60	43.33	24.01	82.91	5.29	77.23	1.46	62.51	11.58
48 h mCh_mRNA _{UTR2}	41.88	1.84	62.51	5.14	53.84	6.60	59.06	1.84	48.63	6.14

	H ₂ O Transf. Ctrl.	error	Untr. Cells Ctrl.	error
6 h H ₂ O Transf. Ctrl.	-1.61	2.84		
6 h Untr. Cells Ctrl.			-4.45	3.83
24 h H ₂ O Transf. Ctrl.	-6.83	3.91		
24 h Untr. Cells Ctrl.			-7.29	3.14
48 h H ₂ O Transf. Ctrl.	-2.45	4.45		
48 h Untr. Cells Ctrl.			-4.30	1.99

Table 83. Mean values [ng *mCherry* protein/well] and standard deviation of duplicate samples, background subtracted and divided by slope of linear standard curve for *mCh_mRNA* or *mCh_mRNA_{UTR2}* variants and controls from exp. #1.

	WT	error	1 CP	error	2 CP	error	1 PM	error	2 PM	error
6 h mCh_mRNA	4.08	2.72	0,00	0,00	0.68	0.68	4.08	4.08	4.76	4.76
6 h mCh_mRNA _{UTR2}	6.25	6.25	6,53	2,18	0.00	0.00	12.37	8.29	11.28	0.14
24 h mCh_mRNA	94.90	13.32	53,97	16,72	93.13	1.77	88.23	3.13	67.57	0.68
24 h mCh_mRNA _{UTR2}	62.13	11.28	72,74	2,31	49.35	2.86	61.32	8.29	62.81	7.34
48 h mCh_mRNA	134.05	6.25	78,45	0,95	140.71	3.13	111.62	27.33	101.15	5.98
48 h mCh_mRNA _{UTR2}	93.81	0.54	105,91	2,31	61.18	6.80	101.29	3.13	67.03	27.60

	H ₂ O Transf. Ctrl.	error	Untr. Cells Ctrl.	error
6 h H ₂ O Transf. Ctrl.	0.00	0.00		
6 h Untr. Cells Ctrl.			0.00	0.00
24 h H ₂ O Transf. Ctrl.	0.00	0.00		
24 h Untr. Cells Ctrl.			0.00	0.00
48 h H ₂ O Transf. Ctrl.	0.68	0.68		
48 h Untr. Cells Ctrl.			3.53	3.53

Table 84. Mean values [ng *mCherry* protein/well] and standard deviation of duplicate samples, background subtracted and divided by slope of linear standard curve for *mCh_mRNA* or *mCh_mRNA_{UTR2}* variants and controls from exp. #2.

	WT	error	1 CP	error	2 CP	error	1 PM	error	2 PM	error
6 h mCh_mRNA	18.04	1.85	-1.85	6.74	20.65	2.50	13.80	7.17	-0.65	3.15
6 h mCh_mRNA _{UTR2}	9.13	1.20	-3.37	2.83	2.72	0.43	5.43	5.54	0.22	1.20
24 h mCh_mRNA	176.18	4.56	57.49	15.00	112.92	3.70	140.75	11.52	111.84	10.87
24 h mCh_mRNA _{UTR2}	74.34	12.28	74.45	17.17	47.39	8.15	82.82	9.67	63.58	0.65
48 h mCh_mRNA	234.97	15.54	82.82	19.67	142.81	19.45	219.22	20.00	156.94	14.02
48 h mCh_mRNA _{UTR2}	98.03	0.33	91.08	2.72	85.10	11.52	96.08	9.89	87.27	6.74

	H ₂ O Transf. Ctrl.	error	Untr. Cells Ctrl.	error
6 h H ₂ O Transf. Ctrl.	2.17	4.89		
6 h Untr. Cells Ctrl.			-1.09	7.28
24 h H ₂ O Transf. Ctrl.	-6.74	1.20		
24 h Untr. Cells Ctrl.			0.33	0.65
48 h H ₂ O Transf. Ctrl.	-2.39	0.54		
48 h Untr. Cells Ctrl.			-2.83	5.76

Table 85. Mean values [ng *mCherry* protein/well] and standard deviation of duplicate samples, background subtracted and divided by slope of linear standard curve for *mCh_mRNA* or *mCh_mRNA_{UTR2}* variants and controls from exp. #3.

	WT	error	1 CP	error	2 CP	error	1 PM	error	2 PM	error
6 h mCh_mRNA	5.68	2.48	-3.10	7.13	16.73	5.47	7.85	1.14	-1.34	3.51
6 h mCh_mRNA _{UTR2}	0.72	4.54	1.24	0.72	-2.69	4.03	8.26	2.38	4.54	3.82
24 h mCh_mRNA	202.56	9.30	75.72	19.21	158.14	11.16	192.54	3.00	131.70	6.40
24 h mCh_mRNA _{UTR2}	107.94	7.23	91.11	10.85	72.31	7.54	100.82	4.65	81.91	8.26
48 h mCh_mRNA	298.11	14.15	101.75	10.33	244.19	5.68	280.55	14.98	218.78	12.71
48 h mCh_mRNA _{UTR2}	157.83	7.75	121.06	7.33	108.15	5.37	146.47	12.09	111.25	5.16

	H ₂ O Transf. Ctrl.	Error	Untr. Cells Ctrl.	Error
6 h H ₂ O Transf. Ctrl.	-3.10	5.27		
6 h Untr. Cells Ctrl.			-5.68	4.54
24 h H ₂ O Transf. Ctrl.	-3.31	5.27		
24 h Untr. Cells Ctrl.			-2.69	0.52
48 h H ₂ O Transf. Ctrl.	-4.03	2.69		
48 h Untr. Cells Ctrl.			-1.34	6.82

Table 86. Mean values [ng *mCherry* protein/well] and standard deviation of duplicate samples, background subtracted and divided by slope of linear standard curve for *mCh_mRNA* or *mCh_mRNA_{UTR 2}* variants and controls from exp. #4.

	WT	error	1 CP	error	2 CP	error	1 PM	error	2 PM	error
6 h <i>mCh_mRNA</i>	11.42	6.58	0.71	0.48	13.64	0.87	1.67	2.22	13.40	0.32
6 h <i>mCh_mRNA_{UTR2}</i>	-0.79	1.03	3.09	1.59	-1.82	0.00	7.30	5.00	4.92	0.08
24 h <i>mCh_mRNA</i>	106.34	1.90	38.38	21.65	118.39	11.89	112.44	9.75	89.84	0.63
24 h <i>mCh_mRNA_{UTR2}</i>	69.07	6.34	55.90	5.07	36.95	11.34	65.74	7.14	50.59	0.24
48 h <i>mCh_mRNA</i>	174.61	12.93	75.81	18.48	176.04	15.46	191.58	2.30	140.67	14.67
48 h <i>mCh_mRNA_{UTR2}</i>	91.43	3.49	90.71	2.14	54.56	5.47	100.31	1.43	77.95	3.65

	H ₂ O Transf. Ctrl.	error	Untr. Cells Ctrl.	error
6 h H ₂ O Transf. Ctrl.	-1.82	0.00		
6 h Untr. Cells Ctrl.			-1.82	0.00
24 h H ₂ O Transf. Ctrl.	-1.74	0.08		
24 h Untr. Cells Ctrl.			-1.82	0.00
48 h H ₂ O Transf. Ctrl.	-0.63	1.19		
48 h Untr. Cells Ctrl.			-1.27	0.56

Table 87. Mean values [ng *mCherry* protein/well] and standard deviation of duplicate samples, background subtracted and divided by slope of linear standard curve for *mCh_mRNA* or *mCh_mRNA_{UTR 2}* variants and controls from exp. #5.

	WT	error	1 CP	error	2 CP	error	1 PM	error	2 PM	error
6 h <i>mCh_mRNA</i>	18.63	1.45	7.05	3.19	31.96	2.41	19.69	2.32	9.56	9.75
6 h <i>mCh_mRNA_{UTR2}</i>	9.07	0.58	10.81	1.74	8.11	2.51	8.30	1.35	8.11	1.93
24 h <i>mCh_mRNA</i>	131.30	6.76	57.25	14.00	166.15	21.72	138.44	4.44	103.59	14.58
24 h <i>mCh_mRNA_{UTR2}</i>	76.07	2.51	78.01	3.48	55.42	6.37	88.34	0.48	60.44	3.09
48 h <i>mCh_mRNA</i>	183.53	23.07	76.75	23.27	229.48	10.14	227.26	3.28	160.36	6.47
48 h <i>mCh_mRNA_{UTR2}</i>	110.93	6.47	106.39	0.39	65.94	4.92	111.41	6.95	94.80	1.74

	H ₂ O Transf. Ctrl.	error	Untr. Cells Ctrl.	error
6 h H ₂ O Transf. Ctrl.	5.70	6.08		
6 h Untr. Cells Ctrl.			3.19	3.57
24 h H ₂ O Transf. Ctrl.	3.77	4.15		
24 h Untr. Cells Ctrl.			4.83	3.48
48 h H ₂ O Transf. Ctrl.	5.99	5.60		
48 h Untr. Cells Ctrl.			4.44	2.32

Table 88. Mean values [ng *mCherry* protein/well] and standard deviation of duplicate samples, background subtracted and divided by slope of linear standard curve for *mCh_mRNA* or *mCh_mRNA_{UTR 2}* variants and controls from exp. #6.

	WT	error	1 CP	error	2 CP	error	1 PM	error	2 PM	error
6 h <i>mCh_mRNA</i>	8.70	3.59	2.56	0.35	6.01	1.59	11.47	3.04	8.01	1.93
6 h <i>mCh_mRNA_{UTR2}</i>	3.73	2.07	8.70	0.41	4.35	2.83	6.01	1.45	6.91	1.38
24 h <i>mCh_mRNA</i>	71.57	4.97	41.10	12.23	35.78	10.78	69.91	0.97	54.78	2.42
24 h <i>mCh_mRNA_{UTR2}</i>	64.66	1.52	80.07	1.45	49.60	4.01	57.06	2.07	45.18	2.63
48 h <i>mCh_mRNA</i>	90.71	0.07	46.56	9.81	40.28	0.90	91.47	4.01	72.26	6.22
48 h <i>mCh_mRNA_{UTR2}</i>	66.11	0.35	88.77	5.87	48.77	1.52	67.36	1.04	47.11	2.76

	H ₂ O Transf. Ctrl.	error	Untr. Cells Ctrl.	error
6 h H ₂ O Transf. Ctrl.	-3.39	1.31		
6 h Untr. Cells Ctrl.			1.66	1.93
24 h H ₂ O Transf. Ctrl.	-1.52	1.24		
24 h Untr. Cells Ctrl.			9.53	2.21
48 h H ₂ O Transf. Ctrl.	-1.66	2.07		
48 h Untr. Cells Ctrl.			3.52	2.14

Table 89. Mean values [ng *mCherry* protein/well] and standard deviation of duplicate samples, background subtracted and divided by slope of linear standard curve for *mCh_mRNA* or *mCh_mRNA_{UTR 2}* variants and controls from exp. #7.

	WT	error	1 CP	error	2 CP	error	1 PM	error	2 PM	error
6 h <i>mCh_mRNA</i>	9.23	0.89	-1.41	3.80	-3.13	1.19	1.04	0.45	-2.38	1.64
6 h <i>mCh_mRNA_{UTR2}</i>	-0.37	1.41	8.26	0.82	-2.53	0.74	4.91	1.94	6.18	0.52
24 h <i>mCh_mRNA</i>	84.35	2.16	40.13	10.94	43.11	9.60	74.75	0.15	59.93	6.33
24 h <i>mCh_mRNA_{UTR2}</i>	61.05	0.30	81.52	5.58	45.12	5.06	55.54	1.94	40.35	0.45
48 h <i>mCh_mRNA</i>	93.96	5.06	60.45	11.17	42.44	2.08	100.14	2.31	84.72	3.57
48 h <i>mCh_mRNA_{UTR2}</i>	68.87	7.67	98.72	2.38	60.53	4.84	68.42	3.05	52.49	2.01

	H ₂ O Transf. Ctrl.	error	Untr. Cells Ctrl.	error
6 h H ₂ O Transf. Ctrl.	0.37	0.52		
6 h Untr. Cells Ctrl.			-0.37	1.86
24 h H ₂ O Transf. Ctrl.	-0.37	4.84		
24 h Untr. Cells Ctrl.			-2.61	2.61
48 h H ₂ O Transf. Ctrl.	-4.62	0.60		
48 h Untr. Cells Ctrl.			-2.46	2.75

Table 90. Mean values [ng *mCherry* protein/well] and standard deviation of duplicate samples, background subtracted and divided by slope of linear standard curve for *mCh_mRNA* or *mCh_mRNA_{UTR 2}* variants and controls from exp. #8.

	WT	error	1 CP	error	2 CP	error	1 PM	error	2 PM	error
6 h <i>mCh_mRNA</i>	0.19	0.19	5.72	5.72	0.39	0.39	6.88	0.68	3.97	3.97
6 h <i>mCh_mRNA_{UTR2}</i>	0.78	0.78	0.87	0.87	6.69	3.97	1.74	1.74	6.88	4.17
24 h <i>mCh_mRNA</i>	108.28	5.91	55.45	24.24	51.57	1.94	91.03	16.58	72.13	1.16
24 h <i>mCh_mRNA_{UTR2}</i>	73.97	10.76	107.51	5.53	61.46	8.14	84.44	1.07	55.26	0.00
48 h <i>mCh_mRNA</i>	107.70	2.04	57.58	17.84	52.74	5.04	108.28	2.42	82.40	12.99
48 h <i>mCh_mRNA_{UTR2}</i>	63.40	5.43	102.66	3.59	62.53	0.68	64.27	13.09	46.92	2.71

	H ₂ O Transf. Ctrl.	error	Untr. Cells Ctrl.	error
6 h H ₂ O Transf. Ctrl.	0.00	0.00		
6 h Untr. Cells Ctrl.			0.00	0.00
24 h H ₂ O Transf. Ctrl.	0.00	0.00		
24 h Untr. Cells Ctrl.			0.00	0.00
48 h H ₂ O Transf. Ctrl.	0.00	0.00		
48 h Untr. Cells Ctrl.			0.00	0.00

Table 91. Mean values [ng *mCherry* protein/well] and standard deviation of duplicate samples, background subtracted and divided by slope of linear standard curve for *mCh_mRNA* or *mCh_mRNA_{UTR 2}* variants and controls from exp. #9.

	WT	error	1 CP	error	2 CP	error	1 PM	error	2 PM	error
6 h <i>mCh_mRNA</i>	2.01	1.80	2.65	2.65	0.64	0.64	2.01	2.01	5.41	5.41
6 h <i>mCh_mRNA_{UTR2}</i>	2.23	2.23	5.62	0.95	5.73	5.73	2.23	2.23	5.73	5.73
24 h <i>mCh_mRNA</i>	123.53	15.37	63.51	15.16	77.83	14.42	141.55	9.44	98.82	12.09
24 h <i>mCh_mRNA_{UTR2}</i>	96.49	13.57	118.12	5.94	83.24	2.01	99.88	7.42	71.78	4.35
48 h <i>mCh_mRNA</i>	114.30	7.00	71.25	11.24	66.59	3.39	114.52	2.97	90.66	6.47
48 h <i>mCh_mRNA_{UTR2}</i>	79.84	2.86	127.24	3.18	76.98	10.82	77.72	6.26	54.08	0.21

	H ₂ O Transf. Ctrl.	error	Untr. Cells Ctrl.	error
6 h H ₂ O Transf. Ctrl.	0.00	0.00		
6 h Untr. Cells Ctrl.			0.00	0.00
24 h H ₂ O Transf. Ctrl.	0.00	0.00		
24 h Untr. Cells Ctrl.			0.00	0.00
48 h H ₂ O Transf. Ctrl.	0.00	0.00		
48 h Untr. Cells Ctrl.			0.00	0.00

Table 92. Mean values [ng *mCherry* protein/well] and standard deviation of duplicate samples, background subtracted and divided by slope of linear standard curve for *mCh_mRNA* or *mCh_mRNA_{UTR 2}* variants and controls from exp. #10.

	WT	error	1 CP	error	2 CP	error
6 h <i>mCh_mRNA</i>	16.44	1.49	10.68	2.78	19.96	1.81
24 h <i>mCh_mRNA</i>	198.57	22.85	109.85	2.46	162.38	8.43
48 h <i>mCh_mRNA</i>	287.49	16.12	161.95	6.30	247.14	0.11

	WT $\Psi+5mC$	error	1 CP $\Psi+5mC$	error	2 CP $\Psi+5mC$	error
6 h <i>mCh_mRNA</i>	34.16	3.42	17.51	0.43	19.22	1.71
24 h <i>mCh_mRNA</i>	399.05	13.88	123.41	2.78	184.37	4.16
48 h <i>mCh_mRNA</i>	529.19	3.31	184.69	2.14	235.18	1.39

	H ₂ O Transf. Ctrl.	error	Untr. Cells Ctrl.	error
6 h H ₂ O Transf. Ctrl.	-0.85	6.19		
6 h Untr. Cells Ctrl.			2.03	2.46
24 h H ₂ O Transf. Ctrl.	-6.83	2.56		
24 h Untr. Cells Ctrl.			3.52	0.32
48 h H ₂ O Transf. Ctrl.	-0.96	1.39		
48 h Untr. Cells Ctrl.			-0.85	1.07

Table 93. Mean values [ng *mCherry* protein/well] and standard deviation of duplicate samples, background subtracted and divided by slope of linear standard curve for *mCh_mRNA* with or without natural base modifications and controls from exp. #1.

	WT	error	1 CP	error	2 CP	error
6 h <i>mCh_mRNA</i>	19.79	2.08	16.99	0.36	31.63	2.53
24 h <i>mCh_mRNA</i>	242.49	19.07	127.70	7.14	248.36	5.60
48 h <i>mCh_mRNA</i>	388.27	38.32	218.72	1.63	381.31	41.48

	WT $\Psi+5mC$	error	1 CP $\Psi+5mC$	error	2 CP $\Psi+5mC$	error
6 h <i>mCh_mRNA</i>	43.38	1.63	22.05	2.89	50.88	11.66
24 h <i>mCh_mRNA</i>	318.67	14.82	221.43	1.63	330.97	6.87
48 h <i>mCh_mRNA</i>	509.46	18.53	382.48	44.83	474.31	27.66

	H ₂ O Transf. Ctrl.	Error	Untr. Cells Ctrl.	Error
6 h H ₂ O Transf. Ctrl.	1.63	1.63		
6 h Untr. Cells Ctrl.			0.18	0.18
24 h H ₂ O Transf. Ctrl.	2.98	1.90		
24 h Untr. Cells Ctrl.			3.25	3.25
48 h H ₂ O Transf. Ctrl.	3.98	0.54		
48 h Untr. Cells Ctrl.			1.17	1.17

Table 94. Mean values [ng *mCherry* protein/well] and standard deviation of duplicate samples, background subtracted and divided by slope of linear standard curve for *mCh_mRNA* with or without natural base modifications and controls from exp. #2.

	WT	error	1 CP	error	2 CP	error
6 h mCh_mRNA	9.65	9.65	2.83	2.83	11.85	4.09
24 h mCh_mRNA	148.98	64.27	102.43	11.85	241.14	1.89
48 h mCh_mRNA	215.87	91.32	168.38	1.89	302.15	7.55

	WT Ψ+5mC	error	1 CP Ψ+5mC	error	2 CP Ψ+5mC	error
6 h mCh_mRNA	16.36	2.73	14.57	1.15	34.07	3.25
24 h mCh_mRNA	312.32	44.98	226.25	0.21	348.91	4.40
48 h mCh_mRNA	368.94	15.20	319.24	3.88	226.98	157.79

	H ₂ O Transf. Ctrl.	Error	Untr. Cells Ctrl.	Error
6 h H ₂ O Transf. Ctrl.	0.00	0.00		
6 h Untr. Cells Ctrl.			0.00	0.00
24 h H ₂ O Transf. Ctrl.	0.00	0.00		
24 h Untr. Cells Ctrl.			0.00	0.00
48 h H ₂ O Transf. Ctrl.	0.00	0.00		
48 h Untr. Cells Ctrl.			0.00	0.00

Table 95. Mean values [ng *mCherry* protein/well] and standard deviation of duplicate samples, background subtracted and divided by slope of linear standard curve for *mCh_mRNA* with or without natural base modifications and controls from exp. #3.

	WT	error	1 CP	error	2 CP	error
6 h mCh_mRNA	4.86	1.30	7.85	4.45	15.79	2.35
24 h mCh_mRNA	86.95	36.27	77.72	6.64	164.75	3.00
48 h mCh_mRNA	153.26	71.65	149.53	4.29	225.23	31.25

	WT Ψ+5mC	error	1 CP Ψ+5mC	error	2 CP Ψ+5mC	error
6 h mCh_mRNA	24.94	3.72	15.30	2.67	33.44	6.40
24 h mCh_mRNA	175.60	0.40	157.95	10.77	244.42	25.50
48 h mCh_mRNA	261.82	27.69	237.54	4.05	317.12	15.63

	H ₂ O Transf. Ctrl.	error	Untr. Cells Ctrl.	error
6 h H ₂ O Transf. Ctrl.	0.00	0.00		
6 h Untr. Cells Ctrl.			4.21	4.21
24 h H ₂ O Transf. Ctrl.	0.40	0.40		
24 h Untr. Cells Ctrl.			1.21	1.21
48 h H ₂ O Transf. Ctrl.	4.45	4.45		
48 h Untr. Cells Ctrl.			0.00	0.00

Table 96. Mean values [ng *mCherry* protein/well] and standard deviation of duplicate samples, background subtracted and divided by slope of linear standard curve for *mCh_mRNA* with or without natural base modifications and controls from exp. #4.

	WT	error	1 CP	error	2 CP	error
6 h mCh_mRNA	15.85	3.10	9.85	1.78	19.70	0.19
24 h mCh_mRNA	110.30	15.94	47.55	7.03	182.15	3.94
48 h mCh_mRNA	129.34	75.50	109.17	6.38	268.25	5.63

	WT $\Psi+5mC$	error	1 CP $\Psi+5mC$	error	2 CP $\Psi+5mC$	error
6 h mCh_mRNA	18.29	2.34	20.54	5.72	27.86	4.22
24 h mCh_mRNA	190.31	18.66	122.87	2.25	185.24	6.85
48 h mCh_mRNA	300.98	15.85	181.40	1.50	280.16	8.35

	H ₂ O Transf. Ctrl.	error	Untr. Cells Ctrl.	error
6 h H ₂ O Transf. Ctrl.	0.00	0.00		
6 h Untr. Cells Ctrl.			0.00	0.00
24 h H ₂ O Transf. Ctrl.	1.88	1.88		
24 h Untr. Cells Ctrl.			0.00	0.00
48 h H ₂ O Transf. Ctrl.	0.00	0.00		
48 h Untr. Cells Ctrl.			0.00	0.00

Table 97. Mean values [ng *mCherry* protein/well] and standard deviation of duplicate samples, background subtracted and divided by slope of linear standard curve for *mCh_mRNA* with or without natural base modifications and controls from exp. #5.

	WT	error	1 CP	error	2 CP	error
6 h mCh_mRNA	16.18	0.09	6.92	1.12	16.56	4.96
24 h mCh_mRNA	108.99	11.51	64.37	3.74	206.66	6.46
48 h mCh_mRNA	240.62	33.49	142.67	4.40	313.69	13.38

	WT $\Psi+5mC$	error	1 CP $\Psi+5mC$	error	2 CP $\Psi+5mC$	error
6 h mCh_mRNA	15.53	3.93	10.95	2.15	19.18	4.02
24 h mCh_mRNA	206.75	6.92	130.41	2.43	223.41	8.42
48 h mCh_mRNA	345.78	26.38	218.54	0.75	283.38	12.44

	H ₂ O Transf. Ctrl.	error	Untr. Cells Ctrl.	error
6 h H ₂ O Transf. Ctrl.	-0.56	0.00		
6 h Untr. Cells Ctrl.			-0.56	0.00
24 h H ₂ O Transf. Ctrl.	-0.56	0.00		
24 h Untr. Cells Ctrl.			-0.37	0.19
48 h H ₂ O Transf. Ctrl.	-0.56	0.00		
48 h Untr. Cells Ctrl.			-0.56	0.00

Table 98. Mean values [ng *mCherry* protein/well] and standard deviation of duplicate samples, background subtracted and divided by slope of linear standard curve for *mCh_mRNA* with or without natural base modifications and controls from exp. #6.

	WT	error	1 CP	error	2 CP	error
6 h mCh_mRNA	4.52	5.22	9.80	1.07	5.84	0.25
24 h mCh_mRNA	84.26	10.93	97.27	0.19	107.45	6.85
48 h mCh_mRNA	136.16	20.61	175.94	2.95	172.36	2.14

	WT $\Psi+5mC$	error	1 CP $\Psi+5mC$	error	2 CP $\Psi+5mC$	error
6 h mCh_mRNA	43.04	0.13	32.80	0.19	31.10	3.27
24 h mCh_mRNA	350.24	19.42	246.82	14.14	236.45	11.31
48 h mCh_mRNA	535.92	7.54	355.33	0.50	359.54	8.36

	H ₂ O Transf. Ctrl.	error	Untr. Cells Ctrl.	error
6 h H ₂ O Transf. Ctrl.	-6.10	1.76		
6 h Untr. Cells Ctrl.			-0.38	0.57
24 h H ₂ O Transf. Ctrl.	-1.70	1.89		
24 h Untr. Cells Ctrl.			-1.19	0.38
48 h H ₂ O Transf. Ctrl.	1.01	1.45		
48 h Untr. Cells Ctrl.			-2.20	0.13

Table 99. Mean values [ng *mCherry* protein/well] and standard deviation of duplicate samples, background subtracted and divided by slope of linear standard curve for *mCh_mRNA* with or without natural base modifications and controls from exp. #7.

	WT	error	1 CP	error	2 CP	error
6 h mCh_mRNA	8.71	1.79	12.78	3.74	9.52	4.23
24 h mCh_mRNA	107.02	11.07	124.11	5.05	126.96	1.87
48 h mCh_mRNA	181.90	24.42	217.54	8.30	214.78	0.16

	WT $\Psi+5mC$	error	1 CP $\Psi+5mC$	error	2 CP $\Psi+5mC$	error
6 h mCh_mRNA	47.45	0.65	37.19	0.33	42.32	0.57
24 h mCh_mRNA	433.38	24.90	290.63	14.97	302.35	16.44
48 h mCh_mRNA	667.44	15.79	438.83	2.69	440.95	6.59

	H ₂ O Transf. Ctrl.	error	Untr. Cells Ctrl.	error
6 h H ₂ O Transf. Ctrl.	-0.24	0.16		
6 h Untr. Cells Ctrl.			-0.41	0.00
24 h H ₂ O Transf. Ctrl.	0.81	1.22		
24 h Untr. Cells Ctrl.			0.49	0.57
48 h H ₂ O Transf. Ctrl.	0.65	1.06		
48 h Untr. Cells Ctrl.			1.95	2.36

Table 100. Mean values [ng *mCherry* protein/well] and standard deviation of duplicate samples, background subtracted and divided by slope of linear standard curve for *mCh_mRNA* with or without natural base modifications and controls from exp. #8.

	WT	error	1 CP	error	2 CP	error
6 h mCh_mRNA	4.68	1.61	14.54	2.41	10.01	0.51
24 h mCh_mRNA	68.33	29.16	122.70	4.17	139.88	12.28
48 h mCh_mRNA	107.72	56.13	183.80	0.07	165.67	8.55

	WT $\Psi+5mC$	error	1 CP $\Psi+5mC$	error	2 CP $\Psi+5mC$	error
6 h mCh_mRNA	14.25	0.51	28.57	5.19	33.32	0.29
24 h mCh_mRNA	102.60	1.32	149.81	16.52	288.45	15.57
48 h mCh_mRNA	159.68	4.90	328.06	38.07	335.00	24.70

	H ₂ O Transf. Ctrl.	error	Untr. Cells Ctrl.	error
6 h H ₂ O Transf. Ctrl.	5.55	3.22		
6 h Untr. Cells Ctrl.			-2.34	0.00
24 h H ₂ O Transf. Ctrl.	-1.02	1.32		
24 h Untr. Cells Ctrl.			-2.34	0.00
48 h H ₂ O Transf. Ctrl.	4.17	3.87		
48 h Untr. Cells Ctrl.			-2.34	0.00

Table 101. Mean values [ng *mCherry* protein/well] and standard deviation of duplicate samples, background subtracted and divided by slope of linear standard curve for *mCh_mRNA* with or without natural base modifications and controls from exp. #9.

	WT	error	1 CP	error	2 CP	error
6 h mCh_mRNA	5.82	4.04	11.15	2.26	11.50	3.97
24 h mCh_mRNA	69.25	31.34	108.80	3.42	121.52	13.27
48 h mCh_mRNA	102.57	49.06	168.67	0.48	149.37	0.75

	WT $\Psi+5mC$	error	1 CP $\Psi+5mC$	error	2 CP $\Psi+5mC$	error
6 h mCh_mRNA	13.14	3.01	28.46	0.68	32.91	0.34
24 h mCh_mRNA	90.59	2.87	143.69	12.04	251.46	9.37
48 h mCh_mRNA	143.42	1.51	289.44	29.56	306.82	2.87

	H ₂ O Transf. Ctrl.	Error	Untr. Cells Ctrl.	Error
6 h H ₂ O Transf. Ctrl.	4.31	5.95		
6 h Untr. Cells Ctrl.			-0.89	3.22
24 h H ₂ O Transf. Ctrl.	-0.89	2.94		
24 h Untr. Cells Ctrl.			1.16	0.21
48 h H ₂ O Transf. Ctrl.	-1.85	1.71		
48 h Untr. Cells Ctrl.			-2.12	6.09

Table 102. Mean values [ng *mCherry* protein/well] and standard deviation of duplicate samples, background subtracted and divided by slope of linear standard curve for *mCh_mRNA* with or without natural base modifications and controls from exp. #10.

	6 h	error	24 h	error	48 h	error
<i>mCh_mRNA</i> ^{WT}	9.18	0.78	118.66	4.86	172.70	8.64
<i>mCh_mRNA</i> ^{1 CP}	5.71	0.88	75.01	2.78	119.56	2.66
<i>mCh_mRNA</i> ^{2 CP}	12.17	0.59	130.80	2.12	182.91	3.11
<i>mCh_mRNA</i> ^{WT, Ψ+5mC}	27.05	0.81	257.95	6.20	382.26	5.13
<i>mCh_mRNA</i> ^{1 CP, Ψ+5mC}	22.80	0.91	181.33	3.13	293.55	6.62
<i>mCh_mRNA</i> ^{2 CP, Ψ+5mC}	32.43	1.53	259.60	3.98	325.94	16.39
<i>mCh_mRNA</i> ^{1 PM}	6.50	1.21	110.69	2.53	152.19	3.78
<i>mCh_mRNA</i> ^{2 PM}	3.64	1.51	83.68	2.40	117.04	3.24
<i>mCh_mRNA</i> ^{WT} _{UTR 2}	3.34	0.46	71.81	0.87	87.21	0.61
<i>mCh_mRNA</i> ^{1 CP} _{UTR 2}	3.80	0.35	78.99	0.83	97.45	0.64
<i>mCh_mRNA</i> ^{2 CP} _{UTR 2}	1.57	0.51	53.00	0.76	67.76	0.77
<i>mCh_mRNA</i> ^{1 PM} _{UTR 2}	6.19	1.29	73.78	1.79	89.24	2.30
<i>mCh_mRNA</i> ^{2 PM} _{UTR 2}	5.33	0.87	56.46	1.39	68.75	3.01
H ₂ O Transfection Ctrl.	0.10	0.69	-1.08	0.54	0.09	0.52
Untreated Cells Ctrl.	-0.34	0.60	0.30	0.34	-0.28	0.63

Table 103. Merged data from both data sets, *mCh_mRNA* with or without natural base modifications or *mCh_mRNA*_{UTR 2}. Mean values [ng *mCherry* protein/well] and standard deviation of duplicate samples, background subtracted and divided by slope of linear standard curve.

	6 h	error	24 h	error	48 h	error
mCh_mRNA ^{WT}	1.00	0.08	12.92	0.53	18.81	0.94
mCh_mRNA ^{1 CP}	0.62	0.10	8.17	0.30	13.02	0.29
mCh_mRNA ^{2 CP}	1.33	0.06	14.24	0.23	19.92	0.34
mCh_mRNA ^{WT, $\Psi+5mC$}	2.95	0.09	28.09	0.67	41.63	0.56
mCh_mRNA ^{1 CP, $\Psi+5mC$}	2.48	0.10	19.75	0.34	31.97	0.72
mCh_mRNA ^{2 CP, $\Psi+5mC$}	3.53	0.17	28.27	0.43	35.50	1.78
mCh_mRNA ^{1 PM}	0.71	0.13	12.05	0.28	16.57	0.41
mCh_mRNA ^{2 PM}	0.40	0.16	9.11	0.26	12.75	0.35
mCh_mRNA ^{WT} _{UTR 2}	0.36	0.05	7.82	0.10	9.50	0.07
mCh_mRNA ^{1 CP} _{UTR 2}	0.41	0.04	8.60	0.09	10.61	0.07
mCh_mRNA ^{2 CP} _{UTR 2}	0.17	0.06	5.77	0.08	7.38	0.08
mCh_mRNA ^{1 PM} _{UTR 2}	0.67	0.14	8.04	0.19	9.72	0.25
mCh_mRNA ^{2 PM} _{UTR 2}	0.58	0.10	6.15	0.15	7.49	0.33
H ₂ O Transfection Ctrl.	0.01	0.07	-0.12	0.06	0.01	0.06
Untreated Cells Ctrl.	-0.04	0.07	0.03	0.04	-0.03	0.07

Table 104. Merged data from both data sets, *mCh_mRNA* with or without natural base modifications or *mCh_mRNA*_{UTR 2}, normalized to mCh_mRNA^{WT}. Mean values [ng *mCherry* protein/well] and standard deviation of duplicate samples, background subtracted and divided by slope of linear standard curve.

Time point [h]	mCh_mRNA ^{WT, $\Psi+5mC$} / mCh_mRNA ^{WT}	error	mCh_mRNA ^{2 CP, $\Psi+5mC$} / mCh_mRNA ^{WT}	error
6	2.95	0.26	3.53	0.34
24	2.17	0.10	2.19	0.10
48	2.21	0.11	1.89	0.13

Table 105. Ratios of *mCherry* protein expression from mCh_mRNA^{WT, $\Psi+5mC$} / mCh_mRNA^{WT} or mCh_mRNA^{2 CP, $\Psi+5mC$} / mCh_mRNA^{WT}.

7.5 RT-qPCR

7.5.1 RT-qPCR full data set figure

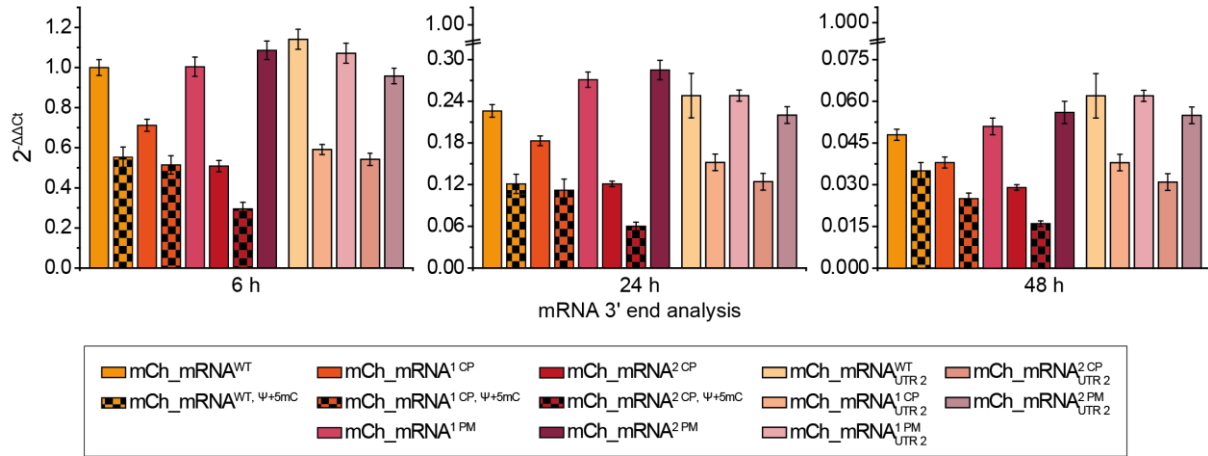


Figure 82. *mCh_mRNA* level analysis by RT-qPCR using the 3'-end primer/probe set of cells transfected with *mCh_mRNA* and *mCh_mRNA*_{UTR 2} sequences at 6, 24 and 48 h after transfection start.

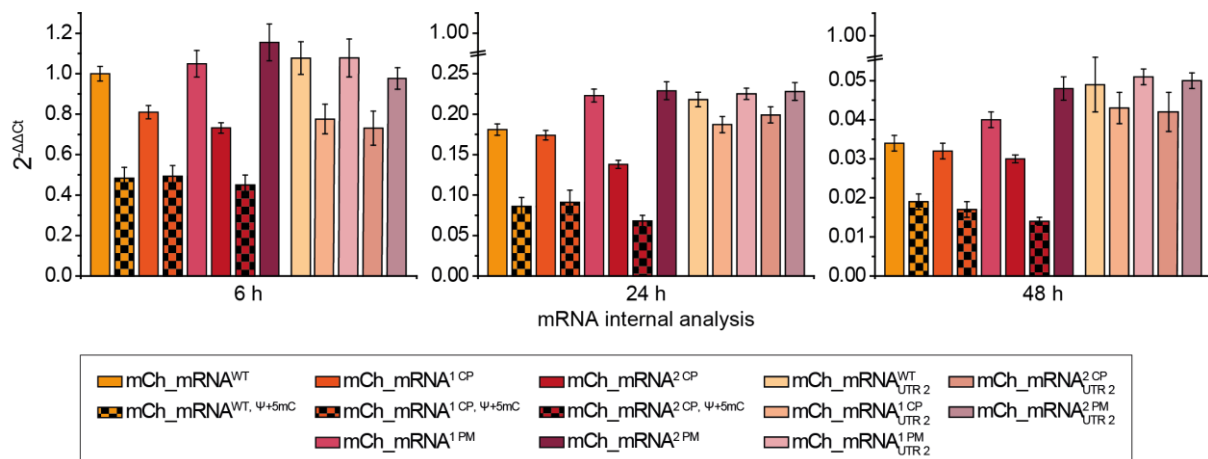


Figure 83. *mCh_mRNA* level analysis by RT-qPCR using the internal primer/probe set of cells transfected with *mCh_mRNA* and *mCh_mRNA*_{UTR 2} sequences at 6, 24 and 48 h after transfection start.

7.5.2 Initial experiments for qPCR efficiencies in singleplex vs. multiplex assays

singleplex mCh_qPCR ^{3'-end}					
V _{CDNA} [μL]	log(V _{CDNA})	C _t Duplicate #1	C _t Duplicate #2	C _t mean value	s.d.
0.156	-0.807	24.40	24.32	24.36	0.04
0.313	-0.504	23.17	23.19	23.18	0.01
0.625	-0.204	22.10	22.01	22.06	0.045
1.25	0.097	20.93	20.98	20.96	0.025
2.5	0.398	19.88	19.86	19.87	0.01
5	0.699	18.73	19.10	18.92	0.185

Ctrls	Ct
NRT	0.0
NTC	0.0

Table 106. Ct values of mCh_qPCR^{3'-end} singleplex qPCR analysis.

multiplex mCh_qPCR ^{3'-end} together w/ β-Actin_qPCR + GAPDH_qPCR					
V _{CDNA} [μL]	log(V _{CDNA})	C _t Duplicate #1	C _t Duplicate #2	C _t mean value	s.d.
0.156	-0.807	24.16	24.07	24.12	0.045
0.313	-0.504	23.10	22.94	23.02	0.08
0.625	-0.204	22.03	21.92	21.98	0.055
1.25	0.097	21.01	20.97	20.99	0.02
2.5	0.398	20.08	19.95	20.02	0.065
5	0.699	18.99	18.92	18.96	0.035

Ctrls	Ct
NRT	0.0
NTC	0.0

Table 107. Ct values of mCh_qPCR^{3'-end} multiplex qPCR analysis together with β-Actin_qPCR and GAPDH_qPCR.

Multiplex mCh_qPCR ^{3'-end} together w/ mCh_qPCR ^{internal} + β-Actin_qPCR + GAPDH_qPCR					
V _{CDNA} [μL]	log(V _{CDNA})	C _t Duplicate #1	C _t Duplicate #2	C _t mean value	s.d.
0.156	-0.807	24.10	24.04	24.07	0.03
0.313	-0.504	23.05	23.08	23.07	0.015
0.625	-0.204	22.00	21.98	21.99	0.01
1.25	0.097	20.96	20.95	20.96	0.005
2.5	0.398	20.01	20.02	20.02	0.005
5	0.699	24.10	24.04	24.07	0.03

Ctrls	Ct
NRT	0.0
NTC	0.0

Table 108. Ct values of mCh_qPCR^{3'-end} multiplex qPCR analysis together with mCh_qPCR^{internal}, β-Actin_qPCR and GAPDH_qPCR.

singleplex mCh_qPCR ^{internal}					
V _{CDNA} [μL]	log(V _{CDNA})	C _t Duplicate #1	C _t Duplicate #2	C _t mean value	s.d.
0.156	-0.807	24.62	24.73	24.68	0.055
0.313	-0.504	23.44	23.51	23.48	0.035
0.625	-0.204	21.71	22.26	21.99	0.275
1.25	0.097	21.21	21.19	21.20	0.01
2.5	0.398	20.12	20.15	20.14	0.015
5	0.699	19.05	19.09	19.07	0.02

Ctrls	Ct
NRT	0.0
NTC	0.0

Table 109. Ct values of mCh_qPCR^{internal} singleplex qPCR analysis.

multiplex mCh_qPCR ^{internal} together w/ β-Actin_qPCR + GAPDH_qPCR					
V _{CDNA} [μL]	log(V _{CDNA})	C _t Duplicate #1	C _t Duplicate #2	C _t mean value	s.d.
0.156	-0.807	25.43	25.48	25.46	0.025
0.313	-0.504	24.18	24.09	24.14	0.045
0.625	-0.204	23.05	23.06	23.06	0.005
1.25	0.097	21.98	21.93	21.96	0.025
2.5	0.398	21.05	20.89	20.97	0.08
5	0.699	20.20	19.85	20.03	0.175

Ctrls	Ct
NRT	0.0
NTC	0.0

Table 110. Ct values of mCh_qPCR^{internal} multiplex qPCR analysis together with β-Actin_qPCR and GAPDH_qPCR.

multiplex mCh_qPCR ^{internal} together w/ mCh_qPCR ^{3'-end} + β-Actin_qPCR + GAPDH_qPCR					
V _{CDNA} [μL]	log(V _{CDNA})	C _t Duplicate #1	C _t Duplicate #2	C _t mean value	s.d.
0.156	-0.807	24.97	25.00	24.99	0.015
0.313	-0.504	23.76	23.79	23.78	0.015
0.625	-0.204	22.64	22.64	22.64	0
1.25	0.097	21.59	21.58	21.59	0.005
2.5	0.398	20.54	20.53	20.54	0.005
5	0.699	24.97	25.00	24.99	0.015

Ctrls	Ct
NRT	0.0
NTC	0.0

Table 111. Ct values of mCh_qPCR^{internal} multiplex qPCR analysis together with mCh_qPCR^{3'-end}, β-Actin_qPCR and GAPDH_qPCR.

singleplex β -Actin_qPCR						
V_{cDNA} [μL]	$\log(V_{\text{cDNA}})$	C_t Duplicate #1	C_t Duplicate #2	C_t mean value	s.d.	
0.156	-0.807	24.27	24.19	24.23	0.04	
0.313	-0.504	23.17	23.07	23.12	0.05	
0.625	-0.204	21.98	21.91	21.95	0.035	
1.25	0.097	20.87	20.85	20.86	0.01	
2.5	0.398	19.73	19.47	19.60	0.13	
5	0.699	18.68	18.46	18.57	0.11	
Ctrls		Ct				
NRT		0.0				
NTC		0.0				

Table 112. Ct values of β -Actin singleplex qPCR analysis.

multiplex β -Actin_qPCR together w/ mCh_qPCR ^{3'-end} + mCh_qPCR ^{internal} + GAPDH_qPCR						
V_{cDNA} [μL]	$\log(V_{\text{cDNA}})$	C_t Duplicate #1	C_t Duplicate #2	C_t mean value	s.d.	
0.156	-0.807	23.37	23.29	23.33	0.04	
0.313	-0.504	22.28	22.54	22.41	0.13	
0.625	-0.204	21.62	21.60	21.61	0.01	
1.25	0.097	20.58	19.42	20.00	0.58	
2.5	0.398	19.54	19.55	19.55	0.005	
5	0.699	23.37	23.29	23.33	0.04	
Ctrls		Ct				
NRT		0.0				
NTC		0.0				

Table 113. Ct values of β -Actin multiplex qPCR analysis together with mCh_qPCR^{3'-end}, mCh_qPCR^{internal} and GAPDH_qPCR.

singleplex GAPDH_qPCR						
V_{cDNA} [μL]	$\log(V_{\text{cDNA}})$	C_t Duplicate #1	C_t Duplicate #2	C_t mean value	s.d.	
0.156	-0.807	25.14	25.20	25.17	0.03	
0.313	-0.504	24.05	24.06	24.06	0.005	
0.625	-0.204	22.83	23.21	23.02	0.19	
1.25	0.097	21.82	21.78	21.80	0.02	
2.5	0.398	20.78	20.82	20.80	0.02	
5	0.699	19.72	19.87	19.80	0.075	
Ctrls		Ct				
NRT		0.0				
NTC		0.0				

Table 114. Ct values of GAPDH singleplex qPCR analysis.

multiplex GAPDH_qPCR together w/ mCh_qPCR ^{3'-end} + mCh_qPCR ^{internal} + β -Actin_qPCR						
V _{CDNA} [μ L]	log(V _{CDNA})	C _t Duplicate #1	C _t Duplicate #2	C _t mean value	s.d.	
0.156	-0.807	24.54	24.58	24.56	0.02	
0.313	-0.504	23.51	23.56	23.54	0.025	
0.625	-0.204	22.50	22.49	22.50	0.005	
1.25	0.097	21.54	21.48	21.51	0.03	
2.5	0.398	20.52	20.45	20.49	0.035	
5	0.699	24.54	24.58	24.56	0.02	

Ctrls	Ct
NRT	0.0
NTC	0.0

Table 115. Ct values of GAPDH multiplex qPCR analysis together with mCh_qPCR^{3'-end}, mCh_qPCR^{internal} and β -Actin_qPCR.

qPCR target	qPCR efficiency [%]	
mCh_qPCR ^{3'-end}	singleplex	88.56
	multiplex (+ β -Actin_qPCR +GAPDH_qPCR)	96.94
	multiplex (+ mCh_qPCR ^{internal} + β -Actin_qPCR + GAPDH_qPCR)	97.07
mCh_qPCR ^{internal}	singleplex	86.8
	multiplex (+ β -Actin_qPCR +GAPDH_qPCR)	90.18
	multiplex (+ mCh_qPCR ^{3'-end} + β -Actin_qPCR + GAPDH_qPCR)	86.85
β -Actin_qPCR	singleplex	83.57
	multiplex (+ mCh_qPCR ^{3'-end} + mCh_qPCR ^{internal} + GAPDH_qPCR)	100.31
GAPDH_qPCR	singleplex	89.81
	multiplex (+ mCh_qPCR ^{3'-end} + mCh_qPCR ^{internal} + β -Actin_qPCR)	97.66

7.5.3 RT-qPCR results for *mCh_mRNA* analysis

	Biological Duplicates	Technical Triplicates	C _t values			
			mCh 3' end: FAM	mCh internal: HEX	β -Actin: ROX	GAPDH: Cy5
mCh_mRNA ^{WT}	#1	#1.1	16.45	16.43	19.04	22.21
		#1.2	16.32	16.32	19.02	22.15
		#1.3	16.29	16.35	19	22.15
	#1 NRT		36.19	34.9	0	0
	#2	#2.1	16.32	16.33	17.69	22.02
		#2.2	16.14	16.17	18.78	22.04
		#2.3	16.1	16.2	18.73	21.92
	#2 NRT		0	0	0	0
	mean		16.27	16.3	18.71	22.08
	s.d.		0.08	0.06	0.26	0.04
mCh_mRNA ^{1 CP}	#1	#1.1	16.96	16.88	17.76	21.89
		#1.2	16.96	16.85	20.34	21.93
		#1.3	16.92	16.89	18.02	21.87
	#1 NRT		0	0	0	38.55

mCh_mRNA^{2CP}	#2	#2.1	16.69	16.6	20.26	21.95
		#2.2	16.64	16.43	20.24	21.79
		#2.3	16.55	16.36	17.23	21.83
	#2 NRT		0	0	0	40.22
	mean		16.79	16.67	18.98	21.88
	s.d.		0.04	0.06	1.29	0.05
	#1	#1.1	17.32	16.72	16.63	21.77
		#1.2	17.2	16.96	15.54	21.66
		#1.3	17.18	16.72	16.52	21.67
		#1 NRT		0	0	0
#2		#2.1	17.12	16.57	16.7	21.78
		#2.2	17.09	16.57	16.57	21.8
	#2.3	17.25	16.87	15.88	21.82	
	#2 NRT		0	0	0	37.14
	mean		17.19	16.74	16.31	21.75
	s.d.		0.07	0.13	0.42	0.03
mCh_mRNA^{1PM}	#1	#1.1	16.43	16.37	16.94	21.91
		#1.2	16.25	16.33	15.23	21.72
		#1.3	16.25	16.32	20.18	21.75
	#1 NRT		0	0	0	0
	#2	#2.1	16.3	16.29	20.19	21.77
		#2.2	16.31	16.9	15.77	21.8
		#2.3	16.35	16.57	15.95	21.82
	#2 NRT		0	0	0	0
	mean		16.32	16.46	17.38	21.80
	s.d.		0.05	0.14	2.05	0.05
mCh_mRNA^{2PM}	#1	#1.1	16.33	16.6	16.61	22.01
		#1.2	16.19	16.18	16.29	21.79
		#1.3	16.23	16.22	17.23	21.89
	#1 NRT		0	0	0	41.51
	#2	#2.1	16.23	16.11	16.34	21.85
		#2.2	16.23	16.54	17.16	21.89
		#2.3	16.24	16.54	16.88	21.83
	#2 NRT		0	0	0	39.46
	mean		16.24	16.37	16.75	21.88
	s.d.		0.03	0.20	0.37	0.06
mCh_mRNA^{UTR2}^{WT}	#1	#1.1	16.06	16.28	16.77	21.86
		#1.2	16.1	16.38	20.61	21.72
		#1.3	16.18	16.49	17	21.86
	#1 NRT		0	0	0	0
	#2	#2.1	16.28	16.83	17.09	21.97
		#2.2	16.17	17.06	17.11	21.92
		#2.3	16.14	16.36	20.75	21.86
	#2 NRT		0	0	0	0
	mean		16.16	16.57	18.22	21.87

	s.d.		0.06	0.19	1.74	0.06
mCh_mRNA_{UTR2}^{1 CP}	#1	#1.1	17.06	17.12	17.27	21.83
		#1.2	17.14	17.35	16.69	21.71
		#1.3	17.15	17.33	15.51	21.78
	#1 NRT		0	0	0	38.62
	#2	#2.1	16.92	17.31	15.54	21.71
		#2.2	16.77	17.11	16.08	21.65
		#2.3	16.81	16.39	16.87	21.53
	#2 NRT		0	0	0	0
	mean		16.98	17.10	16.33	21.70
	s.d.		0.05	0.25	0.64	0.06
mCh_mRNA_{UTR2}^{2 CP}	#1	#1.1	17.22	16.79	15.09	21.72
		#1.2	17.06	16.68	14.99	21.71
		#1.3	16.98	16.66	15.62	21.65
	#1 NRT		0	0	0	0
	#2	#2.1	17.49	17.88	17.18	22.09
		#2.2	17.44	18.06	15.68	22.04
		#2.3	17.21	16.77	16.56	21.82
	#2 NRT		0	0	0	0
	mean		17.23	17.14	15.85	21.84
	s.d.		0.11	0.31	0.45	0.07
mCh_mRNA_{UTR2}^{1 PM}	#1	#1.1	16.19	16.5	20.16	21.82
		#1.2	16.2	16.32	15.48	21.67
		#1.3	16.19	16.15	16.72	21.69
	#1 NRT		0	0	0	38.66
	#2	#2.1	16.24	16.34	16.27	21.8
		#2.2	16.23	16.86	14.61	21.79
		#2.3	16.18	16.3	16.35	21.78
	#2 NRT		0	0	0	0
	mean		16.21	16.41	16.60	21.76
	s.d.		0.02	0.20	1.39	0.04
mCh_mRNA_{UTR2}^{2 PM}	#1	#1.1	16.54	16.86	16.11	21.82
		#1.2	16.47	16.61	16.23	21.77
		#1.3	16.44	17.02	16.96	21.71
	#1 NRT		0	0	0	35.67
	#2	#2.1	16.48	16.56	16.19	21.69
		#2.2	16.4	16.51	15.35	21.7
		#2.3	16.43	16.62	15.51	21.73
	#2 NRT		0	0	0	0
	mean		16.46	16.70	16.06	21.74
	s.d.		0.04	0.11	0.37	0.03
H₂O Ctrl.	#1	#1.1	0	0	18.77	21.57
		#1.2	0	0	16.8	21.54
	#1 NRT		0	0	0	41.76
	#2	#2.1	0	0	15.84	21.41
		#2.2	0	0	16.66	21.38
#2 NRT		0	0	0	37.91	

	mean		0	0	17.02	21.48
	s.d.		0	0	0.70	0.02
Untreated Cells	#1	#1.1	0	0	17.89	21.64
		#1.2	0	0	15.7	21.47
		#1.3	0	0	15.66	21.47
	#1 NRT		0	0	0	39.81
	#2	#2.1	0	0	16.46	21.45
		#2.2	0	0	15.65	21.43
		#2.3	0	0	15.46	21.41
	#2 NRT		0	0	0	0
	mean		0	0	16.14	21.48
	s.d.		0	0	0.74	0.05
NTC	#1		0	0	0	0
	#2		0	0	0	0

Table 116. C_t values of *mCh_mRNA* + *mCh_mRNA_{UTR2}* data set 1, cell lysis 6 h post transfection.

	ΔC_t (mCh 3'end)	error	ΔC_t (mCh internal)	error
mCh_mRNA^{WT}	-5.81	0.09	-5.78	0.07
mCh_mRNA^{1 CP}	-5.09	0.06	-5.21	0.08
mCh_mRNA^{2 CP}	-4.56	0.07	-5.02	0.13
mCh_mRNA^{1 PM}	-5.48	0.07	-5.33	0.15
mCh_mRNA^{2 PM}	-5.64	0.07	-5.51	0.20
mCh_mRNA_{UTR2}^{WT}	-5.71	0.08	-5.30	0.20
mCh_mRNA_{UTR2}^{1 CP}	-4.73	0.08	-4.60	0.26
mCh_mRNA_{UTR2}^{2 CP}	-4.61	0.13	-4.70	0.32
mCh_mRNA_{UTR2}^{1 PM}	-5.55	0.04	-5.35	0.20
mCh_mRNA_{UTR2}^{2 PM}	-5.28	0.05	-5.04	0.11
H₂O Ctrl.	-21.48	0.02	-21.48	0.02
Untreated cells	-21.48	0.05	-21.48	0.05

Table 117. $\Delta C_t = C_t(\text{mCh}) - C_t(\text{GAPDH})$ values of *mCh_mRNA* + *mCh_mRNA_{UTR2}* data set 1, cell lysis 6 h post transfection.

	Biological Duplicates	Technical Triplicates	Ct values			
			mCh 3' end: FAM	mCh internal: HEX	β-Actin: ROX	GAPDH: Cy5
mCh_mRNA^{WT}	#1	#1.1	18.7	19.1	19.15	21.71
		#1.2	18.54	19.1	19.44	21.75
		#1.3	18.54	19.09	19.17	21.73
	#1 NRT		0	0	0	0
	#2	#2.1	19.02	19.59	19.92	22.37
		#2.2	18.9	19.62	19.17	22.33
		#2.3	18.95	19.56	19.01	22.39
	#2 NRT		0	0	0	0
	mean		18.78	19.34	19.31	22.05
	s.d.		0.06	0.01	0.26	0.02

mCh_mRNA ^{1 CP}	#1	#1.1	19.2	19.49	19.43	21.79	
		#1.2	19.16	19.48	18.99	21.75	
		#1.3	19.02	19.44	19.19	21.72	
	#1 NRT		0	0	0	0	
	#2	#2.1	19.21	19.52	18.66	21.84	
		#2.2	19.1	19.6	19.24	21.92	
		#2.3	19.17	19.59	19.18	21.9	
	#2 NRT		0	0	0	36.91	
	mean		19.14	19.52	19.12	21.82	
	s.d.		0.06	0.03	0.22	0.03	
	mCh_mRNA ^{2 CP}	#1	#1.1	19.8	19.82	19.25	21.88
			#1.2	19.72	20.07	19.44	21.81
			#1.3	19.75	19.95	18.26	21.83
#1 NRT			0	0	0	39.9	
#2		#2.1	19.7	19.83	18.61	21.82	
		#2.2	19.59	19.9	18.86	21.74	
		#2.3	19.59	19.92	18.81	21.72	
#2 NRT			0	0	0	0	
mean			19.69	19.92	18.87	21.80	
s.d.			0.04	0.07	0.31	0.04	
mCh_mRNA ^{1 PM}		#1	#1.1	18.82	19.27	19.57	21.98
			#1.2	18.69	19.29	18.76	21.91
			#1.3	18.72	19.29	18.43	21.89
	#1 NRT		0	0	0	0	
	#2	#2.1	18.76	19.29	19.22	22.05	
		#2.2	18.68	19.28	18.71	22	
		#2.3	18.7	19.24	18.43	22.04	
	#2 NRT		0	0	0	41.58	
	mean		18.73	19.28	18.85	21.98	
	s.d.		0.04	0.02	0.40	0.03	
	mCh_mRNA ^{2 PM}	#1	#1.1	18.7	19.2	19.05	21.86
			#1.2	18.52	19.07	18.12	21.71
			#1.3	18.58	19.11	18.67	21.75
#1 NRT			0	0	0	38.95	
#2		#2.1	18.78	19.32	19.18	22.04	
		#2.2	18.64	19.21	19.02	22	
		#2.3	18.62	19.26	18.94	21.96	
#2 NRT			0	39.72	0	37.18	
mean			18.64	19.20	18.83	21.89	
s.d.			0.07	0.05	0.24	0.05	
mCh_mRNA _{UTR2} ^{WT}		#1	#1.1	18.65	19.17	17.69	21.78
			#1.2	18.56	19.15	18.56	21.73
			#1.3	18.6	19.13	18.71	21.76
	#1 NRT		0	0	0	0	
	#2	#2.1	18.42	18.91	18.27	21.69	

		#2.2	18.42	19.09	18.11	21.73
		#2.3	18.33	18.83	18.65	21.66
	#2 NRT		0	0	0	0
	mean		18.50	19.05	18.33	21.73
	s.d.		0.04	0.06	0.34	0.02
mCh_mRNA_{UTR2}^{1CP}	#1	#1.1	19.51	19.47	19.54	22.01
		#1.2	19.27	19.21	18.55	21.74
		#1.3	19.28	19.19	17.51	21.74
	#1 NRT		0	0	0	0
	#2	#2.1	19.35	19.24	18.53	21.73
		#2.2	19.3	19.21	18.02	21.71
		#2.3	19.3	19.24	18.56	21.74
	#2 NRT		0	0	0	0
	mean		19.34	19.26	18.45	21.78
	s.d.		0.07	0.07	0.54	0.07
mCh_mRNA_{UTR2}^{2CP}	#1	#1.1	19.59	19.45	19.02	21.92
		#1.2	19.5	19.36	18.16	21.84
		#1.3	19.44	19.22	18.55	21.76
	#1 NRT		0	0	0	0
	#2	#2.1	19.67	19.44	18.84	21.89
		#2.2	19.62	19.46	18.8	21.86
		#2.3	19.62	19.6	17.74	21.89
	#2 NRT		0	0	0	40.95
	mean		19.57	19.42	18.52	21.86
	s.d.		0.04	0.08	0.43	0.04
mCh_mRNA_{UTR2}^{1PM}	#1	#1.1	18.64	19.14	19.31	21.92
		#1.2	18.53	19.04	18.64	21.85
		#1.3	18.52	19.09	19.12	21.81
	#1 NRT		0	0	0	37.4
	#2	#2.1	18.73	19.22	19.51	22
		#2.2	18.62	19.19	18.31	21.94
		#2.3	18.61	19.19	19.16	21.95
	#2 NRT		0	0	0	38.98
	mean		18.61	19.15	19.01	21.91
	s.d.		0.05	0.03	0.39	0.04
mCh_mRNA_{UTR2}^{2PM}	#1	#1.1	18.74	19.12	18.92	21.94
		#1.2	18.75	19.19	18.67	21.94
		#1.3	18.65	19.04	18.17	21.83
	#1 NRT		0	0	0	0
	#2	#2.1	18.66	19.05	17.87	21.71
		#2.2	18.8	19.23	18.3	22
		#2.3	18.67	19.13	19.03	21.9
	#2 NRT		0	0	0	40.25
	mean		18.71	19.13	18.49	21.89
	s.d.		0.05	0.07	0.40	0.09
H₂O Ctrl.	#1	#1.1	0	0	20.43	22.02
		#1.2	0	0	18.88	21.93

	#1 NRT		0	0	0	0
	#2	#2.1	0	0	18.11	21.84
		#2.2	0	0	18.62	21.67
	#2 NRT		0	0	0	0
	mean		0.00	0.00	19.01	21.87
	s.d.		0.00	0.00	0.52	0.06
Untreated Cells	#1	#1.1	0	0	19.73	21.87
		#1.2	0	0	19.03	21.9
		#1.3	0	0	19.01	21.82
	#1 NRT		0	0	0	0
	#2	#2.1	0	0	18.33	21.93
		#2.2	0	0	19.38	21.86
		#2.3	0	0	18.8	21.88
	#2 NRT		0	0	0	0
	mean		0.00	0.00	19.05	21.88
	s.d.		0.00	0.00	0.38	0.03
NTC	#1		0	0	0	0
	#2		0	0	0	0

Table 118. Ct values of *mCh_mRNA* + *mCh_mRNA_{UTR2}* data set 1, cell lysis 24 h post transfection.

	ΔCt (mCh 3'end)	error	ΔCt (mCh internal)	error
mCh_mRNA^{WT}	-3.27	0.07	-2.70	0.03
mCh_mRNA^{1CP}	-2.68	0.07	-2.30	0.04
mCh_mRNA^{2CP}	-2.11	0.06	-1.89	0.08
mCh_mRNA^{1PM}	-3.25	0.05	-2.70	0.03
mCh_mRNA^{2PM}	-3.25	0.09	-2.69	0.07
mCh_mRNA_{UTR2}^{WT}	-3.23	0.05	-2.68	0.07
mCh_mRNA_{UTR2}^{1CP}	-2.44	0.10	-2.52	0.10
mCh_mRNA_{UTR2}^{2CP}	-2.29	0.06	-2.44	0.09
mCh_mRNA_{UTR2}^{1PM}	-3.30	0.07	-2.77	0.05
mCh_mRNA_{UTR2}^{2PM}	-3.18	0.10	-2.76	0.11
H₂O Ctrl.	-21.87	0.06	-21.87	0.06
Untreated cells	-21.88	0.03	-21.88	0.03

Table 119. ΔCt= Ct(mCh) – Ct(GAPDH) values of *mCh_mRNA* + *mCh_mRNA_{UTR2}* data set 1, cell lysis 24 h post transfection.

	Biological Duplicates	Technical Triplicates	Ct values			
			mCh 3' end: FAM	mCh internal: HEX	β-Actin: ROX	GAPDH: Cy5
mCh_mRNA^{WT}	#1	#1.1	20.92	21.5	19.65	21.68
		#1.2	21.25	21.74	19.65	22.1
		#1.3	21.17	21.66	19.7	22.01
	#1 NRT		0	0	0	0
	#2	#2.1	21.47	22.07	20.17	22.14
		#2.2	21.27	21.85	19	21.94

		#2.3	21.2	21.82	18.56	21.91
	#2 NRT		38.33	40.72	30.2	31.91
	mean		21.21	21.77	19.46	21.96
	s.d.		0.13	0.11	0.35	0.14
mCh_mRNA^{1CP}	#1	#1.1	22.05	22.37	20.06	22.28
		#1.2	21.73	22.15	19.24	22.13
		#1.3	21.55	22.01	19.56	21.96
	#1 NRT		0	0	0	41.42
	#2	#2.1	21.67	22.06	19.14	22.18
		#2.2	21.46	21.82	19.09	22.02
		#2.3	21.33	21.71	19.01	21.9
	#2 NRT		0	0	0	0
	mean		21.63	22.02	19.35	22.08
	s.d.		0.17	0.15	0.20	0.12
mCh_mRNA^{2CP}	#1	#1.1	22.15	22.04	20.01	22.15
		#1.2	22.14	22.08	19.09	22.17
		#1.3	22.14	22.12	19.99	22.16
	#1 NRT		0	0	0	0
	#2	#2.1	22.2	22.15	19.55	22.29
		#2.2	22.05	22.03	18.92	22.17
		#2.3	21.76	21.83	19.15	22.02
	#2 NRT		0	0	0	0
	mean		22.07	22.04	19.45	22.16
	s.d.		0.09	0.08	0.34	0.06
mCh_mRNA^{1PM}	#1	#1.1	21.34	21.77	19.85	22.19
		#1.2	21.06	21.43	18.91	21.77
		#1.3	21.04	21.57	18.82	22.01
	#1 NRT		0	0	0	0
	#2	#2.1	21.28	21.99	19.91	22.28
		#2.2	21.23	21.93	19.87	22.24
		#2.3	21.2	21.99	19.74	22.25
	#2 NRT		0	0	0	0
	mean		21.19	21.78	19.52	22.12
	s.d.		0.08	0.08	0.27	0.09
mCh_mRNA^{2PM}	#1	#1.1	21.13	21.46	19.53	22.09
		#1.2	20.77	21.32	19.44	21.74
		#1.3	21.25	21.69	20.28	22.2
	#1 NRT		0	0	0	0
	#2	#2.1	21.09	21.56	19.6	22.11
		#2.2	20.96	21.34	19.47	22.13
		#2.3	20.83	21.27	19.8	22.01
	#2 NRT		0	0	0	0
	mean		21.01	21.44	19.69	22.05
	s.d.		0.16	0.14	0.26	0.12
mCh_mRNA_{UTR2}^{WT}	#1	#1.1	20.64	21.15	19.06	21.76

		#1.2	20.54	21.07	18.68	21.7
		#1.3	20.86	21.34	19.31	22.1
	#1 NRT		0	0	0	0
	#2	#2.1	20.41	20.92	18.56	21.45
		#2.2	21.3	21.87	20.01	22.37
		#2.3	20.71	21.23	19.32	21.78
	#2 NRT		0	0	0	0
	mean		20.74	21.26	19.16	21.86
	s.d.		0.25	0.25	0.43	0.28
mCh_mRNA_{UTR2}^{1CP}	#1	#1.1	22.03	22.04	19.34	22.28
		#1.2	21.58	21.63	19.04	22
		#1.3	21.6	21.63	18.78	21.97
	#1 NRT		0	0	0	0
	#2	#2.1	21.69	21.8	18.83	22.12
		#2.2	21.47	21.55	19.1	21.92
		#2.3	21.29	21.38	18.86	21.72
	#2 NRT		0	0	0	0
	mean		21.61	21.67	18.99	22.00
	s.d.		0.19	0.18	0.17	0.15
mCh_mRNA_{UTR2}^{2CP}	#1	#1.1	22.3	22.11	19.96	22.29
		#1.2	22.18	21.99	19.27	22.15
		#1.3	21.64	21.52	19.25	21.59
	#1 NRT		0	0	0	0
	#2	#2.1	21.88	21.56	18.99	21.89
		#2.2	22.03	21.76	18.86	22.04
		#2.3	22.14	21.99	19.6	22.21
	#2 NRT		0	0	0	0
	mean		22.03	21.82	19.32	22.03
	s.d.		0.20	0.22	0.33	0.22
mCh_mRNA_{UTR2}^{1PM}	#1	#1.1	21	21.34	19.6	22.11
		#1.2	20.95	21.36	18.57	21.98
		#1.3	20.99	21.41	19.21	22.02
	#1 NRT		0	0	0	39.63
	#2	#2.1	21.09	21.53	19.3	22.18
		#2.2	21	21.43	19.17	22.1
		#2.3	21.06	21.57	19.34	22.18
	#2 NRT		0	0	0	0
	mean		21.02	21.44	19.20	22.10
	s.d.		0.03	0.04	0.25	0.05
mCh_mRNA_{UTR2}^{2PM}	#1	#1.1	21.01	21.25	19.33	22.05
		#1.2	20.77	21.05	19.16	21.85
		#1.3	21.03	21.31	19.1	21.95
	#1 NRT		0	0	0	0
	#2	#2.1	21.08	21.39	19.14	22.04
		#2.2	21.15	21.52	19.29	22.12
		#2.3	21.13	21.5	19.3	22.11

	#2 NRT		0	0	0	0
	mean		21.03	21.34	19.22	22.02
	s.d.		0.07	0.08	0.09	0.06
H₂O Ctrl.	#1	#1.1	0	0	21.35	22.69
		#1.2	0	0	19.81	22.31
	#1 NRT		0	0	0	0
	#2	#2.1	0	0	19.68	22.47
		#2.2	0	0	19.51	22.52
	Untreated Cells	#2 NRT		0	0	0
mean			0.00	0.00	20.09	22.50
s.d.			0.00	0.00	0.43	0.11
#1		#1.1	0	0	20.11	22.89
		#1.2	0	0	19.33	22.34
		#1.3	0	0	19.33	22.35
#1 NRT			0	0	0	0
#2		#2.1	0	0	19.5	22.43
		#2.2	0	0	19.57	22.51
		#2.3	0	0	19.09	22.41
#2 NRT			0	0	0	0
mean			0.00	0.00	19.49	22.49
s.d.		0.00	0.00	0.29	0.15	
NTC	#1		0	0	0	0
	#2		0	0	0	0

Table 120. Ct values of *mCh_mRNA* + *mCh_mRNA_{UTR2}* data set 1, cell lysis 48 h post transfection.

	ΔCt (mCh 3'end)	error	ΔCt (mCh internal)	error
mCh_mRNA^{WT}	-0.75	0.19	-0.19	0.18
mCh_mRNA^{1 CP}	-0.45	0.21	-0.06	0.19
mCh_mRNA^{2 CP}	-0.09	0.11	-0.12	0.10
mCh_mRNA^{1 PM}	-0.93	0.13	-0.34	0.13
mCh_mRNA^{2 PM}	-1.04	0.20	-0.61	0.19
mCh_mRNA_{UTR2}^{WT}	-1.12	0.38	-0.60	0.38
mCh_mRNA_{UTR2}^{1 CP}	-0.39	0.24	-0.33	0.24
mCh_mRNA_{UTR2}^{2 CP}	0.00	0.29	-0.21	0.31
mCh_mRNA_{UTR2}^{1 PM}	-1.08	0.05	-0.65	0.06
mCh_mRNA_{UTR2}^{2 PM}	-0.99	0.09	-0.68	0.10
H₂O Ctrl.	-22.50	0.11	-22.50	0.11
Untreated cells	-22.49	0.15	-22.49	0.15

Table 121. ΔCt= Ct(mCh) – Ct(GAPDH) values of *mCh_mRNA* + *mCh_mRNA_{UTR2}* data set 1, cell lysis 48 h post transfection.

	Biological Duplicates	Technical Triplicates	Ct values			
			mCh 3' end: FAM	mCh internal: HEX	β-Actin: ROX	GAPDH: Cy5
mCh_mRNA^{WT}	#1	#1.1	16.38	16.55	18.7	21.31
		#1.2	16.19	16.37	20.86	21.2

		#1.3	16.22	16.43	18.24	21.21
	#1 NRT		0	0	0	0
	#2	#2.1	16.19	16.44	18.62	21.12
		#2.2	16.2	16.46	18.12	21.2
		#2.3	16.25	16.5	18.15	21.24
	#2 NRT		0	0	0	0
	mean		16.24	16.46	18.78	21.21
	s.d.		0.05	0.05	0.69	0.05
mCh_mRNA^{1 CP}	#1	#1.1	16.97	17.01	18.35	21.25
		#1.2	16.96	16.83	18.48	21.27
		#1.3	16.71	16.82	18.7	21.25
	#1 NRT		0	0	0	0
	#2	#2.1	16.72	16.87	18.17	21.23
		#2.2	16.78	16.98	18.23	21.3
		#2.3	16.68	16.87	17.64	21.22
	#2 NRT		0	0	0	0
	mean		16.80	16.90	18.26	21.25
	s.d.		0.08	0.07	0.20	0.02
mCh_mRNA^{2 CP}	#1	#1.1	17.29	16.84	18.33	21.23
		#1.2	17.28	16.83	18.1	21.24
		#1.3	17.29	16.88	18.52	21.26
	#1 NRT		0	0	0	0
	#2	#2.1	17.28	17.09	18.38	21.14
		#2.2	17.25	17.07	18.36	21.15
		#2.3	17.27	17.1	18.09	21.18
	#2 NRT		0	36.48	0	0
	mean		17.28	16.97	18.30	21.20
	s.d.		0.01	0.02	0.15	0.01
mCh_mRNA^{1 PM}	#1	#1.1	16.45	16.62	18.76	21.46
		#1.2	16.42	16.64	21.39	21.46
		#1.3	16.41	16.61	18.14	21.28
	#1 NRT		0	0	0	0
	#2	#2.1	16.45	16.7	18.2	21.2
		#2.2	16.53	16.75	18.18	21.34
		#2.3	16.57	16.82	18.48	21.35
	#2 NRT		0	0	0	0
	mean		16.47	16.69	18.86	21.35
	s.d.		0.03	0.03	0.77	0.08
mCh_mRNA^{2 PM}	#1	#1.1	16.39	16.57	18.48	21.29
		#1.2	16.34	16.54	18.58	21.27
		#1.3	16.35	16.56	20.92	21.43
	#1 NRT		0	0	0	0
	#2	#2.1	16.31	16.46	18.5	21.32
		#2.2	16.32	16.52	21.36	21.19
		#2.3	16.32	16.54	20.84	21.22

	#2 NRT		0	39.9	0	0
	mean		16.34	16.53	19.78	21.29
	s.d.		0.01	0.02	1.19	0.06
mCh_mRNA_{UTR2}^{WT}	#1	#1.1	16.23	16.51	20.82	21.25
		#1.2	16.13	16.38	20.75	21.16
		#1.3	16.15	16.39	20.8	21.21
	#1 NRT		0	0	0	0
	#2	#2.1	16.14	16.39	18.31	21.08
		#2.2	16.17	16.37	18.42	21.21
#2.3		16.11	16.38	17.83	21.12	
	#2 NRT		0	0	0	0
	mean		16.16	16.40	19.49	21.17
	s.d.		0.03	0.03	0.14	0.05
mCh_mRNA_{UTR2}^{1CP}	#1	#1.1	17.21	16.82	18.45	21.3
		#1.2	17.12	16.71	18.01	21.22
		#1.3	17.09	16.65	17.52	21.19
	#1 NRT		0	37.21	33.7	36.41
	#2	#2.1	17.02	16.59	17.92	21.12
		#2.2	17.02	16.59	17.73	21.14
#2.3		17.03	16.63	18.22	21.13	
	#2 NRT		0	41.37	0	0
	mean		17.08	16.67	17.98	21.18
	s.d.		0.03	0.04	0.29	0.03
mCh_mRNA_{UTR2}^{2CP}	#1	#1.1	17.37	16.94	18.03	21.45
		#1.2	17.28	17.03	18	21.38
		#1.3	17.29	17.03	18.01	21.37
	#1 NRT		0	0	0	0
	#2	#2.1	17.38	17.12	17.7	21.22
		#2.2	17.33	17.11	18.3	21.2
#2.3		17.36	17.12	18.04	21.22	
	#2 NRT		0	0	0	0
	mean		17.34	17.06	18.01	21.31
	s.d.		0.03	0.02	0.13	0.02
mCh_mRNA_{UTR2}^{1PM}	#1	#1.1	16.42	16.64	18.51	21.28
		#1.2	16.37	16.6	18.47	21.26
		#1.3	16.38	16.59	20.76	21.39
	#1 NRT		0	0	0	0
	#2	#2.1	16.4	16.62	18.27	21.49
		#2.2	16.26	16.49	17.9	21.24
#2.3		16.39	16.9	18.37	21.51	
	#2 NRT		0	0	0	0
	mean		16.37	16.64	18.71	21.36
	s.d.		0.04	0.10	0.64	0.09
mCh_mRNA_{UTR2}^{2PM}	#1	#1.1	16.52	16.68	17.98	21.5
		#1.2	16.44	16.63	18.19	21.45
		#1.3	16.45	16.6	18.24	21.43

	#1 NRT		0	41.06	0	40.2
	#2	#2.1	16.51	16.61	18.3	21.3
		#2.2	16.4	16.56	18.3	21.25
		#2.3	16.34	16.79	21.31	21.4
	#2 NRT		0	40.45	0	0
	mean		16.44	16.65	18.72	21.39
	s.d.		0.05	0.07	0.77	0.05
H₂O Ctrl.	#1	#1.1	0	39.85	18.85	21.51
		#1.2	0	40.34	17.97	21.43
	#1 NRT		0	0	0	0
	#2	#2.1	0	0	18.2	21.31
		#2.2	0	0	18.94	21.31
	#2 NRT		0	0	0	0
	mean		0.00	20.05	18.49	21.39
	s.d.		0.00	0.12	0.41	0.02
Untreated Cells	#1	#1.1	34.49	37.09	18.33	21.41
		#1.2	33.39	36.73	17.94	21.34
		#1.3	34.61	37.27	17.95	21.37
	#1 NRT		0	0	0	0
	#2	#2.1	0	0	18.13	21.3
		#2.2	0	0	18.38	21.29
		#2.3	0	0	18.13	21.33
	#2 NRT		0	0	0	0
	mean		17.08	18.52	18.14	21.34
	s.d.		0.27	0.11	0.15	0.02
NTC	#1		0	0	0	0
	#2		0	0	0	0

Table 122. Ct values of *mCh_mRNA* + *mCh_mRNA_{UTR2}* data set 2, cell lysis 6 h post transfection.

	ΔCt (mCh 3'end)	error	ΔCt (mCh internal)	error
mCh_mRNA^{WT}	-4.98	0.07	-4.76	0.07
mCh_mRNA^{1CP}	-4.45	0.08	-4.36	0.07
mCh_mRNA^{2CP}	-3.92	0.02	-4.23	0.02
mCh_mRNA^{1PM}	-4.88	0.08	-4.66	0.08
mCh_mRNA^{2PM}	-4.95	0.06	-4.76	0.07
mCh_mRNA_{UTR2}^{WT}	-5.02	0.06	-4.77	0.06
mCh_mRNA_{UTR2}^{1CP}	-4.10	0.04	-4.52	0.05
mCh_mRNA_{UTR2}^{2CP}	-3.97	0.04	-4.25	0.03
mCh_mRNA_{UTR2}^{1PM}	-4.99	0.10	-4.72	0.13
mCh_mRNA_{UTR2}^{2PM}	-4.95	0.07	-4.74	0.08
H₂O Ctrl.	-21.39	0.02	-1.34	0.12
Untreated cells	-4.26	0.28	-2.83	0.11

Table 123. ΔCt= Ct(mCh) – Ct(GAPDH) values of *mCh_mRNA* + *mCh_mRNA_{UTR2}* data set 2, cell lysis 6 h post transfection.

	Biological Duplicates	Technical Triplicates	Ct values				
			mCh 3' end: FAM	mCh internal: HEX	β -Actin: ROX	GAPDH: Cy5	
mCh_mRNA ^{WT}	#1	#1.1	19.08	19.59	19.12	22.1	
		#1.2	18.94	19.44	18.73	22.03	
		#1.3	19.11	19.68	19.12	22.05	
	#1 NRT		0	0	0	0	
	#2	#2.1	18.78	19.41	18.29	21.93	
		#2.2	18.94	19.43	17.71	21.96	
		#2.3	18.73	19.38	18.34	21.94	
	#2 NRT		0	0	0	0	
	mean		18.93	19.49	18.55	22.00	
	s.d.		0.08	0.06	0.23	0.02	
	mCh_mRNA ^{1 CP}	#1	#1.1	18.95	19.14	18.97	21.69
			#1.2	19.16	19.37	18.32	21.97
			#1.3	19.28	19.53	17.73	22.11
#1 NRT			0	0	0	0	
#2		#2.1	19.47	19.49	18.39	22.07	
		#2.2	19.44	19.46	17.66	22.08	
		#2.3	19.4	19.5	17.84	22.04	
#2 NRT			0	0	0	0	
mean			19.28	19.42	18.15	21.99	
s.d.			0.08	0.09	0.41	0.10	
mCh_mRNA ^{2 CP}		#1	#1.1	19.4	19.25	17.59	21.87
			#1.2	19.46	19.39	17.04	22.01
			#1.3	19.48	19.42	17.48	22.03
	#1 NRT		0	0	0	0	
	#2	#2.1	19.46	19.43	17.8	21.92	
		#2.2	19.49	19.4	17.66	22.01	
		#2.3	19.52	19.48	18.56	22.04	
	#2 NRT		0	0	0	0	
	mean		19.47	19.40	17.69	21.98	
	s.d.		0.03	0.05	0.32	0.06	
	mCh_mRNA ^{1 PM}	#1	#1.1	18.75	19.26	18.23	22.06
			#1.2	18.62	19.13	17.62	21.97
			#1.3	18.65	19.13	16.72	22
#1 NRT			0	0	0	0	
#2		#2.1	18.72	19.21	18.07	22.02	
		#2.2	18.74	19.26	18.18	22.05	
		#2.3	18.79	19.33	18.15	22.12	
#2 NRT			0	0	0	0	
mean			18.71	19.22	17.83	22.04	
s.d.			0.04	0.06	0.33	0.04	
mCh_mRNA ^{2 PM}		#1	#1.1	18.53	19.18	18.07	21.91
			#1.2	18.5	19.09	18.45	21.9

		#1.3	18.63	19.24	18.78	22.02
	#1 NRT		0	0	0	0
	#2	#2.1	18.48	18.96	18.93	22.02
		#2.2	18.56	19.06	18.39	22.12
		#2.3	18.6	19.15	18.55	22.17
	#2 NRT		0	0	0	0
	mean		18.55	19.11	18.53	22.02
	s.d.		0.05	0.07	0.26	0.06
mCh_mRNA_{UTR2}^{WT}	#1	#1.1	18.77	19.31	17.9	22.1
		#1.2	18.62	19.22	17.37	22
		#1.3	18.66	19.27	18.01	22.04
	#1 NRT		0	0	0	0
	#2	#2.1	18.64	19.23	18.04	21.98
		#2.2	18.52	19.13	17.44	21.92
		#2.3	18.58	19.2	17.95	22.01
	#2 NRT		0	0	0	0
	mean		18.63	19.23	17.79	22.01
	s.d.		0.06	0.04	0.27	0.04
mCh_mRNA_{UTR2}^{1CP}	#1	#1.1	19.62	19.66	18.31	22.11
		#1.2	19.45	19.66	18.23	22
		#1.3	19.54	19.73	18.44	22.1
	#1 NRT		0	0	0	0
	#2	#2.1	19.15	19.31	18.48	21.94
		#2.2	19.19	19.37	18.01	22.01
		#2.3	19.19	19.56	17.96	22.07
	#2 NRT		0	0	0	0
	mean		19.36	19.55	18.24	22.04
	s.d.		0.04	0.07	0.16	0.05
mCh_mRNA_{UTR2}^{2CP}	#1	#1.1	19.51	19.3	17.56	22.09
		#1.2	19.47	19.23	17.41	22.04
		#1.3	19.46	19.25	16.82	22.06
	#1 NRT		0	0	0	0
	#2	#2.1	19.43	19.22	18.38	21.92
		#2.2	19.56	19.35	17.49	22.06
		#2.3	19.61	19.38	18.56	22.12
	#2 NRT		0	0	0	0
	mean		19.51	19.29	17.70	22.05
	s.d.		0.05	0.05	0.39	0.05
mCh_mRNA_{UTR2}^{1PM}	#1	#1.1	18.72	19.26	17.77	22.1
		#1.2	18.71	19.24	17.42	22.1
		#1.3	18.74	19.33	17.35	22.14
	#1 NRT		0	0	0	0
	#2	#2.1	18.87	19.45	18.52	22.13
		#2.2	18.86	19.43	18.3	22.19
		#2.3	19	19.45	17.23	22.18
	#2 NRT		0	0	0	0

	mean		18.82	19.36	17.77	22.14	
	s.d.		0.04	0.02	0.37	0.02	
mCh_mRNA_{UTR2}^{2PM}	#1	#1.1	18.86	19.3	17.59	22.12	
		#1.2	19.01	19.3	18.53	22.1	
		#1.3	18.94	19.22	17.98	22.07	
	#1 NRT		0	0	0	0	
	#2	#2.1	18.94	19.19	17.46	22.03	
		#2.2	18.95	19.22	17.42	22.07	
		#2.3	18.91	19.23	17.34	22.04	
	#2 NRT		0	0	0	0	
		mean		18.94	19.24	17.72	22.07
		s.d.		0.04	0.03	0.22	0.02
H₂O Ctrl.	#1	#1.1	0	0	20.2	22.16	
		#1.2	0	0	17.74	22.08	
	#1 NRT		0	0	0	0	
	#2	#2.1	0	0	17.59	22.05	
		#2.2	0	0	18.94	21.98	
	#2 NRT		0	0	0	0	
		mean		0.00	0.00	18.62	22.07
		s.d.		0.00	0.00	0.95	0.04
	Untreated Cells	#1	#1.1	0	0	18.09	22.03
			#1.2	0	0	17.78	21.9
#1.3			0	0	17.24	21.9	
#1 NRT			0	0	0	0	
#2		#2.1	33.54	35.47	17.34	21.92	
		#2.2	32.37	35.14	17.49	21.94	
		#2.3	32.82	35.54	17.87	21.89	
#2 NRT			32.31	34.14	0	33.18	
		mean		16.46	17.69	17.64	21.93
		s.d.		0.24	0.09	0.29	0.04
NTC	#1		0	0	0	0	
	#2		0	0	0	0	

Table 124. Ct values of *mCh_mRNA* + *mCh_mRNA_{UTR2}* data set 2, cell lysis 24 h post transfection.

	Δ Ct (mCh 3'end)	error	Δ Ct (mCh internal)	error
mCh_mRNA ^{WT}	-3.07	0.08	-2.51	0.06
mCh_mRNA ^{1 CP}	-2.71	0.13	-2.58	0.13
mCh_mRNA ^{2 CP}	-2.51	0.07	-2.58	0.08
mCh_mRNA ^{1 PM}	-3.33	0.06	-2.82	0.07
mCh_mRNA ^{2 PM}	-3.47	0.08	-2.91	0.09
mCh_mRNA _{UTR2} ^{WT}	-3.38	0.07	-2.78	0.06
mCh_mRNA _{UTR2} ^{1 CP}	-2.68	0.07	-2.49	0.09
mCh_mRNA _{UTR2} ^{2 CP}	-2.54	0.07	-2.76	0.07
mCh_mRNA _{UTR2} ^{1 PM}	-3.32	0.04	-2.78	0.03
mCh_mRNA _{UTR2} ^{2 PM}	-3.14	0.04	-2.83	0.03
H ₂ O Ctrl.	-22.07	0.04	-22.07	0.04
Untreated cells	-5.48	0.24	-4.24	0.10

Table 125. Δ Ct= Ct(mCh) – Ct(GAPDH) values of mCh_mRNA + mCh_mRNA_{UTR2} data set 2, cell lysis 24 h post transfection.

	Biological Duplicates	Technical Triplicates	Ct values				
			mCh 3' end: FAM	mCh internal: HEX	β -Actin: ROX	GAPDH: Cy5	
mCh_mRNA ^{WT}	#1	#1.1	21.39	22.06	19.44	22.19	
		#1.2	21.24	21.94	19.59	22.11	
		#1.3	21.16	21.93	17.91	22.07	
	#1 NRT		0	0	0	0	
	#2	#2.1	21.24	22.01	17.33	22.1	
		#2.2	21.31	22.08	17.71	22.15	
		#2.3	21.23	22.03	16.84	22.09	
	#2 NRT		0	0	0	0	
	mean		21.26	22.01	18.14	22.12	
	s.d.		0.07	0.04	0.56	0.04	
	mCh_mRNA ^{1 CP}	#1	#1.1	21.73	22.04	17.15	22.11
			#1.2	21.63	22.13	17.98	22.04
			#1.3	21.65	22.19	17.53	22.15
#1 NRT			0	0	0	0	
#2		#2.1	21.66	22.2	17.43	22.26	
		#2.2	21.58	22.11	16.57	22.19	
		#2.3	21.57	22.08	15.28	22.09	
#2 NRT			0	0	0	0	
mean			21.64	22.13	16.99	22.14	
s.d.			0.04	0.06	0.61	0.06	
mCh_mRNA ^{2 CP}		#1	#1.1	21.87	21.9	18.12	22.14
			#1.2	21.81	21.92	17.23	22.12
			#1.3	21.8	21.94	17.83	22.02
	#1 NRT		0	0	0	0	
	#2	#2.1	21.78	21.84	17.86	22.2	
		#2.2	21.75	21.81	16.89	22.17	

		#2.3	21.78	22	16.49	22.18
	#2 NRT		0	0	0	0
	mean		21.80	21.90	17.40	22.14
	s.d.		0.02	0.05	0.47	0.03
mCh_mRNA^{1 PM}	#1	#1.1	21.45	22.08	17.01	22.27
		#1.2	21.43	21.98	17.46	22.26
		#1.3	21.41	21.96	16.64	22.22
	#1 NRT		0	0	0	0
	#2	#2.1	21.35	21.9	16.03	22.09
		#2.2	21.25	21.77	16.94	22.03
		#2.3	21.22	21.91	17.46	22.07
	#2 NRT		0	0	0	0
	mean		21.35	21.93	16.92	22.16
	s.d.		0.04	0.06	0.46	0.02
mCh_mRNA^{2 PM}	#1	#1.1	21.07	21.56	18.31	22.06
		#1.2	20.98	21.5	16.59	21.98
		#1.3	21	21.51	16.67	21.96
	#1 NRT		0	0	0	0
	#2	#2.1	21.05	21.63	16.69	22.06
		#2.2	21.03	21.59	17.85	22.04
		#2.3	20.95	21.55	16.73	22.01
	#2 NRT		0	0	0	0
	mean		21.01	21.56	17.14	22.02
	s.d.		0.04	0.03	0.67	0.03
mCh_mRNA_{UTR2}^{WT}	#1	#1.1	20.94	21.45	18.67	22.09
		#1.2	20.84	21.51	17.25	22.01
		#1.3	20.82	21.46	17.41	22.1
	#1 NRT		0	0	0	0
	#2	#2.1	20.76	21.36	16.05	21.94
		#2.2	20.7	21.33	17.17	21.9
		#2.3	20.7	21.4	13.95	21.9
	#2 NRT		0	38.36	31.23	0
	mean		20.79	21.42	16.75	21.99
	s.d.		0.04	0.03	0.98	0.03
mCh_mRNA_{UTR2}^{1 CP}	#1	#1.1	21.7	21.74	16.79	22.21
		#1.2	21.52	21.57	17.54	22.02
		#1.3	21.52	21.62	15.75	22.08
	#1 NRT		0	0	0	0
	#2	#2.1	21.58	21.66	17.87	22.12
		#2.2	21.63	21.69	17.6	22.06
		#2.3	21.59	21.67	16.69	22.05
	#2 NRT		0	0	0	0
	mean		21.59	21.66	17.04	22.09
	s.d.		0.05	0.04	0.62	0.06
mCh_mRNA_{UTR2}^{2 CP}	#1	#1.1	21.73	21.58	17.69	22.1

		#1.2	21.68	21.55	17.87	22.13
		#1.3	21.66	21.52	17.86	22.05
	#1 NRT		0	0	0	0
	#2	#2.1	21.79	21.66	17.62	22.08
		#2.2	21.77	21.67	16.55	22.13
		#2.3	21.82	21.72	18.04	22.09
	#2 NRT		0	0	0	0
	mean		21.74	21.62	17.61	22.10
	s.d.		0.02	0.03	0.35	0.03
mCh_mRNA_{UTR2}^{1PM}	#1	#1.1	21.16	21.86	17.15	22.3
		#1.2	21.11	21.8	16.68	22.25
		#1.3	21.04	21.71	15.9	22.18
	#1 NRT		0	0	0	0
	#2	#2.1	20.73	21.33	16.62	22.04
		#2.2	20.67	21.31	16.69	22.08
		#2.3	20.71	21.37	17.21	22.04
	#2 NRT		0	0	0	0
	mean		20.90	21.56	16.71	22.15
	s.d.		0.04	0.04	0.39	0.03
mCh_mRNA_{UTR2}^{2PM}	#1	#1.1	21.1	21.61	18.02	22.19
		#1.2	21.06	21.57	17.5	22.08
		#1.3	21.16	21.56	16.51	22.15
	#1 NRT		0	40.5	0	0
	#2	#2.1	21.3	21.71	16.64	22.2
		#2.2	21.12	21.65	17.36	22.15
		#2.3	21.17	21.72	16.57	22.19
	#2 NRT		0	0	0	0
	mean		21.15	21.64	17.10	22.16
	s.d.		0.06	0.03	0.49	0.03
H₂O Ctrl.	#1	#1.1	0	0	19.72	22.23
		#1.2	0	0	15.57	22.25
	#1 NRT		0	0	0	0
	#2	#2.1	0	0	16.72	22.3
		#2.2	0	0	17.6	22.32
	#2 NRT		0	0	0	0
	mean		0.00	0.00	17.40	22.28
	s.d.		0.00	0.00	1.26	0.01
Untreated Cells	#1	#1.1	0	0	17.57	22.37
		#1.2	0	0	18.33	22.29
		#1.3	0	0	17.57	22.32
	#1 NRT		0	0	0	0
	#2	#2.1	0	0	15.8	22.35
		#2.2	0	0	16.72	22.32
		#2.3	0	0	16.55	22.35
	#2 NRT		0	0	0	0
	mean		0.00	0.00	17.09	22.33
	s.d.		0.00	0.00	0.38	0.02
NTC	#1		0	0	0	0
	#2		0	0	0	0

Table 126. Ct values of *mCh_mRNA* + *mCh_mRNA_{UTR2}* data set 2, cell lysis 48 h post transfection.

	Δ Ct (mCh 3'end)	error	Δ Ct (mCh internal)	error
<i>mCh_mRNA^{WT}</i>	-0.86	0.08	-0.11	0.06
<i>mCh_mRNA^{1CP}</i>	-0.50	0.07	-0.02	0.08
<i>mCh_mRNA^{2CP}</i>	-0.34	0.04	-0.24	0.06
<i>mCh_mRNA^{1PM}</i>	-0.81	0.04	-0.22	0.06
<i>mCh_mRNA^{2PM}</i>	-1.01	0.05	-0.46	0.04
<i>mCh_mRNA_{UTR2}^{WT}</i>	-1.20	0.05	-0.57	0.04
<i>mCh_mRNA_{UTR2}^{1CP}</i>	-0.50	0.08	-0.43	0.07
<i>mCh_mRNA_{UTR2}^{2CP}</i>	-0.35	0.04	-0.48	0.04
<i>mCh_mRNA_{UTR2}^{1PM}</i>	-1.24	0.05	-0.58	0.06
<i>mCh_mRNA_{UTR2}^{2PM}</i>	-1.01	0.07	-0.52	0.04
H ₂ O Ctrl.	-22.28	0.01	-22.28	0.01
Untreated cells	-22.33	0.02	-22.33	0.02

Table 127. Δ Ct= Ct(mCh) – Ct(GAPDH) values of *mCh_mRNA* + *mCh_mRNA_{UTR2}* data set 2, cell lysis 48 h post transfection.

	Biological Duplicates	Technical Triplicates	Ct values			
			mCh 3' end: FAM	mCh internal: HEX	β -Actin: ROX	GAPDH: Cy5
<i>mCh_mRNA^{WT}</i>	#1	#1.1	17.09	17.52	20.72	21.88
		#1.2	17.01	17.49	19.52	21.85
		#1.3	17.02	17.51	20.62	21.88
	#1 NRT		0	0	25.71	0
	#2	#2.1	17.27	17.75	21.08	22.27
		#2.2	17.1	17.81	20.3	22.11
		#2.3	17	17.55	20.81	22.02
	#2 NRT		0	0	36.67	0
	mean		17.08	17.61	20.51	22.00
	s.d.		0.07	0.06	0.43	0.06
	<i>mCh_mRNA^{1CP}</i>	#1	#1.1	17.3	17.44	20.41
#1.2			17.29	17.45	20.4	21.78
#1.3			17.28	17.5	20.52	21.81
#1 NRT			0	0	0	0
#2		#2.1	16.91	17.27	20.25	21.69
		#2.2	17.33	17.66	20.9	22.13
		#2.3	17.07	17.41	20.39	21.88
#2 NRT			0	0	0	0
mean			17.20	17.46	20.48	21.85
s.d.			0.09	0.09	0.17	0.10
<i>mCh_mRNA^{2CP}</i>		#1	#1.1	17.75	17.54	20.56
	#1.2		16.69	17.53	20.38	21.75
	#1.3		17.69	17.54	20.38	21.76

	#1 NRT		0	0	0	0
	#2	#2.1	17.77	17.65	19.72	21.83
		#2.2	17.73	17.73	19.4	21.8
		#2.3	17.83	17.68	19.34	21.86
	#2 NRT		0	0	0	0
	mean		17.58	17.61	19.96	21.80
	s.d.		0.26	0.02	0.13	0.02
mCh_mRNA^{WT, Ψ+5mC}	#1	#1.1	17.38	18.05	20.36	21.69
		#1.2	17.31	17.97	19.25	21.62
		#1.3	17.25	17.73	20.29	21.57
	#1 NRT		0	0	0	0
	#2	#2.1	17.47	18.13	19.39	21.67
		#2.2	17.43	18.11	20.4	21.65
		#2.3	17.5	18.19	20.46	21.73
	#2 NRT		0	0	0	0
	mean		17.39	18.03	20.03	21.66
	s.d.		0.04	0.08	0.50	0.04
mCh_mRNA^{1 CP, Ψ+5mC}	#1	#1.1	17.56	18.06	20.51	21.75
		#1.2	17.41	17.96	19.64	21.6
		#1.3	17.42	17.96	20.31	21.65
	#1 NRT		0	0	0	0
	#2	#2.1	17.42	17.76	20.4	21.67
		#2.2	17.43	17.96	20.37	21.68
		#2.3	17.41	17.96	20.3	21.67
	#2 NRT		0	0	0	0
	mean		17.44	17.94	20.26	21.67
	s.d.		0.04	0.07	0.21	0.03
mCh_mRNA^{2 CP, Ψ+5mC}	#1	#1.1	18.62	18.19	20.11	21.88
		#1.2	18.44	18.06	19.05	21.73
		#1.3	18.4	17.89	19.31	21.74
	#1 NRT		0	0	0	0
	#2	#2.1	17.97	17.91	19.55	21.71
		#2.2	18.09	17.92	19.3	21.7
		#2.3	17.93	17.86	20.37	21.7
	#2 NRT		0	0	0	0
	mean		18.24	17.97	19.62	21.74
	s.d.		0.08	0.07	0.45	0.04
Untreated Cells	#1	#1.1	0	0	21.03	21.79
		#1.2	0	0	21.08	21.86
		#1.3	0	0	20.94	21.83
	#1 NRT		0	0	0	0
	#2	#2.1	0	0	20.82	21.61
		#2.2	0	0	20.9	21.75
		#2.3	0	0	20.76	21.53
	#2 NRT		0	0	0	0
	mean		0.00	0.00	20.92	21.73

	s.d.		0.00	0.00	0.06	0.06
H₂O Ctrl.	#1	#1.1	0	0	20.79	21.73
		#1.2	0	0	20.62	21.45
		#1.3	0	0	20.61	21.45
	#1 NRT		0	0	0	0
	#2	#2.1	0	39.35	20.61	21.53
		#2.2	0	38.93	20.66	21.49
		#2.3	0	38.69	18.91	21.68
	#2 NRT		0	0	0	0
	mean		0.00	19.50	20.37	21.56
	s.d.		0.00	0.14	0.45	0.11
NTC	#1		0	0	0	0
	#2		0	0	0	0

Table 128. Ct values of *mCh_mRNA* + *mCh_mRNA*^{ψ+5mC} data set 1, cell lysis 6 h post transfection.

	ΔCt (mCh 3'end)	error	ΔCt (mCh internal)	error
mCh_mRNA^{WT}	-4.92	0.09	-4.40	0.09
mCh_mRNA^{1 CP}	-4.65	0.13	-4.39	0.13
mCh_mRNA^{2 CP}	-4.22	0.26	-4.19	0.03
mCh_mRNA^{WT, ψ+5mC}	-4.27	0.06	-3.63	0.09
mCh_mRNA^{1 CP, ψ+5mC}	-4.23	0.05	-3.73	0.08
mCh_mRNA^{2 CP, ψ+5mC}	-3.50	0.09	-3.77	0.08
H₂O Ctrl.	-21.73	0.06	-21.73	0.06
Untreated cells	-21.56	0.11	-2.06	0.17

Table 129. ΔCt= Ct(mCh) – Ct(GAPDH) values of *mCh_mRNA* + *mCh_mRNA*^{ψ+5mC} data set 1, cell lysis 6 h post transfection.

	Biological Duplicates	Technical Triplicates	Ct values			
			mCh 3' end: FAM	mCh internal: HEX	β-Actin: ROX	GAPDH: Cy5
mCh_mRNA^{WT}	#1	#1.1	19.41	19.71	21.63	22.29
		#1.2	19.3	19.57	21.54	22.22
		#1.3	19.27	19.7	21.54	22.22
	#1 NRT		0	0	0	0
	#2	#2.1	19.12	19.53	21.38	22.02
		#2.2	19.09	19.52	21.35	22.01
		#2.3	19.37	19.92	21.61	22.17
	#2 NRT		0	0	0	0
	mean		19.26	19.66	21.51	22.16
	s.d.		0.09	0.13	0.08	0.05
mCh_mRNA^{1 CP}	#1	#1.1	19.56	19.61	21.41	22.04
		#1.2	19.53	19.63	21.42	22.02
		#1.3	19.53	19.7	21.41	22.06
	#1 NRT		0	0	0	0
	#2	#2.1	19.3	19.53	21.43	22.1

		#2.2	19.28	19.49	21.45	22.1
		#2.3	19.22	19.49	21.38	22.06
	#2 NRT		0	0	0	0
	mean		19.40	19.58	21.42	22.06
	s.d.		0.02	0.03	0.02	0.02
mCh_mRNA^{2 CP}	#1	#1.1	20.19	20.02	21.38	22.03
		#1.2	20.12	20	21.29	21.96
		#1.3	20.1	20.01	21.35	21.95
	#1 NRT		0	0	0	0
	#2	#2.1	20.11	20.11	21.25	21.86
		#2.2	20.22	20.11	21.31	21.9
		#2.3	20.2	20.11	21.35	22
	#2 NRT		0	0	0	0
	mean		20.16	20.06	21.32	21.95
	s.d.		0.04	0.00	0.04	0.05
mCh_mRNA^{WT, $\Psi+5mC$}	#1	#1.1	19.89	20.4	21.34	22.05
		#1.2	19.68	20.15	21.21	21.88
		#1.3	19.67	20.25	21.17	21.86
	#1 NRT		0	0	0	0
	#2	#2.1	19.83	20.4	21.24	21.86
		#2.2	19.92	20.49	21.3	21.97
		#2.3	19.95	20.57	21.38	22.01
	#2 NRT		0	0	0	0
	mean		19.82	20.38	21.27	21.94
	s.d.		0.08	0.09	0.06	0.07
mCh_mRNA^{1 CP, $\Psi+5mC$}	#1	#1.1	20.17	20.52	21.49	22.08
		#1.2	20.03	20.38	21.26	21.93
		#1.3	20.31	21.08	21.61	22.34
	#1 NRT		0	0	0	0
	#2	#2.1	19.86	20.26	21.18	21.78
		#2.2	20.01	20.36	21.31	21.94
		#2.3	19.99	20.4	21.35	21.94
	#2 NRT		0	0	39.47	0
	mean		20.06	20.50	21.37	22.00
	s.d.		0.09	0.18	0.11	0.12
mCh_mRNA^{2 CP, $\Psi+5mC$}	#1	#1.1	21.24	21.13	21.6	22.22
		#1.2	21.13	21.01	21.47	22.13
		#1.3	21.07	20.95	21.46	22.09
	#1 NRT		0	0	0	0
	#2	#2.1	20.8	20.72	21.25	21.89
		#2.2	20.68	20.6	21.22	21.82
		#2.3	20.68	20.63	21.26	21.83
	#2 NRT		0	0	0	0
	mean		20.93	20.84	21.38	22.00
	s.d.		0.06	0.06	0.04	0.04

Untreated Cells	#1	#1.1	0	0	21.58	22.13
		#1.2	0	0	21.41	21.97
		#1.3	0	0	21.42	21.94
	#1 NRT	#2.1	0	0	39.14	0
		#2.2	0	0	21.43	21.98
		#2.3	0	0	21.43	21.95
	#2	#2.1	0	0	21.34	21.89
		#2.2	0	0	0	0
		#2.3	0	0	0	0
	#2 NRT	mean	0.00	0.00	21.44	21.98
s.d.		0.00	0.00	0.06	0.06	
H ₂ O Ctrl.	#1	#1.1	0	0	21.75	22.11
		#1.2	0	0	21.54	22
		#1.3	0	0	21.54	21.96
	#1 NRT	#2.1	0	0	0	0
		#2.2	0	0	21.65	22.07
		#2.3	0	0	21.52	22.08
	#2	#2.1	0	0	21.66	22.12
		#2.2	0	0	0	0
		#2.3	0	0	0	0
	#2 NRT	mean	0.00	0.00	21.61	22.06
s.d.		0.00	0.00	0.08	0.04	
NTC	#1	0	0	0	0	
	#2	0	0	0	0	

Table 130. Ct values of *mCh_mRNA* + *mCh_mRNA*^{ψ+5mC} data set 1, cell lysis 24 h post transfection.

	ΔCt (mCh 3'end)	error	ΔCt (mCh internal)	error
<i>mCh_mRNA</i> ^{WT}	-2.90	0.11	-2.50	0.14
<i>mCh_mRNA</i> ^{1 CP}	-2.66	0.03	-2.49	0.03
<i>mCh_mRNA</i> ^{2 CP}	-1.79	0.06	-1.89	0.05
<i>mCh_mRNA</i> ^{WT, ψ+5mC}	-2.12	0.11	-1.56	0.11
<i>mCh_mRNA</i> ^{1 CP, ψ+5mC}	-1.94	0.15	-1.50	0.22
<i>mCh_mRNA</i> ^{2 CP, ψ+5mC}	-1.06	0.08	-1.16	0.08
H ₂ O Ctrl.	-21.98	0.06	-21.98	0.06
Untreated cells	-22.06	0.04	-22.06	0.04

Table 131. ΔCt= Ct(mCh) – Ct(GAPDH) values of *mCh_mRNA* + *mCh_mRNA*^{ψ+5mC} data set 1, cell lysis 24 h post transfection.

	Biological Duplicates	Technical Triplicates	Ct values			
			mCh 3' end: FAM	mCh internal: HEX	β-Actin: ROX	GAPDH: Cy5
<i>mCh_mRNA</i> ^{WT}	#1	#1.1	21.71	22.47	16.55	22.32
		#1.2	21.6	22.39	17.36	22.26
		#1.3	21.6	22.54	19.02	22.31
	#1 NRT	#2.1	0	0	20.92	0
		#2.2	21.54	22.26	18.69	22.31
		#2.3	21.62	22.54	15.98	22.45

		#2.3	21.65	22.58	15.79	22.48
	#2 NRT		0	0	0	0
	mean		21.62	22.46	17.23	22.36
	s.d.		0.05	0.10	1.18	0.05
mCh_mRNA^{1 CP}	#1	#1.1	22.04	22.49	17.5	22.46
		#1.2	21.97	22.52	17.12	22.4
		#1.3	22.02	22.58	17.31	22.35
	#1 NRT		0	0	0	0
	#2	#2.1	22.03	22.55	13.08	22.42
		#2.2	22.16	22.8	17.78	22.56
		#2.3	22.07	22.81	17.27	22.55
	#2 NRT		0	0	0	0
	mean		22.05	22.63	16.68	22.46
	s.d.		0.04	0.08	1.13	0.05
mCh_mRNA^{2 CP}	#1	#1.1	22.39	22.54	17.33	22.33
		#1.2	22.36	22.57	15.09	22.32
		#1.3	22.25	22.57	16.61	22.28
	#1 NRT		0	0	0	0
	#2	#2.1	22.63	23.04	14.24	22.53
		#2.2	22.65	23.05	17.29	22.57
		#2.3	22.57	23.02	16.21	22.51
	#2 NRT		0	0	24.86	0
	mean		22.48	22.80	16.13	22.42
	s.d.		0.05	0.01	1.10	0.02
mCh_mRNA^{WT, Ψ+5mC}	#1	#1.1	22	23.01	15.1	22.42
		#1.2	21.96	22.9	16.41	22.4
		#1.3	21.94	23.02	15.54	22.35
	#1 NRT		0	0	0	0
	#2	#2.1	21.87	22.98	17.3	22.18
		#2.2	21.87	22.99	16.16	22.26
		#2.3	21.98	22.92	14.92	22.24
	#2 NRT		0	0	0	0
	mean		21.94	22.97	15.91	22.31
	s.d.		0.04	0.04	0.76	0.03
mCh_mRNA^{1 CP, Ψ+5mC}	#1	#1.1	22.49	23.24	17.24	22.45
		#1.2	22.39	23.19	16.87	22.36
		#1.3	22.39	23.15	16.3	22.35
	#1 NRT		0	0	18.07	0
	#2	#2.1	22.11	22.73	14.65	22.2
		#2.2	22.04	22.85	15.48	22.13
		#2.3	22.14	22.75	16.45	22.25
	#2 NRT		0	0	0	0
	mean		22.26	22.99	16.17	22.29
	s.d.		0.04	0.04	0.56	0.05
mCh_mRNA^{2 CP, Ψ+5mC}	#1	#1.1	23.02	23.35	15.06	22.43

		#1.2	22.94	23.31	16.36	22.37
		#1.3	22.96	23.3	17.29	22.42
	#1 NRT		0	0	0	0
	#2	#2.1	22.84	23.23	16.38	22.22
		#2.2	22.88	23.22	15.6	22.33
		#2.3	22.84	23.22	14.83	22.25
	#2 NRT		0	0	0	0
	mean		22.91	23.27	15.92	22.34
	s.d.		0.03	0.01	0.77	0.04
Untreated Cells	#1	#1.1	0	0	17.22	22.65
		#1.2	0	0	18.01	22.64
		#1.3	0	0	16.16	22.52
	#1 NRT		0	0	0	0
	#2	#2.1	0	0	14.48	22.48
		#2.2	0	0	16.46	22.48
		#2.3	0	0	16.26	22.5
	#2 NRT		0	0	0	0
	mean		0.00	0.00	16.43	22.55
	s.d.		0.00	0.00	0.82	0.03
H₂O Ctrl.	#1	#1.1	0	0	17.29	23
		#1.2	0	0	17.99	22.87
		#1.3	0	0	15.55	22.93
	#1 NRT		0	0	0	0
	#2	#2.1	0	0	16.98	22.39
		#2.2	0	0	15.58	22.41
		#2.3	0	0	15.42	22.43
	#2 NRT		0	0	0	0
	mean		0.00	0.00	16.47	22.67
	s.d.		0.00	0.00	0.86	0.03
NTC	#1		0	0	14.31	0
	#2		0	0	0	0

Table 132. Ct values *mCh_mRNA* + *mCh_mRNA*^{ψ+5mC} data set 1, cell lysis 48 h post transfection.

	ΔCt (mCh 3'end)	error	ΔCt (mCh internal)	error
mCh_mRNA^{WT}	-0.73	0.07	0.11	0.11
mCh_mRNA^{1 CP}	-0.41	0.07	0.17	0.10
mCh_mRNA^{2 CP}	0.05	0.05	0.38	0.03
mCh_mRNA^{WT, ψ+5mC}	-0.37	0.05	0.66	0.05
mCh_mRNA^{1 CP, ψ+5mC}	-0.03	0.06	0.70	0.06
mCh_mRNA^{2 CP, ψ+5mC}	0.58	0.04	0.93	0.04
H₂O Ctrl.	-22.55	0.03	-22.55	0.03
Untreated cells	-22.67	0.03	-22.67	0.03

Table 133. ΔCt= Ct(mCh) – Ct(GAPDH) values *mCh_mRNA* + *mCh_mRNA*^{ψ+5mC} data set 1, cell lysis 48 h post transfection.

	Biological Duplicates	Technical Triplicates	Ct values			
			mCh 3' end: FAM	mCh internal: HEX	β -Actin: ROX	GAPDH: Cy5
mCh_mRNA ^{WT}	#1	#1.1	17.04	17.14	18.34	21.99
		#1.2	16.94	17.18	18.07	21.93
		#1.3	16.86	17.04	18.39	21.89
	#1 NRT		0	0	0	0
	#2	#2.1	16.95	17.25	18.35	21.91
		#2.2	16.94	17.25	18.07	21.92
		#2.3	16.96	17.12	18.12	21.96
	#2 NRT		0	0	0	0
	mean		16.95	17.16	18.22	21.93
	s.d.		0.04	0.06	0.13	0.03
	mCh_mRNA ^{1 CP}	#1	#1.1	17.43	17.38	18.12
#1.2			17.34	17.36	18.6	21.78
#1.3			17.32	17.36	17.81	21.82
#1 NRT			0	39.02	21.22	0
#2		#2.1	17.36	17.41	17.24	22.05
		#2.2	17.35	17.36	18.87	21.94
		#2.3	17.28	17.31	18.15	21.85
#2 NRT			0	0	0	0
mean			17.35	17.36	18.13	21.89
s.d.			0.04	0.03	0.50	0.07
mCh_mRNA ^{2 CP}		#1	#1.1	17.78	17.39	17.94
	#1.2		17.68	17.32	18.72	21.79
	#1.3		17.71	17.23	17.32	21.84
	#1 NRT		0	0	0	0
	#2	#2.1	17.81	17.44	18.53	21.85
		#2.2	17.76	17.4	17.15	21.82
		#2.3	17.79	17.44	18.11	21.84
	#2 NRT		0	0	0	0
	mean		17.76	17.37	17.96	21.84
	s.d.		0.03	0.04	0.58	0.03
	mCh_mRNA ^{WT, Ψ+5mC}	#1	#1.1	17.39	17.59	18.86
#1.2			17.27	17.4	17.87	21.64
#1.3			17.27	17.48	18.84	21.66
#1 NRT			0	0	0	0
#2		#2.1	17.33	17.64	18.01	21.69
		#2.2	17.31	17.63	17	21.67
		#2.3	17.34	17.65	17.61	21.73
#2 NRT			0	0	0	0
mean			17.32	17.57	18.03	21.69
s.d.			0.03	0.04	0.44	0.04
mCh_mRNA ^{1 CP, Ψ+5mC}		#1	#1.1	17.61	17.73	17.69
	#1.2		17.44	17.55	18.52	21.6

		#1.3	17.4	17.52	18.28	21.54
	#1 NRT		0	0	0	0
	#2	#2.1	17.5	17.61	16.55	21.68
		#2.2	17.51	17.6	18.47	21.69
		#2.3	17.51	17.63	16.97	21.88
	#2 NRT		0	40.05	0	0
	mean		17.50	17.61	17.75	21.69
	s.d.		0.05	0.05	0.59	0.09
mCh_mRNA^{2 CP, $\Psi+5mC$}	#1	#1.1	18.49	18.05	18.52	21.79
		#1.2	18.32	17.88	17.58	21.62
		#1.3	18.31	17.83	17.39	21.64
	#1 NRT		0	0	0	0
	#2	#2.1	18.26	17.91	17.6	21.67
		#2.2	18.28	17.78	17.82	21.6
		#2.3	18.3	17.8	18	21.59
	#2 NRT		0	0	0	0
	mean		18.33	17.88	17.82	21.65
	s.d.		0.05	0.08	0.33	0.06
Untreated Cells	#1	#1.1	0	0	19.11	21.95
		#1.2	0	0	18.23	21.84
		#1.3	0	0	18.59	21.85
	#1 NRT		0	0	0	0
	#2	#2.1	0	0	18.37	21.76
		#2.2	0	0	18.22	21.71
		#2.3	0	0	20.64	22.61
	#2 NRT		0	0	0	0
	mean		0.00	0.00	18.86	21.95
	s.d.		0.00	0.00	0.73	0.23
H₂O Ctrl.	#1	#1.1	0	40.51	17.78	21.94
		#1.2	0	39.82	18.35	21.82
		#1.3	0	40.53	17	21.76
	#1 NRT		0	0	0	0
	#2	#2.1	0	0	17.23	21.8
		#2.2	0	0	17.67	21.69
		#2.3	0	0	17.23	21.8
	#2 NRT		0	0	0	0
	mean		0.00	20.14	17.54	21.80
	s.d.		0.00	0.17	0.38	0.06
NTC	#1		0	0	0	0
	#2		0	0	0	0

Table 134. Ct values of *mCh_mRNA* + *mCh_mRNA ^{$\Psi+5mC$}* data set 2, cell lysis 6 h post transfection.

	ΔCt (mCh 3'end)	error	ΔCt (mCh internal)	error
mCh_mRNA ^{WT}	-4.99	0.05	-4.77	0.07
mCh_mRNA ^{1 CP}	-4.54	0.08	-4.53	0.07
mCh_mRNA ^{2 CP}	-4.08	0.04	-4.47	0.05
mCh_mRNA ^{WT, $\Psi+5mC$}	-4.37	0.05	-4.13	0.06
mCh_mRNA ^{1 CP, $\Psi+5mC$}	-4.20	0.10	-4.08	0.10
mCh_mRNA ^{2 CP, $\Psi+5mC$}	-3.33	0.07	-3.78	0.09
H ₂ O Ctrl.	-21.95	0.23	-21.95	0.23
Untreated cells	-21.80	0.06	-1.66	0.18

Table 135. $\Delta Ct = Ct(mCh) - Ct(GAPDH)$ values of *mCh_mRNA* + *mCh_mRNA* ^{$\Psi+5mC$} data set 2, cell lysis 6 h post transfection.

	Biological Duplicates	Technical Triplicates	Ct values			
			mCh 3' end: FAM	mCh internal: HEX	β -Actin: ROX	GAPDH: Cy5
mCh_mRNA ^{WT}	#1	#1.1	19.14	19.83	19.56	21.93
		#1.2	18.98	19.63	19.08	21.8
		#1.3	18.98	19.68	19.21	21.82
	#1 NRT		0	0	41.14	0
	#2	#2.1	19.09	19.79	19.24	22.02
		#2.2	19.07	19.96	17.54	22.02
		#2.3	19.09	19.97	19.47	22.04
	#2 NRT		0	0	0	0
	mean		19.06	19.81	19.02	21.94
	s.d.		0.04	0.08	0.53	0.03
	mCh_mRNA ^{1 CP}	#1	#1.1	19.5	20.02	19.5
#1.2			19.42	19.97	18.62	22.16
#1.3			19.3	19.82	19.47	22.14
#1 NRT			0	0	41.52	0
#2		#2.1	19.24	19.88	19.15	22.12
		#2.2	19.23	19.9	18.24	22.14
		#2.3	19.19	19.86	19.33	22.11
#2 NRT			0	0	0	0
mean			19.31	19.91	19.05	22.15
s.d.			0.05	0.05	0.44	0.02
mCh_mRNA ^{2 CP}		#1	#1.1	20.08	20.26	19.22
	#1.2		19.97	20.16	17.87	22.08
	#1.3		20.01	20.2	19.16	22.09
	#1 NRT		0	0	0	0
	#2	#2.1	20.03	20.2	18.37	22.13
		#2.2	19.97	20.15	18.56	22.09
		#2.3	19.99	20.21	19.04	22.13
	#2 NRT		0	0	0	0
	mean		20.01	20.20	18.70	22.11
	s.d.		0.04	0.03	0.45	0.02

mCh_mRNA^{WT, Ψ+5mC}	#1	#1.1	19.69	20.57	18.47	21.72	
		#1.2	19.58	20.48	18.73	21.69	
		#1.3	19.55	20.45	18.35	21.64	
	#1 NRT		0	0	0	0	
	#2	#2.1	19.7	20.59	19.15	21.78	
		#2.2	19.69	20.75	18.45	21.93	
		#2.3	19.74	20.71	18.98	21.99	
	#2 NRT		0	0	0	0	
	mean		19.66	20.59	18.69	21.79	
	s.d.		0.04	0.06	0.23	0.06	
	mCh_mRNA^{1 CP, Ψ+5mC}	#1	#1.1	19.83	20.41	19.01	21.97
			#1.2	19.66	20.27	18.28	21.75
			#1.3	19.71	20.29	19.13	21.77
#1 NRT			0	0	0	0	
#2		#2.1	20.01	20.78	19.24	22.06	
		#2.2	20.03	20.66	18.48	22.08	
		#2.3	20	20.69	18.07	22.08	
#2 NRT			0	0	0	0	
mean			19.87	20.52	18.70	21.95	
s.d.			0.04	0.06	0.43	0.05	
mCh_mRNA^{2 CP, Ψ+5mC}		#1	#1.1	20.94	21.15	18.49	22.03
			#1.2	20.79	21.07	18.73	21.82
			#1.3	20.73	21.01	18.2	21.74
	#1 NRT		0	0	0	0	
	#2	#2.1	20.57	20.83	18.25	21.88	
		#2.2	20.53	20.81	18.55	21.87	
		#2.3	20.51	20.7	16.81	21.85	
	#2 NRT		0	0	0	0	
	mean		20.68	20.93	18.17	21.87	
	s.d.		0.06	0.06	0.49	0.07	
	Untreated Cells	#1	#1.1	0	0	18.32	22.06
			#1.2	0	0	18.34	21.96
			#1.3	0	0	18.36	21.89
#1 NRT			0	0	0	0	
#2		#2.1	0	0	18.27	22.11	
		#2.2	0	0	18.89	22.12	
		#2.3	0	0	17.56	22.14	
#2 NRT			0	0	0	0	
mean			0.00	0.00	18.29	22.05	
s.d.			0.00	0.00	0.28	0.04	
H₂O Ctrl.		#1	#1.1	0	0	18.49	22.11
			#1.2	0	0	18.26	22.01
			#1.3	0	0	17.67	21.97
	#1 NRT		0	0	0	0	
	#2	#2.1	0	0	18.21	21.99	
		#2.2	0	0	18.12	21.92	

		#2.3	0	0	18.15	21.93
	#2 NRT		0	0	0	0
	mean		0.00	0.00	18.15	21.99
	s.d.		0.00	0.00	0.19	0.04
NTC	#1		0	0	0	0
	#2		0	0	0	0

Table 136. Ct values *mCh_mRNA* + *mCh_mRNA*^{ψ+5mC} data set 2, cell lysis 24 h post transfection.

	ΔCt (mCh 3'end)	error	ΔCt (mCh internal)	error
<i>mCh_mRNA</i> ^{WT}	-2.88	0.05	-2.13	0.09
<i>mCh_mRNA</i> ^{1 CP}	-2.83	0.06	-2.24	0.05
<i>mCh_mRNA</i> ^{2 CP}	-2.10	0.04	-1.91	0.04
<i>mCh_mRNA</i> ^{WT, ψ+5mC}	-2.13	0.07	-1.20	0.08
<i>mCh_mRNA</i> ^{1 CP, ψ+5mC}	-2.08	0.07	-1.44	0.08
<i>mCh_mRNA</i> ^{2 CP, ψ+5mC}	-1.19	0.09	-0.94	0.09
H ₂ O Ctrl.	-22.05	0.04	-22.05	0.04
Untreated cells	-21.99	0.04	-21.99	0.04

Table 137. ΔCt= Ct(mCh) – Ct(GAPDH) values *mCh_mRNA* + *mCh_mRNA*^{ψ+5mC} data set 2, cell lysis 24 h post transfection.

	Biological Duplicates	Technical Triplicates	Ct values			
			mCh 3' end: FAM	mCh internal: HEX	β-Actin: ROX	GAPDH: Cy5
<i>mCh_mRNA</i> ^{WT}	#1	#1.1	21.38	22.18	19.77	22.39
		#1.2	21.42	22.15	19.65	22.37
		#1.3	21.37	22.15	20.34	22.35
	#1 NRT		0	0	0	0
	#2	#2.1	21.84	22.74	20.09	22.45
		#2.2	21.8	22.74	20.39	22.43
		#2.3	21.83	22.78	21.11	22.47
	#2 NRT		0	0	0	0
	mean		21.61	22.46	20.23	22.41
	s.d.		0.02	0.02	0.36	0.02
<i>mCh_mRNA</i> ^{1 CP}	#1	#1.1	22.19	22.7	20.19	22.54
		#1.2	22.16	22.72	20.31	22.5
		#1.3	22.04	22.68	20.44	22.49
	#1 NRT		0	0	0	0
	#2	#2.1	21.87	22.4	19.7	22.37
		#2.2	21.88	22.52	20.29	22.39
		#2.3	21.78	22.38	19.63	22.41
	#2 NRT		0	0	29.18	0
	mean		21.99	22.57	20.09	22.45
	s.d.		0.05	0.04	0.20	0.02
<i>mCh_mRNA</i> ^{2 CP}	#1	#1.1	22.86	23.11	20.47	22.73

		#1.2	22.77	23.11	19.52	22.64
		#1.3	22.77	23.1	19.57	22.65
	#1 NRT		0	0	0	0
	#2	#2.1	22.65	23.01	19.43	22.5
		#2.2	22.58	22.96	19.77	22.47
		#2.3	22.59	22.97	18.97	22.46
	#2 NRT		0	0	0	0
	mean		22.70	23.04	19.62	22.58
	s.d.		0.04	0.01	0.38	0.03
mCh_mRNA^{WT, Ψ+5mC}	#1	#1.1	22.22	23.35	20.39	22.54
		#1.2	21.97	23.25	19.87	22.45
		#1.3	21.96	23.2	19.73	22.42
	#1 NRT		0	0	0	0
	#2	#2.1	22.5	23.8	20.36	22.64
		#2.2	22.52	23.71	20.37	22.68
		#2.3	22.57	23.94	19.83	22.75
	#2 NRT		0	0	0	0
	mean		22.29	23.54	20.09	22.58
	s.d.		0.07	0.08	0.27	0.05
mCh_mRNA^{1 CP, Ψ+5mC}	#1	#1.1	23.17	24.05	20.13	22.73
		#1.2	22.88	23.85	20.24	22.59
		#1.3	22.88	23.73	18.67	22.59
	#1 NRT		0	0	0	0
	#2	#2.1	23	23.99	20.19	22.73
		#2.2	23.01	24.03	19.52	22.73
		#2.3	22.98	24.02	20.46	22.74
	#2 NRT		0	0	0	0
	mean		22.99	23.95	19.87	22.69
	s.d.		0.07	0.07	0.56	0.04
mCh_mRNA^{2 CP, Ψ+5mC}	#1	#1.1	23.86	24.34	19.43	22.8
		#1.2	23.68	24.23	20.31	22.63
		#1.3	23.64	24.21	19.77	22.62
	#1 NRT		0	0	0	0
	#2	#2.1	23.66	24.19	19.69	22.61
		#2.2	23.56	24.11	19.33	22.57
		#2.3	23.58	24.14	19.4	22.62
	#2 NRT		0	0	0	0
	mean		23.66	24.20	19.66	22.64
	s.d.		0.07	0.05	0.26	0.05
Untreated Cells	#1	#1.1	0	0	20.75	23
		#1.2	0	0	19.86	22.84
		#1.3	0	0	20.28	22.81
	#1 NRT		0	0	0	0
	#2	#2.1	0	0	20.75	22.86
		#2.2	0	0	20.86	22.9
		#2.3	0	0	20.5	22.86

	#2 NRT		0	0	0	0
	mean		0.00	0.00	20.50	22.88
	s.d.		0.00	0.00	0.26	0.05
H₂O Ctrl.	#1	#1.1	0	0	20.42	22.57
		#1.2	0	0	19.55	22.46
		#1.3	0	0	19.23	22.47
	#1 NRT		0	0	0	0
	#2	#2.1	0	0	20.15	22.53
		#2.2	0	0	19.41	22.47
		#2.3	0	0	20.15	22.47
	#2 NRT		0	0	0	0
	mean		0.00	0.00	19.82	22.50
	s.d.		0.00	0.00	0.43	0.04
NTC	#1		0	0	0	0
	#2		0	0	0	0

Table 138. Ct values of *mCh_mRNA* + *mCh_mRNA*^{ψ+5mC} data set 2, cell lysis 48 h post transfection.

	ΔCt (mCh 3'end)	error	ΔCt (mCh internal)	error
mCh_mRNA^{WT}	-0.80	0.03	0.05	0.02
mCh_mRNA^{1 CP}	-0.46	0.06	0.12	0.04
mCh_mRNA^{2 CP}	0.13	0.05	0.47	0.03
mCh_mRNA^{WT, ψ+5mC}	-0.29	0.09	0.96	0.09
mCh_mRNA^{1 CP, ψ+5mC}	0.30	0.08	1.26	0.08
mCh_mRNA^{2 CP, ψ+5mC}	1.02	0.09	1.56	0.07
H₂O Ctrl.	-22.88	0.05	-22.88	0.05
Untreated cells	-22.50	0.04	-22.50	0.04

Table 139. ΔCt= Ct(mCh) – Ct(GAPDH) values of *mCh_mRNA* + *mCh_mRNA*^{ψ+5mC} data set 2, cell lysis 48 h post transfection.

	6 h		24 h		48 h	
	ΔCt (mCh 3'end)	error	ΔCt (mCh 3'end)	error	ΔCt (mCh 3'end)	error
mCh_mRNA^{WT}	-5.17	0.04	-3.03	0.04	-0.79	0.05
mCh_mRNA^{1 CP}	-4.68	0.05	-2.72	0.04	-0.46	0.06
mCh_mRNA^{2 CP}	-4.20	0.07	-2.13	0.03	-0.06	0.03
mCh_mRNA^{WT, ψ+5mC}	-4.32	0.12	-2.12	0.17	-0.33	0.12
mCh_mRNA^{1 CP, ψ+5mC}	-4.21	0.12	-2.01	0.20	0.14	0.13
mCh_mRNA^{2 CP, ψ+5mC}	-3.41	0.15	-1.13	0.15	0.80	0.11
mCh_mRNA^{1 PM}	-5.18	0.06	-3.29	0.04	-0.87	0.07
mCh_mRNA^{2 PM}	-5.29	0.05	-3.36	0.06	-1.02	0.10
mCh_mRNA^{UTR2}^{WT}	-5.36	0.05	-3.30	0.04	-1.16	0.19
mCh_mRNA^{UTR2}^{1 CP}	-4.41	0.04	-2.56	0.06	-0.45	0.13
mCh_mRNA^{UTR2}^{2 CP}	-4.29	0.07	-2.41	0.05	-0.18	0.15
mCh_mRNA^{UTR2}^{1 PM}	-5.27	0.05	-3.31	0.04	-1.16	0.04
mCh_mRNA^{UTR2}^{2 PM}	-5.11	0.04	-3.16	0.06	-1.00	0.06

Table 140. Averaged ΔCt values of *mCh_mRNA* 3' end primer + probe set.

	6 h		24 h		48 h	
	ΔCt (mCh internal)	error	ΔCt (mCh internal)	error	ΔCt (mCh internal)	error
mCh_mRNA ^{WT}	-4.93	0.04	-2.46	0.04	-0.04	0.05
mCh_mRNA ^{1 CP}	-4.62	0.05	-2.40	0.04	0.05	0.06
mCh_mRNA ^{2 CP}	-4.48	0.04	-2.07	0.03	0.12	0.03
mCh_mRNA ^{WT, $\Psi+5mC$}	-3.88	0.16	-1.38	0.17	0.81	0.12
mCh_mRNA ^{1 CP, $\Psi+5mC$}	-3.91	0.15	-1.47	0.24	0.98	0.13
mCh_mRNA ^{2 CP, $\Psi+5mC$}	-3.77	0.15	-1.05	0.14	1.25	0.10
mCh_mRNA ^{1 PM}	-5.00	0.08	-2.76	0.04	-0.28	0.07
mCh_mRNA ^{2 PM}	-5.13	0.11	-2.80	0.06	-0.53	0.10
mCh_mRNA ^{UTR2^{WT}}	-5.03	0.10	-2.73	0.04	-0.58	0.19
mCh_mRNA ^{UTR2^{1 CP}}	-4.56	0.13	-2.50	0.07	-0.38	0.12
mCh_mRNA ^{UTR2^{2 CP}}	-4.47	0.16	-2.60	0.06	-0.34	0.15
mCh_mRNA ^{UTR2^{1 PM}}	-5.03	0.12	-2.77	0.03	-0.62	0.04
mCh_mRNA ^{UTR2^{2 PM}}	-4.89	0.07	-2.79	0.06	-0.60	0.06

Table 141. Averaged ΔCt values of *mCh_mRNA* internal primer + probe set.

	6 h		24 h		48 h	
	$\Delta\Delta Ct$ (mCh 3'end)	error	$\Delta\Delta Ct$ (mCh 3'end)	error	$\Delta\Delta Ct$ (mCh 3'end)	error
mCh_mRNA ^{WT}	0.00	0.06	2.14	0.06	4.39	0.07
mCh_mRNA ^{1 CP}	0.49	0.06	2.45	0.06	4.72	0.07
mCh_mRNA ^{2 CP}	0.98	0.08	3.04	0.05	5.11	0.05
mCh_mRNA ^{WT, $\Psi+5mC$}	0.85	0.13	3.05	0.17	4.84	0.13
mCh_mRNA ^{1 CP, $\Psi+5mC$}	0.96	0.13	3.16	0.20	5.31	0.14
mCh_mRNA ^{2 CP, $\Psi+5mC$}	1.76	0.16	4.05	0.15	5.97	0.12
mCh_mRNA ^{1 PM}	-0.01	0.07	1.89	0.06	4.30	0.08
mCh_mRNA ^{2 PM}	-0.12	0.06	1.81	0.07	4.15	0.11
mCh_mRNA ^{UTR2^{WT}}	-0.19	0.06	1.87	0.06	4.02	0.19
mCh_mRNA ^{UTR2^{1 CP}}	0.76	0.06	2.61	0.07	4.73	0.13
mCh_mRNA ^{UTR2^{2 CP}}	0.88	0.08	2.76	0.06	5.00	0.15
mCh_mRNA ^{UTR2^{1 PM}}	-0.10	0.07	1.86	0.06	4.01	0.05
mCh_mRNA ^{UTR2^{2 PM}}	0.06	0.06	2.02	0.07	4.17	0.07

Table 142. $\Delta\Delta Ct = \Delta Ct(mCh_mRNA \text{ modified, any time}) - \Delta Ct(mCh_mRNA^{WT}, 6h)$ values of *mCh_mRNA* 3' end primer + probe set.

	6 h		24 h		48 h	
	$\Delta\Delta Ct$ (mCh internal)	error	$\Delta\Delta Ct$ (mCh internal)	error	$\Delta\Delta Ct$ (mCh internal)	error
mCh_mRNA ^{WT}	0.00	0.05	2.47	0.06	4.89	0.07
mCh_mRNA ^{1 CP}	0.30	0.06	2.53	0.05	4.98	0.07
mCh_mRNA ^{2 CP}	0.45	0.05	2.86	0.05	5.05	0.05
mCh_mRNA ^{WT, $\Psi+5mC$}	1.05	0.16	3.55	0.18	5.74	0.13
mCh_mRNA ^{1 CP, $\Psi+5mC$}	1.02	0.15	3.46	0.24	5.90	0.14
mCh_mRNA ^{2 CP, $\Psi+5mC$}	1.15	0.16	3.88	0.15	6.17	0.11
mCh_mRNA ^{1 PM}	-0.07	0.09	2.17	0.05	4.64	0.08
mCh_mRNA ^{2 PM}	-0.21	0.11	2.13	0.07	4.39	0.10
mCh_mRNA _{UTR2} ^{WT}	-0.11	0.11	2.20	0.06	4.34	0.19
mCh_mRNA _{UTR2} ^{1 CP}	0.37	0.14	2.42	0.08	4.55	0.13
mCh_mRNA _{UTR2} ^{2 CP}	0.45	0.17	2.33	0.07	4.58	0.16
mCh_mRNA _{UTR2} ^{1 PM}	-0.11	0.13	2.15	0.05	4.31	0.06
mCh_mRNA _{UTR2} ^{2 PM}	0.03	0.08	2.13	0.07	4.32	0.07

Table 143. $\Delta\Delta Ct = \Delta Ct(mCh_mRNA \text{ modified, any time}) - \Delta Ct(mCh_mRNA^{WT}, 6h)$ values of *mCh_mRNA* internal primer + probe set.

	6 h		24 h		48 h	
	$2^{-\Delta\Delta Ct}$ (mCh 3'end)	error	$2^{-\Delta\Delta Ct}$ (mCh 3'end)	error	$2^{-\Delta\Delta Ct}$ (mCh 3'end)	error
mCh_mRNA ^{WT}	1.00	0.04	0.23	0.01	0.048	0.002
mCh_mRNA ^{1 CP}	0.71	0.03	0.18	0.01	0.038	0.002
mCh_mRNA ^{2 CP}	0.51	0.03	0.12	0.00	0.029	0.001
mCh_mRNA ^{WT, $\Psi+5mC$}	0.55	0.05	0.12	0.01	0.035	0.003
mCh_mRNA ^{1 CP, $\Psi+5mC$}	0.51	0.05	0.11	0.02	0.025	0.002
mCh_mRNA ^{2 CP, $\Psi+5mC$}	0.30	0.03	0.06	0.01	0.016	0.001
mCh_mRNA ^{1 PM}	1.00	0.05	0.27	0.01	0.051	0.003
mCh_mRNA ^{2 PM}	1.09	0.05	0.28	0.01	0.056	0.004
mCh_mRNA _{UTR2} ^{WT}	1.14	0.05	0.27	0.01	0.062	0.008
mCh_mRNA _{UTR2} ^{1 CP}	0.59	0.02	0.16	0.01	0.038	0.003
mCh_mRNA _{UTR2} ^{2 CP}	0.54	0.03	0.15	0.01	0.031	0.003
mCh_mRNA _{UTR2} ^{1 PM}	1.07	0.05	0.28	0.01	0.062	0.002
mCh_mRNA _{UTR2} ^{2 PM}	0.96	0.04	0.25	0.01	0.055	0.003

Table 144. Fold change $2^{-\Delta\Delta Ct}$ values of *mCh_mRNA* 3' end primer + probe set.

	6 h		24 h		48 h	
	$2^{-\Delta\Delta Ct}$ (mCh internal)	error	$2^{-\Delta\Delta Ct}$ (mCh internal)	error	$2^{-\Delta\Delta Ct}$ (mCh internal)	error
mCh_mRNA ^{WT}	1.00	0.04	0.18	0.01	0.034	0.002
mCh_mRNA ^{1 CP}	0.81	0.03	0.17	0.01	0.032	0.002
mCh_mRNA ^{2 CP}	0.73	0.03	0.14	0.00	0.030	0.001
mCh_mRNA ^{WT, $\Psi+5mC$}	0.48	0.05	0.09	0.01	0.019	0.002
mCh_mRNA ^{1 CP, $\Psi+5mC$}	0.49	0.05	0.09	0.02	0.017	0.002
mCh_mRNA ^{2 CP, $\Psi+5mC$}	0.45	0.05	0.07	0.01	0.014	0.001
mCh_mRNA ^{1 PM}	1.05	0.07	0.22	0.01	0.040	0.002
mCh_mRNA ^{2 PM}	1.15	0.09	0.23	0.01	0.048	0.003
mCh_mRNA ^{UTR2^{WT}}	1.08	0.08	0.22	0.01	0.049	0.007
mCh_mRNA ^{UTR2^{1 CP}}	0.78	0.07	0.19	0.01	0.043	0.004
mCh_mRNA ^{UTR2^{2 CP}}	0.73	0.08	0.20	0.01	0.042	0.005
mCh_mRNA ^{UTR2^{1 PM}}	1.08	0.09	0.22	0.01	0.051	0.002
mCh_mRNA ^{UTR2^{2 PM}}	0.98	0.05	0.23	0.01	0.050	0.002

Table 145. Fold change $2^{-\Delta\Delta Ct}$ values of *mCh_mRNA* internal primer + probe set.

Time point [h]	3' end			
	$mCh_mRNA^{WT, \Psi+5mC} /$ mCh_mRNA^{WT}	error	$mCh_mRNA^{2 CP, \Psi+5mC} /$ mCh_mRNA^{WT}	error
6	0.55	0.05	0.30	0.03
24	0.54	0.07	0.27	0.03
48	0.73	0.07	0.33	0.03

Table 146. Fold change ratios of $mCh_mRNA^{WT, \Psi+5mC} / mCh_mRNA^{WT}$ and $mCh_mRNA^{2 CP, \Psi+5mC} / mCh_mRNA^{WT}$, 3'-end data set.

Time point [h]	internal			
	$mCh_mRNA^{WT, \Psi+5mC} /$ mCh_mRNA^{WT}	error	$mCh_mRNA^{2 CP, \Psi+5mC} /$ mCh_mRNA^{WT}	error
6	0.48	0.06	0.45	0.05
24	0.48	0.06	0.38	0.04
48	0.56	0.07	0.41	0.04

Table 147. Fold change ratios of $mCh_mRNA^{WT, \Psi+5mC} / mCh_mRNA^{WT}$ and $mCh_mRNA^{2 CP, \Psi+5mC} / mCh_mRNA^{WT}$, internal data set.

7.6 MT cell viability assay

7.6.1 MT cell viability assay data tables

Time [h]	6	8	22	24	25	26
mCh	2432900	2554490	2685350	2725420	2643830	3255060
mRNA^{2 CP}	2409160	2454330	2416200	2704730	2627880	3233770
	2215920	2334510	2075270	1997020	2117430	2593080
mCh	1174660	1244560	1518930	1614330	1498030	1851460
mRNA^{1 CP}	2209430	2340810	2635460	2690920	2606540	3198450
	2313670	2557930	2356800	2328160	2263850	2738030
mCh	1919750	2165110	2217530	2378180	2129170	2592010
mRNA^{WT}	2374180	2623030	2778790	2795050	2621650	3105210
	2375480	2632540	2659840	2673440	2511330	3019900
mCh	811560	867730	982170	1093620	1086630	1333650
mRNA^{1 PM}	1662180	1650180	2121930	2190380	2079090	2522180
	2375030	2292610	2313820	2208820	2273910	2703040
mCh	2465640	2948460	2843250	3069840	2907870	3503480
mRNA^{2 PM}	2267220	2469010	2588280	2641080	2614210	3016440
	2225750	2308760	2195970	2126190	2256640	2572390
mCh	2378570	2421430	2494960	2693910	2531250	2891690
mRNA^{2 CP, Ψ+5mC}	2673200	2673550	2888130	2934110	3023130	3366430
	2315690	2415560	2473890	2379340	2568100	2872290
mCh	2454960	2895930	3934790	4433470	3916380	4539120
mRNA^{1 CP, Ψ+5mC}	2396240	2719690	3944030	3894430	4032920	4598720
	2394170	2368090	3467600	3222260	3701690	4242190
mRNA^{WT, Ψ+5mC}	2425740	3039910	3654140	4121950	3681070	4491290
	2531230	2851830	3692630	3662330	3625490	4330610
	2272830	2423550	3053540	2851040	3180800	3664090
H₂O Ctrl.	2665420	2951370	4445670	4552470	4314760	4921590
	2630750	3039010	4510970	4609090	4443640	4992870
	2414720	2826700	4067910	3980930	4136510	4375440
Untreated	2494110	3062580	4509860	4963310	4550240	5130990
Cells Ctrl.	2434950	3093910	4744170	4961430	4458690	5104830
	2320500	2757400	4225280	4297340	4199930	4548590
Lysed	2456100	3169160	4836790	5141860	1665630	128210
Cells Ctrl.	2659520	3270530	4929130	5146020	1627770	137680
	2552340	3029590	4627390	4643430	1558040	120080
Medium	13060	14430	13740	14260	13840	17180
Only	14230	16360	14560	15280	15720	19340
	16280	16350	16070	16170	17570	20180
	16420	16480	16710	16790	17800	21280
	17400	16640	16940	16600	19010	21020

Table 148. Raw luminescence values (RLU) measured from cells transfected with *mCh_mRNA* variants and control values.

Time [h]	mCh mRNA ^{2 CP}	mCh mRNA ^{1 CP}	mCh mRNA ^{WT}	mCh mRNA ^{1 PM}	mCh mRNA ^{2 PM}	mCh mRNA ^{2 CP, Ψ+5mC}	mCh mRNA ^{1 CP, Ψ+5mC}	mCh mRNA ^{WT, Ψ+5mC}	H ₂ O Ctrl.	Untreated Cells Ctrl.	Lysed Cells Ctrl.
6	2337182	1883775	2207659	1600779	2304059	2440342	2399645	2394455	2554819	2401042	2540509
8	2431725	2031715	2457508	1587455	2559358	2487461	2645185	2755711	2922975	2955245	3140375
22	2376669	2154793	2536449	1790369	2526896	2603389	3766536	3451166	4325913	4477499	4782166
24	2459903	2195317	2599737	1815120	2596550	2653300	3834233	3529287	4365010	4724873	4961283
25	2446259	2106019	2403929	1796422	2576119	2690705	3866875	3478999	4281515	4386165	1600359
26	3007503	2576180	2885907	2166490	3010970	3023670	4440210	4142197	4743500	4908337	108857

Table 149. Background subtracted mean values of luminescence (RLU).

Time [h]	mCh mRNA ^{2 CP}	mCh mRNA ^{1 CP}	mCh mRNA ^{WT}	mCh mRNA ^{1 PM}	mCh mRNA ^{2 PM}	mCh mRNA ^{2 CP, Ψ+5mC}	mCh mRNA ^{1 CP, Ψ+5mC}	mCh mRNA ^{WT, Ψ+5mC}	H ₂ O Ctrl.	Untreated Cells Ctrl.	Lysed Cells Ctrl.
6	97174	514129	214527	639109	104689	155840	28181	106082	110916	72064	83086
8	89926	574828	218142	582640	271778	120258	219418	257918	87114	151788	98775
22	249638	474496	241477	587761	266226	190503	222445	292620	195297	212167	126237
24	338600	447238	175039	521418	385778	227161	495469	525426	283715	313499	235949
25	244475	463407	211017	519889	266290	223695	137189	223882	125924	148345	44561
26	307165	559005	224535	607412	380251	228505	155932	358132	275798	268592	7192

Table 150. Standard deviation values of luminescence (RLU).

7.6.2 MT cell viability assay linearity validation

		Time [h]				
		6	8	24	30	48
H ₂ O transfection Ctrl.	#1	1074680	1447690	2362210	3153390	3186110
	#2	1188590	1616460	2502170	3459110	3596940
	#3	1205030	1581820	2505510	3487990	3608430
Untreated Cells Ctrl.	#1	550250	740640	1296000	2006640	2321030
	#2	571330	740220	1302030	2037690	2444350
	#3	714620	912360	1513940	2291650	2631250

Table 151. Raw luminescence values (RLU) for assay linearity validation.

		Time [h]				
		6	8	24	30	48
H ₂ O transfection Ctrl.		1153123	1545787	2453970	3363880	3459843
Untreated Cells Ctrl.		609090	794870	1367997	2109043	2461560

Table 152. Background subtracted mean values of luminescence (RFU) for assay linearity validation.

		Time [h]				
		6	8	24	30	48
H ₂ O transfection Ctrl.		57963	72781	66779	151385	196431
Untreated Cells Ctrl.		73025	81049	101347	127667	127530

Table 153. Standard deviation values of luminescence (RFU) for assay linearity validation.

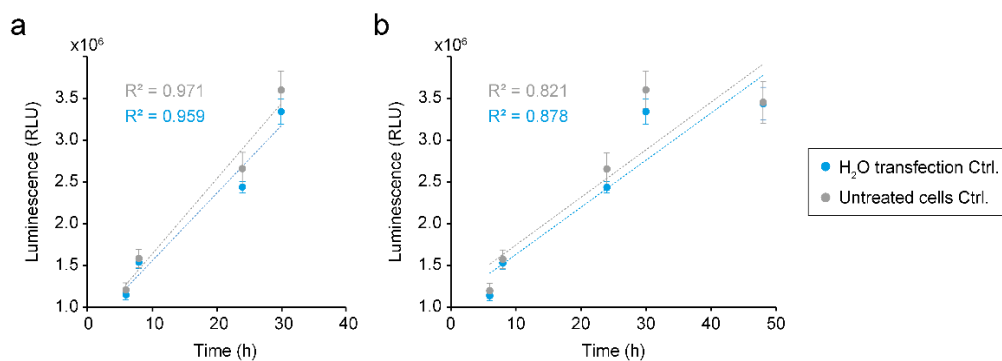


Figure 84. Plotted luminescence values for assay linearity validation. a) Linear regression and coefficient of determination for 30 h assay measurement time. b) Linear regression and coefficient of determination for 48 h assay measurement time.

7.7 cNLS mapper results for *mCherry* protein sequence

For prediction of nuclear localization signals (NLS) specific to the importin $\alpha\beta$ pathway^[445] the cNLS Mapper tool was used (http://nls-mapper.iab.keio.ac.jp/cgi-bin/NLS_Mapper_form.cgi). The result for the *mCherry* protein coding amino acid (AA) sequence is displayed in Figure 85. The cut-off score for prediction was set to 3.0 as a protein with scores of 3, 4 and 5 (scale range from 1 to 10) is localized to both the nucleus and the cytoplasm. It was searched for bipartite NLS with a long linker (13-20 AA) throughout the entire region. Two predicted bipartite NLS were found with a score of 3 and 3.3, additional predicted bipartite NLS were found with scores of 4.1, 4.3 and 4.5.

cNLS Mapper Result

Predicted NLSs in query sequence		
MVSKGEEDNMAIIKEFMRFKVHMEGSVNGHEFEIEGEGEGRPEYEGTQAK	50	
LKVTKGGPLPFAWDILSPQFMYGSKAYVKHPADIPDYLKLSFPEGFKWER	100	
VMNFEDGGVVTVTQDSSLQDGEFIYKVKLRGTNFPSDGPFVMQKKTMGWEA	150	
SSERMYPEDGALKGEIKQRLKLDGGHYDAEVKTTYKAKKPVQLPGAYNV	200	
NIKLDITSHNEDYTIVEQYERAEGRHSTGGMDELYK	236	

Predicted monopartite NLS		
Pos.	Sequence	Score

Predicted bipartite NLS		
Pos.	Sequence	Score
51	LKVTKGGPLPFAWDILSPQFMYGSKAYVK	3
74	SKAYVKHPADIPDYLKLSFPEGFKWERV	4.1
142	QKKTMGWEASSERMYPEDGALKGEIKQRLK	3.3
163	KGEIKQRLKLDGGHYDAEVKTTYKAKKP	4.3
163	KGEIKQRLKLDGGHYDAEVKTTYKAKKPV	4.5

Figure 85. cNLS mapper results for *mCherry* protein coding amino acid sequence.

7.8 Sequences

7.8.1 Plasmid sequences

pmCherry-N1_AA-insert (4724 bp), insertion of two nucleotides **AA** at position 1388 (bold and underlined) in comparison to *pmCherry-N1*, silent mutation of stop codon, no influence on *mCherry* protein coding sequence (underlined with dotted line)

```

5'-TAGTTATTAATAGTAATCAATTACGGGGTCATTAGTTCATAGCCCATATATGGAGTTCC
GCGTTACATAACTTACGGTAAATGGCCCGCCTGGCTGACCGCCCAACGACCCCGCCC
ATTGACGTCAATAATGACGTATGTTCCCATAGTAACGCCAATAGGGACTTTCCATTGACG
TCAATGGGTGGAGTATTTACGGTAAACTGCCCACTTGGCAGTACATCAAGTGTATCATAT
GCCAAGTACGCCCCCTATTGACGTCAATGACGGTAAATGGCCCGCCTGGCATTATGCC
CAGTACATGACCTTATGGGACTTTCCTACTTGGCAGTACATCTACGTATTAGTCATCGCT
ATTACCATGGTGTATGCGTTTTTGGCAGTACATCAATGGGCGTGGATAGCGGTTTGACTC
ACGGGGATTTCCAAGTCTCCACCCATTGACGTCAATGGGAGTTTGTGGTGGCACCAA
ATCAACGGGACTTTCCAAAATGTCGTAACAACCTCCGCCCATGACGCAAATGGGCGGT
AGGCGTGTACGGTGGGAGGTCTATATAAGCAGAGCTGGTTTGTGAACCGTCAGATCC
GCTAGCGCTACCGGACTCAGATCTCGAGCTCAAGCTTCGAATTCTGCAGTCGACGGTA
CCGCGGGCCCGGGATCCACCGGTGCCACCATGGTGAGCAAGGGCGAGGAGGATAAC
ATGGCCATCATCAAGGAGTTCATGCGCTTCAAGGTGCACATGGAGGGCTCCGTGAACG
GCCACGAGTTCGAGATCGAGGGCGAGGGCGAGGGCCGCCCTACGAGGGCACCCAG
ACCGCCAAGCTGAAGGTGACCAAGGGTGGCCCCCTGCCCTTCGCCTGGGACATCCTGT
CCCCTCAGTTCATGTACGGCTCCAAGGCCTACGTGAAGCACCCCGCCGACATCCCCGA
CTACTTGAAGCTGTCTTCCCGAGGGCTTCAAGTGGGAGCGCGTGATGAACTTCGAG
GACGGCGGCGTGGTGACCGTGACCCAGGACTCCTCCCTGCAGGACGGCGAGTTCATC
TACAAGGTGAAGCTGCGCGGCACCAACTTCCCCTCCGACGGCCCCGTAATGCAGAAGA
AGACCATGGGCTGGGAGGCCTCCTCCGAGCGGATGTACCCCGAGGACGGCGCCCTGA
AGGGCGAGATCAAGCAGAGGCTGAAGCTGAAGGACGGCGGCCACTACGACGCTGAGG
TCAAGACCACCTACAAGGCCAAGAAGCCCGTGCAGCTGCCCGGGCGCCTACAACGTCAA
CATCAAGTTGGACATCACCTCCACAACGAGGACTACACCATCGTGGAACAGTACGAAC
GCGCCGAGGGCCGCCACTCCACCGGCGGCATGGACGAGCTGTACAAGTAAAGCGGCC
GCGACTCTAGATCATAATCAGCCATACCACATTTGTAGAGGTTTTACTTGCTTTAAAAA
CCTCCCACACCTCCCCTGAACCTGAAACATAAAATGAATGCAATTGTTGTTGTTAACTT
GTTTATTGCAGTTATAATGGTTACAAATAAAGCAATAGCATCACAAATTTACAAATAAA
GCATTTTTTTCACTGCATTCTAGTTGTGGTTTGTCCAAACTCATCAATGTATCTTAAGGC
TAAATTGTAAGCGTTAATATTTTGTAAAATTTCGCGTTAAATTTTTGTTAAATCAGCTCATT
TTTTAACCAATAGGCCGAAATCGGCAAAATCCCTTATAAATCAAAGAATAGACCGAGAT
AGGGTTGAGTGTGTTCCAGTTTGGAAACAAGAGTCCACTATTAAGAACGTGGACTCCA
ACGTCAAAGGGCGAAAAACCGTCTATCAGGGCGATGGCCCACTACGTGAACCATCACC
CTAATCAAGTTTTTTGGGGTTCGAGGTGCCGTAAAGCACTAAATCGGAACCCTAAAGGGA
GCCCCCGATTTAGAGCTTGACGGGGAAAGCCGGCGAACGTGGCGAGAAAGGAAGGGA
AGAAAGCGAAAGGAGCGGGCGCTAGGGCGCTGGCAAGTGTAGCGGTCACGCTGCGCG
TAACCACCACACCCGCCGCGCTTAATGCGCCGCTACAGGGCGCGTTCAGGTGGCACTTT
TCGGGGAAATGTGCGCGGAACCCCTATTTGTTTATTTTTCTAAATACATTCAAATATGTAT
CCGCTCATGAGACAATAACCCTGATAAATGCTTCAATAATATTGAAAAAGGAAGAGTCCT
GAGGCGGAAAGAACCAGCTGTGGAATGTGTGTGAGTTAGGGTGTGGAAAGTCCCCAGG
CTCCCCAGCAGGCAGAAGTATGCAAAGCATGCATCTCAATTAGTCAGCAACCAGGTGTG
GAAAGTCCCCAGGCTCCCCAGCAGGCAGAAGTATGCAAAGCATGCATCTCAATTAGTCA

```

GCAACCATAGTCCCGCCCCTAACTCCGCCCATCCCGCCCCTAACTCCGCCCAGTTCCG
 CCCATTCTCCGCCCCATGGCTGACTAATTTTTTTTATTTATGCAGAGGCCGAGGCCGCC
 TCGGCCTCTGAGCTATTCCAGAAGTAGTGAGGAGGCTTTTTTGGAGGCCTAGGCTTTTG
 CAAAGATCGATCAAGAGACAGGATGAGGATCGTTTCGCATGATTGAACAAGATGGATTG
 CACGCAGGTTCTCCGGCCGCTTGGGTGGAGAGGCTATTCGGCTATGACTGGGCACAAC
 AGACAATCGGCTGCTCTGATGCCGCCGTGTTCCGGCTGTCAGCGCAGGGGGCGCCCGG
 TTCTTTTTGTCAAGACCGACCTGTCCGGTGCCCTGAATGAACTGCAAGACGAGGCAGCG
 CGGCTATCGTGGCTGGCCACGACGGGCGTTCCTTGCGCAGCTGTGCTCGACGTTGTCA
 CTGAAGCGGGAAGGGACTGGCTGCTATTGGGCGAAGTGCCGGGGCAGGATCTCCTGT
 CATCTCACCTTGCTCCTGCCGAGAAAGTATCCATCATGGCTGATGCAATGCGGCGGCTG
 CACACGCTTACCGGCTACCTGCCATTTCGACCACCAAGCGAAACATCGCATCGAGC
 GAGCACGTAATCGGATGGAAGCCGGTCTTGTGATCAGGATGATCTGGACGAAGAGCA
 TCAGGGGCTCGCGCCAGCCGAACTGTTCCGCCAGGCTCAAGGCGAGCATGCCCGACGG
 CGAGGATCTCGTCGTGACCCATGGCGATGCCTGCTTGCCGAATATCATGGTGGAAAAT
 GGCCGCTTTTTCTGGATTCATCGACTGTGGCCGGCTGGGTGTGGCGGACCGCTATCAGG
 ACATAGCGTTGGCTACCCGTGATATTGCTGAAGAGCTTGGCGGCGAATGGGCTGACCG
 CTTCTCGTGCTTTACGGTATCGCCGCTCCCGATTTCGCAGCGCATCGCCTTCTATCGCC
 TTCTTGACGAGTTCTTCTGAGCGGGACTCTGGGGTTCGAAATGACCGACCAAGCGACG
 CCAACCTGCCATCACGAGATTTTCGATTCCACCGCCGCTTCTATGAAAGGTTGGGCTT
 CGGAATCGTTTTCCGGGACGCCGGCTGGATGATCCTCCAGCGCGGGGATCTCATGCTG
 GAGTTCTTCGCCACCCTAGGGGGAGGCTAACTGAAACACGGAAGGAGACAATACCGG
 AAGGAACCCGCGCTATGACGGCAATAAAAAGACAGAATAAAACGACGCGGTGTTGGGTC
 GTTTGTTCATAAACGCGGGGTTCCGGTCCCAGGGCTGGCACTCTGTGATACCCACCG
 AGACCCCATTTGGGGCCAATACGCCCGGTTTTCTTCTTTTCCCACCCACCCCCCAAG
 TTCGGGTGAAGGCCAGGGCTCGCAGCCAACGTCGGGGCGGCAGGCCCTGCCATAGC
 CTCAGGTTACTCATATATACTTTAGATTGATTTAAACTTCATTTTTAATTTAAAAGGATCT
 AGGTGAAGATCCTTTTTGATAATCTCATGACCAAATCCCTAACGTGAGTTTTCGTTCC
 ACTGAGCGTCAGACCCCGTAGAAAAGATCAAAGGATCTTCTTGAGATCCTTTTTTTCTGC
 GCGTAATCTGCTGCTTGCAAACAAAAAACCACCGCTACCAGCGGTGGTTTGGTTGCCG
 GATCAAGAGCTACCAACTCTTTTTCCGAAGGTAAGTGGCTTCAGCAGAGCGCAGATAACC
 AAATACTGTCCTTCTAGTGTAGCCGTAGTTAGGCCACCACTTCAAGAACTCTGTAGCAC
 CGCCTACATACCTCGCTCTGCTAATCCTGTTACCAGTGGCTGCTGCCAGTGGCGATAAG
 TCGTGTCTTACCGGGTTGGACTCAAGACGATAGTTACCGGATAAGGCGCAGCGGTCCG
 GCTGAACGGGGGTTTCGTGCACACAGCCCAGCTTGGAGCGAACGACCTACACCGAACT
 GAGATACCTACAGCGTGAGCTATGAGAAAGCGCCACGCTTCCCGAAGGGAGAAAGGCG
 GACAGGTATCCGGTAAGCGGCAGGGTCGGAACAGGAGAGCGCACGAGGGAGCTTCCA
 GGGGAAACGCCTGGTATCTTTATAGTCTGTCCGGTTTTCCGCACCTCTGACTTGAGCG
 TCGATTTTTGTGATGCTCGTCAGGGGGGCGGAGCCTATGGAAAACGCCAGCAACGCG
 GCCTTTTTACGTTTCTGGCCTTTTGTGTCGCTTTTGTGCTCACATGTTCTTCTGCGTTA
 TCCCCTGATTCTGTGGATAACCGTATTACCGCCATGCAT-3'

pCMV-Xist-PA (18958 bp, Addgene #26760), *M. musculus Xist gene exon 1* (GenBank NR_001463.3, underlined with dotted line), *Xist A repeat region*^[446] (underlined)

5'-GACATTGATTATTGACTAGTTATTAATAGTAATCAATTACGGGGTCATTAGTTCATAGC
 CCATATATGGAGTTCGCGTTACATAACTTACGGTAAATGGCCCGCCTGGCTGACCGCC
 CAACGACCCCGCCATTGACGTCAATAATGACGTATGTTCCCATAGTAACGCCAATAG
 GGACTTTCCATTGACGTCAATGGGTGGAGTATTTACGGTAAACTGCCCACTTGGCAGTA
 CATCAAGTGTATCATATGCCAAGTACGCCCCCTATTGACGTCAATGACGGTAAATGGCC
 CGCCTGGCATTATGCCAGTACATGACCTTATGGGACTTTCTACTTGGCAGTACATCT
 ACGTATTAGTCATCGCTATTACCATGGTGTGCGGTTTTGGCAGTACATCAATGGGCGT
 GGATAGCGGTTTACTCACGGGGATTTCCAAGTCTCCACCCCACTTACGTCATGGGA

GTTTGTGTTTGGCACCAAATCAACGGGACTTTCCAAAATGTCGTAACAACCTCCGCCCCAT
TGACGCAAATGGGCGGTAGGCGTGTACGGTGGGAGGTCTATATAAGCAGAGCTCGTTT
AGTGAACCGTCAGATCGCCTGGAGACGCCATCCACGCTGTTTTGACCTCCATAGAAGAC
ACCGGGACCGATCCAGCCTCCGCGGATCAGTTAAGGCGTGCAACGGCTTGCTCCAGC
CATGTTTGGCTCGTTTCCCGTGGATGTGCGGTTCTTCCGTGGTTTCTCTCCATCTAAGGA
GCTTTGGGGGAACATTTTTAGTTCCCCTACCACCAAGCCTTATGGCTTATTTAAGAAAAC
ATATCAAATTCACGAGATTTTTGACGTTTTGATATGTTCTGGTAAGATTTTTTTTTGAC
ATGTCCTCCATACTTTTTGATATTTGTAATTTTTGAGTCAATTTTTATTTTAAGGAATA
TTTTCTTGTGTGCTTTTGGTTGATACTTGTGTGTGTATGGTGGACTTACCTTTCTTTCA
TTGTTTATATATTCTTGCCCATCGGGGCCACGGATACCTGTGTGTCTCCCGCCATTC
CATGCCAACGGGGTTTTGGATACTTACCTGCCTTTTTATTCTTTTTTTTTCTTATTATTT
TTTTCTAACTTGCCCATCTGGGCTGTGGATACCTGCTTTTATTCTTTTTTTCTTCTCCT
TAGCCCNATCGGGGCCATGGATACCTGCTTTTTGTAAAAAAAAAAAAAAAAAAAAAAAAAAC
CTTCTCGGTCCATCGGGACCTCGGATACCTGCGTTTAGTCTTTTTTTCCCATGCCAAC
GGGGCTCGGATACCTGCTGTTATTATTTTTTTTTCTTTTTCTTTTGCCCATCGGGGCTG
TGGATACCTGCTTTAAATTTTTTTTTCACGGCCCAACGGGGCGCTTGGTGGATGGAAAT
ATGGTTTTGTGAGTTATTGCACTACCTGGAATATCTATGCCTCTTATTTGCGTGTACTGTT
GCTGCTGATCGTTGGTGTGTGTGAGTGAACCTATGGCTTAGAAAAACGACTTTGCTC
TTAAACTGAGTGGGTGTTGAGGGCGTGGAGAGCCCGCGTCCGCCATTATGGCTTCTGC
GTGATACGGCTATTCTCGAGCCAGTTACGCCAAGAATTAGGACACCGAGGAGCACAGC
GGACTGGATAAAAGCAACCAATTGCGCTGCGCTAGCTAAAGGCTTTCTTTATATGTGCG
GGTTGCGGGATTGCGCTTGATTTGTGGTAGCATTGCGGGGTTGTGCTAGCCGGAAG
TAGAAAGCCAAGGAGTGTCTGATTAGTGTGCGGTGTTGCGCGGAAGCCGCAGAGGAC
TAGGGGATAGGGCTCAGCGTGGGTGTGGGGATTGGGCAGGGTGTGTGTGCATATGGA
CCCCTGGCGCGGTCCCCCGTGGCTTTAAGGGCTGCTCAGAAGTCTATAAAATGGCGGC
TCGGGGGCTCCACCCGAGGCTCGACAGCCCAATCTTTGTTCTGGTGTGTAGCAATGGA
TTATAGGACATTTAGGTGCTACAGGAAAAGATGGCGGCTCAAGTTCTTGGTGCGGTATA
ACGCAAAGGGCTTTGTGTGTACATGTCAGCTTCATGTCTGAGTTAGCCTGGAGAGGTG
GCACATGCTCTTGAATGTGTCTAAGATGGCGGAAGTCATGTGACCTGCCCTCTAGTGGT
TTCTTTCAGTGATTTTTTTTTGGCGGGCTTTAGCTACTTGGCGGGCTTTGCCCGAGGGT
ACACTTGGTGCATTATGGTAGGGTGTGGTTGGTCTACCTTGTGCCACTCGAAGCTGAG
GCAAGGCTAAGTGAAGTGTGGTTGCCACTTACGTAACCTCGTCAGAAATGGGCACAA
GTGTGAAAGTGTGGTGTGGCTTACTTCCAGTTAGAAATGTGCATTATTGCTTGGTGG
CCAGGATGGAATTAGACTGTGATGAGTCACTGTCCATAAGGACGTGAGTTTCGCTTGG
TACTTCACGTGTGCTTTAGTCATCATTTTTTCGAAGTGCCTGCCAGGTCGGGAGAGC
GCATGCTTGAATTCTAACACTGAAGTGTGGATGATGTGCGGATCCGATTGAGAGACC
GAGGCTGCGGGTCTTGGTGCATGTAATCATTGAAACCTCACCTATTAAGAAAGAA
AAGTATCTAAGGCCATTTCAAGGACATTTGACTCATCCGCTTGCCTTCATAGTCTCTTAC
AGTGCTCTATACGTGGCGGTGCAAACTAAACTCAGCCCGTTCATTCTTTGATTGTT
CAGTGGCTAGTCTACTTACACCTTGGCCTCTGATTTAGCCAGCACTGATCTCAAGCGGT
TCTCTAAGCCTACTGGGTATAAGTGGTGACTTTGGCCAGAGTCATAGTGGATCACAAAT
CACTGGTGAAGAGGTAGAATCCTACCTTCTTCCAAAATCTACCCCATGACTATTGCTGG
GGTTGCATTTGATTTCAATGAATTTTTGGATGCCAACGACACGTCTGATAGTGTGCTT
TGCTAGTGTGTTGAATTTAAACCGAAGTGATTGTTTTCAAATGTATTTACGGATTTGCTT
ACTTGTGTAATTCATTTAATTACCTTGTGTAATGTTACTTTGGAGTCTTAAAGTTTTC
AATAATTTTTTTGGCAGATGATACTCAAATTACTTGGCACTTAAATGTACTTTCTTTCAA
CTCATCCACCGAGCTACTCTTCAAATTTTTAAGTCTTATAACACAGATACTGTTAATGTAA
AGTGAACATTATGACTGGATGTCAGGAGTATTTGAGGTTCTATACCAGTTCAGGCTTTGC
TTTTGTTGCTATTGTTGATGCTATATTGACTAATGGTTTTACTTGTGAGCAAGAGCCTTGA
ATTGTAATGCTCTGTGCTCTATCAGACTTACTGTTATAATAGTAATATTAAGGCCTACA
TTTCAACTTTCTGTGTGTTCTTGCTTTATGGCATCTAGATTCTCCTCAAGACTCAGCAA
TAGTGCTGCTGCTATTGCTGCCCCAGCCCGAGCCCGAGCCCGAGCCCTGCCCCAGCC

CCAGCCCCAGCCCCTGCCCCAGCCCCAGCCCCTGCCCCCTGCCCCAGCCCCTGCCCCA
GCCCCAGCCCCAGCCCCTACCCCTGCCCCCTGCCCCCTGCCCCACCCAACCAACCCAATC
CAGTCCAGCCCCTGCCCCAGCCCAGTCTTAGCCCCAGGCCAGATACTTTTCAGACCTAT
CCCAAGCCCACCTTCTACTTAGAGAAATTCGAATCTTCATTGATTGAGTGTAAAATGCAG
TGTCATCACTCAGCCTATAAGACTGAGACAGCCCATCTATACCCCCTCCATACTGACTT
CTAGAGTCATGGAATTTCACTTAATGCATAGAATCGTATTGCTAAAATGCAGTGCCCATC
ACTCAGCCTATAAGACTGAGATAGCCCATCTATACCCCCTCCATACTGACTTACAGAGTC
ATGGAGTTTCACCTAATGCATGCAGTCTATTGCTAAAATGCAGTGCCCATAACTCAGCC
TATAAGACTGAGATAGCCCATTATACCCCATAACCCCCTCCATACTGACTTCTAGGGTCA
TGGAATTTCACTTAATACATAGAATCGTATTGCTAAAATGCAGTGCCCATCACTCAGTCTA
TAAGACTGAGATATCCCTATGTATACCCCATACTCCCTCCATACTGACTTCCAGAGTCAT
AGAATTTCACTTTGCATACGGTCCTATTGCTAAAATGCAGTGCCCATCACTCAGTCTATA
AGACTGAGATATCCCTATGTATACCCCATACTCCCTCCATACTGACTTCCAGAGTCATAG
AATTTCACTTTGCATACGGTCCTATTGCTAAAATGCAGTGCCCATCACTCAGCCTATAAG
ACTGAGATAGCCCATCTATACCCCCTCCATACTGACTTCCAGAGTCATGGAATTTCACTT
AATGCATGCAGTCTATTGCTAAAATGCAGTGCCCATCACTCAGCCTATAAGACTGAGAT
AGCCCATCTATACCCCATAACCCCCTCCATACTGACTTCCAGAGTCATGGAATTTCACTTA
ATGCATGCAGTCTATTGCTAAAATGCAGTGCCCATCACTCAGCCTATAAGACTGAGATA
GCCCATCTATACCCACTCCATACTGACTTCCAGAGTCATGGAATTTCACTTAATGCATGC
AGTCCCTATTGCTAAAATGCAGTGCCCATCACTCAGCCTATAAGACTGAGATAGCCCATCT
ATACCCACTCCATACTGACTTCCAGAGTCATGGAGTTTCACCTAATGCATGCAGTCTAT
TGCTAAAATGCAGTGCCCATAACTCAGCCTATAAGACTGAGATAGCCCATTATACCCCA
TACCCCCTCCATACTGACTTCTAGGGTCATGGAATTTCACTTAATGCATAGAATCGTATT
GCTAAAATGCAGTGCCCATCACTCAGCCTATAAGACTGAGATATCCCTATGTATACCCCA
TACCCCCTCCATACTGACTTCCAGAGACATAGAATTTCACTTTGCATACGGTCCTATTGC
TAAAATGCAGTGCCCATCACTCAGCCTATAAGACTGAGATATCCCTATCTATACCCCTCTA
CCCCCTCCATACTGACTTCCAGAGTCATGGAATTTACATAATGTATAGATTTCTATTGC
TAAAATGCAGTGCCCATAACTCAGCCTATAAGACTGAGATAGCCCATCTATACCCCCTC
CATACTGAGTCCAGAGTCATGGAATTTCACTTAATGCATAGAATCGTATTGCTAAAATG
CAGTGCCCATCACTCAGCCTATAAGACTGAGCCCATCTATACCCCATAACCCCCTCCATA
CTGACTTCCAGAGTCATGGAATTTCACTTTGCATACAGTCTACTTTACTTGTCCATGGA
CAAGTAAACAAGAAGTCTTGTCCTTCATGTTAATCAAGATACACCAATCAAACAAGAGT
TTTATATCAGAGACTTGCCATGGAGGTATCATCTCTCAAGTCTCCTTTCTTTAAGGAAA
GAAAACCATTTCTGTCATTGCTGTAGTAGTCACAGTCCCAAGTTTCTAAGCAGTGTTGAGT
CGTCTTTTCTCATGTATTACCTTGAGTACTGAATAATTCTGTCAGAAATATTTTGTCCATT
GGATTAGACTTTAGCTAGTCCAGCCCTGTGTGCATTTAGCAAAGGGGCAACACAGGTC
TGTTATCAGACAGTTAAAGTGCTCAGTCCCAATTTCAAGGCATTGGCCATTAAGGGG
GTAGAATACTATATACTGTTGGCATGCTGTCATGGGTGCTATCGCCCCAGGTCACATCT
TTCTAACTGATGGAGATACATTTATTTGCTCATGATATTGTATACTAGTCTCACATGCTTT
CTTATTTAGCCAAAAACCTCTGCACTGGAACATTTTATGTGGATAATCCTGACTAGGAA
TTGAGTCTTTTCTCAAGGTCTAATACTACCCTTGCTTTATGTAAAGAGGGTGCTGATTA
CTTAATGCCTCTTACACAATTGTGCAAAATTGCAGTTGTTCAAGTCCCCTTCTGTTAGTAA
CCAAGATCCCATACCCTCATACCCTAATGGGTGACAATCAAGGGTGCCAACCAATGAGA
CCACTTCTCTGTTCTGGTCTTTCTGCTGTGCTGGGGAATCAAACCTTGAGTCTTGTGTAC
GCTAGTAAAGCACTGTCATAGAGCTACAGCCCCACCGTGTGGTGGTTTGAGAGAACAG
CCTCTTATGTAGCCTGGGCTGGGCGGGACTTACAGGCATTGCCACCTGTAATGTAACA
TATTTGTGCCTGTTGTGTGCACAGCTGCATTTGTCCCTCTTCTAAGCATTGGATAAAGA
AACCAAACTAAGTCAAGTCATTTGTTGGTAATCAAGAAGACCTTTGATCTGTCCTGTTTT
TAACTTCCAGGCTGGCCTGGAACCTTAGCATATAACCCAGGCTAGCCTTGAGCTCAGGAT
CTAGCCTGCGTTTAAACAAGTGTGGCATATCTGGTTCCTACCCTATGCCCTGCATGCA
GTCTTTTCATATTGTGAATGTGCATATGTCATTTCACTGTAGTAATCTGCATCTGGTGAAG
ACTTATTTGTATTGCAGCAGTATTTAAGATCCTTAACATAGTAAATGTGCACAGTGTTAAC

TCTATTGTACATATTCTCATGTCCACAGTTGTGCCTTTTAGATCAGGACTCCTGTACTTAG
CAAAGCAAAGAGGCTCACTAATAAAGCTTCTTTTCATGAGACTATAGATTGAAACGATT
CCAATACGGTCAATGGTCTTCAAGGTAAGACTTCTGTCTCTGATCATTTCATATCCTCTT
TGCTTTATGGAATTATGTATGTGCTGTGCACTTGAAACCCCTTCTCAAACCTATTTATGTA
CATACTGGCAATTTTAGTAGGATCAATTTACTCTTAACTTTGAAGTACAGAAGTGGTGT
GACCTATAAGGTCCCATTTGTGGCTTGCTAATAATAATGACTGATTGTAGTAGGCCTT
TCTGTTCACTACAGAAGGAAACCTGAACAGCGTAAACTGTAATGGCCATAAACATGTAC
CTTGCAATATTAGTATGCATTTACTGCACACATCTCATTCCATTTGGATACGATCCTACTCT
CAAACCCTTTTGCAGTACAGCAAGGGTCACTAATCTTTGGCTTCTTCATCTTCTGGAC
ACTGGATAAGGCTGTCCCCTCTTCCACTCTTAAATTTCCAGGACTATTACTTTAAAGA
CTTAATATTTGCATAAAGGATGGGGTTTTAATTGATAACATGTCCCTTGAACATTAATGT
ATATAACAGGGACATGATCCATTCATTTAATAAAAATACTTGGCCAGTTAATGTGTA
TTACACTTATCCACAACCTTATTACTTTTCGGACCATTGTATCTCTTGCACCTGCAAGG
GATACCGTTTATCTCCAAGGTCCCTGCTAGTGGACCATTAATATACAGTGAATCTTCT
TTGTCTTTGCCAGTAAACAAAGGCCATACTCCTTCGCCTTTCATTTGCACTATATCAGGA
TATGCTGATCAACAAGGCCGATTCTTTTGGACTGTTATCATATATAAATGTATGCGTAT
GCACTGCCACCTGCTCTGTGCACTTGAAAGGATCCCCTCACTTCTTAGCACCTTCAG
CAGGAAGTGATAATAAGCTCAAGACTTTCATTTGGAAAGTTCACATGTCTAAGCACTTCT
CTAAGAACTACTGTACCCTCTTCTCCGCTTAAAGCAGAAAGAGGGTTGTACGAAGTGC
TCTTCATTTGGACTTAAGTGCATTAATGCAGTTAGTTGTCCATCATTACCTTTGGAGTTG
GATTTTACATCCTTGTACTCTTTTGCACACCAGAGGCATATTAATTATTTCTGAGCACTTCT
CTTGTCATATTAATCTGTACCCTTACACATATGACCTGTGCGGCAGCAAAGGTTCTGAA
ATGCCTACCTTTTACTGGGGCTGCTGAGTGGTAGTAACCTATTAGTAACCTCAGCATTG
GATGATTACTATGCAAAAATGTCAAGGACCTGTGTGCTCTCTTTGCATACCATCAAGGCT
ACTGAGTCCCAGAATTAATTGCTAAGTTATGCGTATTTATAACTATGAATGTCTGGAATAT
TTTGTCCCCTTACATTATTGCAGAGGTTGCTGAGCCCCGAAACTACCCGGTACTGTC
AATGAGCACAGGGGCTCTGACGAATGACCTGCTCTTCTTAAACTGATTTTGGGACT
CTTAATAGGCACAATGGCAGTTCTGGATGGTTATTTTCTACTCCAACCTTGAGCAAATCC
CCTGCTAGTTCCCAATGATATAATAAAGTACAGCAGTATGTACACCCAACAATGACCCG
GATTTGACCCCTTTTGCATTGCTTTAATATATACAATCCTAATAGTCACAATCTCACAC
TTTATAGTGTTCCCTTTTGCCTGGCCTCTAGTTTGTCCATTGACCACCTTTTCTGAATCACTA
ATTCTCACAAACCCATCATTAAAGGAAGAGTTTGTGCCCTTTCTCAATTCCATCATGCCAT
CCCTTTTGCCTCTTTGTTTGAACAGTATTGACTGGGCAAAGCCCTTCTCTTACTTAAAG
TCAACAACACCAGTTTACTCACTTCATATGGCTACAGTGTCTCAGTTGCCTTCTCCTTGC
TCCCCTGAACAGAGACACCTCGAATTCTTACATTATTCTGGGTAATGTTAATTACCCCA
AACACCCTATGTGTCATTAATAAATTTTGGTGTATTTATACACTGAATAGCAAAGCAGG
CCAAACTAGGTGGATGAGCCTTCAATCTTAACTTGCACCTTCTAAATTATCCAATTCCA
ACTGCTGGCACATTCTAGGGCCAGGAACCATTCTTGCCTACCTTTATTAATGCTTTATTG
TGCAAAAATATTGCAGGCAAGTAGCTCAGGGAGTTGGATTGCCACCTTTTACTTGGGGCT
TTCCTTTACAGTATGAACTGAAAATTGTCTTCTGAGAAGGAAGCTTAGCACTTTTCTTTC
CATTCTTCTCCAGGAAGGAGCCAACCTGTCTGCTTAAAGAACTTTAAGCCCGATTTTGT
TATTGCTACTGTACAGGACCAACTGCCAGAAAAGTTATTGATAATTTTATTCTTAAAGAA
GGCATTGGATTGCAAGGTGGATTGACTGTGAGATCATTAGCTTTTGTGAAGTAAAATA
GCCATTTGTGTCATGTTTCTGAAGACTAAGCAGTGTCTCAGTGTACTGAGGGTGATGAG
TCTGTGAAAGATCAGTGCACCTATTGCAGAATGTTAAGACAAGTATCTTTGCTTGGTC
TTTACTACAAGTTTAAACAAAACGAAAAGTCAATCTTTGTGTGGCCTTTAGTATGATTAAC
TTTTTGGAAAGATGACCTAAGCCTTCTAATCATTATATTTTGTCTGACATTGGTCACCAGTC
CTTGCTTATTTTTAAAGGTGACTGGATGGATTAATTTGAGAACATGTCAAGTCGCCTT
TGAAAATTATATAGGCCATCACATTTAATTAATTCATTCTATCCACCATTAACTCTGGCA
ATAATTTGAAGTAGCTTGAAAATTCCTAAAGTGGGAATTTATTTAGAGATGATAGAACCT
GTTTCCCCTTACATTTTAAATATGTCTGCCAGGATCTAATCATTCTTTAAACGTAC
ACTTCAAAGAGAGATTTTCTAGTAAGAAAAGAGCTTCTCTAGTGTGAAGGGTGCTTTG

TAGCCGCCGAGTACTTAGGTCTTTTTGGGAGCTATTGTGTATGAGTGTATGTATGTGTG
TGTGTACATGCATGTTGCTGCGCGCAGTCATTATTACATGGTGTCTCAGACAACAATG
GGAGCTGGTTCGTCTATCTTGTGGGTCCTGGAGATCAAAGTGAGATCATCAGGCTTGGC
AGCAAGTGCCTTCACCCTCCGCGTGCCATCTTGCCATCCCGCTGCTGAGTGTGTTGATAT
GACATTGCTGATGAAAATAATCATCACAAACAGCAGTTCTCCCGGCATTACTGAGAAATGA
TACTATTTTTCTGAGGAGGATGTTCAAGTAACTCATCCAGTGCAGGATCCTGCTTGA
ACTGCTCCTCCGTTACATCAGACTCTGGCTGTTAGACTACAGGATGAATTTGGAGTCT
GTTTTGTGCTCCTGCCTCAAGAAGAAGGATTGCCTGGATTTAGAGGAGTGAAGAGTGT
GGAGAGAGCCCAAAGGGACAAACAATCCCTATGTGAGATTCAAGGACTGCCAGCAGCC
TATACAGCTACATTACATCTCAGCAGAACTTCTCTTCAAGTCTCGCTACTCTGAACAAA
AAGCTTACAGGCCACATGGAGAAAAAAGATCTCCCCCAGAATTGTGGGCTTGTGCT
TTGCAGTGTGGCGACCTATTCCCTTTGACGATCCCTAGGTGGAGATGGGGCATGAGG
ATCCTCCAGGGGAATAGCTCACCACCCTGGGCAACAGGCCTAGCCCAGATTTTCAAGT
AGACGCTTTCCTGAACCCAGCAAGGAAGACAAAGGCTCAAAGAATGCCACCCTACATCA
AAGTAGGAGAAAAGCTGCTGCAATAGTGGCACTGACCTTCCGAGGAAGCCATTCTGCTC
TATTTGGTTCCTCTCCAGAAGTTAGGAGAACTTTGCCAGCTGTTTACATACTTCAAGAT
GCACTGCTACCCTACTCATGCCATATAATACACAATGCCATCTACCAAATATTACCCTTC
CCCAAAGCAGCACAGAAAAGTGGGCTTTCAGCATGATCAAGCAATGTGAACACACAAAA
GGAAGGCAGCTTTATAAATGACCCGAGGATCAACATGCCTGACTGCAGCATCTTAAAAG
CAATAGAATGAGTGTGTATTGTGTTGTGTGTCTATTTCTTGTTTTATGTATCTATTTTTCC
TTGGTCTGTGTGTCTAATTCTTTGTTACACCTATTTCTTCCCTTGCTTTGTGTGTCTATTTCT
TCCTTGCATTGTGTCTAATTCTTTGTTATATCTATTTCTTCCCTTGCTTCGTGTGTCTGTCTT
CCTTGCTTTGTGTCTATTTCTTCCCTTGCAGTTGTGTCTAATTCTTTGTTACATCTATTTCTT
CCTTGCTTTTGTGTCTTTCTTTCTTGCTTTTGTGTGTCTATTTCTTCCCTTGCAGTTGTG
TCTAATTCTTTGTTACATCTATTTCTTCCCTTGCTTTTGTGTCTATTTCTTCCCTTGCATTGTG
TCTAATTCTTTGGCATATATATTTCTTCAATTGCTTTGTGTGTCTATGTCTCCTTGTGTTGTG
TAATTCGTTGTTGCATCTATTTCTTCCCTTGCTTTGTGTCTATGTCTTCCCTGTTTTGTGTAT
CTACTTCTTCCCTTGTGTGTCTAATTCTTTGTTACATCTATTTCTTCCCTTCCCTTGCATGTCT
CCTTCTTCCCTTGTGTGTCTTTCTGTCTGCAGTGTGCCTTACCTATTCCCATGTTTCTC
CTGCATGTTCTTTCTTGCAGAGCTTTGAGCTTTGTTTCACTTTCTCTGGTGCCTGTGTGG
TCTGCTTTGTCTTCACTAGCTATGGCTCTCTGTTTTATCTATCTGATTGCTATTTCTCTTA
GCTTTTCTTTACTCCTGCCTTTCTGTGACTCCCCTTTGGGTCACATGTTGCATGCATCCC
TCTTTTTTCTTGTGCTCACCCCACTTGTCTTTGTTCAAGTTCTTTGTGAGTCCATTT
CAGTTTTCTTTCTGCTGCTTCTATCCTTAGTGAATTCTTGTTTACATTTCTTCCCTGCCTTT
CTTGGGCCACTTTCTCTGTTTTCTTTGTATTTGTGTCTCTTTGCTATTGGTGGATTTCTT
ATCTCAGCATCATTCTGTTGCTTTGTGTTGCTTGTGTTTCTATCTTCTACTTTCCTCCTTT
CTGTTCACTTTGAGCATTTCATCTCTTTACAAGTCTGTGTCTCTCTTGTATTCTAAAGTAA
TCCTTTCTTGGATGTTTCTTTGTATGTACATGTGCGTGTGTGCATGTGTGTTATGTGTGT
CATGTGTGAGAGGAGCTTCATAGCCCCTTCCAATAGGTCCAGAATGTCACCCGTGGA
GCCGTTCTCACACCAGACTGCCCTGAGAAATAATCTAAGACAAAATACATCATTCCGTC
CGGTCAGGATTCAAGTGGCTCTGAAGTGAACGCCCAAGTAGAAGACAGAAGTTTTGCG
ACTTGAGATTTAAAAGGACCAAAATACACAGATGGCCCGTCTTGAGCTGGCTGGACAGA
ATGCTGACAACCCAAAGAAGAGGAACTGTTTCTACAGGACACCTGTGACTTCCAAGAGC
GGGGAACACTACGTATGTCATAAGACACAAAACCTGAGCTAAGTCCAAGCATAAGACCTAA
GGACCAATCCTATATGGACAGAATATTTAAGAGATAAAGGCCTATGGCCCAGAACTCT
GGAAGGATATTTCTATCCTTCTATCCCCAAGACCAAGAAGGGAAATTCGAAGATGAGAC
CTGCCCCCAACCCAGCATCCCTTTCCATTTCTTATATTTCTATTTAAGCTGTCTTCACT
TGAGATGTAATTTTTTATTGTTGCCATTGCCATAAAGGAATACGTTTTTAGCTGGATAGT
ATTGTGCAAGGGTCTGTTTTAACTGGGCTTAGCCATTTGTTAAATTGTTGATGTTTTAC
AACTTCCATTTCTTTCACATCTGCTCCACTTGAGACGGAACTAAATCCAGCCAGTGTAT
ATAGCCTGACTATTGAACTTCCCTAGGAATAAGCATGCATACAGATATGCATACTGCCA
TCCTCCCTACCTCAGAAGCCCTAGGCTGACAAGAAAAGGAAAGCATCAGGTTGTTAGGG

GGAAAACAATGTCAGGCTATCTAGAGAAAATATAAAGAGTTGTTCCAGACCAATGAGAA
GAATTAGACAAGCAATATGCAGATGTGCCAACCCCTCTGAGAAGCACCAGCCAGTGTAC
CTTCTTTCTTTGGGCTTAGGTGAGCAGGGTATGGTTTTCTAATAATGGTTTGGGGACAAA
ATGAGGTCTGAACTCCCTGCTCATAGTAGTGCCGAGTAATTTGGTGCATTTACCCAAA
GAACTCCTGGGTCTAATACCTACCTTTAAAATTAATGATGAGAGACTCTAAGGACTACT
TAACGGGCTTAATCTTTTTCGTGCCCTCCTCTTCTCTGTAAGAGGGAAGTTAAATGACA
CAGGATGAAAAAGTAACATGCTCATAGCACATTGGCAATTATACATGGTTATTATCTGAA
AGTGTAGAGCTTTTCTATAAGGCATCAGACTAAGTACCTGAAGCTTTGTGGGTTTCATG
GTCTTAGTTGCATATTCCTTAGTTGCAAATCCTTTTTCAAAGGTAAGAAAAAGGCACACT
GGTCTATTGCCTGACTTGATCAAGCCCTGATATGAATGCCAGGGAATGTCTGAGTAAC
ATTAATTTCCCTCCCTGCATATTTTTTTGTGCTGAATACTAAGGCTGTGATGCTTCACTGTG
GTCACCCCCAGGTAACAAGATATTACCAGGTAACCAGGAAACGTATGAATACGTAACC
ATGAAGCCTACTGTAACCTCCAAGTCAGTGTGAGTATGTATTACATAGTAGCTGAAGTC
TACGCCTCTGTGTGCTATAGGCACAAAGATTGCTCTAGGAATAACATGCTTTGTAAAAAC
AAATATATGAACATAACGGGGCTTGAATGAATAACAGTCCATATACTTAAGGCCAGTGTG
TTTTCTTCTGCTTTGGTGAGGCTCAGTAAGTTATATTATACCAGGTAGCAGAAGAGAAAAC
ACATGGAACTGATTTTAACTACAACTAGGTCACTAATGCAGGTGATTGATTACCCTA
TTCTGATCACCTTCTAATTTCTGAATACCCATGTTTCAGCACTGGGAATAACAAAGGGGGA
CATTACCACAGAACTAGAATTTACAAAAGAATGCATTAAATAAAGCATTATACAGCTATCA
ATTGTTCCATGTGTGCAAATGAATGACTACTAACTACCTCTGATGTATCCGATATTGTTTT
GGGTACATGAAATATTCATGAGTAACTGCCATGAAATAAGAATGTTTGCATTCCATACTA
TTCATAAGGAATGAGCCAATGCTTAATTTAATCAGTCAAACCTTGAGTGATAAGGGCATG
TTAATACAAGAACATTTGCCCAGGTCACATTATGGTTGTGGGTACTTTCTTAACTATAAA
GCAGTTCAGTAGTATAAGACAAGACAAATTTTCTATAGAAATAAAGCTGCCTATAAAATA
GGCATAGTCTCTACAAAATTTTCAATTGTACTTTTTAGCCCATAAATGGGAAGAGTACAGTT
ACAAGCTGGGTGTGGTAGCATGTGCTCTGAGCTGAAGCAACAGGACCCTTGAGCCC
AGAAATTGGAGGCTAGCCTGGGAAGACCATAAGGTCAATCTCAAACCTGGAGGCTAAAT
ATTGTCTCCCATGTGTATATTCTCTTTTATGGGTACTGGAGAGATACACAGACGTACATT
TCAGTGTGTCCACACTTGAGAATAATATGTACGTTGGCATTTTATGAACTCGGAGGTACC
ATATAAATGTAACAATTCATTTTCTTACTTGGTATCAATTTCCAGGCTTTTAAAATTCTGCC
ACATTTATTATACTGTGAAAATAAAGTAAATAAGTAACTGTGAACCACTGAATATATGAAG
CATTCAATACTTGATGAGTACATACTGAATGGCAGTCATTTATTACAAAACAGTGCCCTT
GCTAGGCACTGGGATGCAAAGAGCATTCTCATTGTCTGTATCTAAAGAAATTATGCA
TGAGATTAATTTATAATTTGTAAACTGCCATATATATGTGTATATATGCAATATTTGCCTG
GTGTGCAATGACTTTGCTTTTATCCCAGGCATGCACAACAGATCTGTGTGGAGCTTTGT
GAAGTCTACAGTTCTATAAAGCCGGGACCTAACTGTTGGCTTTATCAGTGAACAGTGATT
ACTTTCTAAGTTTCATAATGGCTGAACTTAATCATAATGCTTATCACCTAACACCACCTA
ATAATAATTTTACCATGCTATGTGTTGAGCGAACACATAGATTGCTTTCTAGCATTATGTA
GCACTTATAGGAGTGAAATCTAGACCAAACTTCAATTCATTCATGAGGAAATGAAAA
CAGAAAAAATAATGGATTTGTGCAAGGCAGTGTGCTAAATGTTACACTGAGTGGACTAT
GCTGTCTAGGATACTTCCCAGATCAAGCTTATCGATACCGTCGACGGCCCCCCCCGACC
GATGTCAGCCTGGGGGACGAGCTCCACTTAGACGGCGAGGACGTGGCGATGGCGCAT
GCCGACGCGCTAGACGATTTGATCTGGACATGTTGGGGGACGGGGATTCCCCGGGT
CCGGGATTTACCCCCACGACTCCGCCCCCTACGGCGCTCTGGATATGGCCGACTTCG
AGTTTGAGCAGATGTTTACCGATGCCCTTGAATTGACGAGTACGGTGGGTAGGGGGC
GCGAGGATCCTCTAGAGCTGAGAACTTCAAGGTGAGTTTGGGGACCCTTGATTGTTCTT
TCTTTTTCGCTATTGTAATAATTCATGTTATATGGAGGGGGCAAAGTTTTCAGGGTGTGT
TTAGAATGGGAAGATGCCCTTGTATCACCATGGACCCTCATGATAATTTTGTTCCTTTC
ACTTTCTACTCTGTTGACAACCATTGTCTCCTCTTATTTTCTTTTCAATTTCTGTAACCTTT
TCGTTAACTTTAGCTTGCATTTGTAACGAATTTTAAATTCATTTTGTATTTGTCAGA
TTGTAAGTACTTTCTCTAATCACTTTTTTTTTCAAGGCAATCAGGGTATATTATATTGACTT
CAGCACAGTTTTAGAGAACAATTGTTATAATTAATGATAAGGTAGAATATTTCTGCATAT

AAATTCTGGCTGGCGTGGAAATATTCTTATTGGTAGAAACAACCTACACCCTGGTCATCAT
CCTGCCTTTCTCTTTATGGTTACAATGATATACACTGTTTGAGATGAGGATAAAAATACTCT
GAGTCCAAACCGGGCCCCTCTGCTAACCATGTTTCATGCCTTCTTCTCTTTCCCTACAGCT
CCTGGGCAACGTGCTGGTTGTTGTGCTGTCTCATCATTTTTGGCAAAGAATCACTCCTC
AGGTGCAGGCTGCCTATCAGAAGGTGGTGGCTGGTGTGGCCAATGCCCTGGCTCACAA
ATACCACTGAGATCTTTTTCCCTCTGCCAAAATTATGGGGACATCATGAAGCCCCTTGA
GCATCTGACTTCTGGCTAATAAAGGAAATTTATTTTCATTGCAATAGTGTGTTGGAATTTT
TTGTGTCTCTCACTCGGAAGGACATATGGGAGGGCAAATCATTTAAAACATCAGAATGA
GTATTTGGTTTAGAGTTTGGCAACATATGCCCATATGCTGGCTGCCATGAACAAAGGTT
GGCTATAAAGAGGTCATCAGTATATGAAACAGCCCCCTGCTGTCCATTCTTATTCCATA
GAAAAGCCTTGACTTGAGGTTAGATTTTTTTTTATATTTTGTGTTATTTTTTTCTTTA
ACATCCCTAAAATTTTCTTACATGTTTTACTAGCCAGATTTTTCTCCTCTCCTGACTAC
TCCCAGTCATAGCTGTCCCTCTTCTCTTATGGAGATCCCTCGACTGCATTAATGAATCGG
CCAACGCGCGGGGAGAGGGCGTTTGCATATTGGGCGCTCTTCCGCTTCTCGCTCACT
GACTCGCTGCGCTCGGTCTCGGCTGCGGCGAGCGGTATCAGCTCACTCAAAGGCG
GTAATACGGTTATCCACAGAATCAGGGGATAACGCAGGAAAGAACATGTGAGCAAAGG
CCAGCAAAGGCCAGGAACCGTAAAAAGGCCGCGTTGCTGGCGTTTTTCCATAGGCTC
CGCCCCCTGACGAGCATCACAAAATCGACGCTCAAGTCAGAGGTGGCGAAACCCGA
CAGGACTATAAAGATACCAGGCGTTTTCCCCTGGAAGCTCCCTCGTGCGCTCTCCTGTT
CCGACCCTGCCGTTACCGGATACCTGTCCGCCTTTCTCCCTTCGGGAAGCGTGGCGC
TTTCTCATAGCTCACGCTGTAGGTATCTCAGTTCGGTGTAGGTCGTTTCGCTCCAAGCTG
GGCTGTGTGCACGAACCCCCGTTTCAGCCCCGACCGCTGCGCCTTATCCGGTAACTATC
GTCTTGAGTCCAACCCGGTAAGACACGACTTATCGCCACTGGCAGCAGCCACTGGTAA
CAGGATTAGCAGAGCGAGGTATGTAGGCGGTGCTACAGAGTTCTTGAAGTGGTGGCCT
AACTACGGCTACACTAGAAGAACAGTATTTGGTATCTGCGCTCTGCTGAAGCCAGTTAC
CTTCGGAAAAAGAGTTGGTAGCTCTTGATCCGGCAAACAAACCACCGCTGGTAGCGGT
GGTTTTTTTTGTTTGAAGCAGCAGATTACGCGCAGAAAAAAGGATCTCAAGAAGATCCT
TTGATCTTTTCTACGGGGTCTGACGCTCAGTGGAACGAAAACCTCACGTTAAGGGATTTT
GGTCATGAGATTATCAAAAAGGATCTTCACCTAGATCCTTTTAAATTAATAAATGAAGTTTT
AAATCAATCTAAAGTATATATGAGTAAACTTGGTCTGACAGTTACCAATGCTTAATCAGTG
AGGCACCTATCTCAGCGATCTGTCTATTTCTGTTTCATCCATAGTTGCCTGACTCCCCGTC
GTGTAGATAACTACGATACGGGAGGGCTTACCATCTGGCCCCAGTGCTGCAATGATACC
GCGAGACCCACGCTCACCGGCTCCAGATTTATCAGCAATAAACCAGCCAGCCGGAAGG
GCCGAGCGCAGAAGTGGTCTGCAACTTTATCCGCCTCCATCCAGTCTATTAATTGTTG
CCGGGAAGCTAGAGTAAGTAGTTCGCCAGTTAATAGTTTGCGCAACGTTGTTGCCATTG
CTACAGGCATCGTGGTGTACGCTCGTCTTTGGTATGGCTTCATTACGCTCCGGTTCC
CAACGATCAAGGCGAGTTACATGATCCCCATGTTGTGCAAAAAAGCGGTTAGCTCCTT
CGGTCTCCGATCGTTGTCAGAAGTAAGTTGGCCGCAGTGTTATCACTCATGGTTATGG
CAGCACTGCATAATTCTCTTACTGTCATGCCATCCGTAAGATGCTTTTCTGTGACTGGTG
AGTACTCAACCAAGTCATTCTGAGAATAGTGTATGCGGGCAGCCGAGTTGCTCTTGCCCG
GCGTCAACACGGGATAATACCGCGCCACATAGCAGAACTTTAAAAGTGCTCATCATTGG
AAAACGTTCTTCGGGGCGAAAACCTCTCAAGGATCTTACCGCTGTTGAGATCCAGTTCTGA
TGTAACCACTCGTGCACCCAACCTGATCTTCAGCATCTTTTACTTTACCAGCGTTTCTG
GGTGAGCAAAAACAGGAAGGCAAAATGCCGCAAAAAAGGGAATAAGGGCGACACGGAA
ATGTTGAATACTCATACTCTTCTTTTTCAATATTATTGAAGCATTTATCAGGGTTATTGTC
TCATGAGCGGATACATATTTGAATGTATTTAGAAAAATAAACAATAGGGGTTCCGCGCA
CATTTCCCCGAAAAGTGCCACCTGACGTCTAAGAAACCATTATTATCATGACATTAACCT
ATAAAAATAGGCGTATCACGAGGCCCTTTCGTCTTCACTCGAGGAGCTTGGCCATTGC
ATACGTTGTATCCATATCATAATATGTACATTTATATTGGCTCATGTCCAACATTACCGCC
ATGTT-3'

7.8.2 DNA Primers for PCR, qPCR and Sequencing

Xist_FW (36 nt, T7 promotor sequence underlined, one additional nucleotide **G** underlined with dotted line)

5'-TAATACGACTCACTATAGGTCCCCGCCATTCCATGC-3'

Xist_FW^{1 d5SICS} (36 nt, T7 promotor sequence underlined, one additional nucleotide **G** underlined with dotted line, **Z=d5SICS**)

5'-TAATACGACTCACTATAGGTCCCCGCCA**Z**TCCATGC-3'

Xist_RV^{1 dNaM} (23 nt, **X=dNaM**)

5'-(OMe-)A(OMe-)T**X**TCCATCCACCAAGCGCCCCG-3'

Xist_RV^{2 dNaM} (23 nt, **X=dNaM**)

5'-(OMe-)A(OMe-)T**X**TCCATCCACCA**X**GCGCCCCG-3'

mCh_FW (39 nt, T7 promotor sequence underlined, two additional nucleotides **GG** underlined with dotted line)

5'-TAATACGACTCACTATAGGGCTCAAGCTTCGAATTCTGC-3'

mCh_RV (24 nt)

5'-ACAAATGTGGTATGGCTGATTATG-3'

mCh_RV^{1 dNaM} (**N=dNaM**) or ***mCh_RV^{1 PM}*** (**N=C**) (24 nt)

5'-ACAAATGTGGTAN**G**GCTGATTATG-3'

mCh_RV^{2 dNaM} (**N=dNaM**) or ***mCh_RV^{2 PM}*** (**N=C**) (24 nt)

5'-ACAAAN**G**TGGTATGGCTGAN**T**ATG-3'

mCh_RV_{UTR 2} (40 nt, alternative 5' end overhang sequence marked with dashed line)

5'- ATAACAAGTTAACAACAACTATGATCTAGAGTCGCGGCC-3'

mCh_RV_{UTR 2}^{1 dNaM} (**N=dNaM**) or ***mCh_RV_{UTR 2}^{1 PM}*** (**N=C**)
(alternative 5' end overhang sequence marked with dashed line, 40 nt)

5'-ATAACAAGTTAACAACAACTATGATC**N**AGAGTCGCGGCC-3'

mCh_RV_{UTR 2}^{2 dNaM} (N=dNaM) or ***mCh_RV_{UTR 2}^{2 PM}*** (N=C)
(alternative 5' end overhang sequence marked with dashed line, 40 nt)
5'- ATAACAAGTTAACAACAACTANGATCTAGAGNCGCGGCC -3'

mCh_qPCR^{internal}_FW (21 nt)
5'-CCCGACTACTTGAAGCTGTCC-3'

mCh_qPCR^{internal}_RV (22 nt)
5'-TCACCTTGTAGATGAACTCGCC-3'

mCh_qPCR^{3'-end}_FW (22 nt)
5'-ATCAAGTTGGACATCACCTCCC-3'

mCh_qPCR^{3'-end}_RV (22 nt)
5'-CGCTTTACTTGTACAGCTCGTC-3'

GAPDH_qPCR_FW (22 nt)
5'-AGCCTCAAGATCATCAGCAATG-3'

GAPDH_qPCR_RV (23 nt)
5'-ATGGACTGTGGTCATGAGTCCTT-3'

β-Actin_qPCR_FW (20 nt)
5'-GGTCATCACCATTGGCAATG-3'

β-Actin_qPCR_RV (23 nt)
5'-CGTCACACTTCATGATGGAGTTG-3'

ext-qPCR_FW (17 nt)
5'-GCGTTTACCCGCCATCC-3'

mCh_ext-qPCR^{internal}_RV (21 nt)
5'-TCACCTTGTAGATGAACTCGC-3'

mCh_ext-qPCR^{3'-end}_RV (22 nt)

5'-CGCTTTACTTGTACAGCTCGTC-3'

GAPDH_ext-qPCR_RV (21 nt)

5'-ATGGACTGTGGTCATGAGTCC-3'

β -Actin_ext-qPCR_RV (23 nt)

5'-CGTCACACTTCATGATGGAGTTG-3'

mCh_Seq (17 nt)

5'-GTGGAACAGTACGAACG-3'

T7_Seq (20 nt)

5'-TAATACGACTCACTATAGGG-3'

7.8.3 DNA Hydrolysis Probes for qPCR

mCh_qPCR^{internal}_probe (23 nt)

5'-HEX-TGACCGTGACCCAGGACTCCTCC-BMN-Q535-3'

mCh_qPCR^{3'-end}_probe (26 nt)

5'-FAM-ACACCATCGTGGAACAGTACGAACGC-BMN-Q535-3'

GAPDH_qPCR_probe (23 nt)

5'-Cyanine 5-CCAACTGCTTAGCACCCCTGGCC-BMN-Q620-3'

β -Actin_qPCR_probe (29 nt)

5'-Cyanine 3.5-ATGGAGTCCTGTGGCATCCACGAAACTAC-BMN-Q590-3'

7.8.4 Adapter and splint sequences for qPCR extension

qPCR_adapter (130 nt)

5'-GCGTTTACCCGCCATCCGCACATGCCACCCTCCAGATATATTCGTCTCGACCAAATCA
CTTGGCAGTCTAGGCGATCGCGATGGCCTGAGTCTAGAGCTCGAGTTCGAAGCTTAAG
ACGTCAGCTGCCAT-3'

mCh_qPCR^{internal}_splint (30 nt)

5'-GCTTCAAGTAGTCGGGATGGCAGCTGACGT-3'

mCh_qPCR^{3'-end}_splint (32 nt)

5'-GGTGATGTCCAACCTTGATATGGCAGCTGACGT-3'

GAPDH_qPCR_splint (31 nt)

5'-CTGATGATCTTGAGGCTATGGCAGCTGACGT-3'

β -Actin_qPCR_splint (30 nt)

5'-GCCAATGGTGATGACCATGGCAGCTGACGT-3'

7.8.5 DNA sequences

Xist_DNA^{2UBP}_5_3 (394 bp, **Y**=dTPT3, **Z**=d5SICS)

5'-TAATACGACTCACTATAGGTCCCCGCCA**Z**TCCATGCCCAACGGGGTTTTGGATACTTA
CCTGCCTTTTCATTCTTTTTTTTTCTTATTATTTTTTTTTCTAAACTTGCCCATCTGGGCTG
TGGATACCTGCTTTTATTCTTTTTTTCTTCTCCTTAGCCCATCGGGGCCATGGATACCTG
CTTTTTGTAIAAAAAAAAAAAAAAAAAACAAAAAAAAACCTTTCTCGGTCCATCGGGACCTCGGA
TACCTGCGTTTAGTCTTTTTTTCCCATGCCCAACGGGGCCTCGGATACCTGCTGTTATTA
TTTTTTTTCTTTTTCTTTTGCCCATCGGGGCTGTGGATACCTGCTTTAAATTTTTTTTTTC
ACGGCCCAACGGGGCGCTTGGTGGATGGAY**AT**-3'

Xist_DNA^{2UBP}_3_3 (394 bp, **Y**=dTPT3)

5'-TAATACGACTCACTATAGGTCCCCGCCATTCCATGCCCAACGGGGTTTTGGATACTTA
CCTGCCTTTTCATTCTTTTTTTTTCTTATTATTTTTTTTTCTAAACTTGCCCATCTGGGCTG
TGGATACCTGCTTTTATTCTTTTTTTCTTCTCCTTAGCCCATCGGGGCCATGGATACCTG
CTTTTTGTAIAAAAAAAAAAAAAAAAAACAAAAAAAAACCTTTCTCGGTCCATCGGGACCTCGGA
TACCTGCGTTTAGTCTTTTTTTCCCATGCCCAACGGGGCCTCGGATACCTGCTGTTATTA
TTTTTTTTCTTTTTCTTTTGCCCATCGGGGCTGTGGATACCTGCTTTAAATTTTTTTTTTC
ACGGCCCAACGGGGCGC**Y**TGGTGGATGGAY**AT**-3'

mCh_DNA^{WT} (834 bp, *mCherry* protein coding region underlined)

5'-TAATACGACTCACTATAGGGCTCAAGCTTCTGAATTCTGCAGTCGACGGTACCGCGGG
 CCCGGGATCCACCGGTGCGCCACCATGGTGAGCAAGGGCGAGGAGGATAACATGGCCA
 TCATCAAGGAGTTCATGCGCTTCAAGGTGCACATGGAGGGCTCCGTGAACGGCCACGA
 GTTCGAGATCGAGGGCGAGGGCGAGGGCCGCCCTACGAGGGCACCCAGACCGCCA
 AGCTGAAGGTGACCAAGGGTGGCCCCCTGCCCTTCGCCTGGGACATCCTGTCCCCTCA
 GTTCATGTACGGCTCCAAGGCCTACGTGAAGCACCCCGCCGACATCCCCGACTACTTG
 AAGCTGTCCTTCCCCGAGGGCTTCAAGTGGGAGCGCGTGATGAACTTCGAGGACGGCG
 GCGTGGTGACCGTGACCCAGGACTCCTCCCTGCAGGACGGCGAGTTCATCTACAAGGT
 GAAGCTGCGCGGCACCAACTTCCCCTCCGACGGCCCCGTAATGCAGAAGAAGACCATG
 GGCTGGGAGGCCTCCTCCGAGCGGATGTACCCCGAGGACGGCGCCCTGAAGGGCGA
 GATCAAGCAGAGGCTGAAGCTGAAGGACGGCGGCCACTACGACGCTGAGGTCAAGAC
 CACCTACAAGGCCAAGAAGCCCGTGCAGCTGCCCGGCGCCTACAACGTCAACATCAAG
 TTGGACATCACCTCCCACAACGAGGACTACACCATCGTGGAACAGTACGAACGCGCCG
 AGGGCCGCCACTCCACCGCGGCATGGACGAGCTGTACAAGTAAAGCGGCCGCGACT
 CTAGATCATAATCAGCCATACCACATTTGT-3'

mCh_DNA^{1UBP} (N=dTPT3) or ***mCh_DNA^{1PM} (N=G)***
 (834 bp, *mCherry* protein coding region underlined)

5'-TAATACGACTCACTATAGGGCTCAAGCTTCTGAATTCTGCAGTCGACGGTACCGCGGG
 CCCGGGATCCACCGGTGCGCCACCATGGTGAGCAAGGGCGAGGAGGATAACATGGCCA
 TCATCAAGGAGTTCATGCGCTTCAAGGTGCACATGGAGGGCTCCGTGAACGGCCACGA
 GTTCGAGATCGAGGGCGAGGGCGAGGGCCGCCCTACGAGGGCACCCAGACCGCCA
 AGCTGAAGGTGACCAAGGGTGGCCCCCTGCCCTTCGCCTGGGACATCCTGTCCCCTCA
 GTTCATGTACGGCTCCAAGGCCTACGTGAAGCACCCCGCCGACATCCCCGACTACTTG
 AAGCTGTCCTTCCCCGAGGGCTTCAAGTGGGAGCGCGTGATGAACTTCGAGGACGGCG
 GCGTGGTGACCGTGACCCAGGACTCCTCCCTGCAGGACGGCGAGTTCATCTACAAGGT
 GAAGCTGCGCGGCACCAACTTCCCCTCCGACGGCCCCGTAATGCAGAAGAAGACCATG
 GGCTGGGAGGCCTCCTCCGAGCGGATGTACCCCGAGGACGGCGCCCTGAAGGGCGA
 GATCAAGCAGAGGCTGAAGCTGAAGGACGGCGGCCACTACGACGCTGAGGTCAAGAC
 CACCTACAAGGCCAAGAAGCCCGTGCAGCTGCCCGGCGCCTACAACGTCAACATCAAG
 TTGGACATCACCTCCCACAACGAGGACTACACCATCGTGGAACAGTACGAACGCGCCG
 AGGGCCGCCACTCCACCGCGGCATGGACGAGCTGTACAAGTAAAGCGGCCGCGACT
 CTAGATCATAATCAGCCNTACCACATTTGT-3'

mCh_DNA^{2UBP} (N=dTPT3) or ***mCh_DNA^{2PM} (N=G)***
 (834 bp, *mCherry* protein coding region underlined)

5'-TAATACGACTCACTATAGGGCTCAAGCTTCTGAATTCTGCAGTCGACGGTACCGCGGG
 CCCGGGATCCACCGGTGCGCCACCATGGTGAGCAAGGGCGAGGAGGATAACATGGCCA
 TCATCAAGGAGTTCATGCGCTTCAAGGTGCACATGGAGGGCTCCGTGAACGGCCACGA
 GTTCGAGATCGAGGGCGAGGGCGAGGGCCGCCCTACGAGGGCACCCAGACCGCCA
 AGCTGAAGGTGACCAAGGGTGGCCCCCTGCCCTTCGCCTGGGACATCCTGTCCCCTCA
 GTTCATGTACGGCTCCAAGGCCTACGTGAAGCACCCCGCCGACATCCCCGACTACTTG
 AAGCTGTCCTTCCCCGAGGGCTTCAAGTGGGAGCGCGTGATGAACTTCGAGGACGGCG
 GCGTGGTGACCGTGACCCAGGACTCCTCCCTGCAGGACGGCGAGTTCATCTACAAGGT
 GAAGCTGCGCGGCACCAACTTCCCCTCCGACGGCCCCGTAATGCAGAAGAAGACCATG
 GGCTGGGAGGCCTCCTCCGAGCGGATGTACCCCGAGGACGGCGCCCTGAAGGGCGA
 GATCAAGCAGAGGCTGAAGCTGAAGGACGGCGGCCACTACGACGCTGAGGTCAAGAC

CACCTACAAGGCCAAGAAGCCCGTGCAGCTGCCCGGCCCTACAACGTCAACATCAAG
 TTGGACATCACCTCCCACAACGAGGACTACACCATCGTGGAACAGTACGAACGCGCCG
 AGGGCCGCCACTCCACCGGCCGGCATGGACGAGCTGTACAAGTAAAGCGGCCGCGACT
 CTAGATCATANTCAGCCTTACCACNTTTGT-3'

mCh_DNA^{WT}_{UTR 2}

(834 bp, mCherry protein coding region underlined)

5'-TAATACGACTCACTATAGGGCTCAAGCTTCTGAATTCTGCAGTCGACGGTACCGCGGG
 CCCGGGATCCACCGGTGCCACCATGGTGAGCAAGGGCGAGGAGGATAACATGGCCA
 TCATCAAGGAGTTCATGCGCTTCAAGGTGCACATGGAGGGCTCCGTGAACGGCCACGA
 GTTCGAGATCGAGGGCGAGGGCGAGGGCCGCCCTACGAGGGCACCCAGACCGCCA
 AGCTGAAGGTGACCAAGGGTGGCCCCCTGCCCTTTCGCCTGGGACATCCTGTCCCCTCA
 GTTCATGTACGGCTCCAAGGCCTACGTGAAGCACCCCGCCGACATCCCCGACTACTTG
 AAGCTGTCCTTCCCCGAGGGCTTCAAGTGGGAGCGCGTGATGAACTTCGAGGACGGCG
 GCGTGGTGACCGTGACCCAGGACTCCTCCCTGCAGGACGGCGAGTTCATCTACAAGGT
 GAAGCTGCGCGGCACCAACTTCCCCTCCGACGGCCCCGTAATGCAGAAGAAGACCATG
 GGCTGGGAGGCCTCCTCCGAGCGGATGTACCCCGAGGACGGCGCCCTGAAGGGCGA
 GATCAAGCAGAGGCTGAAGCTGAAGGACGGCGGCCACTACGACGCTGAGGTCAAGAC
 CACCTACAAGGCCAAGAAGCCCGTGCAGCTGCCCGGCCCTACAACGTCAACATCAAG
 TTGGACATCACCTCCCACAACGAGGACTACACCATCGTGGAACAGTACGAACGCGCCG
 AGGGCCGCCACTCCACCGGCCGGCATGGACGAGCTGTACAAGTAAAGCGGCCGCGACT
 CTAGATCATAGTTGTTGTTAACTTGTAT-3'

***mCh_DNA^{1UBP}_{UTR 2}* (N=dTPT3) or *mCh_DNA^{1PM}_{UTR 2}* (N=G)**

(834 bp, mCherry protein coding region underlined)

5'-TAATACGACTCACTATAGGGCTCAAGCTTCTGAATTCTGCAGTCGACGGTACCGCGGG
 CCCGGGATCCACCGGTGCCACCATGGTGAGCAAGGGCGAGGAGGATAACATGGCCA
 TCATCAAGGAGTTCATGCGCTTCAAGGTGCACATGGAGGGCTCCGTGAACGGCCACGA
 GTTCGAGATCGAGGGCGAGGGCGAGGGCCGCCCTACGAGGGCACCCAGACCGCCA
 AGCTGAAGGTGACCAAGGGTGGCCCCCTGCCCTTTCGCCTGGGACATCCTGTCCCCTCA
 GTTCATGTACGGCTCCAAGGCCTACGTGAAGCACCCCGCCGACATCCCCGACTACTTG
 AAGCTGTCCTTCCCCGAGGGCTTCAAGTGGGAGCGCGTGATGAACTTCGAGGACGGCG
 GCGTGGTGACCGTGACCCAGGACTCCTCCCTGCAGGACGGCGAGTTCATCTACAAGGT
 GAAGCTGCGCGGCACCAACTTCCCCTCCGACGGCCCCGTAATGCAGAAGAAGACCATG
 GGCTGGGAGGCCTCCTCCGAGCGGATGTACCCCGAGGACGGCGCCCTGAAGGGCGA
 GATCAAGCAGAGGCTGAAGCTGAAGGACGGCGGCCACTACGACGCTGAGGTCAAGAC
 CACCTACAAGGCCAAGAAGCCCGTGCAGCTGCCCGGCCCTACAACGTCAACATCAAG
 TTGGACATCACCTCCCACAACGAGGACTACACCATCGTGGAACAGTACGAACGCGCCG
 AGGGCCGCCACTCCACCGGCCGGCATGGACGAGCTGTACAAGTAAAGCGGCCGCGACT
 CTNGATCATAGTTGTTGTTAACTTGTAT-3'

***mCh_DNA^{2UBP}_{UTR 2}* (N=dTPT3) or *mCh_DNA^{2PM}_{UTR 2}* (N=G)**

(834 bp, mCherry protein coding region underlined)

5'-TAATACGACTCACTATAGGGCTCAAGCTTCTGAATTCTGCAGTCGACGGTACCGCGGG
 CCCGGGATCCACCGGTGCCACCATGGTGAGCAAGGGCGAGGAGGATAACATGGCCA
 TCATCAAGGAGTTCATGCGCTTCAAGGTGCACATGGAGGGCTCCGTGAACGGCCACGA
 GTTCGAGATCGAGGGCGAGGGCGAGGGCCGCCCTACGAGGGCACCCAGACCGCCA

AGCTGAAGGTGACCAAGGGTGGCCCCCTGCCCTTCGCCTGGGACATCCTGTCCCCTCA
 GTTCATGTACGGCTCCAAGGCCTACGTGAAGCACCCCGCCGACATCCCCGACTACTTG
 AAGCTGTCCTTCCCCGAGGGCTTCAAGTGGGAGCGCGTGATGAACTTCGAGGACGGCG
 GCGTGGTGACCGTGACCCAGGACTCCTCCCTGCAGGACGGCGAGTTCATCTACAAGGT
 GAAGCTGCGCGGCACCAACTTCCCCTCCGACGGCCCCGTAATGCAGAAGAAGACCATG
 GGCTGGGAGGCCTCCTCCGAGCGGATGTACCCCGAGGACGGCGCCCTGAAGGGCGA
 GATCAAGCAGAGGCTGAAGCTGAAGGACGGCGGCCACTACGACGCTGAGGTCAAGAC
 CACCTACAAGGCCAAGAAGCCCGTGCAGCTGCCCGGCCCTACAACGTCAACATCAAG
 TTGGACATCACCTCCCACAACGAGGACTACACCATCGTGGAACAGTACGAACGCGCCG
 AGGGCCGCCACTCCACCGGCGGCATGGACGAGCTGTACAAGTAAAGCGGCCGCGNCT
 CTAGATCN₁TAGTTGTTGTTAACTTGT₁TAT-3'

mCh_qPCR^{internal} (130 bp)

5'-CCCGACTACTTGAAGCTGTCCTTCCCCGAGGGCTTCAAGTGGGAGCGCGTGATGAA
 CTTGAGGACGGCGGCGTGTTGACCGTGACCCAGGACTCCTCCCTGCAGGACGGCGA
 GTTCATCTACAAGGTGA-3'

mCh_qPCR^{3'-end} (112 bp)

5'-ATCAAGTTGGACATCACCTCCCACAACGAGGACTACACCATCGTGGAACAGTACGAA
 CGCGCCGAGGGCCGCCACTCCACCGGCGGCATGGACGAGCTGTACAAGTAAAGCG-3'

GAPDH_qPCR (111 bp)

5'-AGCCTCAAGATCATCAGCAATGCCTCCTGCACCACCAACTGCTTAGCACCCCTGGCC
 AAGGTCATCCATGACAAC₁TTGGTATCGTGGAAGGACTCATGACCACAGTCCAT-3'

β-Actin_qPCR (122 bp)

5'-GGTCATCACCATTGGCAATGAGCGGTTCCGCTGCCCTGAGGCACTCTTCCAGCCTTC
 CTTCTGGGCATGGAGTCTGTGGCATCCACGAAACTACCTTCAACTCCATCATGAAGT
 GTGACG-3'

mCh_ext-qPCR^{internal} (260 bp)

5'-GCGTTTACCCGCCATCCGCACATGCCACCCTCCAGATATATTCGTCTCGACCAAATCA
 CTTGGCAGTCTAGGCGATCGCGATGGCCTGAGTCTAGAGCTCGAGTTCGAAGCTTAAG
 ACGTCAGCTGCCATCCCGACTACTTGAAGCTGTCCTTCCCCGAGGGCTTCAAGTGGGA
 GCGCGTGATGAACTTCGAGGACGGCGGCGTGTTGACCGTGACCCAGGACTCCTCCCT
 GCAGGACGGCGAGTTCATCTACAAGGTGA-3'

mCh_ext-qPCR^{3'-end} (242 bp)

5'-GCGTTTACCCGCCATCCGCACATGCCACCCTCCAGATATATTCGTCTCGACCAAATCA
 CTTGGCAGTCTAGGCGATCGCGATGGCCTGAGTCTAGAGCTCGAGTTCGAAGCTTAAG
 ACGTCAGCTGCCATATCAAGTTGGACATCACCTCCCACAACGAGGACTACACCATCGTG

GAACAGTACGAACGCGCCGAGGGCCGCCACTCCACCGGCGGCATGGACGAGCTGTAC
AAGTAAAGCG-3'

GAPDH_ext-qPCR (241 bp)

5'-GCGTTTACCCGCCATCCGCACATGCCACCCTCCAGATATATTCGTCTCGACCAAATCA
CTTGGCAGTCTAGGCGATCGCGATGGCCTGAGTCTAGAGCTCGAGTTCGAAGCTTAAG
ACGTCAGCTGCCATAGCCTCAAGATCATCAGCAATGCCTCCTGCACCACCAACTGCTTA
GCACCCCTGGCCAAGGTCATCCATGACAACCTTGGTATCGTGGAAGGACTCATGACCAC
AGTCCAT-3'

β-Actin_ext-qPCR (252 bp)

5'-GCGTTTACCCGCCATCCGCACATGCCACCCTCCAGATATATTCGTCTCGACCAAATCA
CTTGGCAGTCTAGGCGATCGCGATGGCCTGAGTCTAGAGCTCGAGTTCGAAGCTTAAG
ACGTCAGCTGCCATGGTCATCACCATTGGCAATGAGCGGTTCCGCTGCCCTGAGGCAC
TCTTCCAGCCTTCTTCTGGGCATGGAGTCCTGTGGCATCCACGAACTACCTTCAAC
TCCATCATGAAGTGTGACG-3'

7.8.6 RNA sequences

Xist_RNA^{2NO}_5_3 (377 nt, **Y**=rTPT3^{NO})

5'-GGUCCCCGCCAYUCCAUGCCCAACGGGGUUUUGGAUACUUACCUGCCUUUUCAUU
CUUUUUUUUUUCUUUAUUUUUUUUUUUCUAAACUUGCCCAUCUGGGCUGUGGAUACCU
GCUUUUAUUCUUUUUUUCUUCUCCUUAAGCCCAUCGGGGCCAUGGAUACCUGCUUUU
UGUAAAAAAAAAAAAAAAAAAAAACAAAAAACCUUUCUGGUCCAUCGGGACCUCGGAUAC
CUGCGUUUAGUCUUUUUUUCCCAUGCCCAACGGGGCCUCGGAUACCUGCUGUUUU
AUUUUUUUUUUCUUUUUCUUUUUGCCCAUCGGGGCUGUGGAUACCUGCUUUAAAAUUU
UUUUUUCACGGCCCAACGGGGCGCUUGGUGGAUGGAYAU-3'

Xist_RNA^{2NO}_3_3 (377 nt, **Y**=rTPT3^{NO})

5'-GGUCCCCGCCAUUCCAUGCCCAACGGGGUUUUGGAUACUUACCUGCCUUUUCAUU
CUUUUUUUUUUCUUUAUUUUUUUUUUUCUAAACUUGCCCAUCUGGGCUGUGGAUACCU
GCUUUUAUUCUUUUUUUCUUCUCCUUAAGCCCAUCGGGGCCAUGGAUACCUGCUUUU
UGUAAAAAAAAAAAAAAAAAAAAACAAAAAACCUUUCUGGUCCAUCGGGACCUCGGAUAC
CUGCGUUUAGUCUUUUUUUCCCAUGCCCAACGGGGCCUCGGAUACCUGCUGUUUU
AUUUUUUUUUUCUUUUUCUUUUUGCCCAUCGGGGCUGUGGAUACCUGCUUUAAAAUUU
UUUUUUCACGGCCCAACGGGGCGCYUGGUGGAUGGAYAU-3'

mCh_mRNA^{WT} (817 nt, mCherry protein coding region underlined)

5'-ARCA-GGGCUCAAGCUUCGAAUUCUGCAGUCGACGGUACCGCGGGCCCGGGAUCC
ACCGGUCGCCACCAUGGUGAGCAAGGGCGAGGAGGAUAACAUGGCCAUCAUCAAGG
AGUUCAUGCCGCUUCAAGGUGCACAUGGAGGGCUCCGUGAACGGCCACGAGUUCGAG
AUCGAGGGCGAGGGCGAGGGCCGCCCUACGAGGGCACCAGACCGCCAAGCUGAA
GGUGACCAAGGGUGGCCCCUCGCCUUCGCCUGGGACAUCCGUCCCUAGUUCA

UGUACGGCUCCAAGGCCUACGUGAAGCACCCCGCCGACAUCCCCGACUACUUGAAGC
 UGUCCUUCCCCGAGGGCUUCAAGUGGGAGCGCGUGAUGAACUUCGAGGACGGCGGC
 GUGGUGACCGUGACCCAGGACUCCUCCUGCAGGACGGCGAGUUCAUCUACAAGGU
 GAAGCUGCGCGGCACCAACUUCUUCCGACGGCCCCGUAAUGCAGAAGAAGACCAU
 GGGCUGGGAGGCCUCCUCCGAGCGGAUGUACCCCGAGGACGGCGCCCUGAAGGGC
 GAGAUCAAGCAGAGGCUGAAGCUGAAGGACGGCGGCCACUACGACGCUGAGGUCAA
 GACCACCUACAAGGCCAAGAAGCCCUGGCAGCUGCCCCGGCGCCUACAACGUCAACAU
 CAAGUUGGACAUCACCUCCACAACGAGGACUACACCAUCGUGGAACAGUACGAACG
 CGCCGAGGGCCGCCACUCCACCGGCGGCAUGGACGAGCUGUACAAGUAAAGCGGCC
 GCGACUCUAGAUCAUAAUCAGCCAUACCACAUUUGU-poly(A)-3'

***mCh_mRNA*^{1 CP} (N=rTPT3^{CP}) or *mCh_mRNA*^{1 PM} (N=G)**
 (817 nt, mCherry protein coding region underlined)

5'-ARCA-GGGCUCAAGCUUCGAAUUCUGCAGUCGACGGUACCGCGGGCCCGGGAUCC
 ACCGGUCGCCACCAUGGUGAGCAAGGGCGAGGAGGAUAACAUGGCCAUCAUCAAGG
 AGUUCAUGCGCUUCAAGGUGCACAUGGAGGGCUCCGUGAACGGCCACGAGUUCGAG
 AUCGAGGGCGAGGGCGAGGGCCGCCCUACGAGGGCACCCAGACCGCCAAGCUGAA
 GGUGACCAAGGGUGGGCCCCUGCCUUCGCCUGGGACAUCUCCUGUCCCUAGUUCA
 UGUACGGCUCCAAGGCCUACGUGAAGCACCCCGCCGACAUCCCCGACUACUUGAAGC
 UGUCCUUCCCCGAGGGCUUCAAGUGGGAGCGCGUGAUGAACUUCGAGGACGGCGGC
 GUGGUGACCGUGACCCAGGACUCCUCCUGCAGGACGGCGAGUUCAUCUACAAGGU
 GAAGCUGCGCGGCACCAACUUCUUCCGACGGCCCCGUAAUGCAGAAGAAGACCAU
 GGGCUGGGAGGCCUCCUCCGAGCGGAUGUACCCCGAGGACGGCGCCCUGAAGGGC
 GAGAUCAAGCAGAGGCUGAAGCUGAAGGACGGCGGCCACUACGACGCUGAGGUCAA
 GACCACCUACAAGGCCAAGAAGCCCUGGCAGCUGCCCCGGCGCCUACAACGUCAACAU
 CAAGUUGGACAUCACCUCCACAACGAGGACUACACCAUCGUGGAACAGUACGAACG
 CGCCGAGGGCCGCCACUCCACCGGCGGCAUGGACGAGCUGUACAAGUAAAGCGGCC
 GCGACUCUAGAUCAUAAUCAGCCNUACCACAUUUGU-poly(A)-3'

***mCh_mRNA*^{2 CP} (817 nt, N=rTPT3^{CP}) or *mCh_mRNA*^{2 PM} (817 nt, N=G)**
 (817 nt, mCherry protein coding region underlined)

5'-ARCA-GGGCUCAAGCUUCGAAUUCUGCAGUCGACGGUACCGCGGGCCCGGGAUCC
 ACCGGUCGCCACCAUGGUGAGCAAGGGCGAGGAGGAUAACAUGGCCAUCAUCAAGG
 AGUUCAUGCGCUUCAAGGUGCACAUGGAGGGCUCCGUGAACGGCCACGAGUUCGAG
 AUCGAGGGCGAGGGCGAGGGCCGCCCUACGAGGGCACCCAGACCGCCAAGCUGAA
 GGUGACCAAGGGUGGGCCCCUGCCUUCGCCUGGGACAUCUCCUGUCCCUAGUUCA
 UGUACGGCUCCAAGGCCUACGUGAAGCACCCCGCCGACAUCCCCGACUACUUGAAGC
 UGUCCUUCCCCGAGGGCUUCAAGUGGGAGCGCGUGAUGAACUUCGAGGACGGCGGC
 GUGGUGACCGUGACCCAGGACUCCUCCUGCAGGACGGCGAGUUCAUCUACAAGGU
 GAAGCUGCGCGGCACCAACUUCUUCCGACGGCCCCGUAAUGCAGAAGAAGACCAU
 GGGCUGGGAGGCCUCCUCCGAGCGGAUGUACCCCGAGGACGGCGCCCUGAAGGGC
 GAGAUCAAGCAGAGGCUGAAGCUGAAGGACGGCGGCCACUACGACGCUGAGGUCAA
 GACCACCUACAAGGCCAAGAAGCCCUGGCAGCUGCCCCGGCGCCUACAACGUCAACAU
 CAAGUUGGACAUCACCUCCACAACGAGGACUACACCAUCGUGGAACAGUACGAACG
 CGCCGAGGGCCGCCACUCCACCGGCGGCAUGGACGAGCUGUACAAGUAAAGCGGCC
 GCGACUCUAGAUCAUNUACGCCAUACCACNUUUGU-poly(A)-3'

mCh_mRNA^{WT}_{UTR 2} (817 nt, mCherry protein coding region underlined)

5'-ARCA-GGGCUCAAGCUUCGAAUUCUGCAGUCGACGGUACCGCGGGCCCGGGAUCC
 ACCGGUCGCCACCAUGGUGAGCAAGGGCGAGGAGGAUAACAUGGCCAUCAUCAAGG
 AGUUCAUGCGCUUCAAGGUGCACAUGGAGGGCUCCGUGAACGGCCACGAGUUCGAG
 AUCGAGGGCGAGGGCGAGGGCCGCCCUACGAGGGCACCCAGACCGCCAAGCUGAA
 GGUGACCAAGGGUGGGCCCCUGCCCUUCGCCUGGGACAUCCUGUCCCCUCAGUUCA
 UGUACGGCUCCAAGGCCUACGUGAAGCACCCCGCCGACAUCCCGACUACUUGAAGC
 UGUCCUUCCCCGAGGGCUUCAAGUGGGAGCGCGUGAUGAACUUCGAGGACGGCGGC
 GUGGUGACCGUGACCCAGGACUCCUCCUUGCAGGACGGCGAGUUCAUCUACAAGGU
 GAAGCUGCGCGGCACCAACUUCUCCUCCGACGGCCCCGUAAUGCAGAAGAAGACCAU
 GGGCUGGGAGGCCUCCUCCGAGCGGAUGUACCCCGAGGACGGCGCCUGAAGGGC
 GAGAUCAAGCAGAGGCUGAAGCUGAAGGACGGCGGCCACUACGACGCUGAGGUCAA
 GACCACCUACAAGGCCAAGAAGCCCGUGCAGCUGCCCGGCCUACAACGUCAACAU
 CAAGUUGGACAUCACCUCCACAACGAGGACUACACCAUCGUGGAACAGUACGAACG
 CGCCGAGGGCCGCCACUCCACCGGCGGCAUGGACGAGCUGUACAAGUAAAGCGGCC
 GCGACUCUAGAUCAUAGUUGUUGUUAACUUGUUUAU-poly(A)-3'

mCh_mRNA^{1 CP}_{UTR 2} (N=rTPT3^{CP}) or *mCh_mRNA*^{1 PM}_{UTR 2} (N=G)
 (817 nt, mCherry protein coding region underlined)

5'-ARCA-GGGCUCAAGCUUCGAAUUCUGCAGUCGACGGUACCGCGGGCCCGGGAUCC
 ACCGGUCGCCACCAUGGUGAGCAAGGGCGAGGAGGAUAACAUGGCCAUCAUCAAGG
 AGUUCAUGCGCUUCAAGGUGCACAUGGAGGGCUCCGUGAACGGCCACGAGUUCGAG
 AUCGAGGGCGAGGGCGAGGGCCGCCCUACGAGGGCACCCAGACCGCCAAGCUGAA
 GGUGACCAAGGGUGGGCCCCUGCCCUUCGCCUGGGACAUCCUGUCCCCUCAGUUCA
 UGUACGGCUCCAAGGCCUACGUGAAGCACCCCGCCGACAUCCCGACUACUUGAAGC
 UGUCCUUCCCCGAGGGCUUCAAGUGGGAGCGCGUGAUGAACUUCGAGGACGGCGGC
 GUGGUGACCGUGACCCAGGACUCCUCCUUGCAGGACGGCGAGUUCAUCUACAAGGU
 GAAGCUGCGCGGCACCAACUUCUCCUCCGACGGCCCCGUAAUGCAGAAGAAGACCAU
 GGGCUGGGAGGCCUCCUCCGAGCGGAUGUACCCCGAGGACGGCGCCUGAAGGGC
 GAGAUCAAGCAGAGGCUGAAGCUGAAGGACGGCGGCCACUACGACGCUGAGGUCAA
 GACCACCUACAAGGCCAAGAAGCCCGUGCAGCUGCCCGGCCUACAACGUCAACAU
 CAAGUUGGACAUCACCUCCACAACGAGGACUACACCAUCGUGGAACAGUACGAACG
 CGCCGAGGGCCGCCACUCCACCGGCGGCAUGGACGAGCUGUACAAGUAAAGCGGCC
 GCGACUCUNGAUCAUAGUUGUUGUUAACUUGUUUAU-poly(A)-3'

mCh_mRNA^{2 CP}_{UTR 2} (N=rTPT3^{CP}) or *mCh_mRNA*^{2 PM}_{UTR 2} (N=G)
 (817 nt, mCherry protein coding region underlined)

5'-ARCA-GGGCUCAAGCUUCGAAUUCUGCAGUCGACGGUACCGCGGGCCCGGGAUCC
 ACCGGUCGCCACCAUGGUGAGCAAGGGCGAGGAGGAUAACAUGGCCAUCAUCAAGG
 AGUUCAUGCGCUUCAAGGUGCACAUGGAGGGCUCCGUGAACGGCCACGAGUUCGAG
 AUCGAGGGCGAGGGCGAGGGCCGCCCUACGAGGGCACCCAGACCGCCAAGCUGAA
 GGUGACCAAGGGUGGGCCCCUGCCCUUCGCCUGGGACAUCCUGUCCCCUCAGUUCA
 UGUACGGCUCCAAGGCCUACGUGAAGCACCCCGCCGACAUCCCGACUACUUGAAGC
 UGUCCUUCCCCGAGGGCUUCAAGUGGGAGCGCGUGAUGAACUUCGAGGACGGCGGC
 GUGGUGACCGUGACCCAGGACUCCUCCUUGCAGGACGGCGAGUUCAUCUACAAGGU
 GAAGCUGCGCGGCACCAACUUCUCCUCCGACGGCCCCGUAAUGCAGAAGAAGACCAU
 GGGCUGGGAGGCCUCCUCCGAGCGGAUGUACCCCGAGGACGGCGCCUGAAGGGC

GAGAUCAAGCAGAGGCUGAAGCUGAAGGACGGCGGCCACUACGACGCUGAGGUCAA
GACCACCUACAAGGCCAAGAAGCCCGUGCAGCUGCCCGGCCUACAACGUCAACAU
CAAGUUGGACAUCACCUCCCACAACGAGGACUACACCAUCGUGGAACAGUACGAACG
CGCCGAGGGCCGCCACUCCACCGGCGGCAUGGACGAGCUGUACAAGUAAAGCGGCC
GCGNCUCUAGAUCNUAGUUGUUGUUAACUUGUUUUAU-poly(A)-3'

7.9 List of abbreviations

Abbreviation	Full word(s)
°C	°Celsius
1mA	<i>N1</i> -Methyladenosine
1mΨ	<i>N1</i> -methylpseudouridine
3mC	3-Methylcytidine
4acC	<i>N4</i> -Acetylcytidine
5hmC	5-Hydroxymethylcytidine
5mC	5-Methylcytidine
5mC	5-Methylcytidine
5mU	5-methyluridine
6fA	<i>N6</i> -Formyl-adenosine
6hmA	<i>N6</i> -Hydroxymethyladenosine
6mA	<i>N6</i> -Methyl-adenosine
7mG	7-Methyl-guanosine
A	Adenine
A ₂₆₀	Absorption at 260 nm wavelength
AA	Amino acid
Ac	Acetate
AEGIS	artificially expanded genetic information system
AEGIS-LIVE	AEGIS laboratory <i>in vitro</i> evolution
ARCA	Anti-reverse cap analog
AU	Airy unit
BPB	Bromphenol blue
BSA	Bovine serum albumin
C	Cytosine
CAR	Chimeric antigen receptor
Cas9	CRISPR associated protein 9
cDNA	Complementary DNA
CEP	Cyanoethyl phosphoramidite
circRNA	Circular RNA
conc.	Concentration
CP	Cyclopropene
CRISPR	Clustered regularly interspaced short palindromic repeats
C _t	Threshold cycle
CuAAC	Copper-catalyzed Alkyne-Azide cycloaddition
cw-EPR	Continuous wave EPR
DAPI	4',6-Diamidino-2-phenylindole
DC	Dendritic cell
ddH ₂ O	Ultrapure water
DMEM	Dulbecco's modified eagle medium
DNA	Deoxyribonucleic acid
DOPE	Dioleoylphosphatidylethanolamine
DPBS	Dulbecco's phosphate buffered saline
dsDNA	Double-stranded DNA
dsRNA	Double-stranded RNA
DTT	Dithiothreitol
<i>e.g.</i>	<i>exempli gratia</i>
EDTA	Ethylenediaminetetraacetic acid
EPR	Electron paramagnetic resonance
EtBr	Ethidium bromide
EtOH	Ethanol
FCS	Foetal calf serum

G	Guanine
g	g Force
GAPDH	<i>Glycerinaldehyd-3-phosphat-dehydrogenase</i>
GENAEXT	Genetic alphabet expansion transcription
gRNA	Guide RNA
h	Hour
HPLC	High-performance liquid chromatography
<i>i.e.</i>	<i>id est</i>
iEDDA	Inverse electron-demand Diels-Alder cycloaddition
iPP	Inorganic pyrophosphatase
isoC	Isocytosine
isoG	Isoguanine
IVT	In vitro transcription
L	Liter
LiCl	Lithium chloride
lncRNA	Long non-coding RNA
LNP	Lipid nanoparticle
<i>mCh_mRNA</i>	<i>mCherry</i> protein encoding mRNA
MD	Molecular dynamics
MEM	Minimum essential medium
min	Minute
miRNA	MicroRNA
mRNA	Messenger RNA
MT	Metabolism
n.a.	Not available
ncAA	Non-canonical amino acids
ncRNA	Non-coding RNA
NEAA	Non-essential amino acids
N-N	Inter-nitroxide
NO	Nnitroxide
NRT	No-reverse-transcriptase-control
NTC	No-template-control
NTP	Nucleoside triphosphates
o/n	Overnight
PA	Propargyl amine
PC	Phosphatidylcholine
PCR	Polymerase chain reaction
PEG	Polyethylene glycol
PELDOR	Pulsed electron-electron double resonance
PKR	RNA-dependent protein kinase
PM	Point mutation
PMSF	Phenylmethylsulfonylfluoride
PP	Polypropylen
pre-mRNA	Precursor mRNA
PS	Polystyrene
qPCR	Quantitative PCR
RBP	RNA-binding protein
RIG-I	Retinoic acid inducible gene I
RISC	RNA-induced silencing complex
RNA	Ribonucleic acid
RNAi	RNA interference
RNP	Ribonucleoprotein
rpm	Revolutions per minute
rRNA	Ribosomal RNA
rt	Room temperature
RT	Reverse transcription

RT-qPCR	Reverse transcription coupled with quantitative PCR
s	Second
s.d.	Standard deviation
SAR	Structure-activity relationship
saRNA	Self-amplifying RNA
SDS	Sodium dodecyl sulfate
SDSL	Site-directed spin labeling
SELEX	Systematic Evolution of Ligands by Exponential Enrichment
siRNA	Small interfering RNA
snRNA	Small nuclear RNA
SPAAC	Strain-promoted azide-alkyne cycloadditions
SSO	Semi-synthetic organism
T	Thymine
TBE	Tris-Borate EDTA
TC	Tissue culture
TET-FL	Tetrazine-conjugated AF 488 fluorophore
TLR	Toll-like receptor
TP	Triphosphate
tRNA	Transfer RNA
U	Uracil
U	Enzyme unit
UB	Unnatural base
UBP	Unnatural base pair
UTR	Untranslated region
WT	Wild type
XC	Xylene cyanol
Xist	X inactive specific transcript
λ_{em}	Emission wavelength
λ_{ex}	Excitation wavelength
Ψ	Pseudouridine

7.10 List of tables

Table 1. 3'-UTR sequences of different mCh_mRNA sequence constructs.	34
Table 2. Calculated protein/ mRNA ratios for selected mCh_mRNA sequence variants as analyzed by RT-qPCR using the 3'-end primer/probe set at 48 h after transfection start and mCherry protein fluorescence quantification.	52
Table 3. Software applications used in this study.	75
Table 4. Databases used in this study.	75
Table 5. Equipment used in this study.	75
Table 6. Consumables used in this study.	77
Table 7. Reagents used in this study.	78
Table 8. Solutions used in this study.	79
Table 9. Buffers used in this study.	79
Table 10. Media used in this study.	80
Table 11. Enzymes used in this study.	80
Table 12. Plasmids used in this study.	81
Table 13. Kits used in this study.	81
Table 14. Organism used in this study.	82
Table 15. Pipetting scheme for diagnostic restriction digest.	86
Table 16. Primer combinations for different mCh_DNA and mCh_DNA _{UTR2} sequences.	92
Table 17. Pipetting scheme for mCh_DNA PCR reaction mixes.	92
Table 18. PCR cycling conditions for different mCh_DNA and mCh_DNA _{UTR2} sequences. ..	93
Table 19. PCR cycling conditions for mCh_DNA _{UTR2} UBP 1 and mCh_DNA _{UTR2} UBP 2.	93
Table 20. Primer combinations for different Xist_DNA sequences.	94
Table 21. Pipetting scheme for Xist_DNA PCR reaction mixes.	94
Table 22. PCR cycling conditions for different Xist_DNA sequences.	95
Table 23. Pipetting scheme for capped mCh_RNA IVT reaction mixes.	96
Table 24. Pipetting scheme for poly(A) tailing reactions.	96
Table 25. Pipetting scheme for Xist_RNA IVT reaction mixes.	97
Table 26. Pipetting scheme for DNase I digestion reaction mixes.	97
Table 27. Exemplary pipetting scheme for mCh_mRNA in vitro click labeling.	98
Table 28. Overview of cell numbers and corresponding amounts to prepare mRNA-lipid complexes for cell transfection.	100
Table 29. Pipetting scheme for RT reaction mixes or NRT controls.	104
Table 30. Thermal program for RT reactions.	104
Table 31. Pipetting scheme for qPCR reaction mixes.	105
Table 32. PCR cycling conditions for qPCR analysis.	105

Table 33. Pipetting scheme for PCR amplification of qPCR products.	106
Table 34. PCR cycling conditions for PCR amplification of qPCR products.	107
Table 35. General pipetting scheme for T4 PNK phosphorylation reactions.	107
Table 36. Incubation steps for T4 PNK phosphorylation reactions.	108
Table 37. General pipetting scheme for splinted ligation reactions.	108
Table 38. Incubation steps for T4 DNA ligase splinted ligation reaction.	109
Table 39. General pipetting scheme for PCR amplification of extended qPCR products.	109
Table 40. PCR cycling conditions for PCR amplification of extended qPCR products.	110
Table 41. Pipetting scheme for BigDye Terminator v3.1 Cycle Sequencing reaction mixes.	110
Table 42. Cycling conditions for BigDye Terminator v3.1 Cycle Sequencing reaction mixes.	111
Table 43. Raw fluorescence values measured from cells transfected with mCh_mRNA or mCh_mRNA _{UTR2} variants and control values from exp. #1.	163
Table 44. mCherry protein standard curve values and calculated parameters from mCh_mRNA or mCh_mRNA _{UTR2} exp. #1.	164
Table 45. Raw fluorescence values measured from cells transfected with mCh_mRNA or mCh_mRNA _{UTR2} variants and control values from exp. #2.	164
Table 46. mCherry protein standard curve values and calculated parameters from mCh_mRNA or mCh_mRNA _{UTR2} exp. #2.	164
Table 47. Raw fluorescence values measured from cells transfected with mCh_mRNA or mCh_mRNA _{UTR2} variants and control values from exp. #3.	165
Table 48. mCherry protein standard curve values and calculated parameters from mCh_mRNA or mCh_mRNA _{UTR2} exp. #3.	165
Table 49. Raw fluorescence values measured from cells transfected with mCh_mRNA or mCh_mRNA _{UTR2} variants and control values from exp. #4.	165
Table 50. mCherry protein standard curve values and calculated parameters from mCh_mRNA or mCh_mRNA _{UTR2} exp. #4.	165
Table 51. Raw fluorescence values measured from cells transfected with mCh_mRNA or mCh_mRNA _{UTR2} variants and control values from exp. #5.	166
Table 52. mCherry protein standard curve values and calculated parameters from mCh_mRNA or mCh_mRNA _{UTR2} exp. #5.	166
Table 53. Raw fluorescence values measured from cells transfected with mCh_mRNA or mCh_mRNA _{UTR2} variants and control values from exp. #6.	166
Table 54. mCherry protein standard curve values and calculated parameters from mCh_mRNA or mCh_mRNA _{UTR2} exp. #6.	167

Table 55. Raw fluorescence values measured from cells transfected with mCh_mRNA or mCh_mRNA _{UTR 2} variants and control values from exp. #7.	167
Table 56. mCherry protein standard curve values and calculated parameters from mCh_mRNA or mCh_mRNA _{UTR 2} exp. #7.	167
Table 57. Raw fluorescence values measured from cells transfected with mCh_mRNA or mCh_mRNA _{UTR 2} variants and control values from exp. #8.	168
Table 58. mCherry protein standard curve values and calculated parameters from mCh_mRNA or mCh_mRNA _{UTR 2} exp. #8.	168
Table 59. Raw fluorescence values measured from cells transfected with mCh_mRNA or mCh_mRNA _{UTR 2} variants and control values from exp. #9.	168
Table 60. mCherry protein standard curve values and calculated parameters from mCh_mRNA or mCh_mRNA _{UTR 2} exp. #9.	168
Table 61. Raw fluorescence values measured from cells transfected with mCh_mRNA or mCh_mRNA _{UTR 2} variants and control values from exp. #10.	169
Table 62. mCherry protein standard curve values and calculated parameters from exp. mCh_mRNA or mCh_mRNA _{UTR 2} exp. #10.	169
Table 63. Raw fluorescence values measured from cells transfected with mCh_mRNA variants with or without natural base modifications and control values from exp. #1.	170
Table 64. mCherry protein standard curve values and calculated parameters from exp. mCh_mRNA variants with or without natural base modifications exp. #1.	170
Table 65. Raw fluorescence values measured from cells transfected with mCh_mRNA variants with or without natural base modifications and control values from exp. #2.	170
Table 66. mCherry protein standard curve values and calculated parameters from exp. mCh_mRNA variants with or without natural base modifications exp. #2.	171
Table 67. Raw fluorescence values measured from cells transfected with mCh_mRNA variants with or without natural base modifications and control values from exp. #3.	171
Table 68. mCherry protein standard curve values and calculated parameters from exp. mCh_mRNA variants with or without natural base modifications exp. #3.	171
Table 69. Raw fluorescence values measured from cells transfected with mCh_mRNA variants with or without natural base modifications and control values from exp. #4.	172
Table 70. mCherry protein standard curve values and calculated parameters from exp. mCh_mRNA variants with or without natural base modifications exp. #4.	172
Table 71. Raw fluorescence values measured from cells transfected with mCh_mRNA variants with or without natural base modifications and control values from exp. #5.	172
Table 72. mCherry protein standard curve values and calculated parameters from exp. mCh_mRNA variants with or without natural base modifications exp. #5.	173

Table 73. Raw fluorescence values measured from cells transfected with mCh_mRNA variants with or without natural base modifications and control values from exp. #6.....	173
Table 74. mCherry protein standard curve values and calculated parameters from exp. mCh_mRNA variants with or without natural base modifications exp. #6.....	173
Table 75. Raw fluorescence values measured from cells transfected with mCh_mRNA variants with or without natural base modifications and control values from exp. #7.....	174
Table 76. mCherry protein standard curve values and calculated parameters from exp. mCh_mRNA variants with or without natural base modifications exp. #7.....	174
Table 77. Raw fluorescence values measured from cells transfected with mCh_mRNA variants with or without natural base modifications and control values from exp. #8.....	174
Table 78. mCherry protein standard curve values and calculated parameters from exp. mCh_mRNA variants with or without natural base modifications exp. #8.....	175
Table 79. Raw fluorescence values measured from cells transfected with mCh_mRNA variants with or without natural base modifications and control values from exp. #9.....	175
Table 80. mCherry protein standard curve values and calculated parameters from exp. mCh_mRNA variants with or without natural base modifications exp. #9.....	175
Table 81. Raw fluorescence values measured from cells transfected with mCh_mRNA variants with or without natural base modifications and control values from exp. #10.....	176
Table 82. mCherry protein standard curve values and calculated parameters from exp. mCh_mRNA variants with or without natural base modifications exp. #10.....	176
Table 83. Mean values [ng mCherry protein/well] and standard deviation of duplicate samples, background subtracted and divided by slope of linear standard curve for mCh_mRNA or mCh_mRNA _{UTR 2} variants and controls from exp. #1.....	176
Table 84. Mean values [ng mCherry protein/well] and standard deviation of duplicate samples, background subtracted and divided by slope of linear standard curve for mCh_mRNA or mCh_mRNA _{UTR 2} variants and controls from exp. #2.....	177
Table 85. Mean values [ng mCherry protein/well] and standard deviation of duplicate samples, background subtracted and divided by slope of linear standard curve for mCh_mRNA or mCh_mRNA _{UTR 2} variants and controls from exp. #3.....	177
Table 86. Mean values [ng mCherry protein/well] and standard deviation of duplicate samples, background subtracted and divided by slope of linear standard curve for mCh_mRNA or mCh_mRNA _{UTR 2} variants and controls from exp. #4.....	178
Table 87. Mean values [ng mCherry protein/well] and standard deviation of duplicate samples, background subtracted and divided by slope of linear standard curve for mCh_mRNA or mCh_mRNA _{UTR 2} variants and controls from exp. #5.....	178

Table 88. Mean values [ng mCherry protein/well] and standard deviation of duplicate samples, background subtracted and divided by slope of linear standard curve for mCh_mRNA or mCh_mRNA _{UTR 2} variants and controls from exp. #6.....	179
Table 89. Mean values [ng mCherry protein/well] and standard deviation of duplicate samples, background subtracted and divided by slope of linear standard curve for mCh_mRNA or mCh_mRNA _{UTR 2} variants and controls from exp. #7.....	179
Table 90. Mean values [ng mCherry protein/well] and standard deviation of duplicate samples, background subtracted and divided by slope of linear standard curve for mCh_mRNA or mCh_mRNA _{UTR 2} variants and controls from exp. #8.....	180
Table 91. Mean values [ng mCherry protein/well] and standard deviation of duplicate samples, background subtracted and divided by slope of linear standard curve for mCh_mRNA or mCh_mRNA _{UTR 2} variants and controls from exp. #9.....	180
Table 92. Mean values [ng mCherry protein/well] and standard deviation of duplicate samples, background subtracted and divided by slope of linear standard curve for mCh_mRNA or mCh_mRNA _{UTR 2} variants and controls from exp. #10.....	181
Table 93. Mean values [ng mCherry protein/well] and standard deviation of duplicate samples, background subtracted and divided by slope of linear standard curve for mCh_mRNA with or without natural base modifications and controls from exp. #1.....	181
Table 94. Mean values [ng mCherry protein/well] and standard deviation of duplicate samples, background subtracted and divided by slope of linear standard curve for mCh_mRNA with or without natural base modifications and controls from exp. #2.....	182
Table 95. Mean values [ng mCherry protein/well] and standard deviation of duplicate samples, background subtracted and divided by slope of linear standard curve for mCh_mRNA with or without natural base modifications and controls from exp. #3.....	182
Table 96. Mean values [ng mCherry protein/well] and standard deviation of duplicate samples, background subtracted and divided by slope of linear standard curve for mCh_mRNA with or without natural base modifications and controls from exp. #4.....	183
Table 97. Mean values [ng mCherry protein/well] and standard deviation of duplicate samples, background subtracted and divided by slope of linear standard curve for mCh_mRNA with or without natural base modifications and controls from exp. #5.....	183
Table 98. Mean values [ng mCherry protein/well] and standard deviation of duplicate samples, background subtracted and divided by slope of linear standard curve for mCh_mRNA with or without natural base modifications and controls from exp. #6.....	184
Table 99. Mean values [ng mCherry protein/well] and standard deviation of duplicate samples, background subtracted and divided by slope of linear standard curve for mCh_mRNA with or without natural base modifications and controls from exp. #7.....	184

Table 100. Mean values [ng mCherry protein/well] and standard deviation of duplicate samples, background subtracted and divided by slope of linear standard curve for mCh_mRNA with or without natural base modifications and controls from exp. #8.	185
Table 101. Mean values [ng mCherry protein/well] and standard deviation of duplicate samples, background subtracted and divided by slope of linear standard curve for mCh_mRNA with or without natural base modifications and controls from exp. #9.	185
Table 102. Mean values [ng mCherry protein/well] and standard deviation of duplicate samples, background subtracted and divided by slope of linear standard curve for mCh_mRNA with or without natural base modifications and controls from exp. #10.	186
Table 103. Merged data from both data sets, mCh_mRNA with or without natural base modifications or mCh_mRNA _{UTR 2}	186
Table 104. Merged data from both data sets, mCh_mRNA with or without natural base modifications or mCh_mRNA _{UTR 2} , normalized to mCh_mRNA ^{WT}	187
Table 105. Ratios of mCherry protein expression from mCh_mRNA ^{WT, Ψ+5mC} / mCh_mRNA ^{WT} or mCh_mRNA ^{2 CP, Ψ+5mC} / mCh_mRNA ^{WT}	187
Table 106. Ct values of mCh_qPCR ^{3'-end} singleplex qPCR analysis.	189
Table 107. Ct values of mCh_qPCR ^{3'-end} multiplex qPCR analysis together with β-Actin_qPCR and GAPDH_qPCR.	189
Table 108. Ct values of mCh_qPCR ^{3'-end} multiplex qPCR analysis together with mCh_qPCR ^{internal} , β-Actin_qPCR and GAPDH_qPCR.	189
Table 109. Ct values of mCh_qPCR ^{internal} singleplex qPCR analysis.	190
Table 110. Ct values of mCh_qPCR ^{internal} multiplex qPCR analysis together with β-Actin_qPCR and GAPDH_qPCR.	190
Table 111. Ct values of mCh_qPCR ^{internal} multiplex qPCR analysis together with mCh_qPCR ^{3'-end} , β-Actin_qPCR and GAPDH_qPCR.	190
Table 112. Ct values of β-Actin singleplex qPCR analysis.	191
Table 113. Ct values of β-Actin multiplex qPCR analysis together with mCh_qPCR ^{3'-end} , mCh_qPCR ^{internal} and GAPDH_qPCR.	191
Table 114. Ct values of GAPDH singleplex qPCR analysis.	191
Table 115. Ct values of GAPDH multiplex qPCR analysis together with mCh_qPCR ^{3'-end} , mCh_qPCR ^{internal} and β-Actin_qPCR.	192
Table 116. C _t values of mCh_mRNA + mCh_mRNA _{UTR2} data set 1, cell lysis 6 h post transfection.	195
Table 117. ΔC _t = C _t (mCh) – C _t (GAPDH) values of mCh_mRNA + mCh_mRNA _{UTR2} data set 1, cell lysis 6 h post transfection.	195
Table 118. Ct values of mCh_mRNA + mCh_mRNA _{UTR2} data set 1, cell lysis 24 h post transfection.	198

Table 119. $\Delta Ct = Ct(mCh) - Ct(GAPDH)$ values of mCh_mRNA + mCh_mRNA _{UTR2} data set 1, cell lysis 24 h post transfection.	198
Table 120. Ct values of mCh_mRNA + mCh_mRNA _{UTR2} data set 1, cell lysis 48 h post transfection.	201
Table 121. $\Delta Ct = Ct(mCh) - Ct(GAPDH)$ values of mCh_mRNA + mCh_mRNA _{UTR2} data set 1, cell lysis 48 h post transfection.	201
Table 122. Ct values of mCh_mRNA + mCh_mRNA _{UTR2} data set 2, cell lysis 6 h post transfection.	204
Table 123. $\Delta Ct = Ct(mCh) - Ct(GAPDH)$ values of mCh_mRNA + mCh_mRNA _{UTR2} data set 2, cell lysis 6 h post transfection.	204
Table 124. Ct values of mCh_mRNA + mCh_mRNA _{UTR2} data set 2, cell lysis 24 h post transfection.	207
Table 125. $\Delta Ct = Ct(mCh) - Ct(GAPDH)$ values of mCh_mRNA + mCh_mRNA _{UTR2} data set 2, cell lysis 24 h post transfection.	208
Table 126. Ct values of mCh_mRNA + mCh_mRNA _{UTR2} data set 2, cell lysis 48 h post transfection.	211
Table 127. $\Delta Ct = Ct(mCh) - Ct(GAPDH)$ values of mCh_mRNA + mCh_mRNA _{UTR2} data set 2, cell lysis 48 h post transfection.	211
Table 128. Ct values of mCh_mRNA + mCh_mRNA ^{$\Psi+5mC$} data set 1, cell lysis 6 h post transfection.	213
Table 129. $\Delta Ct = Ct(mCh) - Ct(GAPDH)$ values of mCh_mRNA + mCh_mRNA ^{$\Psi+5mC$} data set 1, cell lysis 6 h post transfection.	213
Table 130. Ct values of mCh_mRNA + mCh_mRNA ^{$\Psi+5mC$} data set 1, cell lysis 24 h post transfection.	215
Table 131. $\Delta Ct = Ct(mCh) - Ct(GAPDH)$ values of mCh_mRNA + mCh_mRNA ^{$\Psi+5mC$} data set 1, cell lysis 24 h post transfection.	215
Table 132. Ct values mCh_mRNA + mCh_mRNA ^{$\Psi+5mC$} data set 1, cell lysis 48 h post transfection.	217
Table 133. $\Delta Ct = Ct(mCh) - Ct(GAPDH)$ values mCh_mRNA + mCh_mRNA ^{$\Psi+5mC$} data set 1, cell lysis 48 h post transfection.	217
Table 134. Ct values of mCh_mRNA + mCh_mRNA ^{$\Psi+5mC$} data set 2, cell lysis 6 h post transfection.	219
Table 135. $\Delta Ct = Ct(mCh) - Ct(GAPDH)$ values of mCh_mRNA + mCh_mRNA ^{$\Psi+5mC$} data set 2, cell lysis 6 h post transfection.	220
Table 136. Ct values mCh_mRNA + mCh_mRNA ^{$\Psi+5mC$} data set 2, cell lysis 24 h post transfection.	222

Table 137. $\Delta Ct = Ct(mCh) - Ct(GAPDH)$ values mCh_mRNA + mCh_mRNA ^{$\Psi+5mC$} data set 2, cell lysis 24 h post transfection.	222
Table 138. Ct values of mCh_mRNA + mCh_mRNA ^{$\Psi+5mC$} data set 2, cell lysis 48 h post transfection.	224
Table 139. $\Delta Ct = Ct(mCh) - Ct(GAPDH)$ values of mCh_mRNA + mCh_mRNA ^{$\Psi+5mC$} data set 2, cell lysis 48 h post transfection.	224
Table 140. Averaged ΔCt values of mCh_mRNA 3' end primer + probe set.	224
Table 141. Averaged ΔCt values of mCh_mRNA internal primer + probe set.	225
Table 142. $\Delta\Delta Ct = \Delta Ct(mCh_mRNA \text{ modified, any time}) - \Delta Ct(mCh_mRNA^{WT}, 6h)$ values of mCh_mRNA 3' end primer + probe set.	225
Table 143. $\Delta\Delta Ct = \Delta Ct(mCh_mRNA \text{ modified, any time}) - \Delta Ct(mCh_mRNA^{WT}, 6h)$ values of mCh_mRNA internal primer + probe set.	226
Table 144. Fold change $2^{-\Delta\Delta Ct}$ values of mCh_mRNA 3' end primer + probe set.	226
Table 145. Fold change $2^{-\Delta\Delta Ct}$ values of mCh_mRNA internal primer + probe set.	227
Table 146. Fold change ratios of mCh_mRNA ^{$WT, \Psi+5mC$} / mCh_mRNA ^{WT} and mCh_mRNA ^{$2CP, \Psi+5mC$} / mCh_mRNA ^{WT} , 3'-end data set.	227
Table 147. Fold change ratios of mCh_mRNA ^{$WT, \Psi+5mC$} / mCh_mRNA ^{WT} and mCh_mRNA ^{$2CP, \Psi+5mC$} / mCh_mRNA ^{WT} , internal data set.	227
Table 148. Raw luminescence values (RLU) measured from cells transfected with mCh_mRNA variants and control values.	228
Table 149. Background subtracted mean values of luminescence (RLU).	228
Table 150. Standard deviation values of luminescence (RLU).	228
Table 151. Raw luminescence values (RLU) for assay linearity validation.	229
Table 152. Background subtracted mean values of luminescence (RFU) for assay linearity validation.	229
Table 153. Standard deviation values of luminescence (RFU) for assay linearity validation.	229

7.11 List of figures

Figure 1. Genetic information flow according to the central dogma of molecular biology.	1
Figure 2. Extended view on the genetic information flow including catalytic and regulatory RNAs.....	2
Figure 3. Schematic illustration of a DNA or RNA oligonucleotide strand (on the left) and the formation of a double strand via base pairing (on the right).	3
Figure 4. Artificial base pairs to expand the genetic alphabet.	5
Figure 5. Functionalized unnatural bases for site-specific labeling.....	8
Figure 6. Structural features of mRNA.	9
Figure 7. mRNA cap structures.	10
Figure 8. Structural mRNA features and their effects on mRNA translation and stability.....	11
Figure 9. Modified natural nucleobases found in mRNA.	12
Figure 10. Nucleobase modifications and their effects on mRNA translation and stability.....	15
Figure 11. Endosomal take-up of encapsulated mRNA.	17
Figure 12. Overview of mRNA therapeutic strategies.	18
Figure 13. Composition and structure of lipid-based transport vehicles for mRNA.....	20
Figure 14. Reaction cascade for iEDDA click reactions between strained alkenes and tetrazines.....	22
Figure 15. Turn-on effect of tetrazine-conjugated green fluorophores upon iEDDA reaction.	23
Figure 16. Chemical structures of norbornene-modified nucleobase building blocks.	24
Figure 17. Nitroxide spin labels and energy diagram for nitroxides in an external magnetic field.	25
Figure 18. Relationship between relaxation times of differently mobile spin labels with exemplary corresponding cw-EPR spectra.	26
Figure 19. PELDOR experiments for inter-spin distance measurements.	26
Figure 20. Schematic overview of the cellular application and analysis of CP-modified mCh_mRNA.....	32
Figure 21. Chemical structure of the nucleoside triphosphate rTPT3 ^{CP} developed and synthesized by Dr. F. Eggert.	33
Figure 22. Schematic illustration for the sequence design of mCh_mRNA.	33
Figure 23. Schematic illustration for preparation of mCh_DNA by six-letter PCR, followed by GENAEXT for preparation of mCh_mRNA.	35
Figure 24. Agarose gel of different mCh_DNA sequences prepared by PCR.	35
Figure 25. Sanger sequencing results of UBP-modified mCh_DNA.....	36
Figure 26. Agarose gels of mCh_mRNA transcripts without or with additional natural base modifications.	37

Figure 27. Schematic illustration of fluorescent iEDDA click labeling of CP-modified mCh_mRNA.	37
Figure 28. Agarose gel of in vitro click reaction of CP-modified mCh_mRNA.	38
Figure 29. Agarose gel of in vitro click reaction checking for unspecific rTPT3 ^{CP} incorporation into unmodified mCh_mRNA ^{WT}	38
Figure 30. Confocal fluorescence microscopy images of cells transfected with CP-modified mCh_mRNA for live-cell click labeling and fluorescence mRNA visualization.	40
Figure 31. Z-stack series of mCh_mRNA ^{2CP} transfected cells at 6 h after transfection start.	41
Figure 32. Close-up images of mCh_mRNA ^{2CP} transfected cells at 6 h after transfection start.	42
Figure 33. Schematic illustration for the two different sequence sections on mCh_mRNA chosen for RT-qPCR analysis.	44
Figure 34. Results for RT-qPCR analysis of mCh_mRNA level in transfected cells at different time points.	45
Figure 35. Decreased transfection efficiencies by different mCh_mRNA modification patterns.	46
Figure 36. Increased mRNA stability by different mCh_mRNA modification patterns.	47
Figure 37. mCherry protein quantification analysis of cells transfected with different mCh_mRNA sequence variants at different time points.	49
Figure 38. Increased protein yields expressed from mCh_mRNA with different modification patterns.	50
Figure 39. Comparison between cellular mCh_mRNA and mCherry protein levels for selected mCh_mRNA sequence variants.	52
Figure 40. Increased translation efficiencies by different mCh_mRNA modification patterns.	53
Figure 41. Cell viability evaluation of mCh_mRNA transfection and live-cell click labeling.	57
Figure 42. Different models for folding of the mouse Xist RNA A-repeat region.	60
Figure 43. Chemical structure of the nucleoside triphosphate rTPT3 ^{NO} developed and synthesized by Dr. C. Domnick.	61
Figure 44. Structure predictions of truncated Xist A-repeat region RNA sequences.	62
Figure 45. Xist A-repeat region folding as proposed by Fang et al. showing the selected spin labeling positions and the resulting inter-label distances of Xist_RNA ^{2NO} _3_3 or Xist_RNA ^{2NO} _5_3.	62
Figure 46. Alternative proposed structures of Xist A-repeat region with amplified substructures showing the spin label positions of Xist_RNA ^{2NO} _3_3 or Xist_RNA ^{2NO} _5_3.	63

Figure 47. Preparation of UB-modified Xist_DNA by 6-letter PCR amplification and subsequent preparation of spin label modified Xist_RNA by GENAEXT for inter-spin distance measurements by PELDOR.	64
Figure 48. Agarose gel of PCR products of Xist_DNA ^{2UBP} _5_3 and Xist_DNA ^{2UBP} _3_3.	65
Figure 49. Agarose gel of Xist_RNA ^{2NO} _5_3 and Xist_RNA ^{2NO} _3_3 yielded by GENAEXT.	65
Figure 50. Representative snapshots (cluster analysis) of 1 ms MD simulation of the Xist_RNA duplex structures together with schematic illustrations for their label positions and inter-label distances.	66
Figure 51. cw-EPR spectra for Xist_RNA ^{2NO} _3_3 and Xist_RNA ^{2NO} _5_3 with integrated signal peaks for spin counting.	67
Figure 52. PELDOR derived distances for Xist_RNA ^{2NO} _3_3 and Xist_RNA ^{2NO} _5_3.	68
Figure 53. Applications of modified UBs and GENAEXT for site-specific RNA labeling.	71
Figure 54. Agarose gel of unmodified and UB-modified mCh_DNA PCR products.	145
Figure 55. Agarose gel of unmodified and point mutated mCh_DNA and mCh_DNA _{UTR2} PCR products.	145
Figure 56. Agarose gel of UB-modified mCh_DNA _{UTR2} PCR products.	146
Figure 57. Agarose gel of unmodified, UB-modified and point mutated mCh_mRNA.	146
Figure 58. Agarose gel of mCh_mRNA with natural base modifications and UB modifications.	146
Figure 59. Agarose gel of unmodified, UB-modified and point mutated mCh_mRNA _{UTR2}	147
Figure 60. Agarose gel for in vitro fluorescent click labeling of mCh_mRNA with CP-modifications and point mutations.	147
Figure 61. Agarose gel for in vitro fluorescent click labeling of mCh_mRNA _{UTR2} with CP-modifications and point mutations.	148
Figure 62. Agarose gel for analysis of specific rTPT3 ^{CP} incorporation and in vitro fluorescent click labeling of mCh_mRNA.	148
Figure 63. Agarose gel of RT-qPCR products for 6 h analysis of cells transfected with mCh_mRNA sequence variants.	149
Figure 64. Agarose gel of RT-qPCR products for 24 h analysis of cells transfected with mCh_mRNA sequence variants.	149
Figure 65. Agarose gel of RT-qPCR products for 48 h analysis of cells transfected with mCh_mRNA sequence variants.	149
Figure 66. Agarose gel of RT-qPCR products for 6 h analysis of cells transfected with mCh_mRNA and mCh_mRNA _{UTR2} sequence variants.	150
Figure 67. Agarose gel of RT-qPCR products for 24 h analysis of cells transfected with mCh_mRNA and mCh_mRNA _{UTR2} sequence variants.	150

Figure 68. Agarose gel of RT-qPCR products for 48 h analysis of cells transfected with mCh_mRNA and mCh_mRNA _{UTR 2} sequence variants.	151
Figure 69. Agarose gel of PCR amplified RT-qPCR products for sequence elongation.	151
Figure 70. Agarose gel of extended RT-qPCR products after ligation with adapter sequences.	152
Figure 71. Agarose gel of PCR amplified extended RT-qPCR products.	152
Figure 72. Agarose gel of UB-modified Xist_DNA PCR products.....	153
Figure 73. Agarose gel of NO-modified Xist_RNA.	153
Figure 74. Confocal fluorescence microscopy images of cells transfected with mCh_mRNA variants at 6 h after transfection start.....	159
Figure 75. Confocal fluorescence microscopy images of cells transfected with mCh_mRNA variants at 24 h after transfection start.....	159
Figure 76. Confocal fluorescence microscopy images of cells transfected with mCh_mRNA variants at 48 h after transfection start.....	160
Figure 77. Confocal fluorescence microscopy images of cells transfected with mCh_mRNA _{UTR 2} variants at 6 h after transfection start.....	160
Figure 78. Confocal fluorescence microscopy images of cells transfected with mCh_mRNA _{UTR 2} variants at 24 h after transfection start.....	161
Figure 79. Confocal fluorescence microscopy images of cells transfected with mCh_mRNA _{UTR 2} variants at 48 h after transfection start.....	161
Figure 80. Confocal fluorescence microscopy images of transfection controls and untreated cell controls at 6, 24 and 48 h after transfection start.....	162
Figure 81. mCherry protein quantification of cells transfected with mCh_mRNA and mCh_mRNA _{UTR 2} sequences analyzed at 6, 24 and 48 h after transfection start.	163
Figure 82. mCh_mRNA level analysis by RT-qPCR using the 3'-end primer/probe set of cells transfected with mCh_mRNA and mCh_mRNA _{UTR 2} sequences at 6, 24 and 48 h after transfection start.....	188
Figure 83. mCh_mRNA level analysis by RT-qPCR using the internal primer/probe set of cells transfected with mCh_mRNA and mCh_mRNA _{UTR 2} sequences at 6, 24 and 48 h after transfection start.....	188
Figure 84. Plotted luminescence values for assay linearity validation.	229
Figure 85. cNLS mapper results for mCherry protein coding amino acid sequence.	230

8 Eidesstattliche Erklärung

Hiermit versichere ich an Eides statt, dass ich die vorliegende Dissertation mit dem Titel „*Developing new methods for specific RNA modification*“ selbstständig und ohne die Benutzung anderer als der angegebenen Hilfsmittel und Literatur angefertigt habe. Alle Stellen, die wörtlich oder sinngemäß aus veröffentlichten und nicht veröffentlichten Werken dem Wortlaut oder dem Sinn nach entnommen wurden, sind als solche kenntlich gemacht. Ich versichere an Eides statt, dass diese Dissertation noch keiner anderen Fakultät oder Universität zur Prüfung vorgelegen hat; dass sie - abgesehen von unten angegebenen Teilpublikationen und eingebundenen Artikeln und Manuskripten - noch nicht veröffentlicht worden ist sowie, dass ich eine Veröffentlichung der Dissertation vor Abschluss der Promotion nicht ohne Genehmigung des Promotionsausschusses vornehmen werde. Die Bestimmungen dieser Ordnung sind mir bekannt. Darüber hinaus erkläre ich hiermit, dass ich die Ordnung zur Sicherung guter wissenschaftlicher Praxis und zum Umgang mit wissenschaftlichem Fehlverhalten der Universität zu Köln gelesen und sie bei der Durchführung der Dissertation zugrundeliegenden Arbeiten und der schriftlich verfassten Dissertation beachtet habe und verpflichte mich hiermit, die dort genannten Vorgaben bei allen wissenschaftlichen Tätigkeiten zu beachten und umzusetzen. Ich versichere, dass die eingereichte elektronische Fassung der eingereichten Druckfassung vollständig entspricht.

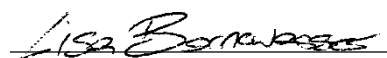
Teilpublikationen:

Bornewasser, L.; Domnick, C.; Kath-Schorr, S., Stronger together for in-cell translation: natural and unnatural base modified mRNA, *Chem. Sci.* **2022**, *13*, 4753-4761 (doi: 10.1039/D2SC00670G).

Bornewasser, L.; Kath-Schorr, S., Preparation of Site-Specifically Spin-Labeled RNA by in Vitro Transcription Using an Expanded Genetic Alphabet, *Methods in Molecular Biology (Clifton, N.J.)* **2022**, *2439*, 223-240 (doi: 10.1007/978-1-0716-2047-2_15).

Domnick, C.; Eggert, F.; Wuebben, C.; Bornewasser, L.; Hagelueken, G.; Schiemann, O.; Kath-Schorr, S., EPR Distance Measurements on Long Non-coding RNAs Empowered by Genetic Alphabet Expansion Transcription, *Angew. Chem. Int. Ed.* **2020**, *59*, 7891-7896 (doi: 10.1002/anie.201916447).

Köln, den 17.12.2022



Lisa Bornewasser